Imperfect upheaval subsea pipeline buckling

TRAN, Vinh Cong

ERRATA

- p 10, l 4 : delete ' both '
- p 19, l 11 : insert ' that ' after ' show '
- p 38, l -3 : delete ' % '
- p 41, eqn (3.3) more sensibly reads

$$q' = \gamma D h \left(1 + 1.17\left[\frac{h}{D}\right] - 0.17\left[\frac{h}{D}\right]^2\right)$$

- p 71, l 13 : delete first ' a '
- p 94, l -3 : note that the prop force is given by $2F_i$ in this context (ref p 149)
- p 103, l 4 : replace ' together with the neglection of ' with ' and neglecting the '
- p 187, l -2 : replace ' is ' with ' are '
- p 246, l 10 : replace ' regarding the neglection of ' with ' by neglecting '

IMPERFECT UPHEAVAL SUBSEA PIPELINE BUCKLING

VINH CONG TRAN

B.Eng (Hons.)

A thesis submitted in partial fulfilment of the

requirements of

Sheffield Hallam University

for the degree of Doctor of Philosophy

March 1994

Contents

List of Figures

List of Tables

List of Plates

Abstract (V C TRAN)

Imperfect Upheaval Subsea Pipeline Buckling

The objective of the research programme has been to develop a set of theoretical models suited to the perceived needs of industrial practice with regard to in-service, subsea pipeline buckling. The role of imperfections is shown to be of central importance. These factors are considered in the context of modern offshore engineering practice, including the particular employment of trenching and/or burial for purposes of protection.

Novel, small scale, full thermo-mechanical system testing is presented, the design and construction of the actual experimental set-up being a key feature of the research programme. Subsidiary geotechnical experimentation is also undertaken. Theoretical studies employing the empirical data provided by latter are assessed against the resulting full system experimental data.

With an introduction to the purpose of the research programme and the physical problem and its mechanical demands given in Chapter 1, Chapter 2 serves to clarify the factors involved. Although novelty involving the testing of burial pipe elements is present in the experimental studies of Chapter 3 the majority of original work lies in the theoretical studies of Chapters 4 to 6 and the full system experimentation reported in Chapter 7. The results of forty-five tests are therein provided and theoretical/experimental correlation considered.

Definition of the upheaval state, crucial to offshore engineering requirements, is considered to be effectively provided for with regard to symmetric prototype configurations and a software suite of complementary models has been developed.

Acknowledgement

The author would like to take this opportunity to express his appreciation to Dr N Taylor, Director of Studies, and Professor A C Walker, External Supervisor, for their help and guidance. Appreciation is also expressed to Mr D A Richardson for his invaluable contribution to the Geotechnical Experimentation.

The author also wishes to thank Messrs N Tidswell, R Brown, J Bickers, P F Lonsborough, T Fox and A Denton for laboratory assistance.

NOMENCLATURE

A	Cross-sectional area
D	Pipe diameter
E	Direct modulus
F, F_i	Shear force at prop
F_A	Resultant axial friction force
F_{fap}	Anchor shear capacity
F_e	End-effects force
F_f	Frictional resistance force
F_p	Pull-Out Force
I	Second moment of area of cross-section
L, L_1, L_2	Buckle lengths
L_D	Dumping interval
L_{fap}	Anchorage spacing
L_o, L_i	Buckle lengths of the imperfection topology
L_s, L_{s1}, L_{s2}	Slip lengths
L_u	Buckle length at upheaval
L^*	Lower limit on buckle length re axial friction force response through slip length
M_x	Bending moment of the buckle at x
M_i	Bending moment of the imperfection curve
M_m	Maximum bending moment of the buckle curve
N_i	Maximum bending moment of the imperfection curve
P	Buckle force

P_a	Axial force component
P_c	Critical buckle force
P_{max}	Maximum buckle force
P_o	Pre-buckling force
P_{qi}	Buckle force at quasi-idealised state
P_s	Weight of soil cover above the pipe
P_u	Buckle force at upheaval
P_w	Pipe weight
Q	Disturbing force
R	Orthogonally applied force to the pipe's surface
T	Temperature rise
T'	Pressure-equivalent temperature rise
T_c	Critical temperature rise
T_{max}	Maximum temperature rise
T_{min}	Minimum safe temperature rise
T_u	Upheaval temperature rise
V	Total potential energy
f	Geotechnical variable
f_A	Friction force parameter
h	Cover depth
k_i	Exponent (i=1,2,3...etc)
k_5, k_6	Geotechnical constants
m	Effective inertial force
n	$\sqrt{P/EI}$
p	Pressure
q	Submerged self-weight of pipeline per unit length
q'	Submerged self-weight of pipeline cover per unit length
r	Pipe radius

t	Wall thickness of pipe
u	Axial displacement of the pipe
u_f	Resultant flexurally induced end shortening
u_s	Resultant longitudinal movement at buckle/slip length interface (peel point)
u_ϕ	Fully mobilised axial displacement
v	Vertical displacement of the pipe
v_i, v_o	Vertical displacement of the imperfection topologies
v_m	Maximum vertical amplitude of the buckled pipe
v_{om}	Maximum vertical amplitude of the imperfection topology
w_m	Maximum lateral amplitude
w_o, w_1, w_2	Buckle amplitudes
x	Spatial coordinate
α	Coefficient of linear thermal expansion
δ	Inclination of pulling-out failure surface to vertical
γ	Specific weight of the soil
ν	Poisson's ratio
ϕ_A	Axial friction coefficient
ϕ'_A	Axial friction coefficient of overburden
ϕ_L	Lateral friction coefficient
Ψ_i	Contact undulation coefficient (i=1,2,3)
σ_m	Maximum compressive longitudinal direct stress
σ_{yld}	Yield stress
θ	Trench angle

nb: Re differential notation - $dv/dx \equiv v_{,x}$ etc

Chapter 1

Introduction

1.1 Research Objective

The present study concentrates on rationalising imperfection types and proposing improved and novel models, incorporating specific features, with respect to upheaval buckling. Both energy and equilibrium based analyses are conducted and these are assessed against alternative established models and full system (model) experimentation, with subsidiary geotechnical testing providing the necessary insight into the associated non-conservative pull-out and friction force characteristics.

1.2 The Physical Problem

The increase in demand for hydrocarbon deposits has led, during the past two decades, to the development of substantial offshore infrastructure. The establishment of oil and gas platforms and subsea pipelines, together with the concomitant ancillary equipment and services in the North Sea, is perhaps the most notable development in question. More recently, marginal offshore fields have been exploited employing unmanned satellite facilities.

Hydrocarbon export frequently employs subsea pipelines which can either simply rest on the sea bed or lie in excavated trenches, with or without burial. The pipes are constructed from steel of high strength and ductility with sufficient wall thickness to withstand the high stresses incurred during installation and operation. The steel is coated for protection against the corrosion associated with the hostile environment and further coated with concrete to provide weight. Overall pipe diameters range typically between 1m (large bore) and 100mm (compact); see Fig 1.1. Compact pipes can feature insulation coating.

Pipeline installation is both sophisticated and expensive and investment is substantial. Failure of a pipeline is costly both in terms of lost production and repair. Great care must therefore be exercised in the design of subsea pipelines and it is with the key aspect of in-service buckling prevention that the present study is concerned.

In-service buckling of subsea pipelines can occur due to the institution of axial compressive forces caused by the constrained thermal and pressure actions. With hydrocarbon transportation temperatures up to $100^{o}C$ above that of the water environment and operating pressures over $10N/mm^2$, these forces can be substantial given the ability of the pipeline/seabed interface to generate the necessary frictional resistance to axial movement.

1.3 Stability basics

In idealised terms, therefore, the pipeline is considered to adopt a straight lie on a flat, rigid surface. Following an initialisation of hydrocarbon flow, the pipe heats up and attempts to expand. If frictional resistance between the pipe and the surface is sufficiently high, axial compression will onset leading to the possibility of buckling wherein lateral flexure, or vertical flexure if circumstances permit, of the pipe will occur. This phenomenon comes under the remit

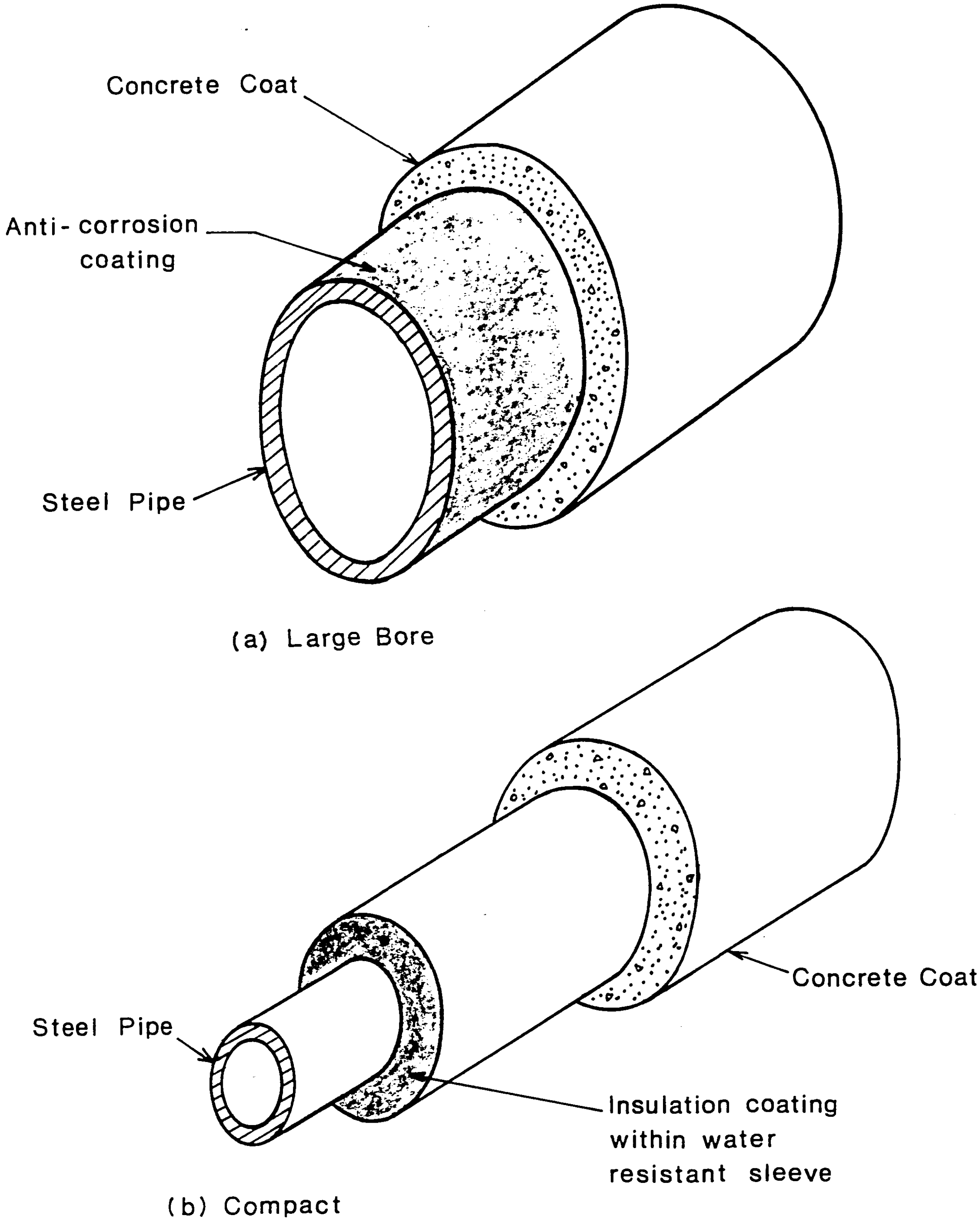

Fig 1.1 Pipe Sections

of Thermo-Mechanical Contact Surface Buckling. Allied studies include rail track buckling and the flexure of steel flats[1,2].

Prior to consideration of the foregoing phenomenon, it is perhaps prudent to briefly discuss the concept of elastic structural stability[3]. Initially, and on the basis of idealised Linear Systems Theory wherein deformations are indefinitely small and constitutive properties linear and elastic, a straight rod, composed of isotropic and homogenous material and subject to axial compression, will suffer axial shortening in direct proportion to the force applied. All system action-response relationships are linear up to some linear elastic system limit.

It is more realistic to study the statics of the rod, however, by considering its loaded equilibrium behaviour in terms of the respective deformed state[3]. If the rod is sufficiently slender and if during the gradually applied axial loading some small, transient, disturbing force (mathematically ill-defined) is additionally applied non-axially to the rod, deformed state studies suggest lateral flexure suddenly becomes the primary system response at some specific value of axial compression. Consider Fig 1.2 (a). The potentially unstable rod or strut, of idealised datum length L, will initially flex or buckle at an axial compression $P=P_c$, the critical load. Fully non-linear kinematic mathematical modelling affords definitive post-buckling characteristics[3,4]. Action-response behaviour is shown in Fig 1.2 (b). For $P<P_c$, linear axial behaviour, represented by equilibrium path 0-1, is obeyed, the disturbing force Q having no measurable effect. At $P=P_c$ and in the presence of Q, path 1-2 is then followed, system flexure being represented by the central and maximum lateral displacement w_m. Paths 0-1 and 1-2 are stable in the presence of Q. Theoretically, if Q is suppressed from the system, axial behaviour alone continues for $P>P_c$; this is an unstable path which

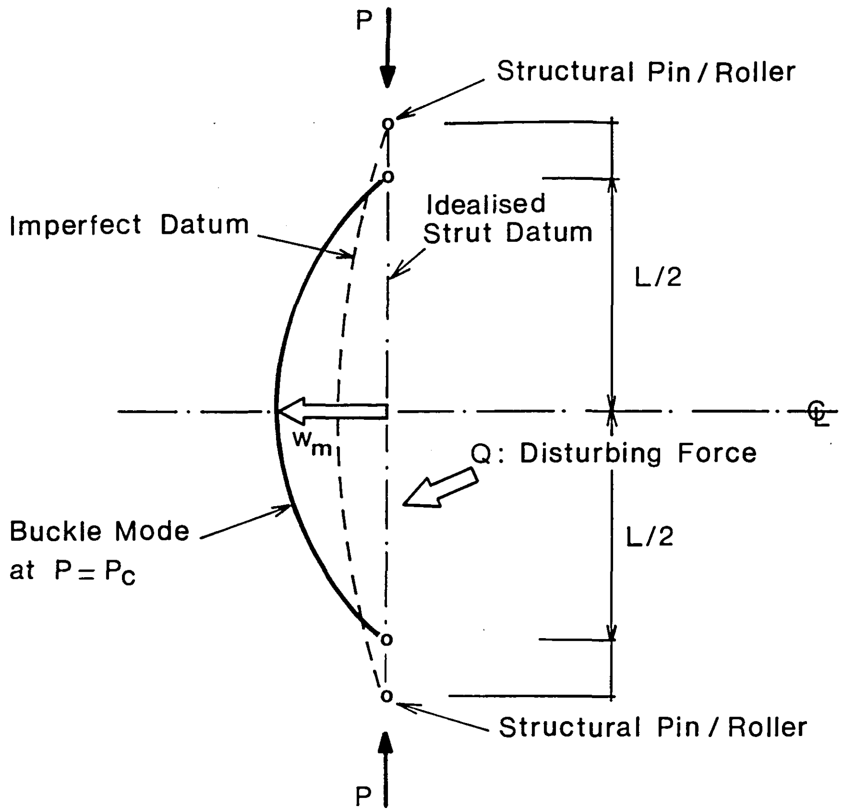

(a) Strut Topology

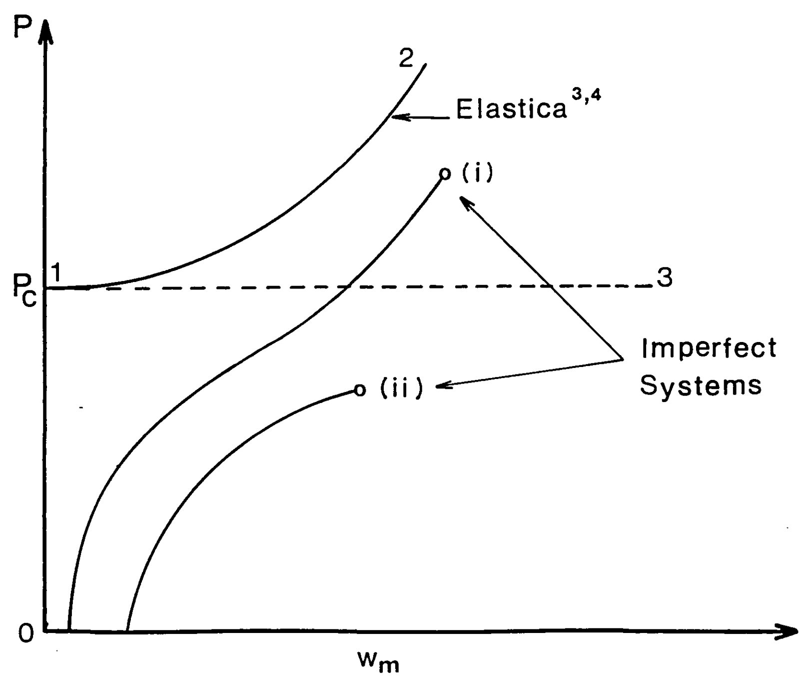

(b) Action - Response Loci

Fig 1.2 Structural Stability

would degenerate into path 1-2 if provoked (ie. Q applied); note that path 1-3 relates to the most basic non-linear kinematic modelling[3,4].

With respect to the slender strut, therefore, idealised and linear theory predicts linear axial behaviour throughout whilst quasi-idealised (ie. ill-defined Q present), non-linear theory suggests this to be potentially unstable and predicts the possibility of buckling and predominantly flexural behaviour. Physically, Q represents some system imperfection such as initial curvature as represented by the imperfect datum in Fig 1.2(a); physically imperfect strut behaviour is typified by loci (i) and (ii) in Fig 1.2(b). Other physical imperfections include material inhomogeneity and anisotropy (eg. residual stresses in formed steelwork) and loading eccentricity. Regardless of their nature, imperfections are conceptually equivalent in their effect[5] and, logically, all struts must be assumed to suffer imperfections.

Accordingly, experimentation generates structural response of the form typified by loci (i) and (ii), shown terminating at the elastic limit, in Fig 1.2(b). Applying great care to minimise the physical imperfections invariably present, such loci can lie very close to their respective, stable quasi-idealised counterparts (ie path 0-1-2). Path (ii) relates to a less slender and/or more imperfect prototype than does path (i). *The study of stability is the study of the effect of imperfections*; imperfections serve to trigger buckling response. For brevity and in accordance with established practice, the classical, quasi-idealised studies incorporating only non-physical or ill-defined imperfections will henceforth be termed 'idealised' buckling studies[3,4].

Classically, the strut is considered to exhibit symmetric bifurcation as path 0-1-2 could equally well adopt negative values of w_m, subject to the compliance of Q, there being no physical restraint upon the strut for all P except for the pinned and rollered boundary conditions. In subsea pipeline buckling, to which attention is now to be turned, there are a number of additional, complicating factors with respect to the above. First, the presence of a contact surface precludes symmetric bifurcation and a variety of buckling modes requires attention. Second, the buckle length L is variable (and unknown), the boundary conditions not being physically fixed. Third, the compression is thermally induced. Fourth, seabed irregularities or undulations generate imperfections of particular forms.

1.4 Idealised Subsea Pipeline Buckling

Figure 1.3(a) shows a straight pipeline, formed from homogenous and isotropic material, lying on a flat, horizontal and rigid surface. The basic section shown in Fig 1.3(b) indicates that buckling can be in either the vertical v or lateral w sense given sufficient length L in which to buckle and sufficient axial compression P to cause buckling. Recent offshore developments have led to the use of trenching and/or burial as suggested in Fig 1.3(c) and (d) whereby the considerations of vertical buckling, following the path of least resistance, predominate .

With regard to the general case indicated by Fig 1.3(a) and (b), six primary buckling modes have been identified as shown in Fig 1.4 [6]. The following computations relate to the idealised analysis of the vertical mode and it is intended that they serve to introduce the key mechanics involved in subsea pipeline buckling.

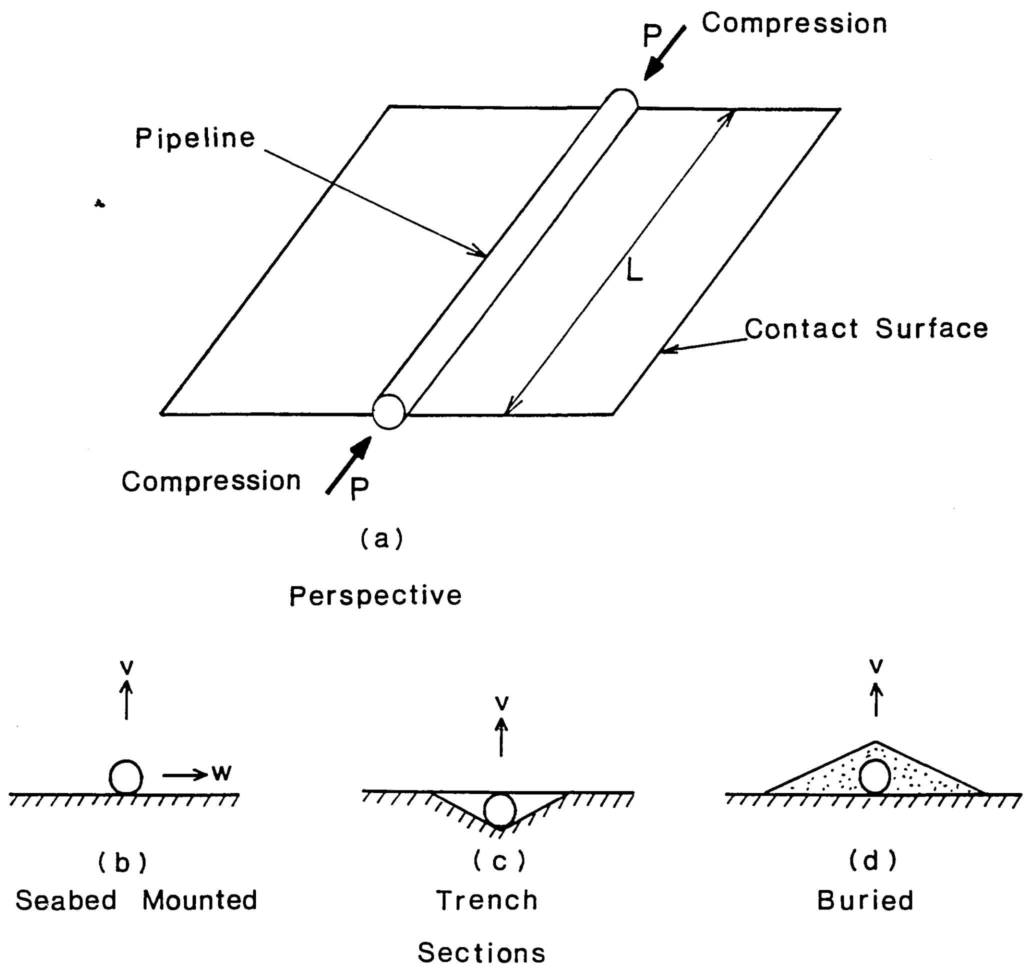

Fig 1.3 Pipeline Lie

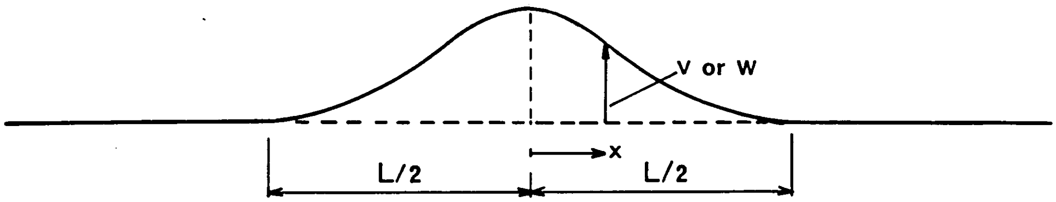

(a) Vertical Buckling / Lateral Mode 1

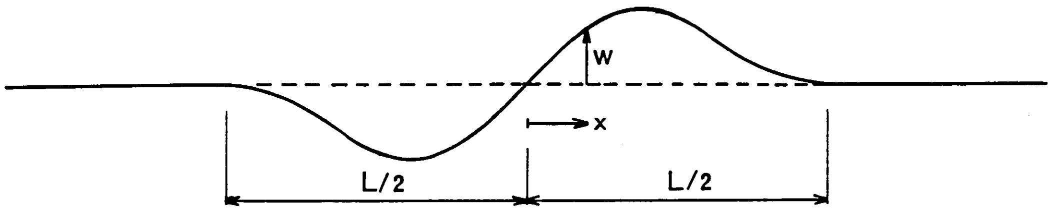

(b) Lateral Mode 2

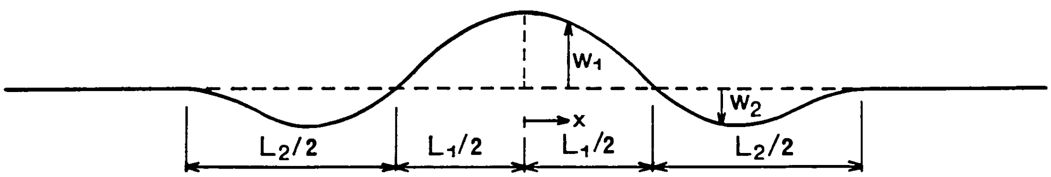

(c) Lateral Mode 3

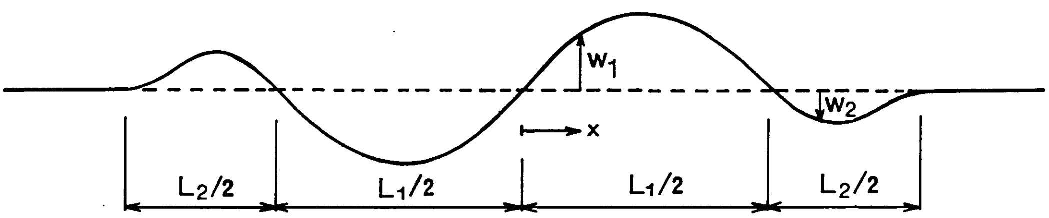

(d) Lateral Mode 4

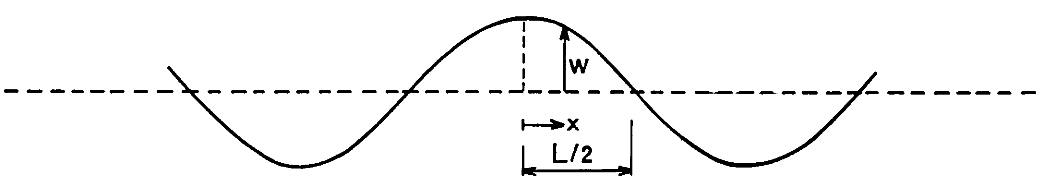

(e) Lateral Mode 5

Fig 1.4 Primary Buckling Modes

Figure 1.5 depicts the respective topology. The seabed is taken to be rigid, the deformations relatively small and the constitutive properties linear elastic. The datum topology involves a straight lie when unstressed and unstrained. Following the initialisation of both hydrocarbon flow, uniform increases in temperature T and pressure p are incurred generating an axial compressive force P_0 in the straight pipeline of the form[6]

$$P_0 = AE\alpha T + \frac{Ap}{t}\left(\frac{D}{2} - t\right)(0.5 - \nu) \tag{1.1}$$

where A denotes the effective cross-sectional area of the steel pipe of wall thickness t and outer diameter D, E the appropriate direct modulus and α the coefficient of linear thermal expansion. This is effectively a pre-stressing force with the axial deformation u and strain remaining zero.

At some critical value of P_0, buckling suddenly occurs with the constrained thermal expansion being released within the buckled length of region L with compensation occurring within the adjacent slip lengths L_s. That is, the 'compressive' force within the buckled length, buckling force P, reduces from P_0 as the pipe slips inwards towards the buckle whose arc length exceeds the corresponding datum chord length. The upwards movement of the buckle is resisted by the submerged self-weight of the pipe (ie zero overburden currently assumed - see later) of q/unit length whilst the inwards movement generating tension in the slip length is resisted by axial friction at the seabed/pipeline interface .

For the symmetrical system involved, the post-buckling boundary conditions relating directly to the buckle length L become,

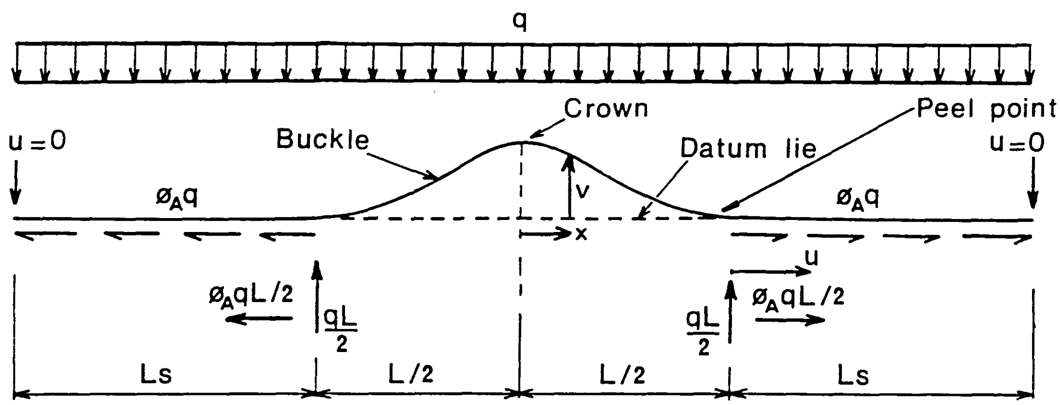

(a) Topology

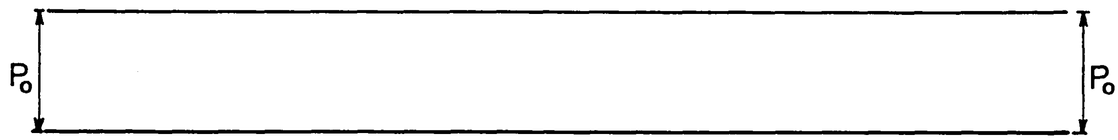

(b) Axial Force Distribution Pre-Buckling

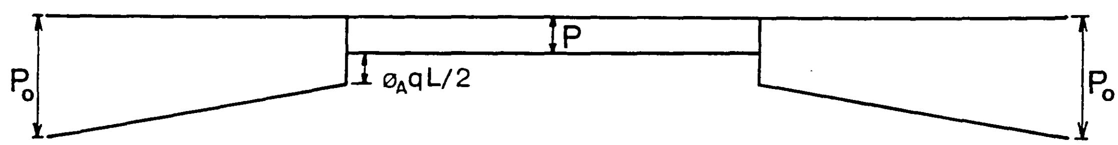

(c) Axial Force Distribution Post-Buckling

Fig 1.5 Vertical Mode – Idealised Modelling ($P = P_{qi}$)

$$v|_{x=0} = v_m \quad ; \quad v,_x|_{x=0} = 0$$
$$v|_{L/2} = v,_x|_{L/2} = v,_{xx}|_{L/2} = 0 \tag{1.2}$$

where x=0 and x=L/2 denote the crown and peel point locations respectively.

The associated linearised differential equation takes the form

$$EIv,_{xx}+Pv+q(4x^2-L^2)/8=0 \tag{1.3}$$

where I denotes the second moment of area of the steel pipe wall. (It is assumed that the seabed is capable of providing the point reaction qL/2 at the peel points[7].) Solving eqns (1.2) and (1.3) affords, with n^2=P/EI,

$$v=\frac{q}{EIn^4}\left(1+\frac{n^2L^2}{8}-\frac{n^2x^2}{2}-\frac{\cos nx}{\cos(nL/2)}\right) \tag{1.4}$$

and,

$$\tan(nL/2)=nL/2 \tag{1.5}$$

for which the lowest root provides

$$nL=8.9868 \tag{1.6}$$

or

$$P=80.76\frac{EI}{L^2}=P_{qi} = 3.962(\frac{EIq}{v_m})^{1/2} \tag{1.7}$$

Key derivative expressions include

$$v_m=v|_0=v_{\max}=2.407.10^{-3}\frac{qL^4}{EI} \tag{1.8}$$

for amplitude,

$$v,_x|_{\max} = 8.657.10^{-3}\frac{qL^3}{EI} \tag{1.9}$$

for maximum slope (≤0.1 rads) and,

$$u|_{L/2}=\frac{(P_o-P)L}{2AE}-\frac{1}{2}\int_0^{L/2}(v,_x)^2\,dx \tag{1.10}$$

ie

$$u|_{L/2}=\frac{(P_o-P)\,L}{2AE}-7.9883.10^{-6}\left(\frac{q}{EI}\right)^2 L^7 \tag{1.11}$$

for longitudinal movement at the peel point (at any L), where a negative value for $u|_{L/2}$ indicates compressive flexural end shortening exceeding the accompanying tensile extension within the buckle length .

With particular reference to the slip lengths and with ϕ_A representing the respective fully mobilised axial friction coefficient[8], longitudinal equilibrium affords

$$P_o-P=\frac{\phi_A qL}{2}+\phi_A qL_s \tag{1.12}$$

whilst, with boundary conditions

$$u|_{\frac{L}{2}+L_s}=u,_x|_{\frac{L}{2}+L_s}=0 \tag{1.13}$$

the tensile relief or extension of the slip length at any L is given by

$$u|_{\frac{L}{2}}=-\frac{\phi_A qL_s^2}{2AE} \tag{1.14}$$

Matching eqns (1.11) and (1.14) thereby gives

$$\frac{(P_o-P)\,L}{2AE}-u_f+\frac{\phi_A qL_s^2}{2AE}=0 \tag{1.15}$$

where $u_f=\int_0^{L/2} v,_x^{\,2}\, dx/2=7.9883.10^{-6}(q/EI)^2L^7$ denotes flexural end-shortening through the half buckle length such that solutions for v, P, L and L_s are obtained from eqns (1.4) and (1.7) [from eqns (1.2) and (1.3)], (1.12) and (1.15), together with eqn (1.1) in terms of T and $p(P_0)$.

For the parametric values given in Table 1.1, primary action/response behaviour is typified in Fig 1.6 which includes the classical *garland* curve. This

Parameter	Symbol	Value	Unit
External diameter	D	650	mm
Wall thickness	t	15	mm
Direct modulus	E	206000	N/mm^2
Effective inertial self-weight	q	3.8	N/mm
Yield stress	σ_{yld}	448	N/mm^2
Thermal coefficient	α	$11x10^{-6}$	$/^oC$
Axial friction coefficient	ϕ_A	0.7	
Poisson's ratio *	ν	0.3	

Table 1.1 Pipe parameters (seabed mounted h=0 and D=650mm)

Note: * ν employed for the evaluation of pressure component as required.

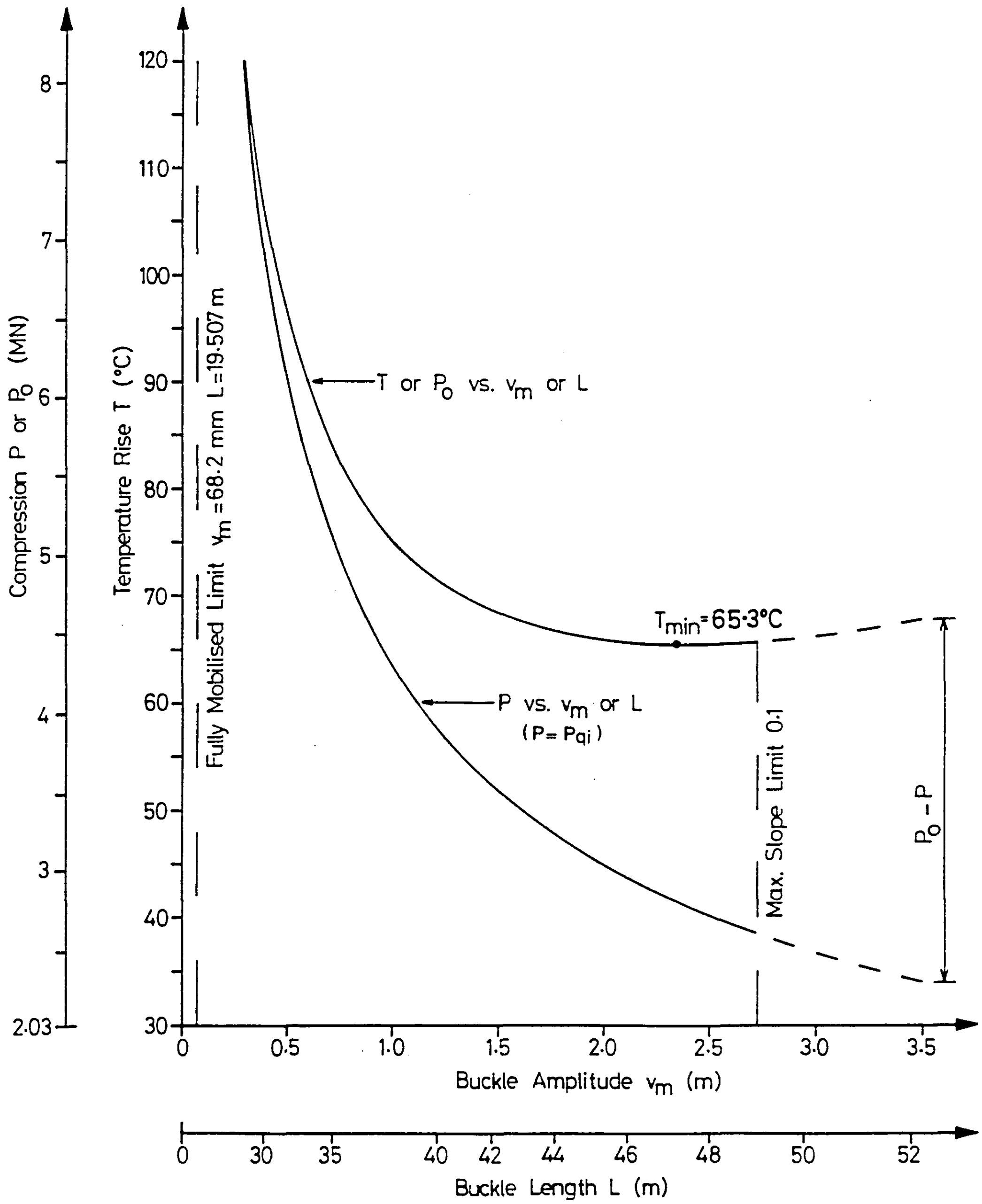

Fig 1.6 Fully Mobilised Loci

exhibits a nominally asymptotic relationship with the ordinate due to the assumption of seabed rigidity[9,10]. The key factors to note include the minimum safe temperature rise state T_{min}, below which idealised buckling will not occur and therefore of major importance to designers, and the continuing decay of the buckling force . Only the rising thermal path is stable. Resistance to buckling is encouraged by the inertial force q and the axial friction coefficient ϕ_A.

It should be noted from eqn (1.1) that action can be wholly considered in terms of either temperature rise T or pressure rise p or both. Merging the known action parameters T and p leads to computational convenience such that eqn (1.1) can be written

$$P_o = AE\alpha T + AE\alpha T' \tag{1.16}$$

where

$$T' = \frac{pD(0.5-\nu)}{2E\alpha t} \tag{1.17}$$

with $T' \approx pD/(24t)$ for typical material values (N,mm units). Herein, action T alone is thereby considered, with pressure equivalent T' to be applied as a back-end reduction as necessary.

Having set out the basics of the subsea pipeline buckling mechanism, attention will now be turned to establishing an historical context for the present study .

1.5 Historical Context

The first published work in the field of subsea pipeline buckling surfaced in 1980 [7]; duly noted reference was therein paid to earlier studies in the related field of rail track buckling. The foregoing vertical buckling analysis leans heavily on the work of Martinet published in 1936 [2]. Early subsea pipeline studies dealt with idealised analyses[6-11].

The first imperfection-based analyses were published in 1986 [12,13], the same year seeing the output of studies on the nature of the seabed/pipeline topology[14]. Since this time an increasing number of publications have been produced, concentration being placed on the vertical mode[15-27]. These publications include various types of analysis corresponding to the variety of subsea topologies deemed to be viable (see below). Only one study extant has involved energy as opposed to equilibrium modelling[12].

In the earlier years, large bore pipes simply lying on the seabed were the focus of attention. As lateral mode buckling in this situation occurs at lower temperatures than vertical mode buckling, the former mode received much consideration. Comparing the vertical mode with lateral mode 1, for example, the primary mathematical variation hinges on the inertial loading term which in the latter case is denoted by $\phi_L q$, rather than q, where ϕ_L represents the fully mobilised lateral friction coefficient; recall Figs 1.4 and 1.5. With $\phi_L < 1$ [10,11], the implications are obvious. Further, so long as the elastic properties of the pipeline are not violated, lateral mode snaking can be interpreted as a relief mechanism should it occur .

With the later employment of smaller bore pipes for in-field hydrocarbon transportation from marginal fields employing satellite technology[21], the vertical mode has become of paramount importance as such pipes must be trenched and/or buried to protect them, for example, from damage by anchors and/or trawling gear - the latter can weigh up to 100 tonnes. Trenching/burial largely obviate lateral mode buckling as noted previously, see Fig 1.3(c) and (d). Additional system refinements include partial burial, the use of fixed anchorage points and trench-incline buckling possibilities, all of which will be considered in the following. It should be noted that the vertical mode buckling of buried pipelines is termed upheaval buckling. In practice, there are a variety of imperfection configurations each with their own causes and consequences. These can, however, be simplified into two basic forms, that in which a vertical pipe undulation is continuously supported[12,19] by the sea bed or trench bottom and that where the pipe lies over a discrete or isolated prop with voids to either side between the pipe and the sea bed or trench bottom[13,18]. The respective responses to thermal loading are quite different and this important matter is further discussed below.

Experimentation to-date has been primarily concerned with the geotechnical factors involved in the problem[8,28-35]. Their very nature is more variable than that of the synthetic pipeline itself and empirical formulae have been provided for various seabed lie configurations for ϕ_A, ϕ_L and q', where q' relates to the inertial force characteristics enjoyed by buried pipelines. Enhanced geotechnical experimentation is reported herein[36].

Full system testing, which is relatively expensive even at small scale, has only recently been reported[37,38]. Indeed, the difficulty of full scale testing is illustrated by the fact that the buckle lengths involved are considerable; field failure case studies[13,27] cite wavelengths of 24m-70m together with amplitudes of 0.5m-2m.

Considering subsea pipeline buckling problems to possess two distinct mechanical fields, the buckling and slip lengths respectively, then the key idiosyncratic features of most mathematical models have been concerned with the interpretation of the buckling field. This reflects the greater mathematical complexity associated with the analysis of this field and the various physical imperfections postulated by the authors concerned. The simplification in slip length (L_s) modelling provided by assuming axial frictional resistance to be fully mobilised - frictional resistance is deformation - or movement-dependent as will be shown - tempts most authors to adopt this feature thereby standardising their slip length field models[6,13,19,39]. There have been a small number of deformation-dependent slip length studies; to-date, these show little change in primary response characteristics (T vs v_m,L) is thereby incurred[9,10]. These latter models do not generate finite slip lengths, however, and are therefore incomplete, particularly as each slip length can, according to the *non-conservative* fully mobilised modelling approach, be of the same order of magnitude as the respective buckle length. The importance here is that the length $L+2L_s$ demanded by whichever modelling is employed must be physically available for the model to be valid. The scale of testing required is again relevant here.

1.6 Imperfect Upheaval Buckling

As noted in Sections 1.3 and 1.5, imperfections are of central importance in stability studies and three archetypal seabed imperfections are herein considered as illustrated in Fig 1.7. In the first case, the pipeline remains in continuous contact with some vertical undulation in an otherwise idealised horizontal and straight lie. The isolated prop alternatively features a sharp and distinct vertical irregularity such that voids (sea-filled) exist to either side. The

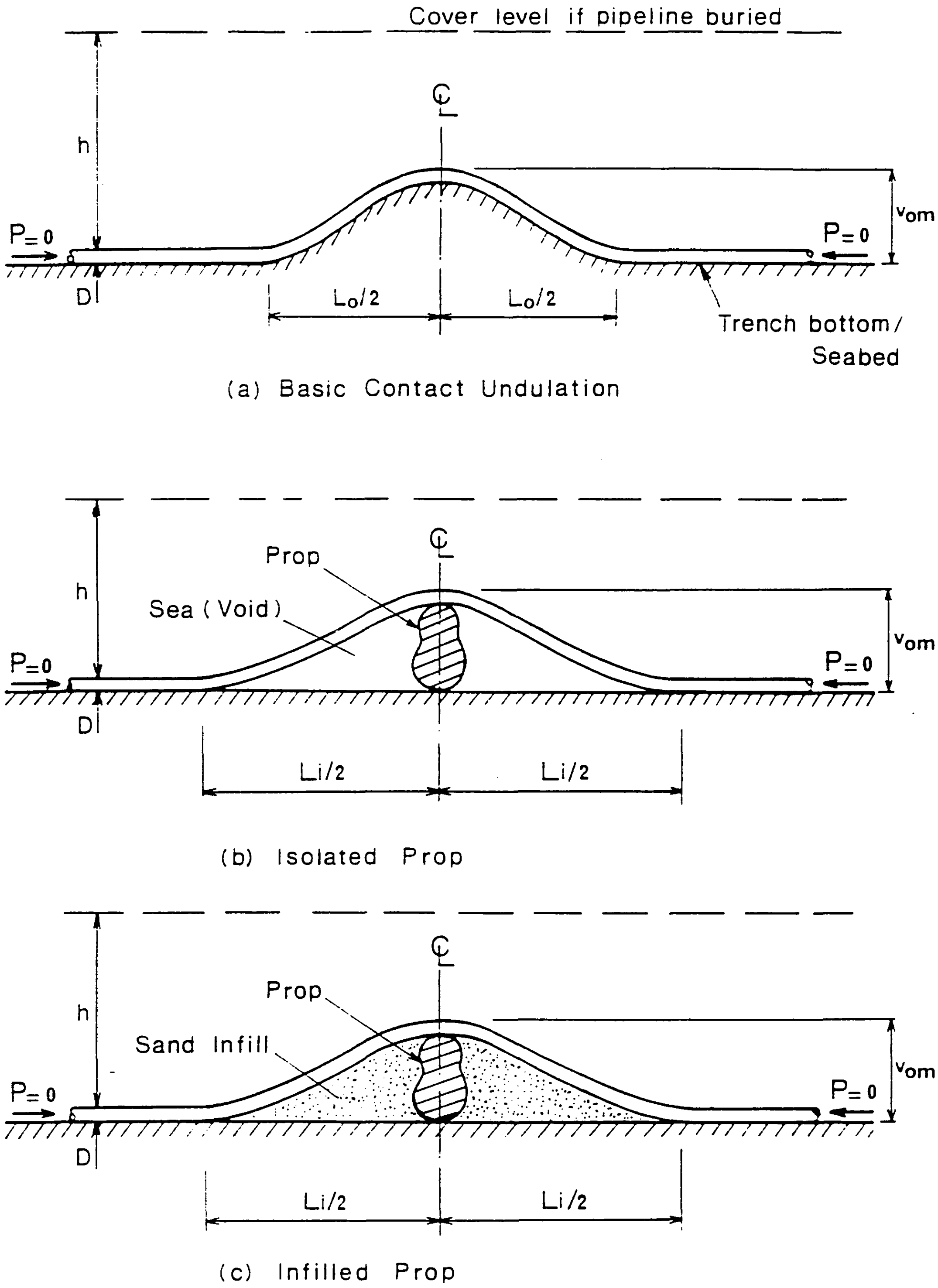

Fig 1.7 Typical Imperfection Configurations

third case occurs where the above voids become infilled with leaching sand and represents a special sub-case of the first. The initial imperfection is denoted by amplitude v_{om} and wavelength L_o or L_i as shown. Whilst L_i is determined from simple statics, L_o is subject to individual engineering judgement[12]. All cases are presumed to be physically symmetric in keeping with most subsea pipeline buckling studies reported to-date with asymmetry presently a very restricted field[40].

Initial physical imperfections serve to trigger buckling as discussed in section 1.3; resistance to buckling in prototype situations is less than that according to corresponding idealised studies as suggested in Fig 1.2(b) [3]. One of the first published and most conservative subsea pipeline buckling imperfection models is typified in Fig 1.8 [12] and relates to the configuration given in Fig 1.7(a). It attempts to represent the worst case scenario in the manner adopted by Perry for strut stability studies and now well-established as the basis for the respective European Design Code[3]. It is herein termed the *Empathetic* model as the geometry of the imperfection

$$v_o=v_{om}\left(0.707-0.26176\frac{\pi^2x^2}{L_o^2}+0.293\cos\left(2.86\frac{\pi x}{L_o}\right)\right) \tag{1.18}$$

is empathetic to the idealised buckling mode given by eqn (1.4) noting eqn (1.6), ie.

$$v=v_m\left(0.707-0.26176\frac{\pi^2x^2}{L^2}+0.293\cos\left(2.86\frac{\pi x}{L}\right)\right) \tag{1.19}$$

with the amplitude/wavelength ratio v_{om}/L_o uniquely in agreement with the idealised expression v_m/L, ie.

$$\frac{v_{om}}{L_o^4}=\frac{2.407.10^{-3}q}{EI}=\frac{v_m}{L^4} \tag{1.20}$$

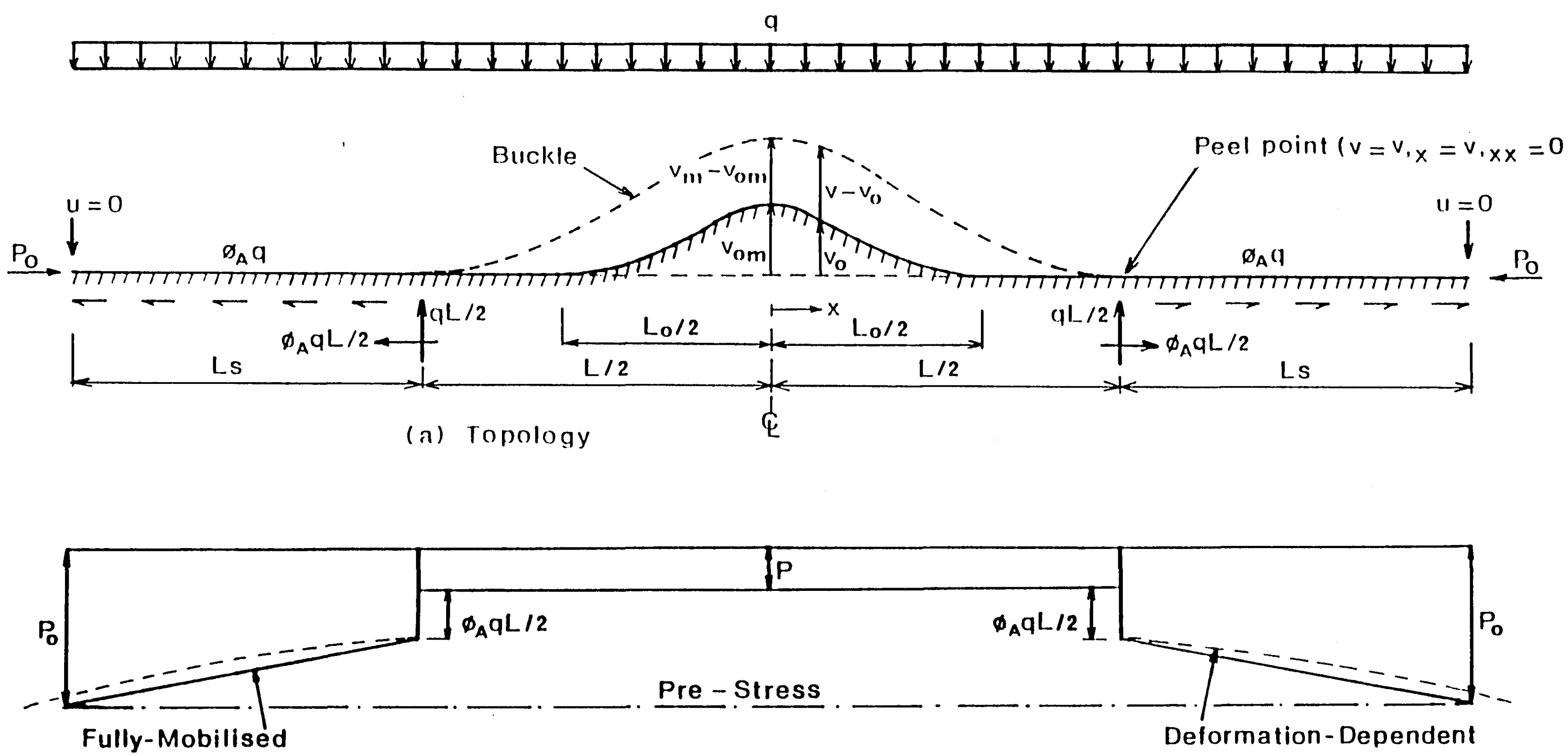

(b) Axial Force Distribution – Post Buckling

Fig 1.8 Fully Mobilised Post - Buckling
Empathetic Imperfection Modelling (Vertical Mode)

The modelling logic is considered clear with the amplitude v_{om} being achieved at zero load P=0. The imperfect system is *unstressed when initially deformed* [3] whilst the idealised system is unstressed when (initially) straight; empathetic energy exchange occurs in a minimalised manner.

From Fig 1.8, therefore, the pipeline is taken to be gradually heated above ambient with upheaval or lift-off, ie $v_m > v_{om}$, occurring at some value of axial force $P=P_u$, with buckling occurring for $P_u < P_{qi}|_{vm=vom}$. The quintessential buckling model employs a Potential Energy (V) approach with

$$V = \int_0^{L_o/2} \frac{EI}{2}(v,_{xx}-v_o,_{xx})^2\,dx + \int_{L_o/2}^{L/2} \frac{EI}{2}(v,_{xx}-v_o,_{xx})^2\,dx$$
$$+ \int_0^{L_o/2} q(v-v_o)\,dx + \int_{L_o/2}^{L/2} q(v-v_o)\,dx \tag{1.21}$$
$$- \int_0^{L_o/2} \frac{P}{2}(v,_x^2-v_o^2,_x)\,dx - \int_{L_o/2}^{L/2} \frac{P}{2}(v,_x^2-v_o^2,_x)\,dx$$

for $L>L_o$, the corresponding equilibrium state being given by $V,_{vm}=0$. Noting that for $0<x<L_o/2$, the derivatives of initial curvature, slope and deflection with respect to v_m are null, as are the actual values of initial curvature, slope and deflection for $L_o/2<x<L/2$, then applying the statics criterion affords the characteristic equation

$$\frac{45.35486EIv_m}{L^3} - \psi_1\frac{EIv_{om}}{LL_o^2} + 0.072785qL - 0.93605\frac{Pv_m}{L} = 0 \tag{1.22}$$

where

$$\psi_1 = 4.60314\sin k_1k_2 + 10.59445k_2\left(\frac{\sin k_1k_3}{k_3} + \frac{\sin k_1k_4}{k_4}\right) \tag{1.23}$$

with $k_1=4.4934$, $k_2=L_o/L$, $k_3=1+k_2$, and $k_4=1-k_2$

In accordance with the Stationary Potential Energy Theorem, kinematic parameter v_m is considered an independent variable, with eqn (1.20) not being applied prior to the calculus of $V'_{vm}=0$ - ie; L is not a kinematic variable within V. Substituting eqn (1.20) into eqns (1.22) and (1.23) yields

$$P=P_{qi}\left(1-\frac{\psi_1}{75.6}\left(\frac{L_o}{L}\right)^2\right) \tag{1.24}$$

where $P_{qi}=80.76EI/L^2=3.962(EIq/v_m)^{\frac{1}{2}}$ denotes the idealised buckle force,with $L \geq L_o$ and $v_m \geq v_{om}$ regarding imperfection studies, with the dependent bending moment

$$M=EI(v,_{xx}-v_o,_{xx}) \tag{1.25}$$

affording the maximum moment (x=0) to be

$$M_m=-0.06938q(L^2-L_o^2) \tag{1.26}$$

Maximum compressive longitudinal direct stress can then be obtained from

$$\sigma_m=\frac{P}{A}+\frac{M_mD}{2I} \tag{1.27}$$

with $\sigma_m \leq \sigma_{yld}$ the limiting elasto-plastic yield stress.

Flexural end shortening now takes the form

$$\begin{aligned} u_f &= \frac{1}{2}\left(\int_0^{L/2}(v,_x)^2\,dx-\int_0^{L_o/2}(v_o,_x)^2\,dx\right) \\ &= 7.9883.10^{-6}\left(\frac{q}{EI}\right)^2(L^7-L_o^7) \end{aligned} \tag{1.28}$$

replacing the idealised u_f term of eqn (1.15).

In summary, eqns (1.20) and (1.27) relate amplitude v_m and wavelength L to axial compression P for $v_m > v_{om}$ and $L > L_o$. Of particular interest is the upheaval state to which eqn (1.24) can only approach *in the limit.* Numerical computations give, as $L \to L_o$

$$P_u = 40\% \, P_{qi}\big|_{L=L_o} \tag{1.29}$$

clearly a severe reduction in buckling onset or upheaval resistance from the idealised state as per eqn (1.7). The uniqueness of eqn (1.20) assures the uniqueness of eqn (1.29) with $v_m \rightarrow v_{om}$ as $L \rightarrow L_0$ as $v \rightarrow v_0$. That is, the pipeline separates or lifts off from the seabed over the whole of L_0 uniquely - the first peel point occurs at $x = \pm L_0/2$ for $P = P_u$.

The complete system requires the incorporation of eqns (1.1), noting eqns (1.12), (1.15), (1.16), (1.17) as modified above, and (1.24), together with eqns (1.18), (1.19) and (1.20) - ie five equations for v, P, L and L_s in terms of $T(P_0)$. As noted previously, other imperfection models extant[13,18,19] differ primarily in possessing their own idiosyncratic alternative expressions to eqns (1.18) and (1.24) and thereby eqn (1.29), of particular interest to practising designers in their desire to preclude buckling behaviour.

Figure 1.9 shows typical empathetic modelling action/response loci, data being as per Table 1.1. Imperfection loci lie within the respective idealised envelope to which they converge, maximum stress and deformation system constraints not withstanding, in the limit as the relative effects of the initial imperfection decays [note Fig 1.2 (b) also]. Fully stable behaviour occurs for larger imperfections whilst stiffer resistance occurs for lesser cases, but this is at the risk of snap or dynamic action[12,13] following attainment of some maximum temperature rise T_{max} being incurred together with the concomitant high stressing penalties. The idealised locus is non-conservative.

Whilst the *Empathetic* model originates elsewhere[12], the foregoing

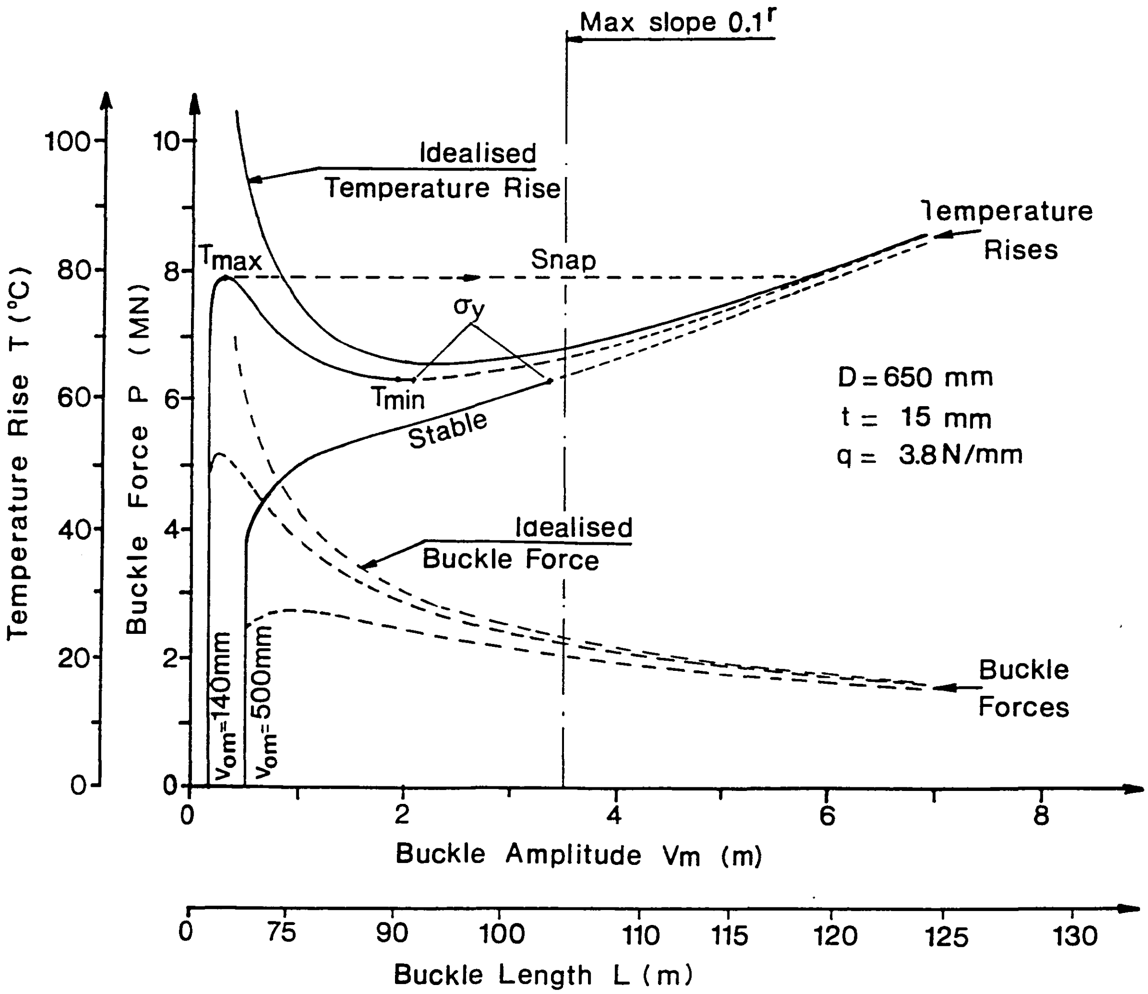

Fig 1.9 Parametric Responses for Empathetic Model
Effect of Initial Imperfection Height

definitively associates it with fully mobilised friction modelling and the model is further enhanced in the following study.

1.7 Summary

The physical problem together with the key conceptual and mathematical factors have been set out in temporal context. The important role of the system imperfection in buckling studies has been particularly identified. A classification is now proposed which will indicate the forward path of the programme initially identified in Section 1.1.

Chapter 2

Upheaval Buckling Classification

2.1 Purpose

By attempting a Systems Analysis for the research programme it is hoped to clarify and unify the factors involved. Throughout, only symmetric, elastic buckling relative to a rigid infinite half-space is considered. Analysis is thereby limited to rotations <0.1 rads and stress $<$ yield. Buckling and slip lengths are so large that singular (St Venant) *end effects* - eg sea-bed vertical reaction of $qL/2$ in Fig 1.8 - are considered to be negligible. Both theoretical and experimental studies are employed.

2.2 Systems Analysis Interpretation

Figure 2.1 details the breakdown of the programme. Activities 1 and 2 have been introduced in Chapter 1 together with some consideration of Activity 3a; novel developments of the *Empathetic* model are proposed in Chapter 4 regarding Activities 3a and 3b. Activity 3 can be seen to largely concern the key imperfection modelling studies and it is useful to recall Fig 1.7 here. The proposed Isolated Prop model (*Isoprop*) of 3d is of novel form and a related Infilled Prop model (*Blister*) is also formulated in Activity 3c.

Activity 4 suggests the eventual production of a user-friendly software suite, typical graphical output being already indicated by Figs 1.6 and 1.9. All digital computing was conducted employing a PC Emulator (note Appendix A).

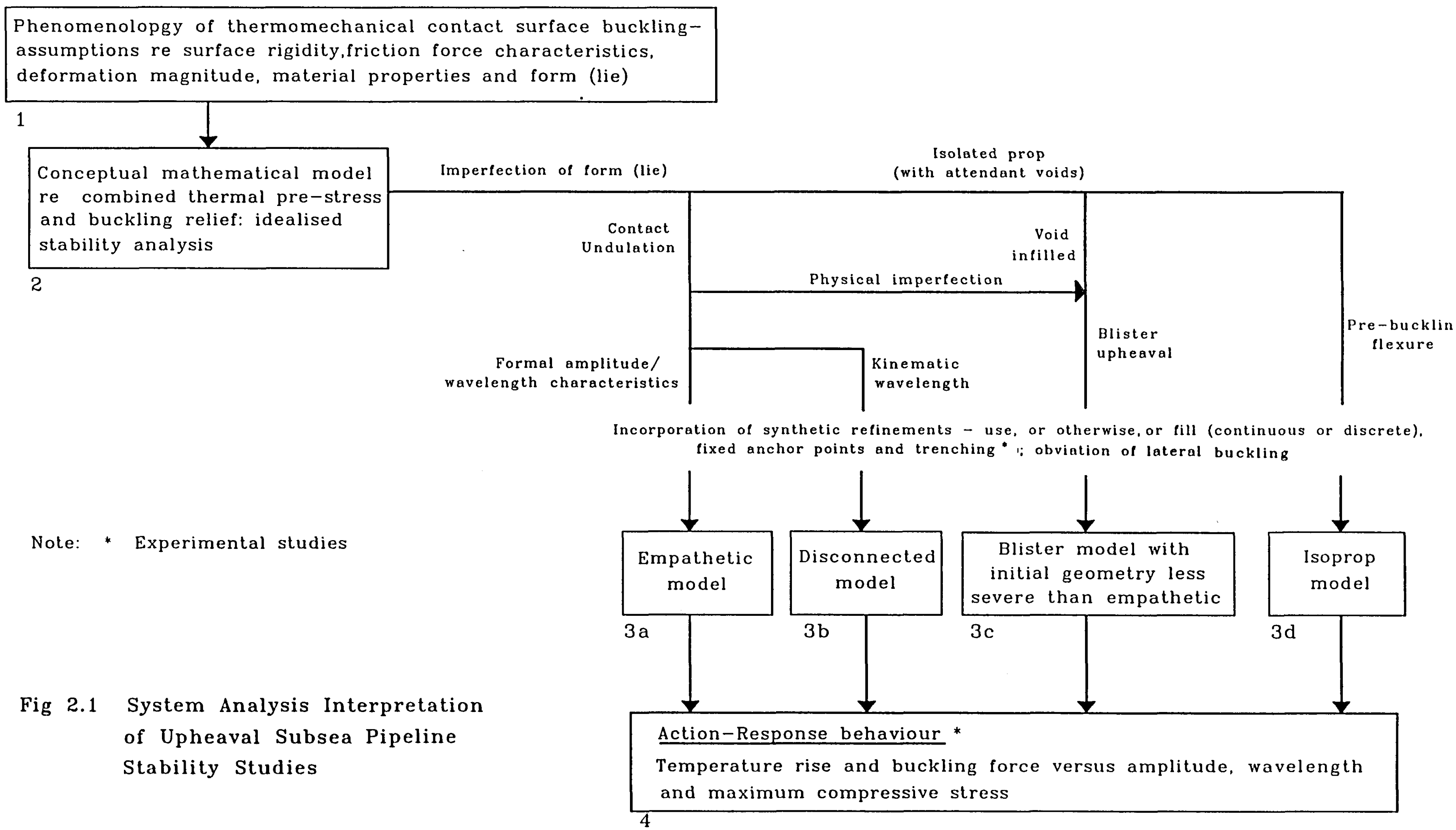

Note: * Experimental studies

Fig 2.1 System Analysis Interpretation of Upheaval Subsea Pipeline Stability Studies

2.3 Preliminary Observations

The overbend of an imperfect subsea pipe serves to trigger upheaval buckling wherein the pipe lifts off the imperfection whilst resistance to this is provided by the respective effective download (ie self-weight, burial overburden) and pipe stiffness.

Whilst the assumption of *stress-free when initially deformed* possesses obvious appeal in the case of the contact undulation imperfection as illustrated in Fig 1.7(a) due to continuous bearing being available for example, this familiar strut-associated characteristic[3] is perhaps a less attractive proposition in the case of the isolated prop hanging under submerged self-weight - note Fig 1.7(b). However, given the complex procedures accompanying pipe laying[41] and the lack of associated accurate residual stress data, claims of accurate stress modelling regarding subsea pipeline buckling must surely be somewhat questionable until appropriate and definite data are made available[42-44]. Accordingly, higher-order non-linear modelling which would admittedly enable ratchetting analysis to be undertaken is not herein considered in detail[19] - pipelines suffer heating/cooling cycles during routine or in-service operation. Further, in the case of the infilled prop imperfection illustrated in Fig 1.7(c), the manner of the actual infilling process will also surely affect initial inertial loading (nb q) considerations; North Sea conditions are typically of granular form (ie sand/silt) rather than of consolidated form (clay)[45]. Although asymmetric buckling[40] can occur with, say, $v,_x|_0 \neq 0$ and $v_0,_x|_0 \neq 0$, it is felt that more remains to be answered with respect to the more basic symmetric modelling cases at this stage.

The key concept is thereby considered to be that of the modelling of a rational set of symmetric imperfections of form. Whilst it is considered that the *Empathetic* model possesses valid, mathematical *worst-case scenario* credentials as previously noted, the distinct prop-based imperfections are clearly feasible as physical probabilities[18,19]; as will be shown, these latter imperfections lead to models whose mathematics obey quite distinct physics and Fig 2.2, developed from Fig 1.7, serves to clarify the respective distinctions. To the design engineer, these theoretically less conservative but potentially more realistic models possess a more attractive definition of rationality. Furthermore, the respective upheaval state, of primary interest to the design engineer, is a function of the imperfection definition.

Regarding the important matter of experimentation, two sets of tests are implemented, these also being identified in Fig 2.1. Geotechnical tests relating to buried configurations and developed from previous, similar but contact surface mounted experimental study[8] are initially reported as they provide insight into the theoretical studies of Activity 3; these tests are to determine inertial and friction force characteristics in the presence of burial. Second, novel 'full' system testing is undertaken later in the programme in order to test the various hypotheses (Activity 4).

2.4 Summary

The research programme has been set out in the context of the perceived engineering problem. The novel geotechnical experimental studies regarding buried pipes are now presented in order to set the ensuing vertical buckling theoretical studies in physical context.

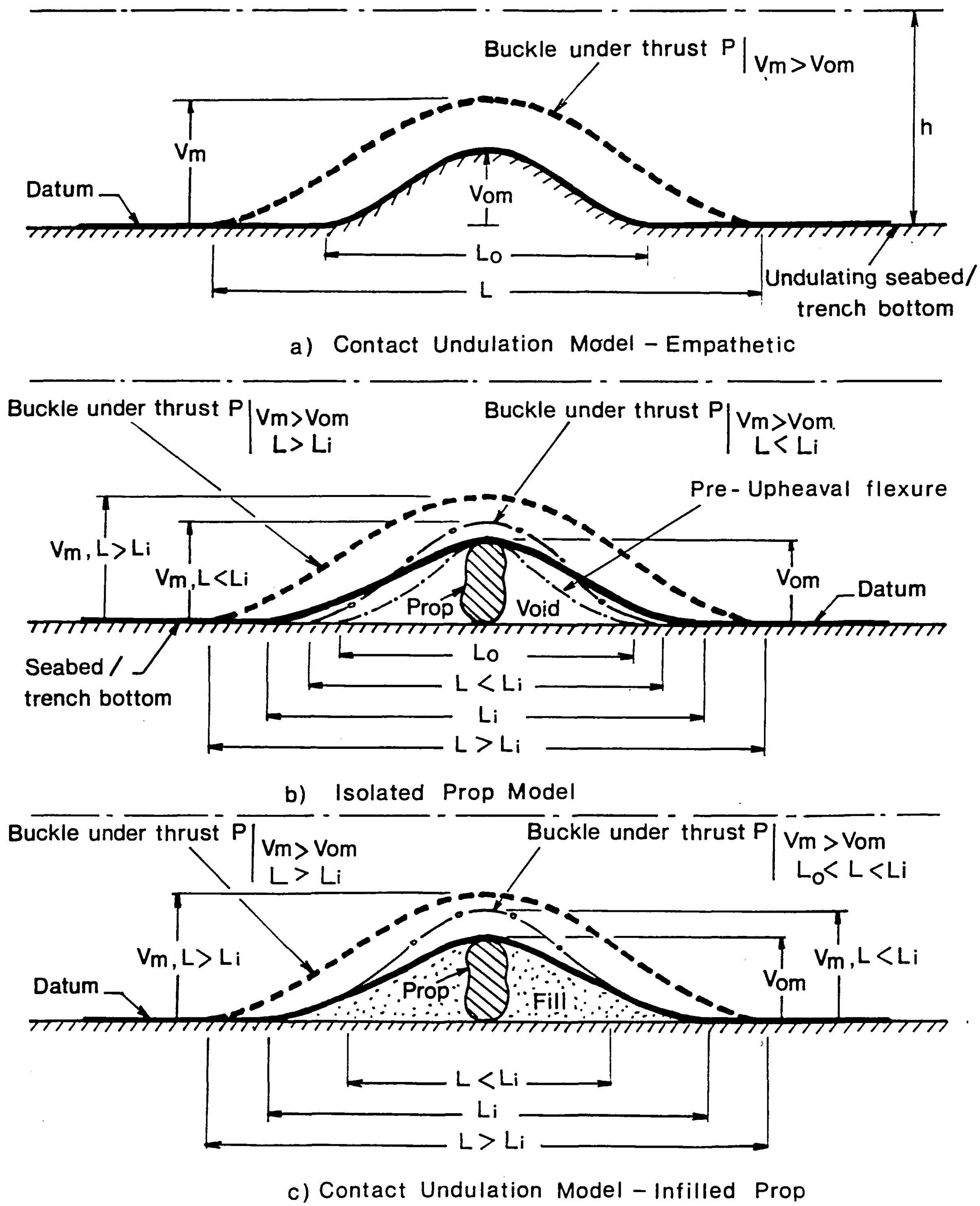

Fig 2.2 Basic Upheaval Buckling Imperfection Topologies

Chapter 3

Geotechnical Experimentation

3.1 Introduction

With reference to Figs 1.5 and 1.8 which typify vertical mode buckling, the axial friction force coefficient ϕ_A and the inertial loading q relate to the geotechnical parameters involved in upheaval buckling. It should be noted that inertial loading is only of geotechnical (and deformation-dependent) form if the pipeline is buried and herein the total inertial loading is taken to be q+q' per unit length where q' denotes the *effective* submerged self-weight of the overburden or fill employed when pipelines are buried within or upon the seabed. Whilst inertial and friction force data appertaining to seabed-mounted pipelines can be claimed to be reasonably well-established[13,46], that for buried pipelines is of limited form[19,20]. Inertial loading characteristics have been considered in terms of geotechnical pull-out tests for a restricted range of burial topologies[13,46] whilst values for axial friction force coefficient ϕ_A have been similarly suggested for buried configurations[19,20]. Surface mounted friction testing has previously suggested that bearing pressure, also a function of cover depth, affects the pipeline/seabed interface and thereby ϕ_A[8]. Herein, values for, and the deformation-dependent nature of, q+q' and ϕ_A appertaining to semi-infinite buried pipelines are determined from geotechnical testing on pipe elements of finite length, due allowance being made for the associated end effects. Data from a set of thirty-six novel small-scale pull-out and axial friction tests is assessed with respect to previously unreported burial topologies.

3.2 Geotechnical Factors

Small scale testing was employed to facilitate the establishment of a substantial data base for a variety of pipeline/burial topologies. Sand was chosen as the supporting medium in view of North Sea conditions and a sieve analysis identified the requisite medium-to-fine sand[35]. Dry testing was employed for convenience, noting that a Coulomb medium was involved. Recalling the basic sections of Fig 1.3 and noting that the imperfection configurations of Fig 1.7 can relate to pipelines being buried or trenched or both or neither, then Fig 3.1 shows three typical prototype burial topologies, cover being of the order $D \leq h \leq 3D$ [13]. Testing sought to replicate type (a) given that data on type (b) already exists. Throughout, tests were far longer in the preparation than the execution.

3.3 Pull-Out Tests - Set-Up and Procedure

The requisite experimental topology is shown in Fig 3.2. A discrete element of 48.3mm O.D. steel pipe represented the pipeline, the pipe being of 3.2mm wall-thickness and possessing a self-weight of 35.3N/m. The sand was first compacted to a typical density, ascertained later, of 1680kg/m^3. A horizontal trench was then cut to the required depth and the pipe (with enclosed ends and lifting straps) emplaced, to be covered with a loose sand fill of typical density 1510kg/m^3. The lifting straps were connected to a spreader beam and transducers mounted to read directly from the buried specimen.

Clearly, as the pipe is pulled vertically, some cover will be disturbed at the ends of the pipe - so called *end effects.* These effects must be catered for if the pipe specimen is to relate to an *infinitely* long pipeline prototype.

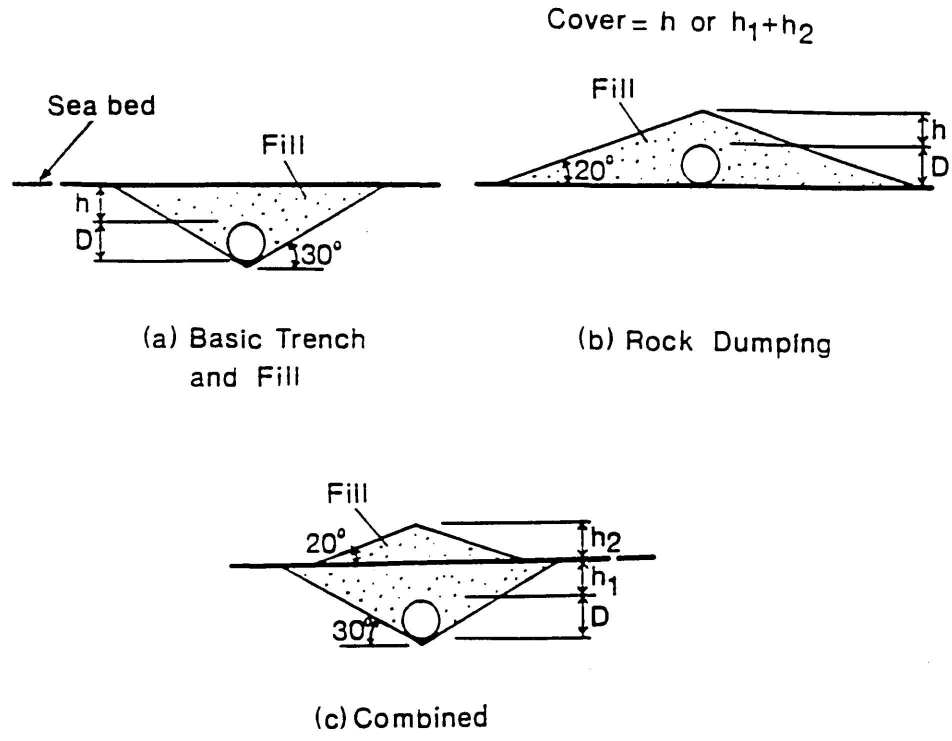

Fig 3.1 Typical burial topologies

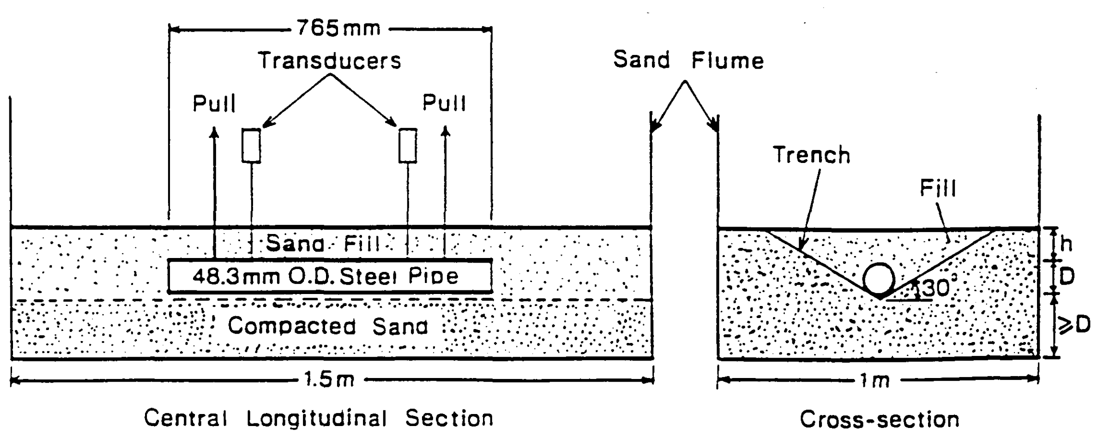

Fig 3.2 Pull-Out Topology

End-effects are dealt with by ensuring the specimen is considerably shorter than the accommodating flume and by experimental identification of the ensuing effects for future deletion from the gross vertical pull values. A plane strain condition is thereby approached[13].

Stroke loading was applied to the lifting straps and the appropriate vertical pull/displacement characteristics recorded until substantial post-maximum pull-out force state deformation had been achieved. Dry testing enabled accurate assessment of the fill failure boundary on the sand surface, this boundary becoming distinct as the maximum pull-out force state was approached. Nine tests were undertaken, careful flume re-filling and sand compaction being implemented with each test.

3.4 Pull-Out Tests - Results

Averaged pull-out characteristics are illustrated in normalised terms in Fig 3.3 for cases of h/D=1.5, 2.25 and 3, strap pull being denoted by F_p, pipe weight by P_w. The loci show that only small deformations are onset up to the maximum pull-out state, deflection then increasing rapidly down the post-maximum falling branch. The loci bear comparison with that given elsewhere[13]; although of generally similar form, the falling branch gradients herein are less severe, this reflecting the different burial topology under investigation - recall Figs 3.1(a) and (b). The maximum pull-out values are indicative of the mechanical effect of pipeline burial, the (submerged) self-weight being effectively increased by factors ranging between 9.7 and 3.7 for covers of 3D and 1.5D respectively; these are non-conservative ratios as due allowance must be made for the end-effects present in the discrete pipe test. This allowance is best undertaken

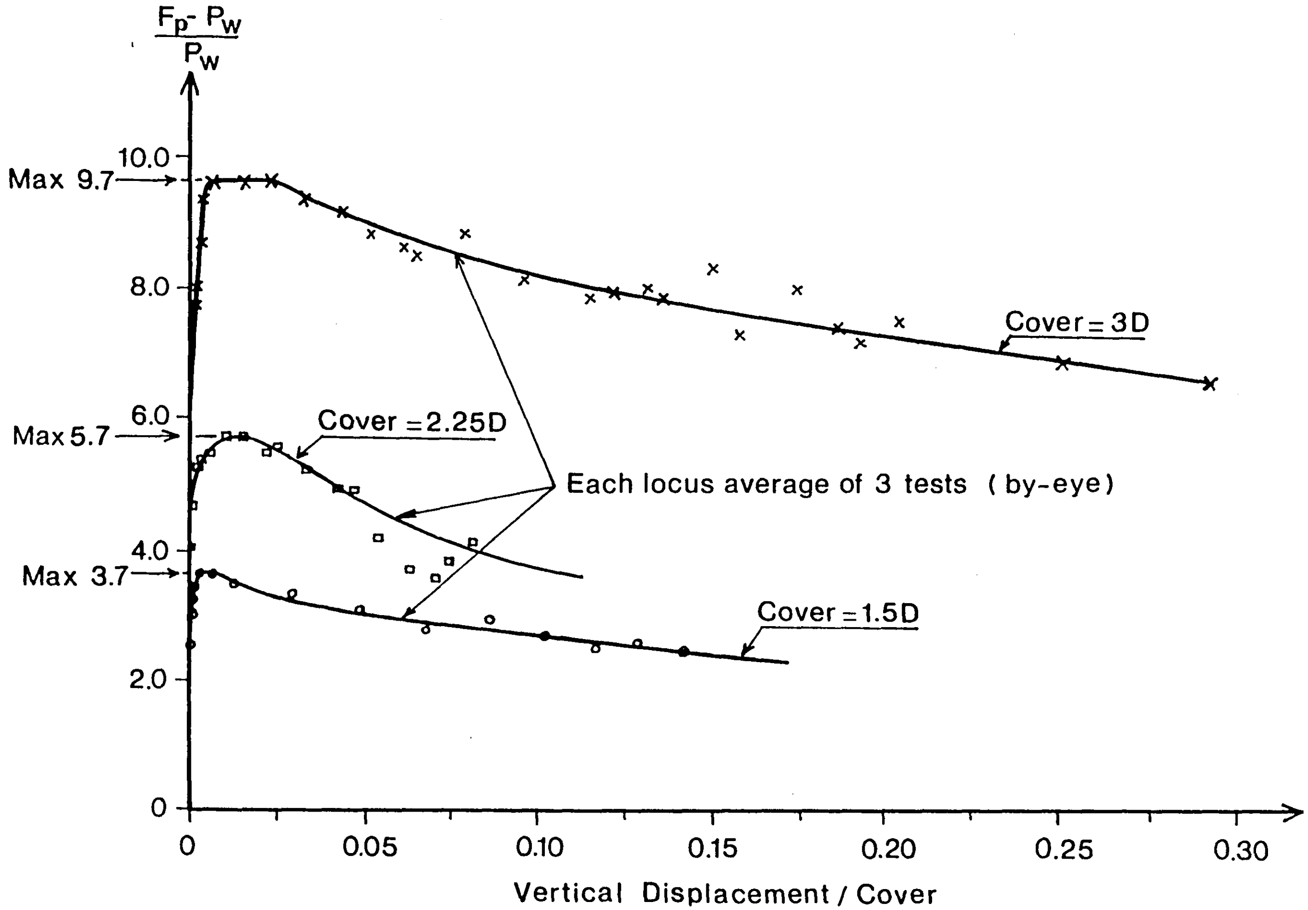

Fig 3.3 Pull-Out Tests Results For 48.3mm O.D. Pipe

when considering the maximum pull-out values in terms of cover height provided. Figure 3.4 illustrates the appropriate data. The section detail shows the failure boundary rising at θ to the vertical through the sand. The net maximum pull-out force relates to the weight of cover fill, identified by shading in Fig 3.4, contained within the failure boundaries and above the pipe, together with the vertical component of the surface tractions active on the failure boundaries. For a discrete length L of pipe, the geometry added to Fig 3.5 readily enables the net pull-out force to be given by

$$F_p-P_w-F_e= L\gamma\left(Dh+Dh\tan\theta+H^2\tan\theta+\frac{D^2}{2}+\left(\frac{D^2}{4}\right)\tan\theta-\frac{\pi D^2}{8}\right) +L\gamma\left((1-k_5)\frac{(h+D/2)^2}{2}\sin 2\theta\right) \tag{3.1}$$

where γ represents the specific weight of the soil, k_5 is a geotechnical constant and F_e denotes the end-effects force

$$F_e= \left(\pi\gamma\left[Dh(\tan^2\theta+\tan\theta)+h^2\tan^2\theta+\frac{D^2}{4}(1+\tan^2\theta+2\tan\theta)\right]\frac{(h+D/2)}{3}\right) +\left(\pi\gamma\left[(1-k_5)\frac{(h+D/2)^3}{6}\sin 2\theta\tan\theta\right]\right) \tag{3.2}$$

F_e corresponds to sand surface semi-circular failure boundary profiles of radius $D/2+(h+D/2)\tan\theta$ being achieved at each end of the pipe. In each of eqns (3.1) and (3.2) the former bracketed term refers to the fill weight component, the latter to the failure boundary tractions.

With $\theta=20^o$ from observation, evaluations of eqns (3.1) and (3.2) employing $k_5=0.33$ (geotechnical value for active pressure) show $100F_e/F_p \leq 10\%$ and a locus corresponding to eqns (3.1) and (3.2) with L=1m is shown in Fig 3.5 together with net experimental values at h/D=1.5, 2.25 and 3. These values are adjusted to take

Note Zone I relates to net pull-out force
Zone II relates to additional end-effect force

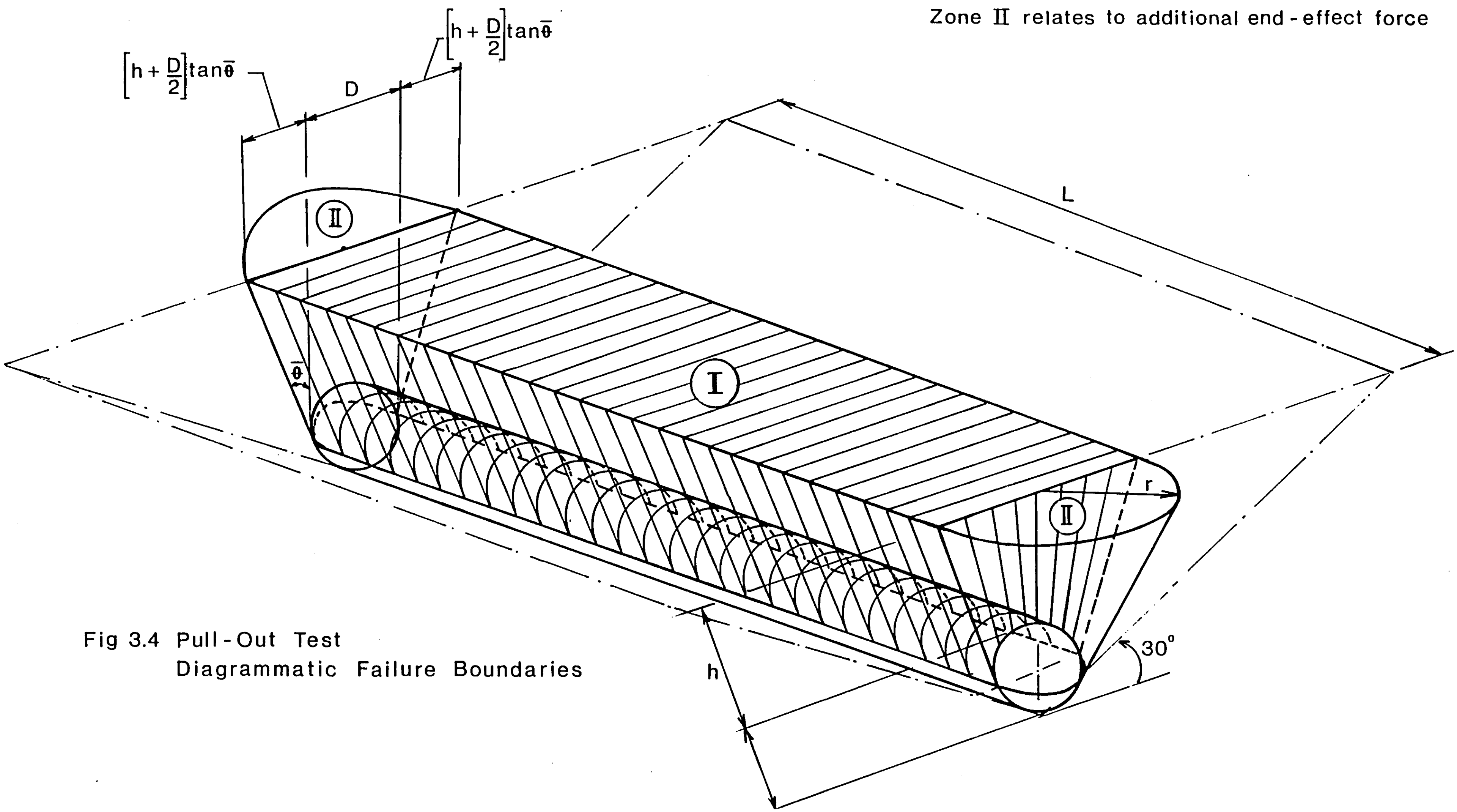

Fig 3.4 Pull-Out Test
Diagrammatic Failure Boundaries

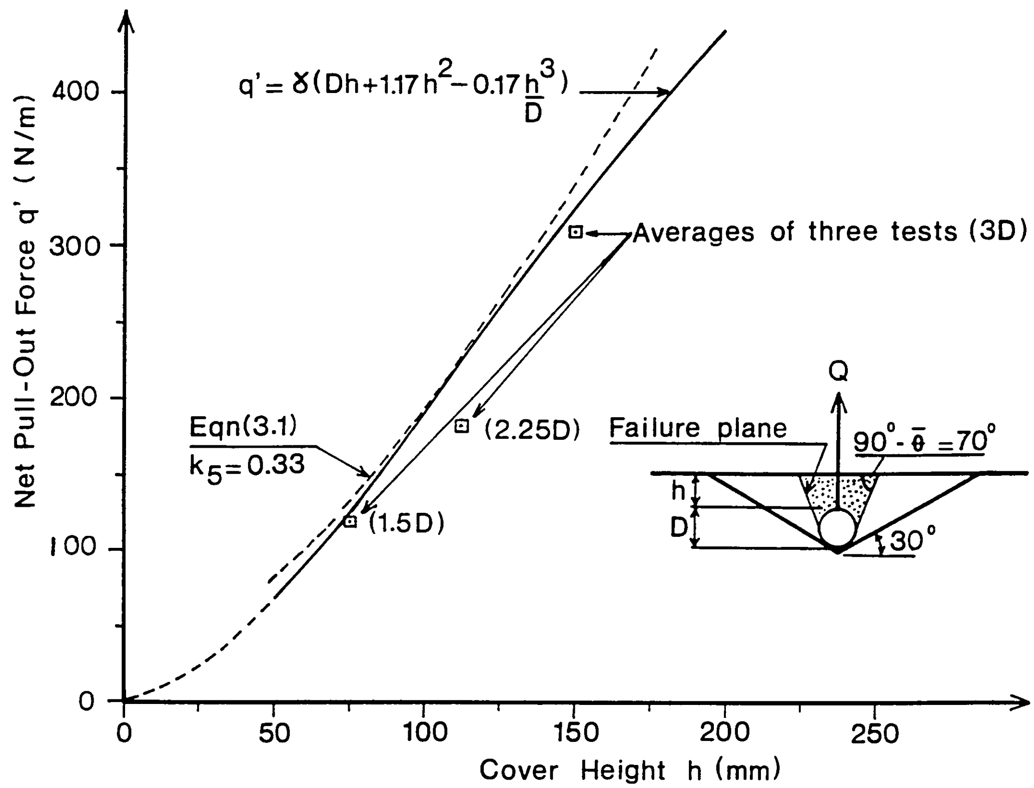

Fig 3.5 Pull-Out Force _ Cover Height Results

account of the end-effects term of eqn (3.2) and to provide convenient per metre data, factoring P_w by 0.765^{-1} recalling Fig 3.2. That is, the graphical ordinate $q'=F_p-P_w-F_e$ in Fig 3.5 represents the net maximum pull-out resistance force per metre of pipeline. Accordingly, the use of eqns (1.3) and (1.4), for example, in the context of continuously buried pipelines would require the substitution of q+q' for q regarding inertial loading characteristics. An empirical design formula

$$q'=\gamma\left[Dh+1.17h^2-0.17\frac{h^3}{D}\right] \tag{3.3}$$

relating net pull-out force to cover depth and pipe diameter is suggested and added to the figure.

Equation (3.3) is similar to its equivalent[13] elsewhere although the coefficient of h^2 is suitably enhanced. Further support for eqn (3.3) comes from the general shallow anchor pull-out expression

$$q'=\gamma Dh\left(1+\frac{h}{D}f\right) \tag{3.4}$$

where f is a geotechnical variable. For the experimental values at h=1.5D and 3D, f=0.9 and 0.69 respectively, these values again being consistent with those given elsewhere[13].

Finally, two wet tests were undertaken employing a clear water depth of D and with h=D. A corresponding dry test gave a pull-out force which to within $\pm$ +10% of the average wet value. Plates 1-5 show instrumentation and testing work.

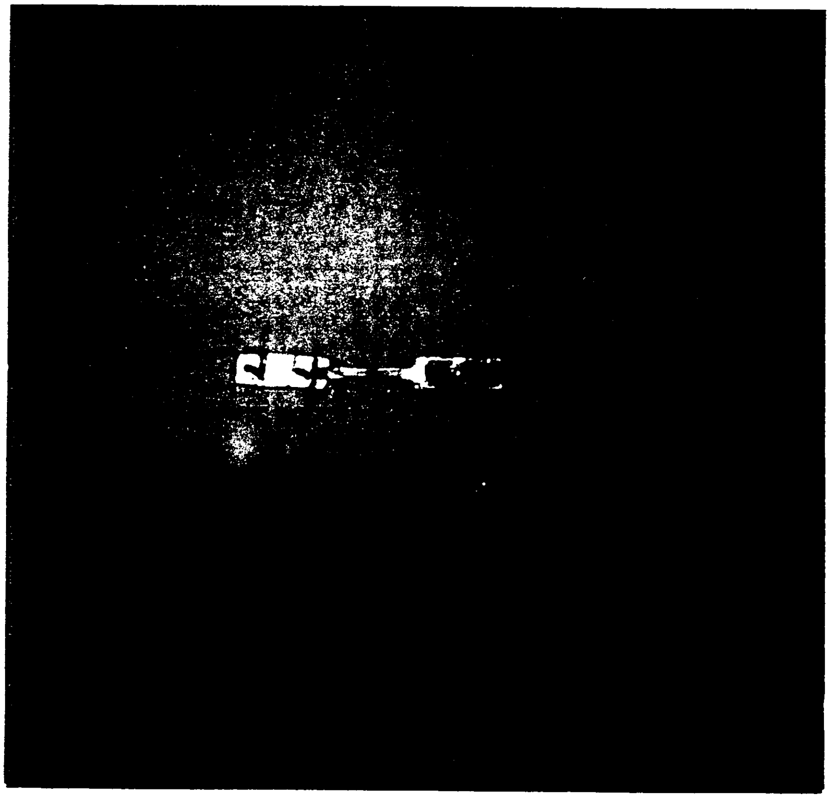

Plate 1   In-House "Load" Cell

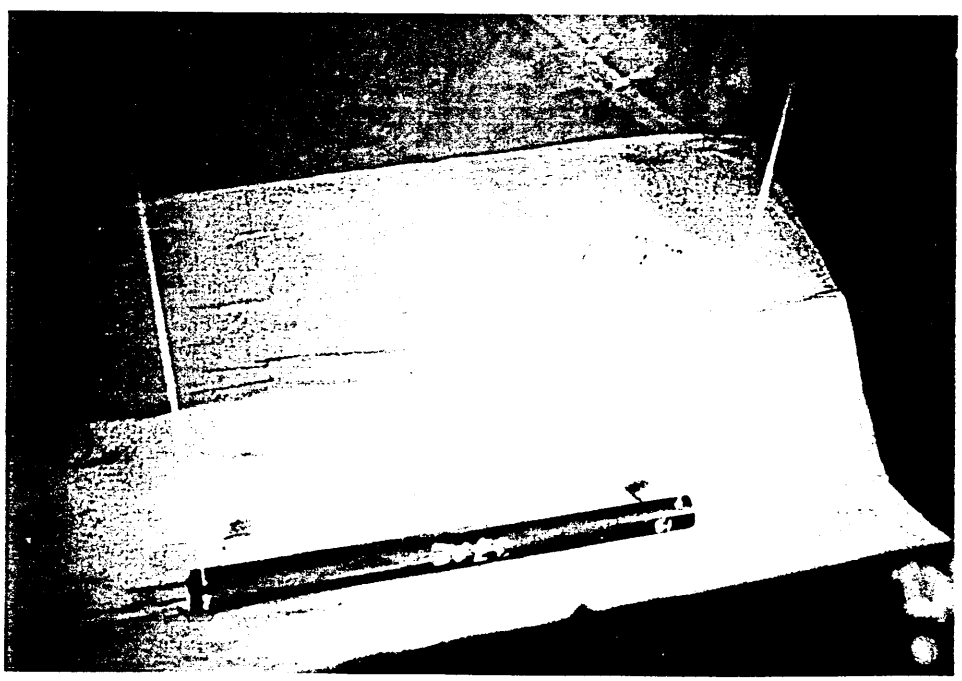

Plate 2   Trench Excavation In Compacted Sand

For Pull-Out Test

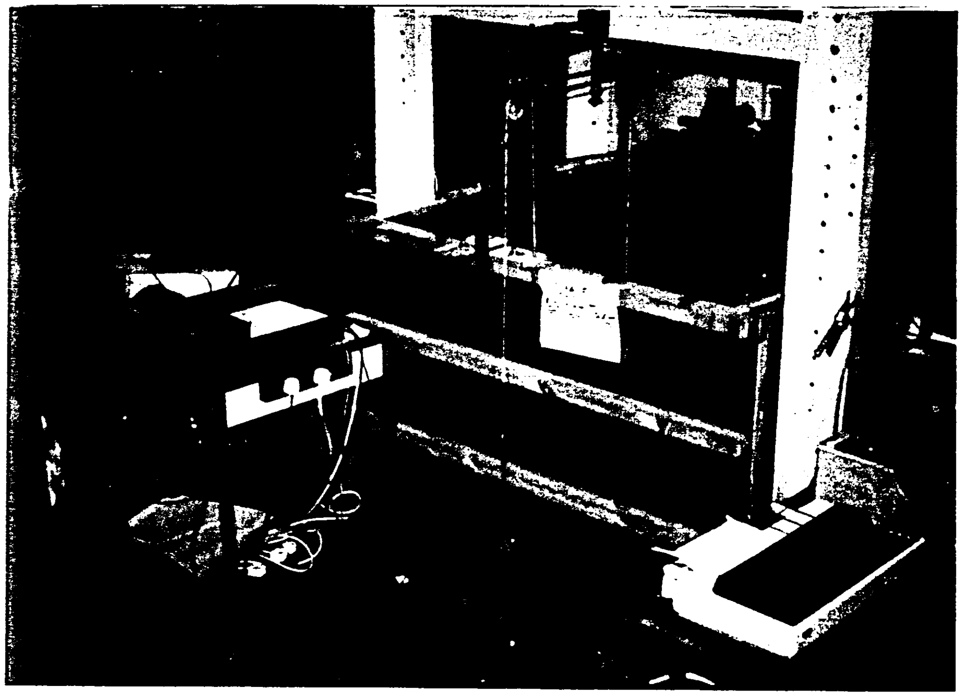

Plate 3 Ready To Test

Plate 4 Under Test

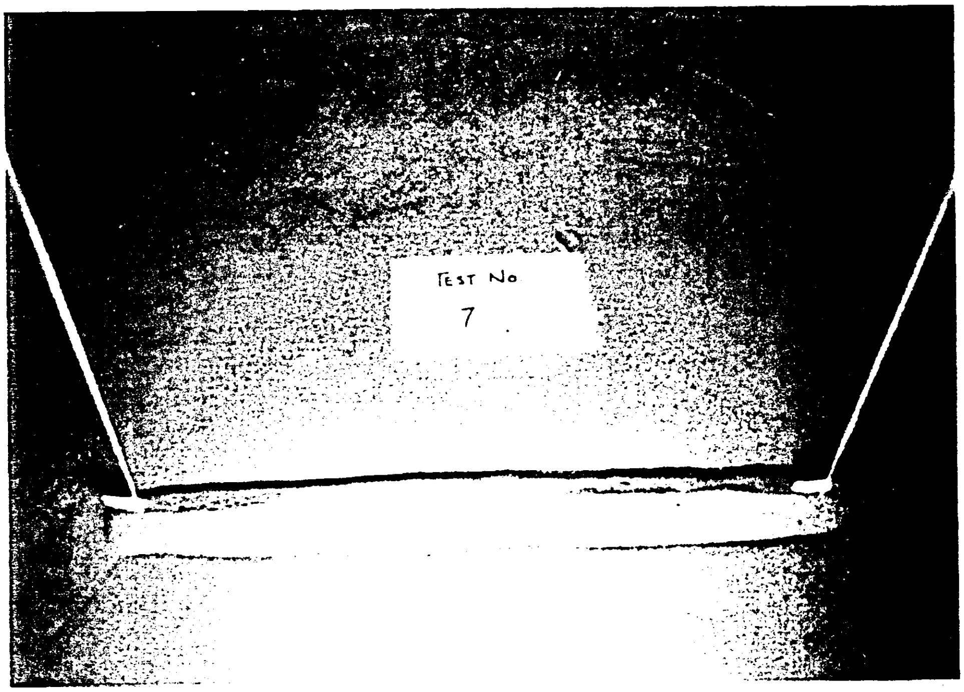

Plate 5 Upheaval Showing "Circular" End Profiles

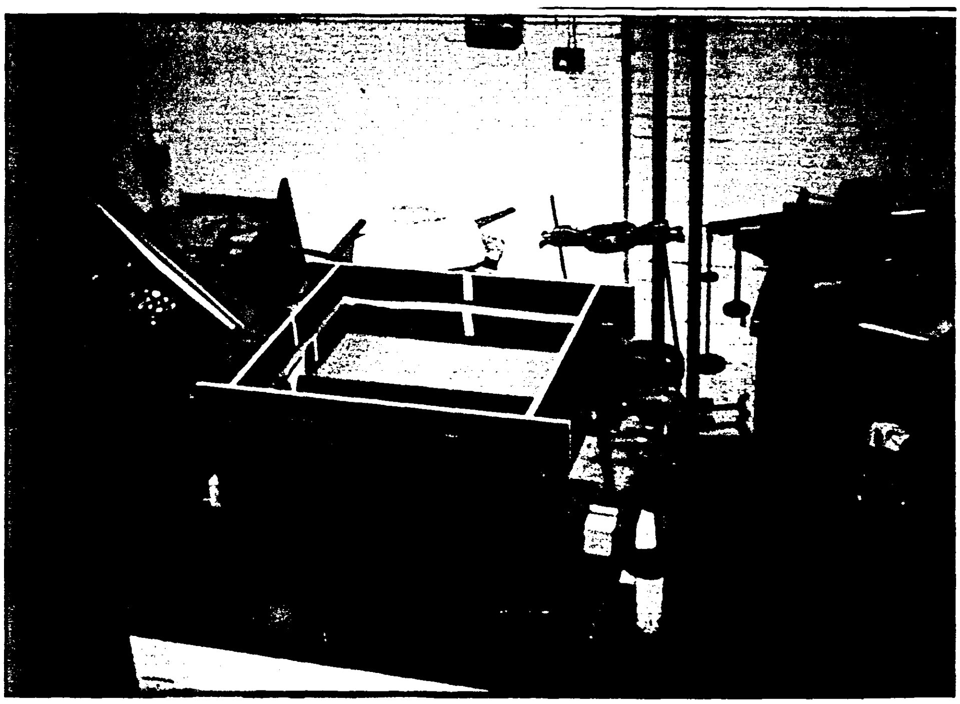

Plate 6 Flume Before Infill For Axial Friction Test Note Paper Valves

3.5 Axial Friction Tests - Set-Up and Procedure

The experimental topology is shown in Fig 3.6. A discrete element of pipe was again employed although in this case the pipe's length of 870mm exceeded the sand flume's corresponding dimension of 715mm providing for axial movement free from end-effects for all proposed axial movements. The sand was compacted and trenched as previously, the pipe and fill then being emplaced. The pipe was connected by wire to a weight hanger at one end, the other end's axial movement being monitored.

Loading was incrementally applied to the hanger and the corresponding displacement monitored. This procedure was initially terminated when the frictional resistance was fully mobilised, i.e. when displacement response became dynamic. However, given that prototype pipelines experience heating/pressurising-cooling/depressurising cycles[19,20], loading was then reversed in order to detect any *burrowing* effect whereby ϕ_A will decrease due to interface wearing[8], a feature perhaps particularly relevant to buried pipelines. Nine key tests were undertaken employing the same 48.3mm O.D. section and burial configuration as previously with three values of cover, h=D, 2D and 3D, each case-test being repeated three times. A significant reduction in friction resistance upon reversal of movement was observed and for h=3D, two further reversed loading half-cycles were implemented in an attempt to determine any lower limiting value for ϕ_A. Eighteen additional simple load reversal tests employing D=15mm and 25mm at h=D, 2D and 3D were also undertaken. Plates 6-8 illustrate various aspects of the testing undertaken.

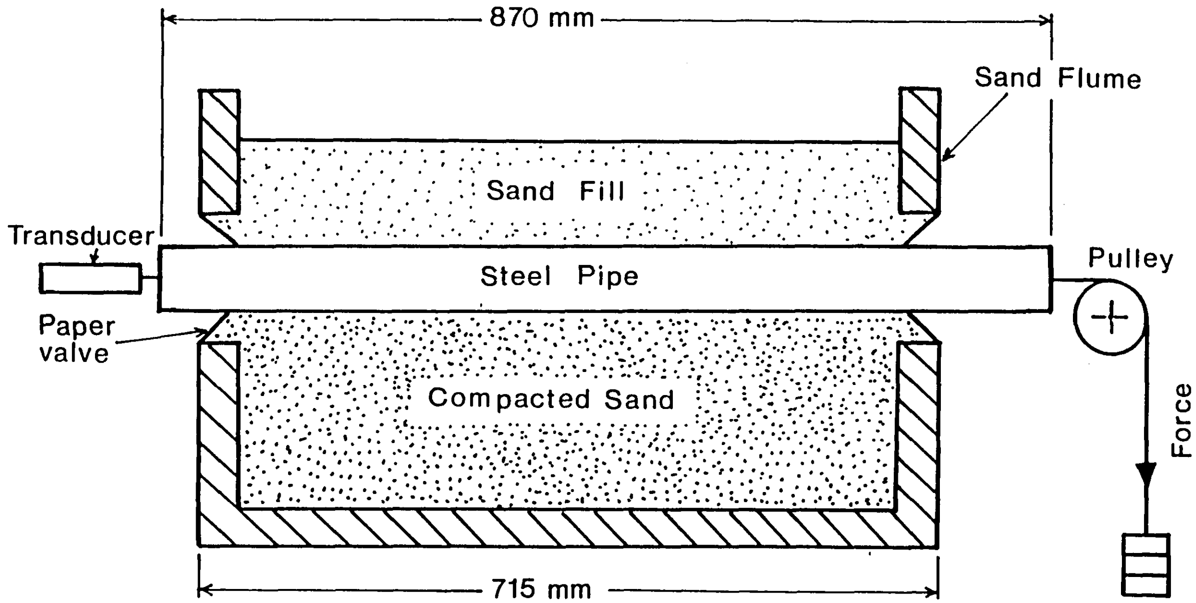

Central Longitudinal Section

Cross-Section as Fig 3.2 ("Breadth" = 720 mm)

Fig 3.6 Axial Friction Topology

Plate 7   Levelling Off

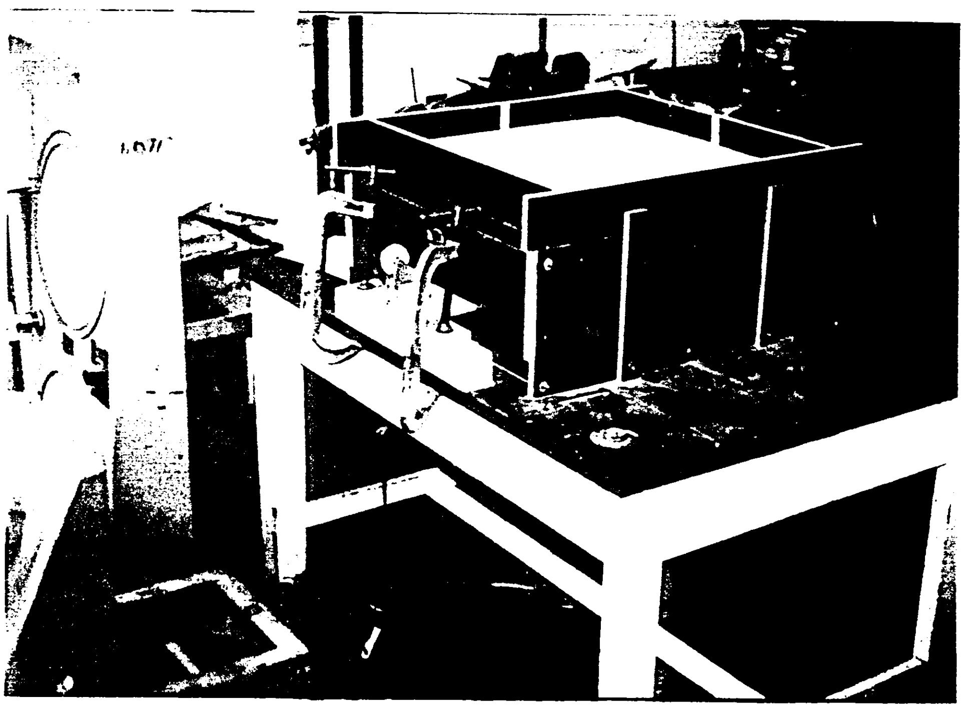

Plate 8   Under Test - No Visible Surface Effects

3.6 Axial Friction Tests - Results

Figure 3.7 displays the averaged axial friction force/displacement loci for D=h/3=48.3mm. First considerations lie with the initial movement locus and the determination of the respective fully mobilised friction coefficient ϕ_A. Frictional resistance initially maximises at 191 Newtons, the corresponding displacement at which this full mobilisation of ϕ_A occurs being u_ϕ=2mm. ϕ_A itself is obtained from

$$F_f=\phi_A R \tag{3.5}$$

where F_f denotes the maximum loading or frictional resistance force and R represents the forces applied orthogonally to the pipe's surface by the surrounding medium as suggested by Fig 3.8. This is a geotechnical matter and an interpretation of piling studies[45] suggests

$$R=P_s+(P_s+P_w)+2\left(k_6\gamma\left[h+\frac{D}{2}\right]\frac{\pi LD}{4}\right) \tag{3.6}$$

where P_s represents the weight of cover lying directly above the top quarter circumference of the pipe whilst the third (parenthetic) term represents the lateral pressure acting on the two middle quarter circumferences lying to the sides of the pipe; k_6 is a geotechnical constant. The bottom quarter circumference carries the pipe weight P_w in addition to P_s. Vertically-oriented pipe was pulled vertically in a number of ancillary tests to evaluate k_6 [45], general geotechnical data ranging between 0.3 and 3. Herein, k_6=1 was determined.

Accordingly, Table 3.1 provides data for ϕ_A for D=48.3mm, these data being the average of three respective individual tests. With F_f=191N for D=48.3mm=h/3, for example, then, noting eqn (3.6),

$$R=(30.36)+(134.2)+2(57.5)\ N \tag{3.7}$$

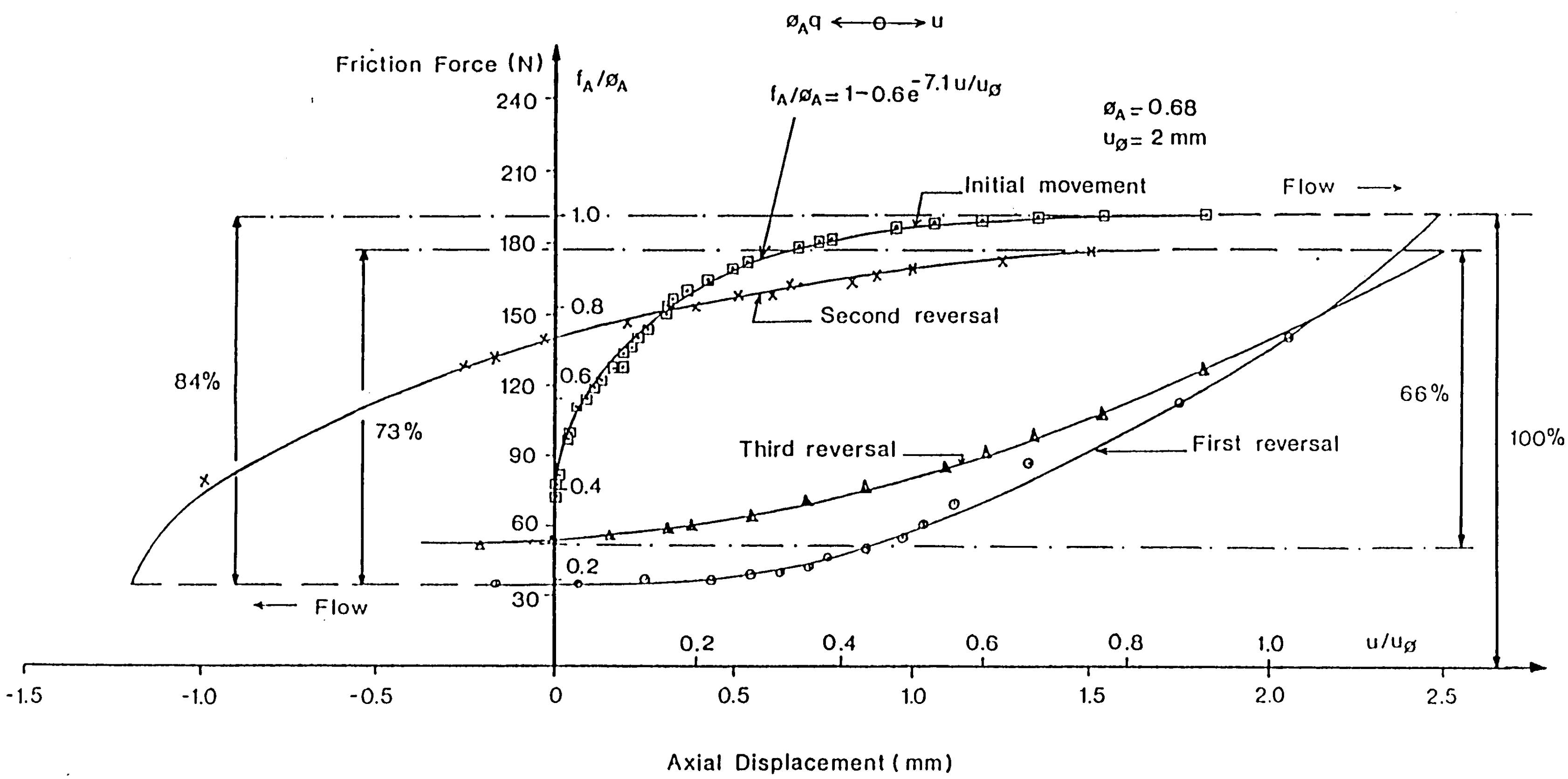

Fig 3.7 Axial Friction Force Characteristics under Cyclic Reversal

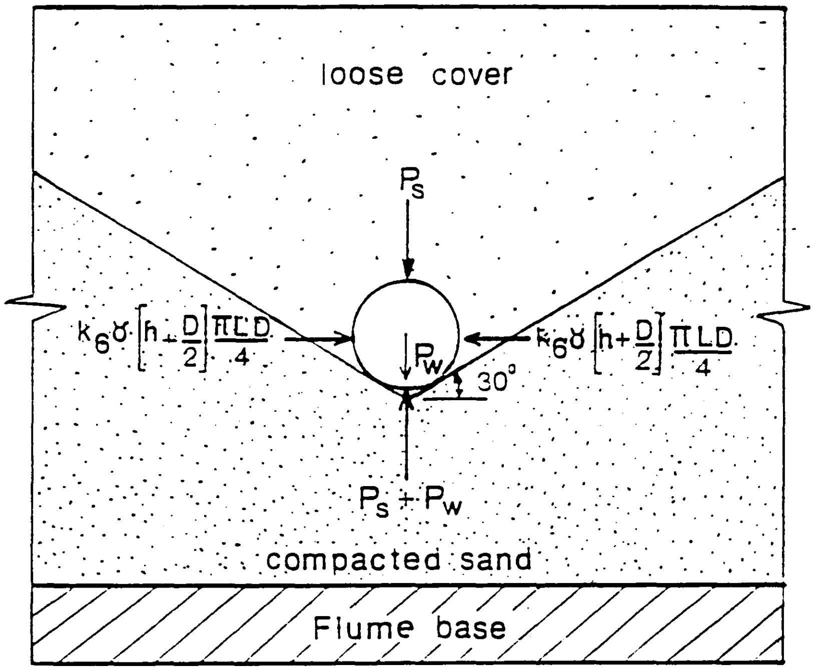

Fig 3.8 Axial Friction Section

	h		
	D	2D	3D
ϕ_A (ϕ_A')	0.55	0.6	0.68

Table 3.1 Buried values for Axial Friction Force Coefficient

so that

$$\phi_A = \frac{191}{279.56} = 0.68 \tag{3.8}$$

Equivalent seabed-mounted tests give values in the range 0.5-0.59 for ϕ_A [8]. The rise in ϕ_A, to ϕ'_A, say, with $\phi'_A|_{h=0}=\phi_A$, for buried pipes is attributed to burial pressure affecting the pipe surface/sand medium interface. This argument is supported by the observation that for surface-mounted pipe, ϕ_A=0.53 for 48.3mm O.D. pipe simply resting on sand against ϕ_A=0.59 for the case of the pipe having been pressed into the sand[8].

The deformation-dependent nature of axial friction force is clearly displayed in Fig 3.7 and an empirical curve

$$f_A = \phi_A(1-0.6e^{k}) \ , \qquad k=-7.1\frac{u}{u_\phi} \tag{3.9}$$

where f_A is a friction force parameter, is employed to fit the initial movement locus data. This is suitably asymptotic to $f_A=\phi_A$ and provides a useful design tool with f_Aq replacing ϕ_Aq in buckling studies to give a consistent deformation-dependent friction model.

Finally, and again consulting Fig 3.7, the effect of reversal is to reduce frictional resistance - the reversal loci are 'by-eye' fits for identification purposes only. It is assumed longitudinal reversal occurs in practice with the opening up/shutting down cycle previously discussed. The reduction in resistance is presumed to relate to the burrowing effect i.e. previous movement smooths the pipeline/seabed interface. Following the initial movement indicated in Fig 3.7, the maximum resistance drops by 16% upon reversal. Two further reversals lead to ensuing reductions of 27% and 34% respectively; Fig 3.9 illustrates this

D(mm)	h		
	D	2D	3D
15	89	87	80
25.4	86	81	75
48.3	83	85	84

Table 3.2 Reduced Fully Mobilised Friction Resistances upon Initial Loading Reversal (Percentages)

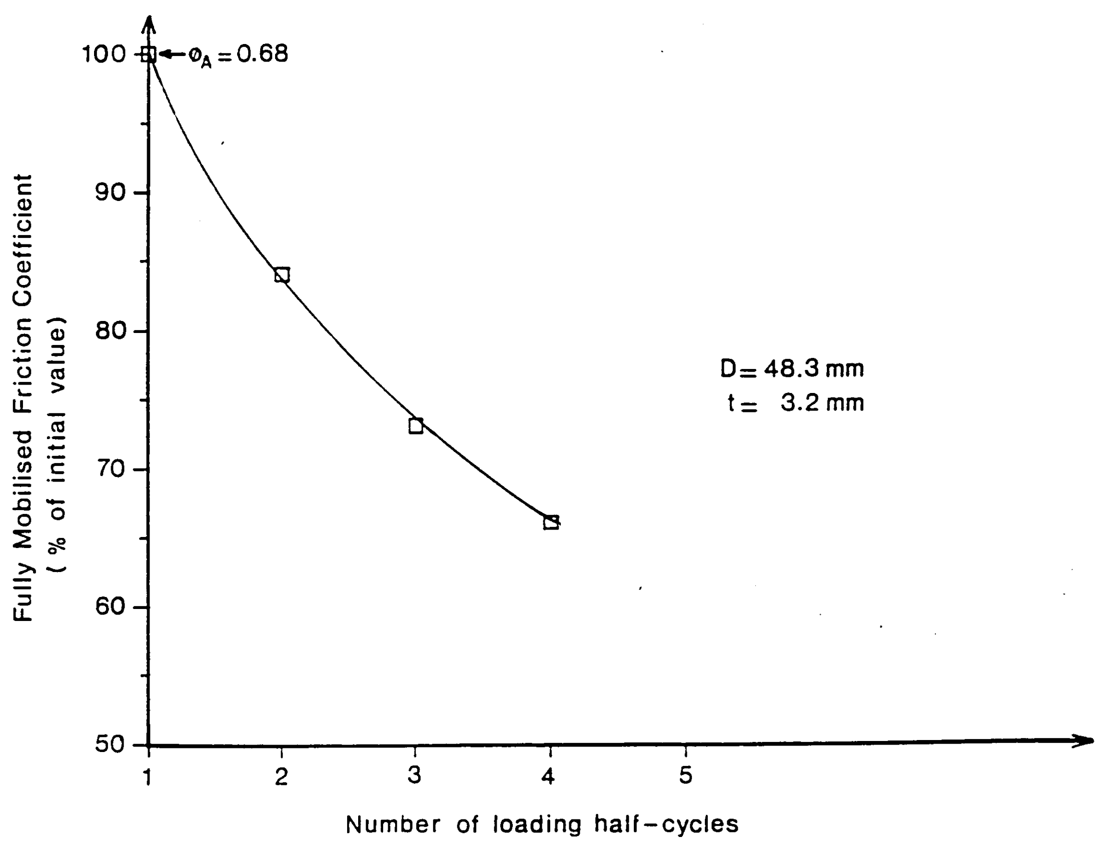

Fig 3.9 Cyclic Reduction in Fully-Mobilised Friction Resistance

effect and suggests a lower limiting value of the order of 60% original ϕ_A. Reduction in friction force resistance upon reversal was obtained in all twenty-seven tests undertaken, recall section 3.5, averaged data being given in Table 3.2.

3.7 Experimental Comments and Conclusions

It is taken that eqns (3.3), (3.8) and (3.9) and the data of Tables 3.1 and 3.2 do not suffer significant scaling factors when applied to relatively small-bore prototypes[19,20]. Scaling is an important matter previously discussed with respect to seabed-mounted pipelines[8,30] which can, however, typically possess up to 1m O.D. The similarity of eqn (3.3) to that concerning a related topology[13], i.e. note Fig 3.1 (b), is reassuring given the equivalent expression is based on D=442mm experimentation. Regarding friction modelling, values ϕ_A=0.5 and u_ϕ=3mm are quoted[19] for D=220mm (h/D=6), adding elsewhere[20] that alternative values for ϕ_A have also been employed.

Figure 3.10 therefore illustrates a suitable *Empathetic* model for continuously buried pipes obeying the configuration of Fig 3.1(a); the deformation-dependent friction force modelling is valid for h=3D. The change in sign of the friction force exponent is due to the overwriting of the convention employed in Fig 3.7 which was therein convenient for experimental purposes. Inertial resistance, initially based on cover h will vary with vertical displacement of the pipe such that q+q'=f(v). However, whilst a deformation-dependent modelling of q+q' is required as an increasing extent of pipe lifts substantially from its initial lie or even breaks through the cover, parametric values in the immediate vicinity of the onset of upheaval will not be significantly affected. Such deformation-de

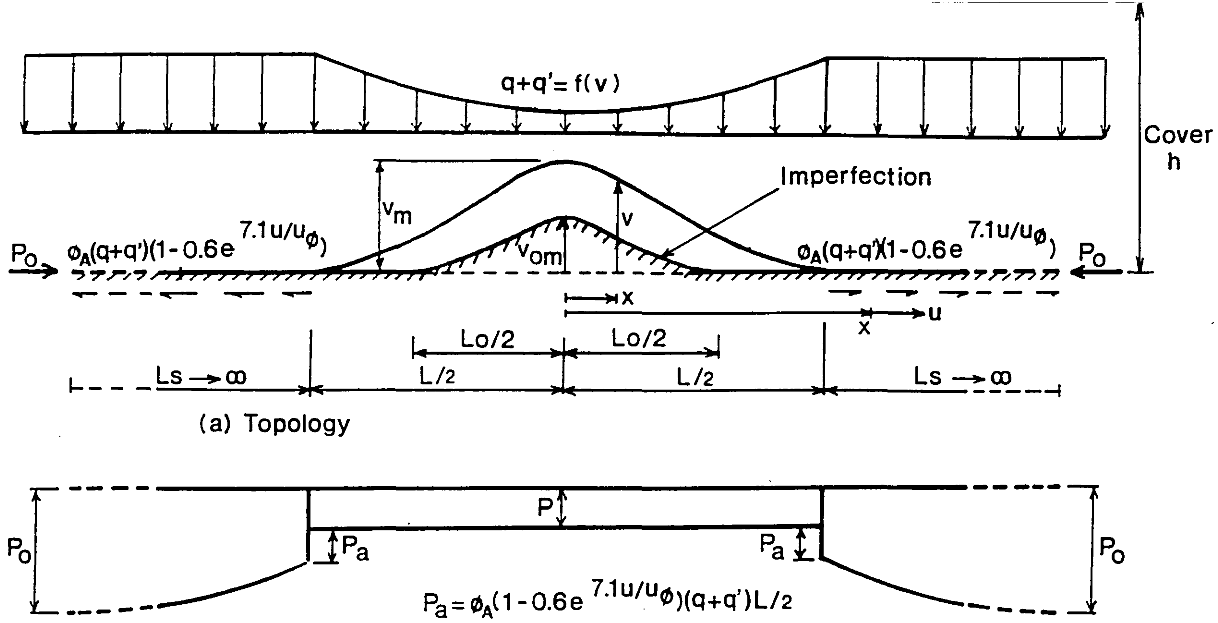

(b) Axial Force Distribution

Fig 3.10 Upheaval Buckling Model

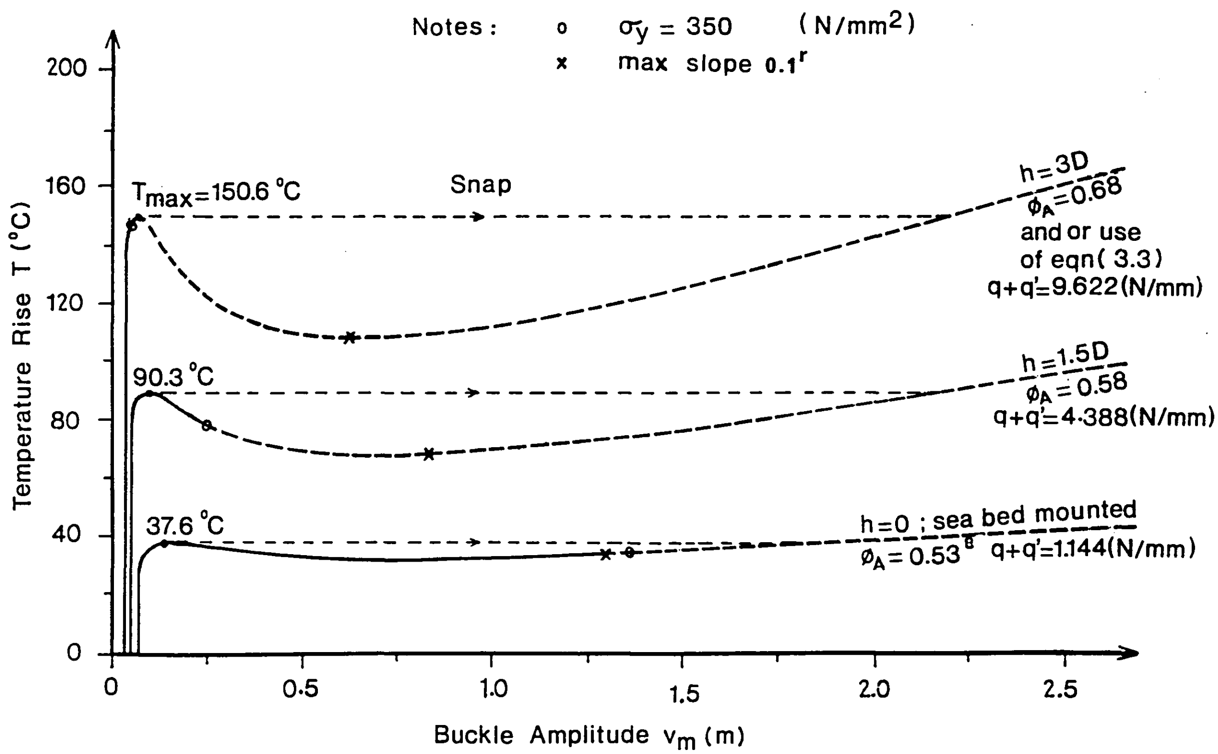

Fig 3.11 Thermal Action Characteristics - Upheaval Buckling Empathetic Model for $v_{om}/L_o = 0.003$

pendent studies would follow in the manner adopted elsewhere for seabed elasticity[8]. Further, employment to-date of deformation-dependent friction parameter f_A in the manner of eqn (3.9) as opposed to the employment of fully mobilised friction parameter ϕ_A in the manner of eqn (3.8) shows little effect[8]. Accordingly, the numerical case studies typified by Fig 3.11 and employing the compact pipe data, more appropriate to upheaval studies, of Table 3.3, consider q+q' to be constant at any h and friction force modelling to be fully mobilised. The data of Table 3.1 and eqn (3.3) are incorporated within the modelling denoted in Section 1.6, q+q' being substituted for q throughout, to give the appropriate data noted on the loci in Fig 3.11, with $\phi_A|_{h=3D/2}=(0.55+0.6)/2$. The overall effect of burial is shown to be the increase in resistance to upheaval although the increased degree of dynamic snap response should buckling occur is to be noted.

3.8 Summary

Two novel sets of upheaval subsea pipeline buckling data have been established and their potential employment briefly identified[36]. Taking eqns (1.1), (1.2), (1.18), (1.19), (1.20) and (1.24) to typify imperfection modelling (Empathetic) then the factors herein discussed relate directly to eqns (1.18)-(1.20), together with eqns (1.12) and (1.15), thereby showing their relevance with particular respect to buried subsea pipes. It is now pertinent to consider the development of the theoretical imperfection models per se.

Parameter	Symbol	Value	Unit
External diameter	D	219	mm
Wall thickness	t	14.3	mm
Direct modulus	E	206000	N/mm^2
Effective inertial self-weight	q	1.144	N/mm
Yield stress	σ_{yld}	350	N/mm^2
Thermal coefficient	α	$11x10^{-6}$	$/^oC$
Axial friction coefficient	ϕ_A	0.53	
Poisson's ratio *	ν	0.3	

Table 3.3 Pipe parameters (seabed mounted h=0 and D=219mm)

Note: * ν employed for the evaluation of pressure component as required.

Chapter 4

Contact Undulation Studies - Empathetic Model

4.1 Introduction to Empathetic Model Enhancements

Initially, Activity 3a of Fig 2.1 is considered wherein acceptance of the *empathetic* expression of eqn (1.20) leads to uniform upheaval of the pipeline from the contact undulation surface - note discussion in Section 1.6. All modelling within this Chapter is of novel form although that contained in Sections 4.7.2 and 4.7.3 has previously been reported in the context of idealised studies[7]. Sections 4.2 to 4.5 consider enhancements of the *Empathetic* model's mathematical construction, whilst Section 4.7 relates to extension of the model's range of application.

4.2 Zero Fully Mobilised Slip Length

Considering further the basic surface mounted topology studies discussed in Section 1.6, it should be recorded that such fully mobilised axial friction studies generate negative slip length values immediately following upheaval. The problem of there being a minimum buckle length below which fully mobilised slip length modelling is invalid has been suggested previously[6,7,9]; see Fig 1.6. The reason for the problem is that the developed slip length topology illustrated in Fig 1.8 is invalid if the frictional resistance demanded by the system can be fully provided by the nominally point reaction force $\phi_A qL/2$ at the peel points[6,7,9] - ie; the presumed finite slip length of Fig 1.8 should not then exist within the model as in the early post-upheaval stage there is no theoretical slip length and eqns (1.12), (1.14) and (1.15) are invalid. That is, from eqns (1.12) and (1.14),

$$P_o - P = (-2\phi_A qAEu_s|_{L/2})^{1/2} + \phi_A \frac{qL}{2} \tag{4.1}$$

and from eqns (1.14) and (1.29),

$$u_s|_{\frac{L}{2}} = \frac{(P_o-P)L}{2AE} - 7.9883\times10^{-6}\left(\frac{q}{EI}\right)^2 (L^7 - L_o^7) \tag{4.2}$$

Eliminating (P_o-P) between eqns (4.1) and (4.2) and re-arranging into a quadratic equation with respect to $(-u_s)^{1/2}$

$$[(-u_s)^{1/2}]^2 + \frac{L}{2AE}[2\phi_A qAE]^{1/2}(-u_s)^{1/2} + \frac{\phi_A qL^2}{4AE} - u_f = 0 \tag{4.3}$$

where the flexural end shortening u_f is given by

$$u_f = 7.9883.10^{-6}\left(\frac{q}{EI}\right)^2 (L^7 - L_o^7) \tag{4.4}$$

and noting tensile relief demands $u_s|_{L/2}$ can never be positive, then from eqns (4.3) and (4.4),

$$\Phi_1 = -\frac{\phi_A qL^2}{4AE} + 7.9883.10^{-6}\left(\frac{q}{EI}\right)^2 \left(L^7 - L_o^7\right) \geq 0 \tag{4.5}$$

Taking $L=L^*$ as the root of eqn (4.5) - ie; R.H.S.=0 - then for the slip length to exist $(u_s<0)$,

$$L > L^* \tag{4.6}$$

Accordingly; for $L \leq L^*$, $u_s=0$ and no slip length exists such that eqn (1.12) is replaced by

$$P_o - P = \phi_A q \frac{L}{2} \tag{4.7}$$

whilst for $L>L^*$, u_s is determined by

$$u_s=-\frac{1}{4}\left(-\left(\frac{\phi_A q}{2AE}\right)^{1/2}L+\left(-\frac{\phi_A qL^2}{2AE}+4u_f\right)^{1/2}\right)^2 \tag{4.8}$$

with

$$L_s=\left(-\frac{2AEu_s}{\phi_A q}\right)^{1/2} \tag{4.9}$$

and

$$P_o=P+\phi_A q\frac{L}{2}+\phi_A qL_s \tag{4.10}$$

The foregoing procedure avoids the problems associated with a minimum case of applicability when employing fully mobilised friction force modelling as typified by L=19.507m in Fig 1.6. Concurrent presentation of the foregoing has been made available elsewhere[12]. Deformation-dependent slip length studies, note the f_A considerations in Chapter 3, are not, by definition, susceptible to this problem.

4.3 Upheaval Temperature Considerations

A second interesting feature relating to the *Empathetic* model at the *onset of upheaval* (zero axial friction force) is that

$$AE\alpha T_u = P_o|_u = P_u \tag{4.11}$$

enables direct evaluation of the upheaval temperature rise from eqn (1.28),

$$T_u = \frac{P_o|_u}{AE\alpha} = \frac{P_u}{AE\alpha} = 32.3\frac{I}{AL_o^2\alpha} \tag{4.12}$$

However, if it is construed that the *peel* point (or otherwise[7]) friction force discussed above indeed exists at upheaval, then, noting eqn (4.7),

$$T_u = \frac{P_o|_u}{AE\alpha} = \left(P_u + \phi_A q \frac{L_o}{2}\right) / (AE\alpha) \qquad (4.13)$$

This essentially philosophical discrepancy is considered to be of minor numerical effect - eg; taking the data of Table 1.1 with v_{om}=140mm and L_0=46.8m, then eqn (4.11) gives T_u=67.6°C whilst eqn (4.13) gives T_u=68.52°C, a difference of only 1.3%. Using eqn (4.11) affords a suitably conservative formulation possessing important computational advantages as discussed below.

4.4 Upheaval Curvature Considerations

From eqn (4.12) it is both possible and potentially useful[18,19] to explicitly relate upheaval temperature T_u to the imperfection crown curvature $v_{o},_{xx}|_0$ on the basis of eqn (4.11) being valid. Employing eqn (1.18),

$$v_{o'xx} = v_{om}\left(-0.5235\frac{\pi^2}{L_o^2} - 2.3966\frac{\pi^2}{L_o^2}\cos\left(2.86\frac{\pi x}{L_o}\right)\right) \qquad (4.14)$$

such that, noting eqn (1.20)

$$v_{o'xx}|_0 = -0.0694\frac{qL_o^2}{EI} \qquad (4.15)$$

Incorporating eqn (4.12)

$$AE\alpha T_u = 32.3\frac{EI}{L_o^2} = (32.3)\,(2.407.10^{-3})\,\frac{qL_o^2}{v_{om}} \qquad (4.16)$$

so that

$$T_u = 0.078q\frac{\left(\frac{L_o^2}{v_{om}}\right)}{AE\alpha} \qquad (4.17)$$

This leads to important implications regarding the physics of upheaval modelling and is further discussed following the ensuing considerations regarding trenching, burial and anchoring; note that $v_{o},_{xx}|_0$ is also the maximum imperfection curvature as required by symmetry.

4.5 Explicit Snap/Stable Differention

A further enhancement consists of the development of a closed-form expression for T_{max}, or its availability, where T_{max} denotes the maximum temperature rise state appropriate to snap response systems - see Figs 1.9 and 3.11. By differentiating eqn (1.16) with respect to buckle length L and noting eqns (4.1), (4.4), and (4.8)

$$
\begin{aligned}
AE\alpha T,_L &= \Phi_2\left(\frac{\phi_A qAE}{2\Phi_3}\right)^{\frac{1}{2}} + P,_L \qquad \textit{for} \quad L>L^* \quad \textit{or} \\
AE\alpha T,_L &= \phi_A q/2 \quad +P,_L \qquad\qquad \textit{for} \quad L<L^* \\
\textit{where} \quad \Phi_2 &= -\frac{\phi_A qL}{2AE} + 111.8362.10^{-6}\left(\frac{q}{EI}\right)^2 L^6 \\
\Phi_3 &= -\frac{\phi_A qL^2}{2AE} + 31.9532.10^{-6}\left(\frac{q}{EI}\right)^2 (L^7-L_o^7)
\end{aligned}
\tag{4.18}
$$

From differentiating eqn (1.24), $P,_L$ is given by

$$
P,_L=80.76\frac{EI}{L^3}\left(-2-\frac{1}{75.6}\left(\frac{L_o}{L}\right)^2 (L\psi_1,_L-4\psi_1)\right) \tag{4.19}
$$

noting that ψ_1 is given by eqn (1.23). Equating eqn (4.18) to zero also affords a closed-form relationship for the maximum temperature rise T_{max} prior to a snap buckling response[12]. Importantly, nonsensical numerical solution implies a fully stable path, recall Fig 1.9, lacking a T_{max} state, and acts as a *flag* - ie; unstable and stable post-buckling behaviour can be differentiated from eqn (4.18) alone, a useful design device as suggested by Fig 4.1 which employs the data of Table 1.1.

A check must be made upon T_{max} occurring in a singular, cusp manner. The maximum buckle force P_{max} can be found by equating eqn (4.19) equal to zero affording

$$L|_{P_{max}} = 1.17115\, L_o \qquad with \qquad P_{max} = 45.36\%\, P_{qi}|_{L=L_o} \tag{4.20}$$

whilst the coefficients Φ_2 and Φ_3 of eqn (4.18) can be expressed as

$$\begin{aligned} \Phi_2 &= \frac{2}{L}\left[\Phi_1 + 7.9883\times10^{-6}\left(\frac{q}{EI}\right)^2 (6L^7+2L_o^7)\right] \\ \Phi_3 &= 2\Phi_1 + 2u_f \end{aligned} \tag{4.21}$$

where u_f and Φ_1 are given by eqns (4.4) and (4.5) respectively. The first implication to be drawn from eqns (4.20) and (4.21) is, noting that coefficients Φ_2 and Φ_3 of eqn (4.21) are always positive for $L>L^*$, *that the slope $T,_L$ of the temperature rise curve typified by eqn (4.18) is greater than zero after the upheaval state*; this situation also becomes obvious for $L<L^*$, ie when eqn (4.18) takes a much simpler form of $AE\alpha T,_L=\phi_A q/2+P,_L>0$. Accordingly, the *Empathetic* model cannot produce a cusp response[39] regardless of the reduction in imperfection ratio ($L|_{T_{max}}>L_o$).

A second implication is that the substitution of $L|_{P_{max}}$ from eqn (4.19) into eqn (4.18) affords $AE\alpha T,_L|_{L|P_{max}}=\Phi_2(\phi_A qAE/2\Phi_3)^{\frac{1}{2}}\neq0$ for $L>L^*$, noting the non-zero coefficients of eqn (4.21), whilst for $L<L^*$, eqn (4.18) becomes $AE\alpha T,_L|_{L|P_{max}}=\phi_A q/2\neq0$. This clearly supports the claim that the states of maximum temperature rise ($AE\alpha T,_L=0$) and maximum buckle force P (rise) are not coincident[1]. A more definitive assessment of the situation is therefore available by comparing $L|_{T_{max}}$ from eqn (4.18) set to zero with $L|_{P_{max}}$ from eqn

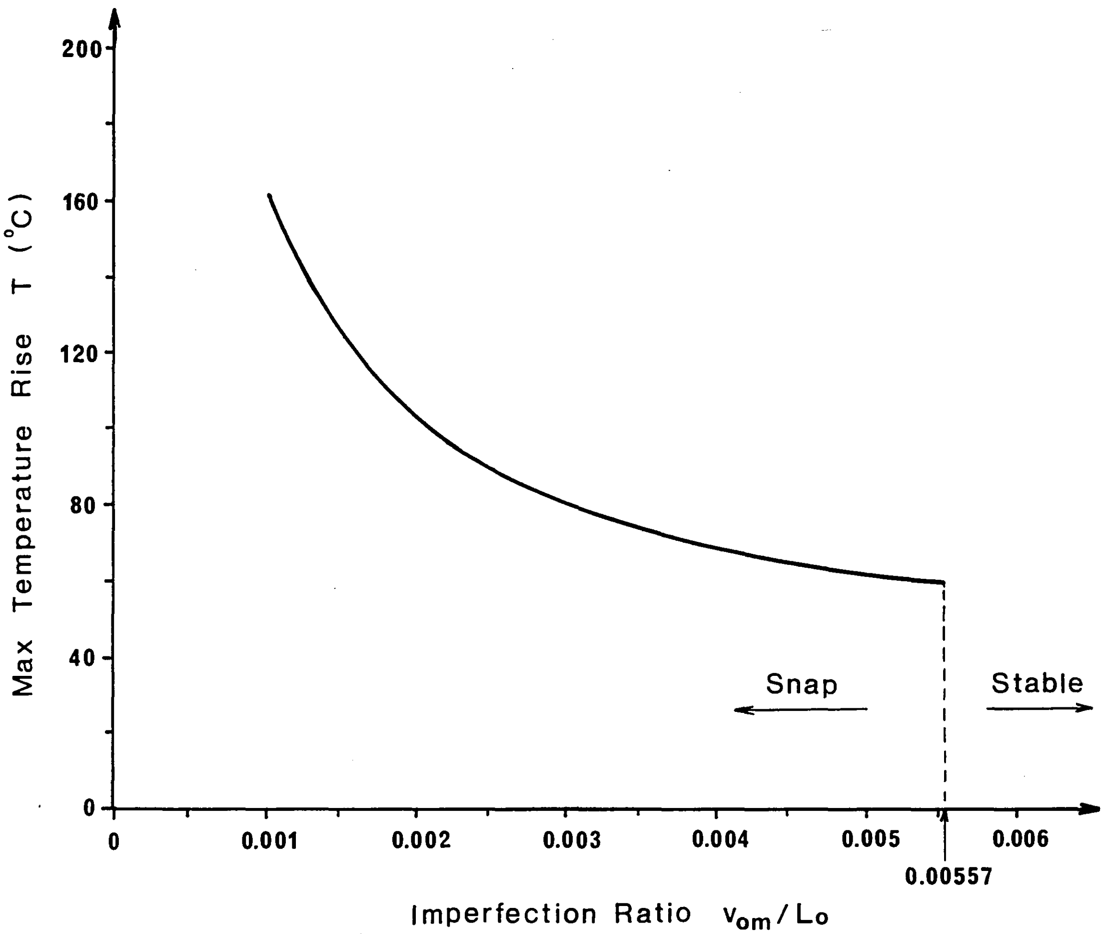

Fig 4.1 Maximum Temperature Rise vs Imperfection Ratio

(4.20) given $L_o<L|_{Tmax}$ and $L_o<L|_{Pmax}$ is demanded from the above. The important feature of the above finding is that the maximum temperature T_{max}, if it occurs, satisfies the condition $T_{max}>T|_{Pmax}>T_u$. The maximum temperature state coincides neither with the upheaval nor the maximum buckling force states[1].

4.6 Standard Model Case Studies (Enhanced Empathetic)

For completeness, Table 4.1 and Fig 4.2 serve to display appropriate upheaval buckling data employing Table 3.3. These data complement that of Fig 3.11 although overburden effects have been neglected for clarity (see next Section).

These data illustrate the key modelling characteristics, involving imperfection amplitude v_{om} ranging from 50mm to 300mm with the corresponding imperfection ratio v_{om}/L_o ranging from 0.0024 to 0.0093 such that L_o ranges from 20.628m to 32.284m. Whilst more precise evaluation of v_{om} at which the transition from snap to stable paths/states has been discussed above, the data confirms that the lesser the imperfection, the less stable the system's potential response to rises in temperature/pressure and that idealised studies are inherently non-conservative.

With regard to the respective temperature rise/buckling amplitude loci and results given in Fig 4.2 and Table 4.1 respectively, it can be seen that only the relatively small imperfections typified by v_{om}=50 and 100mm display a maximum temperature together with the associated snap buckling phenomenon.

v_{om} (mm)	L_o (m)		Upheaval State	Max Temp. State	After snap State	Min. Temp. State	First Yield State	Max slope 0.1rad
50	20.628	T v_m L f	36.62 50 20.628 82.31	42.56 101.6 24.628 125.71	42.56 2639.2 55.600 506.7	(32.26) 829.3 41.628 283.1	(33.50) 1281.8 46.411 350.	(33.54) 1292.4 46.510 351.5
100	24.531	T v_m L f	26.04 100. 24.531 58.2	31.97 239.9 30.531 124.4	31.97 1085.9 44.531 289.2	(30.91) 674.4 39.531 222.3	(34.33) 1531.9 48.531 350.	(32.93) 1292.4 46.510 318.6
150	27.148	T v_m L f	21.36 150. 27.148 47.52	N/A	N/A	N/A	(35.19) 1731.5 50.037 350.	32.29 1292.4 46.510 292.5
200	29.172	T v_m L f	18.58 200. 29.172 41.15	N/A	N/A	N/A	(36.08) 1909.3 51.276 350.	31.62 1292.4 46.510 271.4
250	30.846	T v_m L f	16.69 250. 30.846 36.81	N/A	N/A	N/A	(36.97) 2072.3 52.332 350.	30.87 1292.4 46.510 252.1
300	32.284	T v_m L f	15.29 300. 32.284 33.60	N/A	N/A	N/A	(37.86) 2226.2 53.284 350.	30.22 1292.4 46.510 234.6

Notes :
* N/A - denotes 'stable' buckling path
* T - Temperature rise (^{o}C)
* v_m - Buckle amplitude (mm)
* L - Buckle length (m)
* f - Maximum stress (N/mm^2)

Table 4.1 Fully Mobilised Enhanced *Empathetic* Model - Parametric Studies

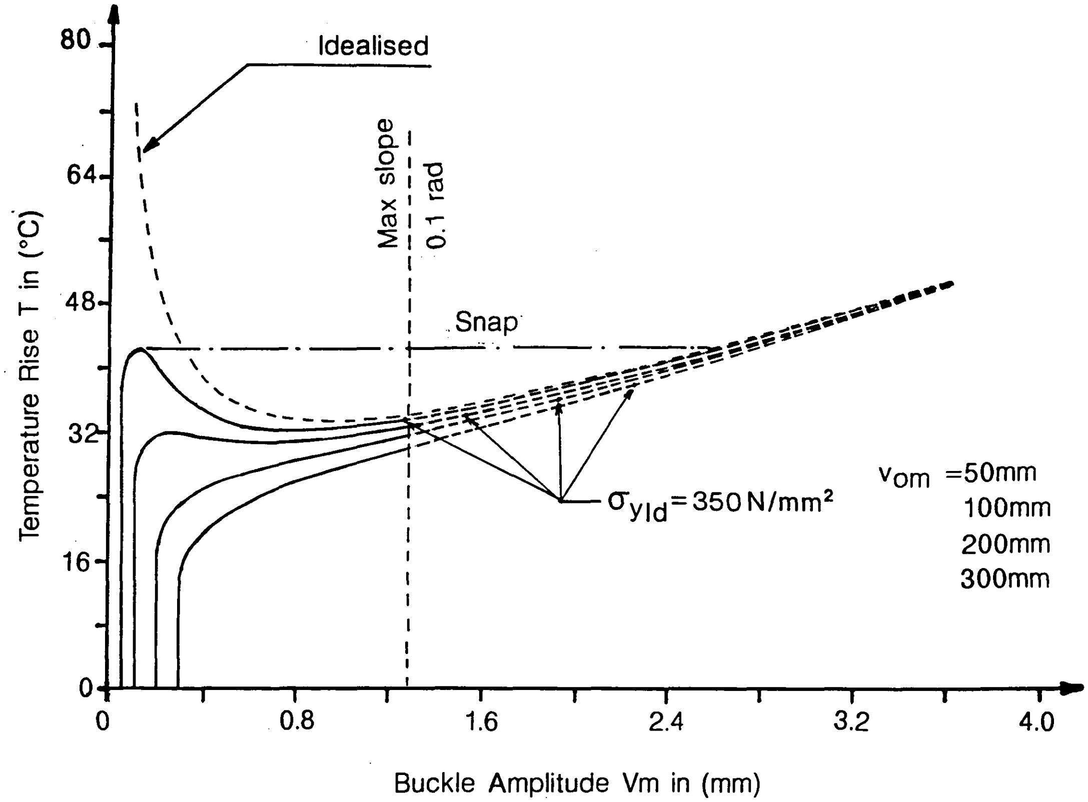

a) Maximum Temperature Rise vs Buckle Amplitude

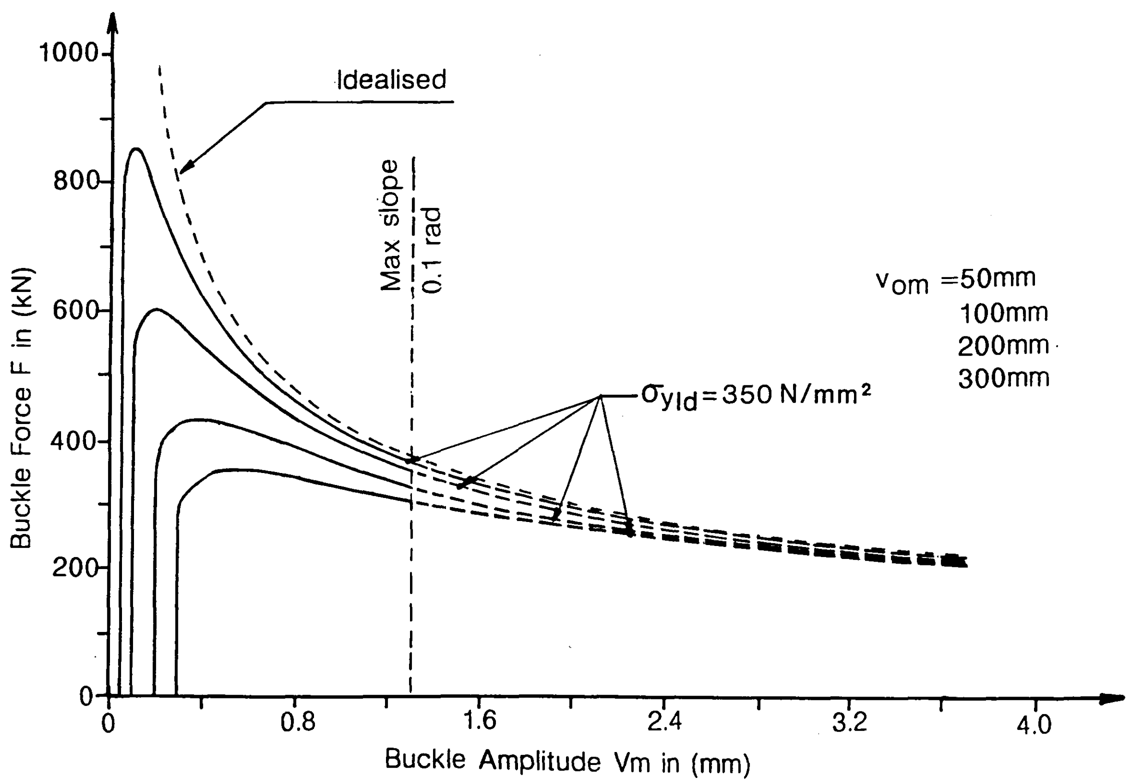

b) Buckle Force vs Buckle Amplitude

Fig 4.2 Thermal Action Characteristics
Fully Mobilised Enhanced Empathetic Model

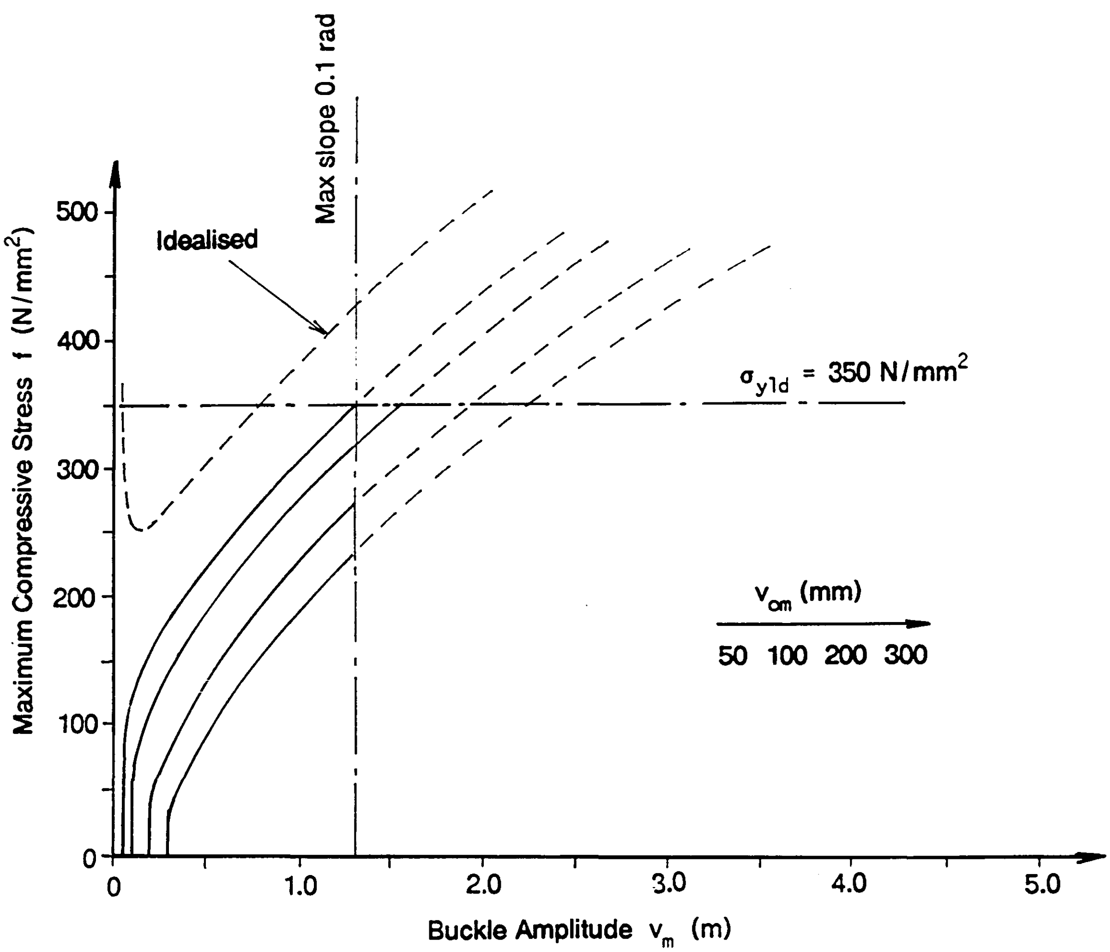

c) Maximum Compressive Stress vs Buckle Amplitude

Fig 4.2 (continued)

The remaining four cases, v_{om}=150 to 300mm, generate stable post-buckling paths. It is to be noted that the onset of slopes in excess of 0.1 radians or of yielding, whichever comes first, is graphically illustrated by dashed loci in Fig 4.2; here, the geometric limit is more restrictive. Operating temperatures should be restricted to either T_u or T_{max} for the snap cases (dynamic action is to be avoided), and to either T_u or $T|_{0.1}r$ for the stable cases.

The general characteristics for the respective buckling force/buckling amplitude and maximum compressive stress/buckling amplitude loci for all cases are again of common form. As illustrated in Fig 4.2(b), all imperfection cases generate maximum buckling force states; it should be noted that in the small imperfection cases, these states do not coincide with the corresponding maximum temperature states, noting the discussion in Section 4.5.

Table 4.1 suggests that for both stable and snap configurations, the temperature rise required for the onset of first yield stress (static) increases with increasing imperfection amplitude whilst with the onset of maximum slope the temperature rise decreases as the imperfection increases. Care must be taken with small imperfections, typically v_{om}=50mm, however, as the first yield or maximum slope state is incurred during snap. This implies that the onset of the respective maximum temperature rise can now be considered as the limiting state for this particular imperfection amplitude.

Three further developments of the *Empathetic* model are now considered. These reflect physical environment rather than mathematical factors, however, and relate to more recent field employment of subsea pipelines. As opposed to adopting a basic seabed lie involving hypothetical vertical buckling, the pipeline is now trenched and/or subject to burial (rock dumping - intermittent or otherwise) and subject to the use of fixing anchors.

4.7 Updated Physical Considerations

The development of marginal offshore fields has required the design of small diameter or compact pipelines to transport hydrocarbon at high pressure and temperatures. Pipelines of this type are highly stressed and vulnerable to accidental damage, and will usually be protected by trenching or dumping techniques. The foregoing 'standard' model case-study relates to a basic seabed lie topology subject to the obviation of lateral mode buckling. Indeed, advances in offshore practice include, in particular, the use of trenching and burial, continuous or discrete, together with the employment of fixed anchorages[26]. Idealised burial and fixed anchorage scenarios have been published previously[47]. The following considerations serve to expand the applicability of the present model accordingly.

4.7.1 Trenching

Trenching serves to protect the pipeline and de-trenching due to in-service upheaval buckling is to be avoided. Noting the basic trench section of Fig 4.3, then the analysis of the fully mobilised *Empathetic* model with trenching is similar to that of the standard case. Variation would only exist should the pipe seek to follow the trench incline requiring substitution for the effective inertial force m, where m is given by

$$m=q(\sin\theta+\phi_L\cos\theta) \qquad (4.22)$$

with θ denoting the trench angle and ϕ_L representing the fully mobilised lateral

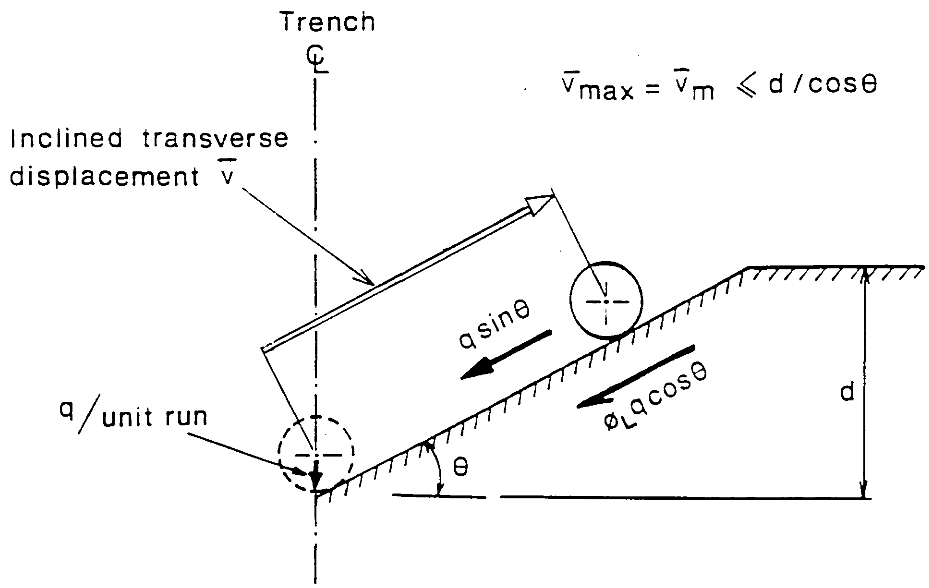

Fig 4.3 Inclined Trenching — Trench section

friction coefficient, in place of q. The effect of trenching upon buckling resistance can be gauged by the fact that with $\theta \leq 30^{o}$ from a geotechnical standpoint[45]

$$(m/q)\big|_{\theta=20^{o}}=1.05 \qquad and \qquad (m/q)\big|_{\theta=30^{o}}=1.15 \tag{4.23}$$

for $\phi_L=0.75$ with transverse deflection $\bar{v}$ inclined as shown in Fig 4.3. Whilst upheaval temperatures are therefore hypothetically enhanced by inspection, purely vertical upheaval would actually dominate as per the standard model case-study.

A more thorough inclined trench slope study would require m to replace q throughout all related equations, herein termed the basic trenching model, with v and v_0 *empathetically* related in terms of orientation $\bar{v}$ of Fig 4.3. A degree of physical compromise is therein incurred for the imperfection v_0 to involve m per se. However, as the *Empathetic* model is ~~a~~ mathematically based upon a worst-case scenario this is not considered to be a significant problem (nb for m>q).

There is a minor difficulty if q rather than m is assumed to be active in the slip length regions, herein termed the refined trenching model. Modelling frictional slip length resistance on the basis of employing q rather than m can be illustrated by recalling eqns (4.1) and (4.2) for the familiar equilibrium and compatibility expressions which now can be written as;

$$P_o-P=[-2\phi_A qAEu_s|_{L/2}]^{1/2}+\phi_A m\frac{L}{2} \tag{4.24}$$

and

$$u_s|_{L/2}=\frac{(P_o-P)\,L}{2AE}-u_f \tag{4.25}$$

respectively, where

$$u_f = 7.9883.10^{-6}\left(\frac{m}{EI}\right)^2 (L^7-L_o^7) \tag{4.26}$$

Similar to eqn (4.3), elimination of (P_o-P) between eqns (4.24) and (4.25) affords the quadratic equation with respect to $(-u_s)^{1/2}$ to be written as

$$[(-u_s)^{1/2}]^2+\frac{L}{2AE}[2\phi_A qAE]^{1/2}(-u_s)^{1/2}+\frac{\phi_A mL^2}{4AE}-u_f=0 \tag{4.26}$$

then the limiting value L^*, ie for the slip length to exist, can be found from (u_s<0)

$$-\left(\frac{\phi_A q}{2AE}\right)^{1/2} L^*+\left[\frac{\phi_A qL^{*2}}{2AE}(1-2\frac{m}{q})+4u_f\right]^{1/2} \geq 0 \tag{4.27}$$

which gives

$$-\frac{\phi_A mL^{*2}}{4AE}+u_f \quad \geq \quad 0 \tag{4.28}$$

For $L \leq L^*$, u_s=L_s=0 and eqn (4.24) is replaced by

$$P_o-P=\phi_A m\frac{L}{2} \tag{4.29}$$

For $L>L^*$

$$\begin{aligned} u_s &= -\frac{1}{4}\left(-\left(\frac{\phi_A q}{2AE}\right)^{1/2} L+\left(\frac{\phi_A qL^2}{2AE}(1-\frac{2m}{q})+4u_f\right)^{1/2}\right)^2 \\ L_s &= \left(-\frac{2AEu_s}{\phi_A q}\right)^{1/2} \\ P_o &= P+\phi_A m\frac{L}{2}+\phi_A qL_s \end{aligned} \tag{4.30}$$

Table 4.2 and Fig 4.4 display appropriate characteristics of the refined trenching model according to the employment of eqns (4.24)-(4.30) for two different imperfections v_{om} of 100mm and 250mm with the trench angles of 20° and 30° and comparative vertical buckling data (ie standard type case-study

v_{om} (mm)	L_o (m)	Trench angle θ (degrees)		Upheaval State	Max. Temp. State	After snap State	Min. Temp. State	First Yield State	Max slope 0.1rad
100	24.531	Standard enhanced model	T	26.04	31.97	31.97	(30.91)	(34.33)	(32.93)
			v_m	100	239.9	1085.9	674.4	1531.9	1292.4
			L	24.531	30.531	44.531	39.531	48.531	46.510
			f	58.2	124.4	289.2	222.3	350.	318.6
	24.252	20	T	26.64	32.68	32.68	(31.49)	(35.14)	(33.36)
			v_m	100	242.1	1135	686.2	1580.6	1273.
			L	24.252	30.252	44.508	39.252	48.354	45.813
			f	59.55	125.3	291.5	221.6	350.	310.6
	23.691	30	T	27.93	34.17	34.17	(32.72)	(36.89)	(34.24)
			v_m	100	246.7	1220.	711.4	1691.6	1233.7
			L	23.691	29.691	44.268	38.691	48.038	44.400
			f	62.4	127.1	293.1	220.2	350.	295.0
250	30.846	Standard enhanced model	T	16.69	N/A	N/A	N/A	(36.97)	30.92
			v_m	250				2072.3	1292.4
			L	30.846				52.332	46.510
			f	36.81				350.	252.1
	30.495	20	T	17.08	N/A	N/A	N/A	(37.92)	31.26
			v_m	250				2132.3	1273.0
			L	30.495				52.108	45.813
			f	37.66				350.	245.3
	29.790	30	T	17.91	N/A	N/A	N/A	(39.96)	31.95
			v_m	250.				2261.8	1233.7
			L	29.790				51.662	44.400
			f	39.46				350.	232.2

Notes :
* N/A - denotes 'stable' buckling path
* T - Temperature rise (°C)
* v_m - Buckle amplitude (mm)
* L - Buckle length (m)
* f - Maximum stress (N/mm^2)

Table 4.2 Fully Mobilised *Empathetic* Model with Refined Trenching Parametric Studies.

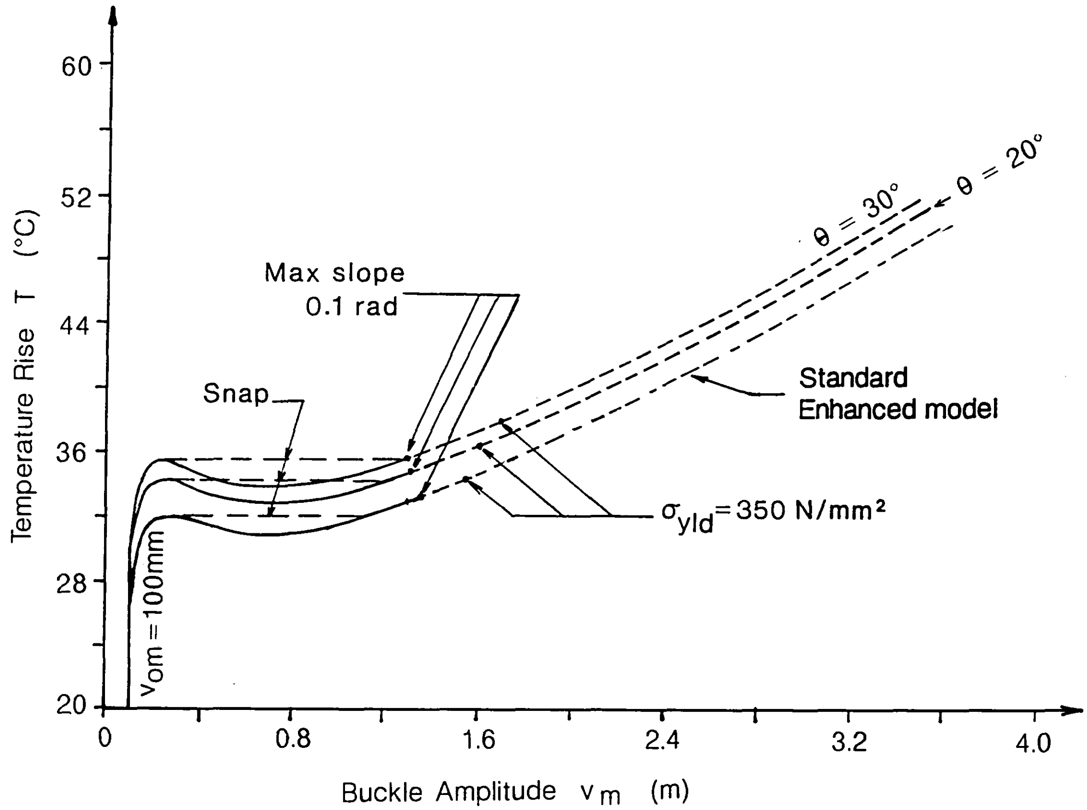

Fig 4.4 Thermal Action Characteristics
Fully Mobilised *Empathetic* Model with Refined Trenching

employing q throughout). It can be seen from Table 4.2 that operating temperatures for the refined trenching model duly provide average theoretical increases, over the corresponding standard case-study, of 2.2% and 7% for $\theta=20^{\circ}$ and 30° respectively. Snap and stable responses remain qualitatively unchanged.

Finally, the refined trenching model could be developed further whereby m replaces q only following the movement of the buckle up the trench slope whilst the imperfection v_0 remains unaltered in terms of q; this would provide a physically more rigorous trenching model. This type of modelling, however, is not valid with respect to the *Empathetic* model as it would violate the *empathetic* relationship between the imperfection and the buckle curves. Such a model will be discussed later in details with respect to the *Blister* and *Isoprop* models.

In summary, the standard case-study (ie vertical buckling in the absence of burial and anchoring) in effect relates to a basic trench lie, so long as the data implications of eqn (4.23) remain typical.

4.7.2 Burial (Continuous)

As introduced in Chapter 3, burial provides damage protection, additional insulation and enhancement of bucking resistance. Three typical burial topologies are illustrated in section in Fig 3.1; two of these involve trenching as shown and, generally, cover h (or h_1+h_2)>D. The submerged self-weight of the pipeline q is now artificially enhanced by an amount q' due to overburden pressure throughout the modelling and empirical formulae for q'/q in terms of cover (h) are available regarding cases (a) and (b)[13,36]. Accordingly, the effect of continuous burial upon imperfect pipeline behaviour is exhibited in Fig 3.11 with regard to burial type (a). The *Empathetic* modelling is as given previously with the simple provision that q is replaced by q+q' throughout with the axial friction coefficient numerically modified as required[36] ($\phi_A=\phi'_A$, say). Herein, for simplicity, the data of Table 3.3 again applies together with that given in Fig 3.11. Upheaval temperatures are enhanced by 140% and 300% for h=1.5D and 3D respectively. Clearly, extended post-upheaval buckling vertical displacement v will require q'=f(v) through the buckle wavelength L as opposed to the constant value given above[13,25]; however, this constant value should suffice in the early and critical, not at least to the designer, stages of upheaval itself. The primary feature of burial is the enhancement of upheaval resistance (T_u) although care must be taken to avoid incurring T_{yld} pre-upheaval as this would become a more constraining operating criterion.

4.7.3 Discrete Dumping or Intermittent Burial

Continuous burial is very expensive. Costs can be reduced by the employment of intermittent burial whereby rock dumping is undertaken at judicious locations along the pipeline[47]. Cost-effectiveness is served by additional friction force generation within the slip length ie $\phi'_A(q+q')$ with buckling, should it occur, initiating in the unburied regions.

The topology is illustrated in Fig 4.5(a) whilst Fig 4.5(b) shows the axial force distribution applicable upon full activation of the peel point friction reaction $\phi_A qL/2$ and of the slip length $(L_{s1}+L_{s2})$ distributed friction forces. (Prior to this stage, analysis proceeds as previously discussed for the standard model). With a dumping interval or intermittency distance L_D and $L<L_D$,

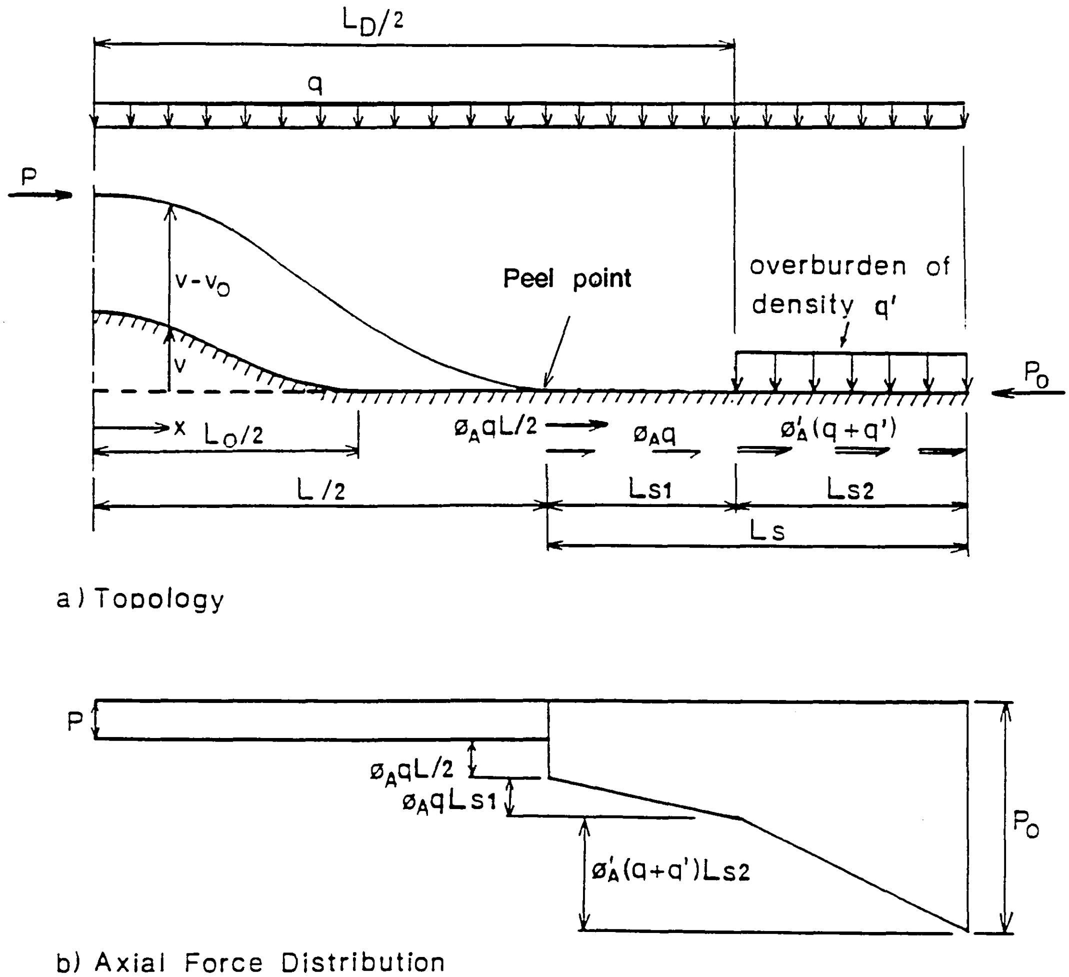

Fig 4.5 *Empathetic* Model with Discrete Dumping ($L > L_o$ shown)

together with a burial length $\geq L_{s2}$ such that axial friction resistance is fully mobilised throughout slip length $L_s=L_{s1}+L_{s2}$ as illustrated in Fig 4.5, the basic slip length modelling becomes duly modified. Noting Fig 3.7, the non-linear slip length field equation[12] takes the form

$$AEu,_{xx}=-\phi_A q \tag{4.31}$$

from which the axial shortening u, for $L/2 \leq x \leq L_D/2$, can be written as

$$u=-\frac{\phi_A q}{AE}\frac{x^2}{2}+A_1 x+A_2 \tag{4.32}$$

where A_1 and A_2 are the constants of integration. These can be expressed in terms of $u|_{LD/2}$ and $u,_x|_{LD/2}$ as

$$\begin{aligned} & A_1=u,_x|_{L_D/2}+\frac{\phi_A q L_D}{2AE} \\ \text{and} \quad & A_2=u|_{L_D/2}+\frac{\phi_A q}{2AE}L_D^2-\left(u,_x|_{L_D/2}+\frac{\phi_A q L_D}{2AE}\right)L_D \end{aligned} \tag{4.33}$$

For $L_D/2 \leq x \leq L_D/2+L_{s2}$

$$u=-\frac{\phi'_A(q+q')}{AE}\frac{x^2}{2}+A_3 x+A_4 \tag{4.34}$$

where A_3 and A_4 are the constants of integration which are determined by the boundary conditions

$$\begin{aligned} u|_{L_D/2+L_{s2}} &= 0 \\ u,_x|_{L_D/2+L_{s2}} &= 0 \end{aligned} \tag{4.35}$$

Such that

$$\begin{aligned} A_3 &= \frac{\phi'_A(q+q')}{2AE}\left(\frac{L_D}{2}+L_{s2}\right) \\ A_4 &= -\frac{\phi'_A(q+q')}{2AE}\left(\frac{L_D}{2}+L_{s2}\right)^2 \end{aligned} \tag{4.36}$$

Manipulation of eqns (4.34) - (4.36) and employing matching conditions at

$x=L_D/2$, then $u|_{LD/2}$ and $u_{,x}|_{LD/2}$ are given by

$$
\begin{aligned}
u|_{L_D/2} &= -\frac{\phi'_A(q+q')}{2AE}L_{s2}^2 \\
u_{,x}|_{L_D/2} &= \frac{\phi'_A(q+q')}{AE}L_{s2}
\end{aligned}
\tag{4.37}
$$

Substituting of eqn (4.33) into eqn (4.32), together with eqn (4.37), affords the axial shortening u_s at the buckle slip length interface to be

$$
u_s=u|_{x=L/2}=-\frac{\phi_A q}{2AE}\left(L_{s1}^2+(L_{s2}^2+2L_{s1}L_{s2})\left[1+\frac{q'}{q}\right].\frac{\phi'_A}{\phi_A}\right) \tag{4.38}
$$

The resulting longitudinal equilibrium and compatibility expressions become

$$
P_o-P=\phi_A q\frac{L}{2}+\phi_A q\left(L_{s1}+L_{s2}\left[1+\frac{q'}{q}\right]\frac{\phi'_A}{\phi_A}\right) \tag{4.39}
$$

and

$$
\begin{aligned}
&\frac{(P_o-P)L}{2AE}-7.9883.10^{-6}\left(\frac{q}{EI}\right)^2(L^7-L_o^7) \\
&+\frac{\phi_A q}{2AE}\left(L_{s1}^2+[L_{s2}^2+2L_{s1}L_{s2}]\left[1+\frac{q'}{q}\right]\frac{\phi'_A}{\phi_A}\right)=0
\end{aligned}
\tag{4.40}
$$

respectively. These two equations replace eqns (1.12) and (1.15) once L_{s2} *has become activated.* Eliminating (P_o-P) between eqns (4.39) and (4.40) and re-arranging as a quadratic equation for L_{s2} leads to

$$
(1+\frac{q'}{q})L_{s2}^2+(1+\frac{q'}{q})L_D L_{s2}+\frac{\phi_A}{\phi'_A}\left(\frac{L^2}{2}+LL_{s1}+L_{s1}^2-\frac{2u_f AE}{\phi_A q}\right)=0 \tag{4.41}
$$

where u_f is given by eqn (4.4).

Solution to eqn (4.41) affords

$$L_{s2}=\frac{1}{2}\left(-L_D+\left[L_D^2-\frac{4}{1+(\frac{q'}{q})}\frac{\phi_A}{\phi'_A}\left(\frac{L^2}{2}+LL_{s1}+L_{s1}^2-\frac{2u_fAE}{\phi_A q}\right)\right]^{1/2}\right) \qquad (4.42)$$

noting $L_{s1}=(L_D-L)/2$, for design purposes regarding L_D.

Parametric studies of the *Empathetic* model with discrete dumping, employing the pipe data of Table 3.3 together with the use of overburden q'=8.478 N/mm and its corresponding axial friction coefficient ϕ'_A of 0.68, have been tabulated in Table 4.3 whilst Fig 4.6 illustrates graphical presentation of the results. The investigation has been carried out for an initial imperfection of 100mm associated with two different cases; the first involved overburden q'=8.478N/mm being kept constant whilst the dumping interval L_D varies from 100, 500 and 1000m; in the second case the dumping interval is kept constant at the value of 100m whilst the overburden varies from 1.823 to 3.680N/mm.

That the discrete dumping technique does improve the thermal action response of the buckling curves is clearly shown in Fig 4.6 as the equilibrium path becomes increasing stable as the intermittency distance reduces although upheaval temperature (T_u) values are unchanged as no axial movement occurs pre-upheaval to cause activation of the slip length which includes the overburden effects (see Section 4.3). This indicates that, unlike with continuous burial, discrete dumping causes disproportionate changes in equilibrium path behaviour of a qualitative form dependent upon how soon the enhanced frictional resistance along the buried pipe comes into effect.

v_{om} (mm)	L_o (m)	L_D (m) q' (N/mm) [ϕ'_A]		Upheaval State	Max. Temp. State	After snap State	Min. Temp. State	First Yield State	Max slope 0.1rad
100	24.531	100	T	26.04	N/A	N/A	N/A	(64.58)	57.51
		q'=8.478	v_m	100				1531.9	1292.4
		[0.68]	L	24.531				48.531	46.510
			f	58.20				350.	318.6
		500	T	26.04	31.97	31.97	(30.98)	(41.16)	(37.18)
		q'=8.478	v_m	100.	239.9	845	608.7	1531.9	1292.4
		[0.68]	L	24.531	30.531	41.817	38.531	48.531	46.510
			f	58.20	124.4	251.6	210.1	350	318.6
		1000	T	26.04	31.97	31.93	(30.91)	(34.85)	(33.00)
		q'=8.478	v_m	100.	239.9	1085.9	674.4	1531.9	1292.4
		[0.68]	L	24.531	30.531	44.531	39.531	48.531	46.510
			f	58.20	124.4	289.2	222.2	350.	318.6
100	24.531	standard model	T	26.04	31.97	31.97	(30.91)	(34.33)	(32.93)
		q'=0	v_m	100.	239.9	1085.9	674.4	1531.9	1292.4
			L	24.531	30.531	44.531	39.531	48.531	46.510
			f	58.20	124.4	289.2	222.3	350.	318.9
		100	T	26.04	N/A	N/A	N/A	(43.99)	40.95
		q'=1.823	v_m	100.				1531.9	1292.4
		[0.55]	L	24.531				48.531	46.510
			f	58.20				350.	318.9
		100	T	26.04	N/A	N/A	N/A	(51.44)	47.03
		q'=3.680	v_m	100.				1531.9	1292.4
		[0.60]	L	24.531				48.531	46.510
			f	58.20				350	318.9

Notes :
- * N/A - denotes 'stable' buckling path
- * T - Temperature Rise in (°C)
- * v_m - Buckle Amplitude in (mm)
- * L - Buckle Length in (m)
- * f - Maximum Stress in (N/mm^2)

Table 4.3 Fully Mobilised *Empathetic* Model with Discrete Dumping Parametric Studies.

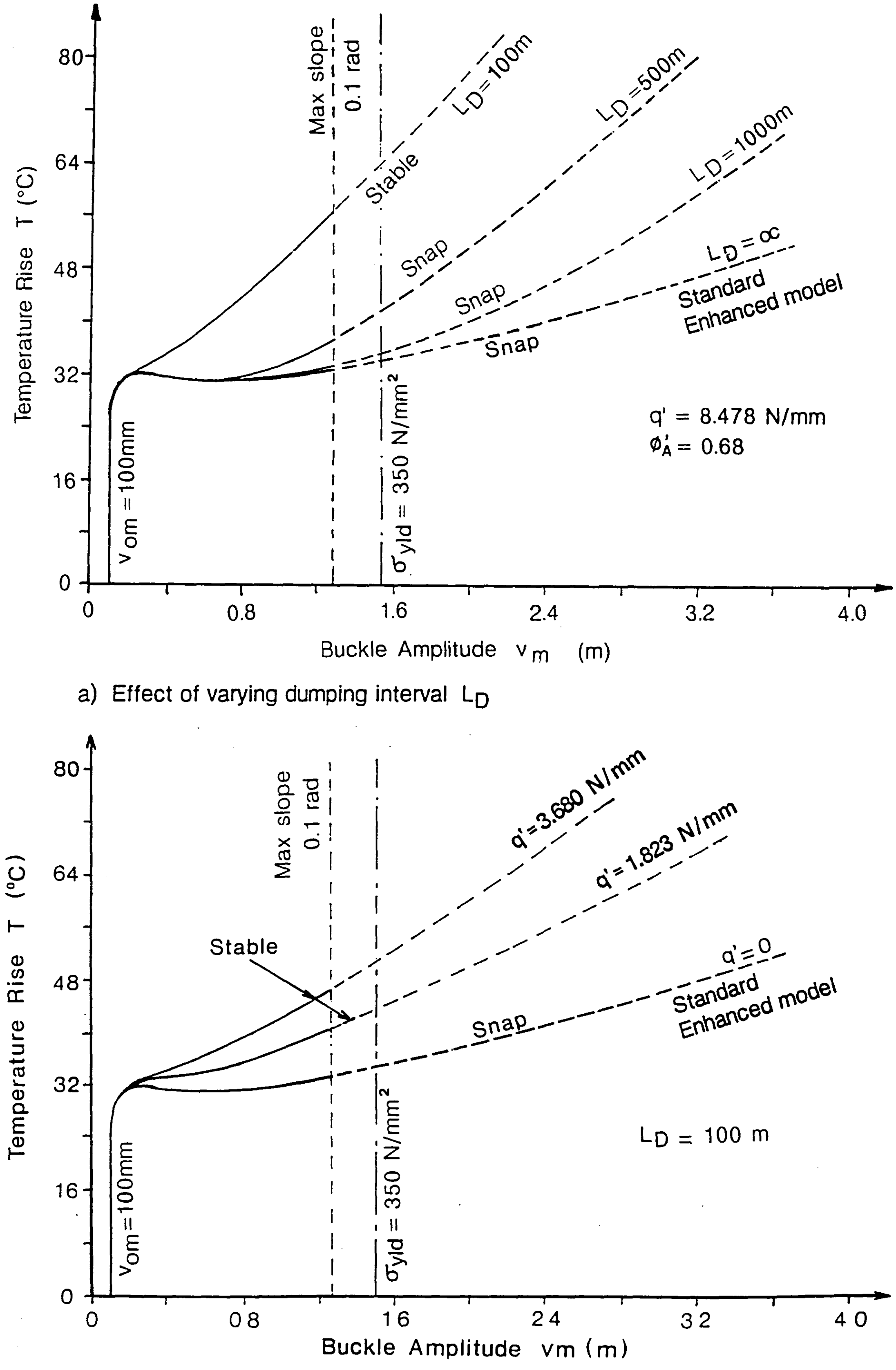

a) Effect of varying dumping interval L_D

b) Effect of varying overburden q'

Fig 4.6 **Thermal Action Characteristics**
Fully Mobilised *Empathetic* Model with Discrete Dumping

4.7.4 Fixed Anchor Points

The use of fixed anchorage points (u=0) which typically possess shearing capacities of 250kN-750kN generates similar effects to that of the previous section, the essential topology and axial force distribution being shown in Fig 4.7. For an anchorage spacing of L_{fap} and for $(L_{fap}-L)/2>0$ and represents a fully-activated slip length before which standard modelling applies, the equivalent expressions to eqns (4.39) and (4.40) take the form

$$P_o-P = \phi_A q\frac{L}{2}+\phi_A q\frac{(L_{fap}-L)}{2}+F_{ap} \tag{4.43}$$

where F_{ap} denotes the required anchorage capacity and

$$\begin{aligned}&\frac{(P_o-P)}{2AE}-7.9883.10^{-6}\left(\frac{q}{EI}\right)^2(L^7-L_o^7)\\&+\left(F_{ap}+\frac{1}{2}\phi_A q\frac{[L_{fap}-L]}{2}\right)\frac{L_{fap}-L}{2AE} = 0\end{aligned} \tag{4.44}$$

respectively, the first two terms in eqn (4.44) representing the total end shortening of the buckle whilst the last term being the axial extension of the slip length. Peel point longitudinal movement u_s takes the form

$$u_s=-\left(F_{ap}+\frac{1}{2}\phi_A q\frac{(L_{fap}-L)}{2}\right)\frac{L_{fap}-L}{2AE} \tag{4.45}$$

Eliminating F_{ap} between eqns (4.43) and (4.44) affords

$$P_o-P=\frac{\phi_A q}{4}\frac{(L_{fap}^2-L^2)}{L_{fap}}+7.9883.10^{-6}\frac{2EA}{L_{fap}}\left(\frac{q}{EI}\right)^2(L^7-L_o^7) \tag{4.46}$$

Table 4.4 and Fig 4.8 present results of a set of *Empathetic* model analyses involving fixed anchor points employing the pipe data of Table 3.3. The results are tabulated for two different values of imperfection of 100 and 250mm with various anchor spacings L_{fap}, ranging from 100 to 1000m. The analysis results displayed in Table 4.4 indicate that the operating temperatures for this

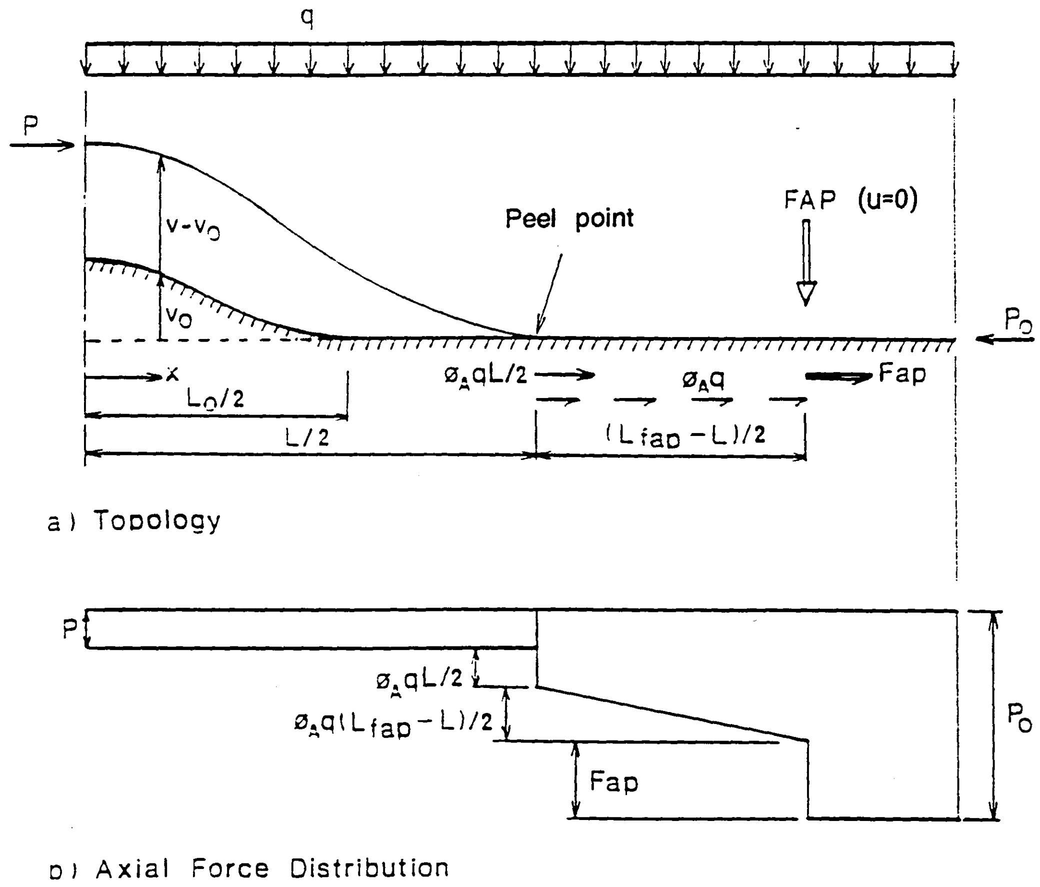

Fig 4.7 Empathetic Model with Fixed Anchor Points ($L_s=(L_{fap}-L)/2$ shown)

v_{om} (mm)	L_o (m)	L_{fap} (m)		Upheaval State	Max. Temp. State	After snap State	Min. Temp. State	First Yield State	Max slope 0.1rad	Max F_{ap} at 750 kN
100	24.531	100	T	26.04	N/A	N/A	N/A	(136.4)	(106.4)	58.14
			v_m	100				1531.9	1292.4	787.2
			L	24.531				48.531	46.510	41.080
			f	58.20				350.	318.6	241.9
		500	T	26.04	31.97	31.97	(31.0)	(43.28)	(38.26)	(57.02)
			v_m	100.	239.9	821.6	608.7	1531.9	1292.4	2034.4
			L	24.531	30.531	41.531	38.531	48.531	46.510	52.091
			f	58.20	124.4	247.7	210.1	350.	318.6	410.4
		1000	T	26.04	31.97	31.97	(30.90)	(34.91)	(33.01)	(61.7)
			v_m	100.	239.9	1085.9	674.4	1531.9	1292.4	3173.5
			L	24.531	30.531	44.531	39.531	48.531	46.510	58.217
			f	58.20	124.4	289.2	222.2	350.	318.6	525.8
250	30.846	100	T	16.69	N/A	N/A	N/A	(302.1)	(100.9)	54.63
			v_m	250.				2072.3	1292.4	834.8
			L	30.846				52.332	46.510	41.692
			f	36.81				350.	252.1	180.2
		500	T	16.69	N/A	N/A	N/A	(56.58)	35.84	(56.12)
			v_m	250.				2072.3	1292.4	2058
			L	30.846				52.332	46.510	52.241
			f	36.81				350.	252.1	348.4
		1000	T	16.69	N/A	N/A	N/A	(40.16)	30.92	(59.39)
			v_m	250.				2072.3	1292.4	3107.3
			L	30.846				52.332	46.510	57.916
			f	36.81				350	252.1	456.0

Notes :
* N/A - denotes 'stable' buckling path
* T - Temperature rise (°C)
* v_m - Buckle amplitude (mm)
* L - Buckle length (m)
* f - Maximum stress (N/mm^2)
* F_{ap} - Anchor shear capacity (kN)

Table 4.4 Fully Mobilised *Empathetic* Model with Fixed Anchor Points Parametric Studies.

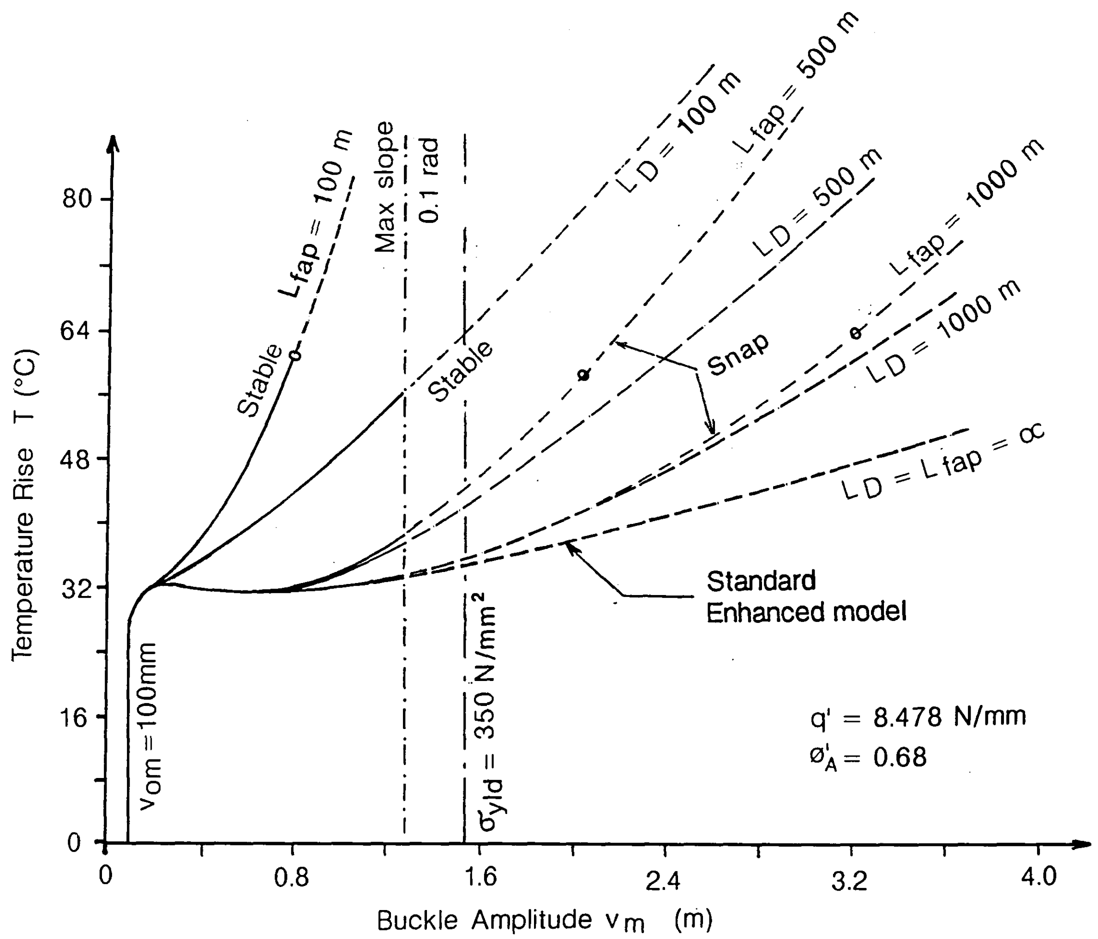

Fig 4.8 Comparison between Discrete Dumping and Fixed Anchor Points Models

o denoting F_{ap} = 750 kN

particular developed model are not only restricted by either T_u or $T|_{max}$ for the snap cases and either T_u or $T|_{0.1}r$ for the stable cases, but that they are also subject to the availability of the anchor shearing capacity F_{ap}; reference should be made to the case where v_{om}=100mm should F_{ap} be limited to 750kN. Figure 4.8, which also includes comparative discrete dumping case data, clearly shows that the use of intermittent burial and fixed anchors are quite effective in stiffening post-upheaval temperature rise behaviour, particular at close spacing. Large anchor spacings, as with large intermittency intervals, produce little improvement over the equivalent standard (trenched) case. Upheaval is not affected by the use of fixed anchor points due to axial movement only occurring with the onset of upheaval in the *Empathetic* model (see Section 4.3).

4.8 Disconnected Model

Referring to Figs 1.7(a) and (2.2(a), The *Empathetic* model requires that initial amplitude and wavelength are uniquely related through eqn (1.20), upheaval occurring uniquely across the entire contact undulation. The physical possibility of any given initial amplitude v_{om} occurring in the presence of a variety of initial wavelength surely exists in practice, however, and the development of an alternative contact undulation formulation involving eqn (1.18) but not eqn (1.20) should be considered.

If wavelength L is considered to be kinematic, eqn (1.20) could be replaced by the statics criterion $V,_L=0$ thereby 'disconnecting' v_{om} and L_o. Noting Section 1.6, the total Potential Energy can be expressed as

$$V = 66.7984EI\left(\frac{v_m^2}{L^3}+\frac{v_{om}^2}{L_o^3}\right)-2.9451EI\frac{v_{om}v_m\psi_1}{LL_o^2}$$
$$+ 0.214359q(Lv_m-L_ov_{om})-1.37849P\left(\frac{v_m^2}{L}-\frac{v_{om}^2}{L_o}\right) \qquad (4.47)$$

so if $V_{'L}=0$ then

$$200.3952\frac{EIv_m}{L^4}-0.214359q-1.37849\frac{Pv_m}{L^2}-\frac{2.9451EIv_{om}}{(LL_o)^2}(\psi_1-\psi_2)=0 \qquad (4.48)$$

where ψ_2 is determined by

$$\psi_2 = -20.68375k_2\cos k_1k_2-10.59446\frac{k_2}{k_3^2}(k_1k_2k_3\cos k_1k_3+\sin k_1k_3)$$
$$+10.59446\frac{k_2}{k_4^2}(k_1k_2k_4\cos k_1k_4-\sin k_1k_4) \qquad (4.49)$$

noting k_i (i=1,..,4) are given by eqn (1.23), provides a second energy-based equation, replacing eqn (1.20).

Manipulation of eqns (1.22) and (4.48), thus affords the maximum buckle amplitude v_m to be written as

$$v_m=2.407.10^{-3}\frac{qL^4}{EI}-0.01102\frac{v_{om}}{L_o^2}L^2(2\psi_2-\psi_1) \qquad (4.50)$$

whilst the buckle force P takes the form

$$P=80.76\frac{EI}{L^2}\left(0.6+9.627.10^{-4}\frac{qL^4}{EIv_m}-0.013227\psi_1\frac{v_{om}}{v_m}\left(\frac{L}{L_o}\right)^2\right) \qquad (4.51)$$

resulting in P_u=50%P_{qi}.

With eqn (4.50) replacing eqn (1.20) of the *Empathetic* model, analysis now involves the independent stipulation of v_{om} and L_o. Clearly, the model requires the incorporation of appropriate longitudinal equilibrium and compatibility expressions similar in form to those of the *Empathetic* model.

Figure 4.9 compares the resulting (hypothetical) Disconnected model performance with its peers employing the data of Table 1.1 with v_{om}=140mm and L_o=46.8m [agrees with eqn (1.20)]. It shows enhanced resistance compared to the *Empathetic* model. This is surely to be expected as additional energy will be required to produce non-empathetic curvatures. The Disconnected model is, however, also considered to be mathematically ill-founded as it appears to violate the *Workless Boundary Conditions* requirement of the Theorem of Stationary Potential Energy[3]. The model is not considered valid and is primarily included to introduce the implications of non-*empathetic* (crown) curvature upon post-buckling behaviour (see next Chapter).

A further alternative model based upon eqn (1.18) was considered with eqn (1.20) substituted prior to application of the statics criterion $V_{,vm}=0$ requiring that v_m and L are completely interchangeable kinematic variables. Briefly, this procedure affords

$$P = P_{qi}\left(1-\frac{\psi_3}{264.4}\left(\frac{L_o}{L}\right)^2\right) \tag{4.52}$$

where

$$\begin{aligned}\psi_3 = {} & 13.80943\sin k_1k_2 - 20.68376\cos k_1k_2 \\ & +21.18893k_2\left(\frac{\sin k_1k_3}{k_3} - \frac{\sin k_1k_4}{k_4}\right) \\ & +21.18893k_2^2\left(\frac{\sin k_1k_3 - k_1k_3\cos k_1k_3}{k_3^2} + \frac{\sin k_1k_4 - k_1k_4\cos k_1k_4}{k_4^2}\right)\end{aligned} \tag{4.53}$$

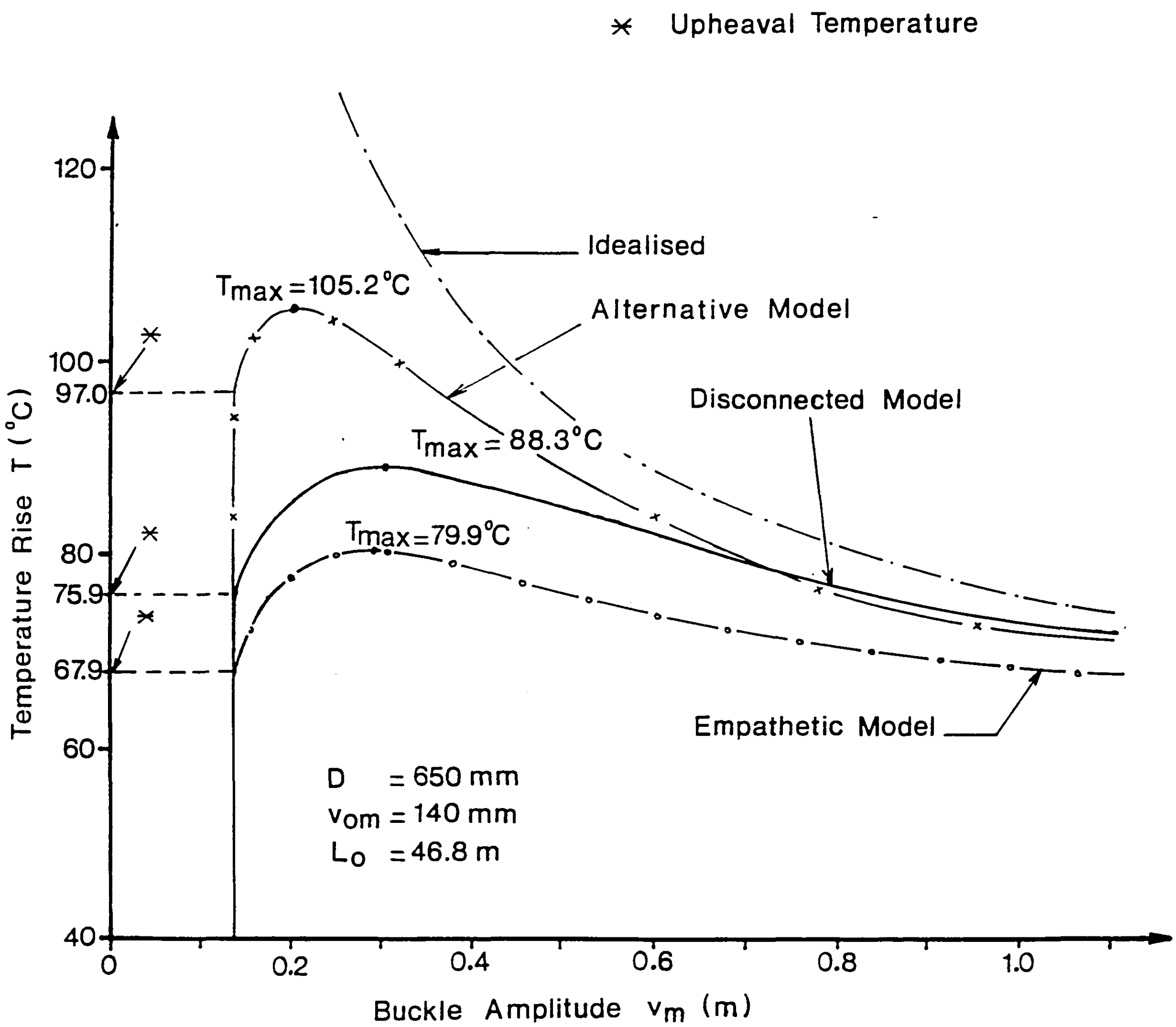

Fig 4.9 Contact Undulation Model Comparisons

resulting in P_u=57.1%P_{qi}. The respective data illustrated in Fig 4.9 again involved the use of equilibrium and compatibility expressions analogous to those developed previously for the standard *Empathetic* model. However, L again varies through the stationary procedure and the model is not considered valid. (Both of the models described in this section relate to frustrated attempts to broaden the scope of the *Empathetic* model.) The ensuing two Chapters relate to more productive studies involving truly alternative models.

4.9 Summary

A number of novel enhancements to the *Empathetic* model have been established and formulations to enable its employment in situations involving updated physical considerations have been developed. An appropriate, enhanced, standard upheaval configuration model has been defined and two erroneous formulations briefly identified to indicate limiting explorations of the *Empathetic* model. A valid alternative treatment of a contact undulation imperfection is now considered.

Chapter 5

Infilled Prop (*Blister* Model)

5.1 Introduction

As discussed in Chapters 1 and 2, an alternative contact undulation model involving the infilling of an isolated prop's attendent voids is to be considered - recall Figs 1.7(c) and 2.2(c). The following relates to Activity 3c of Fig 2.1.

5.2 Datum Establishment

Initially, and as indicated in Figs 1.7 and 2.2, the pre-operational pipeline is taken to lie over a discrete object with *void* (ie; sea water) lying to either side at zero pipeline compression. The appropriate topology is shown in Fig 5.1 with the pipeline effectively being under the contrasting actions of a prop imperfection of amplitude v_{om} and a submerged self-weight loading intensity of q (to which can be added any overburden effect in the case of buried pipes - see later). Note that, initially, q would normally relate to an empty pipe; no such distinction is available in the mathematically based *Empathetic* model. Reactions include a prop shear force F_i, equal to half the prop force, and a bending moment N_i acting at the crown, together with a transverse reaction at the peel point. The boundary conditions are given by

$$v_i|_{L_i/2}=v_{i,x}|_{L_i/2}=v_{i,xx}|_{L_i/2}=v_{i,x}|_0=0 \tag{5.1}$$

and

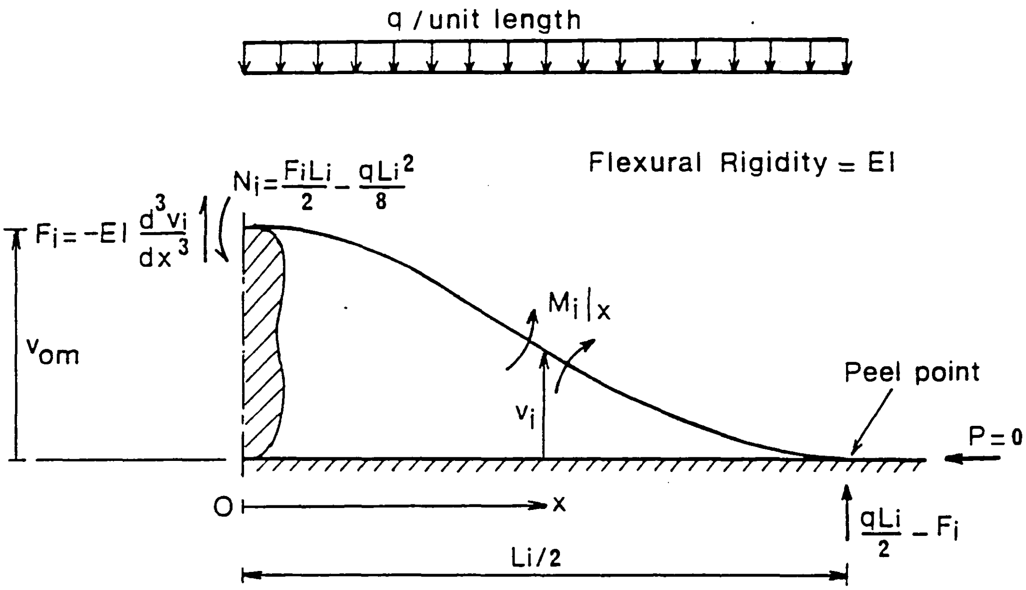

Fig 5.1 Initial Imperfection Topology

$$v_i|_0 = v_{om} \tag{5.2}$$

where v_i denotes initial vertical deflection. From statics, bending moment N_i at the crown (x=0) can be written as

$$N_i = \frac{F_i L_i}{2} - \frac{qL_i^2}{8} \tag{5.3}$$

Equilibrium affords for the general bending moment $M_i|_x$, $0 \leq x \leq L_i/2$

$$M_i|_x = EIv_{i,xx} = \left(\frac{qL_i}{2} - F_i\right)\left(\frac{L_i}{2} - x\right) - q\frac{(L_i/2 - x)^2}{2} \tag{5.4}$$

where subscript i denotes the initial configuration.

The general solution to eqn (5.4) takes the form

$$EIv_i = B_1 + B_2 x + \left(-\frac{F_i L_i}{2} + \frac{qL_i^2}{8}\right)\frac{x^2}{2} + \frac{F_i x^3}{6} - \frac{qx^4}{24} \tag{5.5}$$

where B_1 and B_2 are the constants of integration which are determined as

$$\begin{aligned} v_{i,x}|_0 = 0 \quad &\rightarrow \quad B_2 = 0 \\ v_i|_{L_i/2} = 0 \quad &\rightarrow \quad B_1 = \frac{qL_i^4}{1152} \end{aligned} \tag{5.6}$$

Computational manipulation gives the vertical deflection v_i as

$$v_i = \frac{q}{72EI}\left(2L_i\left[\frac{L_i}{2} - x\right]^3 - 3\left[\frac{L_i}{2} - x\right]^4\right) \tag{5.7}$$

whilst the relationship between the imperfection v_{om} and buckle length is

$$L_i = 5.8259\left(\frac{v_{om}EI}{q}\right)^{1/4} \tag{5.8}$$

The shear force F_i at the crown can be found by employing boundary condition $v_{i,x}|_{Li/2}=0$, which gives

$$\frac{F_i}{EI} = -v_{i,xxx}|_0 = -\frac{qL_i}{3EI} \tag{5.9}$$

From eqn (5.7), the general curvature expression takes the form

$$v_{i},_{xx}=\frac{q}{24EI}(L_i-2x)(6x-L_i) \tag{5.10}$$

thus enabling the curvature at the crown, ie (x=0), to be evaluated as

$$v_{i},_{xx}|_0=v_{i},_{xx}|_{\max}=-\frac{qL_i^2}{24EI}=-0.0417\frac{qL_i^2}{EI} \tag{5.11}$$

Substituting eqn (5.10) into eqn (5.4), then the general bending moment $M_i|_x$ becomes

$$M_i|_x=\frac{q}{12}(\frac{L_i}{2}-x)(6x-L_i) \quad , \quad M_i|_x \leq N_i \tag{5.12}$$

It must be noted, however, that eqn (5.12) is effectively based upon a previous and fictitious *stress-free-when-straight* datum and that it is with the pipe in the above configuration that the voids are now infilled.

Figure 5.2 compares this physically based imperfection with the previously discussed *Empathetic*; for a common imperfection amplitude v_{om}, the initial datum state crown curvatures of this and the *Empathetic* (and *Isoprop*, see later) models are equal from eqns (4.15) and (5.11) respectively. Crown curvatures for symmetric topologies at all states are respective maxima, which remain unchanged for both models prior to upheaval. Given the foregoing and that $L_o<L_i$ ($L_i=1.29L_o$), the possibility of an alternative contact undulation buckling mode to that discussed previously occurring, with upheaval buckling initiating with a '*blister*' of wavelength $L_u<L_i$ and as indicated in Fig 2.2, must be considered. Indeed, contraction upon cooling of an idealised buckle would generate $v_m>v_{om}$ when $L=L_i$, leading to a '*blister*' buckle upon further contraction.

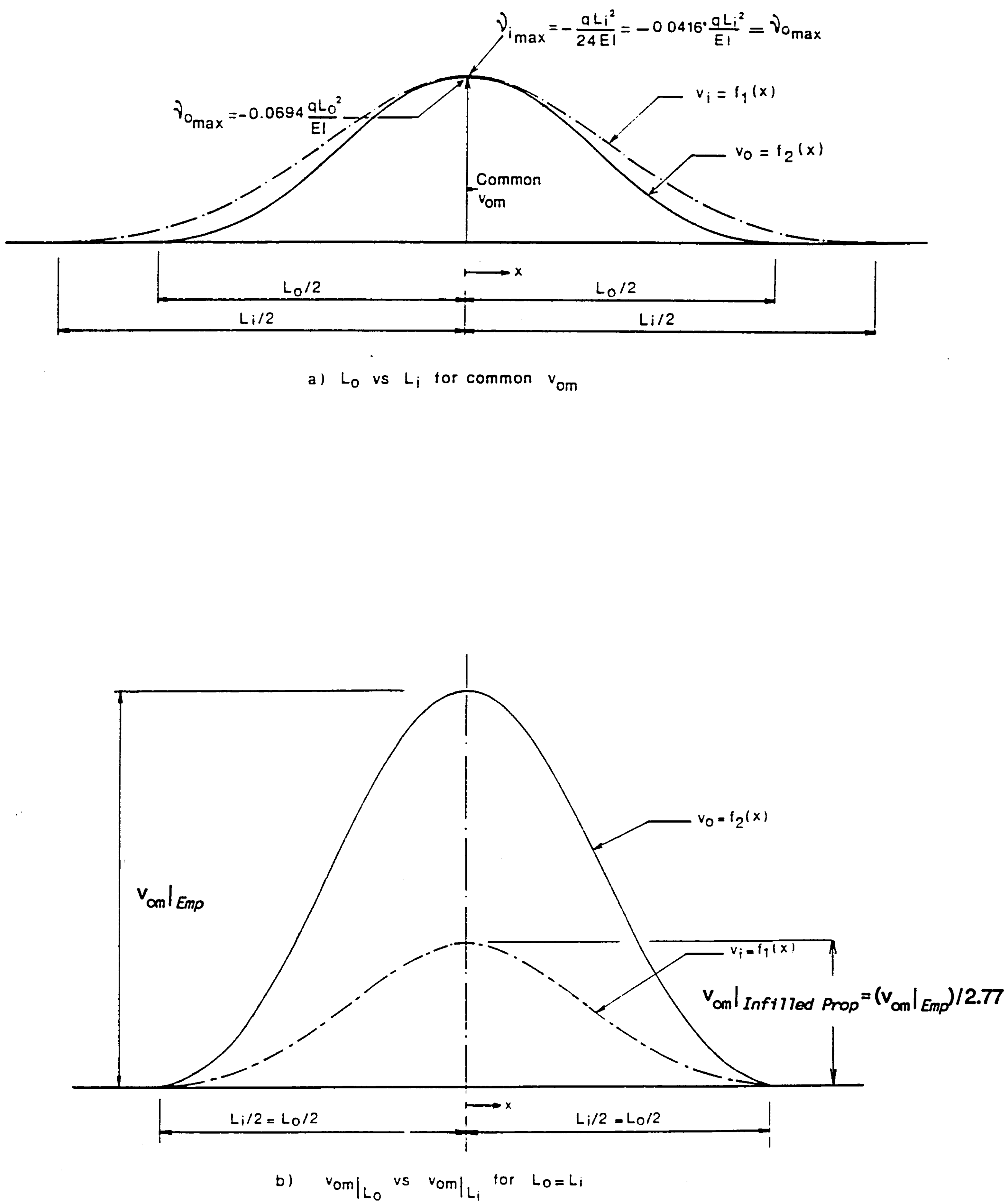

Fig 5.2 Comparison of Initial Imperfection Topologies

5.3 Revised Infilled Prop Topology (*Blister* Model)

The infilling of the voids is an attractive supposition regarding the sandy conditions envisaged in the North Sea, particularly so regarding continuously buried topologies. The infilling will take time to consolidate and the consideration of whether the pipe is full or empty, recall Section 5.2, becomes less precise; submerged self-weight q is therefore taken to relate to the full case. The effect of infilling is to prevent any reduction in spanning prior to upheaval (see *Isoprop* model[39]) and to provide for relief of eqn (5.12) by direct bearing support. Note here that 50%N_i is due to q or q+q', with 50%N_i due to v_{om} itself. In-service residual stress-relieving for this topology has been conceptually propounded elsewhere[17,20] and lends further support to the adoption, as herein, of a *stress-free-when-initially-deformed* datum. That is, whilst eqn (5.7) is henceforth accepted as an imperfection of form, eqn (5.12), considered to be a component of some total residual stressing including fabrication and laying operation, is suppressed. Further discussion of this factor is given in later work. It should be noted that field investigations support the v_{om}/L_i relationship of eqn (5.8) - as for the standard *Empathetic* model (v_{om}/L_o), this is a fixed ratio[12].

5.4 Post Upheaval with $L<L_i$

Figure 5.3 shows the proposed *Blister* model buckling topology in detail with $L<L_i$ in the early post-buckling phase. A vectorial equilibrium-compatibility analysis is employed here employing the moment-curvature relationship

$$M_x=EI(v,_{xx}-v_i,_{xx})=P(v_m-v)-\frac{qx^2}{2}+N \tag{5.13}$$

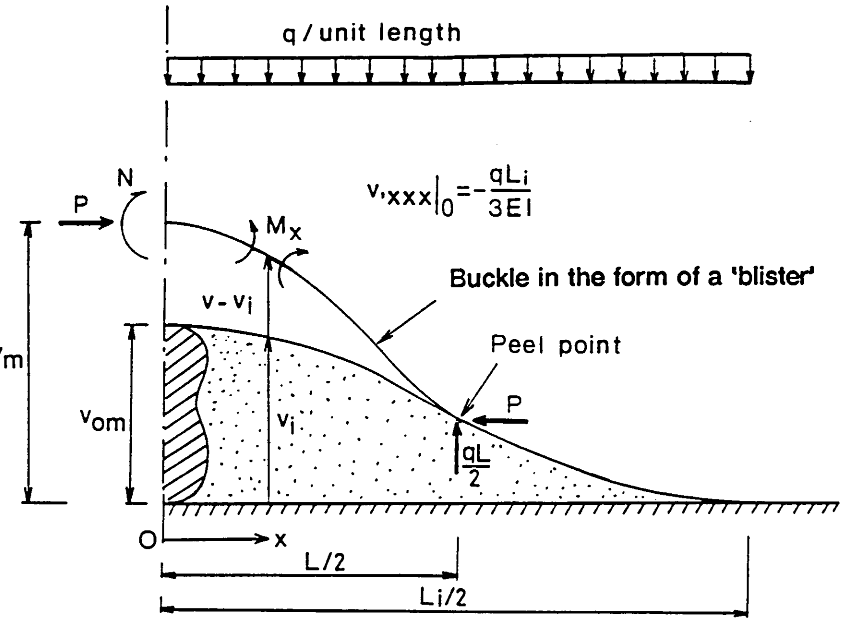

(a) Flexural Range Topology $L \leqslant L_i$

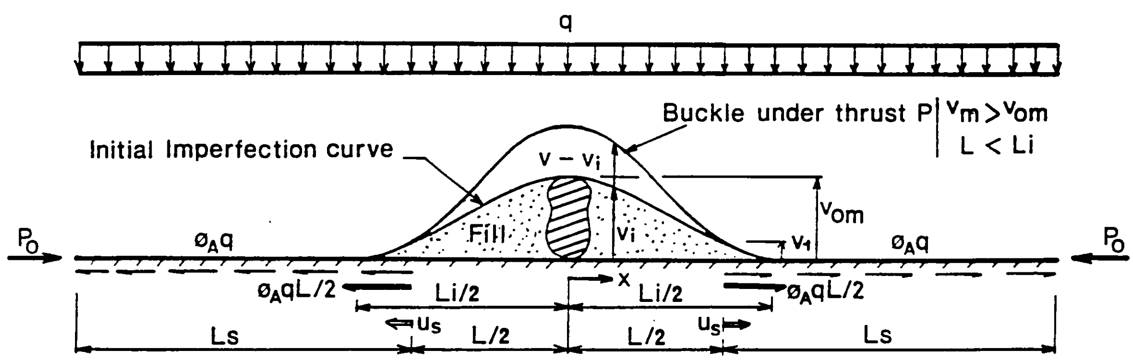

(b) General Topology

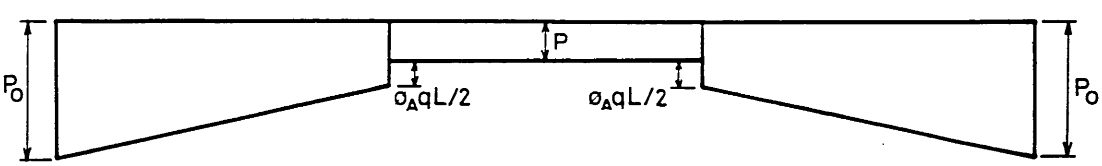

(c) Axial Force Distribution

Fig 5.3 Infilled Prop ; Initial Post Upheaval
Details of Imperfect Fully Mobilised Models $L < L_i$ (*Blister* Model)

where M_x represents the bending moment at x, $0 \le x \le L/2$.

The general solution to eqn (5.13) takes the form

$$v = B_3 \cos nx + B_4 \sin nx + k_7 + \frac{qL_i x}{3EIn^2} - \frac{qx^2}{EIn^2} \tag{5.14}$$

where B_3 and B_4 are the constants of integration, $P=n^2EI$ and k_7 is given by

$$k_7 = v_m + \frac{1}{EIn^2}\left(N - \frac{qL_i^2}{24} + \frac{2q}{n^2}\right) \tag{5.15}$$

Using the boundary conditions

$$\begin{aligned} v|_0 &= v_m \\ v|_{\frac{L}{2}} &= v_i|_{\frac{L}{2}} \\ v,_x|_0 &= 0 \\ v,_x|_{\frac{L}{2}} &= v_i,_x|_{\frac{L}{2}} \\ EIv,_{xx}|_{\frac{L}{2}} &= EIv_i,_{xx}|_{\frac{L}{2}} \end{aligned} \tag{5.16}$$

with $v,_x|_0=0$ then the constant B_4 is determined as

$$B_4 = -\frac{qL_i}{3EIn^3} \tag{5.17}$$

Similarly, the last two boundary conditions given in eqn (5.16) afford the relationship between B_3 and B_4 to be expressed as

$$-nB_3 \sin\frac{nL}{2} + nB_4 \cos\frac{nL}{2} + \frac{qL_i}{3EIn^2} - \frac{qL}{EIn^2} = -\frac{qL^3}{48EI}\left(\frac{L_i}{L} - 1\right)^2 \tag{5.18}$$

and

$$B_3 \cos\frac{nL}{2} + B_4 \sin\frac{nL}{2} + \frac{2q}{EIn^4} = -\frac{qL^2}{24EIn^2}\left(\frac{L_i}{L} - 1\right)\left(\frac{L_i}{L} - 3\right) \tag{5.19}$$

respectively. Combination of eqns (5.18) and (5.19) gives

$$B_3 = \frac{q}{EIn^4}\left(k_8 \cos\frac{nL}{2} + k_9 \sin\frac{nL}{2}\right) \tag{5.20}$$

$$B_4=\frac{q}{EIn^4}\left(k_8\sin\frac{nL}{2}-k_9\cos\frac{nL}{2}\right) \tag{5.21}$$

noting that

$$\begin{aligned} k_8 &= -2+\frac{(nL)^2}{24}\left(\frac{L_i}{L}-1\right)\left(\frac{L_i}{L}-3\right) \\ k_9 &= \frac{nL}{3}\left(\frac{L_i}{L}-3\right)+\frac{(nL)^3}{48}\left(\frac{L_i}{L}-1\right)^2 \end{aligned} \tag{5.22}$$

Furthermore, equating eqns (5.17) and (5.21) yields the characteristic equation for n

$$k_8\sin\frac{nL}{2}-k_9\cos\frac{nL}{2}+\frac{nL_i}{3}=0 \tag{5.23}$$

Values of nL for given values of L_i/L are shown in Table 5.1.

With boundary condition $v|_0=v_m$, then eqn (5.14) becomes

$$B_3+\frac{N}{EIn^2}-\frac{qL_i^2}{24EIn^2}+\frac{2q}{EIn^4}=0 \tag{5.24}$$

Combination of eqns (5.20) and (5.24) affords the bending moment at the crown to be evaluated as

$$N=\frac{q}{n^2}\left(-k_8\cos\frac{nL}{2}-k_9\sin\frac{nL}{2}+\frac{(nL_i)^2}{24}-2\right) \tag{5.25}$$

Lastly, boundary condition $v|_{L/2}=v_i|_{L/2}$ gives

$$B_3\cos\frac{nL}{2}+B_4\sin\frac{nL}{2}+k_7+\frac{qLL_i}{4EIn^2}-\frac{qL^2}{4EIn^2}=v_p \tag{5.26}$$

where peel point height above base level v_p can be found by substituting x=L/2 into eqn (5.7) thus

$$v_p=\frac{qL^4}{1152EI}\left(\frac{L_i}{L}-1\right)^3\left(\frac{L_i}{L}+3\right) \tag{5.27}$$

The vertical deflection v can now be expressed as

	L_i/L	nL	Remarks
Post-Upheaval $L < L_i$	4.670431	1.247017	Upheaval limit at $v_m = 100.05\%\ v_{om}$
	4.0	1.502445	
	2.0	3.764647	
	1.8	4.372683	
	1.6	5.141256	
	1.4	6.046544	
	1.2	6.952257	
	1.0	7.713400	$L = L_i$
Post-Upheaval $L > L_i$	1.0	7.713400	$L = L_i$
	0.9	8.039016	
	0.8	8.327418	
	0.6	8.754047	
	0.5	8.877923	
	0.4	8.946799	
	0.2	8.985391	
	0.1	8.986773	
	.	.	
	.	.	
	0.01	8.9868	$P \rightarrow 80.76\ EI/L^2$

Table 5.1 Typical Buckle Force Solution for *Blister* Model

$$v = \frac{q}{n^4 EI}\Bigg(k_8 \cos n(\frac{L}{2}-x) + k_9 \sin n(\frac{L}{2}-x)$$
$$-k_8 - \frac{(nL)^2}{12}(2\frac{L_i}{L}-3) + \frac{n^2 L_i}{3}x - n^2x^2\Bigg) + v_p \tag{5.28}$$

so that the amplitude v_m takes the form

$$v_m = K_1 \frac{qL^4}{EI} + v_p \tag{5.29}$$

where

$$K_1 = \frac{1}{(nL)^4}\left(k_8 \cos\frac{nL}{2} + k_9 \sin\frac{nL}{2} - k_8 - \frac{(nL)^2}{12}(2\frac{L_i}{L}-3)\right) \tag{5.30}$$

Upheaval, of crucial importance to designers, is usually determined by reducing initial post-buckling amplitude expressions $v_m \to v_{om}$; for example, use is made of eqn (5.29) here. However, numerical limitations affect the *Blister* model as shown by the non-zero upheaval length in Table 5.1 from which upheaval definition is limited to v_m=100.05%v_{om}. At upheaval, buckle length L_u and buckle force P_u become

$$L_u = \frac{L_i}{4.670431} = 21.41\%\ L_i = 27.63\%\ L_o|_{v_{om}} \quad \textit{and}$$
$$nL = 1.247017 \;\rightarrow\; P_u = 25\%\ P_{qi}|_{v_{om}} = 3.962\left(\frac{EIq}{v_{om}}\right)^{1/2} \tag{5.31}$$

and the upheaval temperature T_u can be expressed as

$$T_u = -1.413\frac{q}{AE\alpha}\cdot\frac{1}{v_{i',xx}|_0} = 0.63\left(0.078\frac{q}{AE\alpha}\left[\frac{L_o^2}{v_{om}}\right]\right) \tag{5.32}$$

which contrasts with eqn (4.17).

Having established the buckling force P in terms of wavelength L and amplitude v_m, it is now necessary to employ longitudinal equilibrium and compatibility to relate P to the temperature rise $T=P_0/AE\alpha$; note the system topology and axial force distribution given in Fig 5.3. Employing procedures similar to those adopted in Section 4.2 together with the neglection of slip length's inclination[19,20] for $L<L_i$, then manipulation affords the equilibrium expression to be written as

$$P_o-P=[2\phi_A qAE(-u_s)]^{1/2}+\phi_A\frac{qL}{2} \tag{5.33}$$

where u_s denotes the implied longitudinal movement of the peel point given by the longitudinal compatibility expression

$$u_s=\frac{(P_o-P)L}{2AE}-u_f \tag{5.34}$$

in which u_f denotes the flexural end shortening through the wavelength. This generates

$$u_f=\frac{1}{2}\left(\int_0^{L/2}(v,_x)^2\,dx-\int_0^{L/2}(v_i,_x)^2\,dx\right) \tag{5.35}$$

where

$$\begin{aligned}\int_0^{L/2}(v,_x)^2\,dx = \left(\frac{q}{EI}\right)^2\frac{1}{n^7}\Bigg(&(nL-\sin nL)\frac{k_8^2}{4}\\ &+(nL+\sin nL)\frac{k_9^2}{4}+\frac{k_8k_9}{2}(\cos nL-1)\\ &+\frac{(nL)^3}{18}\left[(L_i/L)^2-3L_i/L+3\right]\\ &+k_8\left[\frac{2nL_i}{3}\left(1-\cos\frac{nL}{2}\right)-2nL+4\sin\frac{nL}{2}\right]\\ &+k_9\left[-\frac{2nL_i}{3}\sin\frac{nL}{2}-4\cos\frac{nL}{2}+4\right]\Bigg)\end{aligned} \tag{5.36}$$

and

$$\int_0^{L/2} (v_{i,x})^2\, dx = \left(\frac{q}{EI}\right)^2 \frac{L^7}{483840}\left[\left(\frac{L_i}{L}\right)^7 - \left(\frac{L_i}{L}-1\right)^5\left(\frac{L_i}{L}\right)^2 - \left(\frac{L_i}{L}-1\right)\left(5\frac{L_i}{L}+15\right)\right] \tag{5.37}$$

Herein, it is necessary to note that the zero fully mobilised slip length consideration in Section 4.2 is still valid for this particular model, apart from the exception that eqn (4.5) used for the evaluation of L^* is to be replaced by

$$-\frac{\phi_A q (L^*)^2}{4AE} + u_f = 0 \tag{5.38}$$

where u_f is given by eqn (5.35). For $L \le L^*$, $u_s=0$ and no slip length exists such that the longitudinal equilibrium expression takes the form of eqn (4.7). Otherwise, the fully developed slip length modelling allows the peel point longitudinal movement u_s, slip length L_s and (P_0-P) to be calculated from eqns (4.8), (4.9) and (4.10) respectively.

5.5 Post Upheaval with $L>L_i$

Figure 5.4 illustrates the key characteristics of the *Blister* model at the developed post-upheaval state. A similar procedure to that employed previously is adopted for this later stage of buckling noting, however, that the transverse deflection $v=f(x,L)$ is not *everywhere* attended by the continuous imperfection $v_i=g(x,L_i)$. For $0 \le x \le L_i/2$, equilibrium affords

$$M_x = EI(v_{,xx} - v_{i,xx}) = P(v_m - v) - \frac{qx^2}{2} + N \tag{5.39}$$

The boundary conditions appertaining to eqn (5.39) are

$$v|_0 = v_m \quad ; \quad v_{,x}|_0 = 0 \tag{5.40}$$

The general solution to eqn (5.39) takes the following form

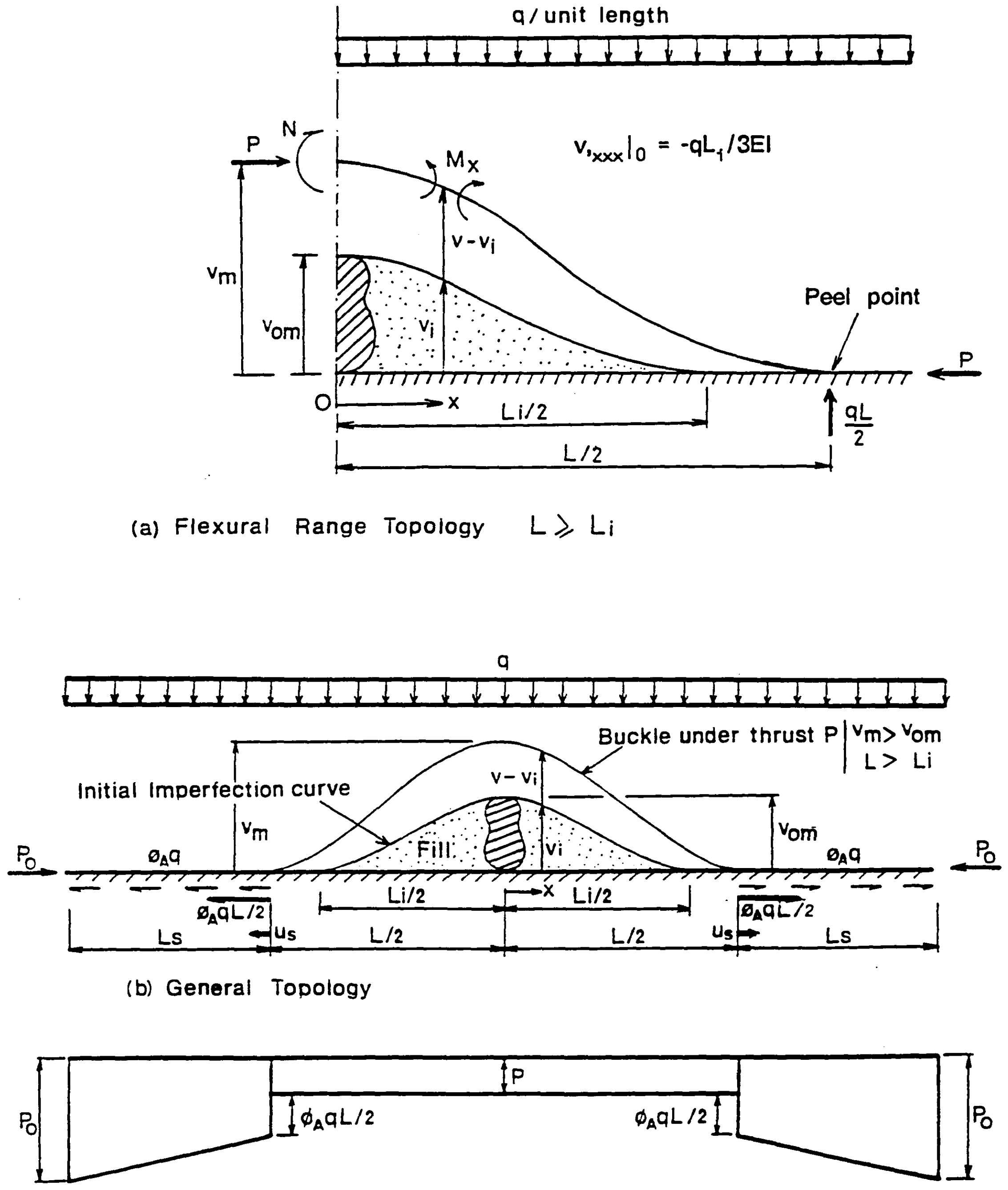

(a) Flexural Range Topology $L \geqslant L_i$

(b) General Topology

(c) Axial Force Distribution

Fig 5.4 Infilled Prop ; Developed Post Upheaval
Details of Imperfect Fully Mobilised Models $L > L_i$ (*Blister* Model)

$$v=B_5\cos nx+B_6\sin nx+k_{10}+\frac{qL_ix}{3EIn^2}-\frac{qx^2}{EIn^2} \tag{5.41}$$

where B_5 and B_6 are the constants of integration and k_{10} is determined by

$$k_{10}=v_m+\frac{1}{EIn^2}\left(N-\frac{qL_i^2}{24}+\frac{2q}{n^2}\right) \tag{5.42}$$

The boundary conditions of eqn (5.40) give

$$n^2EIB_5+N-\frac{qL_i^2}{24}+\frac{2q}{n^2}=0 \tag{5.43}$$

and

$$B_6=-\frac{q}{EIn^4}\frac{nL_i}{3} \tag{5.44}$$

In order to evaluate constant B_5 and consequently the characteristic equation of the buckle force, it is necessary to establish the matching conditions at $x=L_i/2$. First and second derivatives of eqn (5.41) give

$$v,_x|_{L_i/2}=-nB_5\sin\frac{nL_i}{2}+nB_6\cos\frac{nL_i}{2}-\frac{2qL_i}{3EIn^2} \tag{5.45}$$

and

$$v,_{xx}|_{L_i/2}=-n^2B_5\cos\frac{nL_i}{2}-n^2B_6\sin\frac{nL_i}{2}-\frac{2q}{EIn^2} \tag{5.46}$$

whilst for $L_i/2\le x\le L/2$, noting $v_i,_{xx}=0$ within this range, the moment-curvature relationship can be expressed as

$$M_x=EI(v,_{xx})=P(v_m-v)-\frac{qx^2}{2}+N \tag{5.47}$$

with the associated boundary conditions

$$v|_{\frac{L}{2}}=v,_x|_{\frac{L}{2}}=v,_{xx}|_{\frac{L}{2}}=0 \tag{5.48}$$

Similar to eqn (5.41), the general solution to eqn (5.47) takes the form

$$v=B_7\cos nx+B_8\sin nx+v_m+\frac{N}{EIn^2}+\frac{q}{EIn^4}-\frac{qx^2}{2EIn^2} \tag{5.49}$$

where B_7 and B_8 are the constants of integration. Employing boundary conditions $v,_x|_{L/2}=0$ and $v,_{xx}|_{L/2}=0$ then the relationships between B_7 and B_8 can be expressed as

$$-nB_7\sin\frac{nL}{2}+nB_8\cos\frac{nL}{2}-\frac{qL}{2EIn^2}=0 \tag{5.50}$$

and

$$-n^2B_7\cos\frac{nL}{2}-n^2B_8\sin\frac{nL}{2}-\frac{q}{EIn^2}=0 \tag{5.51}$$

Solutions to eqns (5.50) and (5.51) afford

$$B_7=\frac{q}{EIn^4}\left(-\frac{nL}{2}\sin\frac{nL}{2}-\cos\frac{nL}{2}\right) \tag{5.52}$$

and

$$B_8=\frac{q}{EIn^4}\left(\frac{nL}{2}\cos\frac{nL}{2}-\sin\frac{nL}{2}\right) \tag{5.53}$$

Recalling the matching conditions stated in eqns (5.45) and (5.46) then the evaluation of the first and second derivatives of eqn (5.49) at $x=L_i/2$ is essential. From eqns (5.52) and (5.53)

$$v,_x=\frac{q}{EIn^3}\left(-\sin\frac{n}{2}(L-L_i)+\frac{nL}{2}\cos\frac{n}{2}(L-L_i)-\frac{nL_i}{2}\right) \tag{5.54}$$

and

$$v,_{xx}=\frac{q}{EIn^2}\left(\cos\frac{n}{2}(L-L_i)+\frac{nL}{2}\sin\frac{n}{2}(L-L_i)-1\right) \tag{5.55}$$

Matching of eqns (5.45) and (5.54) allows constant B_5 to be written as

$$B_5=\frac{q}{EIn^4}\left(-\frac{nL}{2}\sin\frac{nL}{2}-\cos\frac{nL}{2}-\frac{nL_i}{6}\sin\frac{nL_i}{2}-\cos\frac{nL_i}{2}\right) \tag{5.56}$$

and, similarly, combination of eqns (5.46) and (5.55) affords the characteristic equation of the buckle force

$$\frac{nL}{2}\cos\frac{nL}{2}-\sin\frac{nL}{2}+\frac{nL_i}{6}\cos\frac{nL_i}{2}-\sin\frac{nL_i}{2}+\frac{nL_i}{3}=0 \tag{5.57}$$

Values for nL are obtained in terms of L_i/L and key values are given in Table 5.1. It can be seen from Table 5.1 that the characteristic equations (5.23) and (5.57) smoothly interface at $L=L_i$ and the idealised solution is also obtained, as would be expected, when $L>>L_i$.

Having determined all constants of integration then the equations of the deflected curve take the form

$$v=\frac{q}{EIn^4}\left(k_{11}\cos nx-\frac{nL_i}{3}\sin nx+k_{12}+\frac{n^2L_i}{3}x-n^2x^2\right) \tag{5.58}$$

for $0\leq x\leq L_i/2$, and

$$v=\frac{q}{EIn^4}\left(k_{13}\cos nx+k_{14}\sin nx+1+\frac{(nL)^2}{8}-\frac{n^2x^2}{2}\right) \tag{5.59}$$

for $L_i/2\leq x\leq L/2$
where

$$\begin{aligned}
k_{11}&= -\frac{nL}{2}\sin\frac{nL}{2}-\cos\frac{nL}{2}-\frac{nL_i}{6}\sin\frac{nL_i}{2}-\cos\frac{nL_i}{2}\\
k_{12}&= 2+\frac{(nL)^2}{8}-\frac{(nL_i)^2}{24}\\
k_{13}&= -\frac{nL}{2}\sin\frac{nL}{2}-\cos\frac{nL}{2}\\
k_{14}&= \frac{nL}{2}\cos\frac{nL}{2}-\sin\frac{nL}{2}
\end{aligned} \tag{5.60}$$

The maximum buckle amplitude v_m can be found by substituting x=0 into eqn (5.58)

$$v_m=\frac{q}{EIn^4}\left(2+k_{11}+\frac{(nL)^2}{8}-\frac{(nL_i)^2}{24}\right) \tag{5.61}$$

The bending moment N at the crown can by found by substituting eqn (5.56) into eqn (5.43) thus gives

$$N = \frac{q}{n^2}\left(\frac{nL}{2}\sin\frac{nL}{2}+\cos\frac{nL}{2}+\frac{nL_i}{6}\sin\frac{nL_i}{2}+\cos\frac{nL_i}{2}+\frac{(nL_i)^2}{24}-2\right) \tag{5.62}$$

and the maximum stress

$$\sigma_m=\frac{P}{A}+\frac{ND}{2I} \tag{5.63}$$

The longitudinal equilibrium and compatibility expressions, typified by eqns (5.33) and (5.34) and subject to the zero fully mobilised slip length consideration of Section 4.2 typified by eqn (5.38), still remain valid. The flexural end-shortening u_f of eqns (5.35) and (5.38) is, however, replaced by

$$u_f=\frac{1}{2}\left(\int_0^{L_i/2}(v,_x)^2dx+\int_{L_i/2}^{L/2}(v,_x)^2dx-\int_0^{L_i/2}(v_i,_x)^2dx\right) \tag{5.64}$$

where the third term represents the flexural end-shortening of the initial imperfection curve; a simple manipulation of eqn (5.7) gives

$$\int_0^{L_i/2}(v_i,_x)^2dx=\left(\frac{q}{EI}\right)^2\frac{L_i^7}{483840} \tag{5.65}$$

The first and second terms of eqn (5.64) require lengthy calculation based on eqns (5.58) and (5.59) to give

$$\begin{aligned}\int_0^{L_i/2}(v,_x)^2dx = \left(\frac{q}{EI}\right)^2\frac{1}{n^7}\Bigg(&\frac{k_{11}^2}{4}[nL_i-\sin nL_i]+\frac{(nL_i)^2}{36}[nL_i+\sin nL_i]\\&+\frac{(nL_i)^3}{18}-\frac{nL_ik_{11}}{6}[\cos nL_i-1]\\&+2k_{11}\left[-\frac{2nL_i}{3}\cos\frac{nL_i}{2}+2\sin\frac{nL_i}{2}-\frac{nL_i}{3}\right]\\&+\frac{2nL_i}{3}\left[\frac{2nL_i}{3}\sin\frac{nL_i}{2}+2\cos\frac{nL_i}{2}-2\right]\Bigg)\end{aligned} \tag{5.66}$$

and

$$\int_{L_i/2}^{L/2}(v,_x)^2dx=\left(\frac{q}{EI}\right)^2\frac{1}{n^7}\left(\frac{k_{13}^2}{4}[nL-nL_i-\sin nL+\sin nL_i]\right.$$
$$+\frac{k_{14}^2}{4}[nL-nL_i+\sin nL-\sin nL_i]$$
$$+\frac{(nL)^3}{24}[1-(L_i/L)^3]+\frac{k_{13}k_{14}}{2}[\cos nL-\cos nL_i]$$
$$+2k_{13}\left[-\frac{nL}{2}\cos\frac{nL}{2}+\sin\frac{nL}{2}+\frac{nL_i}{2}\cos\frac{nL_i}{2}-\sin\frac{nL_i}{2}\right]$$
$$\left.-2k_{14}\left[\frac{nL}{2}\sin\frac{nL}{2}+\cos\frac{nL}{2}-\frac{nL_i}{2}\sin\frac{nL_i}{2}-\cos\frac{nL_i}{2}\right]\right)$$
$$(5.67)$$

noting that k_{11}, k_{13} and k_{14} are as per eqn (5.60).

5.6 Standard Model Case Studies

Parametric studies of the fully mobilised standard *Blister* model, employing the data of Table 3.3, have been investigated and tabulations are given in Table 5.2 with graphical comparison illustrated by Fig 5.5 for various initial imperfection amplitudes v_{om}, ranging from 50mm to 300mm as employed in Chapter 4, such that L_i ranges from 26.618m to 41.66m. The upheaval states were assumed to occur when the buckle amplitude v_m=100.05% v_{om}, ie the smallest practical configuration of the buckle curves that could be obtained.

With regard to temperature rise T versus imperfection amplitude v_{om} data, it can be seen that only the relatively small imperfection cases, ie v_{om}=50mm up to 150mm, display a maximum temperature rise, T_{max}, together with the associated snap buckling phenomenon. The remaining three cases, typically from v_{om}=200mm to 300mm, generate stable post-buckling paths. The

v_{om} (mm)	L_i (m)		Upheaval State	Max Temp. State	After snap State	Min. Temp. State	First Yield State	Max slope 0.1rad
50	26.618	T	22.83	49.58	(49.58)	(32.95)	(33.25)	(34.14)
		v_m	50.02	88.1	3380.	916.3	698.1	1348.1
		L	5.597	20.597	58.727	41.618	38.618	46.00
		f	52.0	168.6	666.6	387.6	350.	447.9
100	31.655	T	16.30	36.48	(36.48)	(32.32)	(32.33)	(34.06)
		v_m	100.05	191.2	1630	759.6	751.4	1344.7
		L	6.777	25.277	47.943	38.655	38.533	45.45
		f	37.4	171.0	505.8	351.7	350.	450.6
150	35.032	T	13.49	31.48	(31.48)	(31.22)	(31.56)	(33.77)
		v_m	150.08	341.2	797.	578.	832.	1337.9
		L	7.734	29.734	38.533	35.032	39.032	44.80
		f	31.21	304.4	343.	287.6	350.	443.3
200	37.644	T	11.58	N/A	N/A	N/A	31.02	(33.38)
		v_m	200.1				909.	1332.0
		L	8.087				39.541	44.25
		f	26.93				350.	432.0
250	39.804	T	10.3	N/A	N/A	N/A	30.68	(32.92)
		v_m	250.11				989.4	1324.0
		L	8.379				40.117	43.75
		f	24.06				350.	418.9
300	41.660	T	9.36	N/A	N/A	N/A	30.48	(32.33)
		v_m	300.12				1066.6	1315.5
		L	8.63				40.911	42.30
		f	21.97				350	402.0

Notes :
* N/A - denotes 'stable' buckling path
* T - Temperature rise (^oC)
* v_m - Buckle amplitude (mm)
* L - Buckle length (m)
* f - Maximum stress (N/mm^2)

Table 5.2 Fully Mobilised Standard Infilled Prop (*Blister*) Model Parametric Studies

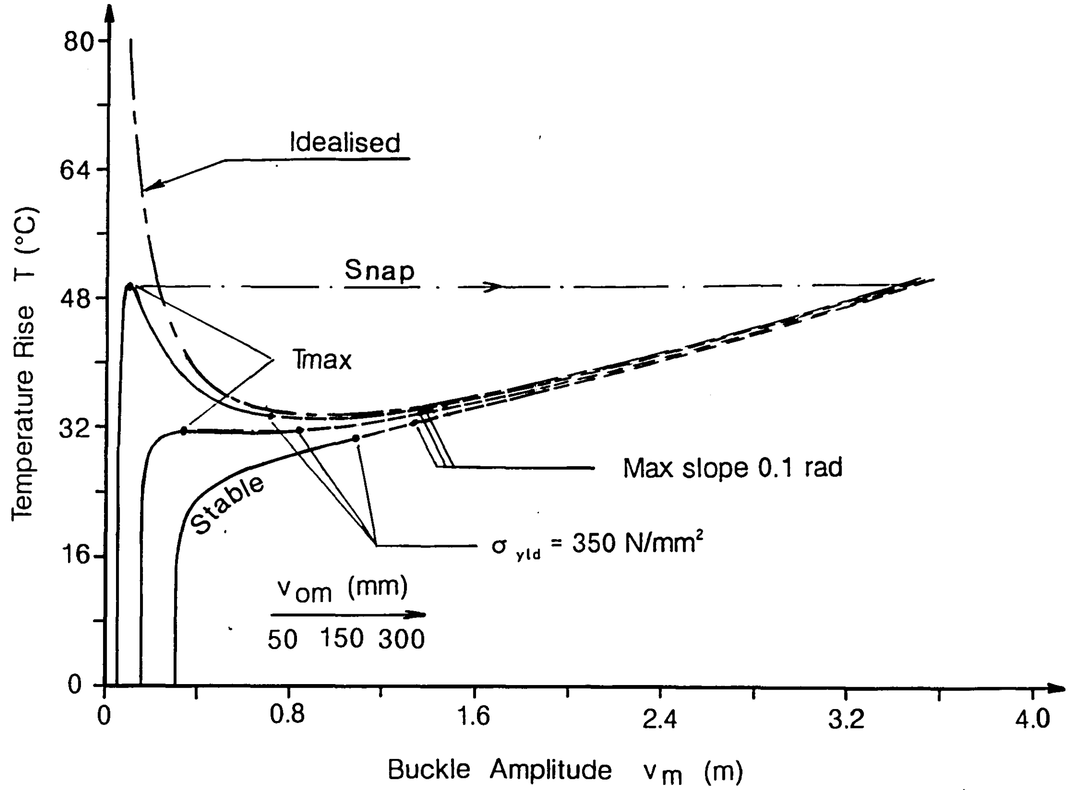

a) Thermal Action Characteristics - T vs v_m

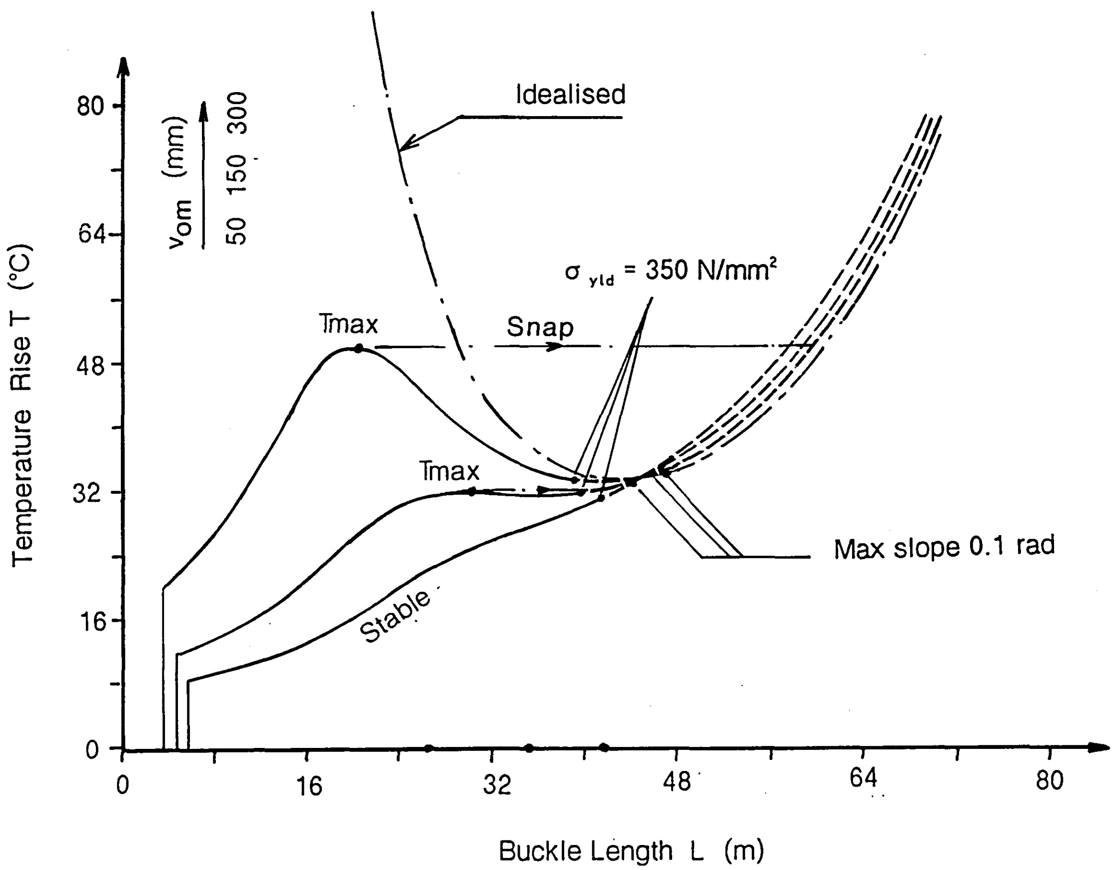

b) Thermal Action Characteristics - T vs L

Fig 5.5 Thermal Action Characteristics
Fully Mobilised Standard Infilled Prop Model *(Blister)*

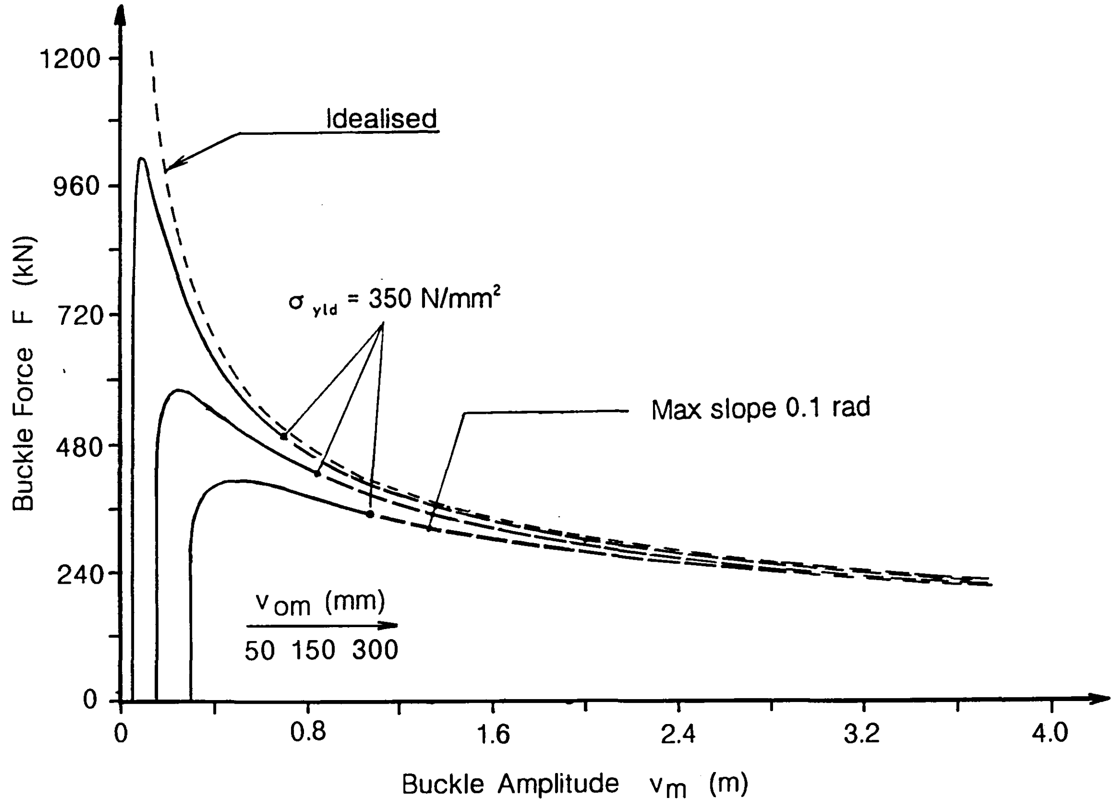

c) Buckle Force Characteristics - P vs v_m

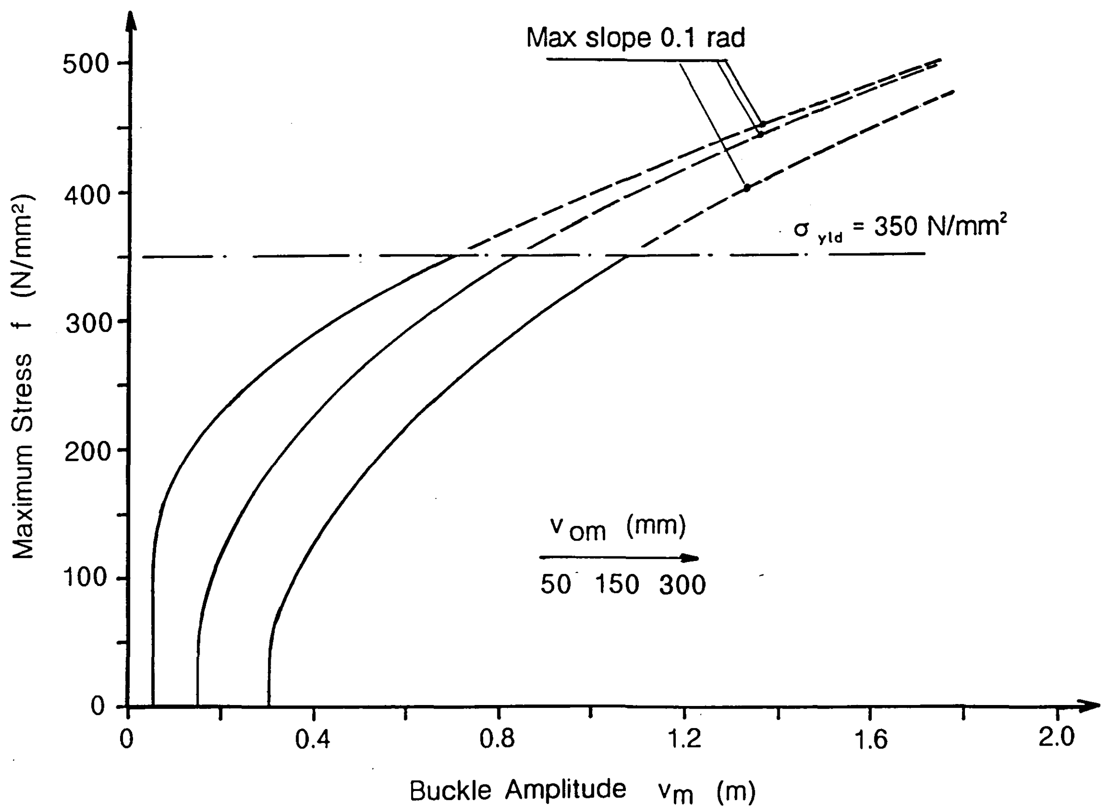

d) Maximum Stress Characteristics - f vs v_m

Fig 5.5 (continued)

onset of slopes in excess of 0.1 radian or yielding limit, whichever comes first, is shown by dashed loci in Fig 5.5; here, the yielding limit is more restrictive. Operating temperatures should be restricted to either T_u or T_{max} for the snap cases and to either T_u or $T|_{\sigma yld}$ for the stable cases.

The analysis results displayed in Table 5.2 confirm that the *Blister* model generates an upheaval state which occurs at lower temperature than that of its respective *Empathetic* equivalent as indicated by eqns (5.31) and (5.32). A closed-form relationship for stable/snap differention of the form given in Section 4.5 is not available given the greater numerical complexity involved in the *Blister* model and each case-study requires numerical analysis. Furthermore, Table 5.2 clearly demonstrates that the upheaval and maximum temperature rise states diverge as imperfect amplitude decreases regarding the snap cases. The implication is that the *Blister* model does not produce a cusp response.

The general characteristics of the respective buckling force/buckling amplitude obey convergence to their idealised equivalent unlike their thermal counterparts with suffer breaches of their idealised equivalent, albeit beyond the geometric and stress limitations; such breaches are further discussed later.

Table 5.2 also suggests that for both stable and snap configuration, $T|_{\sigma yld}$ and $T|_{0.1^r}$ reduce when v_{om} increases. Furthermore, unlike the *Empathetic* model where v_m and L are unique upon the onset of maximum slope ($=0.1^r$) for any particular pipe configuration (D,E,t etc), irrespective of the magnitude of imperfection, the *Blister* model produces a reduction in v_m and L at this state as v_{om} increases. This variation is due to the fact that whilst the characteristic equation of the *Empathetic* model typified by eqn (1.5) generates a unique solution for nL, eqn (5.57) of the *Blister* equivalent provides $nL=f(v_{om})$. On the basis of imperfection amplitude v_{om}, *Empathetic* models more readily generate stable behaviour.

5.7 Updated Physical Considerations

Further developments are now considered in terms of the pipeline being trenched, buried (continuously or otherwise) or subject to the use of fixing anchors.

5.7.1 Trenching

Similar to the discussion in Section 4.7.1, the basic trench section of Fig 4.3 and eqn (4.22) are still valid for this developed *Blister* model. More thoroughly, m could again replace q throughout all related equations for the basic trenching model configuration; vertical buckling would predominate as previously.

A more thorough refined trenching model analysis requires the use of q in the slip length modelling as previously discussed in Section 4.7.1. To this end, modelling the frictional slip length resistance employing by eqns (4.24) - (4.30) is still valid, except that u_f of eqn (4.26) is to be replaced by eqn (5.34) for $L<L_i$ or eqn (5.64) for $L>L_i$ respectively. Table 5.3 displays appropriate characteristics of the analysis for two different imperfections v_{om}=100 and 250mm with trench angles of 20^o and 30^o and a comparative standard case-study (ie trenched vertical buckling in the absence of burial and anchoring). With respect to upheaval temperatures, the refined model generates an average theoretical

v_{om} (mm)	L_i (m)	Trench angle θ (degrees)		Upheaval State	Max. Temp. State	After snap State	Min. Temp. State	First Yield State	Max slope 0.1rad
100	31.655	Standard model	T	16.30	36.48	(36.48)	(32.32)	(32.33)	(34.06)
			v_m	100.05	191.2	1630	759.6	751.4	1344.7
			L	6.777	25.277	47.943	38.655	38.533	45.45
			f	37.4	171.0	505.8	351.7	350.	450.6
	31.295	20	T	16.71	37.32	(37.32)	(32.91)	(32.96)	(34.49)
			v_m	100.05	176.5	1811.3	765.0	713.8	1325.1
			L	6.729	24.229	48.767	38.295	37.528	44.75
			f	38.33	164.9	524.	361.	350.	458.1
	30.571	30	T	17.56	39.05	(39.05)	(34.15)	(34.3)	(35.38)
			v_m	100.05	185.4	1914.8	776.6	643.1	1280.6
			L	6.631	24.131	48.361	37.571	35.571	43.30
			f	40.32	179.3	562.4	380.8	350.	473.0
250	39.804	Standard model	T	10.3	N/A	N/A	N/A	30.68	(32.92)
			v_m	250.1				989.4	1324.0
			L	8.379				40.117	43.75
			f	24.06				350.	418.9
	39.351	20	T	10.55	N/A	N/A	N/A	30.98	(33.24)
			v_m	250.12				954.6	1303.1
			L	8.318				39.244	43.05
			f	24.67				350.	423.7
	38.441	30	T	11.10	N/A	N/A	N/A	31.68	(34.01)
			v_m	250.12				889.8	1261.2
			L	8.195				37.530	41.65
			f	25.96				350.	435.6

Notes :
* N/A - denotes 'stable' buckling path
* T - Temperature rise (°C)
* v_m - Buckle amplitude (mm)
* L - Buckle length (m)
* f - Maximum stress (N/mm^2)

Table 5.3 Fully Mobilised Infilled Prop (*Blister*) Model with Refined Trenching Parametric Studies.

improvements in resistance of 2.4% and 7.7% for $\theta=20^o$ and 30^o respectively, ie of similar order to the *Empathetic* equivalents.

Finally, recalling the discussion of the rigorous trenching model in Section 4.7.1 and given the imperfection of the *Blister* model is generated from physical considerations, then the imperfection formulation should also employ q. This rigorous analysis involves lengthy mathematical procedure. Herein reported is brief consideration of the two distinct stages of the post-upheaval state, noting that the transverse deflection v typified in Fig 4.3 is still valid for this case and the imperfection denoted by eqn (5.7) is also employed here.

For the post-upheaval stage with $L<L_i$, the moment-curvature relationship of eqn (5.13) is replaced by, for $0\le x\le L/2$,

$$M_x=EI(v,_{xx}-v_i,_{xx})=P(v_m-v)-\frac{mx^2}{2}+N \tag{5.68}$$

where $v_i,_{xx}$ is given by eqn (5.10). With the employment of the boundary conditions of eqn (5.16), the solution of eqn (5.68) yields the characteristic equation of the buckling force as

$$k_{15}\sin\frac{nL}{2}-k_{16}\cos\frac{nL}{2}+\frac{nL_i}{3}=0 \tag{5.69}$$

where

$$\begin{aligned} k_{15} &= -1-\frac{m}{q}+\frac{(nL)^2}{24}\left(\frac{L_i}{L}-1\right)\left(\frac{L_i}{L}-3\right) \\ k_{16} &= \frac{nL}{3}\left(\frac{L_i}{L}-3\frac{(q+m)}{2q}\right)+\frac{(nL)^3}{48}\left(\frac{L_i}{L}-1\right)^2 \end{aligned} \tag{5.70}$$

The vertical deflection v of the buckle curve can be expressed as

$$v = v_p + \frac{q}{EIn^4}\left(k_{15}\cos n\left(\frac{L}{2}-x\right) + k_{16}\sin n\left(\frac{L}{2}-x\right) - k_{15} - \frac{(nL)^2}{12}\left[2\frac{L_i}{L} - 3\frac{(q+m)}{2q}\right] + \frac{n^2 L_i}{3}x - n^2 x^2 \frac{(q+m)}{2q}\right) \tag{5.71}$$

where v_p is given by eqn (5.27). The bending moment N at the crown, x=0, takes the form

$$N = \frac{q}{n^2}\left(-k_{15}\cos\frac{nL}{2} - k_{16}\sin\frac{nL}{2} + \frac{(nL_i)^2}{24} - 2\right) \tag{5.72}$$

The expressions for longitudinal equilibrium and compatibility are as per eqns (5.33) and (5.34) respectively, noting that the end reaction $\phi_A qL/2$ of eqn (5.33) is to be replaced by $\phi_A mL/2$, whilst the flexural end-shortening u_f of eqn (5.34) takes a similar form to that of eqns (5.35), (5.36) and (5.37), apart from the fact that coefficients k_8, k_9 of eqn (5.36) are to be replaced by the corresponding k_{15} and k_{16} of eqn (5.70) respectively.

For the post-upheaval stage with $L>L_i$ and for $0 \le x \le L_i/2$, the moment-curvature relationship typified by eqn (5.68) again applies, whilst for $L_i/2 \le x \le L/2$, equilibrium affords

$$M_x = EI(v_{,xx} - v_{i,xx}) = P(v_m - v) - \frac{mx^2}{2} + N \tag{5.73}$$

Again, by employing the boundary conditions of eqn (5.16) in conjunction with matching conditions at $x=L_i/2$ upon the slope and curvature of the buckle curve, then the characteristic equation of the buckle force can be expressed as

$$\frac{m}{q}\left[\frac{nL}{2}\cos\frac{nL}{2} - \sin\frac{nL}{2}\right] + \frac{nL_i}{6}\cos\frac{nL_i}{2} - \sin\frac{nL_i}{2} + \frac{nL_i}{3} = 0 \tag{5.74}$$

It can be seen that eqn (5.74) will regain exactly the same formulation of eqn (5.57) of the standard *Blister* case-study when putting m=q. Typical buckle force solutions for the trench angles of 20^0 and 30^0 are tabulated in Table 5.4. The data of Table 5.4 also confirm that the resistance to buckling increases when the trench slope becomes steeper as would be expected [nb; employing m as in eqn (4.23)]. Convergence to the idealised value is also obtained as $L>>L_i$.

Further manipulation of eqns (5.68), (5.73) and (5.10) yields the equations of the deflected curve as, for $0 \le x \le L_i/2$

$$v=\frac{q}{EIn^4}\left(k_{17}\cos nx-\frac{nL_i}{3}\sin nx+k_{18}+\frac{n^2L_i}{3}x-\frac{(q+m)}{2q}n^2x^2\right) \tag{5.75}$$

and, for $L_i/2 \le x \le L/2$

$$v=\frac{m}{EIn^4}\left(k_{13}\cos nx+k_{14}\sin nx+1+\frac{(nL)^2}{8}-\frac{n^2x^2}{2}\right) \tag{5.76}$$

noting that k_{13} and k_{14} are obtained from eqn (5.60) whilst k_{17} and k_{18} are given by

$$\begin{aligned} k_{17} &= \frac{m}{q}\left[-\frac{nL}{2}\sin\frac{nL}{2}-\cos\frac{nL}{2}\right]-\frac{nL_i}{6}\sin\frac{nL_i}{2}-\cos\frac{nL_i}{2} \\ k_{18} &= 1+\frac{m}{q}\left[1+\frac{(nL)^2}{8}\right]-\frac{(nL_i)^2}{24} \end{aligned} \tag{5.77}$$

The bending moment N at the crown (x=0) is given by

$$N=\frac{q}{n^2}\left(-k_{17}+\frac{(nL_i)^2}{24}-1-\frac{m}{q}\right) \tag{5.78}$$

The longitudinal equilibrium and compatibility expressions, typified by eqns (5.33) and (5.34), still remain valid. The total flexural end shortening u_f and the flexural end shortening of the initial imperfection curve, typified by eqns (5.64) and (5.65) respectively, can also be used with the exception that eqn (5.66) is to be replaced by

	L_i/L	nL		Remarks
		Trench angle $\theta = 20^\circ$	Trench angle $\theta = 30^\circ$	
Post-Upheaval $L<L_i$	4.798396		1.294785	Upheaval limit at v_m=100.05% v_{om}
	4.712016	1.262483	1.322869	
	4.0	1.537079	1.610481	
	2.0	3.846079	4.017273	
	1.8	4.462621	4.650479	
	1.6	5.236316	5.432359	
	1.4	6.135818	6.316142	
	1.2	7.021139	7.157595	
	1.0	7.758224	7.846226	$L=L_i$
Post-Upheaval $L>L_i$	1.0	7.758224	7.846226	$L=L_i$
	0.9	8.073327	8.140455	
	0.8	8.352258	8.400658	
	0.6	8.763677	8.782250	
	0.5	8.882601	8.891583	
	0.4	8.948561	8.951931	
	0.2	8.985455	8.985577	
	0.1	8.986775	8.986779	
	.	.	.	
	.	.	.	
	0.01	8.9868	8.9868	$P \rightarrow 80.76\ EI/L^2$

Table 5.4 Typical Buckle Force Solution for *Blister* Model with Rigorous Trenching.

$$\int_0^{L_i/2} v,_x^2 dx = \left(\frac{q}{EI}\right)^2 \frac{1}{n^7}\left(\frac{k_{19}^2}{4}[nL_i - \sin nL_i] + \frac{(nL_i)^2}{36}[nL_i + \sin nL_i]\right.$$
$$+\frac{(nL_i)^3}{162}\cdot\frac{2q}{(m+q)}\left[1+\frac{1}{8}(1+\frac{3m}{q})^3\right] - \frac{nL_i k_{19}}{6}[\cos nL_i - 1]$$
$$+2k_{19}\left[\frac{-nL_i(1+3m/q)}{6}\cos\frac{nL_i}{2} + \frac{q+m}{q}\sin\frac{nL_i}{2} - \frac{nL_i}{3}\right]$$
$$\left. + \frac{2nL_i}{3}\left[\frac{nL_i(1+3m/q)}{6}\sin\frac{nL_i}{2} + \frac{q+m}{q}\cos\frac{nL_i}{2} - \frac{q+m}{q}\right]\right) \tag{5.79}$$

and the effective submerged self-weight q of eqn (5.67) is also to be replaced by the inertial force m.

Table 5.5 and Fig 5.6 display appropriate characteristics for two different imperfections v_{om}=100 and 250mm with trench angles of 20^o and 30^o and a comparative standard case-study (together with a corresponding *Empathetic* data run for reference), employing the pipe data of Table 3.3. In terms of upheaval temperatures, this rigorous model generates an average improvement of 4.5% and 13.8% for $\theta=20^o$ and 30^o respectively. However, recalling the discussion upon the data of Table 5.4, it can be seen that the refined trenching model associated with Table 5.4 offers a more conservative solution in terms of operating temperatures for both stable and snap cases. Vertical mode buckling would remain predominant, however.

5.7.2 Burial (Continuous)

Recalling the enhanced *Empathetic* model as discussed in Section 4.7.2, the present model has also been investigated for the same three different cover

v_{om} (mm)	L_i (m)	Trench angle θ (degrees)		Upheaval State	Max. Temp. State	After snap State	Min. Temp. State	First Yield State	Max slope 0.1rad
100	31.655	Standard model	T	16.30	36.48	(36.48)	(32.32)	(32.33)	(34.06)
			v_m	100.05	191.2	1630.	759.6	751.4	1344.7
			L	6.777	25.277	47.943	38.655	38.533	45.45
			f	37.4	171.0	505.8	351.7	350.	450.6
	31.654	20	T	17.00	37.43	(37.43)	(32.89)	(32.92)	(35.38)
			v_m	100.05	181.8	1828.7	788.8	720.2	1495.6
			L	6.722	24.522	48.902	38.655	37.655	46.277
			f	39.00	167.74	525.5	364.9	350.	481.7
	31.654	30	T	18.46	39.44	(39.44)	(34.10)	(34.3)	(36.83)
			v_m	100.05	170.7	1971.2	777.9	656.4	1562.8
			L	6.522	23.522	48.768	37.655	35.858	45.777
			f	42.27	167.9	567.6	377.9	350.	512.9
250	39.804	Standard model	T	10.30	N/A	N/A	N/A	30.68	(32.92)
			v_m	250.1				989.4	1324.0
			L	8.379				40.117	43.75
			f	24.06				350.	418.9
	39.804	20	T	10.79	N/A	N/A	N/A	31.01	(34.17)
			v_m	250.12				961.5	1441.5
			L	8.400				39.381	44.379
			f	25.23				350.	446.9
	39.804	30	T	11.78	N/A	N/A	N/A	31.74	(35.53)
			v_m	250.12				907.7	1493.0
			L	8.257				37.940	43.879
			f	27.48				350.	474.3

Notes :
* N/A - denotes 'stable' buckling path
* T - Temperature rise (°C)
* v_m - Buckle amplitude (mm)
* L - Buckle length (m)
* f - Maximum stress (N/mm^2)

Table 5.5 Fully Mobilised Infilled Prop (*Blister*) Model with Rigorous Trenching Parametric Studies.

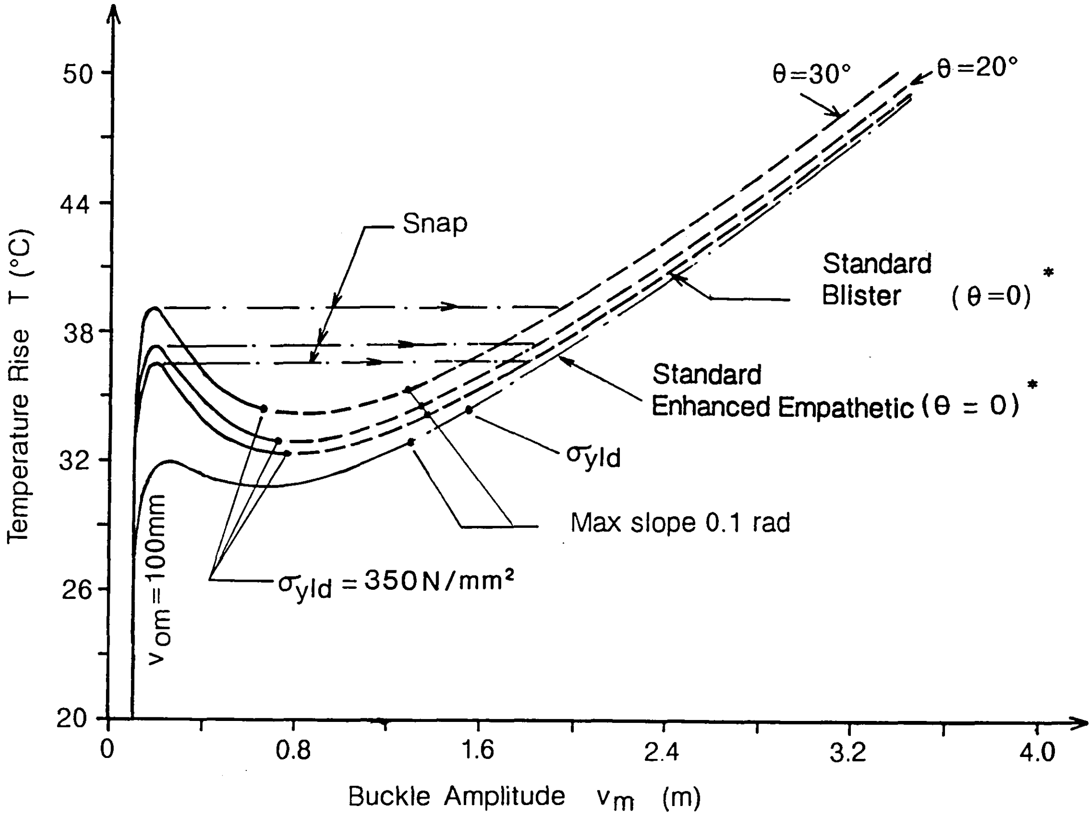

Fig 5.6 Thermal Action Characteristics
Fully Mobilised Infilled Prop (*Blister*) Model with Rigorous Trenching

* nb : Scale prevents explicit illustration
that $T_u|_{\text{Standard Enhanced Emp., }\theta=0} > T_u|_{\text{Standard Blister, }\theta=0}$

depths h=0 (sea bed mounted), 1.5D and 3D, employing pipe data of Table 3.3 and Fig 3.11. The effect of continuous burial upon imperfect pipeline behaviour is shown in Table 5.6 for imperfection amplitude v_{om}=100mm with regard to burial type (a) of Fig 3.1 with q replaced by q+q' throughout the analysis, noting that the fully mobilised axial friction coefficient ϕ_A (ϕ'_A) will vary with depth accordingly. The primary feature of burial is the enhancement of upheaval resistance (T_u) from 16.3°C (h=0) to 32.55°C and 47.48°C, or a percentage improvement of 99.7% and 191.3%, for h=1.5D and 3D respectively. However, Table 5.6 also indicates that the operating temperatures are restricted to either T_u or T_{max} for the seabed mounted (h=0) and cover depth h=1.5D cases, whilst such temperatures are restricted to either T_u or $T|_{\sigma yld}$ for the h=3D case. It can be concluded that any attempts to raise T_{max} by a further increase in cover depth beyond a certain value, typically h=3D for this particular pipe, would not generate a significant improvement upon operating temperatures as material yielding limit begins to take precedence over T_{max} (or even T_u).

5.7.3 Discrete Dumping or Intermittent Burial

Again recalling the equivalent *Empathetic* model studies, Figure 5.7 displays the key characteristics relating to the present model now involving the longitudinal equilibrium expression

$$P_o-P=\phi_A\frac{qL}{2}+\phi_A q\left(L_{s1}+L_{s2}\left[1+\frac{q'}{q}\right]\frac{\phi'_A}{\phi_A}\right) \tag{5.80}$$

and the compatibility expression

$$\frac{(P_o-P)L}{2AE}-u_f+\frac{\phi_A q}{2AE}\left(L_{s1}^2+(L_{s2}^2+2L_{s1}L_{s2})\left[1+\frac{q'}{q}\right]\frac{\phi'_A}{\phi_A}\right)=0 \tag{5.81}$$

where u_f is given by eqn (5.35) for $L\leq L_i$ or eqn (5.62) for $L>L_i$.

v_{om} (mm)	L_i (m)	q+q' (N/mm) [ϕ'_A]		Upheaval State	Max. Temp. State	After snap State	Min. Temp. State	First Yield State	Max slope 0.1rad
100	31.655	1.144 [0.53]	T v_m L f	16.30 100.05 6.777 37.4	36.48 191.2 25.277 171.0	(36.48) 1630 47.943 505.8	(32.32) 759.6 38.655 351.7	(32.33) 751.4 38.533 350.	(34.06) 1344.7 45.45 450.6
	22.619	4.388 [0.58]	T v_m L f	32.55 100.05 5.057 74.6	72.63 191 18.057 334.7	(72.63) 1221.8 31.619 846.7	(67.75) 586.5 25.620 613.4	(72.49) 204.5 18.485 350.	(78.67) 1598 34.056 950
	18.588	9.622 [0.68]	T v_m L f	47.48 100.05 3.940 108.2	(109.27) 216.4 15.512 538.8	(109.27) 825. 23.233 1057.	(105.8) 543.6 20.588 877.1	102.4 130.9 12.359 350.	(116.6) 1145 25.512 1152.3

Notes : * T - Temperature rise (^oC)
* v_m - Buckle amplitude (mm)
* L - Buckle length (m)
* f - Maximum stress (N/mm^2)

Table 5.6 Fully Mobilised Infilled Prop (*Blister*) Model with Continuous Burial Parametric Studies.

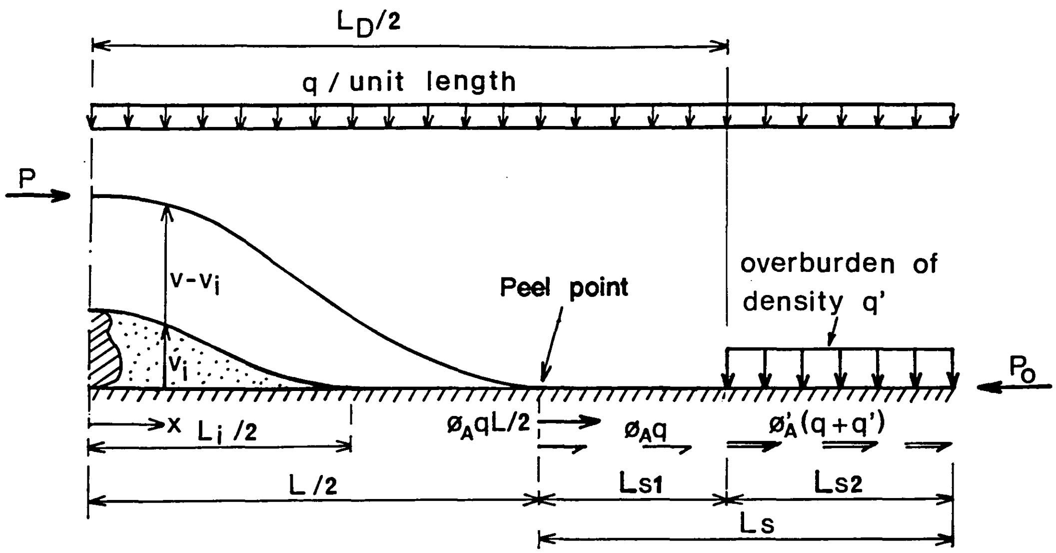

a) Topology

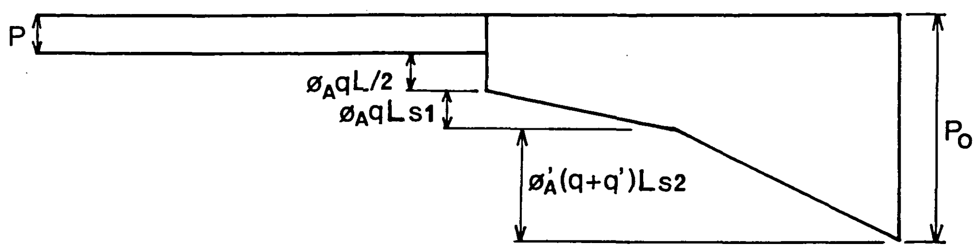

b) Axial Force Distribution

Fig 5.7 Infilled Prop (*Blister*) with Discrete Dumping ($L > L_i$ shown)

Table 5.7 and Fig 5.8 display the characteristics of the foregoing developed model for imperfection v_{om}=100mm, employing the pipe data of Table 3.3. Two different cases have been investigated, the first involving L_D values of 100, 500 and 1000m with overburden q'=8.478N/mm being kept constant; the second relates to the situation where L_D=100m is kept constant throughout whilst q' varies from 1.823 to 3.68N/mm accordingly.

With regard to the first case, Figure 5.8(a) shows that post-buckling characteristics are stiffened as L_D decreases. For L_D=100m, the post buckling response has been so significantly improved that stable behaviour replaces the former snap response. Furthermore, the data in Table 5.7 confirms that the upheaval temperature remains unaffected despite of a significant reduction in L_D from 1000m to 100m as no axial movement occurs prior to upheaval and there is no overburden effect accordingly. This is typical of contact undulation behaviour. Detailed investigation of slip length output confirms this with $L_u=6.777\text{m} \leq L^*=11.777\text{m}$.

Similar to the first case, the variation in overburden from 1.823 to 3.68 N/mm also provides an overall improvement upon the post-buckling or rather post-upheaval behaviour of the respective temperature rise/buckle amplitude curves. The data in Table 5.7 together with further support from Fig 5.8(b) clearly indicate that the enhanced slip length frictional resistance begins to show its effect when $L_u < L < L|_{T_{max}}$, noting a slight improvement in T_{max} whilst T_u remains unaltered as q' increases. (Two corresponding *Empathetic* case-studies showed 'improvement' to fully stable post-upheaval paths.). Finally, in terms of the operating temperatures, T_u or T_{max} are still considered to be the restricting temperatures for these particular cases. The *Empathetic* standard

v_{om} (mm)	L_i (m)	L_D (m) q'(N/mm) [ϕ'_A]		Upheaval State	Max. Temp. State	After snap State	Min. Temp. State	First Yield State	Max slope 0.1rad
			T	16.30				44.76	(60.69)
		100	v_m	100.05	N/A	N/A	N/A	751.4	1344.7
		q'=8.478	L	6.777				38.53	45.45
		[0.68]	f	37.40				350.	450.6
			T	16.30	36.48	(36.48)	(32.64)	(32.87)	(40.98)
100	31.655	500	v_m	100.05	191.2	1156.	632.6	751.4	1344.7
		q'=8.478	L	6.777	25.278	43.567	36.655	38.53	45.45
		[0.68]	f	37.40	171.0	422.1	324.1	350.	450.6
			T	16.30	36.48	(36.48)	(32.32)	(32.83)	(35.14)
		1000	v_m	100.05	191.2	1618.5	759.6	751.4	1344.7
		q'=8.478	L	6.777	25.278	47.834	36.655	38.53	45.45
		[0.68]	f	37.40	171.0	488.	351.7	350.	450.6
			T	16.30	36.48	(36.48)	(32.32)	(32.33)	(34.06)
		standard	v_m	100.05	191.2	1630.	759.6	751.4	1344.7
		model	L	6.777	25.278	47.943	38.655	38.53	45.45
		q'=0	f	37.40	171.0	505.8	351.7	350.	450.6
			T	16.30	36.69	(36.69)	(35.57)	(36.73)	(42.68)
100	31.655	100	v_m	100.05	201.7	744.2	473.3	751.4	1344.7
		q'=1.823	L	6.777	25.778	38.412	33.654	38.53	45.45
		[0.55]	f	37.40	177.4	348.5	283.4	350.	450.6
			T	16.30	36.81	(36.81)	(36.60)	(39.86)	(49.26)
		100	v_m	100.05	201.7	427.6	350.8	751.4	1344.7
		q'=3.680	L	6.777	25.778	32.654	30.778	38.53	45.45
		[0.60]	f	37.40	177.4	269.8	244.4	350.	450.6

Notes :
* N/A - denotes 'stable' buckling path
* T - Temperature Rise in (°C)
* v_m - Buckle Amplitude in (mm)
* L - Buckle Length in (m)
* f - Maximum Stress in (N/mm²)

Table 5.7 Fully Mobilised Infilled Prop (*Blister*) Model with Discrete Dumping Parametric Studies.

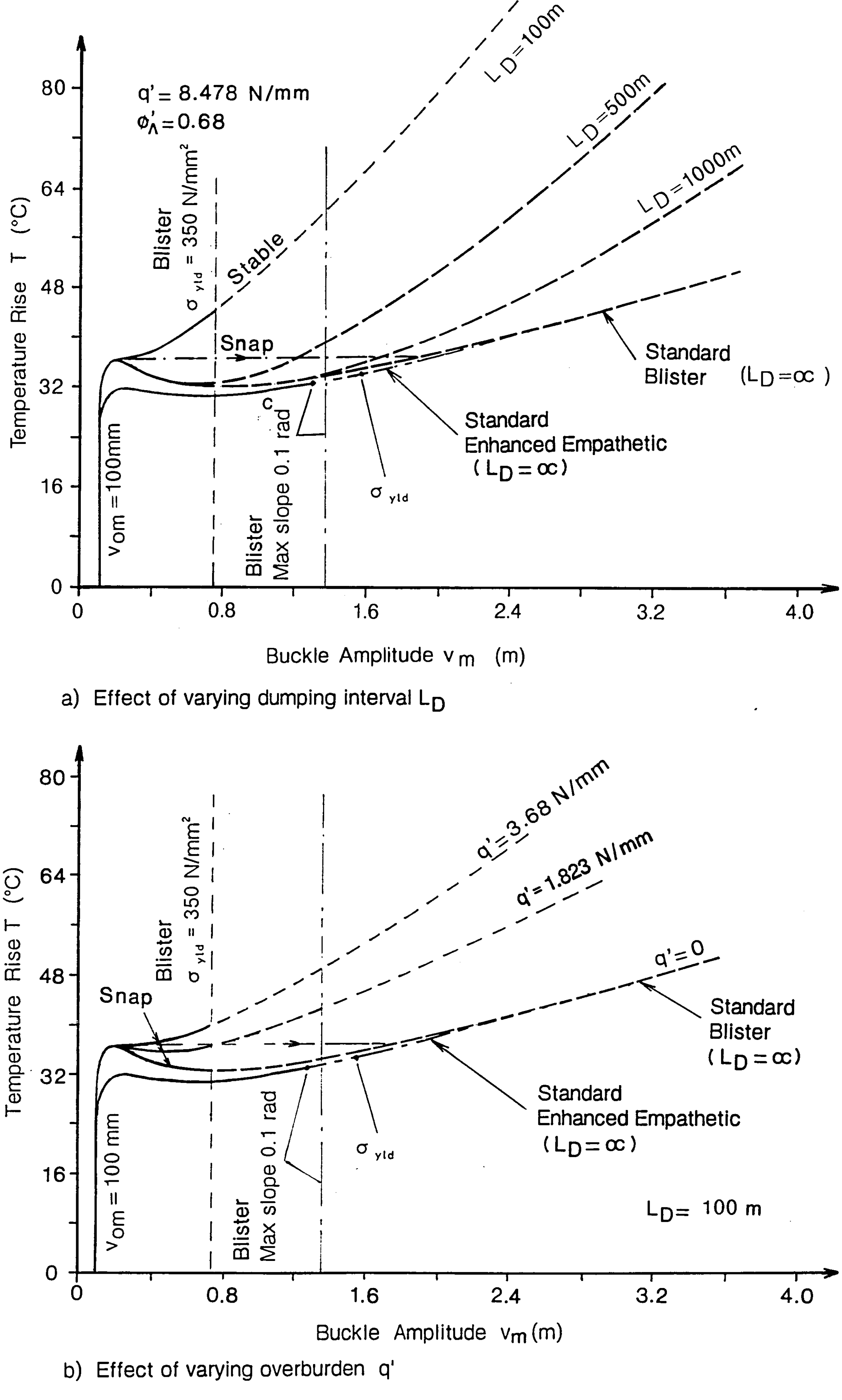

a) Effect of varying dumping interval L_D

b) Effect of varying overburden q'

Fig 5.8 Thermal Action Characteristics
Fully Mobilised Infilled Prop (*Blister*) Model with Discrete Dumping

enhanced model case-studies illustrated in Fig 5.8 are included for comparative purposes.

5.7.4 Fixed Anchor Points

The use of fixed anchor points leads to the following modification of the equilibrium and compatibility expressions; noting Fig 5.9 for the key characteristics, then

$$P_o - P = \phi_A \frac{qL}{2} + \phi_A q \frac{L_{fap} - L}{2} + F_{ap} \tag{5.82}$$

and

$$\frac{(P_o - P)L}{2AE} - u_f + \left(F_{ap} + \frac{1}{2}\phi_A q \frac{L_{fap} - L}{2} \right) \frac{L_{fap} - L}{2AE} = 0 \tag{5.83}$$

respectively

Table 5.8 and Fig 5.10 present results of a set of *Blister* model analyses involving fixed anchor points employing the pipe data of Table 3.3. The results are tabulated for two different values of imperfection v_{om}=100 and 250mm with anchor spacing L_{fap} ranging from 100 to 1000m as per Section 4.7.4.

Figure 5.10 indicates that the developed model similarly generates an overall stiffening improvement with respect to the rising branches of the temperature rise/buckle amplitude curves, the improvement becoming increasingly significant as L_{fap} reduces as is to be expected. However, the data in Table 5.8 show that, in all cases, the temperature rise T_u is again unaffected by anchor provision (ref Table 5.2). Recalling the discussion in Section 5.7.3 with regard to the zero slip length consideration affecting further improvement in T_u, it is

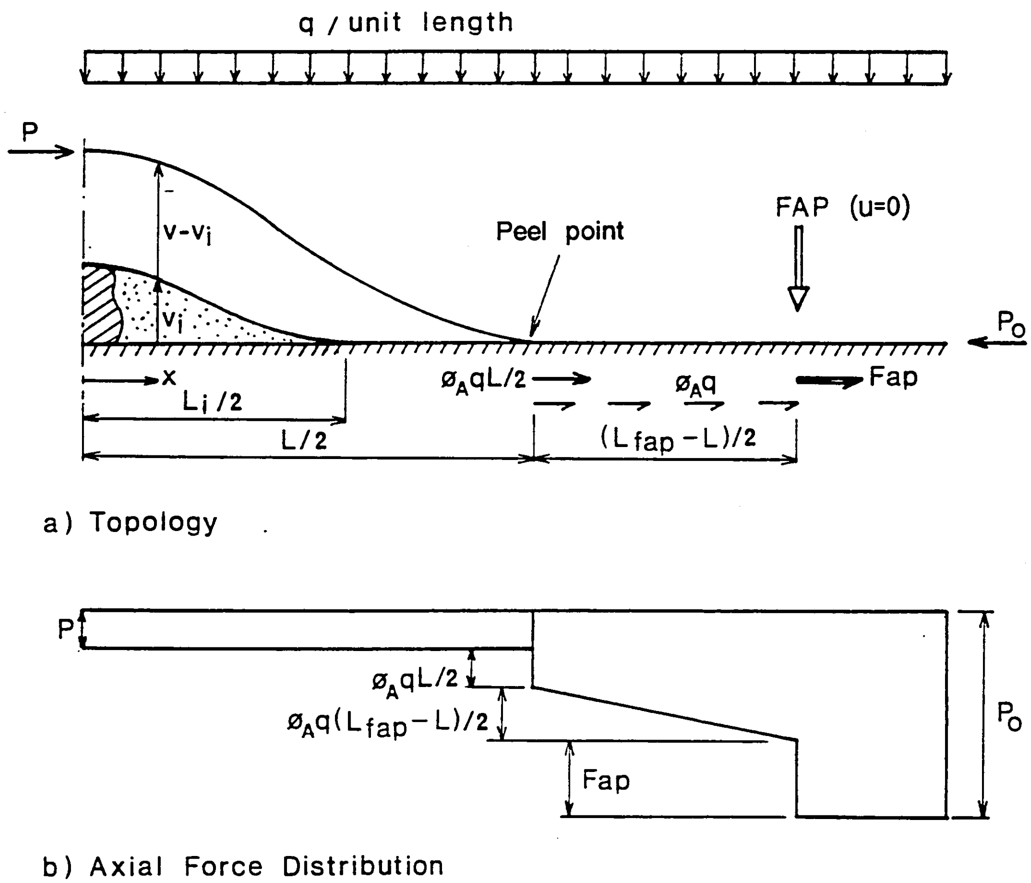

Fig 5.9 Blister Model with Fixed Anchor Points (L_s=(L_{fap}-L)/2 shown)

v_{om} (mm)	L_i (m)	L_{fap} (m)		Upheaval State	Max. Temp. State	After Snap. State	Min. Temp. State	First Yield State	Max slope 0.1rad	Max. F_{ap} at 750 kN
100	31.655	100	T	16.30	N/A	N/A	N/A	59.18	(117.5)	(59.43)
			v_m	100.05				751.4	1344.7	754.9
			L	6.777				38.530	45.45	38.585
			f	37.40				350.	450.6	350.7
		500	T	16.30	36.48	(36.48)	(32.66)	(32.96)	(40.61)	(57.09)
			v_m	100.05	191.2	1072.2	632.6	751.4	1344.7	1995.
			L	6.777	25.277	42.655	36.655	38.530	45.45	50.655
			f	37.40	171.0	408.7	324.2	350	450.6	534.2
		1000	T	16.30	36.48	(36.48)	(32.32)	(32.33)	(34.28)	(61.89)
			v_m	100.05	191.26	1596.	759.6	751.4	1344.7	3152.
			L	6.777	25.277	47.655	38.655	38.530	45.45	57.235
			f	37.40	171.0	485.7	351.7	350.	450.6	652.8
250	39.804	100	T	10.30	N/A	N/A	N/A	(75.63)	(114.4)	56.57
			v_m	250.11				989.3	1324.0	789.3
			L	8.379				40.116	43.75	37.481
			f	24.06				350.	418.9	300.5
		500	T	10.30	N/A	N/A	N/A	32.86	(44.53)	(56.91)
			v_m	250.11				989.3	1324.0	1976.
			L	8.379				40.117	43.75	49.161
			f	24.10				350.	418.9	519.5
		1000	T	10.30	N/A	N/A	N/A	30.68	(35.26)	(61.7)
			v_m	250.11				989.4	1324.0	3106.8
			L	8.379				40.117	43.75	55.904
			f	24.10				350.	418.9	650.6

Notes :
* N/A - denotes 'stable' buckling path
* T - Temperature rise (°C)
* v_m - Buckle amplitude (mm)
* L - Buckle length (m)
* f - Maximum stress (N/mm^2)
* F_{ap} - Anchor shear capacity (kN)

Table 5.8 Fully Mobilised Infilled Prop (*Blister*) Model with Fixed Anchor Points Parametric Studies.

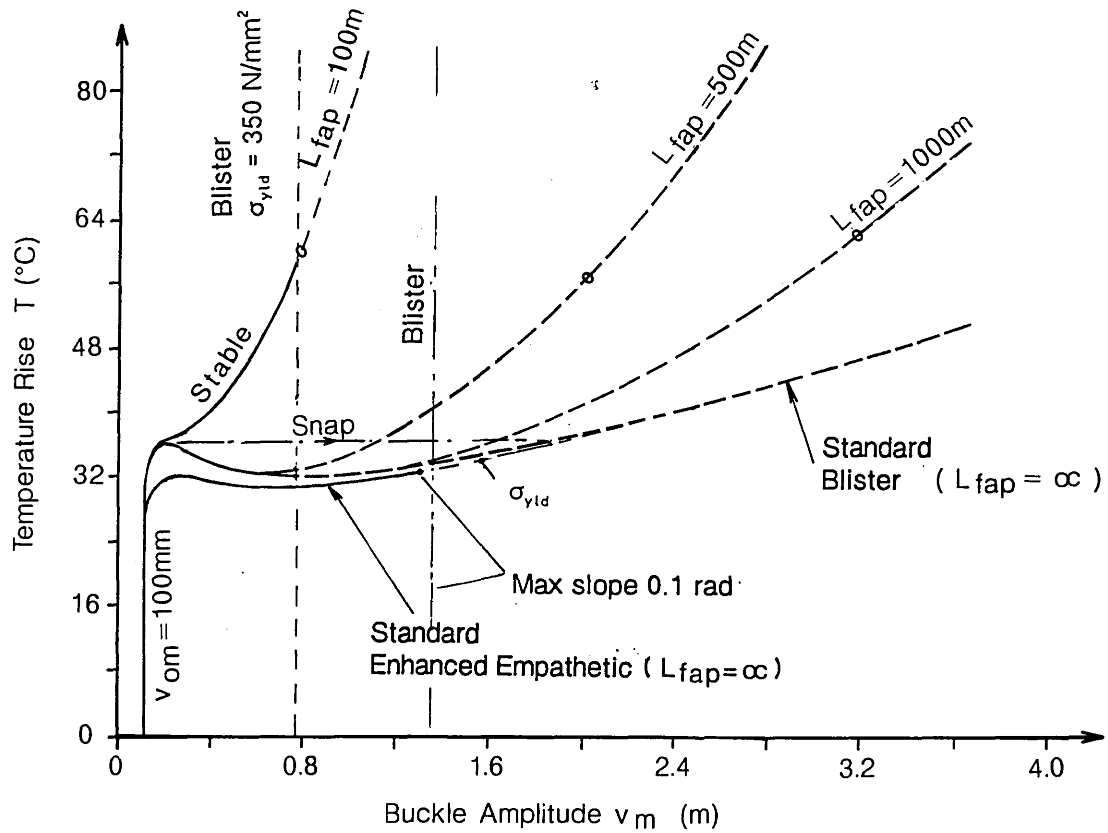

Fig 5.10 **Thermal Action Characteristics**
Fully Mobilised Infilled Prop (*Blister*) Model with Fixed Anchor Points

o denotes $F_{ap} = 750$ kN

obvious to see that the present developed model is also subjected to the same limitation, ie no enhanced effect upon temperature rise is to be obtained for L_u=6.777m<L^*=11.777m. With regard to the smaller imperfection, v_{om}=100mm, response becomes more stabilised by the incorporation of fixed anchors (ref Table 5.2).

Generally, the operating temperatures are restricted to either T_u or T_{max} for the unstable/snap cases and either to T_u or $T_{\sigma yld}$ for the stable cases; however, there is one exception in that for the case of L_{fap}=100m and v_{om}=250mm, the anchor shear capacity F_{ap} of 750kN takes precedence over the material yielding limitation.

5.8 Discussions

The standard *Blister* model herein proposed is quite distinct from the *Empathetic* model. The former is based upon on actual physical imperfection whilst the latter derives from mathematical reasoning. Buckling solutions for nL typified in Table 5.1 not only demonstrate full matching at $L=L_i$ but also converge towards the corresponding idealised solutions; in addition, the model generates a solution in keeping with that provided by an elastic interpretation of an infilled prop formulation available elsewhere[5].

Whilst the *Empathetic* model's upheaval is determined by reducing initial post-buckling amplitude expression $v_m \rightarrow v_{om}$, numerical limitations affect the proposed *Blister* model upheaval definition which involves a nominally zero upheaval length. Practical considerations (ie computational limitations) suggest that the upheaval state be deemed to occur at v_m=100.05%v_{om}. Recalling eqns

(4.17) and (5.32) together with Fig 5.2, whilst the *Blister* model therefore offers the most severe case, for a common v_{om}, comparison with the *Empathetic* model can really only be made in terms of a worst case imperfection scenario on the basis of the respective peel points occupying zero vertical displacement locations (v=0). That is, classical studies of thermo-mechanical contact surface buckling-[7,11] presume flat contact surfaces. For $L=L_i$, therefore, with common initial imperfection amplitude v_{om}

$$P|_{Emp}= 43.8\%\ P_{qi}\ <\ P|_{Blister}= 73.7\%\ P_{qi} \tag{5.84}$$

from eqns (1.29) and (5.31) respectively. Alternatively, for a common initial imperfection wavelength $L_o=L_i$ such that $v_{om}|_{Emp}=2.77v_{om}|_{Blister}$,

$$P_u|_{Emp}=40\%P_{qi}|_{L=L_o=L_i} < 42\%P_{qi}|_{L=L_o=L_i} = P_u|_{Blister} \tag{5.85}$$

Equations (5.84) and (5.85) thereby preserve, mathematically at least, the *Empathetic* model's worst case scenario claim.

The *Blister* model's thermal action/response characteristics are similar to those of the *Empathetic* model with respect to the maximum temperature rise and the upheaval states being non-coincident for the unstable/snap cases, with the maximum temperature rise and the maximum buckling force states also being non-coincident. Explicit snap/stable differention, see Section 4.5, has not been generated for this less computationally amenable model. The two basic parameters nL and u_f required for the formulation of eqn (4.18) were expressed by the simple forms of eqns (1.5) and (1.28) respectively. Conversely, the non-unique nature of the buckling solutions for nL with respect to the *Blister* model as typified in Table 5.1 and the complexity of the u_f expressions typified by eqns (5.35)-(5.37) and (5.64)-(5.67) dictate that a quick and simple solution could not be readily obtained in closed form.

Whilst the standard case-study sea-bed mounted model essentially relates to a purely trenched lie, the effects of employing enhanced burial and anchorage techniques is clearly shown in Figs 5.6, 5.8 and 5.10, with all-round improvements in buckling resistance being provided as anticipated[36,47]. Case-studies with associated operating temperatures are made available in Tables 5.3, 5.5, 5.6, 5.7 and 5.8 for various imperfections, typically v_{om}=100 and 250mm. Clearly, and similarly to the corresponding *Empathetic* models, the upheaval temperature rise T_u generated from the developed *Blister* models could be considered as the safe operating temperature applicable to all cases including the snap and stable cases; however, should the operating temperature be allowed to rise beyond T_u then such temperatures should be restricted to T_{max} for the unstable/snap cases or $T|_{\sigma yld}$ for the stable cases.

5.9 Summary

A theoretical contact undulation model based on a physical imperfection has been established as an alternative to the previously established mathematically-based *Empathetic* model[12]. The assumption of a *stress-free-when-initially-deformed* datum is considered to be appropriate when residual stresses including those due to fabrication and laying operations[41,48] are assumed to be at least partially relieved due to direct bearing between the fill and pipe particularly given the opportunities provided by thermal stress-relieving[19,20,39]. Further support for this model can be obtained from the small-scale laboratory experimentation discussed later. The somewhat lengthy consideration regarding trenching is given upon the basis that whilst vertical buckling would theoretically dictate behaviour, especially at upheaval, extended post-buckling vertical activity could become compromised by perturbations.

An alternative form of physical imperfection, where the prop voids are left unfilled, is now considered.

Chapter 6

Isolated Prop (*Isoprop* Model)

6.1 Introduction

Herein proposed is a mathematical model, termed *Isoprop*, relating to a pipeline whose otherwise horizontal and straight idealised lie is interrupted by an encounter with an isolated prop or point irregularity as illustrated in Figs 1.7(b) and 2.2(b). As noted in Section 5.2, the isolated prop features voids (sea-filled) to either side. With alternative isolated prop models available in literature[13,40,49], the following relates to the Activity 3d of Fig 2.1.

The proposed five key stages in buckling development are illustrated in Fig 6.1. The datum state refers to the initial lie adopted by the pipeline following laying operations whereby a vertical out-of-straightness is caused by the presence of the prop. Subsea conditions are assumed to preclude effective infilling of the adjacent voids with solid matter at any stage of the pre- or post-buckling process.

As the temperature of the pipeline rises due to routine operation, the initial span or imperfection wavelength L_i suffers a reduction as the pipeline *tightens up* under compressive action P ($P<P_0$, see later). The wavelength L reduces to some specific value L_u ($P=P_u$) whereupon the pipeline lifts off the prop. Post-upheaval buckling initially involves wavelength $L_u<L<L_i$, with $L > L_i$ ensuing if circumstances so dictate.

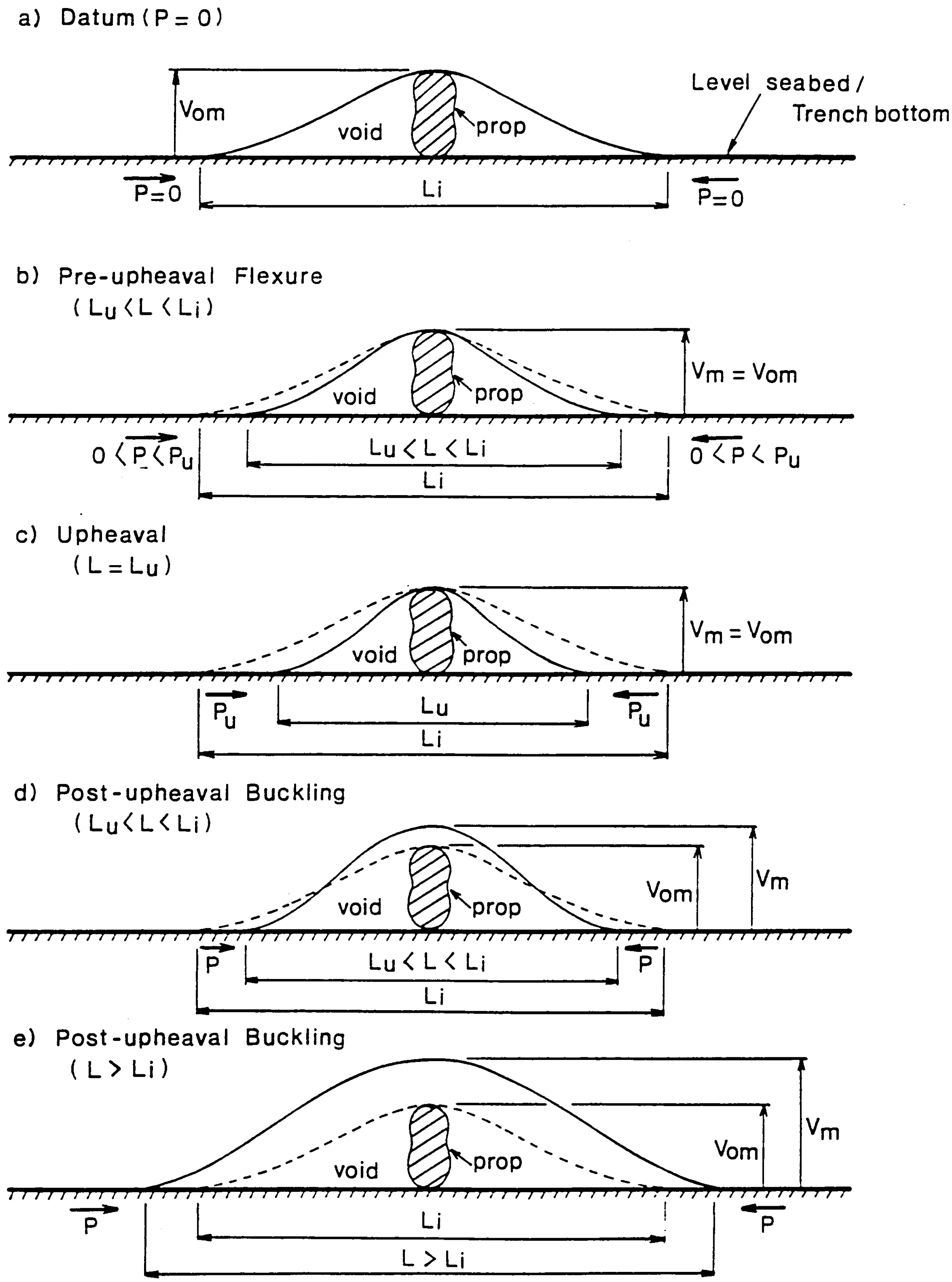

Fig 6.1 Isolated Prop Topologies

6.2 Datum Establishment

The appropriate topology is shown in Fig 5.1 and has been discussed in Section 5.2. Equations (5.1) to (5.12) again apply and the respective equilibrium study, whilst providing an initially curved datum $v_i(x)$ for ensuing stability studies, actually demands a supposedly previous hypothetical or fictitious *stress-free-when-straight* datum with q initially relating to an empty pipe. Accordingly, any isolated prop buckling study which employs eqn (5.7) *in conjunction with* eqn (5.12) is effectively condemned to replicate established idealised study[8,49]. Herein, however, whilst eqn (5.7) is taken to be usefully true following field observations in the North Sea[27], eqn (5.12) is taken to relate to only a *component of* residual stress in the as-laid pipe, other components following from fabrication and laying operations[41,48]. Previous related discussions have introduced such matters in Sections 1.5, 2.3 and 5.3. Given that any residual stresses will surely be subject to in-service thermal stress relieving[20,27,48] and that the 'isolated' inclusion of only the stress data corresponding to eqn (5.12) provides an effectively imperfection-free datum formulation which would then be non-conservative - these features are discussed further in the ensuing - then the familiar engineering *worst case scenario* philosophy is invoked whereby the imperfection--nullifying idealised stress component given by eqn (5.12) is suppressed and a Perry-like datum assumption of *stress-free-when-initially-deformed* is employed[4]. Hereafter, in the absence of comprehensive and definitive as-laid residual stress data[41,48], eqn (5.7) is employed as a kinematic imperfection of form.

6.3 Pre-Upheaval Flexure

Figure 6.2 illustrates the topology adopted upon the onset of in-service axial compression P which is constant through the wavelength $L_u \le L \le L_i$; strictly, q now allows for the pipeline containing hydrocarbons. The argument of the previous section leads to employment of the familiar, imperfect moment-curvature relationship.

$$M_x = EI(v,_{xx} - v_i,_{xx}) = P(v_{om} - v) + N + Fx - \frac{qx^2}{2} \tag{6.1}$$

where M_x represents the bending moment at x, $0 \le x \le L/2$, v_{om} and $v_i,_{xx}$ are given by eqns (5.8) and (5.10) respectively, N denotes the crown moment and shear force F represents half the prop force. The respective boundary conditions take the form

$$\begin{aligned} v|_{L/2} &= v,_x|_{L/2} = v,_{xx}|_{L/2} = v,_x|_0 = 0 \qquad \textit{and} \\ v|_x &= v_{om} \end{aligned} \tag{6.2}$$

The general solution to eqn (6.1) can be written as

$$v = C_1 \cos nx + C_2 \sin nx + k_{19} + k_{20}x - \frac{qx^2}{n^2 EI} \tag{6.3}$$

where C_1 and C_2 are the constants of integration and k_{19}, k_{20} are defined as

$$\begin{aligned} k_{19} &= \frac{qL_i^4}{1152EI} + \frac{1}{n^2 EI}\left(N - \frac{qL_i^2}{24} + \frac{2q}{n^2}\right) \\ k_{20} &= \frac{1}{n^2 EI}\left(\frac{qL_i}{3} + F\right) \end{aligned} \tag{6.4}$$

The presence of the bending moment at the peel point despite the zero curvature transversality requirement is to be noted, however, with

$$M_x|_{L/2} = EIv,_{xx}|_{L/2} - EIv_i,_{xx}|_{L/2} = -EIv_i,_{xx}|_{L/2} \tag{6.5}$$

The curvature $v_i,_{xx}$ of the imperfection curve given by eqn (5.10) enables the

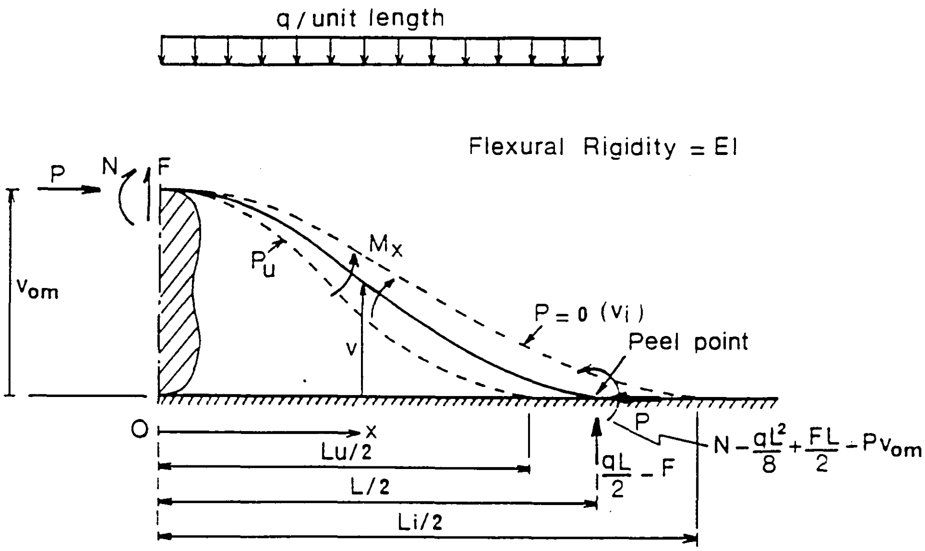

(a) Flexural Range Topology $L_u \leqslant L \leqslant L_i$

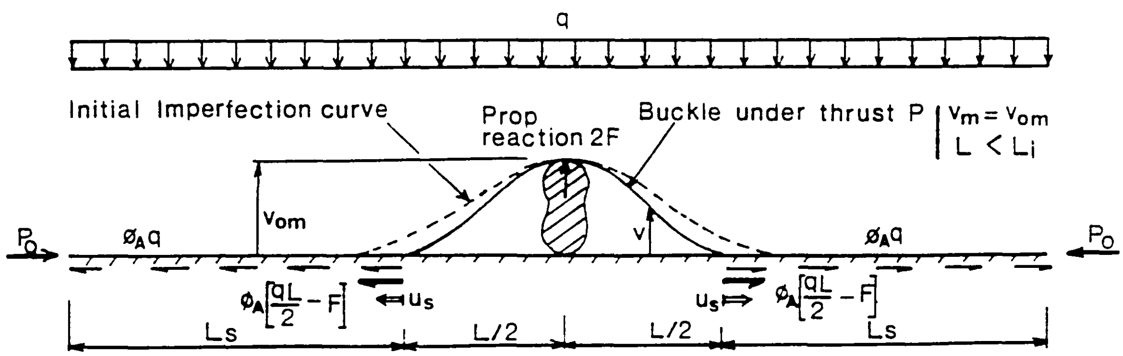

(b) General Topology

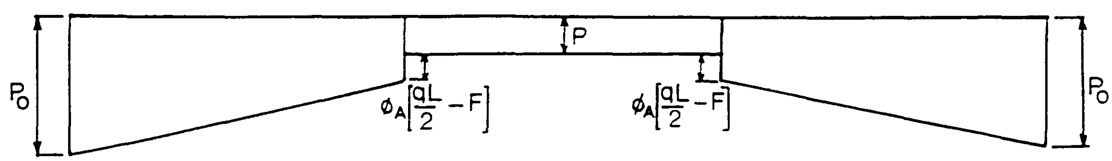

(c) Axial Force Distribution

Fig 6.2 Isolated Prop ; Pre Upheaval
Details of Imperfect Fully Mobilised Model (*Isoprop* Model)

bending moment $M_x|_{L/2}$ of eqn (6.5) to be expressed as

$$M_x|_{L/2}=-\frac{q}{24}(3L-L_i)(L_i-L) \tag{6.6}$$

Alternatively, the boundary condition $v|_{L/2}=0$ of eqn (6.2) allows eqn (6.1) to be expressed as

$$M|_{L/2}=Pv_{om}+N+\frac{FL}{2}-\frac{qL^2}{8} \tag{6.7}$$

Equating $M_x|_{L/2}$ from eqns (6.6) and (6.7), noting v_{om} from eqn (5.8), affords the relationship between N and F to become

$$N+\frac{FL}{2}=\frac{qL^2}{8}-\frac{q}{24}(3L-L_i)(L_i-L)-n^2\frac{qL_i^4}{1152} \tag{6.8}$$

The zero slope condition at x=L/2 of eqn (6.2) enables the first relationship between C_1 and C_2 to be written as

$$-nC_1\sin\frac{nL}{2}+nC_2\cos\frac{nL}{2}+k_{20}-\frac{qL}{n^2EI}=0 \tag{6.9}$$

whilst the boundary condition $v|_{L/2}=0$ provides

$$C_1\cos\frac{nL}{2}+C_2\sin\frac{nL}{2}+\frac{2q}{n^4EI}=0 \tag{6.10}$$

Solving the two simultaneous eqns (6.9) and (6.10) for C_1 and C_2 gives

$$C_1=\frac{q}{n^4EI}\left(-2\cos\frac{nL}{2}+[\frac{nL_i}{3}-nL+\frac{nF}{q}]\sin\frac{nL}{2}\right) \tag{6.11}$$

and

$$C_2=\frac{q}{n^4EI}\left(-2\sin\frac{nL}{2}-[\frac{nL_i}{3}-nL+\frac{nF}{q}]\cos\frac{nL}{2}\right) \tag{6.12}$$

Having evaluated the two constants of integration C_1 and C_2, further employment of boundary condition $v,_x|_0=0$ with eqn (6.3), noting eqn (6.11), affords the crown shear force F to be expressed as

$$\frac{F}{EI} = (-v,_{xxx}|_0) - (-v_i,_{xxx}|_0)$$

$$= \frac{q}{EIn(1-\cos(nL/2))}\left[2\sin\frac{nL}{2} + \left(\frac{nL_i}{3} - nL\right)\cos\frac{nL}{2} - \frac{nL_i}{3}\right] \qquad (6.13)$$

Additionally, the last remaining boundary conditions $v|_0 = v_{om}$ gives, noting eqn (6.15) also,

$$2\cos\frac{nL}{2} - \frac{nL}{3}\left(\frac{L_i}{L} - 3\right)\sin\frac{nL}{2} + k_{21} = -\frac{nF}{q}\left(\frac{nL}{2} - \sin\frac{nL}{2}\right) \qquad (6.14)$$

where

$$k_{21} = -2 - \frac{(nL)^2}{4} + \frac{(nL)^2 L_i}{6L} + \frac{(nL_i)^4}{1152} \qquad (6.15)$$

Eliminating F between eqns (6.13) and (6.14), then the characteristic equation of the buckle force takes the form

$$\frac{L_i}{L} = \frac{5.8259}{nL}\left[\frac{(4-(nL)^2/4)\cos(nL/2) + 2nL\sin(nL/2) - 4 - (nL)^2/4}{\cos(nL/2) - 1}\right]^{\frac{1}{4}}$$

(6.16)

Table 6.1 presents typical values of nL in terms of L_i/L.

The vertical deflection v of eqn (6.3) can be found by employing eqns (6.11) and (6.12), also noting eqn (5.8) for v_{om}, such that

$$v = \frac{q}{n^4 EI}\left(-2\cos n\left(\frac{L}{2} - x\right) + k_{22}\sin n\left(\frac{L}{2} - x\right) + k_{24} + k_{23}nx - n^2x^2\right) \qquad (6.17)$$

where

$$\begin{aligned} k_{22} &= \frac{nL}{3}\left(\frac{L_i}{L} - 3\right) + \frac{nF}{q} \\ k_{23} &= k_{22} + nL \\ k_{24} &= \frac{(nL_i)^4}{1152} + 2\cos\frac{nL}{2} - k_{22}\sin\frac{nL}{2} \end{aligned} \qquad (6.18)$$

	L_i/L	nL	Remarks
Pre-Upheaval $L<L_i$	1.194847	1.5	$P \rightarrow 0$
	1.199310	2.0	
	1.205182	2.5	
	1.212541	3.0	
	1.221515	3.5	
	1.232263	4.0	
	1.259967	5.0	
	1.298091	6.0	
	1.3421	6.857667	Upheaval F=0
Post-Upheaval $L<L_i$	1.3421	6.857667	Upheaval ($v_m=v_{om}$)
	1.3	6.986727	
	1.2	7.262400	
	1.1	7.502238	
	1.0	7.7134	$L=L_i$
Post-Upheaval $L>L_i$	1.0	7.7134	$L=L_i$
	0.9	8.039016	
	0.8	8.327418	
	0.7	8.659057	
	0.6	8.754047	
	.	.	
	.	.	
	0.01	8.9868	$P \rightarrow 80.76\ EI/L^2$ ($L>L_u$)

Table 6.1 Typical Buckle Force Solution for *Isoprop* Model

From eqn (6.17) the maximum buckle amplitude v_m at x=0 can be simply expressed as

$$v_m = K_2 \frac{qL^4}{EI} \tag{6.19}$$

where

$$K_2 = \frac{1}{(nL)^4}\left(-2\cos\frac{nL}{2} + k_{22}\sin\frac{nL}{2} + k_{24}\right) \tag{6.20}$$

Recalling the relationship between the maximum bending moment N at x=0 and the shear force F of eqn (6.8), where F itself can be found from eqn (6.13), then N takes the form

$$N = \frac{q}{n^2}\left(k_{24} - 2 + \frac{(nL_i)^2}{24} - \frac{(nL_i)^4}{1152}\right) \tag{6.21}$$

and the maximum stress becomes

$$\sigma_m = \frac{P}{A} + \frac{ND}{2I} \tag{6.22}$$

Combination of eqns (6.1) and (6.21) affords the general bending moment to be given by

$$M_x = P(v_{om} - v) + \frac{q}{n^2}\left(k_{24} - 2 + \frac{(nL_i)^2}{24} - \frac{(nL_i)^4}{1152}\right) + Fx - \frac{qx^2}{2} \le N \tag{6.23}$$

F being available from eqn (6.13).

Similar to the previously discussed *Empathetic* and *Blister* models, it is now necessary to employ longitudinal equilibrium and compatibility to relate P to the temperature rise $T = P_0/AE\alpha$ employing the system topology and axial force distribution given in Figs 6.2 (b) and (c). At this stage of buckling, recalling the presence of half the prop force F in the expression of peel point reaction, the equilibrium expression takes the form,

$$P_o-P=[2\phi_A qAE(-u_s)]^{1/2}+\phi_A\left(\frac{qL}{2}-F\right) \tag{6.24}$$

where u_s denotes the longitudinal movement of the peel point given by the longitudinal compatibility expression

$$u_s=\frac{(P_o-P)L}{2AE}-u_f \tag{6.25}$$

in which u_f denotes the flexural end-shortening through the wavelength such that

$$u_f=\frac{1}{2}\int_0^{L/2}(v,_x)^2dx-\frac{1}{2}\int_0^{L_i/2}(v_i,_x)^2dx \tag{6.26}$$

Equation (6.26) is somewhat tedious to evaluate with, following computational manipulation,

$$\begin{aligned}\int_0^{L/2}(v,_x)^2dx = &\left(\frac{q}{EI}\right)^2\frac{1}{n^7}\Bigg((4+k_{22}^2)\frac{nL}{4}+\frac{nL}{2}(k_{22}+nL)k_{22}\\ &+\frac{(nL)^3}{6}+\frac{1}{4}(k_{22}^2-4)\sin nL-k_{22}(\cos nL-1)\\ &-4\left[(k_{22}+nL)\left(1-\cos\frac{nL}{2}\right)+2\sin\frac{nL}{2}-nL\right]\\ &+2k_{22}\left[2-2\cos\frac{nL}{2}-(k_{22}+nL)\sin\frac{nL}{2}\right]\Bigg)\end{aligned} \tag{6.27}$$

where k_{22} is given by eqn (6.18), and eqn (5.7) affords the second term of eqn (6.26) to be evaluated as

$$\int_0^{L_i/2}(v_i,_x)^2dx=\left(\frac{q}{EI}\right)^2\frac{L_i^7}{483840} \tag{6.28}$$

Full solution for the pre-upheaval flexure stage is now available from eqns (6.16) - (6.28), although the longitudinal fully mobilised friction modelling employed above fails to allow for the early phase of this stage in which all necessary frictional resistance is (theoretically) provided for by the peel point concentrated reaction ϕ_A[qL/2-F] as discussed previously with regard to the

Empathetic and *Blister* models in Sections 4.2 and 5.4 respectively; ie eqns (6.24) and (6.25) are only valid for $u_s \le 0$, such that elimination of $(P_o - P)$ between these two equations affords

$$u_s = [2\phi_A qAE(-u_s)]^{1/2}\frac{L}{2AE} + \phi_A\left[\frac{qL}{2} - F\right]\frac{L}{2AE} - u_f \tag{6.29}$$

Equation (6.29) can be re-written as a quadratic equation with respect to $(-u_s)^{1/2}$

$$[(-u_s)^{1/2}]^2 + \frac{L}{2AE}(2\phi_A qAE)^{1/2}[(-u_s)^{1/2}] + \phi_A\left(\frac{qL}{2} - F\right)\frac{L}{2AE} - u_f = 0$$

(6.30)

where u_f is given by eqn (6.26). Noting tensile relief demands $u_s|_{L/2}$ can never be positive, then from eqn (6.30),

$$-\frac{\phi_A L}{2AE}\left(\frac{qL}{2} - F\right) + u_f \ge 0 \tag{6.31}$$

Taking $L = L^*$ as the root of eqn (6.31) - ie; R.H.S.=0 - then for the slip length to exist $(u_s < 0)$, $L > L^*$.

For $L \le L^*$, $u_s = 0$ and no slip length exists such that eqn (6.24) is replaced by

$$P_o = P + \phi_A\left(\frac{qL}{2} - F\right) \tag{6.32}$$

whilst for $L > L^*$, u_s is given by

$$\begin{aligned}
u_s &= -\frac{1}{4}\left(-\left(\frac{\phi_A q}{2AE}\right)^{1/2} . L + \left[\frac{\phi_A qL^2}{2AE} - \phi_A\left(\frac{qL}{2} - F\right)\frac{2L}{AE} + 4u_f\right]^{1/2}\right)^2 \\
L_s &= \left(\frac{2AE(-u_s)}{\phi_A q}\right)^{1/2} \\
P_o &= P + \phi_A\left(\frac{qL}{2} - F\right) + \phi_A qL_s
\end{aligned} \tag{6.33}$$

The above formulation is valid for $0 \le P \le P_u$ where P_u denotes the buckle force in the pipe at the onset of upheaval from the prop. Prior to consideration of the important upheaval state (ie $P = P_u$), it is pertinent to appreciate that the present analysis relates to in-service conditions. In comparison with the contact undulation studies of Chapters 4 and 5, the pre-upheaval flexural regime represents an in-service capability for delaying the onset of upheaval; flexural and associated slip length movement can occur without upheaval being induced. Although the physical prototype presently under consideration lacks the self-weight relieving presence provided by the prop-attendent fill of the infilled case, it does share the residual stress relieving mechanism provided by the *actually* complex non-linear axial friction behaviour within the slip lengths[36], ratchetting surely attending the cyclic nature of in-service activity. Given the above noted substantial degree of in-service movement herein concerned, it is contended that thermally-induced residual stress-relieving is thereby similarly available. This important matter will be subject to further deliberation following presentation of the complete model. However, the above lends further support to the adoption, as for the contact undulation models, of a *stress-free-when-initially-deformed* datum[39].

6.4 Upheaval

This state, of crucial importance to the designer, is defined herein as being that at which the prop reaction force (2F) reduces to zero. From eqn (6.13) therefore, with F=0 ,

$$L_u = L|_{F=0} = 0.745L_i = 0.96L_o \qquad and$$
$$P_u = P|_{F=0} = 47.027\frac{EI}{L_u^2} = 63\% P_{qi}|_{v_{om}} \qquad (6.34)$$

where $P_{qi}=80.76EI/L^2=3.962(EIq/v_m)^{\frac{1}{2}}$ denotes the idealised buckling force value[7] ($L \equiv L_u$, $v_m \equiv v_{om}$) whilst the corresponding curvature and upheaval temperature T_u can be respectively expressed as

$$(v,_{xx}|_0)_u = (v,_{xx}|_{max})_u = -0.106\frac{qL_u^2}{EI} = -0.0588\frac{qL_i^2}{EI} = -0.0979\frac{qL_o^2}{EI}$$

$$T_u = -3.53\frac{q}{AE\alpha}\cdot\frac{1}{v_i,_{xx}|_0} = 1.57\left(0.078\frac{q}{AE\alpha}\left[\frac{L_o^2}{v_{om}}\right]\right) \tag{6.35}$$

Equations (6.34) and (6.35) are quite distinct from the upheaval values obtained in previous isolated prop models[13,49] and this factor requires *particular* consideration.

As noted in Section 6.2, the above are explicitly based upon the familiar moment-curvature expression given by eqn (6.5) which incorporates initial imperfection curvature $v_i,_{xx}$ effects. Equation (5.7) is taken to prescribe a *stress-free-when-initially-deformed* datum state, ie eqn (5.12) is suppressed. *If* the internal stressing of eqn (5.12) were to be incorporated within eqn (6.1) apriori with $M_i|_x = EIv_i,_{xx}$, the idealised[7] solutions

$$P_u = 80.76\frac{EI}{L_u^2} = P_{qi}|_{L=L_u} \tag{6.36}$$

and

$$L_u = 4.5147\left(\frac{v_{om}EI}{q}\right)^{1/4} = L|_{P_{qi}} \tag{6.37}$$

would ensue as eqns (5.7), (5.8) and (5.12) represent the deformed state solution of a problem in which the (previous hypothetical) datum state was *stress-free-when-straight.* This is effectively implemented in previous isolated prop models[13,49] ie a *stress-free-when-straight* pipeline has been subjected to displacement v_{om} under inertial loading *q* and *then* compressed by P. These are therefore equivalent to idealised studies[7] in which the pipeline has been 'disturbed' or propelled into the idealised buckling mode at amplitude $v_m|_{Pqi} \equiv v_{om}|_{Pqi}$.

(Regarding overall system modelling, thermal values may be only approximately idealised therein due to the employment of simplified compatibility assumptions[9].)

Summarising, justification for the proposed prop model's *conservative* philosophy which results in the 37% loss in upheaval buckling resistance identified by comparing eqns (6.34) and (6.36) is provided twofold. First, in the absence of comprehensive as-laid residual stress data, it is a *high risk assumption* to be definitive about only that component which nullifies imperfect behaviour and is based upon a *historically non-existent or fictitious state.* Second, whilst the previous in-service considerations are not to be taken to suggest that complete relieving of all residual stress components is thereby provided[20,48], there is surely little doubt that the precise and component-only elastic interpretation given by eqn (5.12) fails, non-conservatively, to replicate a duly definitive in-service imperfect datum state. Should definitive residual stress data become available[41,48], this could be readily accommodated within the present model by suitable modification of eqn (6.1) and thereafter.

Finally, it should be noted that given the *imperfect* force-deformation relationship of eqn (6.13)

$$\frac{F}{EI}=(-v,_{xxx}|_0)-(-v_i,_{xxx}|_0) \tag{6.38}$$

then for F=0, there is the implicit *kinematic* requirement

$$v,_{xxx}|_0=v_i,_{xxx}|_0 \qquad (F=0) \tag{6.39}$$

such that, from eqn (5.7),

$$v,_{xxx}|_0=-\frac{qL_i}{3EI} \tag{6.40}$$

This is true[20] for upheaval and beyond as described in the following.

6.5 Post-Upheaval Buckling ($L_u \le L \le L_i$)

Upon upheaval the tightening-up of the wavelength is reversed with L now growing as buckling ensues with further rise in temperature. As indicated in Fig 6.1, mathematical modelling of post-upheaval buckling again requires a two-phase structure, first with $L<L_i$ and second with $L>L_i$ (see below).

Figure 6.3 illustrates the initial post-upheaval stage with Fig 6.3 (a) detailing the crucial flexural region, boundary conditions taking the form

$$v|_{L/2}=v,_x|_{L/2}=v,_x|_0=v,_{xx}|_{L/2}=0 \tag{6.41}$$

with

$$v|_0=v_m \tag{6.42}$$

Noting that eqns (6.5) and (6.40) remain valid, equilibrium affords for $0 \le x \le L/2$,

$$M_x=EI(v,_{xx}-v_i,_{xx})=P(v_m-v)-\frac{qx^2}{2}+N \tag{6.43}$$

where $v_i,_{xx}$ is given by eqn (5.10).

The general solution to eqn (6.43) takes the form

$$v=C_3\cos nx+C_4\sin nx+k_{25}+\frac{qL_i}{3n^2EI}x-\frac{qx^2}{n^2EI} \tag{6.44}$$

where C_3 and C_4 are the constant of integration and k_{25} can be expressed as

$$k_{25}=v_m+\frac{q}{n^2EI}\left(\frac{2}{n^2}-\frac{L_i^2}{24}\right)+\frac{N}{n^2EI} \tag{6.45}$$

Manipulation of eqns (6.43), (5.10) and boundary condition and $v,_{xx}|_{L/2}=0$ gives

$$Pv_m-\frac{qL^2}{8}+N=-EIv_i,_{xx}|_{L/2}=-\frac{q}{24}(3L-L_i)(L_i-L) \tag{6.46}$$

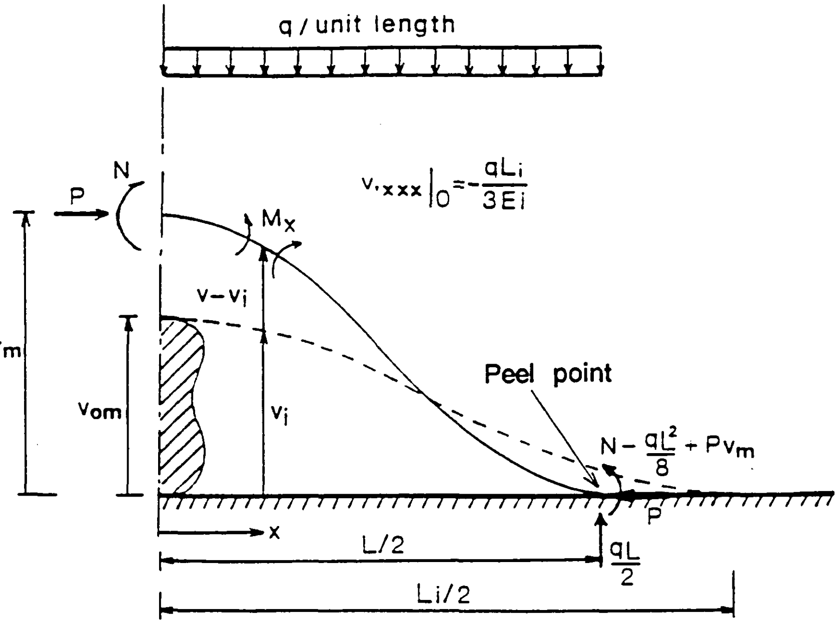

(a) Flexural Range Topology $L \leqslant L_i$

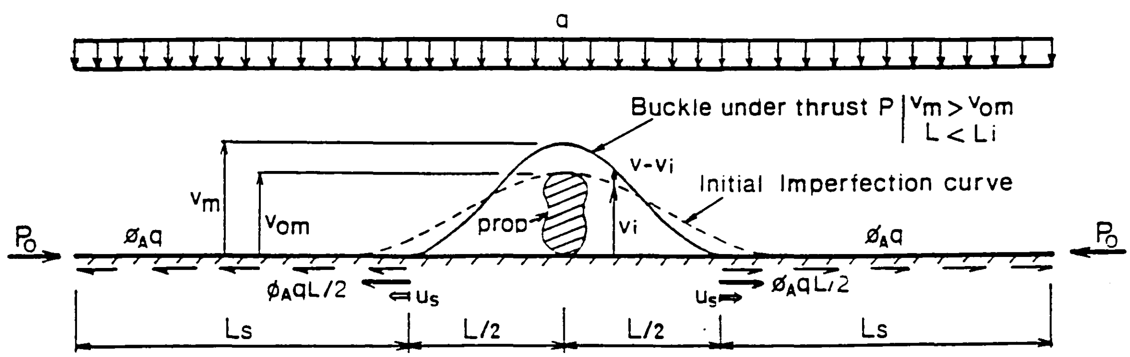

(b) General Topology

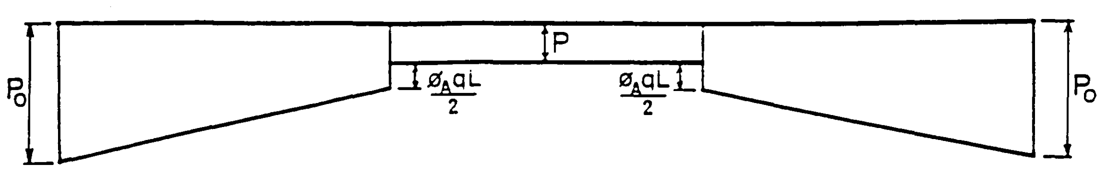

(c) Axial Force Distribution

Fig 6.3 Isolated - Prop ; Initial Post Upheaval
Details of Imperfect Fully Mobilised Model $L < L_i$ **(*Isoprop* Model)**

which affords k_{25} of eqn (6.45) to be expressed as

$$k_{25}=\frac{q}{n^2EI}\left(\frac{2}{n^2}-\frac{LL_i}{6}+\frac{L^2}{4}\right) \tag{6.47}$$

The employment of boundary condition $v|_{L/2}=0$ of eqn (6.41), noting eqn (6.47), affords the first relationship between C_3 and C_4 to be established as

$$C_3\cos\frac{nL}{2}+C_4\sin\frac{nL}{2}+\frac{2q}{n^4EI}=0 \tag{6.48}$$

and similarly, condition $v,_x|_{L/2}=0$ provides

$$-nC_3\sin\frac{nL}{2}+nC_4\cos\frac{nL}{2}+\frac{qL_i}{3n^2EI}-\frac{qL}{n^2EI}=0 \tag{6.49}$$

Solution to eqns (6.48) and (6.49) allows two constants C_3 and C_4 to be written as

$$C_3=\frac{q}{n^4EI}\left(-2\cos\frac{nL}{2}+\frac{nL}{3}\left(\frac{L_i}{L}-3\right)\sin\frac{nL}{2}\right) \tag{6.50}$$

and

$$C_4=\frac{q}{n^4EI}\left(-2\sin\frac{nL}{2}-\frac{nL}{3}\left(\frac{L_i}{L}-3\right)\cos\frac{nL}{2}\right) \tag{6.51}$$

Alternatively, further employment of boundary condition $v,_x|_0=0$ in conjunction with eqn (6.44) gives

$$C_4=-\frac{qL_i}{3n^3EI} \tag{6.52}$$

Equating eqns (6.51) and (6.52) yields the characteristic equation of buckle force as

$$2\sin\frac{nL}{2}+\left(\frac{nL_i}{3}-nL\right)\cos\frac{nL}{2}-\frac{nL_i}{3}=0 \tag{6.53}$$

Equation (6.53) is evaluated for nL for given values of L_i/L - recall the treatment of eqn (6.16) - and key values are given in Table 6.1.

Having evaluated k_{25}, C_3 and C_4 then the deflection v of eqn (6.44) finally becomes

$$v = \frac{q}{EIn^4}\left(-2\cos n\left(\frac{L}{2}-x\right)+\left(\frac{nL_i}{3}-nL\right)\sin n\left(\frac{L}{2}-x\right)\right.$$
$$\left.+2-\frac{(nL)^2}{12}\left(2\frac{L_i}{L}-3\right)+\frac{n^2L_ix}{3}-n^2x^2\right) \qquad (6.54)$$

for $0 \le x \le L/2$; the buckle amplitude v_m is determined from eqn (6.54), noting eqn (6.42).

$$v_m=K_3\frac{qL^4}{EI} \qquad (6.55)$$

where

$$K_3=\frac{1}{(nL)^4}\left(-2\cos\frac{nL}{2}+\left(\frac{nL_i}{3}-nL\right)\sin\frac{nL}{2}+2-\frac{(nL)^2}{12}\left(2\frac{L_i}{L}-3\right)\right) \qquad (6.56)$$

Bending moment N at the crown can be found by employing eqn (6.46) together with eqns (6.55) and (6.56)

$$N=\frac{q}{n^2}\left(2\cos\frac{nL}{2}-\left(\frac{nL_i}{3}-nL\right)\sin\frac{nL}{2}+\frac{(nL_i)^2}{24}-2\right) \qquad (6.57)$$

and similar to eqn (6.22) the maximum stress σ_m is given by

$$\sigma_m=\frac{P}{A}+\frac{ND}{2I} \qquad (6.58)$$

That the present modelling smoothly interfaces, as required, with the pre-upheaval flexure modelling previously discussed at the upheaval state is available from Table 6.1, the respective and alternative statements for upheaval being $v_m=v_{om}$ [ie eqns (6.42) and (6.54)] and F=0 [ie eqns (6.13) and (6.40)]; note $0.745=(1.3421)^{-1}$.

Having related buckling force P to amplitude v_m and wavelength L it is again necessary to relate P to the temperature rise $T(P_0)$. Noting the system topology shown in Fig 6.3 (b) together with the axial force distribution shown in Fig 6.3 (c), then eqns (6.24), with F=0, and (6.25) are again employed with

$$\begin{aligned}
u_f = {} & \frac{1}{2}\int_0^{L/2} (v,_x)^2 dx - \frac{1}{2}\int_0^{L_i/2} (v_i,_x)^2 dx \\
= {} & \frac{1}{2}\left(\frac{q}{EI}\right)^2 \frac{1}{n^7}\left(\frac{n^2}{36}(L_i-3L)^2(nL+\sin nL)+nL-\sin nL\right. \\
& +\frac{nL_i}{3}-\frac{n}{3}(L_i-3L)\cos nL+\frac{n^3L}{18}(L_i^2-3LL_i+3L^2) \\
& +4\left[\frac{nL_i}{3}\left(\cos\frac{nL}{2}-1\right)-2\sin\frac{nL}{2}+nL\right] \\
& \left.+\frac{2n}{3}(L_i-3L)\left[-\frac{nL_i}{3}\sin\frac{nL}{2}-2\cos\frac{nL}{2}+2\right]\right) \\
& -\left(\frac{q}{EI}\right)^2 \frac{L_i^7}{967680}
\end{aligned} \qquad (6.59)$$

Figure 6.3 indicates that fully activated slip lengths are tacitly assumed although should the pre-upheaval flexure stage have resulted in this not being the case, equations (6.31) and (6.32) are employed subject to F=0 in place of eqns (6.24) and 6.25).

6.6 Post-Upheaval Buckling ($L \geq L_i$)

The key features of this stage of buckling are illustrated in Fig 6.4. Similar to the previously discussed *Blister* model that the transverse deflection $v=f(x,L)$ is not *everywhere* attended by the continuous imperfection $v_i=g(x,L_i)$, the flexural region of the buckled pipe shown in Fig 6.4(a), therefore, still needs to be split into two separate zones $0 \leq x \leq L_i/2$ and $L_i/2 \leq x \leq L/2$ for the analysis to be valid. However, the analytical procedure is similar to those discussed in

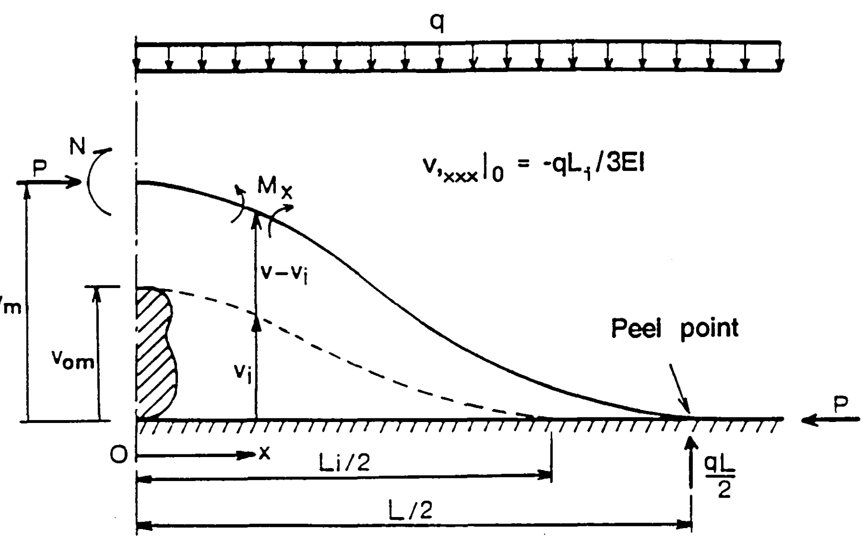

(a) Flexural Range Topology $L \geqslant Li$

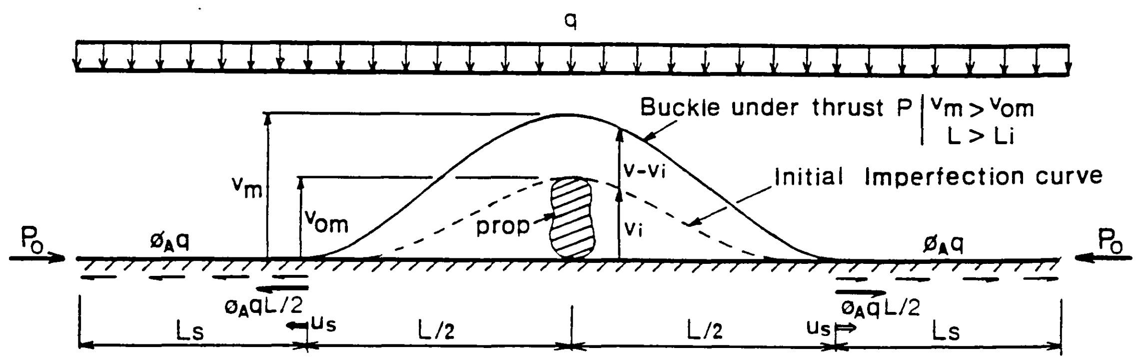

(b) General Topology

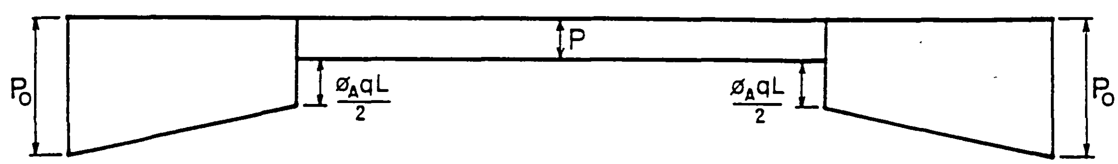

(c) Axial Force Distribution

Fig 6.4 Isolated - Prop : Post Upheaval
Details of Imperfect Fully Mobilised Model $L > Li$ **(*Isoprop* Model)**

Section 5.5, that is, the characteristic equation of the buckle force and the equations of the deflected curve, typified by eqns (5.57) and (5.58) - (5.59) respectively, are still valid for the *Isoprop* model. In addition, the longitudinal equilibrium and compatibility expressions, typified by eqns (5.33) and (5.34) with further support from the zero fully mobilised slip length consideration of eqn (5.38) together with the flexural end-shortening u_f expressions of eqns (5.64) - (5.67), again still apply here.

6.7 Standard Model Case Studies

The parametric data of Table 3.3 is again employed and resulting data is given in Table 6.2 together with graphical presentation in Figs 6.5(a)-(d). The same six magnitudes of imperfection v_{om} have been employed - refer to Sections 4.6 and 5.6 - to distinguish between stable and unstable responses. Note that from eqn (5.8) the initial imperfection lengths L_i ranging from 26.618m 41.66m correspond with v_{om} ranging from 50mm to 300mm.

The overall impression is considered to be consistent with system responses obeying the idealised envelope within the defined range of applicability, being downgraded from the idealised case due to the presence of the prop imperfections. As previously, the smaller the imperfection (v_{om}), the more likely the occurrence of (undesirable) snap buckling with designers preferably maintaining operating temperatures/pressures below the upheaval values for the snap cases at least. In this respect, unlike the previously discussed contact undulation models in Sections 4.6 and 5.6, one of the most interesting features of the isolated prop model is that the maximum temperature state, if occurs, is coincident with the upheaval state; ie the smooth transitional zone of the

v_{om} (mm)	L_i (m)		Upheaval State	Max Temp. State	After snap State	Min. Temp. State	First Yield State	Max slope 0.1rad
50	26.618	T v_m L f	57.59 50 19.833 161.3	57.59 50 19.833 161.3	(57.59) 4480. 63.118 757.3	(32.95) 916.3 41.618 387.6	(33.25) 698.1 38.618 350.	(34.14) 1348.1 46.00 447.9
100	31.655	T v_m L f	41.26 100. 23.586 136.4	41.26 100. 23.586 136.4	(41.26) 2436 53.447 582.7	(32.32) 759.6 38.655 351.7	(32.33) 751.4 38.533 350.	(34.06) 1344.7 45.45 450.6
150	35.032	T v_m L f	34.23 150. 26.102 129.7	34.23 150. 26.102 129.7	(34.23) 1418.6 45.547 455.5	(31.22) 578. 35.032 287.6	(31.56) 832. 39.032 350.	(33.77) 1337.9 44.80 443.3
200	37.644	T v_m L f	30.17 200. 28.049 128.1	30.17 200. 28.049 128.1	(30.17) 705. 36.895 299.7	(29.74) 490.9 34.049 238.2	(31.02) 909. 39.541 350.	(33.38) 1332.0 44.25 432.0
250	39.804	T v_m L f	27.51 250. 29.658 128.7	N/A	N/A	N/A	30.68 989.4 40.117 350.	(32.92) 1324.0 43.75 418.9
300	41.660	T v_m L f	25.63 300. 31.041 130.5	N/A	N/A	N/A	30.48 1066.6 40.911 350	(32.33) 1315.5 43.30 402.0

Notes :
* N/A - denotes 'stable' buckling path
* T - Temperature rise (^oC)
* v_m - Buckle amplitude (mm)
* L - Buckle length (m)
* f - Maximum stress (N/mm^2)

Table 6.2 Fully Mobilised Standard Isolated Prop (*Isoprop*) Model Parametric Studies

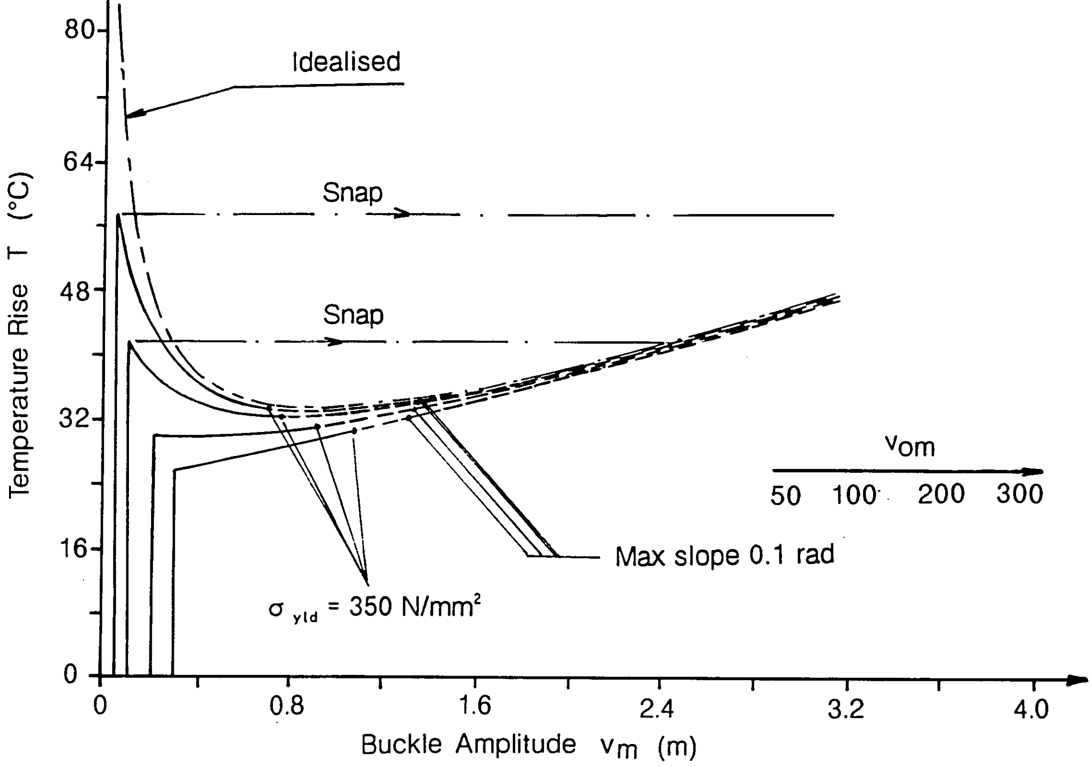

a) Thermal Action Characteristics - T vs v_m

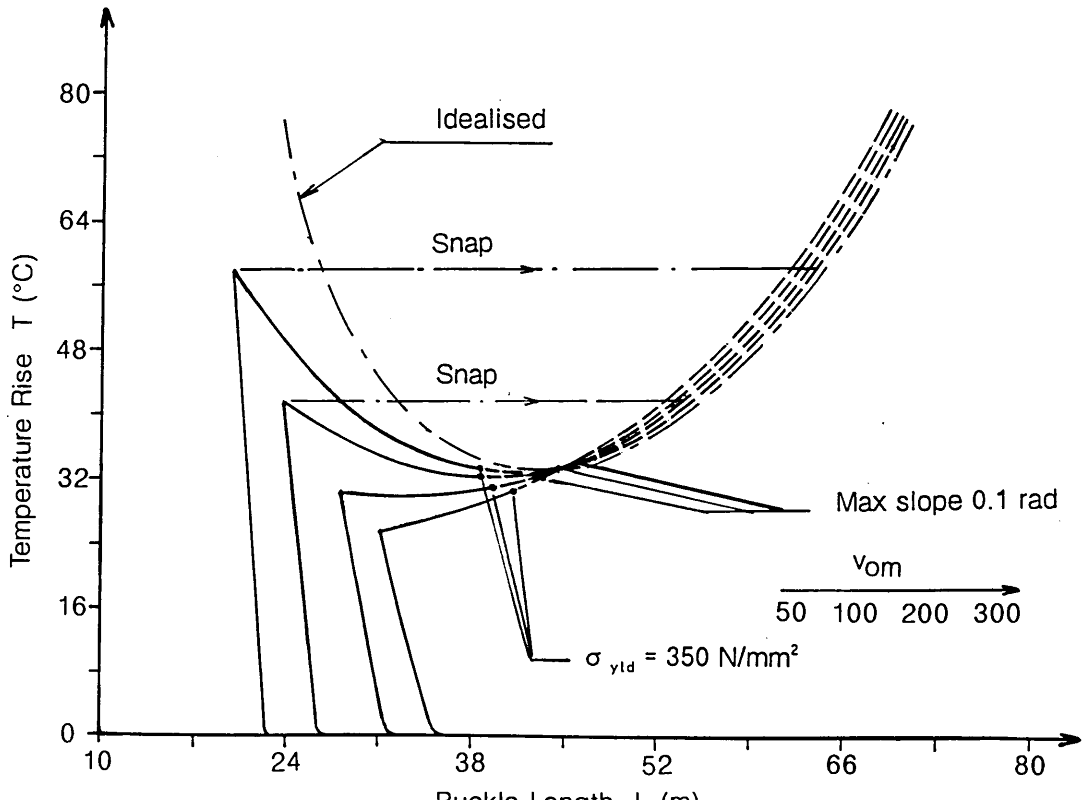

b) Thermal Action Characteristics - T vs L

Fig 6.5 Thermal Action Characteristics
Fully Mobilised Standard Isolated Prop Model *(Isoprop)*

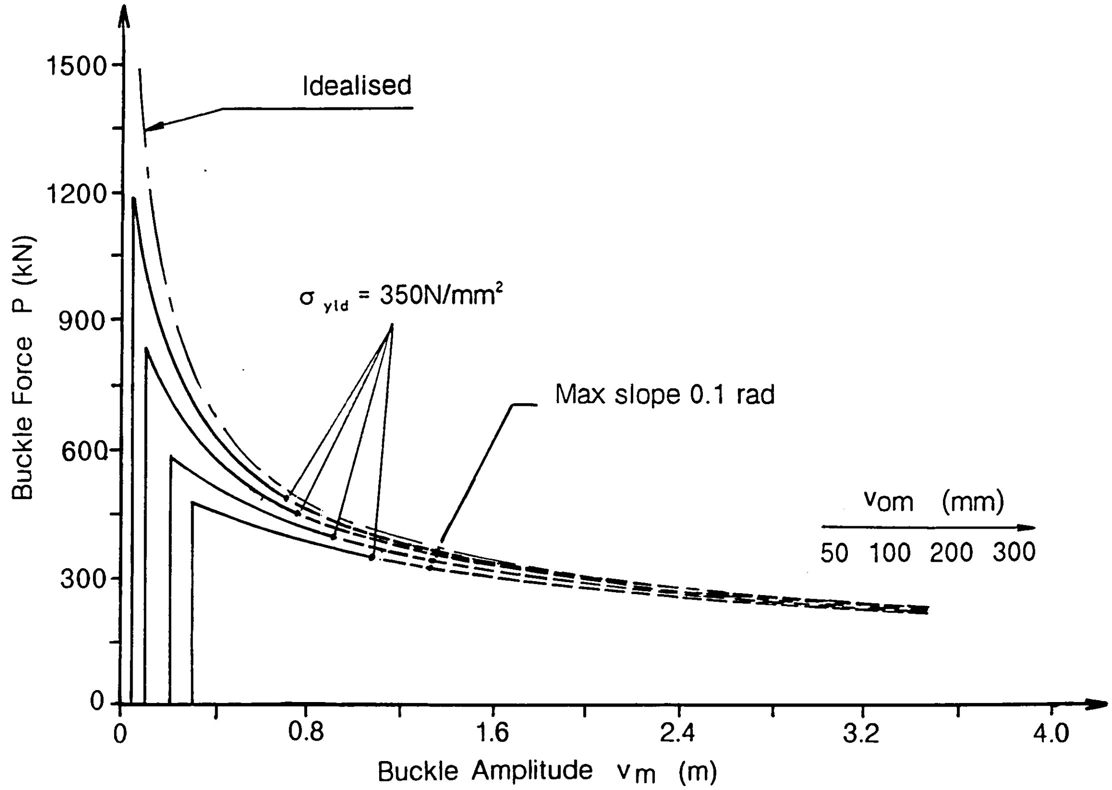

c) Buckle Force Characteristics

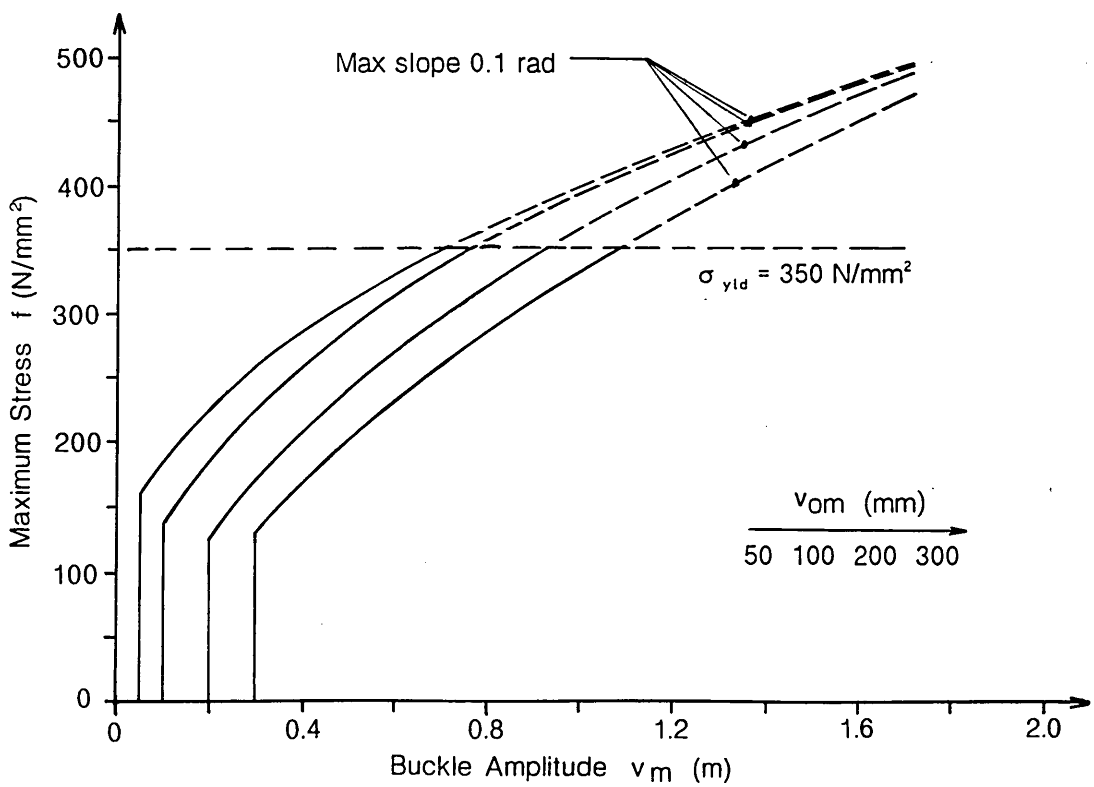

d) Maximum Stress Characteristics

Fig 6.5 (continued)

Empathetic and *Blister* models is replaced by a sharp, distinct cusp.

From theoretical comparison with the analysis results of the contact undulation models recalling Tables 4.1 and 5.2, it can be seen that the *Isoprop* model generates proportionately less stable data cases such that the stable response only occurs at larger imperfections, ie $v_{om} \geq 250$mm, whilst the *Blister* and *Empathetic* model exhibit the same phenomenon at smaller imperfections, ie $v_{om} \geq 200$ and 150mm respectively. With respect to the snap cases, the operating temperatures are to be restricted to either T_u or T_{max} as previously; however, for the stable cases employing the data of Table 3.3, whilst the *Isoprop* and *Blister* models are subject to either T_u or $T|_{\sigma yld}$, the *Empathetic* model is restricted to T_u or $T|_{0.1}r$.

Noting Fig 6.5(c), all *Isoprop* imperfection studies generate maximum buckle force states as for the contact undulation studies. However, in the *Isoprop* studies, involving cusp maxima, these states coincide with maximum temperature rise and/or upheaval states; note Fig 6.5(a).

6.8 Updated Physical Considerations

The foregoing model is applicable to a basic seabed lie topology subject to the obviation of lateral mode buckling. Advances in offshore practice including, in particular, the use of trenching and burial, continuous or discrete, together with the employment of fixed anchorages[26] have already been discussed in Chapters 4 and 5. The following considerations serve to expand the applicability of the present isolated prop imperfection model accordingly.

6.8.1 Trenching

Recalling the discussion of the *Blister* model with respect to trenching in Section 5.7.1, the corresponding development of the *Isoprop* model, being also physically based, requires similar treatment. The trenching characteristics shown in Fig 4.3 and typified by eqn (4.22) are again used.

First, for the basic trenching model with m replacing q in all related equations, vertical buckling would predominate as previously.

Second, for the refined trenching model with the assumption, similar to that used in both contact undulation models, that the slip length resistance should employ q rather than m, use is made of eqns (4.24)-(4.30) with appropriate values of u_f from eqns (6.59) and (5.64) for the post-upheaval stages with $L<L_i$ and $L>L_i$ respectively. However, for the pre-upheaval stage, recalling the zero slip length consideration of Section 4.2 being implemented by eqn (6.35) - (6.37), then L^* is to be found from the following modified equation,

$$-\frac{\phi_A L^*}{2AE}\left(\frac{mL^*}{2}-F\right)+u_f=0 \qquad (6.60)$$

where u_f is given by eqn (6.30).

For $L<L^*$, $u_s=0$ and

$$P_o=P+\phi_A\left(\frac{mL}{2}-F\right) \qquad (6.61)$$

For $L>L^*$, u_s is given by

$$u_s = -\frac{1}{4}\left(-\left(\frac{\phi_A q}{2AE}\right)^{1/2} . L + \left[\frac{\phi_A q L^2}{2AE} - \phi_A\left(\frac{mL}{2} - F\right)\frac{2L}{AE} + 4u_f\right]^{1/2}\right)^2$$
$$L_s = \left(\frac{2AE(-u_s)}{\phi_A q}\right)^{1/2} \qquad (6.62)$$
$$P_o = P + \phi_A\left(\frac{mL}{2} - F\right) + \phi_A q L_s$$

Table 6.3 displays the thermal response characteristics of the refined trenching model for the two imperfections v_{om}=100 and 250mm, employing the pipe data of Table 3.3. For each imperfection, two different trench angles of 20^o and 30^o were again employed; the corresponding standard model (m=q throughout) is also included for comparison. In terms of upheaval temperatures, this particular model offers average increases in T_u of 2.3% and 7% for $\theta=20^o$ and 30^o respectively - these are similar to their *Empathetic* and *Blister* equivalents.

Third, the rigorous trenching model employs similar principles to those used for the derivation of Table 5.5. The *Isoprop* model requires a separate consideration of the pre- and the post-upheaval states; however, the *Isoprop* model is subject to the same mathematical formulation as the corresponding *Blister* model for post-upheaval beyond L_i. Herein reported is the three stage analysis of the rigorous trenching model corresponding to the initial imperfection amplitude of v_{om} given by eqn (5.7).

For the pre-upheaval flexure stage, the imperfect moment-curvature relationship of eqn (6.5) is modified to become

$$M_x = EI(v,_{xx} - v_i,_{xx}) = P(v_{om} - v) + N + Fx - \frac{mx^2}{2} \qquad (6.63)$$

where $v_i,_{xx}$ is given by eqn (5.10). Solution of eqn (6.63) in conjunction with the

v_{om} (mm)	L_i (m)	Trench angle θ (degrees)		Upheaval State	Max. Temp. State	After snap State	Min. Temp. State	First Yield State	Max slope 0.1rad
100	31.655	Standard model	T v_m L f	41.26 100 23.586 126.4	41.26 100 23.586 126.4	(41.26) 2436 53.447 582.7	(32.32) 759.6 38.655 351.7	(32.33) 751.4 38.533 350.	(34.06) 1344.7 45.45 450.6
	31.295	20	T v_m L f	42.21 100 23.318 139.6	42.21 100 23.318 139.6	(42.21) 2496 53.186 602.6	(32.91) 765.0 38.295 361.	(32.96) 713.8 37.528 350.	(34.49) 1325.1 44.75 458.1
	30.571	30	T v_m L f	44.23 100 22.778 146.3	44.23 100 22.778 146.3	(44.23) 2624.5 52.658 645.6	(34.15) 776.6 37.571 380.8	(34.39) 643.1 35.571 350.	(35.38) 1280.6 43.30 473.0
250	39.804	Standard model	T v_m L f	27.51 250 29.658 128.7	27.51 250 29.658 128.7	N/A	N/A	30.68 989.4 40.117 350.	(32.92) 1324.0 43.75 418.9
	39.351	20	T v_m L f	28.13 250 29.321 131.7	28.13 250 29.321 131.7	N/A	N/A	31.00 954.6 39.269 350.	(33.24) 1303.1 43.05 423.7
	38.441	30	T v_m L f	29.44 250. 28.642 138.0	29.44 250. 28.642 138.0	N/A	N/A	31.68 888.6 37.776 350.	(34.01) 1261.2 41.65 435.6

Notes : * N/A - denotes 'stable' buckling path
* T - Temperature rise (°C)
* v_m - Buckle amplitude (mm)
* L - Buckle length (m)
* f - Maximum stress (N/mm^2)

Table 6.3 Fully Mobilised Isolated Prop (*Isoprop*) Model with Refined Trenching Parametric Studies.

boundary conditions of eqn (6.2) affords the crown shear force F to be expressed as

$$\begin{aligned}\frac{F}{EI} &= (-v,_{xxx}) - (-v_i,_{xxx}) \\ &= \frac{q}{EIn(1-\cos(nL/2))}\left[\frac{q+m}{q}\sin\frac{nL}{2} - \frac{nL_i}{3}\right. \\ &\qquad \left. + \left(\frac{nL_i}{3} - nL\frac{q+m}{2q}\right)\cos\frac{nL}{2}\right]\end{aligned} \tag{6.64}$$

with the characteristic equation of the buckle force taking the form

$$\frac{L_i}{L} = \frac{5.8259}{nL}\left[\frac{\left(4-\frac{(nL)^2}{4}\right)\cos\frac{nL}{2}+2nL\sin\frac{nL}{2}-4-\frac{(nL)^2}{4}}{\cos\frac{nL}{2}-1}\frac{q+m}{2q}\right]^{\frac{1}{4}} \tag{6.65}$$

Table 6.4 represents typical values of nL in terms of L_i/L for two different trench angles of 20^o and 30^o. For m=q, equation (6.65) regains the original form of eqn (6.16) of the standard model. Further manipulation of eqn (6.63) allows the vertical deflection v of the buckle curve to be written as

$$\begin{aligned} v = \frac{q}{n^4EI}\Big(&-\frac{q+m}{q}\cos n\left(\frac{L}{2}-x\right) + k_{26}\sin n\left(\frac{l}{2}-x\right) \\ &+k_{28}+k_{27}nx-n^2x^2.\frac{q+m}{2q}\Big)\end{aligned} \tag{6.66}$$

where

$$\begin{aligned} k_{26} &= \frac{nL}{3}\left(\frac{L_i}{L}-3\frac{q+m}{2q}\right)+\frac{nF}{q} \\ k_{27} &= k_{26}+nL \\ k_{28} &= \frac{(nL_i)^4}{1152}+\frac{q+m}{q}\cos\frac{nL}{2}-k_{26}\sin\frac{nL}{2}\end{aligned} \tag{6.67}$$

and the bending moment N at x=0 to be evaluated as

$$N=\frac{q}{n^2}\left(k_{28}-\frac{q+m}{q}+\frac{(nL_i)^2}{24}-\frac{(nL_i)^4}{1152}\right) \tag{6.68}$$

	Trench angle = 20°		Trench angle = 30°		Remarks
	L_i/L	nL	L_i/L	nL	
Pre-Upheaval $L<L_i$	1.201776	1.5	1.216578	1.5	$P \rightarrow 0$
	1.206264	2.0	1.221123	2.0	
	1.212169	2.5	1.227102	2.5	
	1.219571	3.0	1.234594	3.0	
	1.228597	3.5	1.243732	3.5	
	1.239408	4.0	1.254675	4.0	
	1.267272	5.0	1.282883	5.0	
	1.305618	6.0	1.321700	6.0	
	1.353566	6.918436	1.377821	7.039450	Upheaval F=0
Post-Upheaval $L<L_i$	1.353566	6.918436	1.377821	7.039450	Upheaval ($v_m=v_{om}$)
	1.3	7.072919	1.3	7.237694	
	1.2	7.331415	1.2	7.464739	
	1.1	7.557802	1.1	7.666082	
	1.0	7.758224	1.0	7.846226	$L=L_i$
Post-Upheaval $L>L_i$	1.0	7.758224	1.0	7.846226	$L=L_i$
	0.9	8.073327	0.9	8.140455	
	0.8	8.352258	0.8	8.400658	
	0.6	8.763677	0.6	8.782250	
	0.5	8.882601	0.5	8.891583	
	0.4	8.948561	0.4	8.951931	
	0.2	8.985455	0.2	8.985577	
	0.1	8.986775	0.1	8.986779	
	.	.	.	.	
	.	.	.	.	
	0.01	8.9868	0.01	8.9868	$P \rightarrow 80.76\ EI/L^2$ ($L>L_u$)

Table 6.4 Typical Buckle Force Solution for *Isoprop* Model with Rigorous Trenching.

The temperature rise $T(P_0)$ can still be evaluated from eqns (6.24) - (6.28) whereby the peel point reaction $\phi_A(qL/2-F)$ of eqn (6.24) is to be replaced by $\phi_A(mL/2-F)$, and the flexural end shortening of eqn (6.27) takes the form

$$\int_0^{L/2} v,_x^2 dx = \left(\frac{q}{EI}\right)^2 \frac{1}{n^7}\Bigg(\left(\left(\frac{q+m}{q}\right)^2 + k_{26}^2\right)\frac{nL}{4} + \frac{nL}{2}\left(k_{26}+nL.\frac{q+m}{2q}\right)k_{26}$$
$$+\left(\frac{q+m}{2q}\right)^2.\frac{(nL)^3}{6} + \frac{1}{4}\left(k_{26}^2 - \left(\frac{q+m}{q}\right)^2\right)\sin nL$$
$$-k_{26}(\cos nL-1)\frac{q+m}{2q}$$
$$-2\frac{q+m}{q}\left[\left(k_{26}+nL\frac{q+m}{2q}\right)\left(1-\cos\frac{nL}{2}\right) + \left(2\sin\frac{nL}{2}-nL\right)\frac{q+m}{2q}\right]$$
$$+2k_{26}\left[\left(2-2\cos\frac{nL}{2}\right)\frac{q+m}{2q} - \left(k_{26}+nL\frac{q+m}{2q}\right)\sin\frac{nL}{2}\right]\Bigg) \tag{6.69}$$

where k_{26} is given by eqn (6.67).

The zero slip length considerations given previously regarding eqns (6.60)-(6.62) are still valid provided u_f is determined from eqns (6.26), (6.28) and (6.69).

For the post-upheaval buckling ($L_u \le L \le L_i$) stage, the moment curvature relationship of (6.60) becomes,

$$M_x = EI(v,_{xx} - v_i,_{xx}) = P(v_m - v) - \frac{mx^2}{2} + N \tag{6.70}$$

where $v_i,_{xx}$ is given by eqn (5.10). With the employment of the boundary conditions, typified by eqns (6.41) and (6.42), the solution of eqn (6.70) affords the characteristic equation of buckle force to be expressed as

$$\frac{q+m}{q}\sin\frac{nL}{2} + \left(\frac{nL_i}{3} - nL\frac{q+m}{2q}\right)\cos\frac{nL}{2} - \frac{nL_i}{3} = 0 \tag{6.71}$$

Equation (6.71) is evaluated for nL for given values of L_i/L; Table 6.4 shows key values for two different trench angles of 20^o and 30^o. Comments are as previously given regarding Table 5.4. Furthermore, the deflection v of the buckle curve becomes, for $0 \le x \le L/2$,

$$v = \frac{q}{EIn^4}\left(-\frac{q+m}{q}\cos n(\frac{L}{2}-2)+(\frac{nL_i}{3}-nL\frac{q+m}{2q})\sin n(\frac{L}{2}-x) + \frac{q+m}{q}-\frac{(nL)^2}{12}(2\frac{L_i}{L}-3\frac{q+m}{2q})+\frac{n^2L_ix}{3}-n^2x^2\frac{q+m}{2q}\right) \tag{6.72}$$

and the bending moment N at the crown (x=0) takes the form

$$N=\frac{q}{n^2}\left(\frac{q+m}{q}\cos\frac{nL}{2}-(\frac{nL_i}{3}-nL\frac{q+m}{2q})\sin\frac{nL}{2}+\frac{(nL_i)^2}{24}-\frac{q+m}{q}\right) \tag{6.73}$$

Again as per the previously discussed pre-upheaval case, the temperature rise $T(P_0)$ again can be evaluated from eqns (6.24) and (6.25) whereby the peel point reaction ($\phi_A qL/2-F$) of eqn (6.24) is to be replaced by $\phi_A mL/2$ and the flexural end shortening of eqn (6.26) is now replaced by

$$\begin{aligned} u_f = & \frac{1}{2}\int_0^{L/2}(v,_x)^2dx-\frac{1}{2}\int_0^{L_i/2}(v_i,_x)^2dx \\ = & \frac{1}{2}\left(\frac{q}{EI}\right)^2\frac{1}{n^7}\left(\frac{n^2}{36}(L_i-3L)^2(nL+\sin nL)+nL-\sin nL\right. \\ & +\frac{nL_i}{3}-\frac{n}{3}(L_i-3L)\cos nL \\ & +\frac{n^3L}{18}\left[L_i^2-3LL_i(\frac{q+m}{2q})+3L^2.(\frac{q+m}{2q})^2\right] \\ & +4\left[\frac{nL_i}{3}(\cos\frac{nL}{2}-1)+(-2\sin\frac{nL}{2}+nL)\frac{q+m}{2q}\right] \\ & \left.+\frac{2n}{3}(L_i-3L)\left[-\frac{nL_i}{3}\sin\frac{nL}{2}+(-2\cos\frac{nL}{2}+2)\frac{q+m}{2q}\right]\right) \\ & -\left(\frac{q}{EI}\right)^2\frac{L_i^7}{967680} \end{aligned} \tag{6.74}$$

For the post-upheaval buckling ($L>L_i$) stage, the analysis of the rigorous trenching model of Section 5.6.1.2 of the *Blister* model can still be used here.

Table 6.5 and Fig 6.6 present the results of parametric studies of the rigorous trenching model for two different trench angles of 20^{o} and 30^{o} regarding imperfections v_{om} of 100 and 250mm and employing the pipe data of Table 3.3; comparative standard *Isoprop* (m=q throughout) data are also included. The results of Table 6.5 indicate that the rigorous analysis generates an average improvement of 3.5% and 11% in upheaval temperature for $\theta=20^{o}$ and 30^{o} respectively whilst slightly lower than their *Blister* equivalents, they do relate to higher base cases. As for the *Blister* studies, the rigorous model continues the progression of increasing upheaval temperatures as the trench modelling becomes more sophisticated. Theoretically, the standard case vertical modelling remains critical with particular respect to upheaval. Although nominally related to contact undulation imperfections, an *Empathetic* data run is included in Fig 6.6 for comparative purposes upon the basis that its mathematical derivation relates to the *worst case scenario.*

6.8.2 Burial (Continuous)

Similar to the discussions in Sections 4.7.2 and 5.7.2, and again employing the pipe data of Table 3.3 and Fig 3.11, the *Isoprop* model with continuous burial is also considered for three different cover depths of h=0 (seabed mounted), 1.5D and 3D, together with the associated axial friction coefficients of 0.53, 0.58 and 0.68 respectively. The fully mobilised analysis results are shown in Table 6.6 for imperfection amplitude v_{om}=100mm with regard to burial type (a) of Fig 3.1 with q replaced by q+q' throughout the analysis. Similar to the *Empathetic* and *Blister* models, the developed *Isoprop* model generates an enhancement in upheaval temperature of 96.6% and 191.8% for h=1.5D and 3D respectively. Further upheaval enhancement is compromised as the yielding limit state occurs prior to

v_{om} (mm)	L_i (m)	Trench angle θ (degrees)		Upheaval State	Max. Temp. State	After snap State	Min. Temp. State	First Yield State	Max slope 0.1rad
100	31.655	Standard model	T	41.26	41.26	(41.26)	(32.32)	(32.33)	(34.06)
			v_m	100	100	2436	759.6	751.4	1344.7
			L	23.586	23.586	53.447	38.655	38.533	45.45
			f	136.4	136.4	582.7	351.7	350.	450.6
	31.655	20	T	42.72	42.72	(42.72)	(32.89)	(32.92)	(35.38)
			v_m	100	100	2578.2	788.8	720.2	1495.6
			L	23.386	23.386	53.654	38.655	37.655	46.277
			f	141.4	141.4	610.8	364.9	350.	481.7
	31.655	30	T	45.82	45.82	(45.82)	(34.10)	(34.30)	(36.83)
			v_m	100	100	2813.8	777.9	656.4	1562.8
			L	22.975	22.975	53.654	37.655	35.858	45.777
			f	152.2	152.2	664.3	377.9	350.	512.9
250	39.804	Standard model	T	27.51	N/A	N/A	N/A	30.68	(32.92)
			v_m	250				989.4	1324.0
			L	29.658				40.117	43.75
			f	128.7				350.	418.9
	39.804	20	T	28.46	N/A	N/A	N/A	31.0	(34.17)
			v_m	250				960.8	1441.5
			L	29.407				39.593	44.379
			f	133.6				350.	446.9
	39.804	30	T	30.49	N/A	N/A	N/A	31.76	(35.53)
			v_m	250				904.2	1493.0
			L	28.889				38.322	43.879
			f	144.0				350.	474.3

Notes :
* N/A - denotes 'stable' buckling path
* T - Temperature rise (^{o}C)
* v_m - Buckle amplitude (mm)
* L - Buckle length (m)
* f - Maximum stress (N/mm^2)

Table 6.5 Fully Mobilised Isolated Prop (*Isoprop*) Model with Rigorous Trenching Parametric Studies.

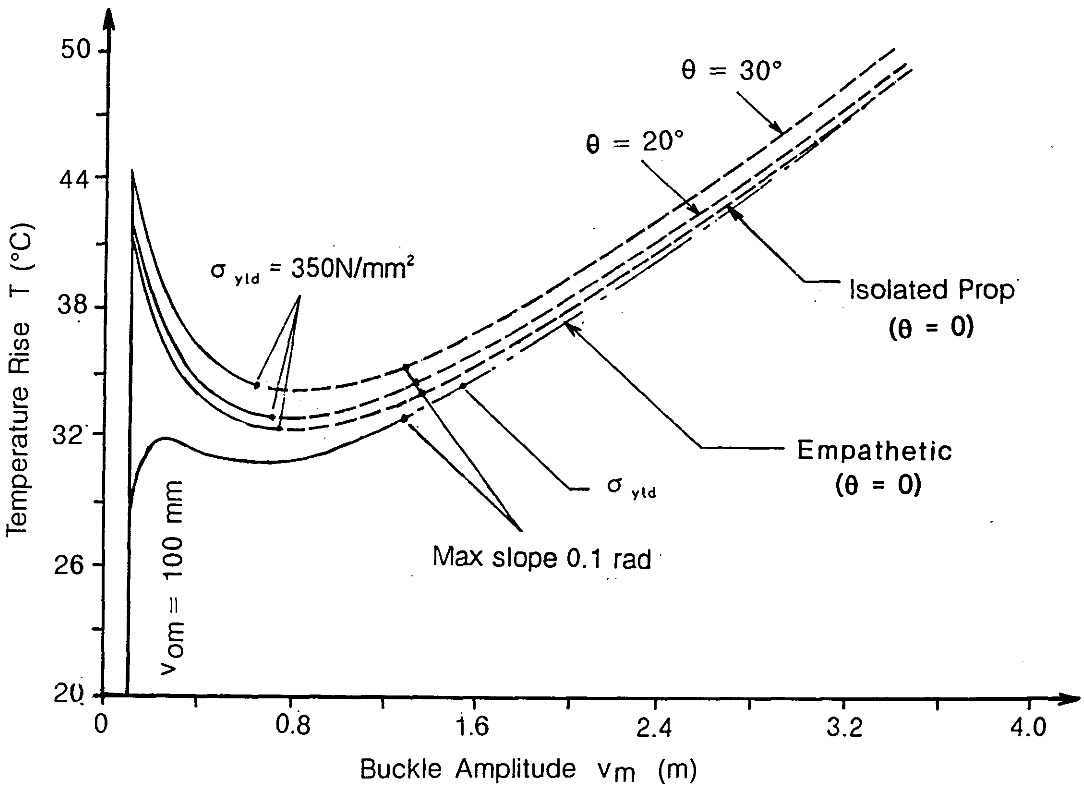

Fig 6.6 **Thermal Action Characteristics**
Fully Mobilised Isolated Prop (*Isoprop*) Model with Rigorous Trenching

v_{om} (mm)	L_i (m)	q+q' (N/mm) [ϕ'_A]		Upheaval State	Max. Temp. State	After snap State	Min. Temp. State	First Yield State	Max slope 0.1rad
100	31.655	1.144 [0.53]	T v_m L f	41.26 100 23.586 136.4	41.26 100 23.586 136.4	(41.26) 2436 53.447 582.7	(32.32) 759.6 38.655 351.7	(32.33) 751.4 38.533 350.	(34.06) 1344.7 45.45 450.6
	22.619	4.388 [0.58]	T v_m L f	81.1 100 16.854 267.2	81.1 100 16.854 267.2	(81.1) 1741 34.866 985.9	(67.75) 586.5 25.619 613.4	(75.86) 182.5 19.152 350.	(78.67) 1598 34.056 950
	18.588	9.622 [0.68]	T v_m L f	(120.43) 100 13.850 395.7	(120.43) 100 13.850 395.7	(120.43) 1279 26.307 1278.2	(105.83) 543.6 20.588 877.1	86.66 100 3.600 350.	(116.6) 1145 25.512 1152.3

Notes :
* N/A - denotes 'stable' buckling path
* T - Temperature rise (°C)
* v_m - Buckle amplitude (mm)
* L - Buckle length (m)
* f - Maximum stress (N/mm^2)

Table 6.6 Fully Mobilised Isolated Prop (*Isoprop*) Model with Continuous Burial Parametric Studies.

the upheaval state.

6.8.3 Discrete Dumping or Intermittent Burial

The topology of intermittent burial is illustrated in Fig 6.7 (a) whilst Fig 6.7 (b) shows the axial force distribution applicable upon full activation of the peel point friction reaction $\phi_A qL/2$ and of the slip length L_{s1} distributed friction force. (Prior to this stage, analysis proceeds as previously discussed for the standard topology unless the overburden slip length L_{s2} is activated for $L<L_i$ whilst checks must also be made upon the pre-upheaval flexure analysis to ascertain as to whether the overburden is also therein involved.)

The mechanics of the system are only modified with respect to the longitudinal equilibrium and compatibility expressions which are similar to those typified by eqns (5.80) and (5.81) respectively. Note that for $L<L_i$, the flexural end shortening u_f of eqn (5.81) can be evaluated from eqn (6.59) whilst for pre-upheaval studies u_f is determined from eqns (6.26) - (6.28). It is assumed, given the purpose of intermittent burial, that $L<L_D$ and $L_i<L_D$.

There are a variety of particular slip length configurations to consider when analysing these systems depending upon when the overburden slip length is activated; a program suite is strictly required for this purpose.

The results of the fully mobilised *Isoprop* model with discrete dumping are tabulated in Table 6.7 and graphically presented in Fig 6.8, the effects of varying dumping intervals and/or varying overburden having been investigated for imperfection amplitude v_{om}=100mm employing the pipe data of Table 3.3. The

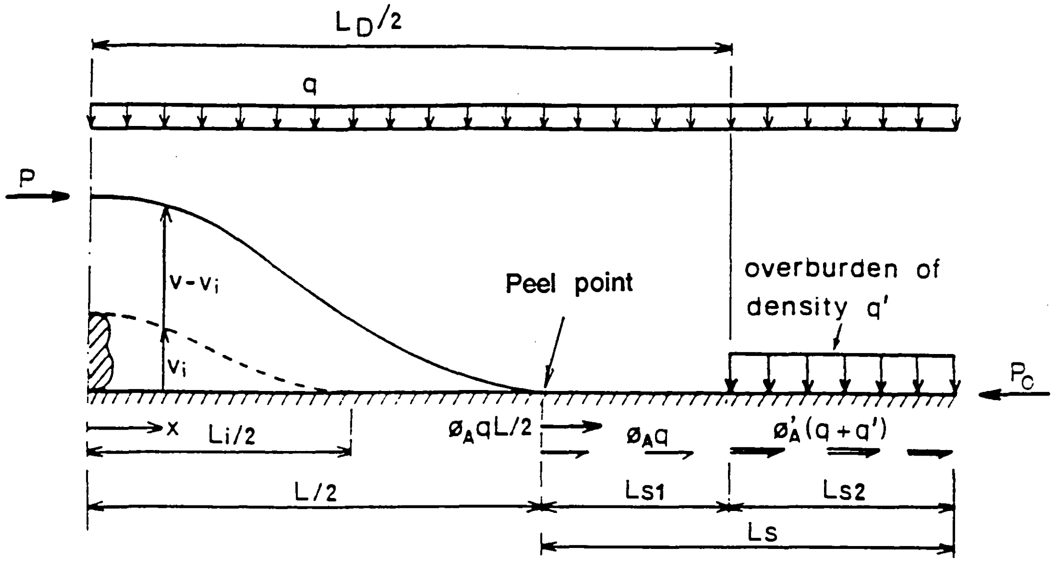

a) Topology

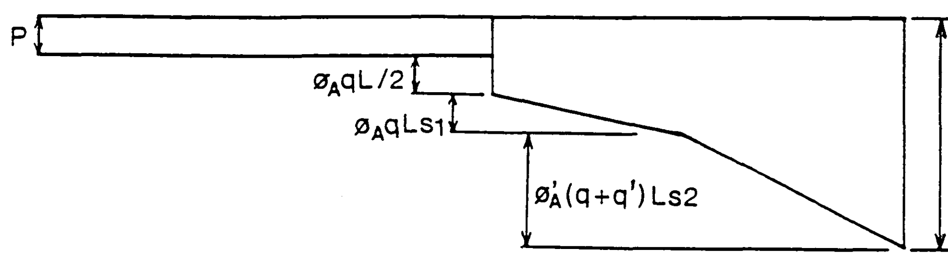

b) Axial Force Distribution

Fig 6.7 Isolated Prop (*Isoprop*) with Discrete Dumping ($L > L_i$ shown)

v_{om} (mm)	L_{-i} (m)	L_D (m) q' (N/mm) [ϕ'_A]		Upheaval State	Max. Temp. State	After snap State	Min. Temp. State	First Yield State	Max slope 0.1rad
100	31.655	100 q'=8.478 [0.68]	T	41.26	41.26	(41.26)	(37.35)	(44.76)	(60.69)
			v_m	100	100	592.2	284.6	751.4	1344.7
			L	23.586	23.586	35.947	29.586	38.530	45.45
			f	136.4	136.4	314.5	220.7	350.	450.6
		500 q'=8.478 [0.68]	T	41.26	41.26	(41.26)	(32.64)	(32.87)	(40.98)
			v_m	100.	100.	1471.8	632.6	751.4	1344.7
			L	23.586	23.586	46.600	36.655	38.530	45.45
			f	136.4	136.4	468.3	324.1	350	450.6
		1000 q'=8.478 [0.68]	T	41.26	41.26	(41.26)	(32.32)	(32.83)	(35.14)
			v_m	100.	100.	2045.5	632.6	751.4	1344.7
			L	23.586	23.586	50.986	36.655	38.530	45.45
			f	136.4	136.4	539.9	351.7	350.	450.6
100	31.655	standard model q'=0	T	41.26	41.26	(41.26)	(32.32)	(32.33)	(34.06)
			v_m	100.	100.	2436.0	759.6	751.4	1344.7
			L	23.586	23.586	53.447	38.655	38.530	45.45
			f	136.4	136.4	582.7	351.7	350.	450.6
		100 q'=1.823 [0.55]	T	41.26	41.26	(41.26)	(35.57)	(36.74)	(42.68)
			v_m	100.	100.	1223.4	473.3	751.4	1344.7
			L	23.586	23.586	44.258	33.654	38.530	45.45
			f	136.4	136.4	432.5	283.4	350.	450.6
		100 q'=3.680 [0.60]	T	41.26	41.26	(41.26)	(36.63)	(39.86)	(49.26)
			v_m	100.	100.	853.5	330.5	751.4	1344.7
			L	23.586	23.586	39.966	30.586	38.530	45.45
			f	136.4	136.4	370.1	237.5	350.	450.6

Notes :
* T - Temperature Rise in (°C)
* v_m - Buckle Amplitude in (mm)
* L - Buckle Length in (m)
* f - Maximum Stress in (N/mm^2)

Table 6.7 Fully Mobilised Isolated Prop (*Isoprop*) Model with Discrete Dumping Parametric Studies.

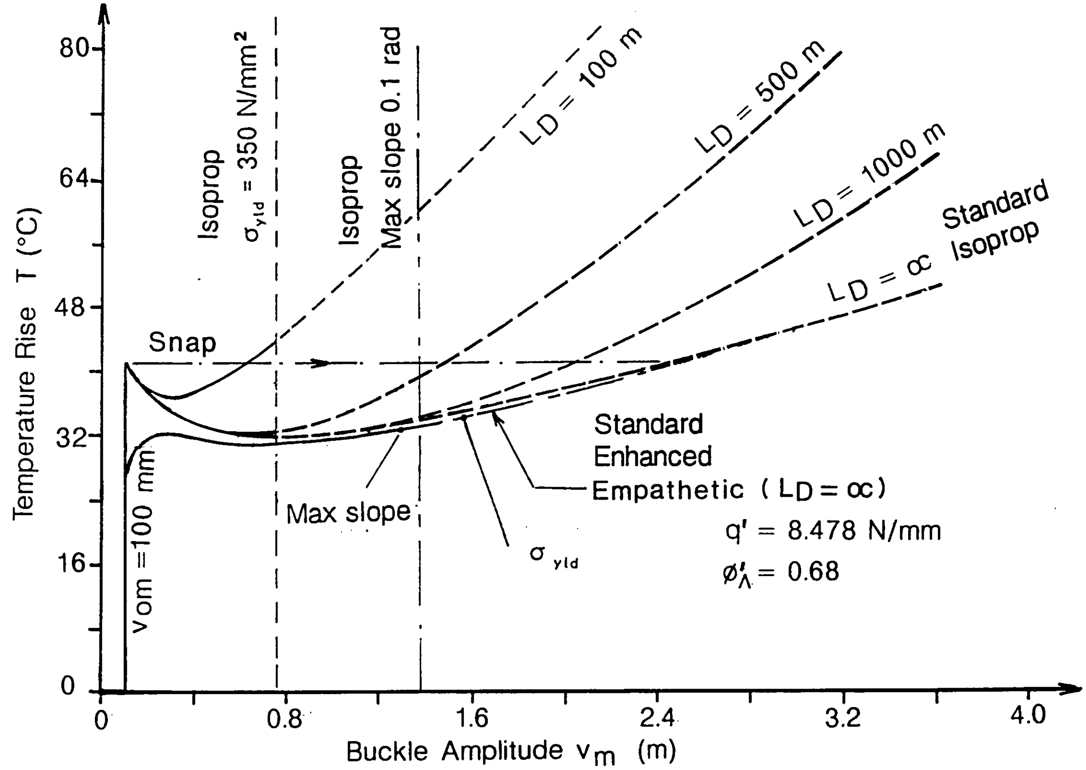

a) Effects of varying Dumping interval L_D

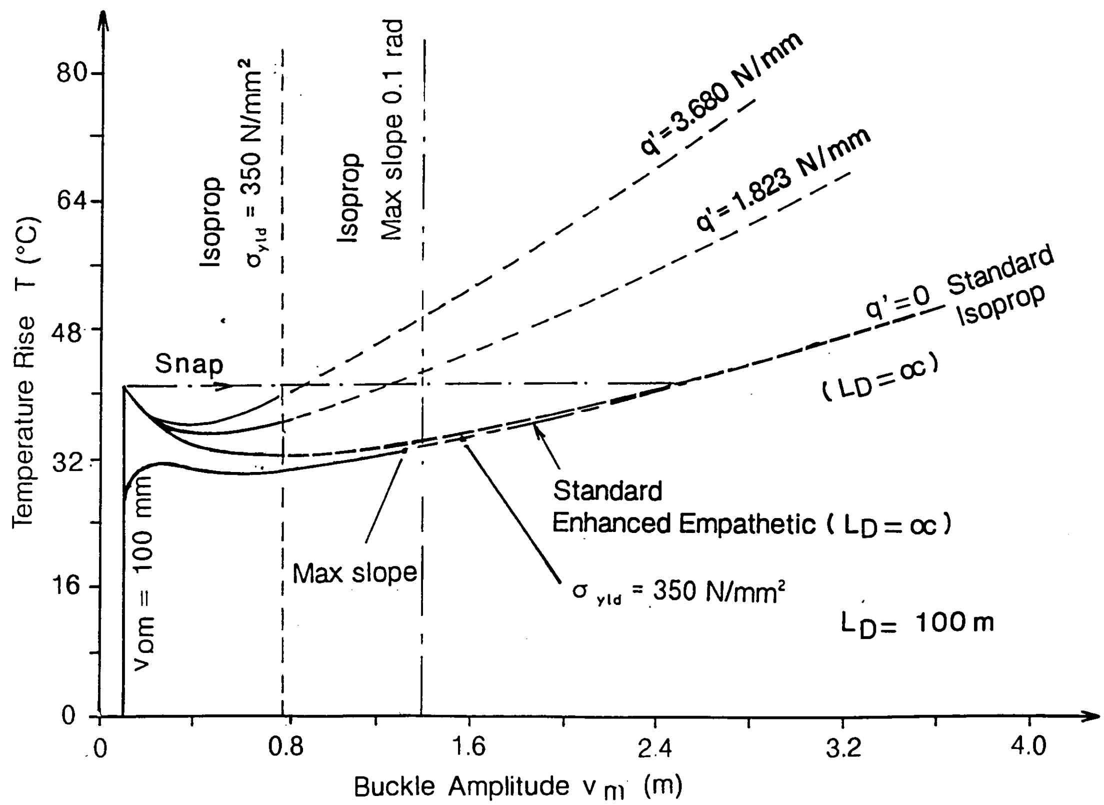

b) Effects of varying overburden q'

Fig 6.8 Thermal Action Characteristics
Fully Mobilised Isolated Prop (*Isoprop*) Model with Discrete Dumping

overall impression from Figs 6.8(a) and (b) is that the developed model generates a stiffer post-upheaval response in all cases. The operating temperatures are generally restricted to T_u=T_{max} for the unstable/snap cases; for stable responses, typically L_D=100m and q'=8.478N/mm, such temperatures may be increased upto $T_{\sigma yld}$ (about 8% higher than T_u) should upheaval be allowed for during operation.

When comparison is made with Tables 4.3 and 5.7 of the respective *Empathetic* and *Blister* models, it can be seen that, for q'=8.478N/mm, all three models exhibit the same snap buckling phenomenon for both the L_D=500 and 1000m cases, noting a little increase in T_{min} (less than 0.4^{o}C) when L_D reduces from 1000m to 500m. However, a further reduction of L_D to 100m would change the state of thermal response from dynamic snap buckling to a stable path configuration, this feature again being common for all three models.

With respect to the effect of varying overburden, Tables 5.7 and 6.7 indicate that both developed *Blister* and *Isoprop* models generate the same snap buckling response in all cases as per the standard model, whilst the corresponding *Empathetic* model exhibits a stable buckling throughout, providing a more efficient enhancement over the respective standard model, noting Table 4.3.

In keeping with the former contact undulation studies of Sections 4.7.3, 4.7.4, 5.7.3 and 5.7.4, no improvement in resistance is recorded until $L+2L_s \geq L_D$ (or L_{fap}, see below). It is not necessarily the case, however, that $L_s|_{Tu}$=0 nor that $L<L^*$ in the proximity of upheaval.

6.8.4 Fixed Anchor Points

Noting the discussions in Sections 4.7.4 and 5.7.4, the respective topology is shown in Fig 6.9 together with the appropriate axial force distribution; the figure relates to the case of the peel point friction force $\phi_A qL/2$ being activated and the fully mobilised axial friction force $\phi_A q$ being generated throughout the slip length $(L_{fap}-L)/2$, where L_{fap} denotes the spacing of the fixed anchors, and $L_{fap}>L>L_i$. The modified longitudinal equilibrium and compatibility expressions of eqns (5.82) and (5.83) can still be used here, and the evaluation of the flexural end shortening u_f is to be carried out in the same manner to that of the discrete dumping case.

Table 6.8 and Fig 6.10 present results of the *Isoprop* model with fixed anchor points employing the pipe data of Table 3.3. The results are tabulated for imperfection amplitudes v_{om} of 100 and 250mm and three different anchorage spacings of 100, 500 and 1000m have been considered for each case. Similar to the discrete dumping case discussed in Section 6.8.3, the developed model shows no effect with respect to the upheaval temperatures for the chosen L_{fap} values. However, with particular emphasis upon the operating temperatures should they not be restricted to T_u for the stable cases, typically v_{om}=250mm, the model does provide a percentage improvement of 6.5% in $T|_{\sigma yld}$ over the standard case ($L_{fap}=\infty$), whilst at closer anchorage spacing of L_{fap}=100m, where the maximum anchor shear capacity state occurs prior to the yielding state, the developed model generates a better enhancement of 84.6%.

Comparison is also to be made with Tables 4.4 and 5.8 of the corresponding *Empathetic* and *Blister* models. It can be seen that both of these models

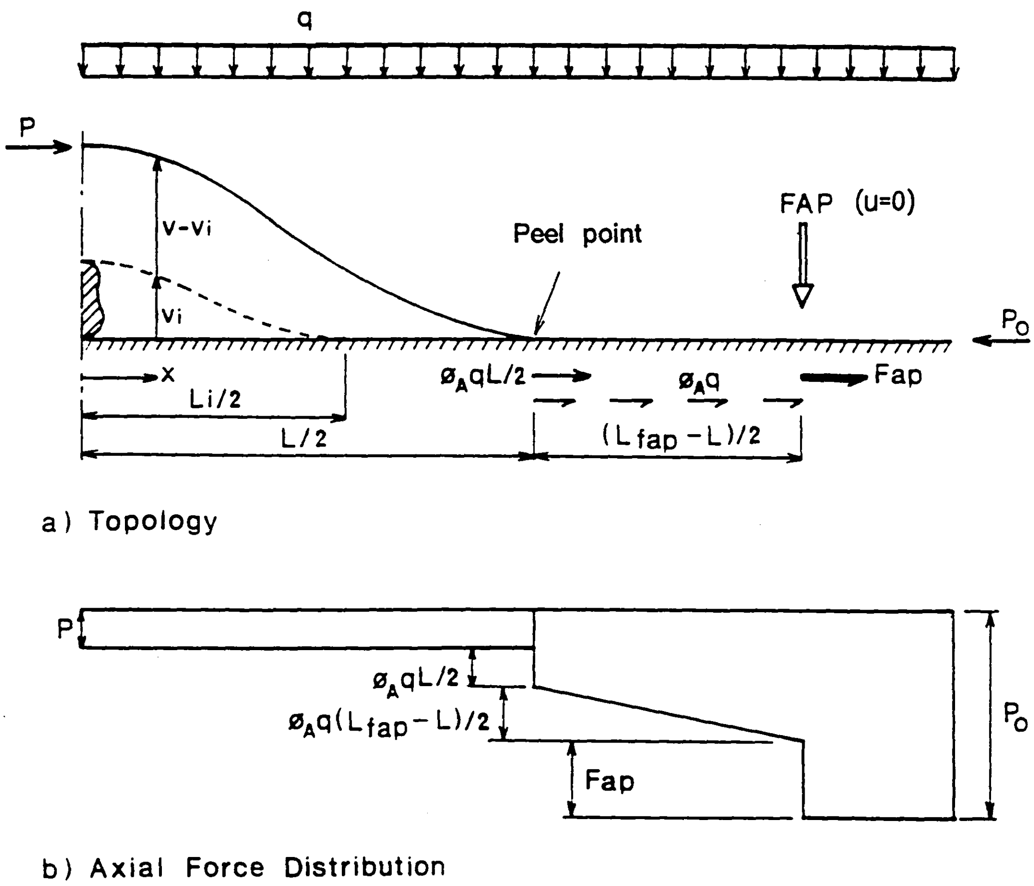

Fig 6.9 Isoprop Model with Fixed Anchor Points $(L_s=(L_{fap}-L)/2$ shown)

v_{om} (mm)	L_i (m)	L_{fap} (m)		Upheaval State	Max. Temp. State	After snap State	Min. Temp. State	First Yield State	Max slope 0.1rad	Max F_{ap} at 750 kN
100	31.655	100	T	41.26	41.26	(41.26)	(37.88)	(59.18)	(117.5)	(59.43)
			v_m	100	100	424.5	243.7	751.4	1344.7	754.9
			L	23.586	23.586	32.581	28.586	38.530	45.45	38.585
			f	136.4	136.4	268.8	204.8	350.	450.6	350.7
		500	T	41.26	41.26	(41.26)	(32.74)	(32.96)	(40.61)	(57.09)
			v_m	100.	100.	1378.	693.8	751.4	1344.7	1995.
			L	23.586	23.586	45.757	37.655	38.530	45.45	50.655
			f	136.4	136.4	454.8	337.8	350	450.6	534.2
		1000	T	41.26	41.26	(41.26)	(32.32)	(32.33)	(34.28)	(61.89)
			v_m	100.	100.	2008.6	759.6	751.4	1344.7	3152.
			L	23.586	23.586	50.740	38.655	38.530	45.45	57.235
			f	136.4	136.4	535.7	351.7	350.	450.6	652.8
250	39.804	100	T	27.51				(75.63)	(114.4)	56.65
			v_m	250.	N/A	N/A	N/A	989.4	1324.0	786.8
			L	29.658				40.117	43.75	38.032
			f	128.7				350.	418.9	301.1
		500	T	27.51				32.86	(44.53)	(56.91)
			v_m	250.	N/A	N/A	N/A	989.4	1324.0	1976.
			L	29.658				40.117	43.75	49.161
			f	128.7				350.	418.9	519.5
		1000	T	27.51				30.68	(35.26)	(61.70)
			v_m	250.	N/A	N/A	N/A	989.4	1324.0	3106.8
			L	29.658				40.117	43.75	55.904
			f	128.7				350	418.9	650.6

Notes :
- * N/A - denotes 'stable' buckling path
- * T - Temperature rise (°C)
- * v_m - Buckle amplitude (mm)
- * L - Buckle length (m)
- * f - Maximum stress (N/mm^2)
- * F_{ap} - Anchor shear capacity (kN)

Table 6.8 Fully Mobilised Isolated Prop (*Isoprop*) Model with Fixed Anchor Points Parametric Studies.

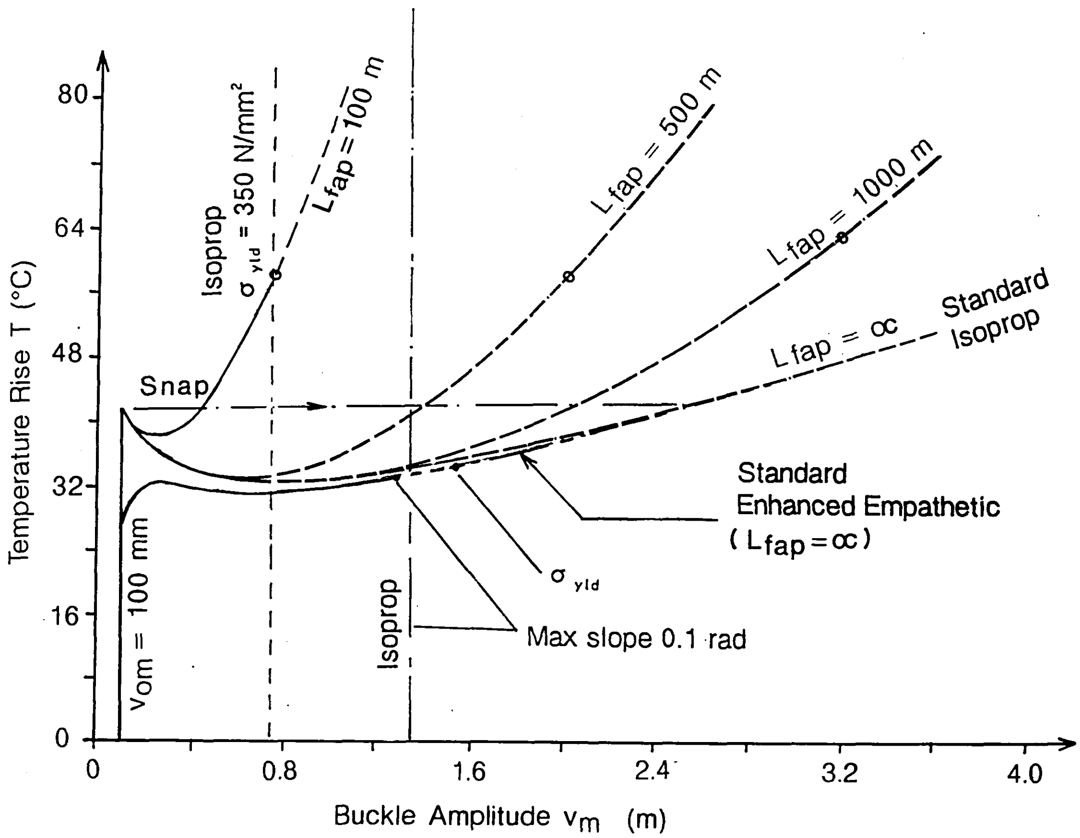

Fig 6.10 **Thermal Action Characteristics**
Fully Mobilised Islated Prop (*Isoprop*) Model with Fixed Anchor Points

o denotes F_{ap} = 750 kN

generate a similar thermal buckling response at the smaller imperfection v_{om}=100mm ie dynamic snap buckling occurred with L_{fap}=100m and stable response occurred at $L_{fap} \geq 500$m. This is contrary to the respective developed *Isoprop* model which still exhibits the same unstable response even as L_{fap} reduces from 1000m to 100m. At the larger imperfection v_{om}=250mm all three models produce the same stable buckling response as per their respective standard models.

6.9 Discussions

The standard *Isoprop* model herein proposed is quite distinct from previously recorded formulations[13,49]; unlike these alternative models, the present proposal affords elastically imperfect behaviour, typified by Figs 6.5, 6.6, 6.8 and 6.10, largely consistent, ie upto yield and large rotation limits, with the concept that imperfect loci are conservative relative to the corresponding idealised solutions. Alternative modelling[13,49] actually suggests that for any prop (imperfection) amplitude v_{om}, the lift-off buckling force corresponds identically to that afforded by idealised (ie non-imperfect) studies for $v_m=v_{om}$ as identified by eqns (6.36) and (6.37)[7,11]. Herein, the lift-off or upheaval state, so important to offshore designers, is shown to suffer a potential 37% degradation in this resistance if the existence of a supposedly previous yet totally hypothetical, indeed fictional, *stress-free-when-straight* state is questioned. Further, the similarity in the respective upheaval lengths L_u as suggested by eqns (6.35) and (6.37) belies more substantial differences in the appropriate action/response characteristics as typified by Fig 6.5.

The deformation characteristics given by eqn (5.7) are accepted for the present model on the basis of the support provided for eqn (5.8) by field observations[27]. However, the precise stressing formulation given by eqn (6.40) is not considered to reflect an accurate assessment of the state of residual stress in the pipe in the as-laid state. Not only does the acceptance of eqn (6.40) in conjunction with eqn (5.7) require the existence of an historically fictitious idealised lie, it also requires that residual stress due to fabrication and laying operations[41,48] can, by comparison, be safely ignored. Given the complexities attending the hostile environment involved[48], it is considered inappropriate and high risk to construct the analysis other than in accord with that well-established principle of elastic stability whereby the datum is prescribed as being *stress-free-when-initially-deformed*[4]. As noted above, the effect is duly conservative. The model could accommodate definitive and comprehensive residual stress data, should it become available.

Further support for this approach is available from infilled prop studies which similarly suppress *any* supposed as-laid residual stressing[20,22,24,48]. Therein, such stressing is considered to be relieved under in-service conditions due to the interaction of non-linear fill accretion and slip length axial friction behaviour with *thermal* cyclic loading[20,36]. The prototypes corresponding to the isolated and infilled prop topologies share the common features of actually complex non-linear axial friction behaviour and the initial bending moments supposedly suggested by eqn (6.40). Therein, idealised theory indicates that 50% N_i, the crown and maximum moment, is due to self-weight considerations, the remainder being due to the prop imperfection *per se* in the form $6EIv_{om}/L_i^2$. Although lacking fill support to assist in cyclic thermal stress-relieving, it is surely inconceivable to suggest these components will accurately reflect in-service residual stress levels following numerous cycles of in-service non-linear axial friction response[20,36]. Indeed, in-service *pre-upheaval* flexural and axial movement can occur by design with this prototype - the buckle length/temperature rise locus of Fig 6.5 is particularly relevant here - and consequent as-laid stress relief due to the onset of localised plasticity under thermal loading must be considered highly probable in a manner similar to that discussed elsewhere[48]. Such 'conversion' into an imperfection of form would clearly be influenced by the out-of-straightness ratio v_{om}/L_i. Noting eqn (5.8), then the ratios corresponding to the case-studies are 1/532 and 1/139 respectively and are considered typical of offshore practice.

Similar to the *Blister* model, the effects of employing enhanced burial and anchorage techniques is clearly shown in Figs 6.6, 6.8 and 6.10 with overall enhancement being achieved as anticipated[36,47]. Imperfection-based data is thereby made available for design purposes; maximum operating temperature/pressure rises - recall the arguments concerning pressure-equivalent parameter T' in eqn (1.16) - clearly cannot exceed $T_u=T_{max}$ for unstable/snap cases, whilst the onset of yield stress or finite rotations ($v,_{xmax}< 0.1^r$) delimits the stable post-buckling cases studies as shown in Figs 6.5, 6.6, 6.8 and 6.10. Whilst a closed-form solution is available for the crucial upheaval buckling force P_u as given by eqn (6.34), closed-form evaluation of T_u is not computationally amenable assuming the development of slip length friction forces during pre-upheaval flexure. Maximum curvature, important to the buckling mechanism, occurs at the crown throughout. It increases from the imperfection value given by eqn (5.11) to $-0.106qL^2/EI$ $(L\equiv L_u)$=$-0.0588qL_i^2/EI$ at upheaval; these latter values are available from eqn (6.21) with $P=P_u$.

Qualitatively, the *Isoprop* model action/response characteristics differ from those associated with contact undulation models, recall Fig 1.7, by virtue of the *cusp* upheaval - note Figs 6.5, 6.6, 6.8 and 6.10. Whilst the interesting asymmetric implications (note below) have been discussed elsewhere[40], the cusp is associated with the fact that the pre-buckling flexure phase, unavailable to contact undulation models, results in a singular change in direction, upon upheaval, of wavelength propagation (L) as amplitude continues its monotonic path. Intriguingly, solution data for the post-buckling $L>L_i$ phase corresponds with that produced by the previously discussed equivalent *Blister* model (for common prop height v_{om}) - recall Fig 1.7(c) and Chapter 5. The implication is that whilst infilling of the voids reduces resistance to upheaval by preventing pre-upheaval flexural energy release, by the post-buckling state $L=L_i$, buckling force behaviour is effectively common for the two cases.

6.10 Summary

By not requiring reference to a fictitious *stress-free-when-straight* datum, the *Isoprop* model described herein is considered to present a consistent elastic interpretation of the corresponding prototype behaviour subject only to the provision of accurate residual, as-laid stressing data; this is a common feature of all elastic subsea pipeline buckling models available in literature. However, this is a complex matter; for example, whilst residual laying tension should improve buckling resistance perhaps beyond idealised values, field observations have shown buckling failures. The proposed model thereby suggests interpreting the prop as generating an imperfection of form on the basis of a *worst case* scenario; whilst it is not suggested that the stress-relieving mechanism discussed would remove *all* as-laid, residual stressing, the fact that some degree of relief is highly probable under in-service, pre-upheaval, cyclic operation demands this *stress-free-when-initially-deformed* proposal must be considered given its relatively conservative implications.

Chapters 4,5 and 6 have set out three particular imperfect subsea pipeline buckling models, two of which, the *Blister* and *Isoprop* models, relate directly to physical configurations. Activity 3 of Fig 2.1 is therefore complete subject to the experimental testing employing these two physical configuration albeit to small scale. Imperfection loci breaches of the corresponding idealised envelopes becomes a more pertinent factor with this reduction in scale and is discussed in the following chapter.

Chapter 7

Thermo-Mechanical System Experimentation

7.1 Introduction

Whilst theoretical studies of upheaval buckling have been available in literature for more than a decade, experimental programmes have to-date been largely restricted to those required for the provision of necessary empirical data. Experiments have focussed upon the geotechnical/structural interface characteristics associated with pull-out and friction tests[8,13,25,36]. Full thermo-mechanical pipeline buckling experimentation is both complex and costly - prototype field parameters include L_i (Fig 1.7) occupying approximately 24m [27] whilst buckling can typically affect upto 100m of pipe[13]. Following the recent disclosure of in-service failures[24,25,26] a number of full system experimental programmes have been established[38,50] and herein presented are the results of a series of model tests involving both isolated and infilled prop topologies - recall Fig 1.7. These results are compared with the respective output from the in-house developed suite of computer-based theoretical models. It is considered that the upheaval state is of crucial or particular importance to design engineers.

The proposed *Isoprop* and *Blister* models discussed in Chapters 5 and 6 are based upon actual physical imperfections whilst the *Empathetic* model derives from mathematical reasoning. Whilst the *Blister* model generates a solution in keeping with that provided by an elastic interpretation of an infilled prop formulation available elsewhere[20], the *Isoprop* model generates a solution at odds with its predecessors[13,49]. However, solutions for nL, $L \geq L_i$ for both the *Isoprop* and *Blister* models are in agreement which supports the case for the former given the latter's support elsewhere[20] and the anticipated reduction of initial imperfection effects as post-upheaval buckling develops[5].

Given the obvious importance to designers of the upheaval state, Table 7.1 summarises the key, individual characteristics of the various models concerned at upheaval for a common imperfection amplitude v_{om}. Upheaval is determined in each case by reducing initial post-buckling amplitude expressions $v_m \rightarrow v_{om}$; for example, use is made of eqns (1.20),and (5.28) here. For the *Isoprop* model, upheaval can also be computed by reducing the pre-upheaval force to zero. Numerical limitations affect the *Blister* model definition as shown by the non-zero upheaval length in Table 7.1. Upheaval curvatures, inversely proportional to the upheaval temperatures as indicated, are themselves proportional to the respective upheaval buckling force.

For a given v_{om}, the *Blister* model is seen to offer the most severe case; as already discussed in Section 5.8, however, the *Empathetic* model can reverse this situation if commonality is based upon a given imperfection wavelength [L_o=L_i as per eqn (5.85)] or upon an idealised-related zero vertical peel point height [ie eqn (5.84)].

The upheaval temperatures quoted in Table 7.1 presume zero frictional resistance as indicated by eqn (4.17). Employing the pipe characteristics given in Table 7.2 with v_{om}=30mm - these values are relevant to the experimental programme discussed shortly - full system numerical analysis affords upheaval

Phenomenon	Model	Upheaval Length $L_{(u)}$ (*) as $v_m \to v_{om}$		% Idealised Buckle Force at Upheaval	Upheaval Temperature (**) Coefficient of respective individual (***)	Upheaval Temperature (**) based on
		$\%L_o$	$\% L_i$	$3.962(EIq/v_{om})^{\frac{1}{2}}$	$(q/AE\alpha)(1/curv)_u\|_{crown}$	$0.078(q/AE\alpha)[L_o^2/v_{om}]$
Isolated Prop	*Isoprop*	96	74.5	63	-4.98	1.57
	Refs 13 and 49	100	77	100	N/A	2.49
Contact Undulation	*Empathetic*	100	77	40	-2.24	1.0
	Blister (****) and Ref 20 (elastic)	27.6	21.4	25.2	-1.42	0.63

Notes:

- $(curv)_u$ denotes $(v_{,xx})_u$ or $v_{o,xx}$ or $v_{i,xx}$
- (*) For common v_{om}, L_i=1.2904 L_o
- (**) Assume L_s=0 and $\phi_A qL/2$ (+F)<< P_u at upheaval
- (***) Employing respective model's $v|_u = f(x)$
- (****) Numerical limitations restrict upheaval to 100.05% v_{om} (see Table 5.1)

Table 7.1 Model Characteristics at Upheaval for Common Initial Amplitude v_{om}

Parameter	Symbol	Value	Unit
External diameter	D	9.53*	mm
Wall thickness	t	1.6*	mm
Direct modulus	E	195000	N/mm^2
Effective inertial self-weight**	q	0.00341	N/mm
Limiting linear stress	σ_y	113	N/mm^2
Thermal coefficient	α	$11x10^{-6}$*	$/^oC$
Axial friction coefficient	ϕ_A	0.2	
Poisson's ratio ***	ν	0.3	

Table 7.2 Pipe parameters (D=9.53mm)

nb * From RJB Stainless, Birmingham

** For dry environment experimental purposes involving lock-off post-flow initiation, q is full weight plus water contents

*** ν employed for the evaluation of pressure component as required.

Laboratory restrictions; $v_m|_{max}$=50mm; L_{fap}=5.68m≥L_{buckle}

temperatures less than 1.5% above those given in Table 7.1 with respect to the *Empathetic* and *Blister* models whilst for the *Isoprop* model the variation is in excess of 10% at v_{om}=30mm as upheaval follows frictional slip length development during the pre-upheaval flexural stage.

It is now proposed to place the foregoing theories within the context of physical testing. Both Isolated Prop and Infilled Prop type physical configurations are investigated. Economic considerations dictate small-scale testing, with additional recourse to the use of *fixed anchor points*[9,39] being demanded to further restrict length-of-pipe requirements (see later). As already discussed, in prototype practice, resistance to upheaval buckling is enhanced by trenching, burial, continuous or discrete, and/or the use of fixed anchors.

7.2 Experimental Programme

7.2.1 General

Initially, a series of theoretical case-studies was conducted to identify the typical overall lengths-of-pipe required ($L+2L_s$) to permit observation of thermo-mechanical contact surface buckling at small scale. A typical case-study for v_{om}=30mm is illustrated in Fig 7.1. It was thereby concluded that a 6m length of seamless ferritic stainless steel pipe of 9.53mm O.D. should prove suitable when used in conjunction with fixed anchor restraints; Fig 7.2 typifies prototype D/t scaling features. Tensile tests showed the roundhouse constitutive locus[51] to be satisfactorily linear upto a stress σ_y=110 N/mm^2 with a direct modulus of 195kN/mm^2 as shown by Fig 7.3. Further pipe data is given in Table 7.2.

Notes: $v_m|_{\sigma_{yld}}$ (*Empathetic*) > $v_m|_{L=L_{fap}=5.68m}$ *

$v_m|_{0.1r}$ (*Empathetic*) = 166.4 mm > v_m = 50mm *

$v_m|_{\sigma_{yld}}$ (*Isoprop & Blister*) = 130.8 mm > v_m = 50 mm *

$v_m|$ (*Isoprop & Blister*) > $v_m|_{L=L_{fap}=5.68m}$ *

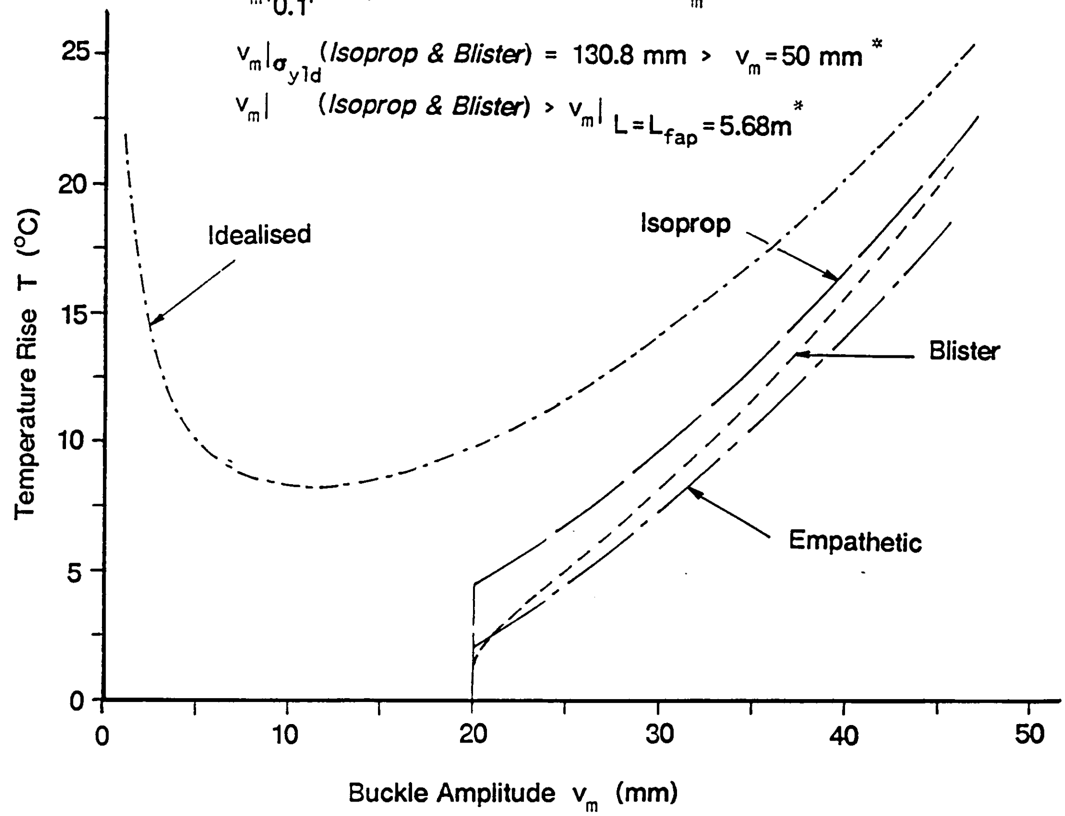

* Refer to Section 7.2.2 for physical limitations of the Test Rig

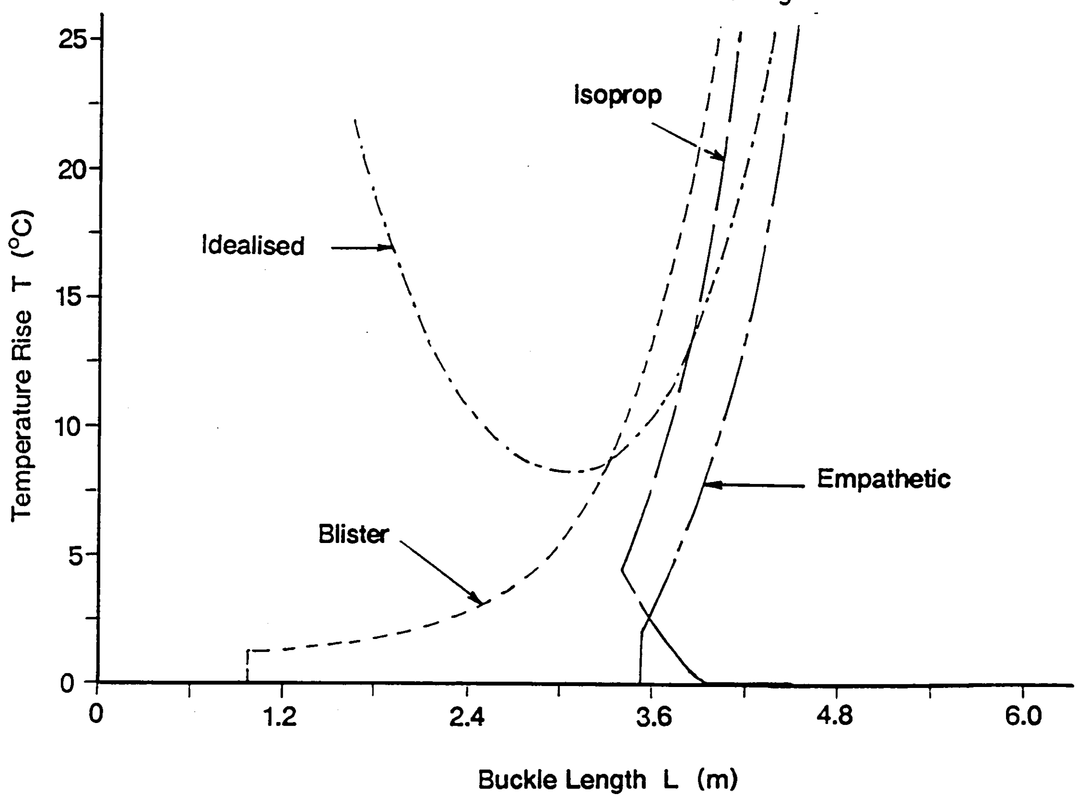

Fig 7.1 Thermal characteristics responses of various models

L_{fap} = 5.68 m

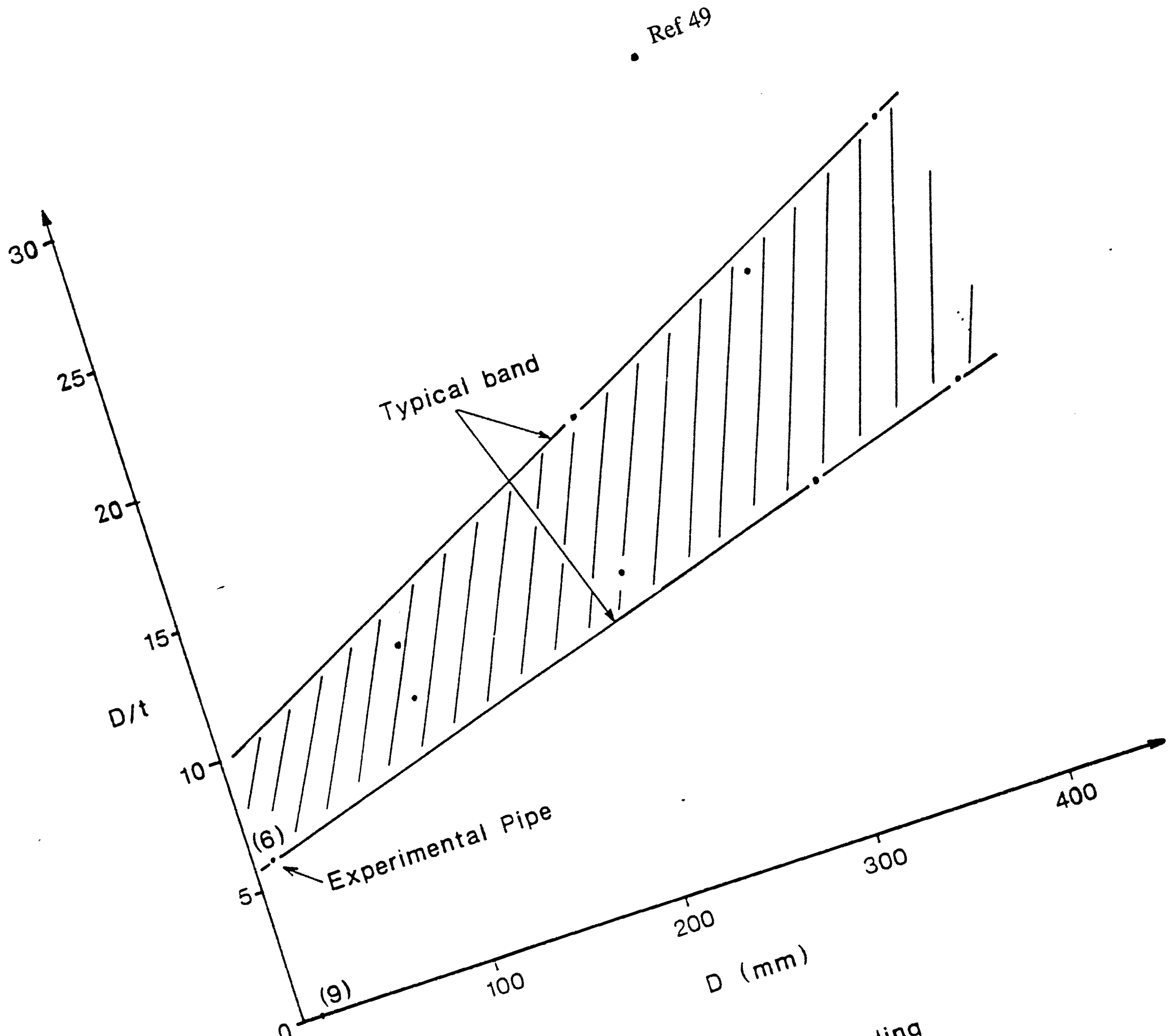

Fig 7.2 Pipe Scaling

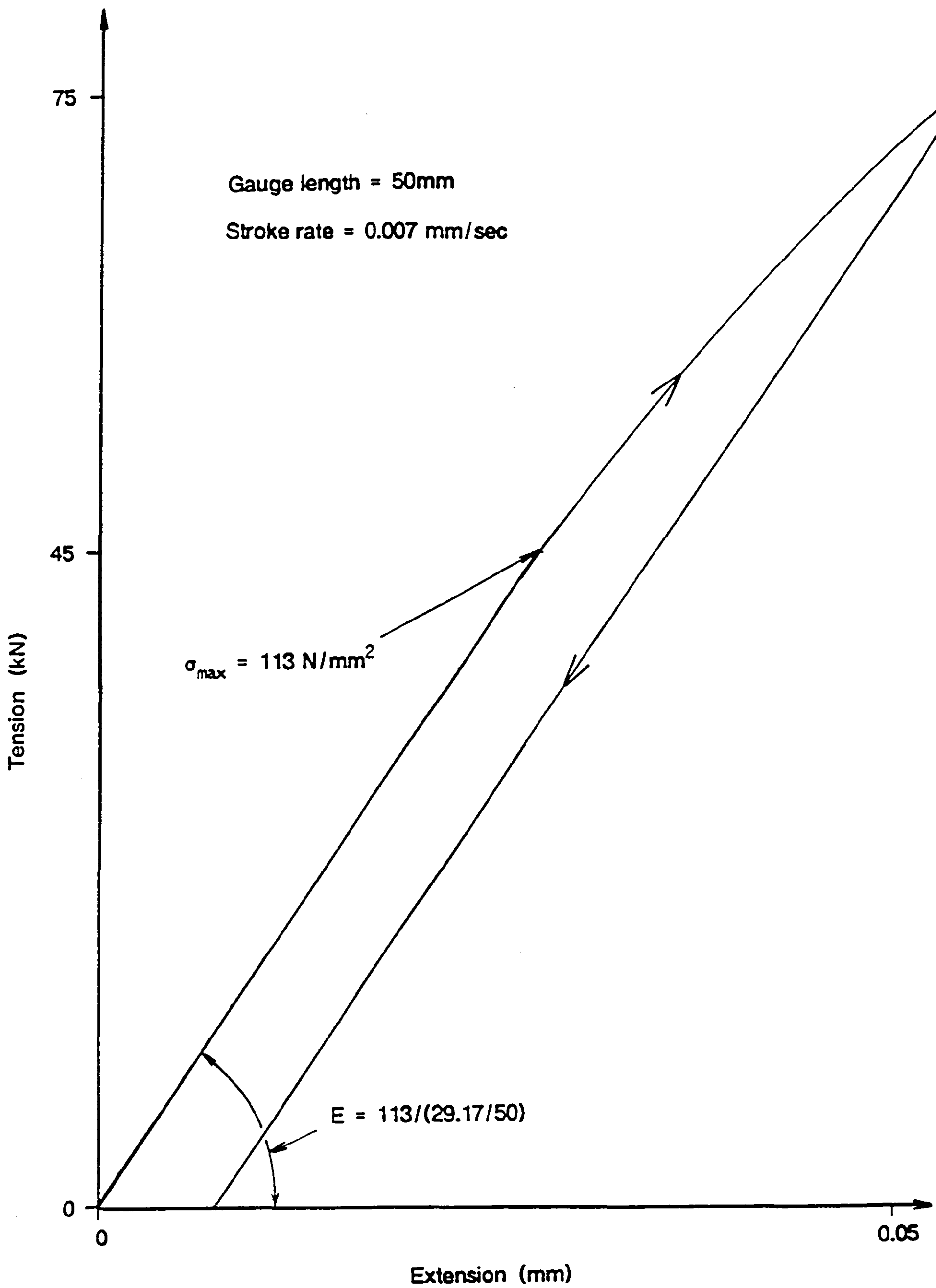

Fig 7.3 Experimental Tensile Tests on 400mm Samples using ESH servo-hydraulic testing machine

7.2.2 The Test Rig

The essential details of the pipeline rig are illustrated in Figs 7.4 and 7.5; although electrical trace heating was considered, design calculations showed heated water could provide the necessary thermal action more cost-effectively. Briefly, the pipe lies in contact with a sheet of phenolic coated 18mm ply and is anchored at approximately 6m centres; the ply is fixed onto a thermally insulated bed or spine consisting of a water filled a 100x100x6.3 RHS. PTFE-coated PVC alignment blades or gates ensure vertical buckling with a minimum of frictional interference whilst, initially regarding isolated prop modelling, a steel blade acts as a centrally located prop. Inlet and outlet pipe wall temperatures (to 0.01^{o}C accuracy) and water pressures are monitored and displacement gauges check for any pipe/anchor slippage. Upheaval or lift-off is precisely monitored by a simple make-or-break electrical contact whilst a second make-or-break enables the $\pm$ 0.02mm digital calliper employed for amplitude measurement to be read with a minimum of physical contact with the pipe, see Plate 9 for details. The water heater/cooler permits the setting of discrete thermal increments. The appropriate pipe/contact surface axial friction coefficient as noted in Table 7.2 was determined from subordinate pre-testing of the form discussed in Chapter 3.

Given the obvious difficulties in acquiring idealised, stress-free, straight subsea pipeline lies following prototype laying operations[41], the 9.53mm O.D. pipe was employed as-delivered although the absence of welding is to be noted. The length of pipe was emplaced on the levelled contact surface and over the prop imperfection to as good a centralised lie as possible without restraint. The gates, which featured adjustable blades, were located with $\leq$1mm clearance to

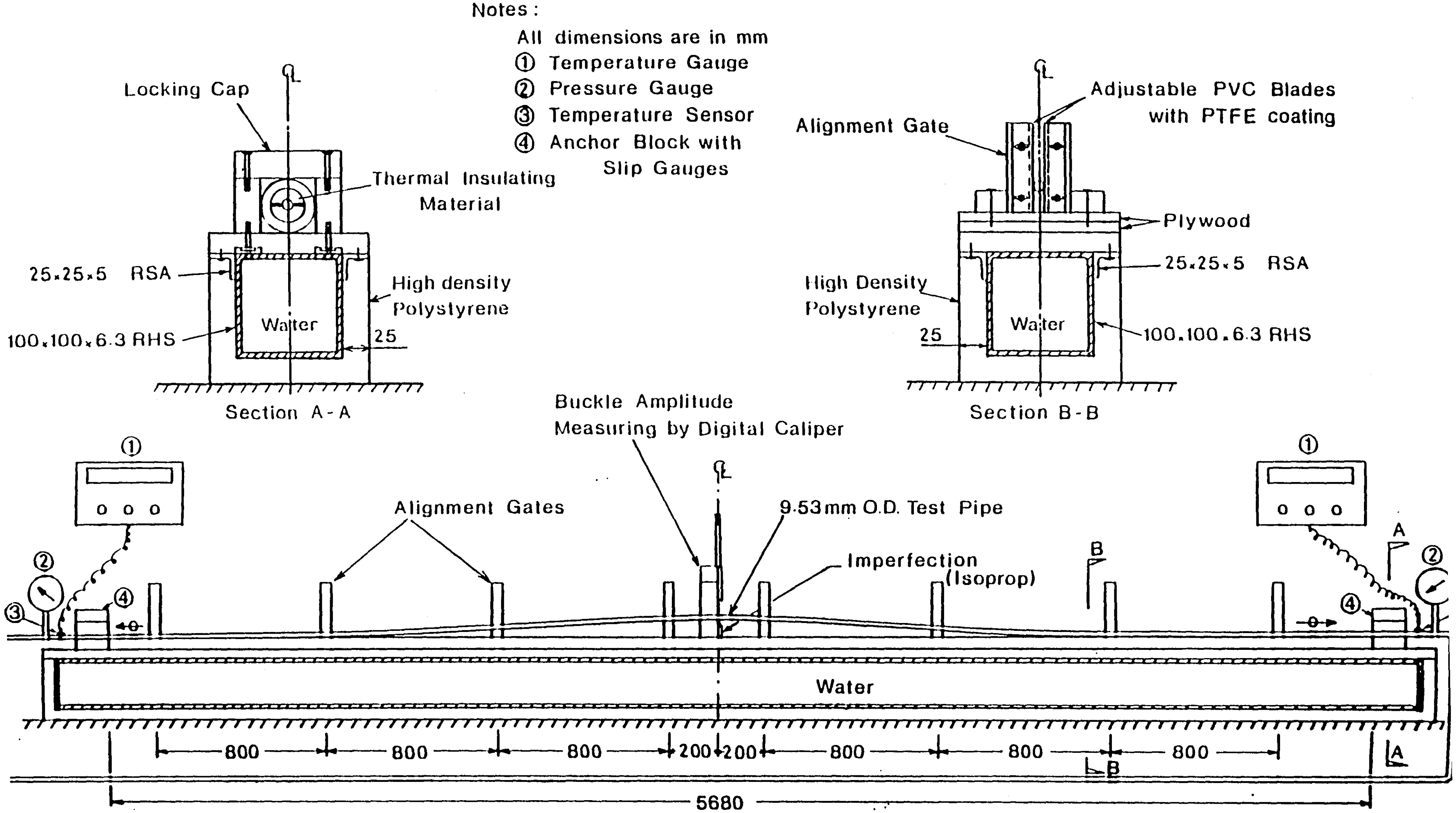

Fig 7.4 Pipe Experimentation

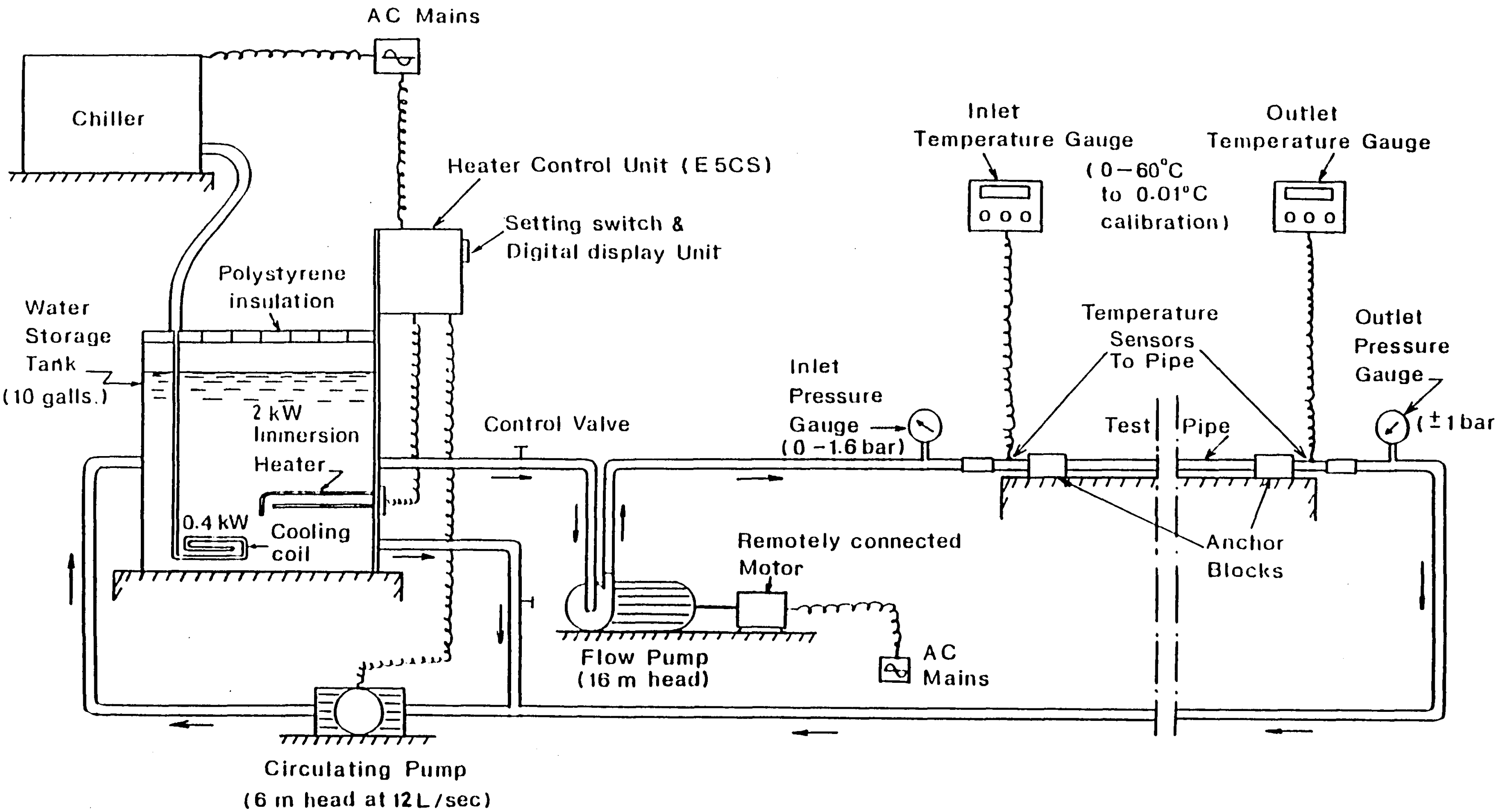

Fig 7.5 Control and Monitoring

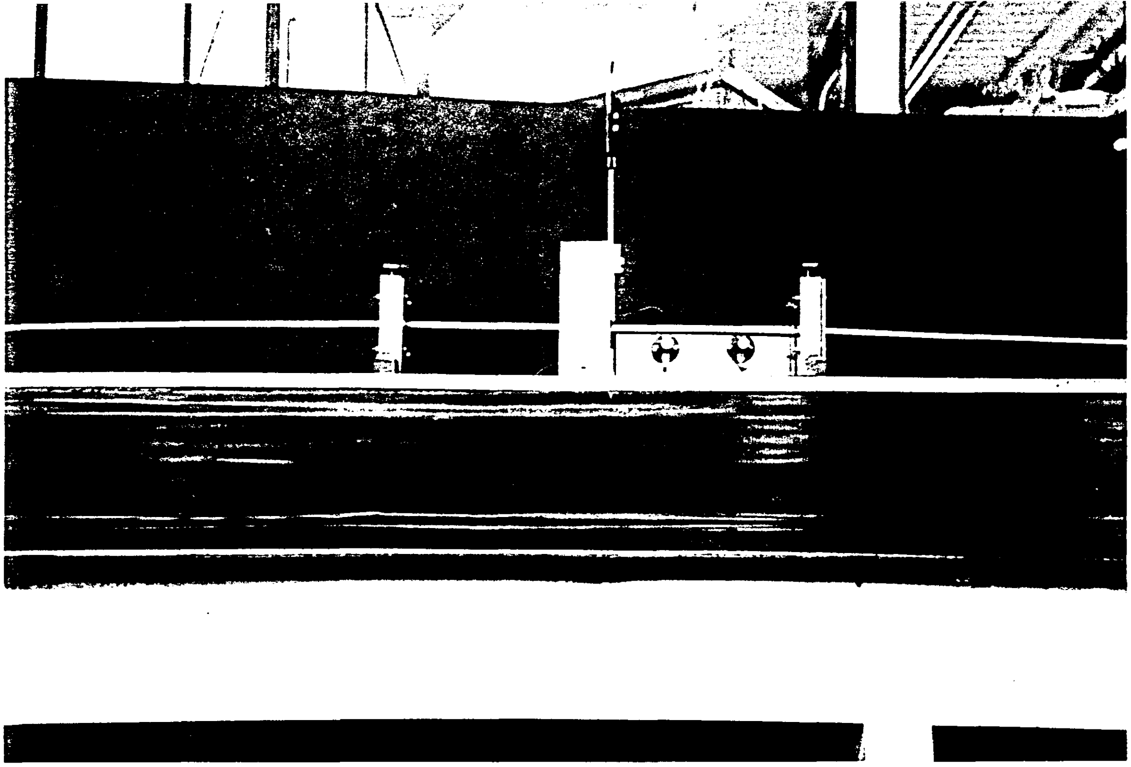

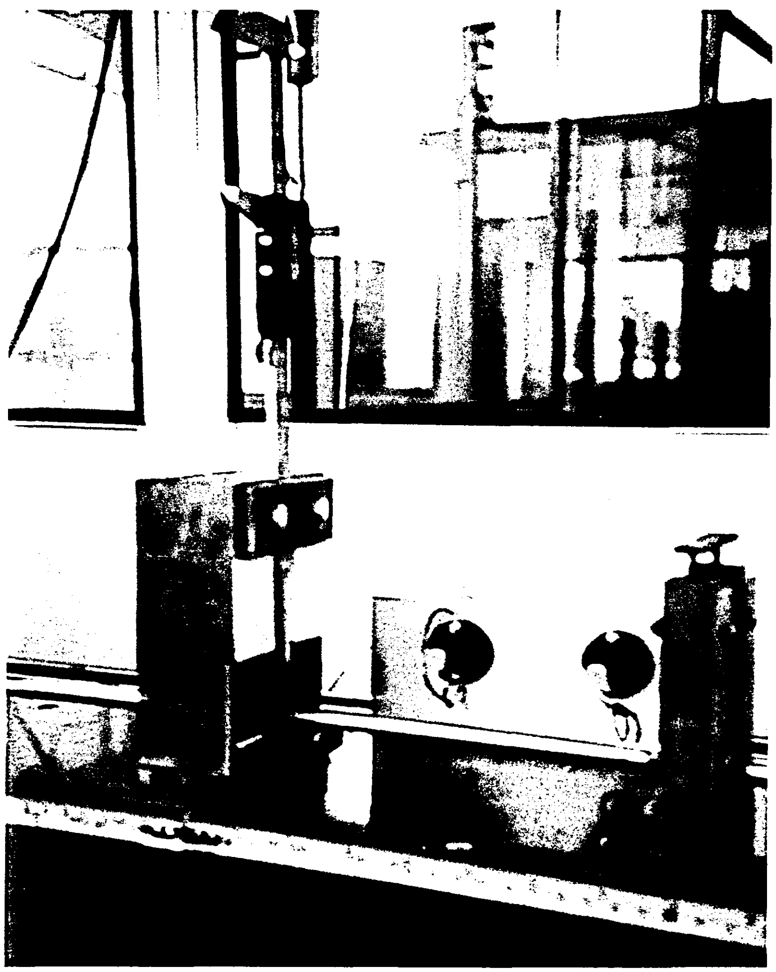

Plate 9 Make-or-break Electrical Contact

(Top) Pipe touches dial gauge reading, noting a single light on the left

(Bottom) Pipe touches both dial gauge and metal prop, both lights are on the pipe. The anchors were then fitted about the pipe, using shims as required. All round clamping action was provided by simply bolting-up a top plate which secured an insulated inner collar that had previously been firmly clamped onto the pipe employing adjusting screws; the inlet end anchor was so secured at the start of each test. With laboratory temperatures fluctuating considerably, pipe ambient was set at an artificially raised level ($\simeq 20^{o}$-30^{o}C), through pre-heating of the circulating water, whereat the outlet end anchor was locked-off. Initial wavelength L_i therefore corresponds to a water filled pipe in an unsubmerged environment. It is considered that L_i did not effectively vary with temperature prior to full anchorage lock-off. Wavelengths were assessed employing a 0.05mm feeler gauge. Under test, target thermal increments of either sign were then prescribed by means of the E5CS control unit, pipe temperature being averaged from the inlet/outlet thermal sensors. Inlet and outlet temperatures hardly differed and no above ambient inlet/outlet pressure changes were observed throughout the testing programme. A pipe flow rate corresponding to an outlet pressure of 1 bar was maintained continuously.

Overall, forty-five experimental case-studies are herein recorded as denoted in Tables 7.3 and 7.4. Brief procedural notes are given below in the context of both stable and unstable (snap) buckling topologies. The physically-based isolated and infilled prop imperfection configurations, recall Fig 1.7(b) and (c), are subject to experimentation in order to test the respective *Isoprop* and *Blister* models; the mathematically-based *Empathetic* model [Fig 1.7(a)] is tested against both experimental imperfection configurations. Experimental limitations restricted amplitude to ≤50mm and buckle length to ≤5.68m whilst compressive stressing was (theoretically) restricted to ≤50% σ_y, say, for linear constitutive modelling correlation purposes; buckle length magnitude is additionally subject

v_{om} (mm)	Remarks	Date Undertaken	Test No.	Pipe * Configuration
30	Stable Isolated Prop Heating Tests	Aug 1991 **	1 2 3	1a 1b 1c
		Jul 1992	4 5 6	2a 2b 2c
20		Aug 1991 **	7 8 9	1a 1b 1c
		Jul 1992	10 11 12	2a 2b 2c
15	Stable Isolated Prop Cyclic Thermal Tests	Jul 1992	13 14 15 16 17 18	1a 1b 1c 2a 2b 2c
10		Jul 1992	19 20 21 22 23 24	1a 1b 1c 2a 2b 2c
2	Snap Isolated Prop Heating Tests	Dec 1991 ***	25 26 27 28 29 30	1a 1b 1c 2a 2b 2c
		Jul 1992	31 32 33	2a 2a 2a
	Snap Isolated Prop Cyclic Thermal Tests	Dec 1991/ Jan 1992 ***	34 35 36 37 38 39	1a 1b 1c 2a 2b 2c
30	Stable Infilled Prop Heating Tests	Aug 1991 **	40 41 42	1a 1b 1c
20		Aug 1991 **	43 44 45	1a 1b 1c

Notes : * Refer to Table 7.4 for details
** Pipe Configuration not definitive
*** Undertaken in absence of candidate

Table 7.3 Summary of Pipe Buckling Experimentation (1991/1992)

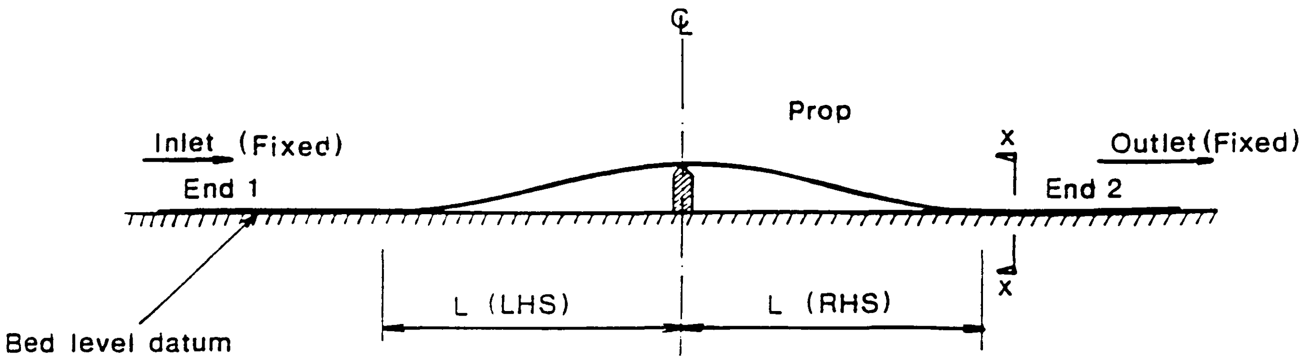

Elevation from East side of laboratory
with End 1 of pipe at Inlet

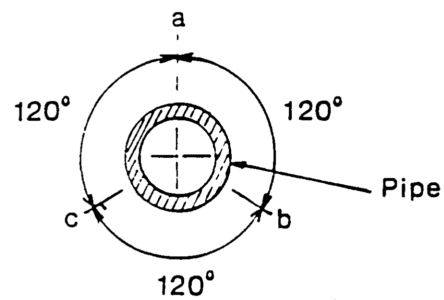

Orientation 'a'
x – x

INLET	Rotation about pipe's axis		
	0^{o}	120^{o}	240^{o}
End 1	1a	1b	1c
End 2	2a	2b	2c

Table 7.4 Experimental Pipe Configuration (1a shown)

to requirements relating to the minimisation of end condition effects (see Discussions). Onset of large rotation (0.1^r) was a less restrictive consideration according to theory with, for v_{om}=10mm for example, this state corresponding to $v_m \simeq 165$mm and $L \simeq 5.82$m, whilst for v_{om}=30mm the maximum slope occurs at $v_m \simeq 153$mm and $L \simeq 5.48$m.

7.2.3 Imperfection Considerations

The presence of undesirable as-delivered imperfections, such as initial pipe out-of-straightness, was unavoidable. To identify and partially overcome this problem the pipe was rotated through 120^o for each test sub-set (normally, but not Tests 31-33, Table 7.4), hence enabling a mean of the individual results to be acquired for better representation. In addition to this, consideration of the possibility of asymmetry within the test rig itself was allowed for by rotating the pipe through 180^o about the imperfection amplitude axis, ie switching the pipe end-to-end, regarding the more numerous isolated prop tests. Finally, the adequacy of the anchorage blocks were also monitored during the test by attaching dial gauges between the pipe and the block, see Fig 7.6, to ensure that there would be no slippage through the thermal insulating material clamps and the clamp collars.

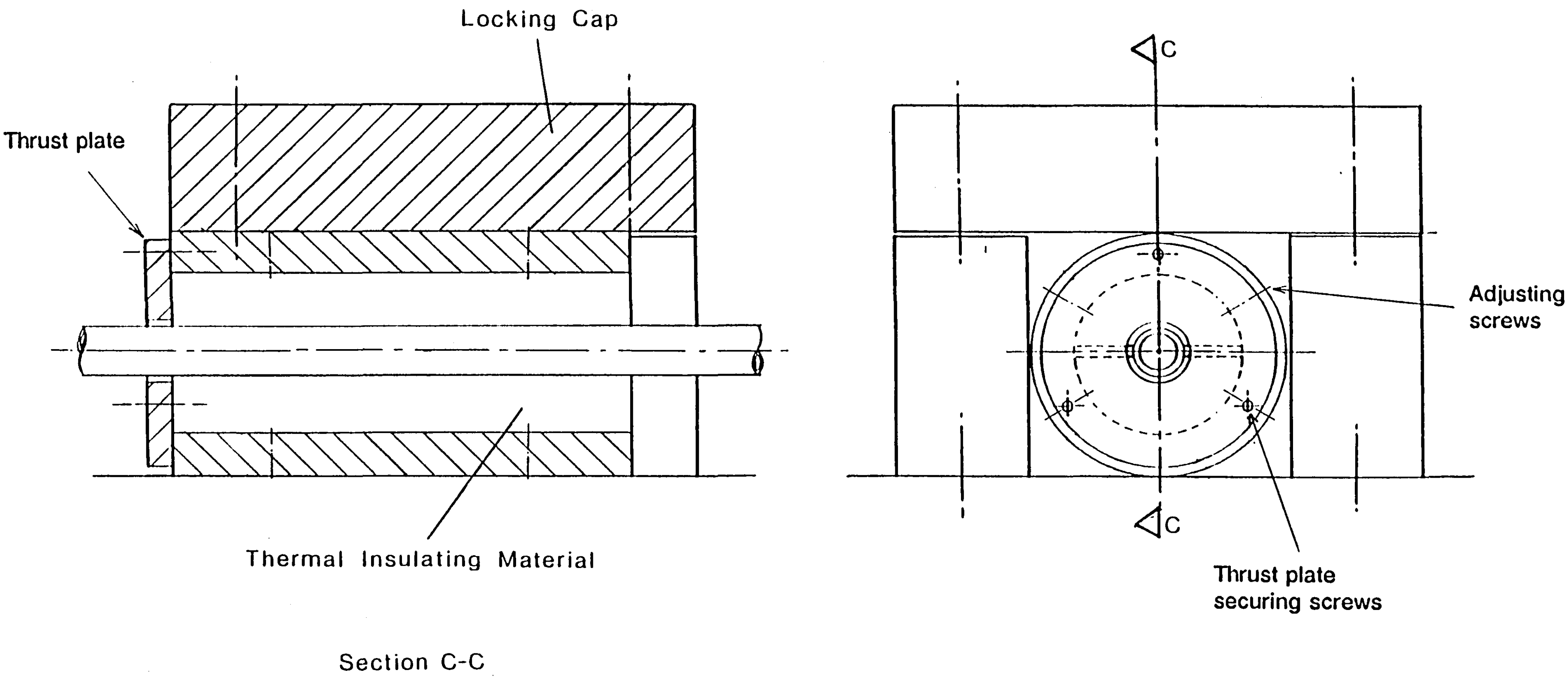

Fig 7.6 Anchor Block

7.3 Stable Buckling Isolated Prop Tests

7.3 1 Test Set-Up and Procedure

With the single blade providing the prop imperfection, temperature rise, buckle amplitude and wavelength data were recorded for imperfections of 30mm$\geq v_{om} \geq$10mm, these values theoretically producing fully stable post-upheaval buckling paths. The larger the prop amplitude, the less effective any as-delivered pipe imperfections were considered to become. For each case of v_{om}=30mm and 20mm, six heating up tests were conducted; test execution time was approximately 1.5 hours. For each of the smaller imperfection cases involving v_{om}=15mm and 10mm, six full heating up/cooling down thermal cycle tests were undertaken, the cooling phase being incrementally monitored through to effective recovery of the ambient state. Each cyclic test took approximately 2.5 hours to execute.

7.3.2 Results (Heating only)

Table 7.5 provides a loci legend for all following experimental/theoretical loci - a comprehensive data display is given in Appendices B and C. A general impression of a pipeline buckling under test is available from Plate 10 whilst key data are given in Table 7.6 and action-response loci are illustrated in Figs 7.7 and 7.8. With regard to the 30mm and 20mm larger imperfection studies (ie Tests 1-12), it is considered that excellent experimental-theoretical correlation is provided regarding *Isoprop* definition of the crucial upheaval state; Table 7.6 further shows that theoretical *Isoprop* upheaval temperatures T_u are conservative and within 7% of the respective average experimental values whilst upheaval

Experimental (By-eye fit)	
Idealised Theory	
Empathetic Theory	
Isoprop Theory	
Blister Theory	

Table 7.5 Loci Legend for Experimental/Theoretical Loci

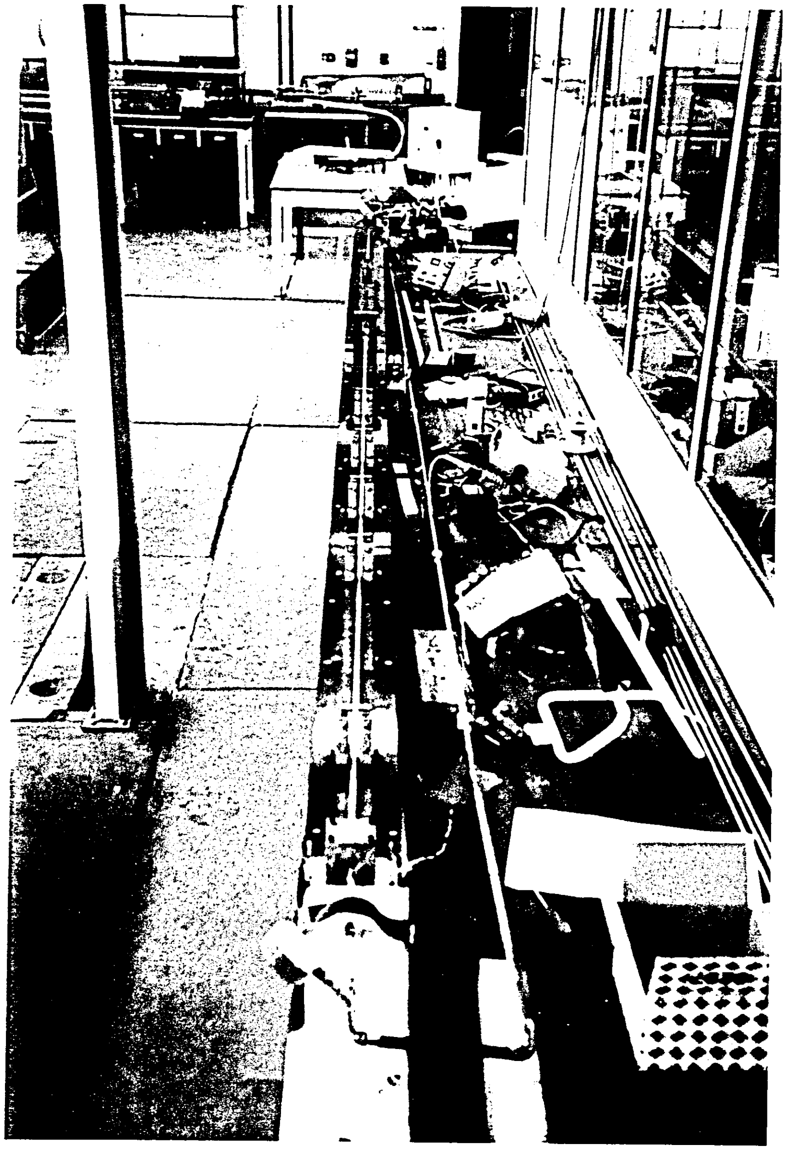

Plate 10 Stable Buckling Isolated Prop Test - Plan view

Test No	Imper-fection (mm)	Loading Status	Parameter	Experimental Data							Isoprop Theory	% Theoretical Discrepancy	Idealised Theory	
				1a	1b	1c	2a	2b	2c	Average			T_{min} (°C)	$T \mid_{v=v_{om}}$ (°C)
1-6	30	Heating	L_i (m)	4.93	4.91	4.74	4.95	4.96	4.86	4.89	5.04	3.07	N/A	N/A
			T_u (°C)	5.10	4.80	5.10	5.91	5.43	5.77	5.35	5.18	-3.18	8.27	9.80
			L_u (m)	3.60	3.78	3.71	3.79	3.51	3.58	3.66	3.75	2.46	N/A	N/A
7-12	20	Heating	L_i (m)	4.18	4.35	4.17	4.31	4.38	4.41	4.30	4.55	5.81	N/A	N/A
			T_u (°C)	4.50	4.20	4.00	5.07	4.96	5.35	4.68	4.37	-6.62	8.27	14.1
			L_u (m)	3.35	3.37	3.40	3.22	3.20	3.26	3.30	3.39	2.73	N/A	N/A

Note : N/A - Not applicable

Table 7.6 Isolated Prop Heating Test Results (Stable cases) - Initial and Upheaval States.

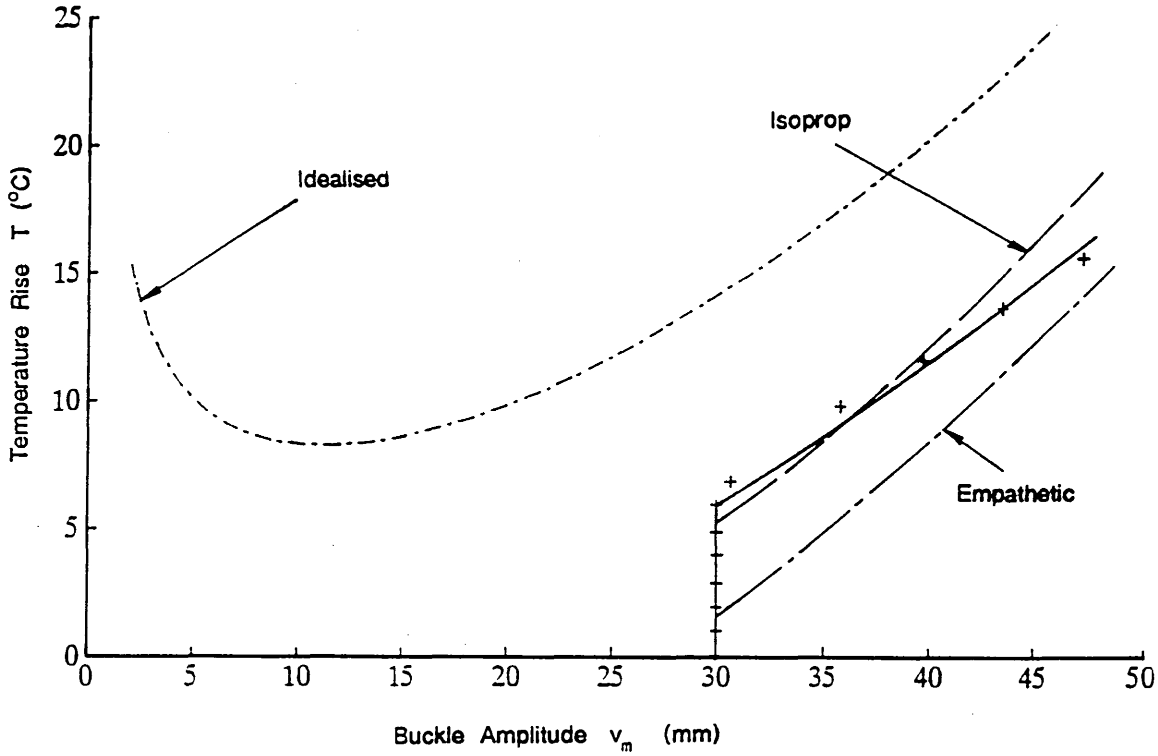

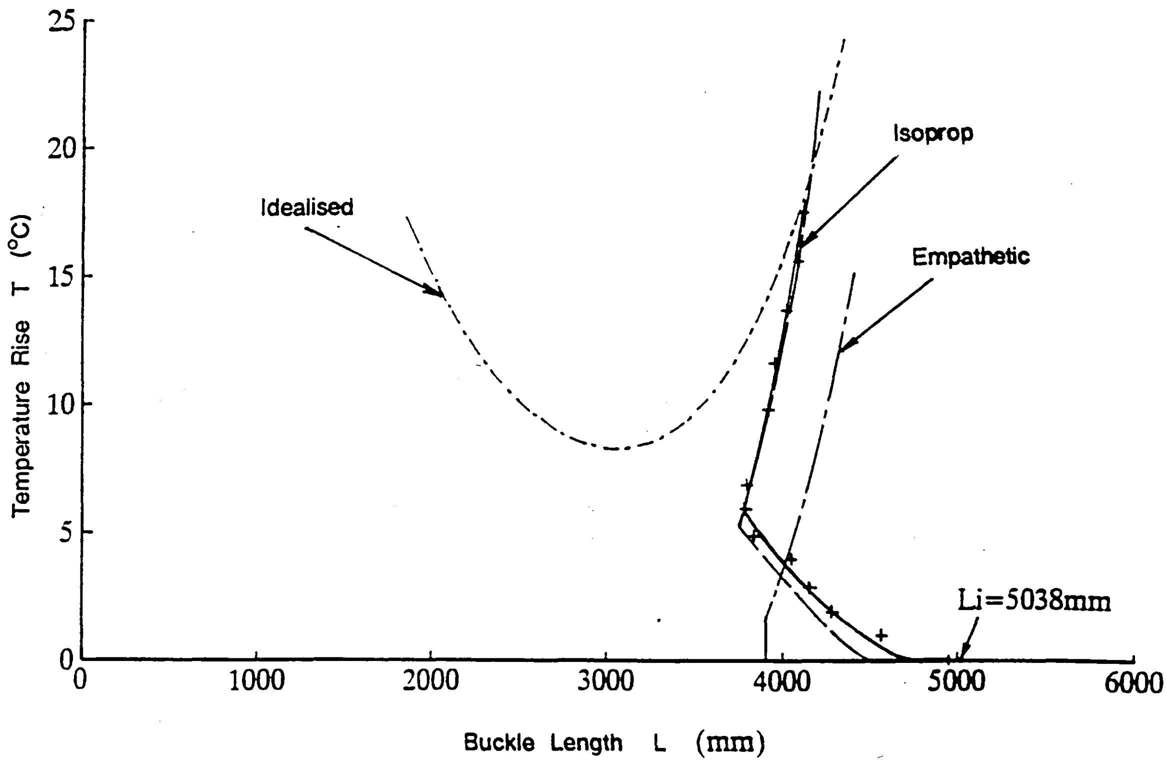

Fig 7.7 Stable Isoprop with Fixed Anchor Points

Thermal Action Characteristics for Heating Test No 4, v_{om}=30mm

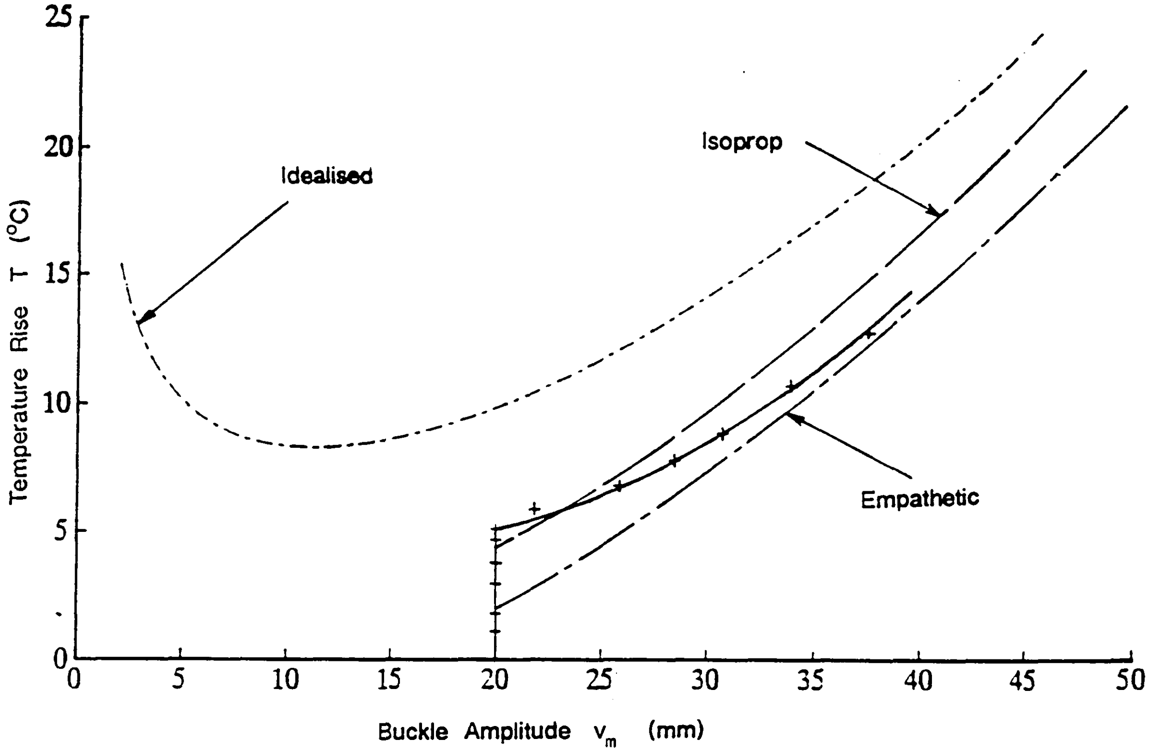

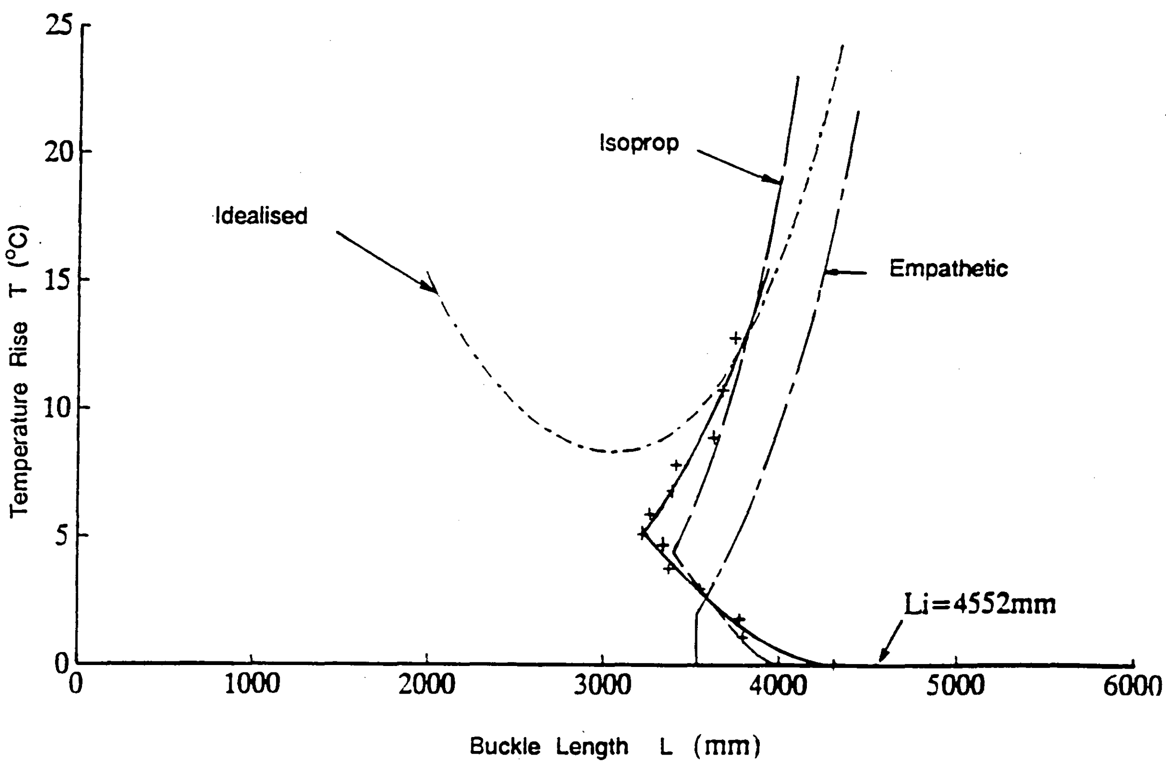

Fig 7.8 Stable Isoprop with Fixed Anchor Points

Thermal Action Characteristics for Heating Test No 10, v_{om} = 20mm wavelengths L_u lie within 3% of their average experimental counterparts. The reduction in wavelength from L_i (initial) to L_u is clearly displayed.

Typical graphical features regarding the twelve larger imperfection amplitude tests are displayed in Figs 7.7 and 7.8, whilst Table 7.7 displays typical test data for an imperfection of 30mm. With the experimental temperature/amplitude data decaying relative to the *Isoprop* theoretical locus with increasing amplitude whilst the temperature/buckle length characteristics are more consistent with *Isoprop*'s theoretical predictions. Idealised and *Empathetic* loci are added for comparative purposes; experimental loci are 'by-eye' fits. For the twelve tests overall, whilst buckle length data are clustered about the *Isoprop* locus, substantially post-upheaval amplitude data breaches the *Empathetic* locus on occasion, although not in Tests No 4 and 10 in Figs 7.7 and 7.8 respectively, particularly in the lower imperfection amplitude, v_{om}=20mm, case.

7.3.3 Cyclic Testing Results

Regarding recovery characteristics in these latter twelve tests (ie Tests 13-24), Table 7.8 indicates that the temperature required to achieve initial return to the prop is generally - 9 tests - lower than that at upheaval (ie $T|v_{om}<T_u$). Average values for the corresponding buckling lengths ($L|v_{om}$ and L_u) vary by less than 1.6%, similarly excellent wavelength recovery being exhibited upon return to ambient (L_i).

Figures 7.9 and 7.10 illustrate typical characteristics regarding the cyclic testing at imperfection amplitudes v_{om}=15mm and 10mm respectively, whilst

Temperature (^oC)				v_m	Buckle length (mm)			
I/L	O/L	Mean	Rise	(mm)	I/L	O/L	Total	Remarks
20.67	20.84	20.75	0	30	2710	2240	4950	
21.78	21.92	21.85	1.0	30	2570	2100	4570	
22.63	22.69	22.66	1.91	30	2280	2100	4280	
23.56	23.68	23.62	2.87	30	2200	2050	4150	
24.70	24.75	24.72	3.97	30	2120	2030	4050	
25.55	25.65	25.60	4.85	30	2100	2010	3840	
26.63	26.70	26.66	5.91	30	1870	1920	3790	Upheaval
27.52	27.68	27.60	6.85	30.66	1880	1820	3800	Apex at 150 LHS
30.54	30.55	30.54	9.79	35.81	2100	1820	3920	Apex at 270 LHS
32.33	32.41	32.37	11.62	39.73	2130	1820	3950	no change
34.42	34.49	34.45	13.70	43.51	2190	1830	4020	Apex at 300 LHS
36.34	36.38	36.36	15.61	47.31	2190	1890	4080	no change
38.18	38.36	38.27	17.52	50.74	2200	1910	4110	no change

Date : 10-7-1992

Time start : 2:20 pm　　Time finish : 3:15 pm

$v_{om} = 30mm$　　$L_i = 4950mm$

Pressure : Inlet (I/L) = 0.90 bar　　Outlet (O/L) = 0

Rotation about imperfection = 180 degrees

Rotation about pipe's axis = 0 degrees

Table 7.7 **Stable Isolated Prop with Fixed Anchor Points Typical Experimental Data for Heating Test No 4, v_{om} = 30mm**

Test No	Imper-fection (mm)	Loading Status	Parameter	Experimental Data							Isoprop Theory	% Theoretical Discrepancy	Idealised Theory	
				1a	1b	1c	2a	2b	2c	Average			T_{min} (°C)	$T \|_{v=v_{om}}$ (°C)
13-18	15	Heating	L_i (m)	3.81	3.88	4.05	3.81	4.05	4.00	3.93	4.24	7.89	N/A	N/A
			T_u (°C)	5.05	4.86	4.81	4.76	4.92	5.49	4.98	4.31	-13.4	8.27	8.6
			L_u (m)	2.96	2.98	2.94	3.20	3.22	3.24	3.09	3.16	2.26	N/A	N/A
		Cooling	$L \|_{v_{om}}$ (m)	2.93	3.00	3.48	3.18	3.02	3.20	3.14	3.16	0.64	N/A	N/A
			$T \|_{v_{om}}$ (°C)	4.96	4.23	5.36	4.91	4.95	5.07	4.91	4.31	-12.2	8.27	8.6
			$L_{i\ return}$ (m)	3.77	3.81	3.94	3.77	3.77	3.89	3.83	4.24	10.7	N/A	N/A
19-24	10	Heating	L_i (m)	3.58	3.56	3.55	3.56	3.56	3.58	3.56	3.83	7.58	N/A	N/A
			T_u (°C)	5.10	4.83	5.53	5.30	4.95	4.92	5.11	4.70	-8.02	8.27	8.3
			L_u (m)	2.61	2.73	3.09	2.76	2.80	2.97	2.83	2.85	0.71	N/A	N/A
		Cooling	$L \|_{v_{om}}$ (m)	2.69	2.72	2.85	2.77	2.90	2.98	2.82	2.85	1.06	N/A	N/A
			$T \|_{v_{om}}$ (°C)	4.68	4.66	5.14	4.89	4.20	4.33	4.65	4.70	1.08	8.27	8.3
			$L_{i\ return}$ (m)	3.56	3.53	3.54	3.36	3.55	3.56	3.52	3.83	8.8	N/A	N/A

Note : N/A - Not applicable

Table 7.8 Isolated Prop Cyclic Thermal Test Results (Stable cases) - Initial, Upheaval, Return to Prop ($v_m = v_{om}$) and Final States.

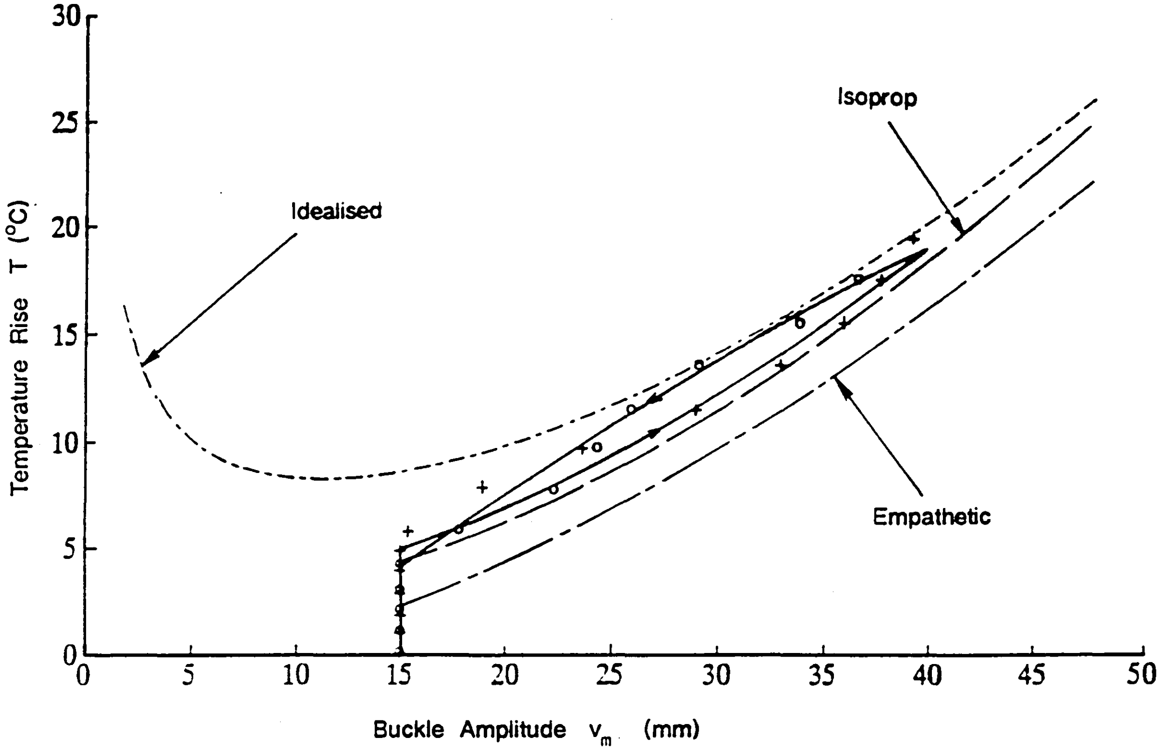

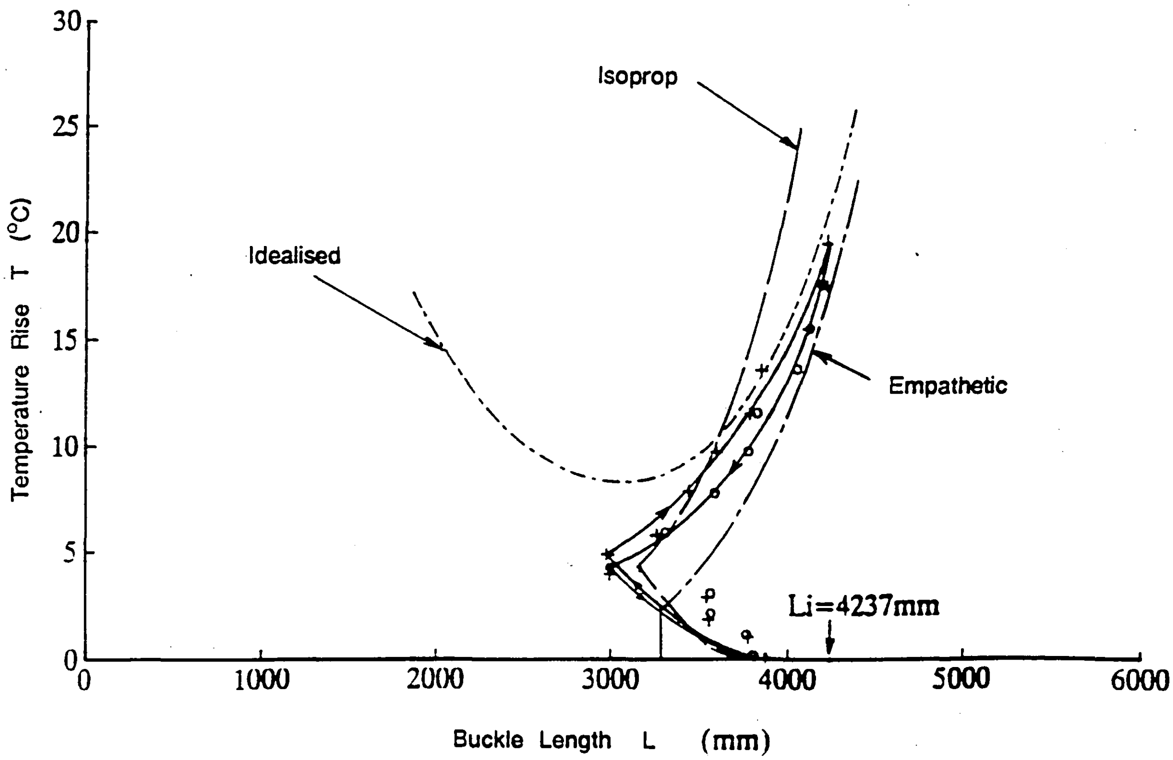

Fig 7.9 Stable Isoprop with Fixed Anchor Points

Thermal Action Characteristics for Cyclic Thermal Test No 14, v_{om} = 15mm

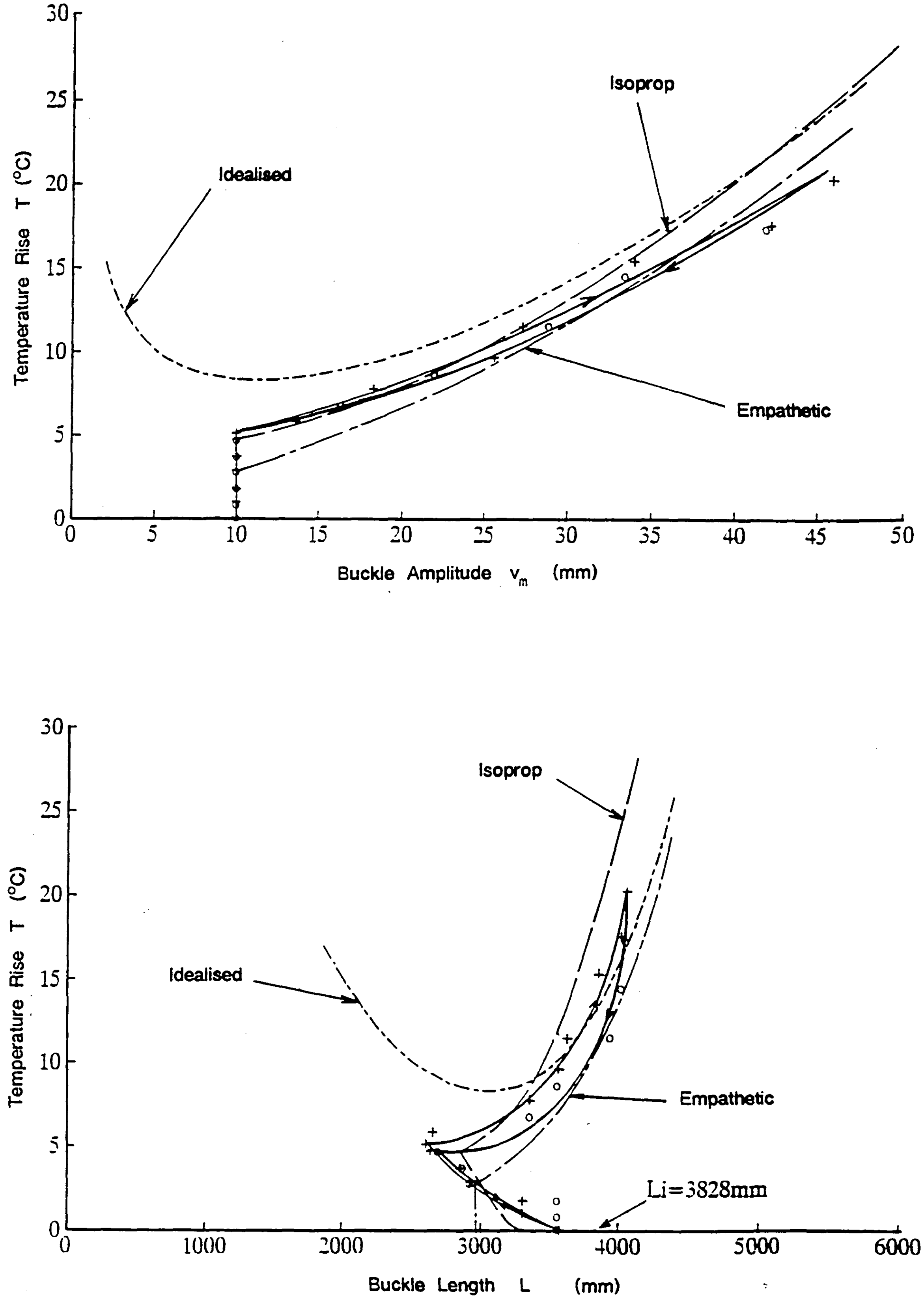

Fig 7.10 Stable Isoprop with Fixed Anchor Points
Thermal Action Characteristics for Cyclic Thermal Test No 19, v_{om} = 10mm

Table 7.9 displays typical test data for imperfection of 15mm. The above comments are again largely applicable with substantially post-upheaval temperature/amplitude data becoming increasingly 'softened' as imperfection amplitude decreases. Table 7.8 clearly shows that the percentage experimental/theoretical discrepancy of the upheaval temperatures T_u is less than 14%, twice of the heating only tests, whilst average upheaval theoretical wavelength L_u still lie within 3% of their experimental counterparts, the same percentage as obtained from the heating only tests. Hysteresis indicates the presence of non-conservative behaviour within the system (eg friction).

7.3.4 Comments

Although experimental-theoretical correlation remains equally good for the upheaval wavelengths corresponding to the smaller 15mm and 10mm imperfection studies (ie Tests 13-24), upheaval temperature correlation numerically suffers as the as-delivered imperfections become proportionately more effective - recall all three theoretical models assume a *stress-free-when-deformed* datum. Fortunately, however, the *Isoprop* model data do become increasingly conservative in these studies and the overall average experimental/theoretical upheaval temperature discrepancy for the twenty-four stable isolated prop tests is less than 8%. Still better correlation would have been obtained were it not for five (of 24) notably higher experimental upheaval temperatures, three of which occur in the same pipe configuration (2c). The four theoretical initial wavelength (L_i) values were also within 8% of their four averaged experimental equivalents; here, the key reason for the discrepancy is considered to lie with the visually obvious, as-delivered, lack of pipe-straightness.

Temperature (^oC)				v_m	Buckle length (mm)			Remarks
I/L	O/L	Mean	Rise	(mm)	I/L	O/L	Total	
20.39	20.41	20.40	0	15	2120	1930	4050	
21.42	21.49	21.45	1.05	15	1870	1710	3580	
22.20	22.29	22.24	1.84	15	1860	1680	3540	
23.38	23.45	23.41	3.01	15	1860	1670	3530	
24.35	24.43	24.39	3.99	15	1850	1490	3340	
25.36	25.40	25.38	4.92	15	1850	1470	3220	Upheaval
26.34	26.42	26.38	5.98	20.78	1450	1810	3260	Apex at 260 RHS
28.05	28.16	28.10	7.7	24.18	1300	2040	3340	Apex at 330 RHS
30.18	30.21	30.20	9.8	26.36	1300	2300	3600	Apex at 360 RHS
32.05	32.08	32.06	11.66	31.72	1350	2480	3830	Apex at 360 RHS
33.94	34.17	34.05	13.65	35.78	1450	2480	3930	Apex at 360 RHS
35.90	35.96	35.93	15.53	38.45	1460	2490	3950	Apex at 400 RHS
37.81	37.92	37.86	17.46	40.03	1460	2500	3960	Apex at 400 RHS
39.90	39.90	39.90	19.5	42.59	1500	2640	4140	Apex at 500 RHS
38.04	38.06	38.05	17.65	40.79	1500	2550	4050	Unloading
36.0	36.06	36.03	15.63	36.31	1460	2550	4010	Apex at 500 RHS
33.93	34.03	33.98	13.58	34.15	1450	2500	4000	Apex at 460 RHS
31.94	32.04	31.99	11.59	28.35	1300	2480	3780	Apex at 460 RHS
30.16	30.18	30.17	9.77	25.39	1290	2450	3740	Apex at 400 RHS
28.05	28.19	28.12	7.72	21.21	1290	2450	3740	Apex at 400 RHS
26.40	26.46	26.43	6.03	18.37	1160	2450	3610	Apex at 400 RHS
25.29	25.42	25.35	4.95	15	1300	1720	3020	Apex at 400 RHS
23.49	23.58	23.54	3.14	15	1460	1720	3180	
22.32	22.43	22.37	1.97	15	1850	1720	3570	
21.45	21.58	21.51	1.11	15	1860	1720	3580	
20.35	20.45	20.40	0	15	1860	1910	3770	

Date : 9-7-1992

Time start : 10:35 am — Time finish : 12:20 pm

$v_{om} = 15mm$ — $L_i = 4050$

Pressure : Inlet (I/L) = 1 bar — Outlet (O/L) = 0

Rotation about imperfection = 180 degrees

Rotation about pipe's axis = 120 degrees

Table 7.9 Stable Isolated Prop with Fixed Anchor Points

Typical Experimental Data for Cyclic Thermal Test No 17, v_{om}=15mm

Finally, asymmetric buckling[40] relative to the prop (x=0) was recorded in all tests, post-upheaval buckle amplitude being displaced to the inlet side in 14 tests, to the outlet side in the remaining 10; see Plate 11. Post-upheaval amplitude offset from the prop was of the order of 0.8m.

Whilst *Empathetic* data remained largely conservative, upheaval temperatures could be criticised as being uneconomic by certain authorities; idealised studies appear to afford little useful data for such topologies.

7.4 Snap Buckling Isolated Prop Tests

7.4.1 Test Set-Up and Procedure

Smaller imperfections produce snap buckling and the *Isoprop* model predicts that an initial amplitude of v_{om}=2mm would produce a moderate snap. As-delivered imperfection effects become proportionately more significant, however, and fifteen tests were conducted at this imperfection amplitude to produce a relatively larger set of upheaval temperature values. Six tests involved full thermal cyclic action. Throughout, dynamic effects associated with snap buckling caused difficulty in securing precise buckle length values in the vicinity of upheaval and its equivalent upon cooling.

7.4.2 Results (Heating only)

Key snap buckling data for the nine heating tests conducted are given in Table 7.10 whilst action-response characteristics are illustrated in Fig 7.11. The reduction of amplitude from the order of 3D (v_{om}=30mm) to D/5 is unsurprisingly

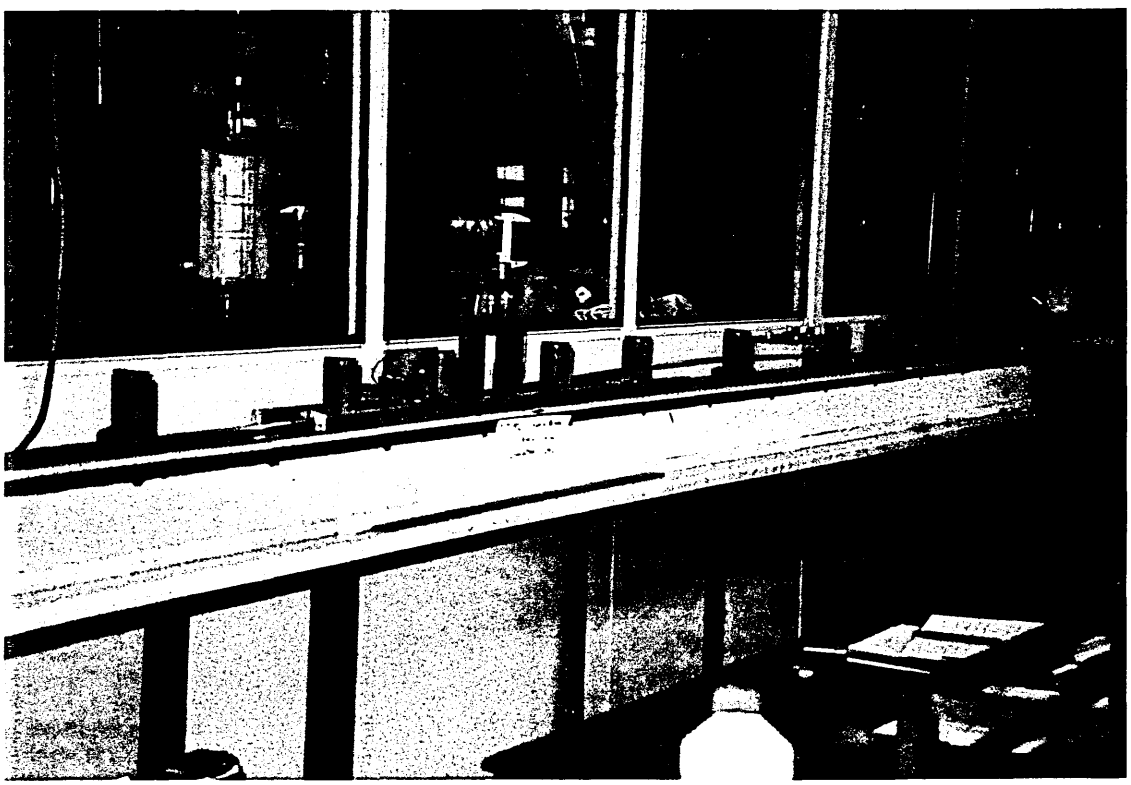

Plate 11 Isolated Prop Test - Asymmetry Details
(Top) Crown moves towards inlet end (LHS)
(Bottom) Crown moves towards outlet end (RHS)

Test No	Imper-fection (mm)	Loading Status	Parameter	Experimental Data										Isoprop Theory	% Theoretical Discrepancy	Idealised Theory	
				1a	1b	1c	2a	2b	2c	2a	2a	2a	Average			T_{min} (^oC)	$T\|_{v=v_{om}}$ (^oC)
			L_i (m)	2.54	2.33	2.28	2.30	2.57	2.29	2.28	2.27	2.29	2.35	2.56	8.94	N/A	N/A
25			T_u (^oC)	9.84	6.36	9.14	6.97	10.2	8.89	7.90	8.13	8.12	8.40	9.64	14.7	8.27	15.35
to	2	Heating	L_u (m)	1.89	2.30	1.50	1.94	1.83	1.68	1.69	1.67	1.75	1.81	1.907	5.36	N/A	N/A
33			v_{snap} (mm)	30.75	13.95	26.38	21.38	31.63	27.02	18.77	25.01	25.73	24.51	19.54	-20.39	N/A	N/A
			L_{snap} (m)	3.58	3.19	3.55	3.49	3.70	3.53	3.44	3.46	3.43	3.49	3.36	-3.72	N/A	N/A

Note : N/A - Not applicable

Table 7.10 Isolated Prop Heating Test Results (Snap cases) - Initial and Upheaval States.

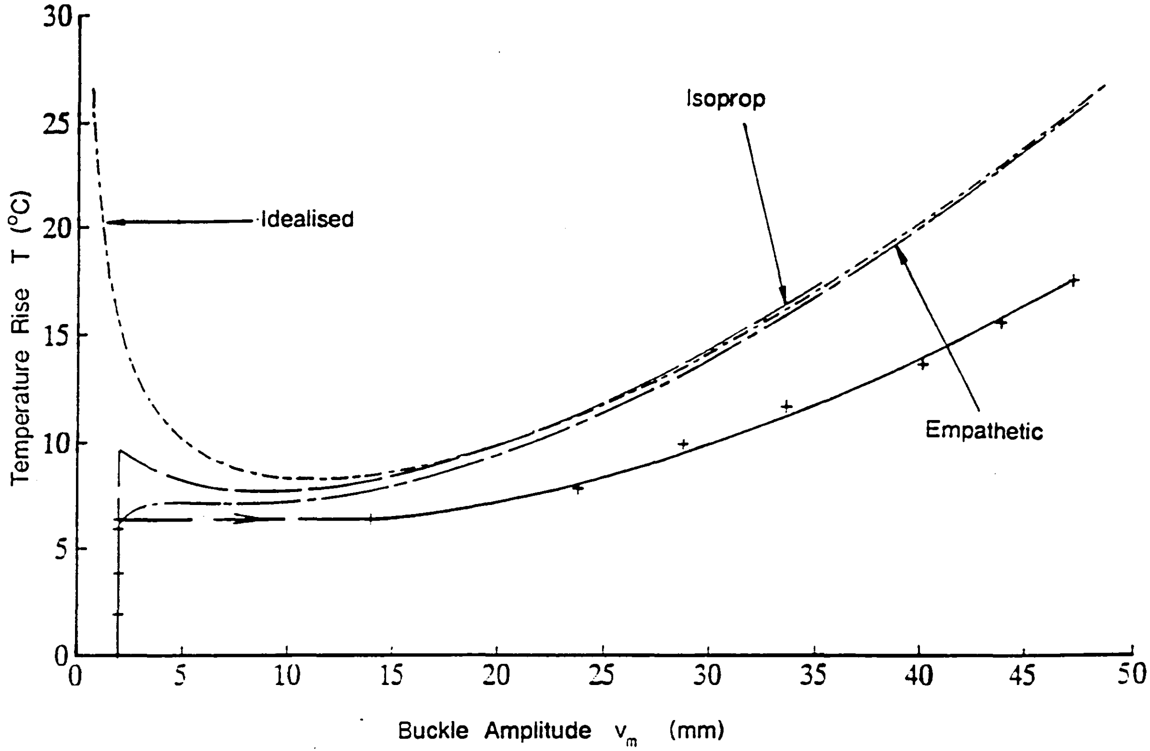

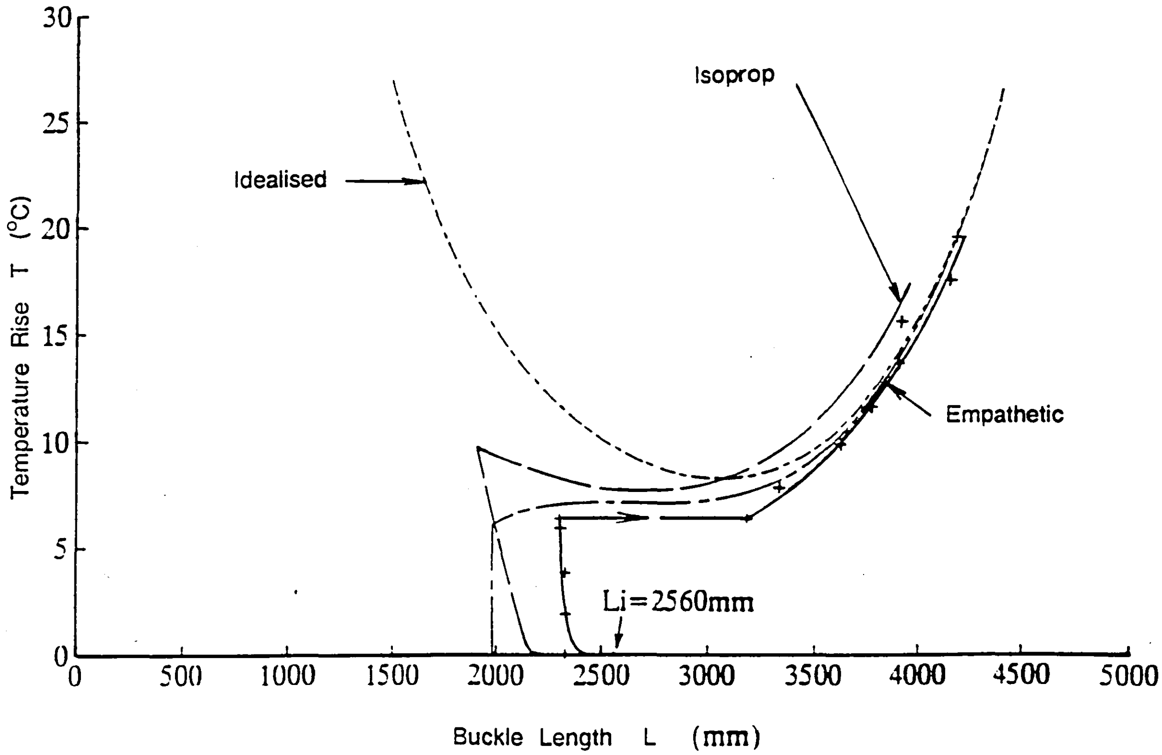

Fig 7.11 Snap Buckling Isoprop with Fixed Anchor Points

Thermal Action Characteristics for Heating Test No 26, v_{om} = 2mm accompanied by an increased experimental/theoretical discrepancy regarding *Isoprop*'s predicted upheaval temperature which is herein non-conservative by some 14.7% with respect to the experimental average, whilst the upheaval length prediction is within 5.36% of the average experimental values. The *Empathetic* model, however, provides a conservative upheaval temperature throughout (6.11^{o}C). The four experimental values which are particularly low occupy configurations 1b and 2a, and Tests 31-33, see Table 7.10, represent an attempt to investigate this factor by concentrating on the latter configuration. The later three tests gave more consistent results although these clearly remain susceptible to the as-laid residual stressing levels discussed previously.

7.4.3 Cyclic Testing Results

Table 7.11 displays the test data for six cyclic thermal tests employing an imperfection amplitude of 2mm and Fig 7.12 illustrates graphical presentation of the results. As in the former tests, the average experimental upheaval temperature is within 12% of the predicted theoretical value whilst the upheaval length prediction correlates excellently with experimental observation, being within 0.16% of the experimental average. Similar accuracy is reflected in the first post-snap buckling length data (ie L_{snap} in Tables 7.10 and 7.11) which is considered particularly notable given the substantial dynamic snap and damping activity attending these tests. Despite the double snap that occurs in the six cyclic tests, experimental upheaval and initial buckle lengths L_u and L_i display remarkable recovery characteristics (97% and 99.6% respectively).

As illustrated by Fig 7.12, recovery (ie cooling) values for upheaval temperature and pre-return-snap amplitude and buckle length are not comparable

Test No	Imperfection (mm)	Loading Status	Parameter	Experimental Data							Isoprop Theory	% Theoretical Discrepancy	Idealised Theory	
				1a	1b	1c	2a	2b	2c	Average			T_{min} (°C)	$T\|_{v=v_{om}}$ (°C)
34-39	2	Heating	L_i (m)	2.56	2.33	2.31	2.29	2.55	2.30	2.39	2.56	7.11	N/A	N/A
			T_u (°C)	9.73	7.60	9.07	7.07	8.82	9.40	8.61	9.64	11.96	8.27	15.35
			L_u (m)	1.89	2.33	1.49	2.07	2.01	1.67	1.91	1.907	-0.16	N/A	N/A
			v_{snap} (mm)	28.96	22.33	24.37	19.81	26.48	28.30	25.04	19.54	-21.9	N/A	N/A
			L_{snap} (m)	3.57	3.33	3.55	3.23	3.41	3.66	3.46	3.36	-2.89	N/A	N/A
		Cooling	$T_{u\ return}$ (°C)	5.89	5.69	6.30	5.95	5.09	6.13	5.84	7.67	31.3	8.27	15.35
			$v_{snap\ return}$ (mm)	22.41	17.63	15.97	10.84	14.22	22.14	17.2	8.76	-49.1	N/A	N/A
			$L_{u\ pre\text{-}snap}$ (m)	3.26	3.18	3.05	2.80	3.23	3.49	3.17	2.66	-16.1	N/A	N/A
			$L_{u\ post\text{-}snap}$ (m)	1.72	2.33	1.53	2.08	2.03	1.69	1.90	1.95	2.63	N/A	N/A
			$L_{i\ return}$ (m)	2.55	2.33	2.30	2.29	2.55	2.37	2.40	2.56	6.67	N/A	N/A

Note: N/A Not applicable

Table 7.11 Isolated Prop Cyclic Thermal Test Results (Snap cases) - Initial, Upheaval, Return to Prop ($v_m = v_{om}$) and Final States.

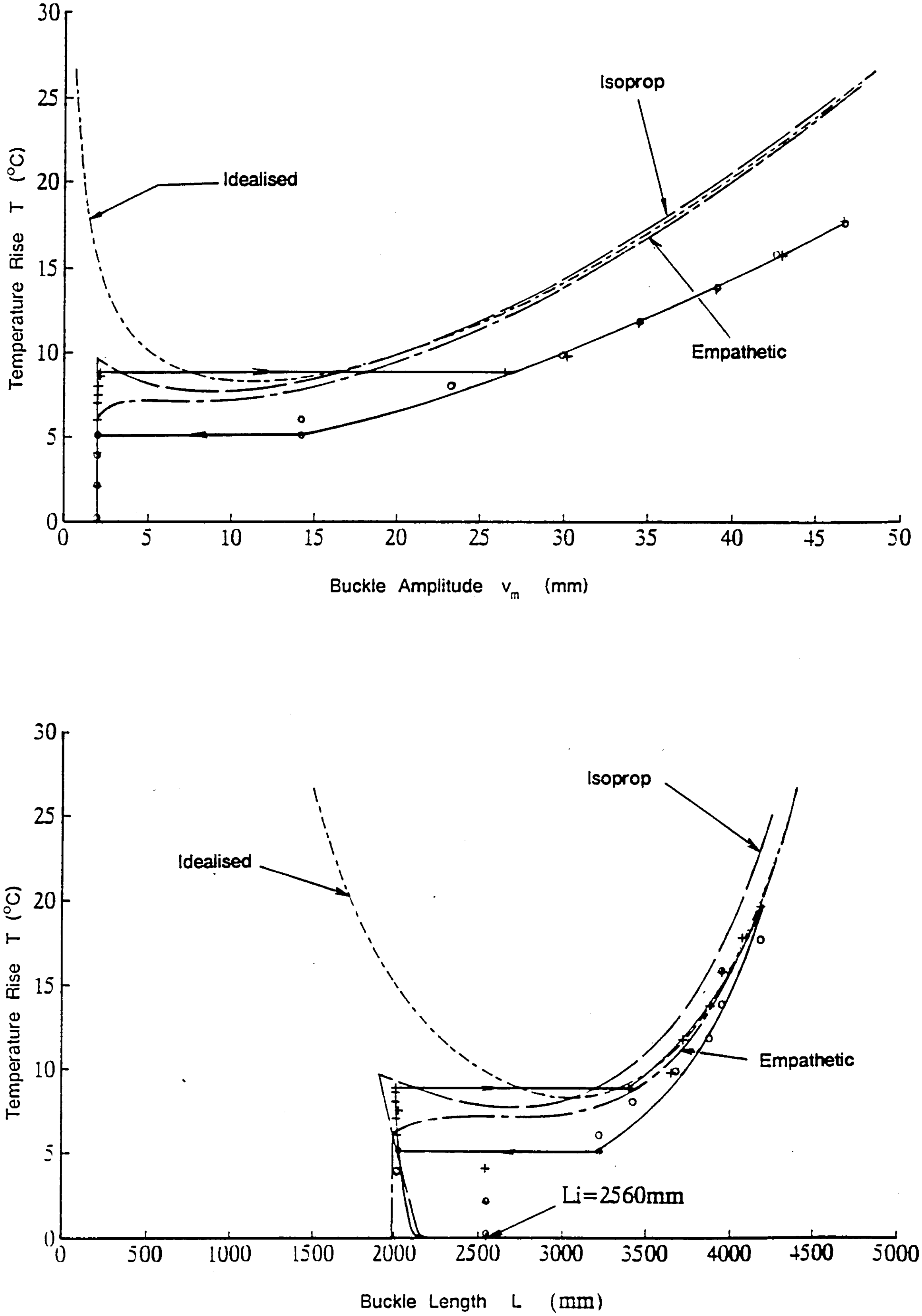

Fig 7.12 Snap Buckling Isoprop with Fixed Anchor Points

Thermal Action Characteristics for Cyclic Thermal Test No 38, v_{om} = 2mm

with their heating-up counterparts by definition. Actual measurement of these geometric variables under test incurs particular difficulties discussed later. The general features of the loci illustrated in Fig 7.12 are fairly typical of the tests concerned with the enforced heating-up/cooling-down snap divergence clearly displayed and following upon any system hysteresis.

7.4.4 Comments

Asymmetry[40] was again present through the tests. Indeed, the substantial dynamic snap activity involved resulted in the interchanging of post-upheaval buckle length bias in four tests. Tests 31-33 which involved consecutive re-testing of the same configuration - the pipe was not detached from the test rig between tests - generated a common post-upheaval bias for the three tests.

Inspection of Tables 7.9 and 7.10 indicates that the average upheaval temperature of fifteen tests is within 13.3% of the theoretical counterpart. A better correlation of 11.7% would have been obtained provided the result of Test 26 was discounted, since snap occurs particularly early in this orientation whilst in the remainder of cases, ie fourteen out of fifteen, snap occurs generally between 7^oC and 10^oC at an average of approximately 8.6^oC as compared to the theoretical prediction of 9.64^oC. Furthermore, Table 7.10 also indicates that the lowest and highest snap values of Tests 26 and 29 respectively have been obtained for the pipe in the same rotational orientation but with the pipe switched round in the test rig, demonstrating the degree of sensitivity of data at such low levels of 'synthetic' (v_{om}) imperfection. (The asymmetry 'bias' was also reversed - see Table 7.14 later.) Figures 7.11 and 7.12 show that experimental amplitude data decay prominently beyond even the *Empathetic* locus although buckle length data are more in line with the *Empathetic* model's predictions. Plate 12 displays the dynamic snap buckling phenomenon being video recorded.

7.5 Stable Buckling Infilled Prop Tests

7.5.1 Test Set-Up and Procedure

Six infilled prop buckling tests were conducted relating to imperfection amplitudes of 30mm and 20mm; *Blister* model data for these magnitudes of imperfection indicated stable buckling characteristics. Otherwise similar to the foregoing isolated prop tests at the same amplitudes, herein the prop-attendant voids were initially infilled with a sand coated balsa framework, a time-consuming process. The variation in the axial friction coefficient along the infilled imperfection lie with respect to that established previously was checked by further subordinate friction testing (recall Chapter 3) and found not to be of major significance, typically affecting theoretical upheaval temperature values by <0.5%. The metal prop remained as an integral part of the imperfection, facilitating lift-off identification as previously. Test execution time lengthened to two hours due to buckle length values being difficult to obtain with the feeler gauge for $L<L_i$ (ie with respect to the curved, sand-coated imperfection surface). It was necessary to establish a 'contour map' of vertical pipe displacement (ie $=v_i$ or $\neq v_i$) at numerous locations for $L<L_i$ in order to determine the respective buckle length values. Plates 13 and 14 display various views of the *Blister* tests.

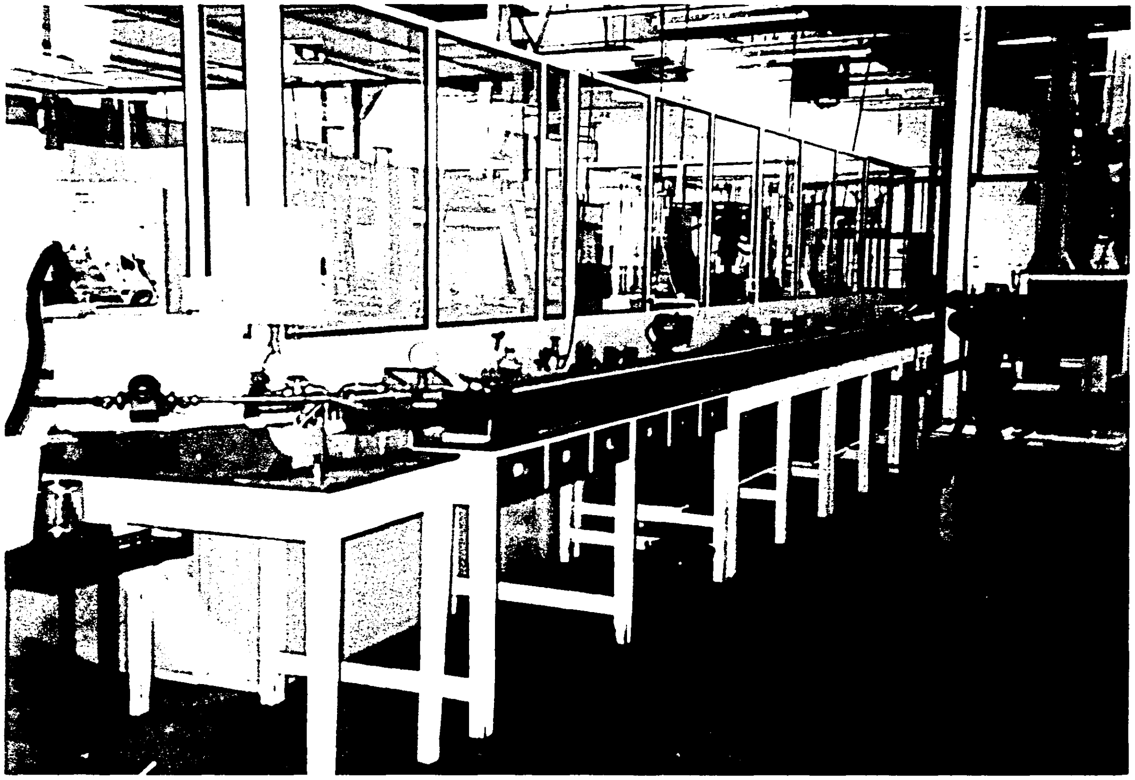

Plate 12 Snap Buckling Isolated Prop Test with video recording

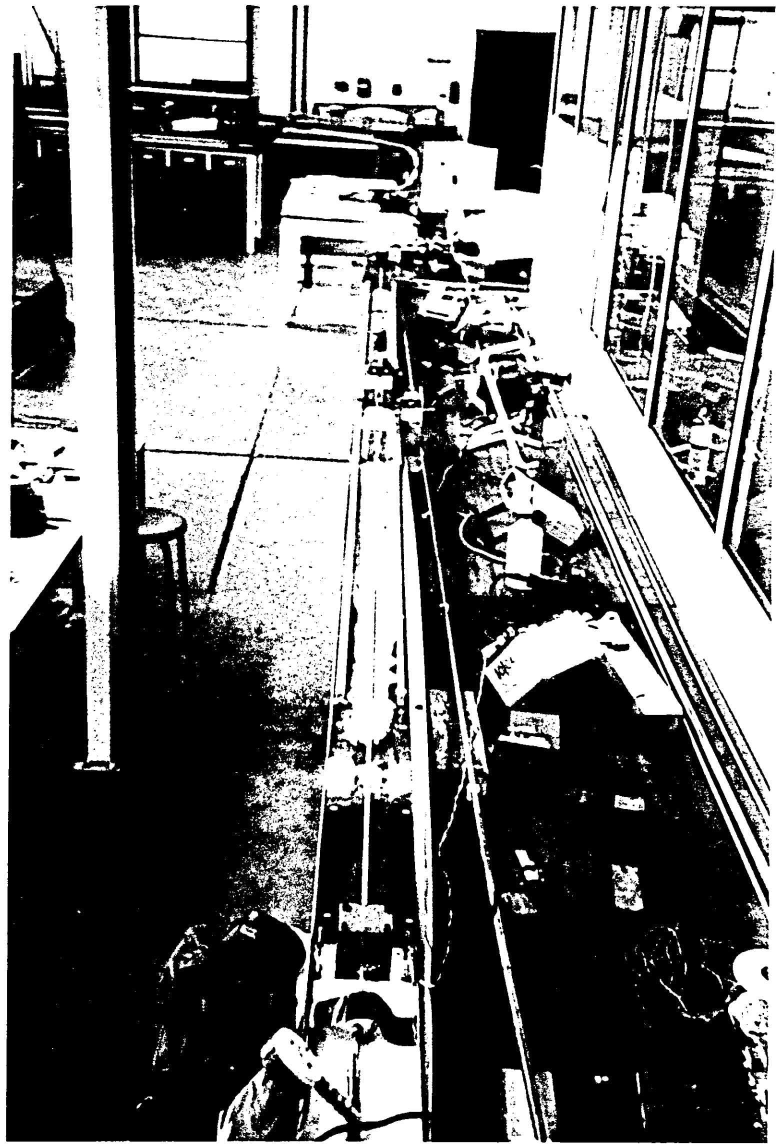

Plate 13 Stable Buckling Infilled Prop Test - Plan view

Plate 14 Stable Buckling Infilled Prop Test
(Top) Isometric view
(Bottom) Front view

7.5.2 Results

Prominent data are summarised in Table 7.12 whilst action-response characteristics are illustrated in Figs 7.13 and 7.14. Experimental upheaval temperatures and buckle lengths are consistent but before further theoretical comparisons are drawn, both the *Blister* model's numerical sensitivity and the experimental system's limitations in the vicinity of the upheaval state must be considered.

The upper and lower theoretical upheaval temperatures and wavelengths given in Table 7.12 for each imperfection case correspond to numerically terminating the search for upheaval as v_m tends to v_{om} at v_m=100.05%v_{om}, recall Table 7.1, and v_m=105%v_{om} respectively. As in the previous isolated prop cases, whilst the corresponding experimental upheaval temperatures are precisely acquired from the make-and-break system discussed previously, the experimental upheaval wavelengths are subject to a discrete delay in acquisition. Temperatures discussed herein are as monitored from the pipe wall whilst the applied or controlled temperature of the water is subject to discrete incremental increase. With upheaval generally occurring mid-increment, the necessary delay in recording the corresponding wavelength with particular regard to the infilled prop is to be noted given the previously discussed difficulty in acquiring the buckle length and the sensitivity of the measurement itself (ie wavelength is increasing rapidly from zero through the thermal increment). This sensitivity is reflected in the *Blister* data; Table 7.12 indicates that as v_m increases by less than 5% post-upheaval, corresponding temperature rise and buckle length data effectively double in magnitude. Accordingly, the acceptable correlation between experimental upheaval data and theoretical values corresponding to v_m=105%v_{om}

Test No	Imper-fection (mm)	Loading Status	Parameter	Experimental Data				Blister Theory **	% Theoretical Discrepancy	Idealised Theory	
				1a	1b	1c	Average			T_{min} (°C)	$T \mid_{v=v_{om}}$ (°C)
40-42	30	Heating	L_i (m)	4.62	4.84	4.76	4.74	5.04	6.33	N/A	N/A
			T_u (°C)	2.30	2.60	2.50	2.47	1.0 → 2.02	-59.5 → -18.2	8.27	14.1
			L_u (m)	2.50*	2.30*	2.40*	2.40*	1.08 → 2.28	-55.0 → -5.0	N/A	N/A
43-45	20	Heating	L_i (m)	4.18	4.39	4.12	4.23	4.55	7.56	N/A	N/A
			T_u (°C)	2.70	2.60	2.90	2.73	1.22 → 2.37	-55.3 → -13.2	8.27	9.80
			L_u (m)	2.40*	2.10*	2.20*	2.23*	0.97 → 2.22	-56.5 → -0.4	N/A	N/A

Notes: N/A Not applicable

* Earliest possible visible/physical measurements

** First number at upheaval is value at 100.05%v_{om}, second at 105%v_{om} - see Table 7.1

Table 7.12 Infilled Prop Test Results (Stable cases) - Initial and Upheaval States.

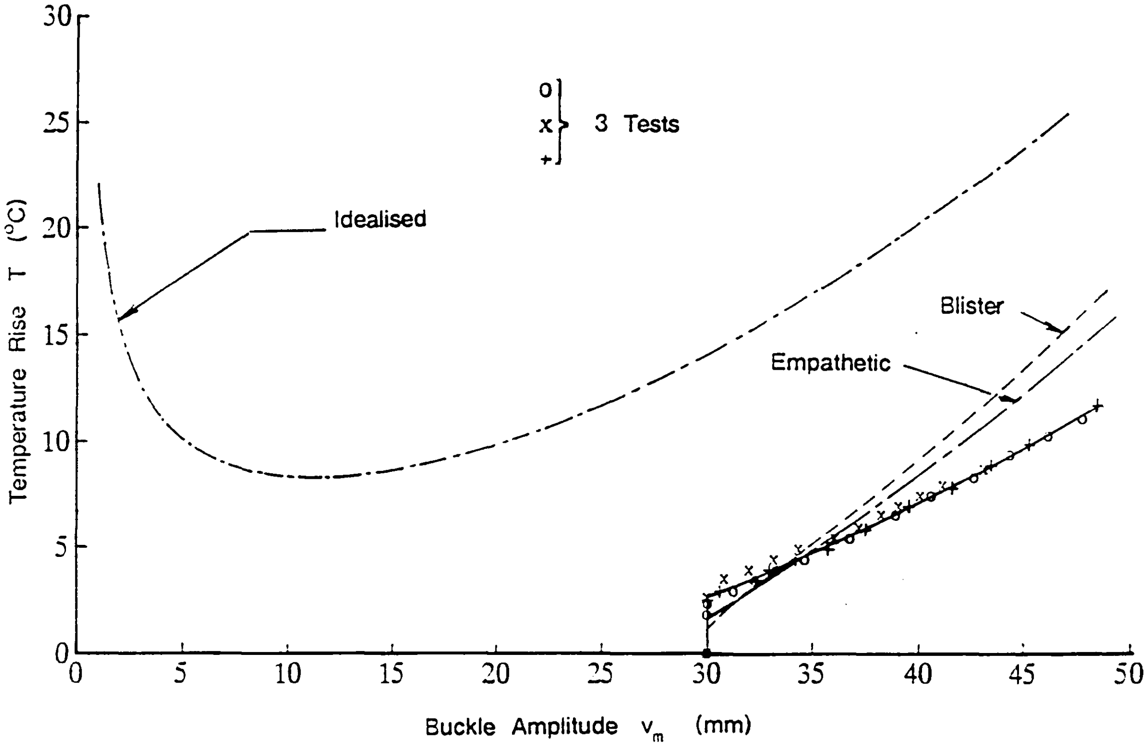

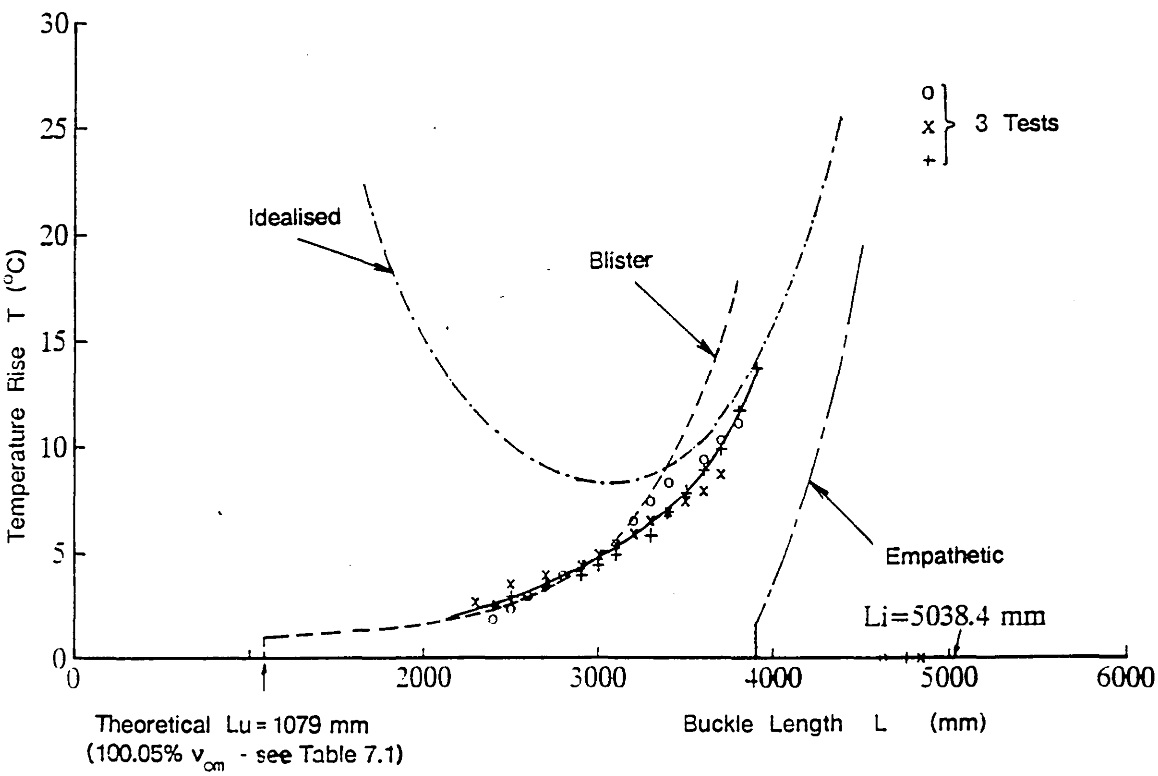

Fig 7.13 Stable Blister with Fixed Anchor Points

Thermal Action Characteristics for Heating Test Nos 40, 41 and 42, v_{om} = 30 mm

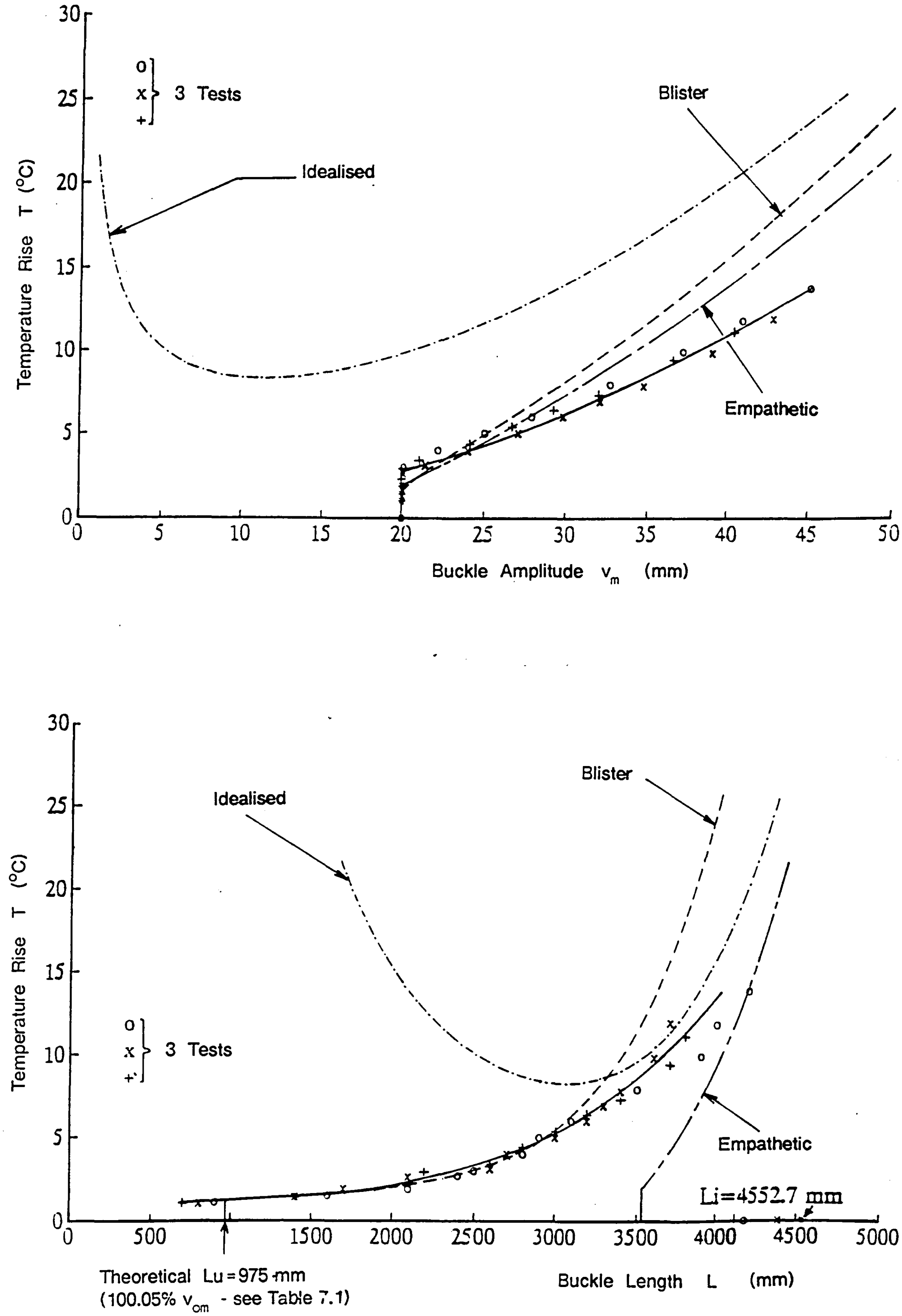

Fig 7.14 Stable Blister with Fixed Anchor Points

Thermal Action Characteristics for Heating Test Nos 43, 44 and 45, v_{om} = 20 mm is considered to provide adequate assessment.

Initial, as-delivered imperfections accounted for a maximum deviation in upheaval temperatures between the tests of 6.2%, whilst the measured upheaval lengths only deviate 5.9% from the corresponding averaged value for both 20mm and 30mm synthetic imperfections. However, the measured initial imperfection wavelengths were less than the theoretical values, typically in the order of 6-7%. Theoretical upheaval temperatures are again conservative (upto 20%) and initial buckle length values are within approximately 5% of their respective experimental averages. Initial wavelength values, both experimental (which are affected by the infilled imperfection 'construction') and theoretical (*Blister*), are of similar form to their *Isoprop* equivalents denoted in Table 7.12.

7.5.3 Comments

The graphical path data illustrated in Figs 7.13 and 7.14 and relating to all six tests exhibits good experimental consistency. Decay of the experimental data from the respective theoretical loci is similar to that previously noted in the *Isoprop* studies.

Asymmetric buckling[40] invariably occurred with the post-upheaval amplitude displaced typically up to 200mm towards the inlet in four of the six tests. The construction of an adequate infilled prop imperfection is clearly far more difficult than that of a simple prop and buckle length monitoring was tedious. (It was considered more productive to undertake cyclic and snap testing employing the former, isolated prop configuration.)

Empathetic model upheaval data was conservative throughout, whilst idealised modelling again appears to have little to offer regarding this form of imperfection with v_{om}>D.

7.6 Discussions

Notwithstanding the experimental considerations given below, particularly with regard to the matter of scaling effects, it is considered that highly satisfactory experimental/theoretical correlation has been established with respect to the crucial upheaval state. Predicted pre-upheaval flexure associated with the isolated prop topology has been observed and the approximately 50% reduction in upheaval temperatures caused by infilling of the attendant voids has been confirmed by experiment. Offshore designers need to prevent infilling wherever possible although this may comprise burial. Snap or stable responses were correctly identified by the *Isoprop* and *Blister* models. The inverse relationship between upheaval temperature and imperfection amplitude recorded in Table 7.1 obtained from eqns (4.17), (5.32) and (6.35) has also been confirmed although there is a consideration to be made, see below, as isolated prop upheaval temperatures, in the presence of fixed anchor points, rise with increasing imperfection amplitude for v_{om}=20 and 30mm (note Table 7.6).

With the thermal data of Table 7.1 dependant upon zero pre-upheaval friction force activation, and therefore zero corresponding axial movement, the foregoing relationship is suitably unaffected by the inclusion of fixed anchor points with respect to the *Blister* and *Empathetic* models. However, the previously discussed limitation upon the inclusion of *Isoprop*'s thermal upheaval expression within Table 7.1 is further supported by the implication that the associated pre-upheaval axial movement may typically include activation of any (additional) fixed anchor points with repercussions for upheaval response being further dependant on variables such as anchor spacing and capacity. Accordingly, a numerical investigation was conducted employing *Isoprop* with the experimental pipe data; Table 7.13 shows that the inverse temperature/imperfection amplitude relationship is valid for $0.5 \leq D/v_{om} \leq 10$ with upheaval temperature mutually increasing with initial imperfection for $0.3 \leq D/v_{om} \leq 0.5$. At upheaval, *Isoprop* model data suggests $0.93N \leq F_{ap} \leq 229N$ as $2mm \leq v_{om} \leq 30mm$.

Given the previously noted status of residual or as-laid stress treatment within the *Isoprop* and *Blister* models, upheaval temperature data experimental/theoretical correlation varies inversely with imperfection amplitude as anticipated. Tables 7.10 and 7.11 suggest that the as-laid, more particularly as-delivered, imperfections become significant for the case of v_{om}=2mm although the concomitant snap action at this amplitude additionally results in increased modelling difficulty. It is considered that this observation supports the *stress-free-when-deformed* assumption made with regard to the synthetic (ie amplitude v_{om}) imperfections; eqns (6.34) and (6.35), for example, would suggest an invariant upheaval experimental/theoretical correlation[13,39], with respect to v_{om}, although the small scale and relatively low static stressing levels are to be noted.

Isolated prop experimentation was more readily constructed to an acceptable standard and upheaval state experimental/theoretical correlation was correspondingly superior to that exhibited in the equivalent (v_{om}) infilled prop studies. Experimental path data display consistency although experimental/theoretical (*Isoprop* and *Blister*) correlation decays with increasing post-

D=9.53mm L_{fap}=5.68m		D=101.6mm L_{fap}=60m		D=219.1mm L_{fap}=130m		D=323.9mm L_{fap}=195m		D=406.4mm L_{fap}=240m	
v_{om} (mm)	T_u (°C)	v_{om} (mm)	T_u (°C)	v_{om} (mm)	T_u (°C)	v_{om} (mm)	T_u (°C)	v_{om} (mm)	T_u (°C)
1	13.61	20	26	50	30.38	50	40.63	100	60.41
2	9.64	30	21.31	80	24.17	100	28.92	200	43.32
3	7.91	40	18.54	100	21.72	150	23.80	300	35.97
4	6.88	50	16.67	120	19.92	200	20.79	355 *	33.40
5	6.21	60	15.31	150	17.96	250	18.77	400	31.74
6 *	5.72	70	14.26	170 *	16.98	260 *	18.45	500	28.97
8	5.08	75 *	13.83	200	15.83	300	17.34	600	27.08
10	4.70	100	12.24	250	14.47	400	15.47	700	25.78
12	4.47	120	11.43	300	13.57	500	14.37	800	24.88
15	4.32	150	10.66	400	12.58	600	13.74	900	24.30
18 **	4.31	170	10.35	500 **	12.26	700	13.42	1000	23.95
20	4.37	200 **	10.10	550	12.27	800 **	13.34	1100 **	23.80
25	4.68	300	10.43	600	12.36	900	13.43	1200	23.82
30	5.18	350	11.05	700	12.78	1000	13.67	1300	23.98
		400	11.90	800	13.45	1100	14.04	1400	24.26
		450	12.94	900	14.32	1200	14.52	1500	24.65
		500	14.15	1000	15.36	1300	15.10		

Notes: * denotes transition from Snap to Stable

** denotes transition from declining to rising of T_u versus v_{om} curve as v_{om} increases.

Table 7.13 Numerical investigation of Upheaval Temperatures of Isolated Prop Model with Fixed Anchor Points ($D/L_{fap} \approx 1/600$)

buckling deformation. Post-upheaval temperature/wavelength characteristics are superior to their temperature/amplitude equivalents in accordance with eqn (1.20) in this respect. Indeed, the cyclic tests displayed high degrees of system recoverability in terms of pipe return to initial wavelength despite the presence of hysteresis perceived to be influenced by friction force action. Further, this friction force activity, when coupled with the snap-related dynamic response in the v_{om}=2mm case, will surely adversely affect the corresponding experimental data.

The key factors involved in subsea pipeline buckling, inertial loading and pipe stiffness opposing thermal action in the presence of an imperfection 'trigger', are not amenable to consistent scaling and it is important to maintain the principal action-response characteristics of the prototype. Figure 7.2 depicts appropriate data appertaining to D/t ratios. Further, whilst some of the lower D/v_{om} ratios employed in the experiments appear excessively so (eg 1/3), taking the D/v_{om} ratio corresponding to the interface between snap and stable response as an indicator shows that the experimental system affords a value of 1.58 against prototype values of $1.35 \geq D/v_{om} \geq 1.15$ relating to pipes in the range $101\text{mm} \leq D \leq 406\text{mm}$. The above ratios involve the use of fixed anchor points employed at a spacing in accordance with $L_{fap}/D \approx 600$ (ie 60m-240m regarding the prototype pipe diameters indicated). It is contended that the foregoing ratios are in accord with acceptable practice. Initial imperfections clearly affect both the experimental and prototype systems although claims for direct equivalence cannot be made. Recourse to an imperfection magnitude v_{om}=2mm, necessary to produce a moderate degree of snap according to the *Isoprop* model, involved an amplitude of only the same order of magnitude of as-laid (on the rigid test bed) undulations elsewhere in the pipe. Attempts to minimise as-laid imperfection effects by increasing the 'synthetic' imperfection whilst maintaining snap response by incorporating, say, constant force 'springs' to represent burial in addition to trenching, were not implemented as snap could not theoretically be produced at v_{om}=10mm even when employing constant force 'springs' which increased the self-weight q by a factor of 150.

Undulations, both vertical and lateral, existed in the respective slip lengths throughout the testing programme and are considered to influence the recorded asymmetric behaviour and system hysteresis. The number of trench-simulating gates employed in a test was minimised for each imperfection amplitude as interference due to lateral as-laid undulations would result in further adverse effects upon asymmetric buckling and system hysteresis. Overall, the buckle amplitude tended to be displaced towards the pipe inlet in 27 of the 45 tests, and towards the outlet in 14, the remaining 4 tests, all for v_{om}=2mm, involving significant pre and post-upheaval amplitude bias 'switching'; see Table 7.14 for details. Pipe wall inlet and outlet temperatures invariably agreed, however, and the above noted proportions of cases regarding amplitude/prop asymmetry surely allay fears of test rig bias per se. The declining degree of experimental/theoretical (ie *Isoprop* and *Blister*) correlation as buckle length and amplitude increase could conceivably be due to ill-defined residual stress affects causing inelastic softening. However, cyclic recovery factors are good and the possibility of adverse 'end effects' must be considered.

End conditions are always important in testing and it was thought that the experimental $L_{fap}/D \approx 600$ ratio appeared very useful in this respect. Furthermore, actual clamping at the prescribed ambient or lock-off temperature involved only transverse pressure, as noted previously, in an attempt to minimise

Test No	Bias	Test No	Bias	Test No	Bias	Test No	Bias	Test No	Bias
1	LHS	10	LHS	19	RHS	28	LHS	37	*
2	RHS	11	LHS	20	RHS	29	LHS	38	LHS
3	LHS	12	LHS	21	LHS	30	LHS	39	LHS
4	LHS	13	RHS	22	RHS	31	LHS	40	LHS
5	LHS	14	RHS	23	RHS	32	LHS	41	RHS
6	LHS	15	LHS	24	RHS	33	LHS	42	LHS
7	LHS	16	LHS	25	LHS	34	*	43	LHS
8	LHS	17	RHS	26	RHS	35	*	44	RHS
9	LHS	18	RHS	27	*	36	RHS	45	LHS

Summary : 27 LHS, 14 RHS and 4 * for a total of 45 Tests.

Notes: LHS, RHS denote asymmetry bias to the inlet or outlet of the test rig respectively. Refer to Table 7.3 for details.

* denotes asymmetry interchanged between inlet and outlet during the test.

Table 7.14 Pipe Buckling Experimentation Bias Table (Post-Upheaval) induced distortion of the pipe-specimen (eg due to twisting, bending, extension or contraction upon clamping). In the context of the pipe specimen possessing the low axial and flexural stiffnesses AE/L_{fap}=0.52 kN/m and EI/L_{fap}=210.8 kNm respectively, the above comments lend confidence. Additional security was obtained by restricting experimental buckle lengths suitably below L_{fap}.

Alternative, full pipeline buckling system testing references have only recently become available[38,50]. These programmes have similarly involved scaled systems employing approximately the same length of specimen. Reference 38 also similarly utilises a synthetic trench configuration whilst Reference 50 considers a buried pipe subject to pressure loading. The limited experimental data available in the former suggest relatively higher upheaval temperatures and stiffer post-upheaval response characteristics than contained herein. Stressing levels appear higher, involving plastic behaviour. However, asymmetry is again prominently displayed.

7.7 Models' Comparisons

The theoretical propositions for the three configurations, ie the *Empathetic*, *Blister* and *Isoprop* models illustrated in Fig 1.7, have already been discussed in Chapters 4, 5 and 6 respectively.

Note should be made regarding the robust performance of the *Empathetic* model which generated conservative upheaval temperatures throughout the forty-five tests. The post-upheaval behavioural loci were also largely conservative, particularly regarding the larger imperfection amplitude tests. Idealised modelling appears to offer little regarding upheaval state definition although it is capable of providing a conservative T_{min} in cases where $T_u > T_{min}$ (ie some cases of low imperfection amplitude snap buckling as typified by Figs 7.11 and 7.12). Furthermore, whilst idealised behavioural loci act as envelopes to respective *Empathetic* model loci, *Isoprop* and *Blister* loci can intersect the associated idealised envelope as shown in Figs 7.10 to 7.14. This would appear to contradict the concept of imperfection loci converging towards idealised systems as post-buckling develops due to the proportionately diminishing effect of the initial imperfection and is worthy of consideration. Whilst all three models display idealised convergence behaviour with regard to buckling force/wavelength characteristics, typified by Tables 5.1 and 6.1 , only the *Empathetic* model insists upon employing the idealised v_m/L^4 relationship of eqn (1.20) throughout. It thereby provides an accurate mathematical interpretation of the contact surface half-space upon which the corresponding idealised modelling is based 'upto' and including the upheaval state - ie $v_m \rightarrow v_{om}$ as $L \rightarrow L_o$ such that $v_{om}/L_o{}^4 = v_m/L^4$.

Importantly, the *Isoprop* and *Blister* models do not provide the same v_m/L^4 relationship; at upheaval, *Isoprop* generates $v_{om}/L_u = v_{om}/(0.96L_o)$ for a common imperfection amplitude v_{om} such that $v_{om}/L_u{}^4 = 1.17v_{om}/L_o{}^4$. These ratios are incompatible with the idealised relationship and suggest that *Isoprop* solutions for amplitude and wavelength will invariably breach the corresponding quasi-idealised envelopes. Additionally, although the *Isoprop* upheaval amplitude/wavelength ratio is within 4% of the idealised value, this is achieved with a crown curvature approximately 50% in excess of the *Empathetic*/idealised equivalent as shown in Table 7.1. Conversely, whilst the *Blister* upheaval amplitude/wavelength ratio is clearly and similarly at odds with its idealised equivalent, be it infinite if based upon a theoretical wavelength $L_u=0$, or equal to $v_{om}/(1.29L_o)$ if rather more nominally based upon the initial infilled prop topology wavelength L_i as illustrated in Fig 5.1. Summarising, only the *Empathetic* model provides for idealised v_m/L^4 - compatible characteristics although both the *Isoprop* and *Blister* models display either amplitude/wavelength or crown curvature characteristics in keeping with their shared physical roots. The underlying physics of these models are, however, neither mutually identical with, nor totally sympathetic to, the perceived idealised equivalent. As discussed previously, the '*Blister*' model relates to a curved non-empathetic half-space for $L<L_i$ whilst the *Isoprop* model provides for flexural action to occur in the absence of upheaval buckling with cusp upheaval occurring upon reversal of wavelength characteristics. The *Blister* model generates idealised loci intersections more readily than the *Isoprop* model, that is they occur at lower temperatures for a common initial amplitude, with, again noting eqn (1.20), temperature/wavelength loci in turn intersecting more readily than their temperature/amplitude counterparts. Indeed, *Isoprop* (and *Blister*) analysis does afford temperature/amplitude loci of a substantially convergent (ie to the respective idealised locus) nature regarding numerical studies to-date employing prototype parameters suffering loci intersection only beyond the elastic range[39] as previously shown in Chapters 5 and 6. That is, the small scale of the tests exaggerates the problem.

7.8 Summary

Improved experimentation, largely concerned with an increase in scale, would involve substantial financial investment although a number of specific improvements suggest themselves. Pre-working or flushing of the pipe at high temperatures could reduce residual stress levels in a prototype-like manner whilst the monitoring of wavelength and amplitude, particularly in the vicinity of upheaval require digital logging. The latter point again implies additional cost, particularly with regard to infilled prop testing where the difficulty of providing a valid scaled imperfection proved substantial. Given that the primary objective was to establish upheaval temperatures by experimentation, however, it is considered that highly satisfactory experimental/theoretical correlation has been achieved.

Both isolated and infilled prop subsea pipeline buckling topologies have been tested. Snap and stable responses have been studied and recovery upon cooling characteristics observed. The three theoretical imperfection models discussed have displayed their own distinct predictive powers within the context of the identified restrictions upon experimentation at small scale. With particular regard to the important upheaval states, the *Empathetic* model is suitably robust whilst the *Isoprop* and *Blister* models afford more economic, whilst remaining *conservative*, data for the larger imperfection cases wherein the as-delivered residual stress effects were minimised. Designers should prevent the infilling of prop-attendant voids wherever possible due to their role in the provision of pre-upheaval flexural energy release in the isolated prop case. Further experimental developments in the field will inevitably depend upon the economic factors involved and the degree of risk considered to exist in offshore practice.

The full system experimental programme and the associated theoretical studies complete Activity 4 of Fig 2.1.

Chapter 8

Comments and Conclusions

8.1 Summary of Findings

In accordance with the comments of Sections 1.1 and 2.3, it is contended that a rational set of complementary, symmetric imperfections, appertaining to subsea pipeline buckling, have been theoretically studied. New models or model developments thereby have been proposed and experimental assessment conducted. The primary activities correspond to the levels 3 and 4 activities of Fig 2.1 and are reported in Chapters 4 to 7 with support provided in Chapter 3.

The two basic (mathematical) forms of imperfection identified, contact undulation and isolated prop, have been considered in terms of three models two of which, *Blister* and *Isoprop*, are based on physical field conditions. The third, *Empathetic* model is based upon a *worst-case-scenario* mathematical conjecture.

The original *Empathetic* model[12] has been subjected to novel developments in Sections 4.3 - 4.5 including the provision of a closed-form upheaval state algorithm which provides a quick guide for design engineers additionally involving explicit snap/stable buckling classification.

The *Blister* model serves as an alternative contact undulation model and although nominally original (ie; an equivalent elsewhere is not available) can, in fact, be considered as a degenerate elastic form of an established inelastic model[19,20]. Its relationship to the *Empathetic* model has served to illustrate the role of crown curvature upon upheaval whilst the equivalence of its formulation with that of the *Isoprop* model once the buckle length develops beyond the imperfection wavelength serves to support this latter, somewhat more contentious model.

The *Isoprop* model, at odds with its predecessors[13,18] elsewhere, provides a completely novel model for design engineers. Without definitive field residual stress data being made available a *worst-case-scenario* type assumption is made regarding the neglection of certain, apparently equilibrium-demanded, initial stressing. This stressing is, however, based upon a historically fictitious state and is also neglected in *Blister* type modelling[19,20]. Given residual stress surely occurs due to fabrication and laying operations, a conservative formulation must be preferred.

Chapters 3 and 7 provide experimental support for and assessment of the three theoretical models, albeit at small scale. The system testing involved the design and construction of a novel experimental rig and showed, with regard to the crucial upheaval state at least, the robust performance of the *Empathetic* model. Should the respective model data be considered too conservative, however, recourse can be made to the less conservative, physically based *Blister* and *Isoprop* model formulations particularly where relatively large imperfections are involved.

Study has been concentrated upon the upheaval state with a view to the prevention of upheaval occurring during in-service operation; ie operating temperatures and pressures are to be maintained below the upheaval threshold wherever possible with any continuous burial clearly compromising recovery characteristics. Caution must also be exercised with regard to pre-upheaval yield occurring in buried topologies in particular, although this enhances the possibility of in-service thermal stress-relieving.

Whilst trenching studies are trench-configuration dependent, the basic Vee-trench studies provide insight into the so-called Standard Model mechanics. For although post-upheaval perturbations would cause trench-incline following behaviour to ensue - hence the additional trench mechanics of Chapters 4, 5 and 6 - upheaval would occur in the vertical mode.

Finally, the ordering of upheaval onset for the various models - *Empathetic* then *Blister* then *Isoprop* [recall eqns (5.84) and (5.85)] - also flags further key behavioural patterns. These importantly include the respective ratios of snap/stable case studies for the standard and updated topologies.

8.2 Further Work

Further experimentation involving a larger scale is required for more definitive study including residual stress considerations. This would involving additional complexity and cost and would depend heavily upon the needs of industry. Additional data could be obtained from the present rig; for example, the tests could be repeated upon further specimens - a single specimen was employed throughout the experimental systems testing in order to restrict the as-delivered imperfection variability. Such data would remain subject to scaling concerns, however.

The development of asymmetric[40] models, possibly including the use of finite elements[20], must surely be undertaken; asymmetry was encountered throughout the systems testing. This is perhaps the most pressing theoretical development need.

Further theoretical developments could include non-linear, inelastic studies including the presence of prototype residual stress data. Clearly, the *Empathetic*, *Blister* and *Isoprop* models could be further developed themselves; here, a slip length formulation which was deformation-dependent[12] but generated finite length slip-length would be useful.

8.3 Closing Remarks

Three model formulations possessing varying degrees of originality have been proposed in the context of modern offshore employment including considerations of trenching and/or burial. Novel experimentation has been conducted and the models accordingly assessed. A software suite has been produced suited to the perceived needs of offshore engineering.

REFERENCES

1. Kerr, A.D., On the stability of the railroad track in the vertical plane, *Rail International*, **2** (February 1974) 131-142.

2. Martinet, A., Flambement des voies sans joints sur ballast et rails de grande longuer, (Buckling of the jointless track on ballast and very long rail - in French). *Revenue Generale des Chemins de Fer*, **10** (1936) 212-230.

3. Allen, H.G. & Bulson, P.S., Background to buckling, McGraw-Hill, 1980, 82-89.

4. Timoshenko, S.P. & Gere, J.M., Theory of Elastic Stability. 2nd Edition, McGraw-Hill, New York, 1961, 76-81.

5. Croll, J.G.A. & Walker, A.C., Elements of structural stability, Macmillan Press 1976.

6. Hobbs, R.E., In-service buckling of heated pipelines,*Journal of Transportation Eng.*, ASCE, **110** (2) (March 1984) 175-188.

7. Hobbs, R.E., Pipeline buckling caused by axial loads, *Journal of Constructional Steel Research*, **1** (2) (January 1981) 2-10.

8. Taylor, N., Richardson, D. & Gan A.B., On submarine pipeline frictional characteristics in the presence of buckling, *Proc. of the 4th Int. Symposium on*

Offshore Mech. and Arc. Eng., ASME, Dallas, Texas, (February 1985) 508-515.

9. Taylor N. & Gan A.B., Refined modelling for the vertical buckling of submarine pipelines, *Journal of Constructional Steel Research*, **7** (1987) 55-74.

10. Taylor N. & Gan A.B., Refined modelling for the lateral buckling of submarine pipelines, *Journal of Constructional Steel Research*, **6** (1989) 143-162.

11. Taylor N. & Gan A.B., Regarding the buckling of pipelines subject to axial loading, *Journal of Constructional Steel Research*, **4** (1) (January 1984) 45-50.

12. Taylor N. & Gan A.B., Submarine pipeline buckling-imperfection studies, *Thin-Walled Structures*, **4** (4) (1986) 295-323.

13. Boer, S.,et al., Buckling considerations in the design of the gravel cover for a high-temperature oil line, *Proc 18th Annual OTC*, Houston, Texas, (May 1986).

14. Richards, D.M. & Andronicou, A., Seabed irregularity effects on the buckling of heated submarine pipelines, *Holland Offshore*, Amsterdam, (November 1986).

15. Yun, H. & Kyriakides, S., Model for beam mode buckling of buried pipelines, *Journal of Eng. Mech.*, ASCE, (February 1985).

16. Friedmann, Y., Some aspects of the design buried hot pipelines, *1986 European Seminar, Offshore Oil and Gas Pipeline Technology*, (January 1986).

17. Nielsen, N.J.R., Pedersen, P.T., Grundy, A.K. & Lyngberg, B.S., New design criteria for upheaval creep of buried sub-sea pipelines, *Seventh Int. Conference on*

Offshore Mechanics and Arctic Eng., Houston, Texas, (February 1988).

18. Yun H. & Kyriakides, S., Thermal buckling of offshore pipelines, *Deparment of Aerospace Eng. and Eng. Mech.*, EMRL Rep. No. 87/1, Un. Texas Austin, (January 1987).

19. Pedersen, P.T. & Michelsen, J., Large deflection upheaval buckling of marine pipelines, *Proc. Behaviour of Offshore Structures (BOSS)*, Trondheim, Norway, **3** (June 1988) 965-980.

20. Pedersen, P.T. & Jensen, J.J., Upheaval creep of buried heated pipeline with initial imperfections, *Journal of Marine Structures*, **1** (1988) 11-22.

21. Ellinas, C.P., Supple, W.J. & Vastenholt, H., Prevention of upheaval buckling of hot submarine pipelines by means of intermittent rock dumping, *Proc 22nd Annual OTC*, Houston, Texas, (May 1990) 7-10.

22. Klever, F.J., Van Helvoirt, L.C. & Sluyterman, A.C., A dedicated Finite-element model for analyzing upheaval buckling response of submarine pipelines, *Proc 22nd Annual OTC*, Houston, Texas, **2** (May 1990) 529-538.

23. Craig, I.G., Nash, N.W. & Oldfield, G.A., Upheaval buckling: A practical solution using hot water flushing technique, *Proc 22nd Annual OTC*, Houston, Texas, (May 1990).

24. Palmer, A.C., Ellinas, C.P., Richards, D.M. & Guijt, J., Design of submarine pipelines against upheaval buckling, *Proc 22nd Annual OTC*, Houston, Texas, **4** (May 1990) 540-550.

25. Schaminee, P.E.L., Zrn, N.F. & Schotman, G.J.M., Soil response for pipeline upheaval buckling analyses: Full-scale laboratory tests and modelling, *Proc 22nd Annual OTC*, Houston, Texas, **4** (May 1990) 563-572.

26. Guijt, J., Upheaval buckling of offshore pipelines; Overview and Introduction, *Proc 22nd Annual OTC*, Houston, Texas, **4** (May 1990) 573-578.

27. Nielsen, N.J.R., Lyngberg, B. & Pedersen, P.T., Upheaval buckling failures of insulated buried pipelines-a Case Story, *Proc 22nd Annual OTC*, Houston, Texas, **4** (May 1990) 581-600.

28. Lyons, C.G., Soil resistance to lateral sliding of marine pipelines, *5th Offshore Technology Conference*, OTC 1876, **2** (1973) 479-484.

29. Gulhati, S.K., Venkatapparao, G. & Varadarajan, A., Positional stability of submarine pipelines, *I.G.S. Conference on Geotechnical Engineering*, **1** (1978) 430-434.

30. Anand, S. & Agarwal, S.L., Field and laboratory studies for evaluating submarine pipeline frictional resistance, *Transaction of the American Society of Civil Engineers*, Journal of Energy Resources Technology, **103** (September 1981) 250-254.

31. Agarwal, S.L. & Malhotra, A.K., Frictional resistance for submarine pipelines in soft clays, *I.G.S. Conference on Geotechnical Engineering*, **1** (1978) 373-379.

32. Grazzaly, O.I. & Lim, S.J., Experimental investigations of pipelines stability in very soft clay, *7th Offshore Technology Conference*, OTC 2277, **2** (1975) 315-326.

33. Wantland, G.M. O'Neill, M.W., Reese, L.C. & Kalajian, E.H., Lateral stability of pipelines in clay, *11th Offshore Technology Conference*, OTC 3477, (1979) 1025-1034.

34. Karal, K., Lateral stability of submarine pipelines, *9th Offshore Technology Conference*, OTC 2967, **4** (1977) 71-78.

35. Bjerrum, L., Geotechnical problems involved in foundations of structures in the North Sea, *Geotechnique 23*, **3** (1973) 319-358.

36. Taylor, N., Tran, V.C. & Richardson, D., Interface modelling for upheaval subsea pipeline buckling, *Proceedings of 4th International Conference on Computational Methods and Experimental Measurements*, Capri, Italy, (May 1989) 269-282.

37. Taylor, N. & Tran, V.C., Experimental and Theoretical Studies in Subsea Pipeline Buckling, Submitted to *Journal of Marine Structures* for publication.

38. Raoof, M. & Maschner, E., Thermal buckling of subsea pipeline, *Proc. Offshore Mech. Arctic Eng. Conf.*, Glasgow, V (June 1993) 21-29.

39. Taylor, N. & Tran, V.C., Prop-Imperfection subsea Pipeline Buckling, *Marine Structures*, **6** (1993) 325-358.

40. Ballet, J.P. & Hobbs, R.E., Asymmetric effects of prop imperfections on the upheaval buckling of pipelines, *Thin-Walled Structures*, **13** (1992) 355-373.

Ells

41. Palmer, A.C., Hutchinson, G. & Ellis, J.W., Configuration of submarine pipelines during laying operations. Transaction of the American Society of Mechanical

Engineers, *Journal of Engineering for Industry*, **96** (1974) 1112-1118.

42. Timmermans, W.J., Deepwater pipelaying techniques improve, *Oil and Gas Journal*, (November 1974) 83-88.

43. Brown, R.J., New methods needed for deep water pipe-laying, *Oil and Gas Journal*, (August 1977) 58-61.

44. Hobbs, R.E., The lifting of pipelines for repair of modification, *Proceedings of the Institution of Civil Engineers*, Part 2, 67, (December 1979) 1003-1013.

45. Bowles, J.E., Foundation Analysis and Design, 3rd Edition, McGraw-Hill, 1982, 59-60.

46. Traumann, C.H. et al., Uplift Force-Displacement Response of Buried Pipe, *ASCE Journal of Geotechnical Engineering*, Vol III, **9**, (Sep 1985).

47. Hobbs, R.E. & Liang, F., Thermal buckling of pipelines close to restraints, *Proc. Offshore Mech. Arctic Eng. Conf.*, The Hague, Paper OMAE-89-812, (1989).

48. Nielsen, N.J.R. et al., New design criteria for upheaval creep of buried subsea pipelines, *Proc 22nd Annual OTC*, Houston, Texas, (May 1990) 243-249.

49. Ju, G.T. & Kyriakides, S., Thermal buckling of offshore pipelines, *Journal of OMAE*, **110** (November 1988) 355-364.

50. Maltby, M., Upheaval of buried pipelines in a model soil, Ph.D. Thesis, Cambridge University (December 1992).

51. Taylor, N. & Hirst, P., Strut behaviour: sub-buckling cyclic excursion effects and risk assessment, Res Mechanics, **28** (1989) 139-189.

Appendix A

GUIDANCE TO COMPUTER PROGRAM

Page

Introduction

In order to support the theoretical formulation described earlier in the previous chapters, a user-friendly PC-based computer program has been developed to perform a non-linear analysis for the imperfection triggered, in-service upheaval of subsea pipeline buckling model. The model is capable of calculating all thermal action characteristics of a geometrically imperfect pipeline subject to pressure and temperature loads. In each model, the imperfection is characterised by an imperfection amplitude and corresponding imperfection wavelength, or alternately by a ratio between imperfection amplitude and wavelength, assuming a symmetrical imperfection shape about the imperfection apex. The analysis has been categorised into four main models, typically classical Quasi-Idealised, Contact Undulation, Isolated Prop and Infilled Prop models. A detailed description of each model will be discussed later.

Method of Analysis

From a specified imperfection amplitude (v_{om}) or imperfection ratio (v_{om}/L_o or v_{om}/L_i), the corresponding initial imperfection length (L_o or L_i) will then be calculated depending whether it is a Contact Undulation or Isolated Prop type model. Taking the value of L_o or L_i as a starting point, the program will perform the calculation process for other values of buckle length L, noting that such incremental changes in buckle lengths can be specified at the beginning of the analysis. In each calculation step, not only temperature rise T and maximum compressive stress σ_m are calculated but other relevant thermal characteristics such as buckle force P, slip length L_s, total end shortening u_s and fixed anchorage force F_{ap}, (if appropriate, are also determined and stored in an array for further use.

In order to increase the degree of accuracy and to minimise the effect of rounding off errors upon the results, double-precision procedure has been used throughout the calculation and where appropriate, a numerical tolerance of 10^{-6} has also been allowed for in all iteration processes.

Its output is also organised in an user-friendly manner, either numerically or graphically. The hard copy of graphical output can be obtained via an Epson dot matrix printer or Color-Pro Plotter.

Computer Program Manual

The foregoing is a step-by-step explanation of the program execution.

Screen Display No 1

```
                    IMPERFECT  UPHEAVAL
              SUBSEA PIPELINE BUCKLING ANALYSIS
            FULLY MOBILISED ISOPROP WITH FAP MODEL


      IMPERFECTION TO BE INPUTTED IN THE FORM OF :

        1. Imperfection ratio vom/Li
        2. Imperfection height vom
   Option : ? 2
```

Screen Display No 2

```
IMPERFECTION HEIGHT :

     *. (Please note ONLY ONE imperfection height is allowed at this stage
     *. Imperfection height vom (mm) = ? 100
     *. Buckle length increment in (mm) = ? 1000
```

Screen Display No 3

```
                    IMPERFECT  UPHEAVAL
              SUBSEA PIPELINE BUCKLING ANALYSIS
            FULLY MOBILISED ISOPROP WITH FAP MODEL
         ************************************************************
         Program is running for
         Imperfection height of  20  (mm)
---------------------------------------------------------------------------
         Initial buckle   amplitude in (mm) Voc =  20
         Initial imperfection length    in (mm) Li  =  37052.75
---------------------------------------------------------------------------
Io. of calculation steps ....

1       2       3       4       5       6       7       8       9       10
11      12      13      14      15      16      17      18      19      20
21      22      23      24      25      26      27      28      29      30
31      32      33      34      35      36      37
```

Screen Display No 4

```
        The FULLY MOBILISED ISOPROP with FAP
             analysis has now completed
              results have been saved
```

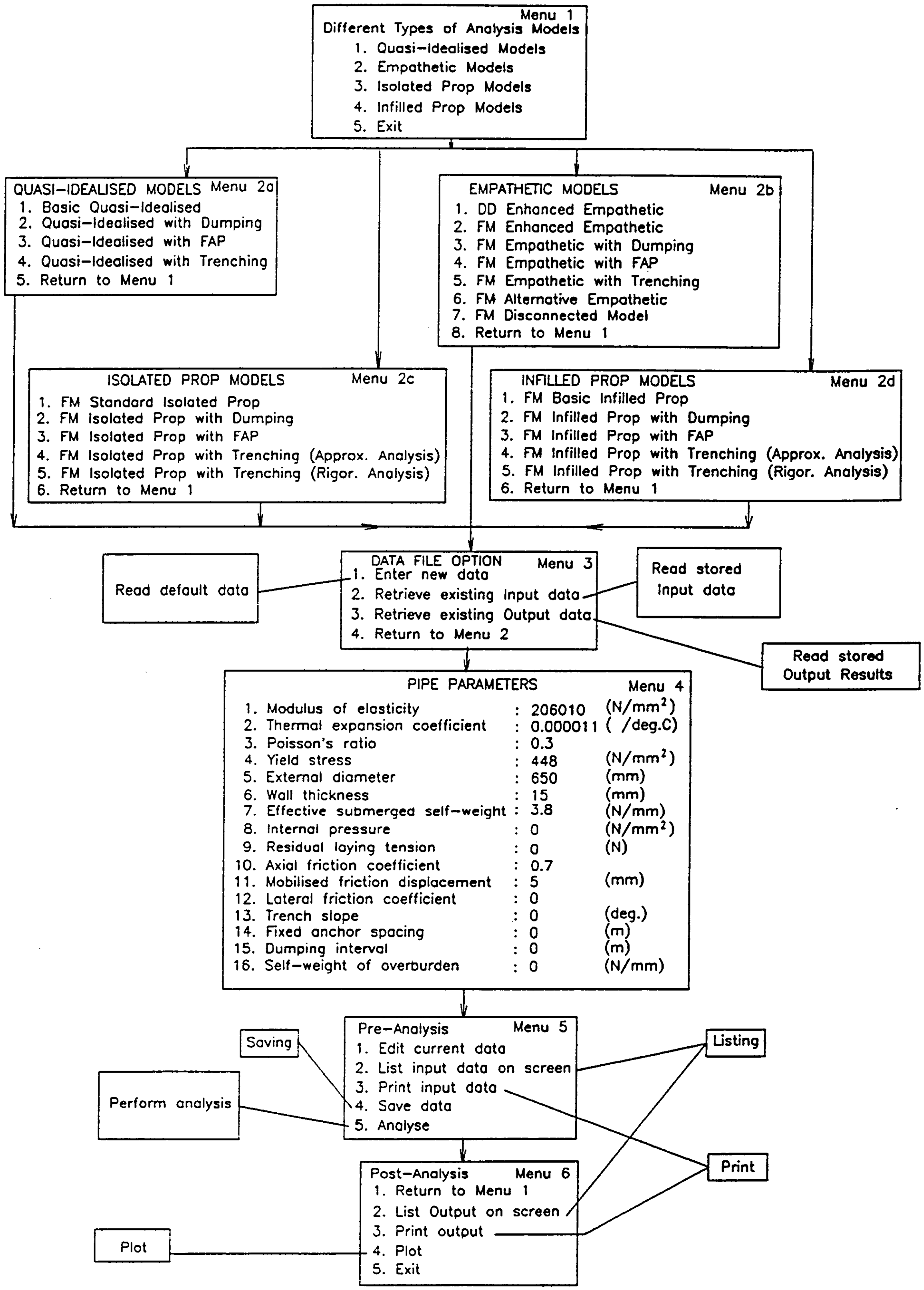

COMPUTER PROGRAM FLOW CHART

Menu 1

Imperfect Upheaval Subsea Pipeline Buckling

DIFFERENT TYPES OF ANALYSIS MODELS

1. Quasi-Idealised Models
2. Empathetic Models
3. Isolated Prop Models
4. Infilled Prop Models
5. Exit

Option 1 : Allow user to perform the analysis based on the classical quasi-idealised model.

Option 2 : Perform the analysis based on the assumption that the pipeline remains in continuous contact with some distinct vertical undulation in an otherwise idealised horizontal and straight lie.

Option 3 : Allow user to carry the analysis where the pipeline crosses a non-parallel pipe or the presence of an intervening rock.

Option 4 : as similar to option 2 but the voids becomes infilled with leaching sand.

Option 5 : Exit.

All analysis models presume system symmetry and seabed or trench bottom rigidity, together with indefinitely small deformation and linear elastic properties. Overall, each model's formulation includes interpreting the in-service temperature and pressure rises over ambient suffered by the pipe. In addition to that, each model possesses unique longitudinal equilibrium and compatibility statements, problem definition being completed in terms of individual buckling/ flexural relationships.

Menu 2

Imperfect Upheaval Subsea Pipeline Buckling

QUASI-IDEALISED MODELS

DIFFERENT TYPES OF ANALYSIS

1. Basic Quasi-Idealised
2. Quasi-Idealised with Dumping
3. Quasi-Idealised with FAP
4. Quasi-Idealised with Refined Trenching
5. Return to Menu 1

Option 1 : Perform analysis of Basic Quasi-Idealised Model based on a quasi-idealised straight lie of the pipeline laid on a flat, rigid surface.

Option 2 : as per Option 1, but in this case the basic model is replaced by the presence of discrete rock dumping, in which the pipe is covered by an additional overburden.

Option 3 : as similar to option 1, but the method of Fixed Anchor Points is used instead.

Option 4 : as per Option 1, the pipe is now laid along the bottom of a trench.

Option 5 : Go back to last Menu.

Menu 2b

Imperfect Upheaval Subsea Pipeline Buckling

EMPATHETIC MODELS

DIFFERENT TYPES OF ANALYSIS

1. Deformation-Dependent Enhanced Empathetic
2. Fully-Mobilised Enhanced Empathetic
3. FM Empathetic with Discrete Dumping
4. FM Empathetic with Fixed Anchor Points
5. FM Empathetic with Refined Trenching
6. FM Alternative Empathetic
7. FM Disconnected Model
8. Return to Menu 1

Option 1 : Perform analysis of Enhanced Empathetic Model with deformation--dependent characteristics of the pipe's friction-displacement.

Option 2 : as per Option 1, but the Fully-Mobilised characteristics of the pipe's friction-displacement is employed instead.

Option 3 : as per Option 2, but the model is now being enhanced by the used of discrete dumping.

Option 4 : as per Option 2, the enhancement is in the form of fixed anchor points.

Option 5 : again as per Option 2, but the pipe's self-weight in this case is being modified by trenching technique.

Option 6 : Perform analysis similar to that of Option 2, but a variation is incorporated on this model by involving substitution of the empathetic relationship before application of the Stationary Principle.

Option 7 : the relationship between the initial buckle amplitude and the buckle length is disconnected.

Option 8 : Go back to last Menu.

Menu 2c

Imperfect Upheaval Subsea Pipeline Buckling

ISOLATED PROP MODELS

DIFFERENT TYPES OF ANALYSIS

1. Fully-Mobilised Standard Isolated Prop
2. FM Isolated Prop with Discrete Dumping
3. FM Isolated Prop with Fixed Anchor Points
4. FM Isolated Prop with Refined Trenching
5. FM Isolated Prop with Rigorous Trenching
6. Return to Menu 1

Option 1 : Perform analysis in which the imperfection is represented by an isolated rock and the Fully-Mobilised characteristics of the pipe's friction-displacement is also incorporated.

Option 2 : as per Option 2, but the model is now being developed further by the used of discrete dumping.

Option 3 : as per Option 2, the development is in the form of fixed anchor points.

Option 4 : again as per Option 2, but the pipe's self-weight in this case is being modified by trenching technique. A refined analysis is employed by replacing, within the buckle, the inertial force m in place of the effective submerged self-weight q throughout the computational procedure of the standard isolated prop model.

Option 5 : in this case, the inertial force m only replaces the effective submerged self-weight q following the movement of the buckled curve along the slope, whilst the initial imperfection curve remains unaltered.

Option 6 : Go back to last Menu.

Menu 2d

Imperfect Upheaval Subsea Pipeline Buckling

INFILLED PROP MODELS

DIFFERENT TYPES OF ANALYSIS

1. Fully-Mobilised Standard Infilled Prop
2. FM Infilled Prop with Discrete Dumping
3. FM Infilled Prop with Fixed Anchor Points
4. FM Infilled Prop with Refined Trenching
5. FM Infilled Prop with Rigorous Trenching
6. Return to Menu 1

Option 1 : Perform analysis in which the imperfection is represented by an isolated rock with the void being filled by leaching sand and the Fully-Mobilised characteristics of the pipe's friction-displacement is also incorporated.

Option 2 : as per Option 2, but the model is now being developed further by the used of discrete dumping.

Option 3 : as per Option 2, the development is in the form of fixed anchor points.

Option 4 : again as per Option 2, but the pipe's self-weight in this case is being modified by trenching technique. Approximate analysis is employed by replacing the inertial force m in place of the effective submerged self-weight q throughout the computational procedure of the standard isolated prop model.

Option 5 : in this case, the inertial force m only replaces the effective submerged self-weight q following the movement of the buckled curve along the slope, whilst the initial imperfection curve remains unaltered.

Option 6 : Go back to last Menu.

Menu 3
Imperfect Upheaval Subsea Pipeline Buckling
FULLY-MOBILISED ISOLATED PROP
DATA FILE OPTIONS
1. Enter new data 2. Retrieve existing input data (.IN) 3. Retrieve existing output data (.OUT) 4. Return to Menu 2

Option 1 : Allow the user to enter data for a completely new model.

Option 2 : Allow the user to retrieve input data created in a previous run under filename extension ********.IN.

When this option is selected, a directory of input data files appears as

Directory of input data files :

AAAA.IN   BBBB.IN   CCCC.IN

Please select input data file name :

Assume that file AAAA.IN is selected, then just typing in AAAA

Option 3 : Allow the user to retrieve output data created in a previous run under filename extension ********.OUT.

When this option is selected, a directory of output data files appears as

Directory of output data files :

AAAA.OUT   BBBB.OUT   CCCC.OUT

Please select output data file name :

Assume that file BBBB.OUT is selected, then just typing in BBBB

Option 4 : Go back to Menu 1.

Menu 4

Imperfect Upheaval Subsea Pipeline Buckling
FM ISOLATED PROP WITH FIXED ANCHOR POINTS
PIPE PARAMETERS

1. Modulus of Elasticity	:	206000	(N/mm^2)
2. Thermal expansion coefficient	:	0.000011	($/^oC$)
3. Poisson's ratio	:	0.3	
4. Yield stress	:	448	(N/mm^2)
5. External diameter	:	650	(mm)
6. Wall thickness	:	15	(mm)
7. Effective submerged self-weight	:	3.8	(N/mm)
8. Internal pressure	:	0	(N/mm^2)
9. Residual laying tension	:	0	(N)
10. Axial friction coefficient	:	0.7	
11. Mobilised friction coefficient	:	5	(mm)
12. Lateral friction coefficient	:	0	
13. Trench slope	:	0	(deg.)
14. Fixed anchor spacing	:	0	(m)
15. Dumping interval	:	0	(m)
16. Self-weight of overburden	:	0	(N/mm)

At this point, a menu is displayed showing all the relevant pipe parameters to the chosen analysis model. This Menu is referred to as the Edit PIPE PARAMETERS Menu and the number of parameters displayed vary from a minimum of 10 for an Enhanced Empathetic Model to a maximum of 16 for a Developed Discrete Dumping Model.

If Option 1 from the previous Menu was selected, then the default pipe parameters will appear on the screen as shown above. To change the default values to your own values, carrying out the following steps,

a. Use "U" or "D" key to move the cursor and press <CR> to accept
b. Type in the new value and press <CR> to accept
c. Repeat the same process for any further changes
d. Press <ESC> to store the entire set of displayed parameters.

Menu 5

Imperfect Upheaval Subsea Pipeline Buckling

FM ISOLATED PROP WITH FIXED ANCHOR POINTS

PRE-ANALYSIS OPTIONS

1. Edit current data
2. List input data on screen
3. Print input data
4. Save data
5. Analyse

Option 1 : Return to Edit Pipe Parameters Menu with the opportunity to modify the current data

Option 2 : Allow the user to view input parameters on screen

Option 3 : Allow the user to obtain hard copy of input data

Option 4 : Save the current input data without analysing it

Option 5 : Perform the same task as per option 4 but in this case the analysis will be carried out after saving input data.

Depending on the type of analysis model being chosen from Menu 2(a), (b), (c) or (d) then the appropriate program will be linked to perform the analysis. At this stage, before the program starts, it allows the user to specify the type of the imperfection topology to be used in the analysis, either in the form of an imperfection height or imperfection ratio. For each type of imperfection selected, the user also has the opportunity to specify the buckle length increment to be used in the calculating process.

A typical analysis programme is displayed on screen as follows (please note that, at this stage of the research programme, only <u>ONE</u> imperfection to be allowed in the analysis at any one time).

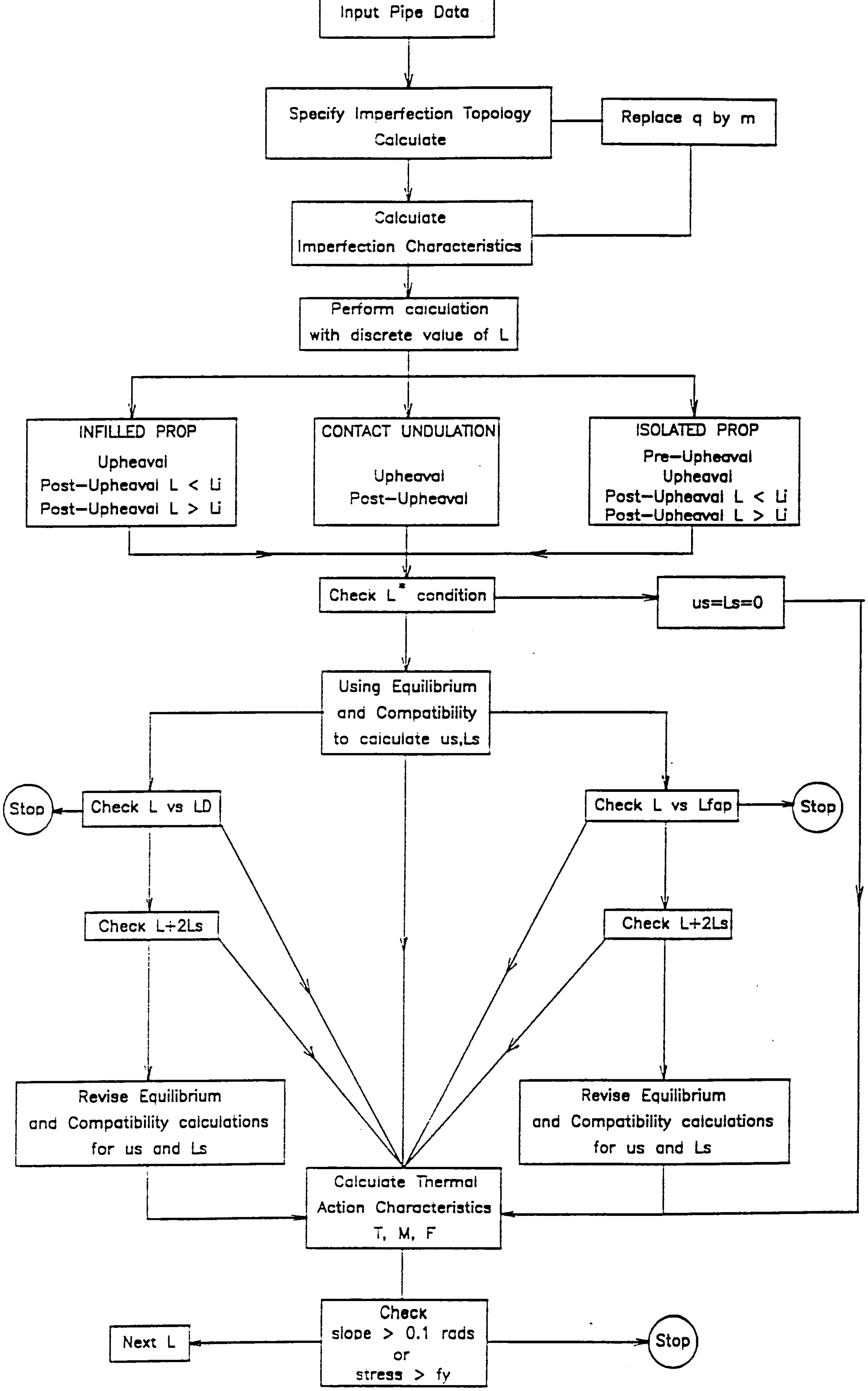

Typical Analytical Model Flow Chart

Menu 6

Imperfect Upheaval Subsea Pipeline Buckling

FM ISOLATED PROP WITH FIXED ANCHOR POINTS POST-ANALYSIS OPTIONS

1. Return to Menu 1
2. List output on screen
3. Print output
4. Draw graph
5. Exit

Option 1 : Return to Models of Analysis Menu 1

Option 2 : Allow the user to view output on screen

Option 3 : Allow the user to obtain numerical output from printer

Option 4 : Allow the user to obtain graphical output of the results

Option 5 : Terminate the analysis and log-off.

Menu 7

Imperfect Upheaval Subsea Pipeline Buckling

GRAPH TYPES

1. Temperature vs Buckle Amplitude T vs v_m
2. Buckle Force vs Buckle Amplitude P vs v_m
3. Total Stress vs Buckle Amplitude f vs v_m
4. Temperature vs Buckle Length T vs L
5. Buckle Force vs Buckle Length P vs L
6. Total Stress vs Buckle Length f vs L
7. Exit

Options 1-6: Allow user to produce the graph of Temperature Rise, or Buckle Force, or Total Stress versus Buckle Amplitude or Buckle Length on screen.

Option 7 : Exit from graph plotting option.

Menu 8

Imperfect Upheaval Subsea Pipeline Buckling

Temperature vs Buckle Amplitude T vs v_m

GRAPH DATA FILE OPTIONS

1. Create new plot file
2. Retrieve existing plot file (.DAT)
3. Retrieve existing output data (.OUT)
4. Return to GRAPH TYPES Menu

Option 1 : Allow the user to enter data for a completely new plot file.

Option 2 : Allow the user to retrieve previously created plot data file under filename extension ********.DAT.

Option 3 : Allow the user to retrieve output data created in a previous analytical run under filename extension ********.OUT.

When this option is selected, a directory of output data files appears as

Directory of output data files :

AAAA.OUT BBBB.OUT CCCC.OUT

Number of files required to plot (1-5) : 1

File name : BBBB

Assume that only one file is required under filename BBBB.OUT

Option 4 : Go back to Menu 7.

Menu 9

Imperfect Upheaval Subsea Pipeline Buckling
Temperature vs Buckle Amplitude T vs v_m
GRAPH PARAMETERS

1. X-axis....	Initial value	: 0	(m)
2.	Final value	: 5	(m)
3.	Step	: 0.5	(m)
4.	Grid (Y=Yes; N=No)	: Y	
5. Y-axis....	Initial value	: 0	(deg.C)
6.	Final value	: 150	(deg.C)
7.	Step	: 10	(deg.C)
8.	Grid (Y=Yes; N=No)	: Y	
9. Number of Curve(s) to be plotted		: 1	
10. Number of plotting points/curve		: 50	
11. Graph Title		: EXAMPLE	
12. Data Output filename (.OUT) #1		: BBBB	
13. Data Output filename (.OUT) #2		: NONE	
14. Data Output filename (.OUT) #3		: NONE	
15. Data Output filename (.OUT) #4		: NONE	
16. Data Output filename (.OUT) #5		: NONE	

Options 1-3: Set the scale on the X-axis by specifying INITIAL and FINAL VALUES with STEP increment by default as shown or entered manually.

Option 4 : Allow vertical grid lines to be drawn at each STEP increment as requested by " Y " option, otherwise no lines will be drawn.

Options 5-8: similar to Options 1-4, but involving scaling on Y-axis.

Option 9 : Allow number of curves to be plotted on the same graph, (maximum of 5).

Option 10 : Allow user specify number of plotting points per curve, noting number of calculation steps when performing the analysis of selected model in Menu 5. (eg Screen 3 on page A14 shows 59 steps in the analysis).

Option 11 : Specify plot name to be saved under extensions *****.DAT.

Options 12-16: Depending on number of OUT files and filenames requested in Option 3 of Menu 8, these names will re-appear again in these options for identification purposes only.

After all, all information contained in this Menu will then be stored as a *****.DAT file whose name has been selected in Option 11, this file can either be retrieved from Option 2 of Menu 8 or altered from Option 1 of Menu 10.

Menu 10

Imperfect Upheaval Subsea Pipeline Buckling

Temperature vs Buckle Amplitude T vs v_m

PLOT OPTIONS

1. Edit current graph parameters
2. Plot on screen
3. Plot on EPSON-Printer
4. Plot on Color-Pro Printer
5. Return to POST-ANALYSIS Menu 6

Option 1 : Return to Graph Parameters Menu with the opportunity to modify the current data

Option 2 : Allow the user to view graph on screen

Option 3 : Allow the user to obtain hard copy from EPSON Printer

Option 4 : Allow user to obtain hard copy from Color-Pro Plotter

Option 5 : Return to POST-ANALYSIS Menu, hence EXIT.

Appendix B

THERMO-MECHANICAL SYSTEM EXPERIMENTATION - TEST DATA

Stable Buckling Isolated Prop with Fixed Anchor Points

Heating Test No 1

Date 15-8-1991
Time start : 11:05 am — Time finish : 12:30 pm
v_{om}=30mm — L_i=4930mm
Pressure: Inlet (I/L)=0.92 bar — Outlet (O/L) = 0
Rotation about imperfection = 0 degrees
Rotation about pipe's axis = 0 degrees

Temperature (°C)			Spine Temp.	v_m (mm)	Buckle length (mm)			Remarks
I/L	O/L	Rise			I/L	O/L	Total	
20.4	20.4	0	23.6	30	2420	2510	4930	
21.6	21.6	1.2	23.6	30	2160	2510	4670	
22.6	22.6	2.2	23.6	30	2120	1990	4110	
23.6	23.6	3.2	23.6	30	1900	1900	3800	
24.4	24.4	4.0	23.6	30	1880	1780	3660	
25.5	25.5	5.1	23.6	30.57	1870	1730	3600	Upheaval
26.5	26.5	6.1	23.6	31.87	1900	1780	3680	Apex @ 200 LHS
29.4	29.4	9.0	23.6	37.02	2170	1780	3950	no change
32.4	32.4	12.0	23.6	43.87	2300	1780	4080	Apex @ 300 LHS
35.2	35.2	14.8	23.6	50.0	2300	1940	4240	Apex @ 200 LHS

Stable Buckling Isolated Prop with Fixed Anchor Points

Heating Test No 2

Date 19-8-1991
Time start : 9:45 am — Time finish : 10:50 am
v_{om}=30mm — L_i=4910mm
Pressure: Inlet (I/L)=0.92 bar — Outlet (O/L) = 0
Rotation about imperfection = 0 degrees
Rotation about pipe's axis = 120 degrees

Temperature (°C)			Spine Temp.	v_m (mm)	Buckle Length (mm)			Remarks
I/L	O/L	Rise			I/L	O/L	Total	
20.5	20.5	0	21.2	30	2410	2500	4910	
21.5	21.5	1.0	21.2	30	2180	2500	4680	
22.5	22.5	2.0	21.2	30	2120	2030	4150	
23.6	23.6	3.1	21.2	30	1860	2000	3860	
24.5	24.5	4.3	21.2	30	1860	1950	3810	
25.3	25.3	4.8	21.2	30	1830	1950	3780	Upheaval
26.3	26.3	5.8	21.2	30.13	1530	2330	3860	Apex @ 350 RHS
28.4	28.3	7.8	21.2	34.16	1510	2460	3970	Apex @ 400 RHS
30.2	30.2	9.7	21.2	38.28	1480	2500	3980	Apex @ 500 RHS

Stable Buckling Isolated Prop with Fixed Anchor Points

Heating Test No 3

Date 19-8-1991
Time start : 11:10 am   Time finish : 12:30 pm
v_{om}=30mm L_i=4740mm
Pressure: Inlet (I/L)=0.92 bar   Outlet (O/L) = 0
Rotation about imperfection = 0 degrees
Rotation about pipe's axis = 240 degrees

Temperature (°C)			Spine Temp.	v_m (mm)	Buckle length (mm)			Remarks
I/L	O/L	Rise			I/L	O/L	Total	
20.5	20.5	0	21.2	30	2410	2330	4740	
21.5	21.5	1.0	21.2	30	2180	2300	4480	
22.4	22.4	1.9	21.2	30	2150	2040	4190	
23.4	23.4	2.9	21.2	30	2120	1940	4060	
24.3	24.3	3.8	21.3	30	1880	1910	3790	
25.3	25.3	4.8	21.3	30	2120	1640	3760	
25.6	25.6	5.1	21.3	30.2	2170	1540	3710	Upheaval
26.4	26.4	5.9	21.3	32.23	2180	1540	3720	Apex @ 300 LHS
28.3	28.3	7.8	21.4	37.35	2210	1540	3750	Apex @ 350 LHS
30.4	30.4	9.9	21.4	41.44	2220	1650	3870	Apex @ 300 LHS
32.2	32.2	11.7	21.4	45.46	2410	1640	4050	Apex @ 370 LHS
34.2	34.2	13.7	21.4	49.31	2480	1650	4130	Apex @ 400 LHS

Stable Buckling Isolated Prop with Fixed Anchor Points

Heating Test No 4

Date 10-7-1992
Time start : 2:20 pm   Time finish : 3:15 pm
v_{om}=30mm L_i=4950mm
Pressure: Inlet (I/L)=0.90 bar   Outlet (O/L) = 0
Rotation about imperfection = 180 degrees
Rotation about pipe's axis = 0 degrees

Temperature (°C)				v_m (mm)	Buckle Length (mm)			Remarks
I/L	O/L	Mean	Rise		I/L	O/L	Total	
20.67	20.84	20.75	0	30	2710	2240	4950	
21.78	21.92	21.85	1.00	30	2570	2100	4570	
22.63	22.69	22.66	1.91	30	2280	2100	4280	
23.56	23.68	23.62	2.87	30	2200	2050	4150	
24.70	24.75	24.72	3.97	30	2120	2030	4050	
25.55	25.65	25.60	4.85	30	2100	2010	3840	
26.63	26.70	26.66	5.91	30	1870	1920	3790	Upheaval
27.52	27.68	27.60	6.85	30.66	1880	1820	3800	Apex @ 150 LHS
30.54	30.55	30.54	9.79	35.81	2100	1820	3920	Apex @ 270 LHS
32.33	32.41	32.37	11.62	39.73	2130	1820	3950	no change
34.42	34.49	34.45	13.70	43.51	2190	1830	4020	Apex @ 300 LHS
36.34	36.38	36.36	15.61	47.31	2190	1890	4080	no change
38.18	38.36	38.27	17.52	50.74	2200	1910	4110	no change

Stable Buckling Isolated Prop with Fixed Anchor Points

Heating Test No 5

Date 10-7-1992
Time start : 3:30 pm   Time finish : 4:10 pm
v_{om}=30mm L_i=4960mm
Pressure: Inlet (I/L)=0.90 bar   Outlet (O/L) = 0
Rotation about imperfection = 180 degrees
Rotation about pipe's axis = 120 degrees

Temperature (°C)				v_m (mm)	Buckle length (mm)			Remarks
I/L	O/L	Mean	Rise		I/L	O/L	Total	
20.77	20.89	20.83	0	30	26.20	2340	4960	
21.84	21.90	21.87	1.04	30	2410	2180	4420	
22.58	22.66	22.62	1.79	30	2120	2030	4150	
23.70	23.75	23.72	2.89	30	2080	1930	4010	
24.68	24.72	24.70	3.87	30	1870	1720	3700	
25.53	25.59	25.56	4.73	30	1870	1690	3620	
26.16	26.37	26.26	5.43	30	1860	1650	3510	Upheaval
27.57	27.64	27.60	6.77	34.88	2100	1610	3710	Apex @ 290 LHS
29.60	29.63	29.61	8.78	39.41	2140	1620	3760	Apex @ 290 LHS
31.34	31.40	31.37	10.54	43.21	2160	1620	3780	Apex @ 350 LHS
33.52	33.52	33.52	12.69	46.61	2180	1680	3860	no change
35.34	35.38	35.36	14.53	49.57	2210	1720	3930	no change

Stable Buckling Isolated Prop with Fixed Anchor Points

Heating Test No 6

Date 10-7-1992
Time start : 4:15 pm   Time finish : 5:30 pm
v_{om}=30mm L_i=4860mm
Pressure: Inlet (I/L)=0.90 bar   Outlet (O/L) = 0
Rotation about imperfection = 120 degrees
Rotation about pipe's axis = 240 degrees

Temperature (°C)				v_m (mm)	Buckle Length (mm)			Remarks
I/L	O/L	Mean	Rise		I/L	O/L	Total	
21.14	21.22	21.18	0	30	2750	2110	4860	
21.96	21.97	21.96	0.78	30	2480	2100	4580	
22.61	22.69	22.65	1.47	30	2110	2020	4130	
24.69	24.74	24.72	3.54	30	1870	1730	3720	
25.84	26.07	25.95	5.77	30	1870	1510	3580	Upheaval
27.60	27.82	27.71	6.53	31.69	2100	1510	3610	Apex @ 360 LHS
28.55	28.59	28.57	7.39	34.44	2120	1510	3630	Apex @ 360 LHS
30.68	30.70	30.69	9.51	38.08	2150	1510	3720	Apex @ 370 LHS
32.42	32.55	32.48	11.30	41.33	2180	1540	3810	no change
34.18	34.32	34.25	13.07	44.67	2210	1570	3900	no change

Stable Buckling Isolated Prop with Fixed Anchor Points

Heating Test No 7

Date 15-8-1991
Time start : 2:15 pm — Time finish : 4:10 pm
v_{om}=20mm — L_i=4180mm
Pressure: Inlet (I/L)=0.92 bar — Outlet (O/L) = 0
Rotation about imperfection = 0 degrees
Rotation about pipe's axis = 0 degrees

Temperature (°C)				v_m (mm)	Buckle length (mm)			Remarks
I/L	O/L	Rise	Spine		I/L	O/L	Total	
20.5	20.5	0	23.9	20	2140	2040	4180	
21.5	21.5	1.0	23.9	20	1880	1930	3810	
22.6	22.6	2.1	23.9	20	1870	1900	3770	
23.5	23.5	3.0	23.9	20	1860	1730	3590	
24.6	24.6	4.1	23.9	20	1860	1510	3370	
24.8	24.8	4.3	23.9	20	1860	1510	3370	
25.0	25.0	4.5	23.9	20.24	1860	1490	3350	Upheaval
26.4	26.4	5.9	24.0	23.74	1960	1500	3460	Apex @ 300 LHS
26.9	26.9	6.4	24.0	25.29	1860	1490	3350	Apex @ 280 LHS
29.3	29.3	8.8	24.1	33.44	2150	1530	3680	no change
32.1	32.1	11.6	24.1	39.22	2170	1740	3810	Apex @ 200 LHS
35.1	35.1	14.6	24.1	45.57	2210	1900	4110	Apex @ 230 LHS

Stable Buckling Isolated Prop with Fixed Anchor Points

Heating Test No 8

Date 19-8-1991
Time start : 1:45 pm — Time finish : 3:00 pm
v_{om}=20mm — L_i=4350mm
Pressure: Inlet (I/L)=0.92 bar — Outlet (O/L) = 0
Rotation about imperfection = 0 degrees
Rotation about pipe's axis = 120 degrees

Temperature (°C)				v_m (mm)	Buckle Length (mm)			Remarks
I/L	O/L	Rise	Spine		I/L	O/L	Total	
20.4	20.4	0	21.7	20	2150	2200	4350	
21.5	21.5	1.1	21.7	20	1900	1940	3840	
22.5	22.5	2.1	21.7	20	1880	1910	3790	
23.5	23.5	3.1	21.7	20	1870	1770	3640	
24.4	24.4	4.0	21.7	20	1870	1510	3380	
24.6	24.6	4.2	21.7	20.32	1870	1500	3370	Upheaval
25.5	25.5	5.1	21.7	21.95	1880	1550	3430	Apex @ 150 LHS
27.5	27.5	7.1	21.7	27.80	2180	1330	3510	Apex @ 370 LHS
29.5	29.5	9.1	21.7	34.06	2180	1500	3680	Apex @ 330 LHS
31.4	31.3	10.95	21.7	38.00	2190	1530	3720	no change
33.3	33.3	12.9	21.7	42.22	2390	1560	3950	Apex @ 400 LHS
35.2	35.2	14.8	21.7	46.32	2410	1640	4050	no change: stop

Stable Buckling Isolated Prop with Fixed Anchor Points

Heating Test No 9

Date 16-8-1991
Time start : 10:35 am Time finish : 12:00 pm
v_{om}=20mm L_i=4170mm
Pressure: Inlet (I/L)=0.92 bar Outlet (O/L) = 0
Rotation about imperfection = 0 degrees
Rotation about pipe's axis = 240 degrees

Temperature (°C)				v_m (mm)	Buckle length (mm)			Remarks
I/L	O/L	Rise	Spine		I/L	O/L	Total	
20.6	20.6	0	23.7	20	2130	2040	4170	
21.5	21.5	0.9	23.7	20	2110	1940	4050	
22.5	22.5	1.9	23.7	20	2110	1930	4040	
23.5	23.5	2.9	23.7	20	2110	1690	3800	
24.0	24.0	4.0	23.7	20.39	1870	1530	3400	Upheaval
25.0	25.0	4.4	23.7	21.45	2020	1500	3520	Apex @ 200 LHS
26.3	26.3	5.7	23.7	36.60	2180	1500	3680	
26.5	26.5	5.9	23.6	24.80	2210	1330	3540	Apex @ 400 LHS
29.4	29.4	8.8	23.6	34.53	2220	1510	3730	Apex @ 380 LHS
32.3	32.3	11.7	23.6	40.55	2310	1640	3950	no change
35.2	35.2	14.6	23.6	46.60	2420	1640	4060	no change
38.2	38.2	17.6	23.6	51.83	2480	1690	4170	stop

Stable Buckling Isolated Prop with Fixed Anchor Points

Heating Test No 10

Date 16-7-1992
Time start : 8:45 am Time finish : 9:25 am
v_{om}=20mm L_i=4310mm
Pressure: Inlet (I/L)=0.90 bar Outlet (O/L) = 0
Rotation about imperfection = 180 degrees
Rotation about pipe's axis = 0 degrees

Temperature (°C)				v_m (mm)	Buckle Length (mm)			Remarks
I/L	O/L	Mean	Rise		I/L	O/L	Total	
20.86	20.97	20.91	0	20	2080	2230	4310	
21.94	22.02	21.98	1.02	20	1870	1930	3800	
22.65	22.74	22.70	1.79	20	1860	1920	3780	
23.82	23.88	23.85	2.94	20	1860	1690	3550	
24.62	24.69	24.65	3.74	20	1860	1510	3370	
25.52	25.60	25.56	4.65	20	1860	1480	3340	
25.96	26.00	25.98	5.07	20	1860	1360	3220	Upheaval
26.74	26.80	26.77	5.86	25.02	1900	1360	3260	Apex @ 300 LHS
27.64	27.71	27.67	6.76	27.68	1900	1490	3390	Apex @ 360 LHS
28.66	28.69	28.68	7.77	30.33	1900	1510	3410	no change
29.72	29.72	29.72	8.81	33.10	2100	1530	3630	Apex @ 400 LHS
31.48	31.69	31.58	10.67	37.52	2160	1520	3680	no chnage
33.64	33.64	33.64	12.73	41.60	2210	1540	3750	no change

Stable Buckling Isolated Prop with Fixed Anchor Points

Heating Test No 11

Date 16-7-1992
Time start : 9:30 am — Time finish : 10:15 am
v_{om}=20mm — L_i=4380mm
Pressure: Inlet (I/L)=0.90 bar — Outlet (O/L) = 0
Rotation about imperfection = 180 degrees
Rotation about pipe's axis = 120 degrees

Temperature (°C)				v_m (mm)	Buckle length (mm)			Remarks
I/L	O/L	Mean	Rise		I/L	O/L	Total	
20.71	20.86	20.78	0	20	2120	2260	4380	
21.84	21.95	21.89	1.11	20	1880	1930	3810	
23.32	23.43	23.37	2.59	20	1860	1710	3570	
24.66	24.76	24.71	3.93	20	1860	1500	3360	
25.72	25.77	25.74	4.96	20	1860	1340	3200	Upheaval
26.75	26.86	26.80	6.02	25.10	1890	1350	3240	Apex @ 400 LHS
27.73	27.77	27.75	6.97	27.94	1890	1480	3370	
28.74	28.74	28.74	7.96	30.39	1900	1500	3400	Apex @ 420 LHS
29.62	29.68	29.65	8.87	33.11	2100	1510	3610	Apex @ 420 LHS
31.57	31.65	31.61	10.83	37.65	2140	1510	3650	no change
33.34	33.36	33.35	12.57	41.32	2170	1520	3690	no change

Stable Buckling Isolated Prop with Fixed Anchor Points

Heating Test No 12

Date 16-7-1992
Time start : 10:25 am — Time finish : 11:15 am
v_{om}=20mm — L_i=4410mm
Pressure: Inlet (I/L)=1.00 bar — Outlet (O/L) = 0
Rotation about imperfection = 180 degrees
Rotation about pipe's axis = 240 degrees

Temperature (°C)				v_m (mm)	Buckle Length (mm)			Remarks
I/L	O/L	Mean	Rise		I/L	O/L	Total	
20.84	20.96	20.90	0	20	2100	2310	4410	
21.90	21.96	21.93	1.03	20	1900	2030	3930	
23.22	23.32	23.27	2.37	20	1860	1930	3610	
24.78	24.82	24.80	3.90	20	1860	1540	3400	
26.21	26.30	26.25	5.35	20	1860	1400	3260	Upheaval
26.61	26.83	26.72	5.82	20.73	1860	1450	3310	Apex @ 350 LHS
27.70	27.74	27.72	6.82	25.42	1890	1450	3340	Apex @ 350 LHS
28.68	28.73	28.70	7.80	28.46	1890	1490	3380	Apex @ 380 LHS
29.52	29.65	29.58	8.65	31.06	1890	1500	3490	no change
30.50	30.53	30.52	9.62	33.81	2110	1500	3610	no change
32.50	32.50	32.50	11.60	37.86	2140	1500	3640	Apex @ 400 LHS
34.52	34.56	34.54	13.64	41.80	2170	1520	3690	no change:stop

Stable Buckling Isolated Prop with Fixed Anchor Points

Cyclic Thermal Test No 13

Date 8-7-1992
Time start : 12:50 pm Time finish : 14:55 pm
v_{om}=15mm L_i=3810mm
Pressure: Inlet (I/L)=1.0 bar Outlet (O/L) = 0
Rotation about imperfection = 0 degrees
Rotation about pipe's axis = 0 degrees

Temperature (°C)				v_m (mm)	Buckle length (mm)			Remarks
I/L	O/L	Mean	Rise		I/L	O/L	Total	
20.50	20.64	20.57	0	15	1880	1930	3810	
21.44	21.59	21.51	0.94	15	1870	1790	3660	
22.29	22.44	22.36	1.79	15	1860	1700	3560	
23.35	23.44	23.40	2.83	15	1860	1700	3560	
24.38	24.40	24.39	3.82	15	1290	1700	2990	
25.30	25.43	25.36	4.79	15	1200	1700	2900	
25.51	25.73	25.62	5.05	15	1170	1790	2960	Upheaval
26.23	26.35	26.29	5.72	15.91	1170	2030	3200	Apex @ 490 RHS
28.12	28.29	28.20	7.63	20.68	1200	2300	3500	Apex @ 490 RHS
30.18	30.23	30.25	9.68	23.19	1200	2460	3660	Apex @ 490 RHS
32.05	32.15	32.10	11.53	26.00	1220	2490	3710	Apex @ 620 RHS
34.08	34.12	34.10	13.53	29.90	1280	2500	3780	Apex @ 620 RHS
35.83	36.09	35.96	15.39	33.08	1290	2620	3910	Apex @ 620 RHS
38.04	38.05	38.04	17.47	36.43	1300	2720	4020	Apex @ 620 RHS
39.92	39.95	39.93	19.36	39.94	1450	2760	4210	Apex @ 620 RHS
37.96	37.94	37.95	17.38	35.28	1310	2720	4030	Unloading
35.96	36.06	36.07	15.44	32.73	1300	2720	4020	Apex @ 620 RHS
34.08	34.19	34.13	13.56	30.37	1300	2700	4000	Apex @ 620 RHS
32.00	32.02	32.07	11.44	28.21	1300	2640	3940	Apex @ 620 RHS
30.11	30.26	30.18	9.61	26.23	1300	2470	3770	Apex @ 620 RHS
28.25	28.30	28.27	7.70	23.70	1300	2190	3490	
26.20	26.36	26.28	5.71	16.86	1170	2030	3200	
25.52	25.54	25.53	4.96	15	1010	1920	2930	
24.30	24.47	24.38	3.81	15	1280	1720	3000	
22.40	22.47	22.43	1.86	15	1850	1700	3550	
21.44	21.54	21.49	0.92	15	1860	1910	3770	
20.45	20.60	20.52	-0.05	15	1870	1930	3800	

Stable Buckling Isolated Prop with Fixed Anchor Points

Cyclic Thermal Test No 14

Date 8-7-1992
Time start : 10:40 am Time finish : 12:45 pm
v_{om}=15mm L_i=3880mm
Pressure: Inlet (I/L)=1.0 bar Outlet (O/L) = 0
Rotation about imperfection = 0 degrees
Rotation about pipe's axis = 120 degrees

Temperature (°C)				v_m (mm)	Buckle Length (mm)			Remarks
I/L	O/L	Mean	Rise		I/L	O/L	Total	
20.40	20.53	20.46	0	15	1900	1980	3880	
21.36	21.55	21.46	1.0	15	1880	1900	3780	
22.24	22.35	22.30	1.84	15	1870	1690	3560	
23.26	23.35	23.31	2.85	15	1870	1680	3550	
24.30	24.46	24.38	3.92	15	1320	1680	3000	
25.29	25.35	25.32	4.86	15	1300	1680	2980	Upheaval
26.18	26.32	26.25	5.79	15.40	1230	2030	3260	Apex @ 420 RHS
28.29	28.35	28.32	7.86	18.86	1230	2210	3440	Apex @ 620 RHS
30.08	30.25	30.16	9.70	23.16	1230	2370	3600	Apex @ 620 RHS
31.96	32.01	31.98	11.52	28.98	1310	2480	3790	Apex @ 620 RHS
33.98	34.04	34.01	13.55	32.92	1350	2500	3850	Apex @ 620 RHS
35.93	36.00	35.96	15.50	35.93	1450	2660	4110	Apex @ 620 RHS
37.86	38.09	37.97	17.15	37.71	1450	2770	4220	Apex @ 620 RHS
39.88	39.97	39.93	19.47	39.23	1450	2770	4220	Apex @ 620 RHS
37.91	38.11	38.01	17.55	36.61	1420	2770	4190	Unloading
35.96	36.01	35.98	15.52	33.80	1350	2770	4120	
34.05	34.10	34.07	13.61	29.11	1300	2750	4050	
31.92	32.08	32.00	11.54	25.92	1300	2530	3830	
30.11	30.31	30.21	9.75	24.32	1290	2490	3780	
28.17	28.29	28.23	7.77	22.24	1290	2300	3590	
26.26	26.45	26.36	5.90	17.77	1290	2020	3310	
24.61	24.78	24.69	4.23	15	1290	1710	3000	
23.42	23.58	23.50	3.04	15	1860	1710	3570	
22.49	22.64	22.56	2.10	15	1860	1710	3570	
21.52	21.65	21.58	1.12	15	1870	1900	3770	
20.53	20.64	20.58	0.12	15	1880	1930	3810	

Stable Buckling Isolated Prop with Fixed Anchor Points

Cyclic Thermal Test No 15

Date 8-7-1992
Time start : 8:30 am — Time finish : 10:30 am
v_{om}=15mm — L_i=4050mm
Pressure: Inlet (I/L)=1.0 bar — Outlet (O/L) = 0
Rotation about imperfection = 0 degrees
Rotation about pipe's axis = 240 degrees

Temperature (^oC)				v_m (mm)	Buckle length (mm)			Remarks
I/L	O/L	Mean	Rise		I/L	O/L	Total	
20.47	20.54	20.50	0	15	2120	1930	4050	
21.41	21.55	21.48	0.98	15	1880	1710	3590	
22.22	22.37	22.30	1.80	15	1880	1680	3560	
23.34	23.40	23.37	2.87	15	1880	1500	3380	
24.18	24.28	24.23	3.73	15	1880	1400	3280	
24.33	24.45	24.39	3.89	15	1880	1340	3220	
25.26	25.36	25.31	4.81	15	1880	1060	2940	Upheaval
26.18	26.35	26.26	5.76	16.72	2120	1060	3180	Apex @ 600 LHS
27.19	27.32	27.25	6.75	18.35	2480	1050	3430	Apex @ 600 LHS
28.30	28.32	28.31	7.81	20.08	2480	1050	3530	Apex @ 600 LHS
29.17	29.23	29.20	8.70	23.74	2700	1060	3760	Apex @ 600 LHS
31.06	31.24	31.15	10.65	26.84	2710	1050	3870	Apex @ 600 LHS
33.00	33.08	33.04	12.54	28.51	2710	1250	4060	Apex @ 600 LHS
34.92	35.05	34.98	14.48	32.54	2780	1380	4160	Apex @ 600 LHS
36.90	37.06	36.98	16.48	35.88	2780	1400	4180	Apex @ 600 LHS
38.90	39.02	38.96	18.46	38.39	2780	1500	4280	Apex @ 600 LHS
37.01	37.09	37.05	16.55	34.74	2780	1330	4110	Unloading
34.93	35.08	35.00	14.50	31.59	2780	1330	4110	
33.10	33.22	33.16	12.66	28.18	2780	1320	4100	
31.05	31.29	31.17	10.67	24.86	2490	1330	3820	
29.21	29.27	29.24	8.74	17.65	2490	1050	3540	
27.53	27.58	27.55	7.05	16.21	2470	1030	3500	
25.88	25.85	25.86	5.36	15	2160	1320	3480	
23.26	23.46	23.36	2.86	15	1870	1500	3370	
22.46	22.49	22.47	1.97	15	1870	1680	3550	
21.42	21.55	21.48	0.98	15	1900	1700	3600	
20.55	20.70	20.62	0.12	15	1900	2040	3940	

Stable Buckling Isolated Prop with Fixed Anchor Points

Cyclic Thermal Test No 16

Date 9-7-1992
Time start : 8:40 am — Time finish : 10:30 am
v_{om}=15mm — L_i=3810mm
Pressure: Inlet (I/L)=1.00 bar — Outlet (O/L) = 0
Rotation about imperfection = 180 degrees
Rotation about pipe's axis = 0 degrees

Temperature (^oC)				v_m (mm)	Buckle Length (mm)			Remarks
I/L	O/L	Mean	Rise		I/L	O/L	Total	
20.51	20.46	20.48	0	15	1880	1930	3810	
21.48	21.54	21.51	1.03	15	1870	1720	3590	
22.32	22.37	22.34	1.86	15	1860	1700	3460	
23.37	23.46	23.42	2.94	15	1860	1500	3360	
24.30	24.36	24.33	3.85	15	1860	1480	3340	
25.16	25.32	25.24	4.76	15	1860	1340	3200	Upheaval
26.13	26.21	26.17	5.69	19.64	1860	1360	3220	Apex @ 320 LHS
28.09	28.15	28.12	7.64	25.49	1890	1490	3380	Apex @ 320 LHS
30.18	30.21	30.20	9.72	31.00	1890	1670	3560	Apex @ 320 LHS
31.93	31.93	31.93	11.45	35.27	2110	1580	3690	Apex @ 320 LHS
34.11	34.08	34.10	13.62	37.92	2140	1680	3820	Apex @ 320 LHS
35.88	35.88	35.88	15.40	41.92	2170	1680	3850	Apex @ 320 LHS
37.85	37.89	37.87	17.39	45.83	2170	1710	3880	Apex @ 320 LHS
40.04	40.01	40.02	19.54	49.64	2280	1790	4070	Apex @ 320 LHS
37.85	37.86	37.85	17.37	46.76	2200	1780	3980	Unloading
35.91	36.04	35.97	15.49	42.29	2200	1700	3900	Apex @ 320 LHS
33.89	34.00	33.94	13.46	37.86	2200	1680	3880	Apex @ 320 LHS
31.94	32.04	32.00	11.52	33.32	1880	1510	3390	Apex @ 320 LHS
30.22	30.27	30.24	9.76	28.40	1880	1480	3360	Apex @ 320 LHS
28.11	28.14	28.12	7.64	21.46	1880	1330	3210	Apex @ 320 LHS
26.39	26.45	26.42	5.94	17.42	1880	1320	3200	Apex @ 320 LHS
25.36	25.42	25.39	4.19	15	1880	1340	3180	
23.27	23.34	23.30	2.82	15	1860	1480	3340	
22.38	22.48	22.43	1.95	15	1860	1500	3360	
21.33	21.46	21.39	0.91	15	1860	1700	3560	
20.48	20.57	20.53	-	15	1860	1910	3220	

Stable Buckling Isolated Prop with Fixed Anchor Points

Cyclic Thermal Test No 17

Date 9-7-1992
Time start : 10:35 am — Time finish : 12:20 pm
v_{om}=15mm — L_i=4050mm
Pressure: Inlet (I/L)=1.0 bar — Outlet (O/L) = 0
Rotation about imperfection = 180 degrees
Rotation about pipe's axis = 120 degrees

Temperature (°C)				v_m (mm)	Buckle length (mm)			Remarks
I/L	O/L	Mean	Rise		I/L	O/L	Total	
20.39	20.41	20.40	0	15	2120	1930	4050	
21.42	21.49	21.45	1.05	15	1870	1710	3580	
22.20	22.29	22.24	1.84	15	1860	1680	3540	
23.38	23.45	23.41	3.01	15	1860	1670	3530	
24.35	24.43	24.39	3.99	15	1850	1490	3340	
25.36	25.40	25.38	4.92	15	1850	1470	3220	Upheaval
26.34	26.42	26.38	5.98	20.78	1450	1810	3260	Apex @ 260 RHS
28.05	28.16	28.10	7.70	24.18	1300	2040	3340	Apex @ 330 RHS
30.18	30.21	30.20	9.80	26.36	1300	2300	3600	Apex @ 360 RHS
32.05	32.08	32.06	11.66	31.72	1350	2480	3830	Apex @ 360 RHS
33.94	34.17	34.05	13.65	35.78	1450	2480	3930	Apex @ 360 RHS
35.90	35.96	35.93	15.53	38.45	1460	2490	3950	Apex @ 400 RHS
37.81	37.92	37.86	17.46	40.03	1460	2500	3960	Apex @ 400 RHS
39.90	39.90	39.90	19.50	42.59	1500	2640	4140	Apex @ 500 RHS
38.04	38.06	38.05	17.65	40.79	1500	2550	4050	Unloading
36.00	36.06	36.03	15.63	36.31	1460	2550	4010	Apex @ 500 RHS
33.93	34.03	33.98	13.58	34.15	1450	2500	4000	Apex @ 460 RHS
31.94	32.04	31.99	11.59	28.35	1300	2480	3780	Apex @ 460 RHS
30.16	30.18	30.17	9.77	25.39	1290	2450	3740	Apex @ 400 RHS
28.05	28.19	28.12	7.72	21.21	1290	2450	3740	Apex @ 400 RHS
26.40	26.46	26.43	6.03	18.37	1160	2450	3610	Apex @ 400 RHS
25.29	25.42	25.35	4.95	15	1300	1720	3020	Apex @ 400 RHS
23.49	23.58	23.54	3.14	15	1460	1720	3180	
22.32	22.43	22.37	1.97	15	1850	1720	3570	
21.45	21.58	21.51	1.11	15	1860	1720	3580	
20.35	20.45	20.40	0	15	1860	1910	3770	

Stable Buckling Isolated Prop with Fixed Anchor Points

Cyclic Thermal Test No 18

Date 9-7-1992
Time start : 12:35 pm — Time finish : 14:15 pm
v_{om}=15mm — L_i=4000mm
Pressure: Inlet (I/L)=1.00 bar — Outlet (O/L) = 0
Rotation about imperfection = 180 degrees
Rotation about pipe's axis = 240 degrees

Temperature (°C)				v_m (mm)	Buckle Length (mm)			Remarks
I/L	O/L	Mean	Rise		I/L	O/L	Total	
20.26	20.37	20.31	0	15	1870	2130	4000	
21.52	21.58	21.55	1.24	15	1860	1920	3780	
22.24	22.33	22.29	1.98	15	1860	1710	3570	
23.40	23.49	23.44	3.13	15	1860	1680	3540	
24.37	24.44	24.40	4.09	15	1500	1880	3380	
25.12	25.16	25.14	4.83	15	1210	1980	3290	
25.78	25.83	25.80	5.49	15	1160	2080	3240	Upheaval
28.06	28.17	28.11	7.80	18.37	990	2470	3460	Apex @ 620 RHS
30.18	30.25	30.21	9.90	26.91	980	2650	3630	Apex @ 810 RHS
32.01	32.09	32.05	11.74	31.53	980	2680	3660	Apex @ 810 RHS
34.00	34.03	34.01	13.70	36.47	960	2730	3690	Apex @ 810 RHS
36.00	36.06	36.03	15.72	40.82	960	2760	3720	Apex @ 810 RHS
37.95	37.98	37.96	17.65	45.32	980	2770	3750	Apex @ 810 RHS
39.82	39.95	39.88	19.57	47.41	1270	2770	4040	Apex @ 810 RHS
37.98	38.00	37.99	17.68	46.18	1200	2770	3970	Unloading
35.95	35.98	35.96	15.65	42.38	1160	2730	3890	Apex @ 720 RHS
34.00	34.12	34.06	13.75	38.97	1160	2710	3870	Apex @ 700 RHS
32.02	32.12	32.07	11.76	33.32	1160	2680	3840	Apex @ 700 RHS
30.33	30.42	30.38	10.07	28.30	1160	2660	3820	Apex @ 620 RHS
28.16	28.26	28.21	7.90	22.25	1160	2630	3790	Apex @ 620 RHS
26.32	26.40	26.36	6.05	19.32	1000	2480	3480	
25.36	25.41	25.38	5.07	15	1220	2020	3200	
23.36	23.47	23.41	3.10	15	1850	2030	3880	
22.45	22.60	22.52	2.21	15	1860	2030	3890	
21.42	21.53	21.47	1.16	15	1860	2030	3890	
20.46	20.56	20.51	0.20	15	1860	2030	3890	

Stable Buckling Isolated Prop with Fixed Anchor Points

Cyclic Thermal Test No 19

Date 7-7-1992
Time start : 8:30 am — Time finish : 10:50 am
v_{om}=10mm — L_i=3580mm
Pressure: Inlet (I/L)=1.0 bar — Outlet (O/L) = 0
Rotation about imperfection = 0 degrees
Rotation about pipe's axis = 0 degrees

Temperature (°C)				v_m (mm)	Buckle length (mm)			Remarks
I/L	O/L	Mean	Rise		I/L	O/L	Total	
20.52	20.66	20.59	0	10	1880	1700	3580	
21.52	21.63	21.57	0.98	10	1680	1630	3310	
22.29	22.46	22.37	1.78	10	1680	1630	3310	
23.38	23.53	23.45	2.86	10	1290	1630	2920	
24.22	24.34	24.28	3.69	10	1220	1630	2850	
25.24	25.36	25.30	4.71	10	1010	1630	2640	
25.60	25.61	25.60	5.10	10	990	1620	2610	Upheaval
26.37	26.45	26.41	5.82	13.58	990	1970	2660	Apex @ 200 RHS
28.28	28.32	28.30	7.71	18.26	1170	2190	3360	Apex @ 460 RHS
30.15	30.25	30.20	9.61	25.57	1260	2310	3570	Apex @ 460 RHS
32.01	32.11	32.06	11.47	27.29	1290	2340	3630	Apex @ 460 RHS
35.90	35.93	35.91	15.32	33.95	1300	2560	3860	Apex @ 600 RHS
38.03	38.13	38.08	17.49	42.14	1300	2720	4020	Apex @ 600 RHS
40.74	40.92	40.83	20.24	45.89	1300	2760	4060	Apex @ 600 RHS
37.83	38.00	37.81	17.22	41.81	1300	2750	4050	Unloading
35.02	35.00	35.01	14.42	33.42	1300	2720	4020	Apex @ 600 RHS
31.96	32.16	32.06	11.47	28.86	1220	2720	3940	Apex @ 460 RHS
29.05	29.27	29.16	8.57	21.94	1220	2340	3560	Apex @ 460 RHS
27.23	27.39	27.31	6.72	16.35	1160	2200	3360	Apex @ 460 RHS
25.12	25.31	25.22	4.68	10	1000	1690	2690	
24.18	24.32	24.25	3.66	10	1180	1690	2870	
23.26	23.43	23.34	2.75	10	1230	1690	2920	
22.26	22.42	22.34	1.75	10	1870	1690	3560	
21.31	21.47	21.39	0.80	10	1870	1690	3560	
20.54	20.66	20.60	0.01	10	1870	1690	3560	

Stable Buckling Isolated Prop with Fixed Anchor Points

Cyclic Thermal Test No 20

Date 7-7-1992
Time start : 11:00 am — Time finish : 13:20 pm
v_{om}=10mm — L_i=3560mm
Pressure: Inlet (I/L)=1.00 bar — Outlet (O/L) = 0
Rotation about imperfection = 0 degrees
Rotation about pipe's axis = 120 degrees

Temperature (°C)				v_m (mm)	Buckle Length (mm)			Remarks
I/L	O/L	Mean	Rise		I/L	O/L	Total	
20.45	20.61	20.53	0	10	1870	1690	3560	
21.37	21.50	21.43	0.9	10	1870	1510	3380	
22.32	22.42	22.37	1.84	10	1860	1500	3360	
23.33	23.49	23.41	2.88	10	1300	1500	2800	
24.34	24.41	24.37	3.84	10	1280	1500	2780	
25.30	25.42	25.36	4.83	10	1020	1710	2730	Upheaval
26.40	26.48	26.44	5.91	13.39	1020	2030	3050	Apex @ 440 RHS
28.30	28.32	28.31	7.78	19.30	1210	2310	3520	Apex @ 440 RHS
30.14	30.21	30.17	9.64	25.83	990	2780	3770	Apex @ 450 RHS
31.20	31.16	31.18	10.65	29.14	1300	2310	3610	Apex @ 400 RHS
33.02	33.16	33.09	12.56	31.90	1350	2550	3900	Apex @ 500 RHS
35.88	36.01	35.94	15.41	36.73	1340	2700	4040	Apex @ 440 RHS
39.00	39.11	39.05	18.52	37.26	1350	2770	4120	Apex @ 610 RHS
35.91	36.08	35.98	15.45	33.32	1300	2760	4060	Unloading
33.09	33.13	33.11	12.58	32.27	1300	2440	3740	Apex @ 400 RHS
31.12	31.14	31.13	10.60	29.65	1300	2290	3590	Apex @ 400 RHS
29.08	29.29	29.18	8.66	24.84	1300	2190	3490	Apex @ 400 RHS
27.21	27.37	27.29	6.76	20.01	1300	2030	3330	Apex @ 400 RHS
25.24	25.35	25.29	4.66	10	1000	1720	2720	
24.36	24.48	24.42	3.89	10	1210	1690	2900	
23.36	23.38	23.37	2.84	10	1300	1550	2850	
22.28	22.44	22.36	1.83	10	1850	1640	3490	
21.42	21.49	21.45	0.92	10	1860	1660	3520	
20.51	20.64	20.57	0.04	10	1860	1670	3530	

Stable Buckling Isolated Prop with Fixed Anchor Points

Cyclic Thermal Test No 21

Date 7-7-1992
Time start : 13:30 pm   Time finish : 15:30 pm
v_{om}=10mm L_i=3550mm
Pressure: Inlet (I/L)=1.0 bar   Outlet (O/L) = 0
Rotation about imperfection = 0 degrees
Rotation about pipe's axis = 240 degrees

Temperature (^oC)				v_m (mm)	Buckle length (mm)			Remarks
I/L	O/L	Mean	Rise		I/L	O/L	Total	
20.30	20.44	20.37	0	10	1870	1680	3550	
21.34	21.45	21.39	1.02	10	1860	1670	3530	
22.15	22.32	22.23	1.86	10	1860	1500	3360	
23.22	23.39	23.30	2.93	10	1860	1350	3210	
24.30	24.46	24.38	4.01	10	1860	1320	3180	
25.16	25.32	25.24	4.83	10	2110	990	3100	
25.79	26.02	25.90	5.53	10	2100	990	3090	Upheaval
26.22	26.42	26.32	5.95	12.13	2410	800	3210	Apex @ 570 LHS
28.03	28.29	28.16	7.79	19.53	2470	800	3270	Apex @ 570 LHS
30.10	30.20	30.15	9.78	25.64	2620	1050	3670	Apex @ 570 LHS
31.85	31.98	31.91	11.54	30.89	2710	1050	3760	Apex @ 830 LHS
34.00	34.10	34.05	13.68	33.20	2710	1140	3850	Apex @ 570 LHS
35.90	35.98	35.94	15.57	35.46	2710	1320	4030	Apex @ 570 LHS
37.88	37.98	37.93	17.56	36.38	2750	1350	4100	Apex @ 570 LHS
35.98	36.09	36.03	15.66	34.21	2750	1300	4050	Unloading
33.91	34.11	34.01	13.64	32.54	2750	1070	3820	Apex @ 570 LHS
31.96	32.10	32.03	11.66	29.33	2750	1000	3750	Apex @ 570 LHS
30.02	30.24	30.13	9.76	26.72	2750	800	3550	Apex @ 570 LHS
28.15	28.25	28.20	7.83	21.24	2480	800	3280	Apex @ 570 LHS
26.21	26.40	26.31	5.94	15.06	2450	790	3240	Apex @ 570 LHS
25.40	25.62	25.51	5.14	10	2050	800	2850	
24.24	24.46	24.35	3.98	10	1870	1320	3190	
23.35	23.46	23.40	3.03	10	1870	1350	3220	
22.28	22.45	22.36	1.99	10	1870	1500	3370	
21.33	21.51	21.42	1.05	10	1870	1530	3400	
20.36	20.53	20.44	0.07	10	1870	1670	3540	

Stable Buckling Isolated Prop with Fixed Anchor Points

Cyclic Thermal Test No 22

Date 10-7-1992
Time start : 10:20 am   Time finish : 12:30 pm
v_{om}=10mm L_i=3560mm
Pressure: Inlet (I/L)=1.00 bar   Outlet (O/L) = 0
Rotation about imperfection = 180 degrees
Rotation about pipe's axis = 0 degrees

Temperature (^oC)				v_m (mm)	Buckle Length (mm)			Remarks
I/L	O/L	Mean	Rise		I/L	O/L	Total	
20.74	20.81	20.77	0	10	1860	1700	3560	
21.75	21.83	21.79	1.02	10	1860	1490	3350	
22.58	22.66	22.62	1.85	10	1860	1480	3340	
23.70	23.76	23.73	2.97	10	1860	1470	3330	
24.53	24.62	24.58	3.81	10	1390	1480	2870	
25.51	25.55	25.53	4.86	10	1290	1480	2770	
26.00	26.14	26.07	5.30	10	1290	1470	2760	Upheaval
26.58	26.65	26.61	5.84	16.60	1310	1510	2820	still symmetry
28.46	28.52	28.49	7.72	23.94	1450	1710	3160	still symmetry
30.44	30.48	30.46	9.69	29.31	1520	2020	3540	Apex @ 140 RHS
32.34	32.38	32.36	11.59	32.09	1460	2270	3730	Apex @ 140 RHS
34.34	34.47	34.40	13.63	35.55	1470	2200	3770	Apex @ 310 RHS
38.18	38.24	38.21	17.44	40.16	1470	2490	3960	Apex @ 310 RHS
36.39	36.44	36.42	15.65	36.04	1450	2490	3940	Unloading
34.32	34.36	34.34	13.57	30.75	1310	2490	3800	Apex @ 310 RHS
32.25	32.52	32.28	11.51	28.31	1200	2490	3600	Apex @ 310 RHS
30.42	30.49	30.45	9.68	23.52	1000	2490	3490	returns symmetry
28.40	28.47	28.43	7.66	20.18	950	2490	3440	
26.52	26.58	26.55	5.88	16.60	1310	1680	2990	
25.54	25.58	25.56	4.89	10	1290	1490	2780	
23.60	23.78	23.69	2.92	10	1300	1490	2780	
22.62	22.71	22.67	1.90	10	1850	1490	3340	
21.61	21.73	21.67	0.9	10	1860	1500	3360	
20.59	20.73	20.66	0	10	1860	1500	3360	

Stable Buckling Isolated Prop with Fixed Anchor Points

Cyclic Thermal Test No 23

Date 10-7-1992
Time start : 8:25 am   Time finish : 10:00 am
v_{om}=10mm L_i=3560mm
Pressure: Inlet (I/L)=1.0 bar   Outlet (O/L) = 0
Rotation about imperfection = 180 degrees
Rotation about pipe's axis = 120 degrees

Temperature (°C)				v_m (mm)	Buckle length (mm)			Remarks
I/L	O/L	Mean	Rise		I/L	O/L	Total	
20.76	20.84	20.80	0	10	1870	1690	3560	
21.72	21.78	21.75	0.95	10	1860	1540	3400	
22.49	22.62	22.55	1.75	10	1860	1490	3350	
23.62	23.69	23.65	2.85	10	1850	1470	3320	
24.44	24.69	24.56	3.76	10	1600	1500	3100	
25.66	25.84	25.75	4.95	10	1100	1700	2800	Upheaval
26.48	26.57	26.53	5.73	16.76	1300	1900	3200	Apex @ 300 RHS
28.37	28.50	28.43	7.63	22.83	1300	2020	3220	Apex @ 330 RHS
30.31	30.44	30.37	9.57	26.69	1310	2200	3510	Apex @ 350 RHS
32.31	32.36	32.34	11.54	31.39	1450	2220	3670	Apex @ 350 RHS
34.21	34.26	34.24	13.44	34.68	1460	2300	3760	Apex @ 370 RHS
36.26	36.26	36.26	15.46	37.55	1470	2480	3950	Apex @ 370 RHS
38.37	38.41	38.39	17.59	39.77	1470	2500	3970	Apex @ 400 RHS
36.40	36.43	36.42	15.62	37.78	1470	2500	3970	Unloading
34.28	34.40	34.44	13.54	32.93	1450	2500	3950	Apex @ 370 RHS
32.16	32.23	32.19	11.39	27.84	1330	2500	3830	Apex @ 370 RHS
30.34	30.51	30.42	9.62	24.80	1300	2500	3800	Apex @ 350 RHS
28.38	28.47	28.43	7.63	18.29	1160	2540	3700	Apex @ 350 RHS
26.60	26.71	26.65	5.85	12.10	960	2540	3500	Apex @ 300 RHS
24.98	25.01	25.00	4.20	10	1260	1700	2900	Apex @ 300 RHS
23.69	23.97	23.74	2.94	10	1300	1500	2800	
22.66	22.70	22.68	1.88	10	1850	1520	3370	
21.70	21.80	21.75	0.95	10	1860	1680	3540	
20.74	20.86	20.80	0	10	1860	1690	3550	

Stable Buckling Isolated Prop with Fixed Anchor Points

Cyclic Thermal Test No 24

Date 9-7-1992
Time start : 14:20 pm   Time finish : 16:10 pm
v_{om}=10mm L_i=3580mm
Pressure: Inlet (I/L)=1.00 bar   Outlet (O/L) = 0
Rotation about imperfection = 180 degrees
Rotation about pipe's axis = 240 degrees

Temperature (°C)				v_m (mm)	Buckle Length (mm)			Remarks
I/L	O/L	Mean	Rise		I/L	O/L	Total	
20.40	20.60	20.50	0	10	1860	1720	3580	
21.34	21.43	21.39	0.89	10	1860	1680	3540	
22.19	22.27	22.23	1.73	10	1860	1680	3540	
23.38	23.38	23.38	2.88	10	1520	1680	3200	
24.42	24.44	24.43	3.93	10	1090	2020	3110	
25.37	25.48	25.42	4.92	10	950	2020	2970	Upheaval
26.38	26.47	26.43	5.93	15.20	970	2300	3270	Apex @ 480 RHS
28.24	28.30	28.37	7.87	19.75	960	2470	3430	Apex @ 620 RHS
30.08	30.32	30.20	9.70	26.40	970	2650	3620	Apex @ 720 RHS
32.05	32.07	32.06	11.56	31.92	980	2660	3640	Apex @ 720 RHS
33.96	34.14	34.05	13.55	36.45	990	2710	3700	Apex @ 800 RHS
35.91	35.97	35.94	15.44	40.53	990	2740	3730	Apex @ 850 RHS
38.04	38.06	38.05	17.55	44.42	990	2760	3750	Apex @ 820 RHS
36.84	36.40	36.37	15.87	41.63	990	2740	3730	Unloading
34.42	34.44	34.43	13.93	38.11	990	2740	3730	Apex @ 750 RHS
32.46	32.51	32.48	11.98	33.23	1160	2700	3860	Apex @ 720 RHS
30.54	30.60	30.57	10.07	28.25	1160	2670	3830	Apex @ 620 RHS
28.39	28.52	28.45	7.95	22.57	1010	2650	3660	Apex @ 620 RHS
26.48	26.60	26.54	6.04	14.09	970	2490	3460	Apex @ 620 RHS
24.80	24.86	24.83	4.33	10	950	2030	2980	Apex @ 620 RHS
23.56	23.68	23.62	3.12	10	1000	1910	2910	
22.60	22.70	22.65	2.15	10	1210	1710	2920	
21.60	21.72	21.66	1.16	10	1850	1700	3550	
20.52	20.64	20.58	0.08	10	1860	1700	3560	

Snap Buckling Isolated Prop with Fixed Anchor Points

Heating Test No 25

Date 1-12-1991
Time start : 9:00 am — Time finish : 10:20 am
v_{om}=2mm — L_i=2540mm
Pressure: Inlet (I/L)=1.0 bar — Outlet (O/L) = 0
Rotation about imperfection = 0 degrees
Rotation about pipe's axis = 0 degrees

Temperature (°C)				v_m (mm)	Buckle length (mm)			Remarks
I/L	O/L	Mean	Rise		I/L	O/L	Total	
20.46	20.51	20.49	0	2	1210	1330	2540	
22.42	22.43	22.43	1.94	2	1210	730	1940	
24.30	24.32	24.31	3.82	2	1200	730	1930	
26.42	26.43	26.43	5.94	2	1190	730	1920	
28.28	28.29	28.29	7.80	2	1170	730	1900	
29.55	29.56	29.56	9.07	2	1170	720	1890	
29.91	29.93	29.92	9.43	2	1160	730	1890	
30.10	30.08	30.09	9.60	2	1160	730	1890	
30.32	30.33	30.33	9.84	2	1160	730	1890	Snap
30.32	30.33	30.33	9.84	30.75	2780	800	3580	
32.10	32.09	32.10	11.61	34.50	2780	900	3680	
34.10	34.09	34.10	13.61	39.74	2780	1050	3830	
36.15	36.10	36.13	15.64	42.88	2790	1060	3850	
38.08	38.05	38.07	17.58	46.64	2790	1070	3860	
39.94	39.90	39.92	19.43	50.49	2790	1330	4120	stop

Snap Buckling Isolated Prop with Fixed Anchor Points

Heating Test No 26

Date 26-11-1991
Time start : 11:00 am — Time finish : 12:00 pm
v_{om}=2mm — L_i=2330mm
Pressure: Inlet (I/L)=1.00 bar — Outlet (O/L) = 0
Rotation about imperfection = 0 degrees
Rotation about pipe's axis = 120 degrees

Temperature (°C)				v_m (mm)	Buckle Length (mm)			Remarks
I/L	O/L	Mean	Rise		I/L	O/L	Total	
20.50	20.55	20.52	0	2	980	1350	2330	
22.42	22.43	22.42	1.90	2	990	1340	2330	
24.34	24.35	24.34	3.82	2	990	1340	2330	
26.45	26.45	26.45	5.93	2	950	1350	2300	
26.86	26.90	26.88	6.36	2	950	1350	2300	Snap
26.86	26.90	26.88	6.36	13.95	1160	2030	3190	
28.34	28.35	28.34	7.82	23.80	1300	2040	3340	
30.41	30.41	30.41	9.89	28.78	1310	2320	3630	
32.16	32.12	32.14	11.62	33.62	1310	2470	3780	
34.18	34.17	34.17	13.65	40.13	1880	2030	3910	
36.15	36.09	36.12	15.60	43.88	1890	2030	3920	
38.10	38.02	38.06	17.54	47.28	2110	2040	4150	
40.16	40.05	40.10	19.58	50.86	2130	2050	4180	stop

Snap Buckling Isolated Prop with Fixed Anchor Points

Heating Test No 27

Date 3-12-1991
Time start : 11:00 am — Time finish : 12:30 pm
v_{om}=2mm — L_i=2280mm
Pressure: Inlet (I/L)=1.0 bar — Outlet (O/L) = 0
Rotation about imperfection = 0 degrees
Rotation about pipe's axis = 240 degrees

Temperature (°C)				v_m (mm)	Buckle length (mm)			Remarks
I/L	O/L	Mean	Rise		I/L	O/L	Total	
20.63	20.58	20.60	0	2	940	1340	2280	
22.48	22.47	22.47	1.87	2	940	1330	2270	
24.30	24.29	24.30	3.69	2	940	1320	2260	
26.50	26.48	26.49	5.89	2	940	1260	2200	
27.40	27.38	27.39	6.79	2	690	1050	1740	
28.42	28.40	28.41	7.81	2	690	890	1580	
29.40	29.36	29.38	8.78	2	690	830	1520	
29.75	29.73	29.74	9.14	2	690	810	1500	Snap
29.75	29.73	29.74	9.14	26.38	1210	2340	3550	
30.18	30.16	30.17	9.57	27.80	1210	2330	3540	
32.10	32.05	32.07	11.47	32.17	1300	2330	3630	
34.04	34.00	34.02	13.42	36.58	1310	2340	3650	
36.06	36.02	36.04	15.44	41.08	1310	2500	3810	
38.10	38.03	38.06	17.46	44.40	1310	2670	3980	
39.96	39.90	39.93	19.33	48.12	1310	2720	4030	
40.07	40.03	40.05	19.45	49.98	2110	2040	4150	stop

Snap Buckling Isolated Prop with Fixed Anchor Points

Heating Test No 28

Date 6-12-1991
Time start : 13:00 pm — Time finish : 14:20 pm
v_{om}=2mm — L_i=2310mm
Pressure: Inlet (I/L)=1.00 bar — Outlet (O/L) = 0
Rotation about imperfection = 180 degrees
Rotation about pipe's axis = 0 degrees

Temperature (°C)				v_m (mm)	Buckle Length (mm)			Remarks
I/L	O/L	Mean	Rise		I/L	O/L	Total	
20.63	20.72	20.68	0	2	950	1360	2310	
22.30	22.36	22.33	1.65	2	950	1340	2290	
24.23	24.28	24.26	3.58	2	940	1340	2280	
26.22	26.27	26.25	5.57	2	720	1340	2060	
27.23	27.28	27.26	6.58	2	450	1500	1950	
27.55	27.61	27.58	6.90	2	440	1500	1940	
27.62	27.67	27.65	6.97	2	440	1500	1940	Snap
27.62	27.67	27.65	6.97	21.38	2150	1340	3490	
28.34	28.30	28.32	7.64	23.91	2170	1490	3660	
30.24	30.27	30.26	9.58	30.19	2440	1490	3930	
32.04	32.06	32.05	11.37	34.90	2470	1490	3960	
34.19	34.17	34.18	13.50	39.85	2760	1490	4250	
36.11	36.11	36.11	15.43	43.64	2750	1510	4260	
38.00	38.02	38.01	17.33	47.93	2770	1510	4280	
39.96	39.90	39.93	19.25	51.20	2770	1550	4320	stop

Snap Buckling Isolated Prop with Fixed Anchor Points

Heating Test No 29

Date 6-12-1991
Time start : 10:00 am — Time finish : 12:00 pm
v_{om}=2mm — L_i=2570mm
Pressure: Inlet (I/L)=1.0 bar — Outlet (O/L) = 0
Rotation about imperfection = 180 degrees
Rotation about pipe's axis = 120 degrees

Temperature (°C)				v_m (mm)	Buckle length (mm)			Remarks
I/L	O/L	Mean	Rise		I/L	O/L	Total	
20.59	20.50	20.54	0	2	1220	1350	2570	
22.42	22.34	22.38	1.84	2	1200	1340	2540	
24.44	24.38	24.41	3.87	2	1050	1330	2380	
26.43	26.40	26.41	5.87	2	1030	1330	2360	
27.88	27.84	27.86	7.32	2	1020	1330	2350	
29.23	29.18	29.20	8.66	2	1030	810	1840	
30.12	30.08	30.10	9.56	2	1030	800	1830	Snap
30.76	30.72	30.74	10.20	2	1030	800	1830	
30.76	30.72	30.74	10.20	31.63	2150	1550	3700	
31.80	31.76	31.78	11.24	35.06	2170	1560	3730	
34.18	34.17	34.17	13.63	39.04	2180	1920	4100	
35.81	35.81	35.81	15.27	43.87	2400	1900	4300	
38.12	38.11	38.11	17.57	47.70	2480	1900	4380	
40.06	40.06	40.06	19.52	51.00	2480	1900	4380	stop

Snap Buckling Isolated Prop with Fixed Anchor Points

Heating Test No 30

Date 3-12-1991
Time start : 13:00 pm — Time finish : 14:20 pm
v_{om}=2mm — L_i=2290mm
Pressure: Inlet (I/L)=0.98 bar — Outlet (O/L) = 0
Rotation about imperfection = 180 degrees
Rotation about pipe's axis = 240 degrees

Temperature (°C)				v_m (mm)	Buckle Length (mm)			Remarks
I/L	O/L	Mean	Rise		I/L	O/L	Total	
20.52	20.44	20.48	0	2	950	1340	2290	
22.21	22.18	22.20	1.72	2	940	830	1770	
24.28	24.24	24.26	3.78	2	940	740	1680	
26.26	26.21	26.24	5.76	2	940	740	1680	
27.27	27.26	27.27	6.79	2	940	740	1680	
28.70	28.69	28.70	8.22	2	940	740	1680	
29.37	29.36	29.37	8.89	2	940	740	1680	Snap
29.37	29.36	29.37	8.89	27.02	2170	1360	3530	
30.19	30.18	30.19	9.71	29.48	2170	1360	3530	
32.04	32.02	32.03	11.55	34.59	2170	1500	3670	
34.06	34.06	34.06	13.58	38.98	2170	1550	3720	
36.10	36.10	36.10	15.62	42.81	2170	1680	3850	
38.02	37.95	37.99	17.51	46.41	2300	1710	4010	
40.10	40.04	40.07	19.59	49.85	2290	1910	4200	stop

Snap Buckling Isolated Prop with Fixed Anchor Points

Heating Test No 31

Date 16-7-1992
Time start : 11:30 am — Time finish : 12:20 pm
v_{om}=2mm — L_i=2280mm
Pressure: Inlet (I/L)=1.0 bar — Outlet (O/L) = 0
Rotation about imperfection = 180 degrees
Rotation about pipe's axis = 0 degrees

Temperature (°C)				v_m (mm)	Buckle length (mm)			Remarks
I/L	O/L	Mean	Rise		I/L	O/L	Total	
20.73	20.83	20.78	0	2	960	1320	2280	
21.94	22.00	21.97	1.19	2	950	1270	2220	
23.84	23.86	23.85	3.07	2	950	940	1890	
25.64	25.72	25.68	4.90	2	960	740	1700	
27.70	27.79	27.74	6.96	2	950	740	1690	
28.65	28.72	28.68	7.90	2	950	740	1690	Snap
28.65	28.72	28.68	7.90	18.77	2120	1320	3440	Apex @ 450 LHS
29.56	29.80	29.68	8.90	28.03	2130	1330	3460	no change
30.65	30.67	30.66	9.88	30.40	2130	1340	3470	no change
31.60	31.61	31.60	10.82	32.72	2140	1470	3610	Apex @ 480 LHS
32.54	32.56	32.55	11.77	34.83	2140	1490	3630	no change
33.48	33.48	33.48	12.70	36.76	2240	1500	3740	no change
35.38	35.55	35.46	14.88	40.89	2400	1500	3900	no change:stop

Snap Buckling Isolated Prop with Fixed Anchor Points

Heating Test No 32

Date 16-7-1992
Time start : 12:30 pm — Time finish : 13:10 pm
v_{om}=2mm — L_i=2270mm
Pressure: Inlet (I/L)=1.00 bar — Outlet (O/L) = 0
Rotation about imperfection = 180 degrees
Rotation about pipe's axis = 120 degrees

Temperature (°C)				v_m (mm)	Buckle Length (mm)			Remarks
I/L	O/L	Mean	Rise		I/L	O/L	Total	
21.01	21.15	21.08	0	2	950	1320	2270	
22.67	22.72	22.70	1.62	2	950	830	1780	
24.76	24.82	24.79	3.71	2	950	780	1730	
26.68	26.71	26.70	4.62	2	960	720	1670	
27.72	27.75	27.73	6.65	2	950	720	1670	
28.70	28.71	28.70	7.62	2	950	720	1670	
29.13	29.27	29.20	8.12	2	950	720	1670	Snap
29.13	29.27	29.20	8.12	25.01	2130	1330	3460	Apex @ 430 LHS
30.60	30.62	30.61	9.53	28.98	2170	1330	3500	Apex @ 440 LHS
31.62	31.63	31.62	10.54	31.44	2170	1340	3510	Apex @ 480 LHS
32.38	32.38	32.38	11.30	33.62	2170	1470	3640	no change
33.60	33.62	33.61	12.53	36.24	2200	1500	3700	no change
34.50	34.48	34.49	13.41	38.14	2200	1580	3780	no change
36.56	36.58	36.57	15.49	41.74	2250	1600	3850	no change:stop

Snap Buckling Isolated Prop with Fixed Anchor Points

Heating Test No 33

Date 16-7-1992

Time start : 13:25 pm   Time finish : 14:05 pm

v_{om}=2mm L_i=2290mm

Pressure: Inlet (I/L)=1.0 bar   Outlet (O/L) = 0

Rotation about imperfection = 180 degrees

Rotation about pipe's axis = 240 degrees

Temperature (°C)				v_m (mm)	Buckle length (mm)			Remarks
I/L	O/L	Mean	Rise		I/L	O/L	Total	
20.80	20.90	20.85	0	2	960	1330	2290	
22.88	22.95	22.91	2.06	2	960	900	1860	
24.70	24.74	24.72	3.87	2	960	850	1810	
26.76	26.81	26.79	5.94	2	960	830	1790	
27.68	27.72	27.70	6.85	2	950	820	1770	
28.64	28.68	28.66	7.81	2	950	800	1750	
28.95	29.16	29.05	8.20	2	950	800	1750	Snap
28.95	29.16	29.05	8.20	25.73	2110	1320	3430	Apex @ 300 LHS
29.64	29.67	29.66	8.81	27.07	2120	1330	3450	Apex @ 300 LHS
30.67	30.67	30.67	9.82	29.53	2120	1410	3530	Apex @ 400 LHS
31.64	31.64	31.64	10.79	32.36	2120	1460	3580	Apex @ 400 LHS
32.40	32.42	32.41	11.56	34.32	2120	1470	3590	Apex @ 420 LHS
33.52	33.56	33.54	12.69	36.73	2180	1500	3680	Apex @ 450 LHS
34.54	34.56	34.55	13.70	38.45	2220	1500	3720	no change
36.42	36.42	36.42	15.57	42.20	2240	1530	3770	no change:stop

Snap Buckling Isolated Prop with Fixed Anchor Points

Cyclic Thermal Test No 34

Date 17-1-1992
Time start : 1:50 pm — Time finish : 3:20 pm
v_{om}=2mm — L_i=2560mm
Pressure: Inlet (I/L)=1.0 bar — Outlet (O/L) = 0
Rotation about imperfection = 0 degrees
Rotation about pipe's axis = 0 degrees

Temperature (°C)				v_m (mm)	Buckle length (mm)			Remarks
I/L	O/L	Mean	Rise		I/L	O/L	Total	
20.67	20.53	20.60	0	2	1230	1330	2560	
22.57	22.45	22.51	1.91	2	1230	740	1970	
24.61	24.50	24.56	3.96	2	1160	740	1900	
26.57	26.46	26.52	5.92	2	1150	740	1890	
27.43	27.33	27.38	6.78	2	1150	740	1890	
28.55	28.44	28.50	7.90	2	1150	740	1890	
29.46	29.36	29.41	8.81	2	1150	740	1890	
30.37	30.28	30.33	9.73	2	1150	740	1890	Snap: loading
30.37	30.28	30.33	9.73	28.96	2760	810	3570	
32.29	32.18	32.24	11.64	32.86	1850	2200	4050	
34.28	34.23	34.26	13.66	37.00	950	2800	3750	
36.27	36.20	36.24	15.64	41.62	1010	2800	3810	
38.22	38.14	38.18	17.58	44.80	1850	2490	4340	
40.10	40.00	40.05	19.45	50.31	1860	2780	4640	
38.23	38.14	38.19	17.59	45.87	1850	2490	4340	
36.40	36.32	36.36	15.76	42.16	1850	2490	4340	
34.39	34.30	34.35	13.75	37.63	1850	2350	4200	
32.33	32.23	32.28	11.68	31.96	710	2800	3510	
30.50	30.37	30.44	9.84	26.74	1320	2200	3520	
28.55	28.43	28.49	7.89	22.41	2460	800	3260	
26.56	26.42	26.49	5.89	22.41	2460	800	3260	
26.56	26.42	26.49	5.89	2	990	730	1720	Snap:unloading
24.64	24.50	24.57	3.97	2	1150	740	1890	
22.58	22.45	22.52	1.92	2	1230	1330	2560	
21.52	21.37	21.45	0.85	2	1220	1330	2550	
20.76	20.63	20.70	0.10	2	1850	1330	3180	

Snap Buckling Isolated Prop with Fixed Anchor Points

Cyclic Thermal Test No 35

Date 21-1-1992
Time start : 12:45 pm — Time finish : 14:30 pm
v_{om}=2mm — L_i=2330mm
Pressure: Inlet (I/L)=1.0 bar — Outlet (O/L) = 0
Rotation about imperfection = 0 degrees
Rotation about pipe's axis = 120 degrees

Temperature (°C)				v_m (mm)	Buckle Length (mm)			Remarks
I/L	O/L	Mean	Rise		I/L	O/L	Total	
20.68	20.55	20.62	0	2	990	1340	2330	
22.55	22.42	22.49	1.87	2	990	1340	2330	
23.88	23.74	23.81	3.19	2	990	1340	2330	
26.43	25.32	26.38	5.76	2	990	1340	2330	
28.26	28.17	28.22	7.60	2	990	1340	2330	Snap: loading
28.26	28.17	28.22	7.60	22.33	1290	2040	3330	
30.34	30.24	30.30	9.68	28.14	1320	2200	3520	
32.38	32.28	32.33	11.71	32.08	1320	2470	3790	
34.31	34.23	34.28	13.66	38.99	1900	2020	3920	
36.16	36.10	36.14	15.52	43.19	1910	2040	3950	
38.25	38.14	38.20	17.58	46.77	2110	2040	4150	
40.12	40.07	40.10	19.48	50.32	2130	2020	4150	
38.19	38.08	38.14	17.52	46.41	2110	2040	4150	
36.16	36.09	36.13	15.51	43.35	2120	2010	4130	
33.95	33.86	33.91	13.29	39.13	2110	1990	4100	
32.29	32.19	32.25	11.63	34.20	2110	1930	4040	
30.29	30.18	30.24	9.62	29.93	2110	1800	3910	
28.48	28.34	28.42	7.80	21.21	1280	2040	3320	
27.25	27.12	27.19	6.57	17.63	1160	2020	3180	
26.35	26.26	26.31	5.69	17.63	1160	2020	3180	
26.35	26.26	26.31	5.69	2	990	1340	2330	Snap:unloading
24.61	24.48	24.55	3.93	2	990	1340	2330	
22.47	22.33	22.40	1.78	2	990	1340	2330	
20.74	20.61	20.68	0.06	2	990	1340	2330	

Snap Buckling Isolated Prop with Fixed Anchor Points

Cyclic Thermal Test No 36

Date 28-1-1992
Time start : 12:15 pm   Time finish : 14:20 pm
v_{om}=2mm L_i=2310mm
Pressure: Inlet (I/L)=1.0 bar   Outlet (O/L) = 0
Rotation about imperfection = 0 degrees
Rotation about pipe's axis = 240 degrees

Temperature (°C)				v_m (mm)	Buckle length (mm)			Remarks
I/L	O/L	Mean	Rise		I/L	O/L	Total	
20.55	20.49	20.52	0	2	960	1350	2310	
22.60	22.48	22.54	2.02	2	950	1340	2290	
24.52	24.39	24.46	3.94	2	740	1340	2080	
26.52	26.40	26.46	5.94	2	720	810	1530	
28.45	28.35	28.40	7.88	2	710	800	1510	
29.43	29.30	29.37	8.85	2	690	800	1490	
29.64	29.53	29.59	9.07	2	690	800	1490	Snap: loading
29.64	29.53	29.59	9.07	24.37	1230	2320	3550	
30.47	30.36	30.42	9.90	26.66	1290	2330	3620	
32.21	32.08	32.15	11.63	31.87	1290	2340	3630	
34.20	34.16	34.18	13.66	36.67	1330	2340	3670	
36.22	36.14	36.18	15.66	40.31	1330	2480	3810	
37.99	37.90	37.95	17.43	46.22	1900	2320	4220	
40.18	40.00	40.09	19.57	49.83	1900	2200	4100	
38.03	37.90	37.97	17.45	45.98	1890	2210	4100	
36.09	35.96	35.03	15.51	40.73	1330	2490	3820	
34.31	34.25	34.28	13.76	36.64	1320	2480	3800	
32.05	31.94	32.00	11.48	31.64	1310	2330	3640	
30.39	30.27	30.33	9.81	26.58	1220	2330	3550	
28.46	28.34	28.40	7.88	19.16	1160	2200	3360	
27.48	27.35	27.42	6.90	15.97	1020	2030	3050	
26.86	26.77	26.82	6.30	15.97	1020	2030	3050	
26.86	26.77	26.82	6.30	2	720	810	1530	Snap:unloading
24.63	24.50	24.57	4.05	2	730	1330	2060	
22.69	22.55	22.62	2.10	2	960	1340	2300	
20.64	20.48	20.56	0.04	2	960	1340	2300	

Snap Buckling Isolated Prop with Fixed Anchor Points

Cyclic Thermal Test No 37

Date 17-12-1991
Time start : 11:30 am   Time finish : 13:10 pm
v_{om}=2mm L_i=2290mm
Pressure: Inlet (I/L)=0.98 bar   Outlet (O/L) = 0
Rotation about imperfection = 180 degrees
Rotation about pipe's axis = 0 degrees

Temperature (°C)				v_m (mm)	Buckle Length (mm)			Remarks
I/L	O/L	Mean	Rise		I/L	O/L	Total	
20.49	20.41	20.45	0	2	950	1340	2290	
22.41	22.34	22.38	1.93	2	950	1340	2290	
24.44	24.40	24.42	3.97	2	740	1340	2080	
26.37	26.32	26.35	5.90	2	730	1340	2070	
27.72	27.31	27.52	7.07	2	730	1340	2070	Snap: loading
27.72	27.31	27.52	7.07	19.81	750	2480	3230	
29.24	29.20	29.22	8.77	27.55	780	2840	3620	
29.39	29.34	29.37	8.92	28.10	2450	1360	3810	
33.30	33.25	33.28	12.83	37.80	2480	1500	3980	
35.20	35.17	35.19	14.74	41.85	2480	1550	4030	
37.23	37.19	37.21	16.76	45.01	1890	2340	4230	
39.24	39.08	39.16	18.71	48.61	1870	2470	4340	
37.24	37.19	37.22	16.77	44.77	1880	2340	4220	
35.27	35.24	35.26	14.81	41.38	2470	1640	4110	
33.30	33.25	33.28	12.83	37.31	2470	1550	4020	
31.30	31.25	31.28	10.83	32.48	2450	1490	3940	
29.30	29.29	29.30	8.85	26.66	2310	1490	3800	
28.37	28.32	28.35	7.90	22.86	2170	1360	3530	
28.07	28.02	28.05	7.60	20.80	2170	1350	3520	
27.88	27.83	27.86	7.41	19.66	2170	1340	3510	
27.67	27.62	27.65	7.20	16.84	780	2340	3120	
26.91	26.90	26.91	6.46	14.56	760	2080	2840	
26.72	26.65	26.69	6.24	10.84	760	2040	2800	
26.42	26.38	26.40	5.95	10.84	760	2040	2800	
26.42	26.38	26.40	5.95	2	720	1360	2080	Snap:unloading
24.63	24.56	24.60	4.15	2	740	1340	2080	
22.51	22.43	22.47	2.02	2	950	1340	2290	

Snap Buckling Isolated Prop with Fixed Anchor Points

Cyclic Thermal Test No 38

Date 14-1-1992
Time start : 10:45 am　　Time finish : 12:10 pm
v_{om}=2mm　　L_i=2550mm
Pressure: Inlet (I/L)=0.98 bar　　Outlet (O/L) = 0
Rotation about imperfection = 180 degrees
Rotation about pipe's axis = 120 degrees

Temperature (°C)				v_m (mm)	Buckle length (mm)			Remarks
I/L	O/L	Mean	Rise		I/L	O/L	Total	
20.50	20.43	20.46	0	2	1220	1330	2550	
22.57	22.50	22.54	2.06	2	1220	1330	2550	
24.53	24.48	24.50	4.04	2	1210	1330	2540	
26.49	26.45	26.47	6.01	2	1210	800	2010	
27.52	27.42	27.47	7.01	2	1220	800	2020	
28.48	28.42	28.45	7.99	2	1220	790	2010	
29.04	29.02	29.03	8.57	2	1220	790	2010	
29.30	29.27	29.28	8.82	2	1220	790	2010	Snap: loading
29.30	29.27	29.28	8.82	26.48	1900	1510	3410	
30.25	30.20	30.22	9.76	30.19	2140	1510	3650	
32.22	32.18	32.20	11.74	34.49	2180	1540	3720	
34.25	34.20	34.22	13.76	39.00	2170	1710	3880	
36.25	36.22	36.23	15.77	42.94	2170	1780	3950	
38.25	38.22	38.23	17.77	46.68	2300	1780	4080	
40.11	40.10	40.10	19.64	50.50	2410	1780	4190	
38.16	38.11	38.13	17.67	46.73	2410	1780	4190	
36.31	36.28	36.29	15.83	42.62	2180	1780	3960	
34.33	34.25	34.29	13.83	39.08	2180	1780	3960	
32.30	32.27	32.28	11.82	34.57	2160	1720	3880	
30.34	30.26	30.30	9.84	29.89	2140	1540	3680	
28.52	28.44	28.48	8.02	23.24	1890	1540	3430	
26.52	26.46	26.49	6.03	14.22	1880	1350	3230	
25.60	25.51	25.55	5.09	14.22	1880	1350	3230	
25.60	25.51	25.55	5.09	2	1230	800	2030	Snap: unloading
24.40	24.35	24.37	3.91	2	1220	800	2020	
22.62	22.53	22.57	2.11	2	1220	1320	2540	
20.71	20.62	20.66	0.2	2	1220	1330	2550	

Snap Buckling Isolated Prop with Fixed Anchor Points

Cyclic Thermal Test No 39

Date 16-12-1992
Time start : 14:00 pm　　Time finish : 15:30 pm
v_{om}=2mm　　L_i=2300mm
Pressure: Inlet (I/L)=0.98 bar　　Outlet (O/L) = 0
Rotation about imperfection = 180 degrees
Rotation about pipe's axis = 240 degrees

Temperature (°C)				v_m (mm)	Buckle Length (mm)			Remarks
I/L	O/L	Mean	Rise		I/L	O/L	Total	
20.61	20.51	20.56	0	2	960	1340	2300	
22.35	22.27	22.31	1.75	2	950	1340	2290	
24.55	24.49	24.52	3.96	2	950	730	1680	
26.42	26.36	26.39	5.83	2	950	730	1680	
28.35	28.28	28.32	7.76	2	950	730	1680	
29.22	29.16	29.19	8.63	2	940	730	1670	
29.72	29.65	29.69	9.13	2	940	730	1670	
29.82	29.74	29.78	9.22	2	940	730	1670	
29.97	29.95	29.96	9.40	2	940	730	1670	Snap: loading
29.97	29.95	29.96	9.40	28.30	2170	1490	3660	
32.09	32.02	32.06	11.50	33.88	2170	1530	3700	
34.20	34.16	34.18	13.62	38.40	2180	1630	3810	
36.12	36.06	36.09	15.53	42.21	2170	1700	3870	
38.10	38.10	38.10	17.54	45.85	2170	1720	3890	
40.08	40.02	40.05	19.49	49.43	2470	1720	4190	
38.26	38.24	38.25	17.69	46.41	2470	1640	4110	
36.26	36.21	36.24	15.68	42.30	2470	1530	4000	
34.48	34.43	34.46	13.90	38.26	2470	1520	3990	
32.54	32.47	32.51	11.95	34.19	2410	1500	3910	
30.64	30.57	30.61	10.05	29.36	2170	1490	3660	
28.73	28.64	28.69	8.13	22.14	2170	1320	3490	
26.73	26.65	26.69	6.13	22.14	2170	1320	3490	
26.73	26.65	26.69	6.13	2	950	740	1690	Snap: unloading
24.77	24.70	24.64	4.18	2	950	740	1690	

Stable Buckling Infilled Prop with Fixed Anchor Points

Heating Test No 40

Date 28-8-1991
Time start : 8:45 am — Time finish : 10:20 am
v_{om}=30mm — L_i=4620mm
Pressure: Inlet (I/L)=0.92 bar — Outlet (O/L) = 0
Rotation about imperfection = 0 degrees
Rotation about pipe's axis = 0 degrees

Temperature (°C)				v_m (mm)	Buckle length (mm)			Remarks
I/L	O/L	Rise	Spine		I/L	O/L	Total	
20.5	20.5	0	23.1	30	2120	2500	4620	
22.3	22.3	1.8	23.1	30				unmeasurable
22.8	22.8	2.3	23.1	30.02	1200	1300	2500	Upheaval
23.4	23.4	2.9	23.1	31.26	1300	1300	2600	Apex @ 100 LHS
23.9	23.9	3.4	23.1	32.29	1400	1300	2700	no change
24.4	24.4	3.9	23.1	33.29	1400	1400	2800	good symmetry
24.9	24.9	4.4	23.1	34.63	1500	1400	2900	Apex @ 100 LHS
25.9	25.9	5.4	23.1	36.74	1600	1500	3100	no change
27.0	27.0	6.5	23.1	30.90	1700	1500	3200	no change
27.9	27.9	7.4	23.0	40.57	1700	1600	3300	no change
28.8	28.8	8.3	23.0	42.61	1700	1700	3400	symmetry
29.9	29.9	9.4	23.0	44.31	1800	1800	3600	no change
30.8	30.8	10.3	23.0	46.15	1900	1800	3700	Apex @ 100 LHS
31.6	31.6	11.1	23.0	47.78	1900	1900	3800	no change

Stable Buckling Infilled Prop with Fixed Anchor Points

Heating Test No 41

Date 28-8-1991
Time start : 11:10 am — Time finish : 12:30 pm
v_{om}=30mm — L_i=4840mm
Pressure: Inlet (I/L)=0.92 bar — Outlet (O/L) = 0
Rotation about imperfection = 0 degrees
Rotation about pipe's axis = 120 degrees

Temperature (°C)				v_m (mm)	Buckle Length (mm)			Remarks
I/L	O/L	Rise	Spine		I/L	O/L	Total	
20.5	20.5	0	22.9	30	2240	2600	4840	
23.1	23.1	2.6	22.8	30.01	900	1400	2300	Upheaval
24.0	24.0	3.5	22.8	30.82	1000	1500	2500	Apex @ 100 RHS
24.4	24.4	3.9	22.8	32.02	1000	1700	2700	Apex @ 200 RHS
24.9	24.9	4.4	22.8	33.19	1100	1800	2900	Apex @ 100 RHS
25.4	25.4	4.9	22.8	34.35	1200	1800	3000	no change
25.9	25.8	5.4	22.8	36.03	1200	1900	3100	more PTFE added
26.4	28.4	5.9	22.8	37.14	1300	1900	3200	Apex @ 100 RHS
27.0	27.0	6.5	22.8	38.21	1400	1900	3300	no change
27.4	27.4	6.9	22.8	39.02	1400	2000	3400	no change
27.9	27.8	7.4	22.8	40.06	1500	2000	3500	no change
28.4	28.4	7.9	22.7	41.12	1600	2000	3600	Apex @ 200 RHS
29.2	29.2	8.7	22.7	43.05	1600	2100	3700	no change

Stable Buckling Infilled Prop with Fixed Anchor Points

Heating Test No 42

Date 28-8-1991
Time start : 13:00 pm　　Time finish : 14:20 pm
v_{om}=30mm　　L_i=4760mm
Pressure: Inlet (I/L)=0.92 bar　　Outlet (O/L) = 0
Rotation about imperfection = 0 degrees
Rotation about pipe's axis = 240 degrees

Temperature (°C)				v_m (mm)	Buckle length (mm)			Remarks
I/L	O/L	Rise	Spine		I/L	O/L	Total	
20.5	20.5	0	22.7	30	2530	2230	4760	
23.0	23.0	2.5	22.7	30.03	1300	1100	2400	Upheaval
23.4	23.4	2.9	22.6	30.60	1400	1100	2500	Apex @ 100 LHS
23.9	23.9	3.4	22.6	32.34	1400	1300	2700	no change
24.4	24.4	3.9	22.6	32.97	1500	1400	2900	no change
24.9	24.9	4.4	22.6	34.23	1600	1400	3000	no change
25.4	25.4	4.9	22.6	35.70	1600	1500	3100	PTFE added
26.3	26.3	5.8	22.6	37.48	1700	1600	3300	Apex @ 100 LHS
27.4	27.4	6.9	22.6	39.53	1800	1600	3400	no change
28.3	28.3	7.8	22.6	41.58	1800	1700	3500	symmetry
29.4	29.4	8.9	22.6	43.42	1800	1800	3600	no change
30.4	30.4	9.9	22.6	45.23	1900	1800	3700	no change
32.2	32.2	11.7	22.6	48.47	1900	1900	3800	no change
34.2	34.2	13.7	22.6	51.92	2000	1900	3900	stop

Stable Buckling Infilled Prop with Fixed Anchor Points

Heating Test No 43

Date 22-8-1991
Time start : 14:10 pm　　Time finish : 16:30 pm
v_{om}=20mm　　L_i=4180mm
Pressure: Inlet (I/L)=0.92 bar　　Outlet (O/L) = 0
Rotation about imperfection = 0 degrees
Rotation about pipe's axis = 0 degrees

Temperature (°C)				v_m (mm)	Buckle Length (mm)			Remarks
I/L	O/L	Rise	Spine		I/L	O/L	Total	
20.5	20.5	0	24.3	20	2140	2040	4180	
21.6	21.6	1.1	24.4	20	400	500	900	
22.0	22.0	1.5	24.4	20	800	800	1600	
22.4	22.4	1.9	24.4	20	1000	1100	2100	
23.2	23.2	2.7	24.5	20.02	1100	1300	2400	Upheaval
23.5	23.5	3.0	24.5	20.08	1200	1300	2500	Apex @ 100 LHS
24.5	24.5	4.0	24.5	22.18	1400	1400	2800	Apex @ 100 LHS
25.5	25.5	5.0	24.5	24.99	1400	1500	2900	no change
26.5	26.5	6.0	24.5	27.87	1500	1600	3100	no change
28.4	28.4	7.9	24.5	32.69	1800	1700	3500	Apex @ 200 LHS
30.4	30.4	9.9	24.6	37.13	1900	2000	3900	no change
32.3	32.3	11.8	24.6	40.86	2000	2000	4000	no change
34.3	34.3	13.8	24.6	45.03	2100	2100	4200	no change

Stable Buckling Infilled Prop with Fixed Anchor Points

Heating Test No 44

Date 23-8-1991
Time start : 9:45 am — Time finish : 11:30 am
v_{om}=20mm — L_i=4390mm
Pressure: Inlet (I/L)=0.92 bar — Outlet (O/L) = 0
Rotation about imperfection = 0 degrees
Rotation about pipe's axis = 120 degrees

Temperature (°C)				v_m (mm)	Buckle length (mm)			Remarks
I/L	O/L	Rise	Spine		I/L	O/L	Total	
20.4	20.4	0	22.8	20	2090	2300	4390	
21.4	21.4	1.0	22.8	20	300	500	800	
21.8	21.8	1.4	22.8	20	400	1000	1400	
22.3	22.3	1.9	22.8	20	500	1200	1700	
23.0	23.0	2.6	22.7	20.12	800	1300	2100	Upheaval
23.5	23.5	3.1	22.7	21.48	1200	1400	2600	Apex @ 100 RHS
24.4	24.4	4.0	22.7	24.00	1200	1500	2700	Apex @ 200 RHS
25.4	25.4	5.0	22.6	27.06	1300	1700	3000	Apex @ 300 RHS
26.4	26.4	6.0	22.6	29.84	1300	1900	3200	Apex @ 200 RHS
27.3	27.3	6.9	22.6	32.14	1300	2000	3300	Apex @ 200 RHS
28.2	28.2	7.8	22.5	34.71	1400	2000	3400	no change
30.2	30.2	9.8	22.5	39.00	1500	2100	3600	no change
32.3	32.3	11.9	22.5	42.80	1600	2100	3700	Apex @ 300 RHS

Stable Buckling Infilled Prop with Fixed Anchor Points

Heating Test No 45

Date 23-8-1991
Time start : 12:00 pm — Time finish : 14:45 pm
v_{om}=20mm — L_i=4120mm
Pressure: Inlet (I/L)=0.92 bar — Outlet (O/L) = 0
Rotation about imperfection = 0 degrees
Rotation about pipe's axis = 240 degrees

Temperature (°C)				v_m (mm)	Buckle Length (mm)			Remarks
I/L	O/L	Rise	Spine		I/L	O/L	Total	
20.5	20.5	0	22.4	20	2100	2020	4120	
21.5	21.5	1.0	22.4	20	400	300	700	
21.9	21.9	1.4	22.4	20	700	700	1400	
22.4	22.4	1.9	22.4	20	900	1000	1900	
22.8	22.8	2.3	22.4	20	1000	1100	2100	
23.4	23.4	2.9	22.4	20.03	1100	1100	2200	Upheaval
23.9	23.9	3.4	22.3	21.09	1300	1300	2600	Apex @ 100 LHS
24.9	24.9	4.4	22.2	24.11	1400	1400	2800	Apex @ 200 LHS
25.9	25.9	5.4	22.2	26.69	1600	1400	3000	Apex @ 100 LHS
26.9	26.9	6.4	22.2	29.24	1700	1500	3200	no change
27.8	27.8	7.3	22.2	32.01	1800	1600	3400	no change
29.9	29.9	9.4	22.1	36.48	2000	1700	3700	Apex @ 200 LHS
31.6	31.6	11.1	22.1	40.33	2100	1700	3800	Apex @ 200 LHS

Appendix C

THERMO-MECHANICAL SYSTEM EXPERIMENTATION
GRAPHICAL PRESENTATION

ISOLATED PROP (Stable) Heating Test No 1 v_{om} = 30 mm

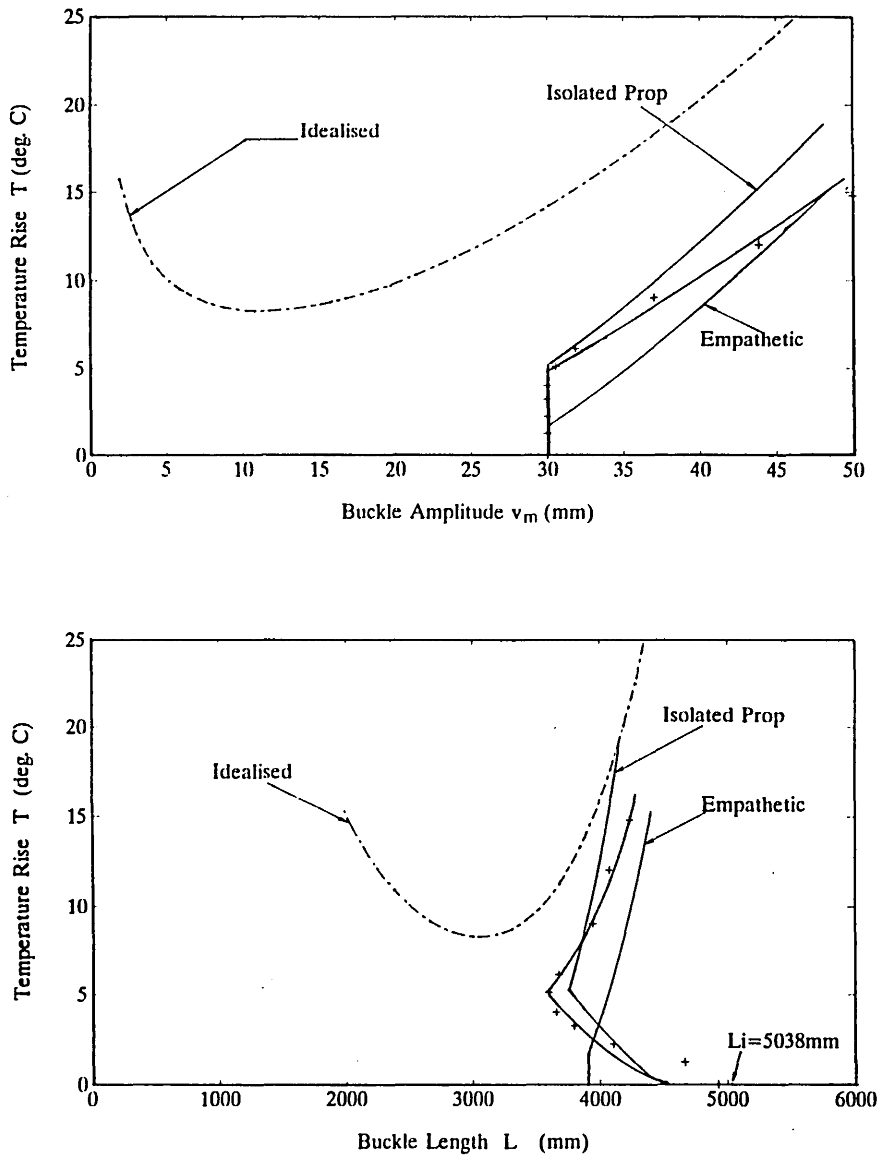

ISOLATED PROP (Stable) Heating Test No 2 v_{om} = 30 mm

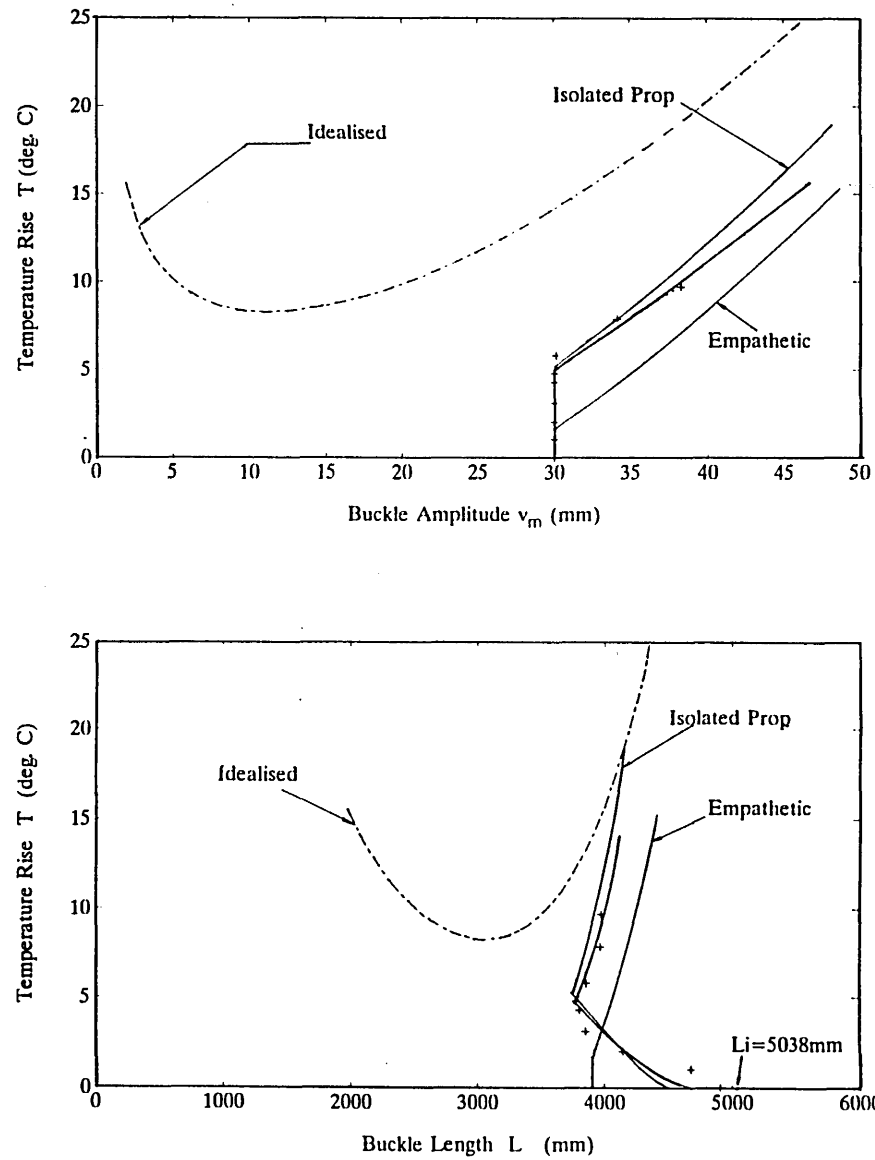

ISOLATED PROP (Stable) Heating Test No 3 v_{om} = 30 mm

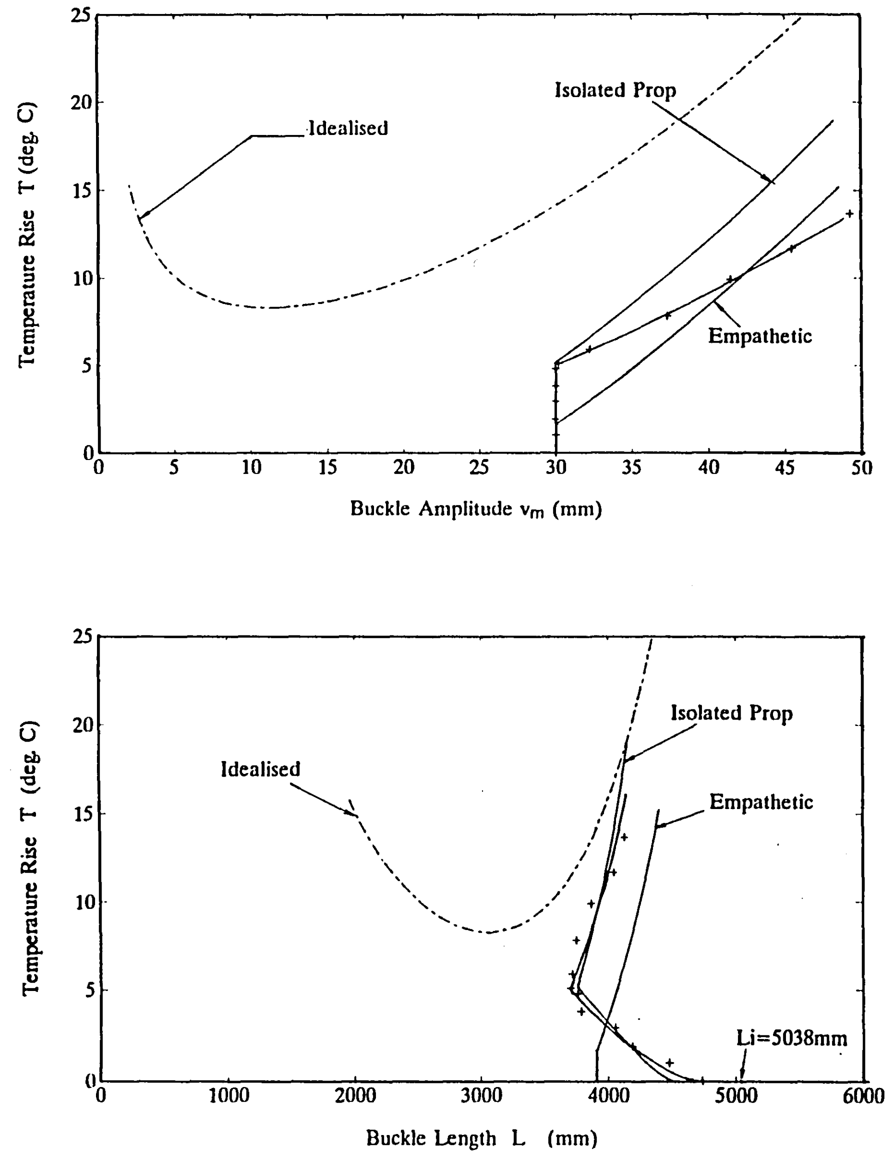

ISOLATED PROP (Stable) Heating Test No 4 v_{om} = 30 mm

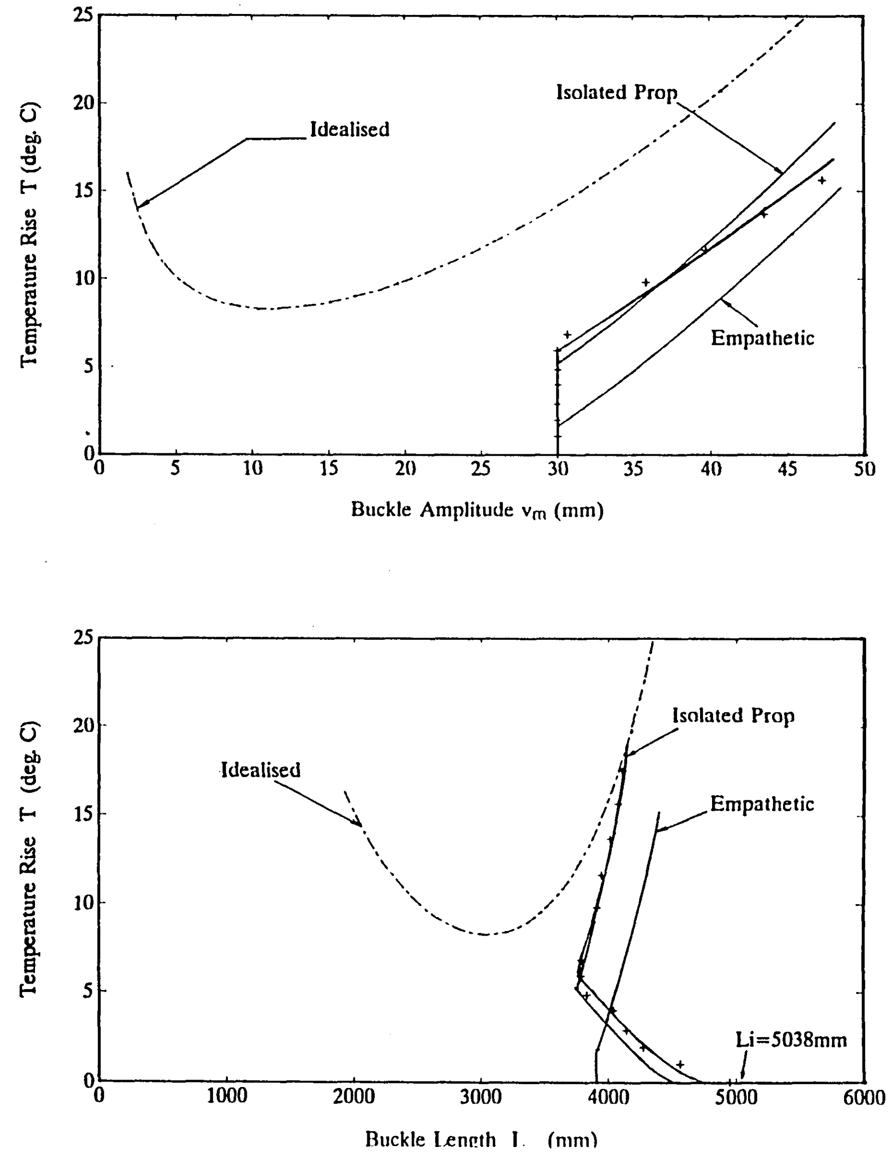

ISOLATED PROP (Stable) Heating Test No 5 v_{om} = 30 mm

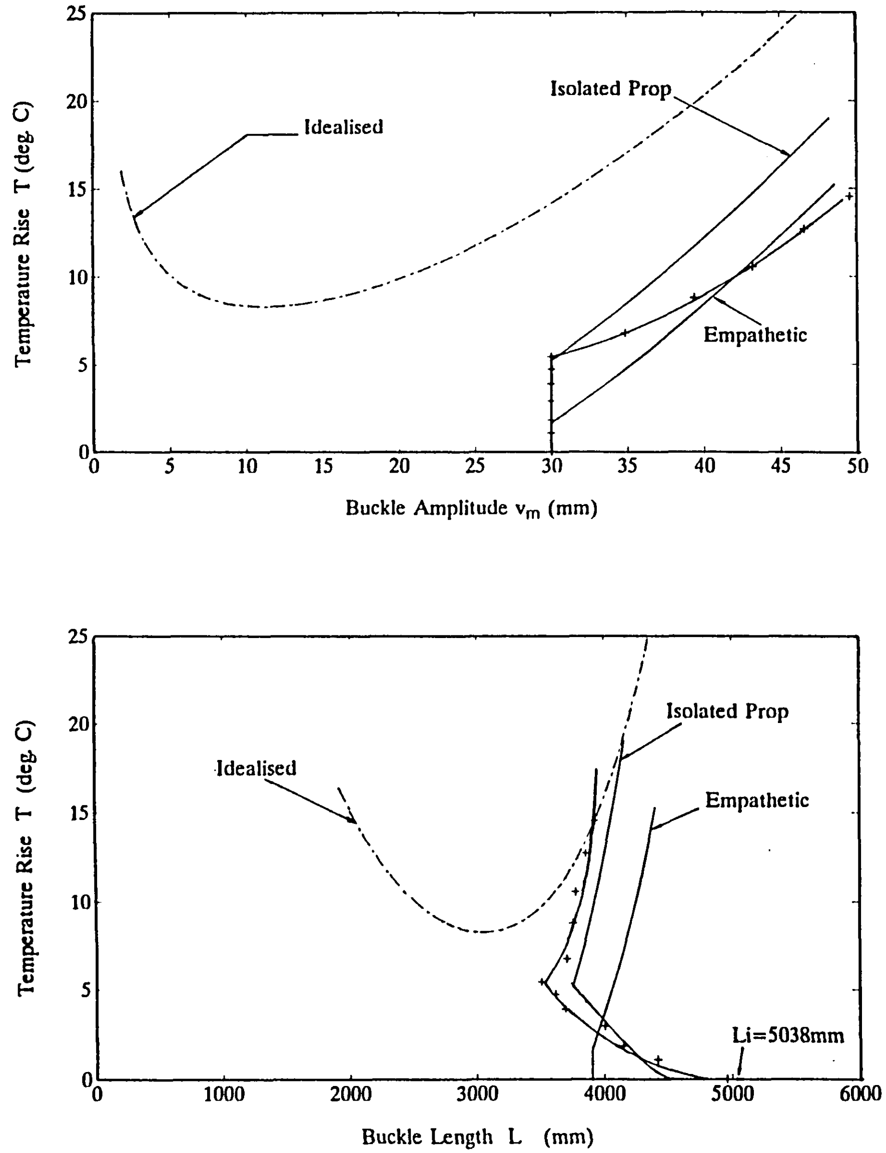

ISOLATED PROP (Stable) Heating Test No 6 v_{om} = 30 mm

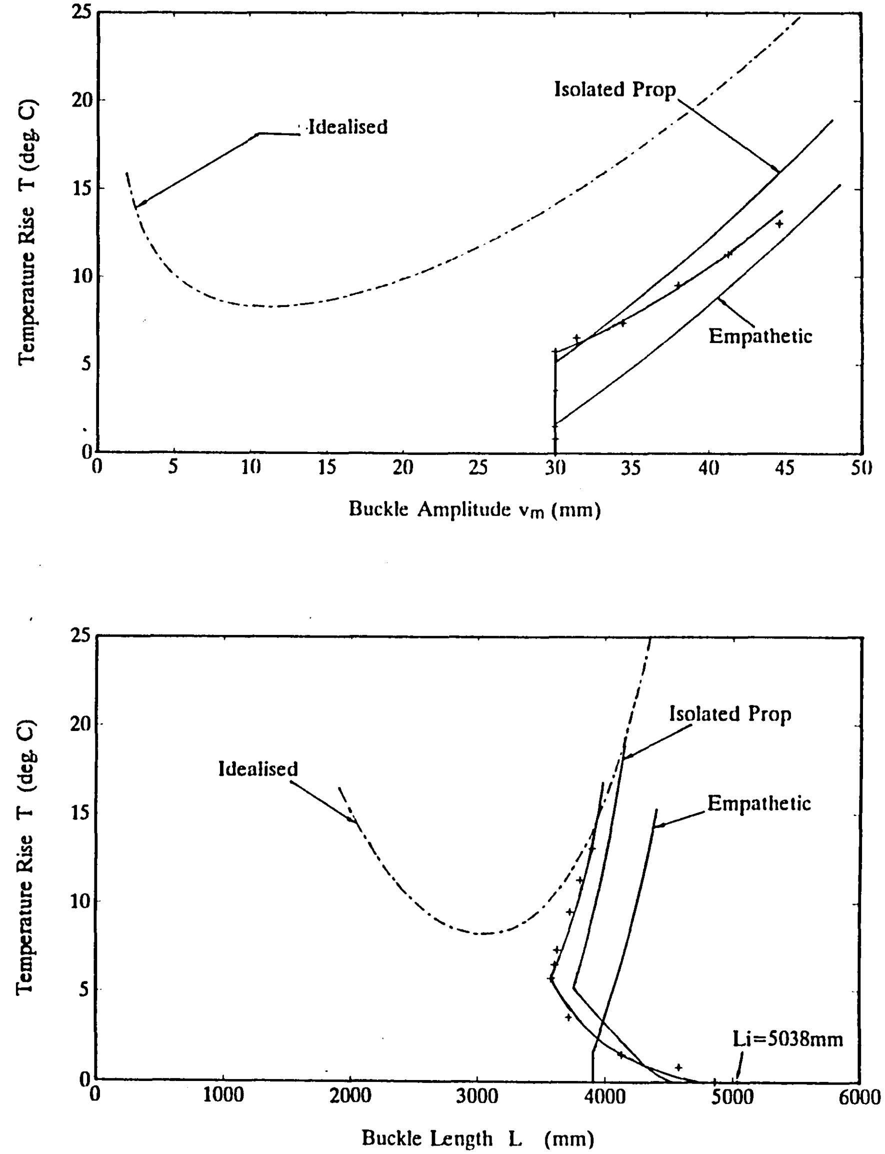

ISOLATED PROP (Stable) Heating Test No 7 v_{om} = 20 mm

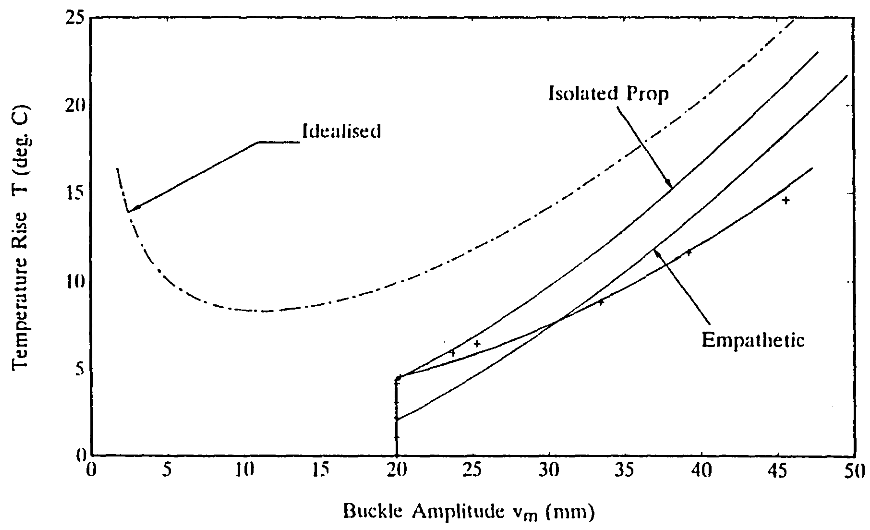

ISOLATED PROP (Stable) Heating Test No 8 v_{om} = 20 mm

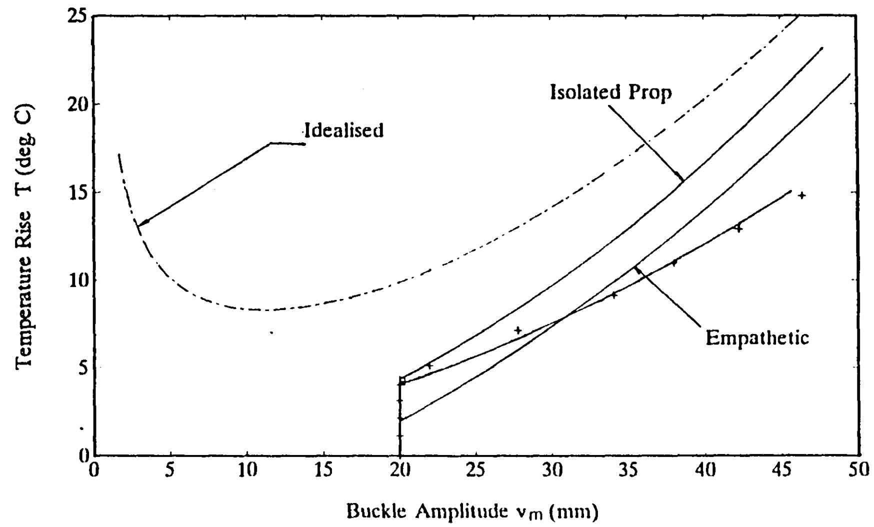

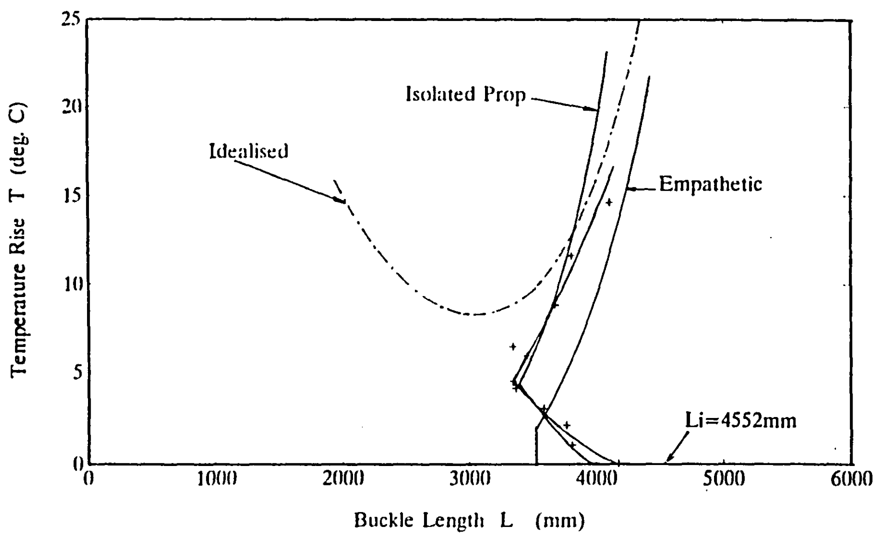

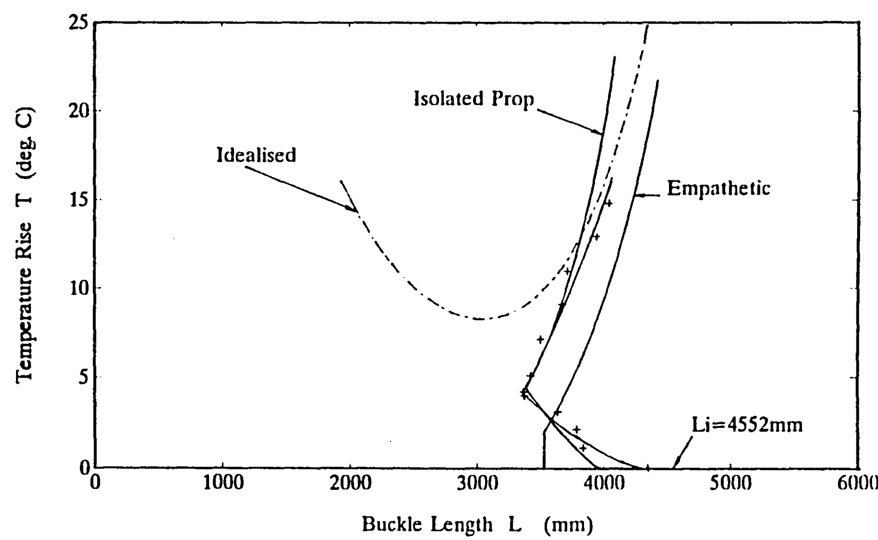

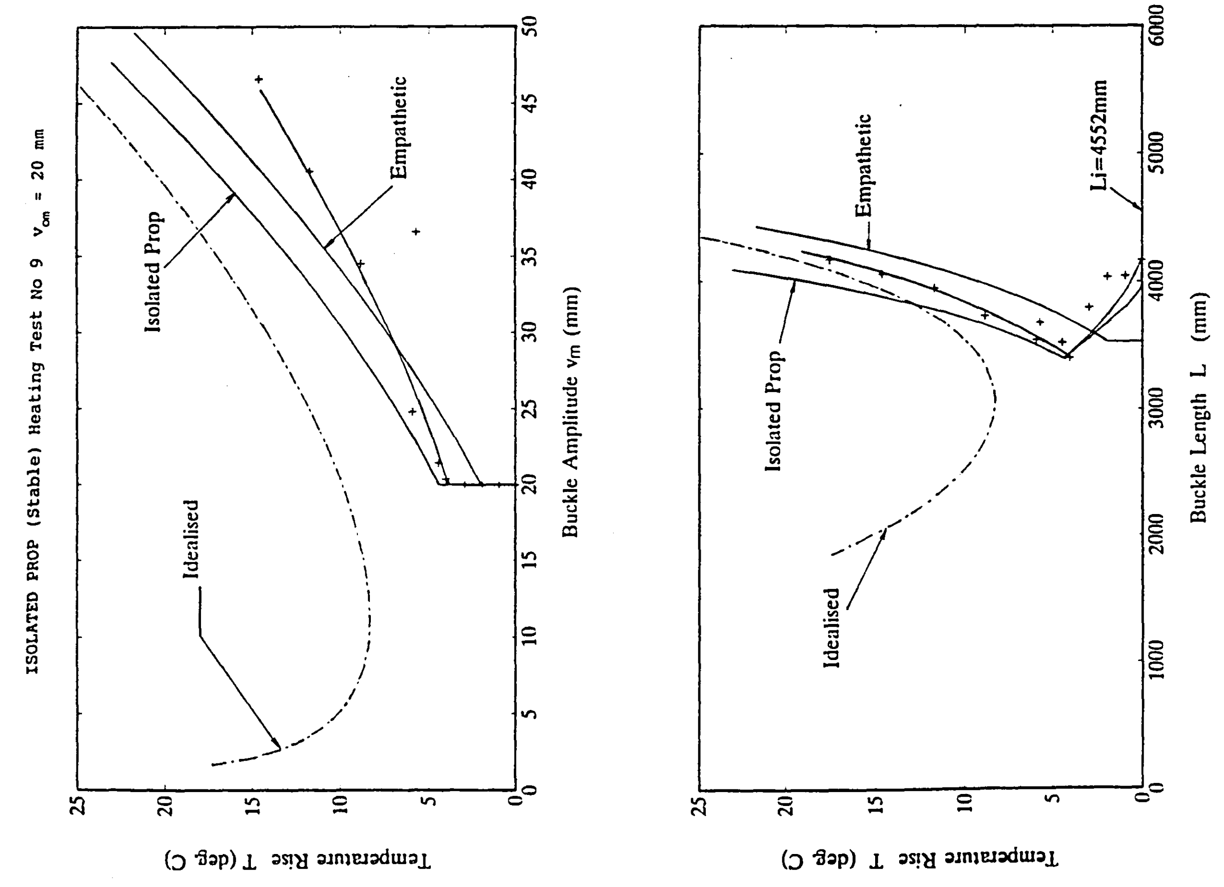
ISOLATED PROP (Stable) Heating Test No 9 v_{om} = 20 mm
Temperature Rise T (deg. C)
Buckle Amplitude v_m (mm)
Buckle Length L (mm)
Idealised
Isolated Prop
Empathetic
Li=4552mm

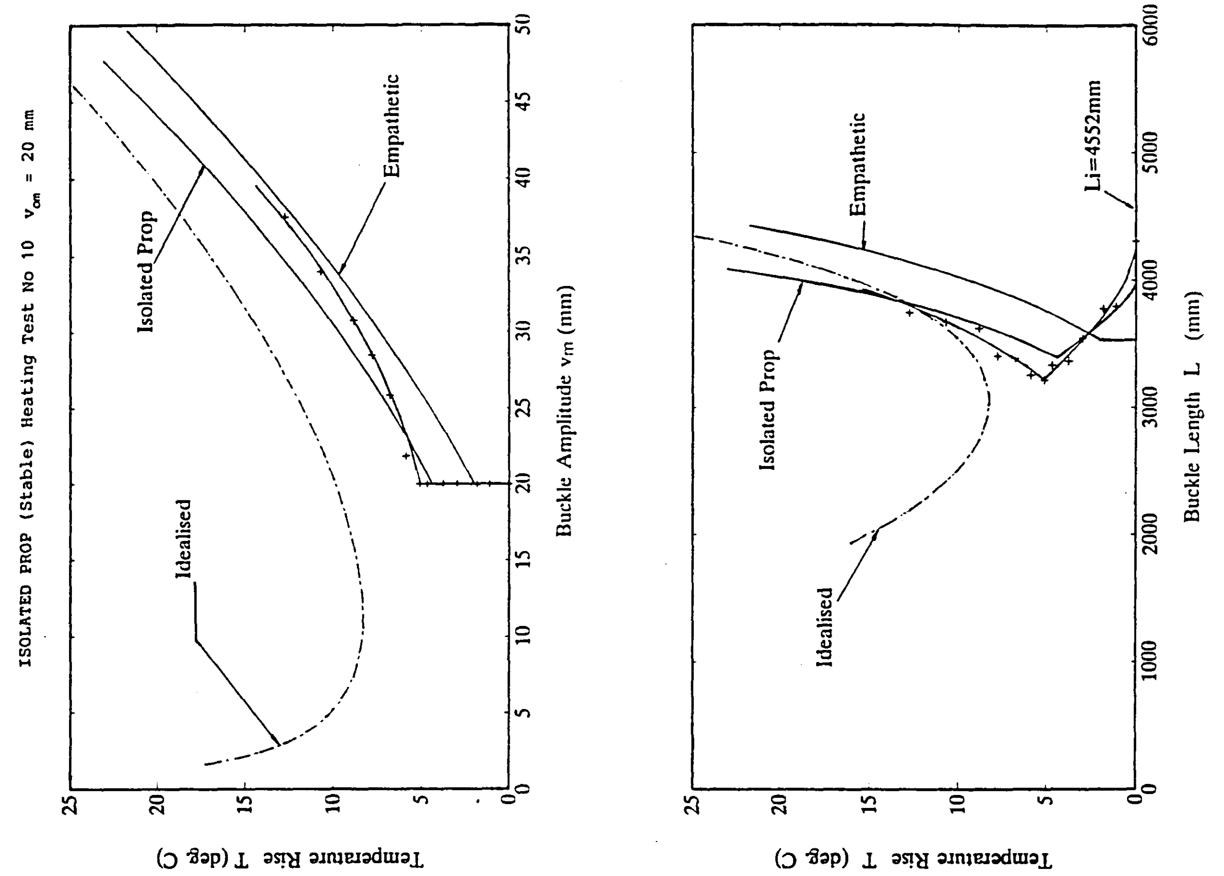
ISOLATED PROP (Stable) Heating Test No 10 v_{om} = 20 mm
Temperature Rise T (deg. C)
Buckle Amplitude v_m (mm)
Buckle Length L (mm)
Idealised
Isolated Prop
Empathetic
Li=4552mm

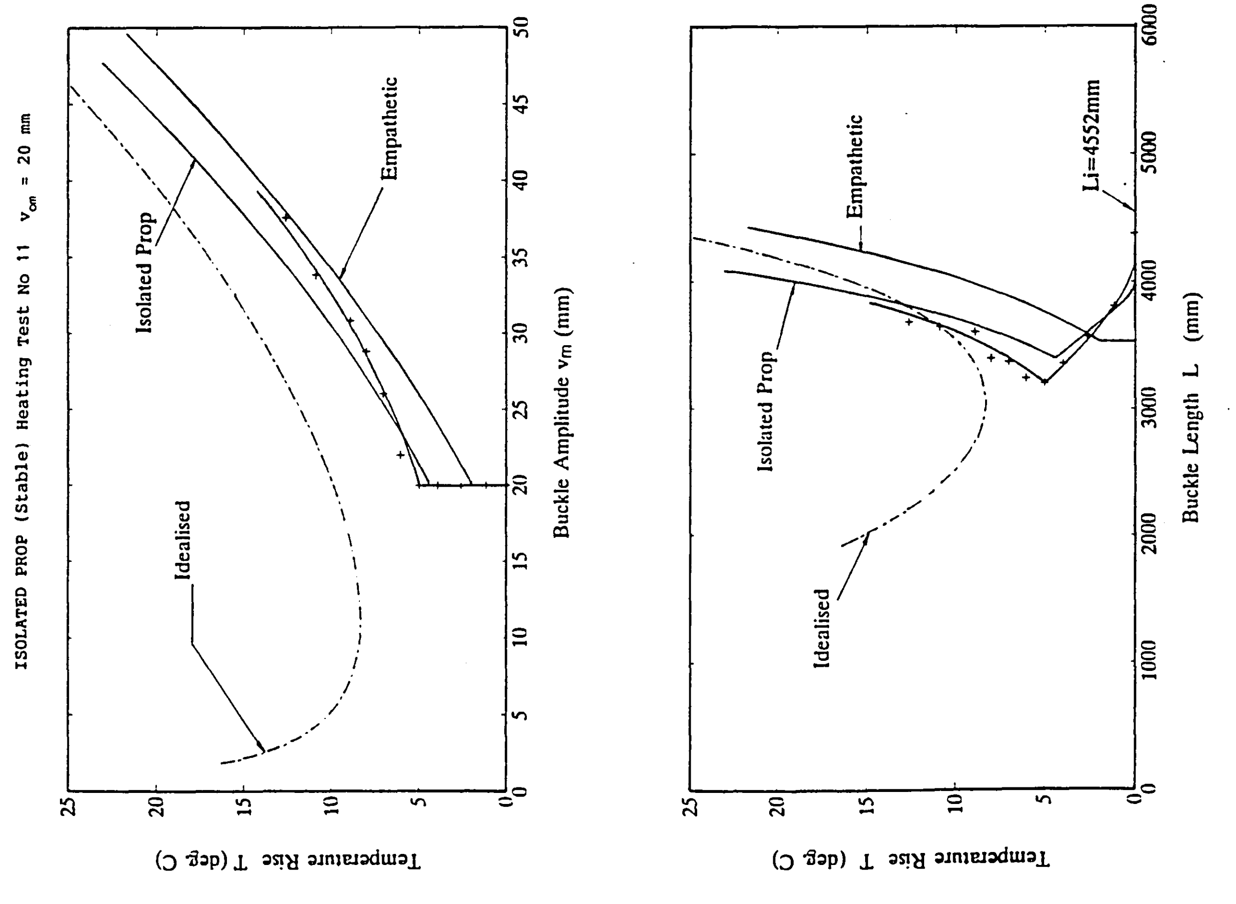

ISOLATED PROP (Stable) Heating Test No 11 v_{om} = 20 mm
Temperature Rise T (deg. C)
Buckle Amplitude v_m (mm)
Idealised
Isolated Prop
Empathetic
Buckle Length L (mm)
Li=4552mm

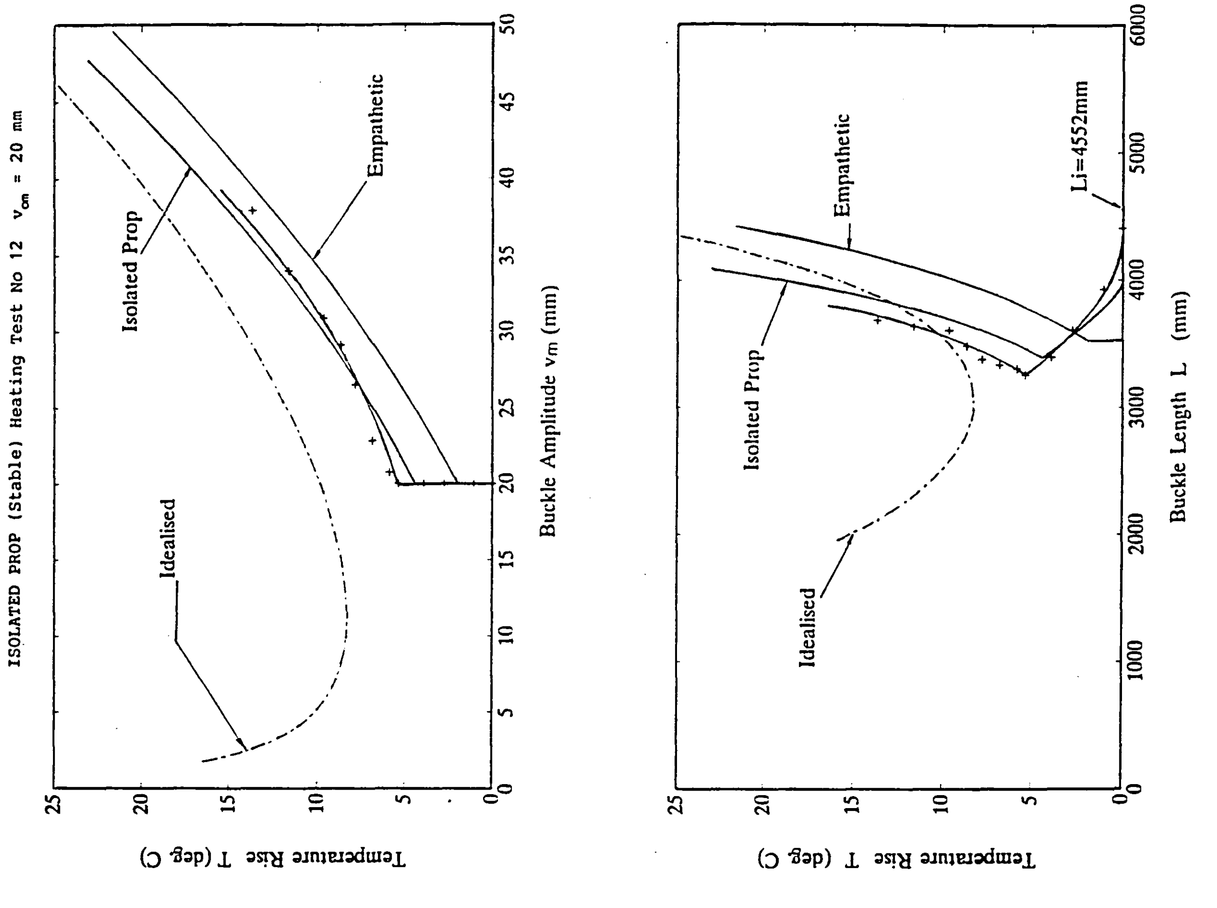

ISOLATED PROP (Stable) Heating Test No 12 v_{om} = 20 mm
Temperature Rise T (deg. C)
Buckle Amplitude v_m (mm)
Idealised
Isolated Prop
Empathetic
Buckle Length L (mm)
Li=4552mm

ISOLATED PROP (Stable) Cyclic Thermal Test No 13 v_{om} = 15 mm

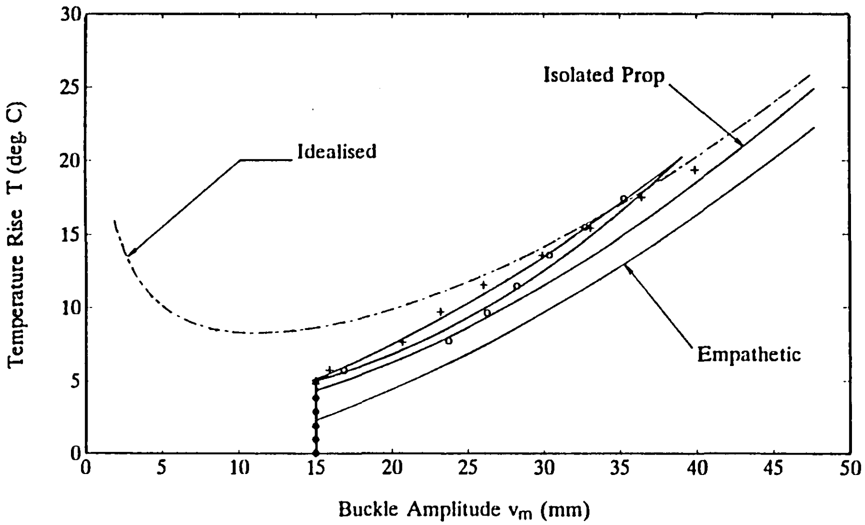

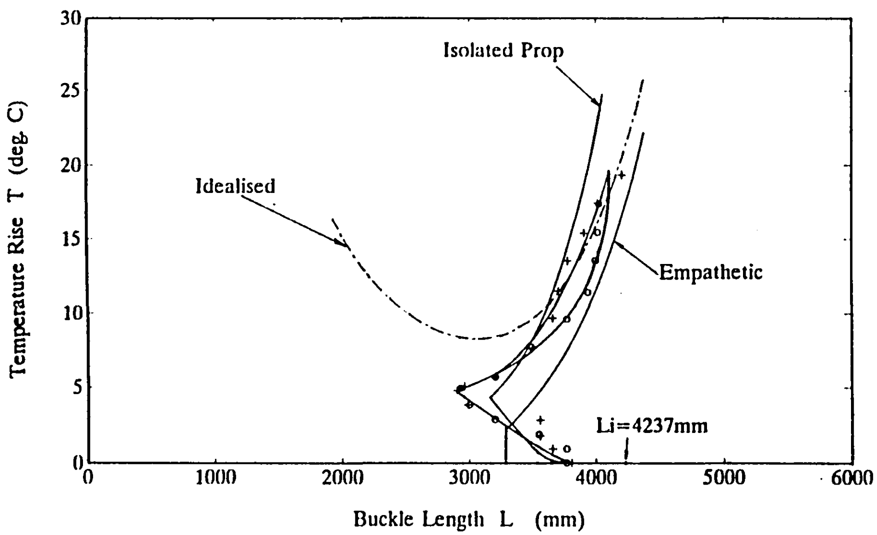

ISOLATED PROP (Stable) Cyclic Thermal Test No 14 v_{om} = 15 mm

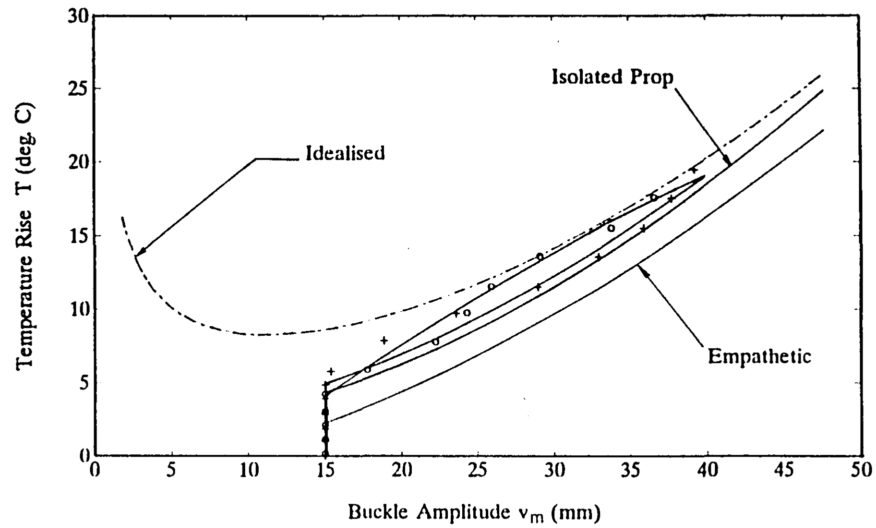

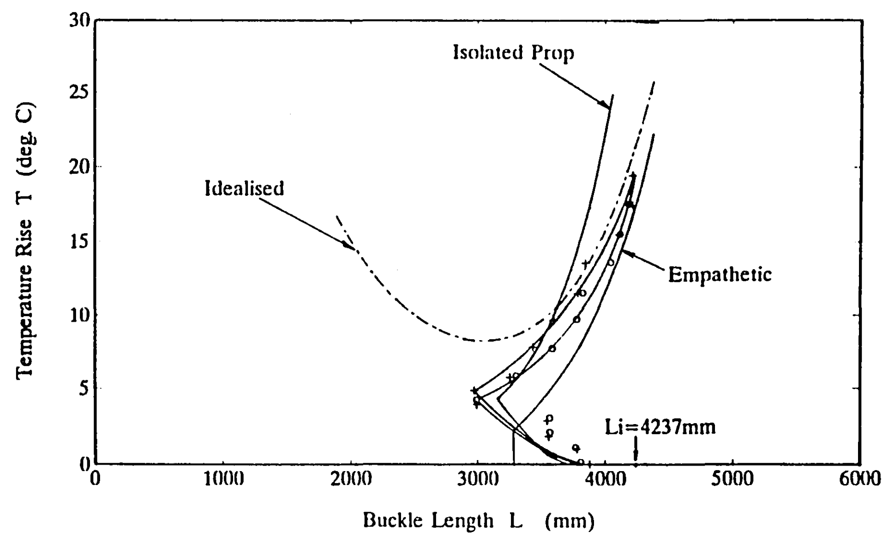

ISOLATED PROP (Stable) Cyclic Thermal Test No 15 v_{om} = 15 mm

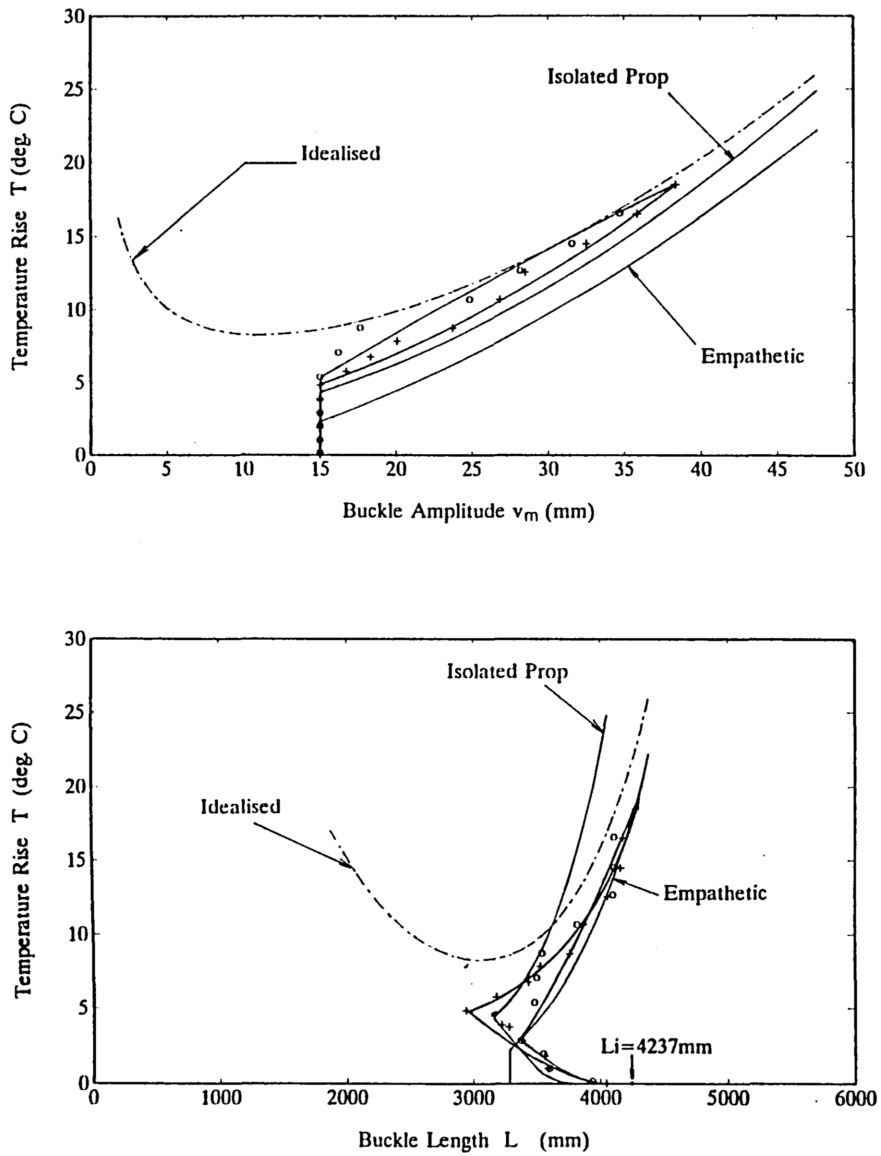

ISOLATED PROP (Stable) Cyclic Thermal Test No 16 v_{om} = 15 mm

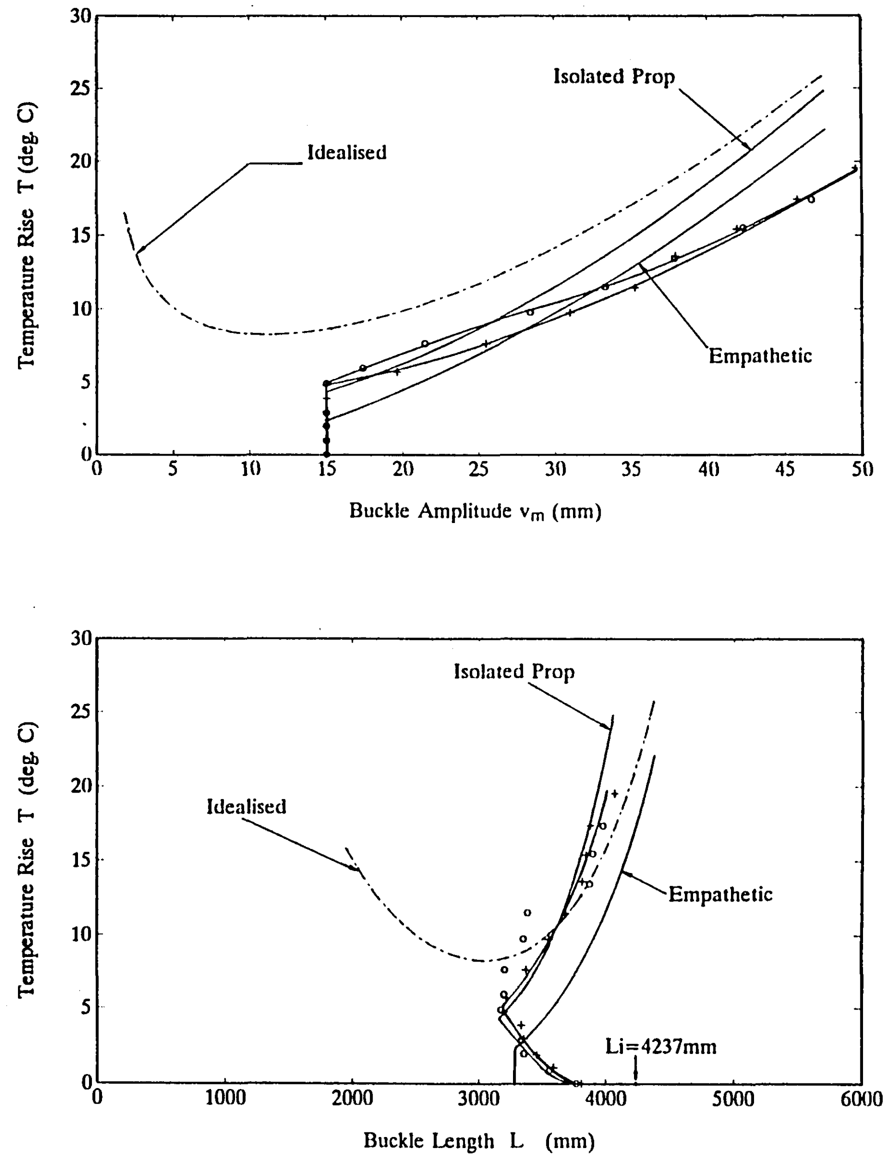

ISOLATED PROP (Stable) Cyclic Thermal Test No 17 v_{om} = 15 mm

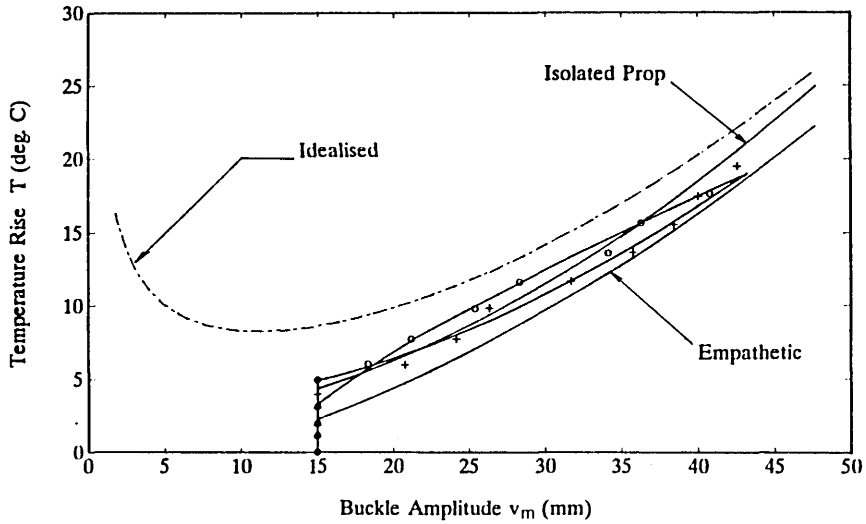

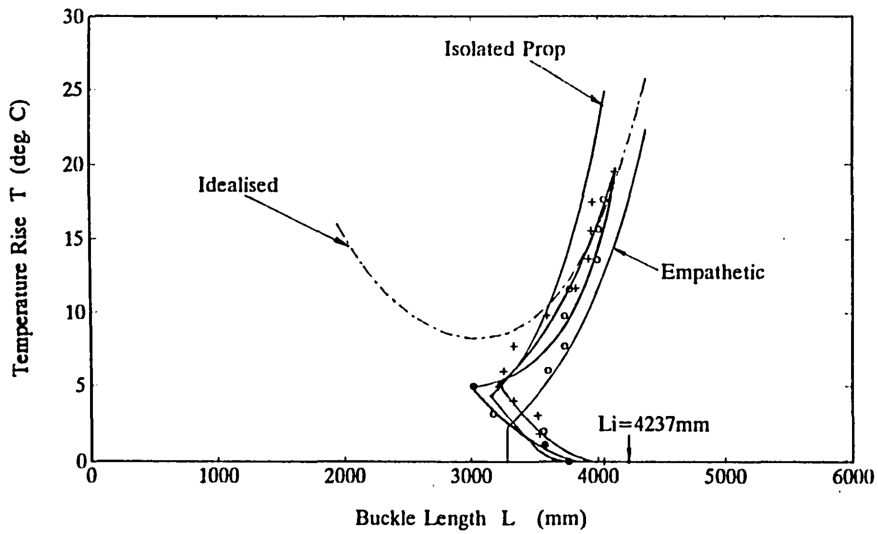

ISOLATED PROP (Stable) Cyclic Thermal Test No 18 v_{om} = 15 mm

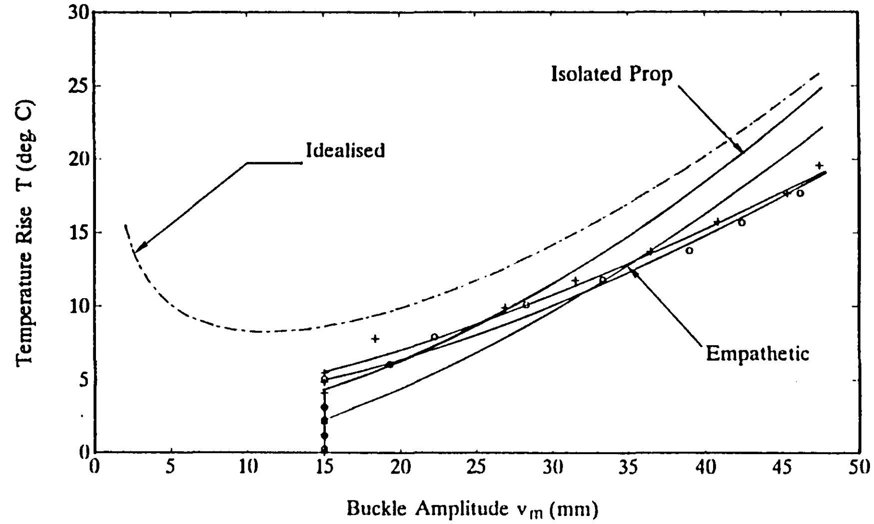

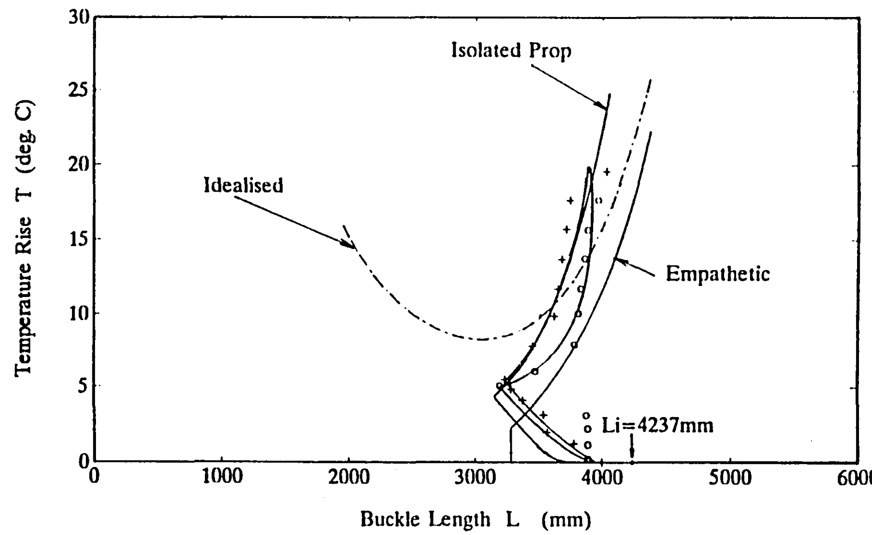

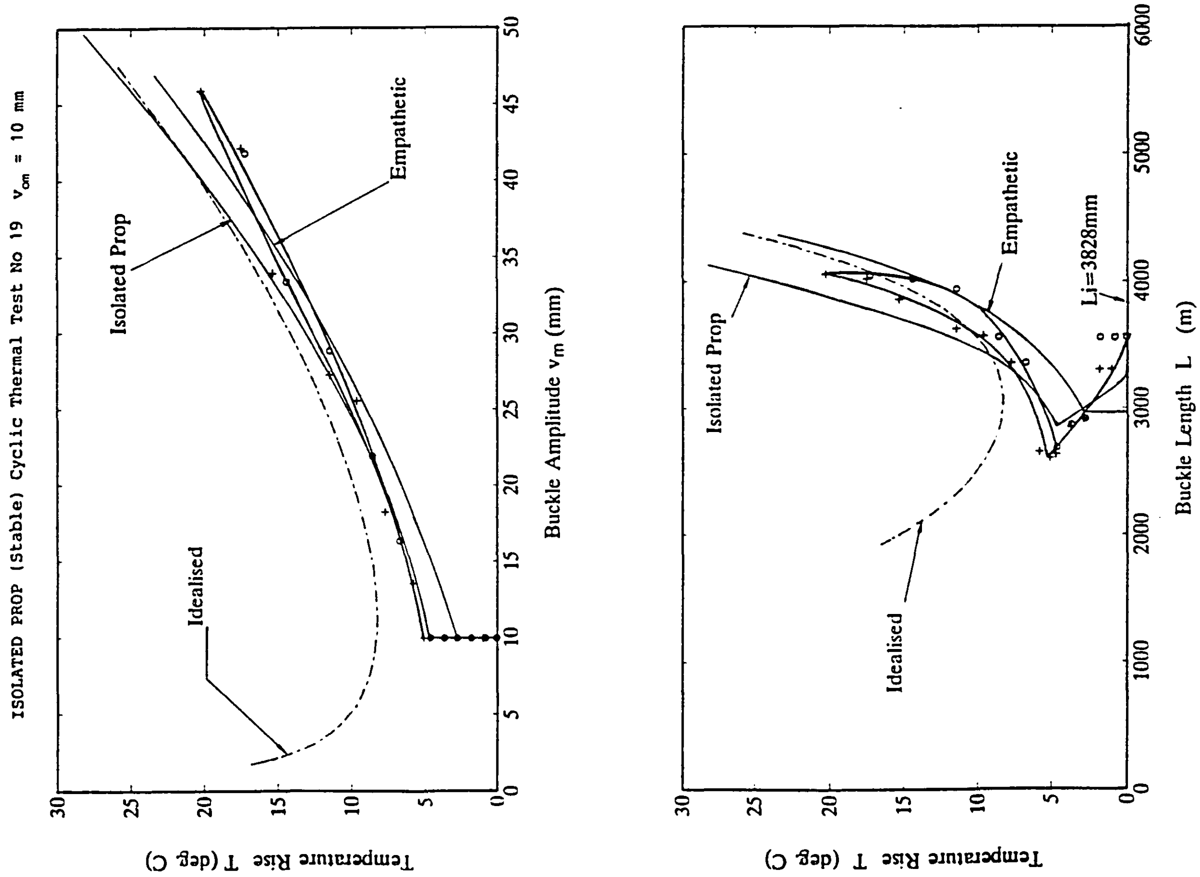

ISOLATED PROP (Stable) Cyclic Thermal Test No 19 v_{om} = 10 mm
Temperature Rise T (deg. C)
Buckle Amplitude v_m (mm)
Idealised
Isolated Prop
Empathetic
Temperature Rise T (deg. C)
Buckle Length L (m)
Isolated Prop
Empathetic
Idealised
Li=3828mm

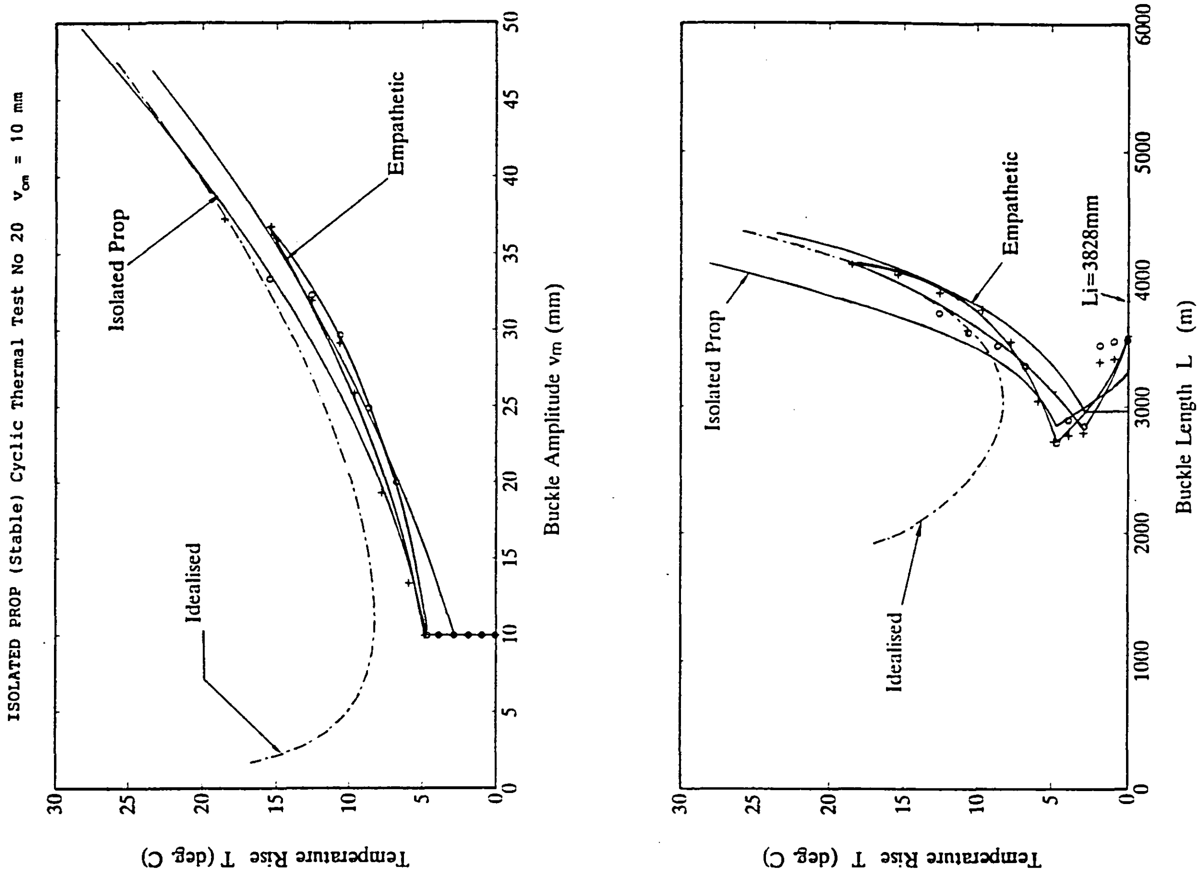

ISOLATED PROP (Stable) Cyclic Thermal Test No 20 v_{om} = 10 mm
Temperature Rise T (deg. C)
Buckle Amplitude v_m (mm)
Idealised
Isolated Prop
Empathetic
Temperature Rise T (deg. C)
Buckle Length L (m)
Isolated Prop
Empathetic
Idealised
Li=3828mm

ISOLATED PROP (Stable) Cyclic Thermal Test No 21 v_{om} = 10 mm

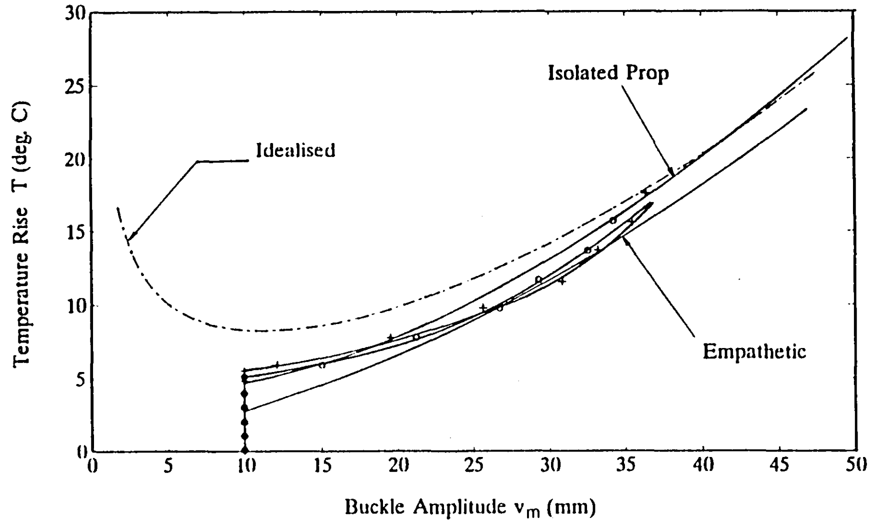

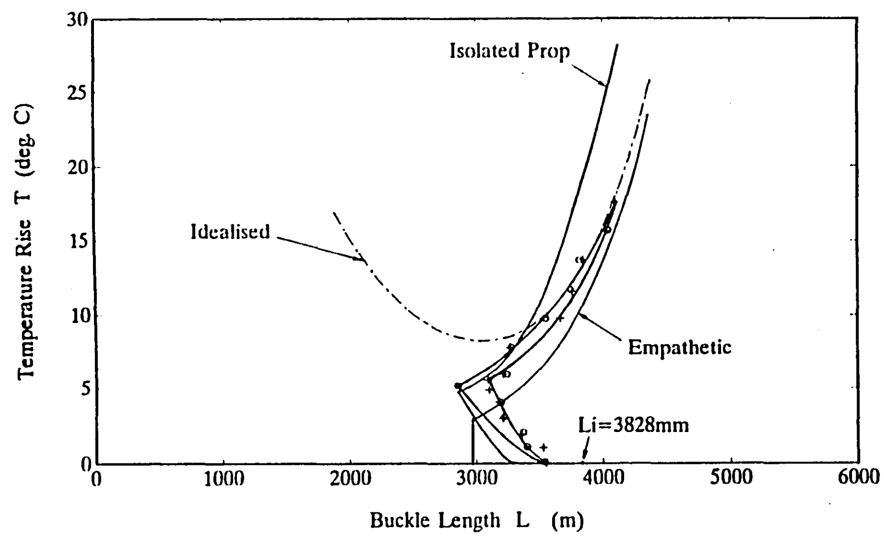

ISOLATED PROP (Stable) Cyclic Thermal Test No 22 v_{om} = 10 mm

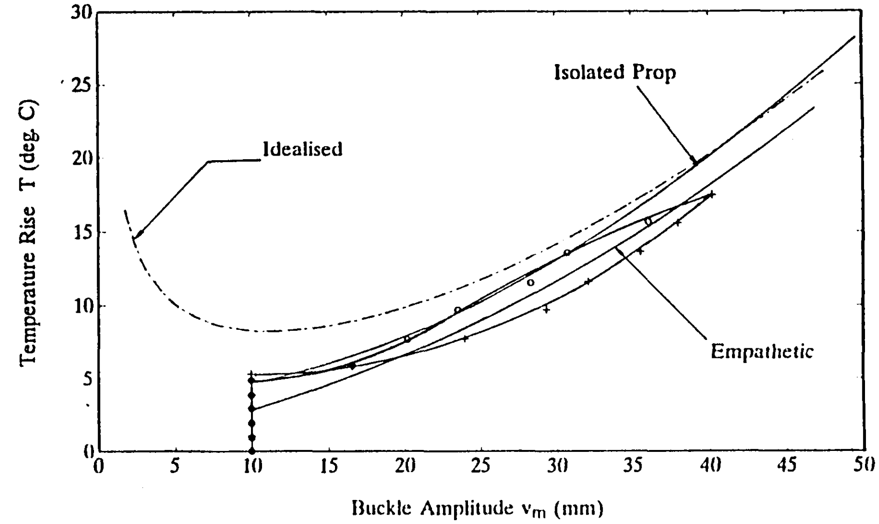

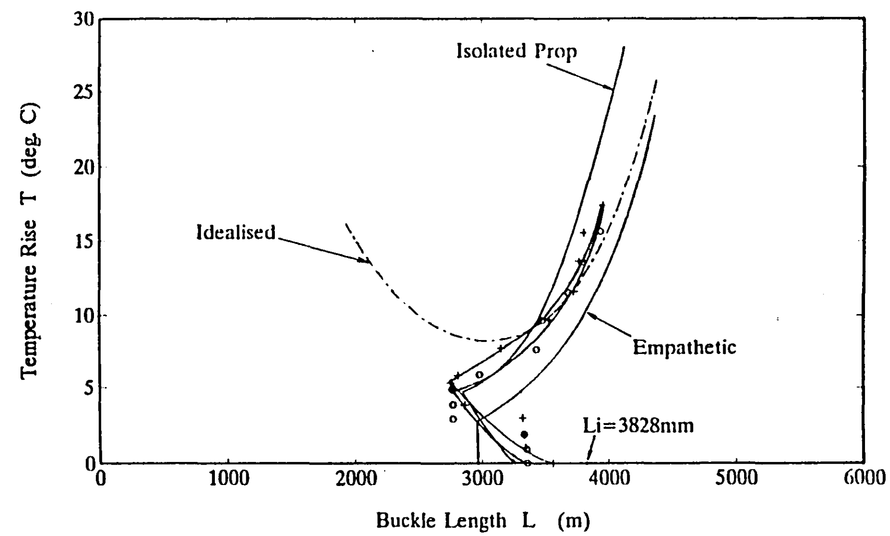

ISOLATED PROP (Stable) Cyclic Thermal Test No 23 v_{om} = 10 mm

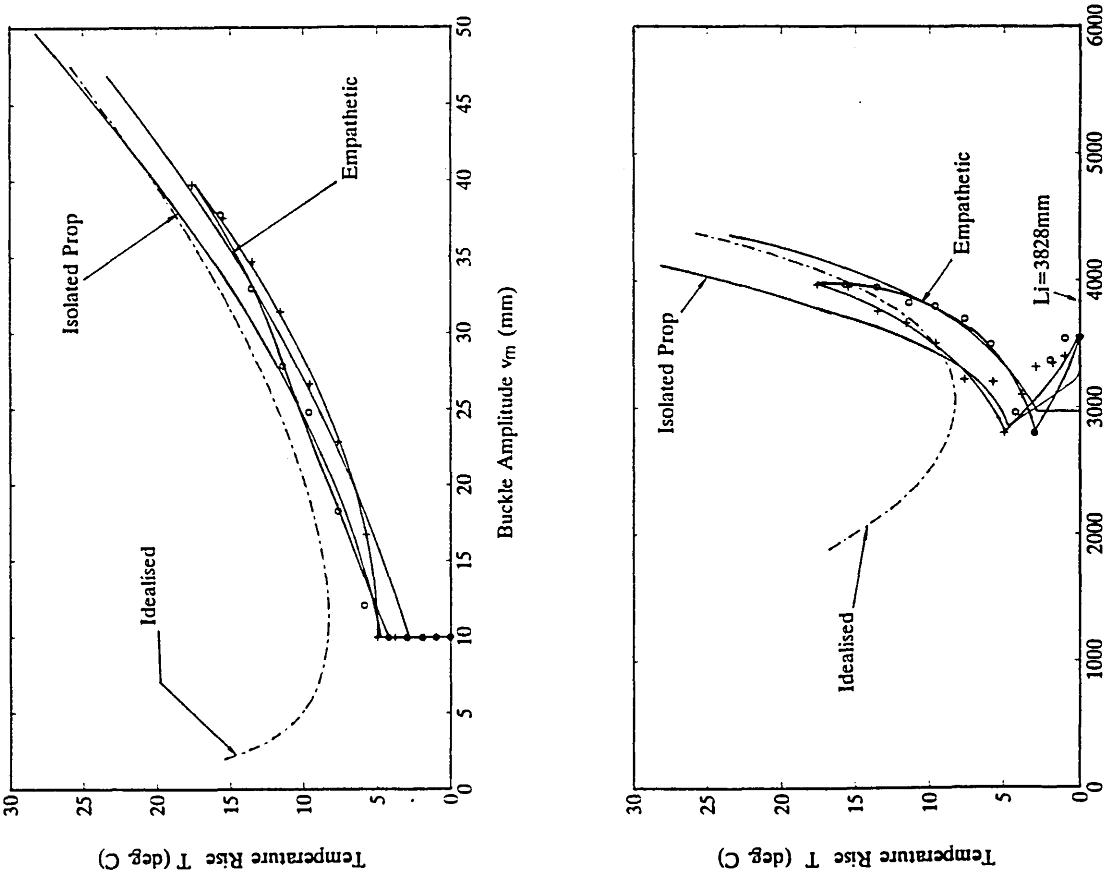

ISOLATED PROP (Stable) Cyclic Thermal Test No 24 v_{om} = 10 mm

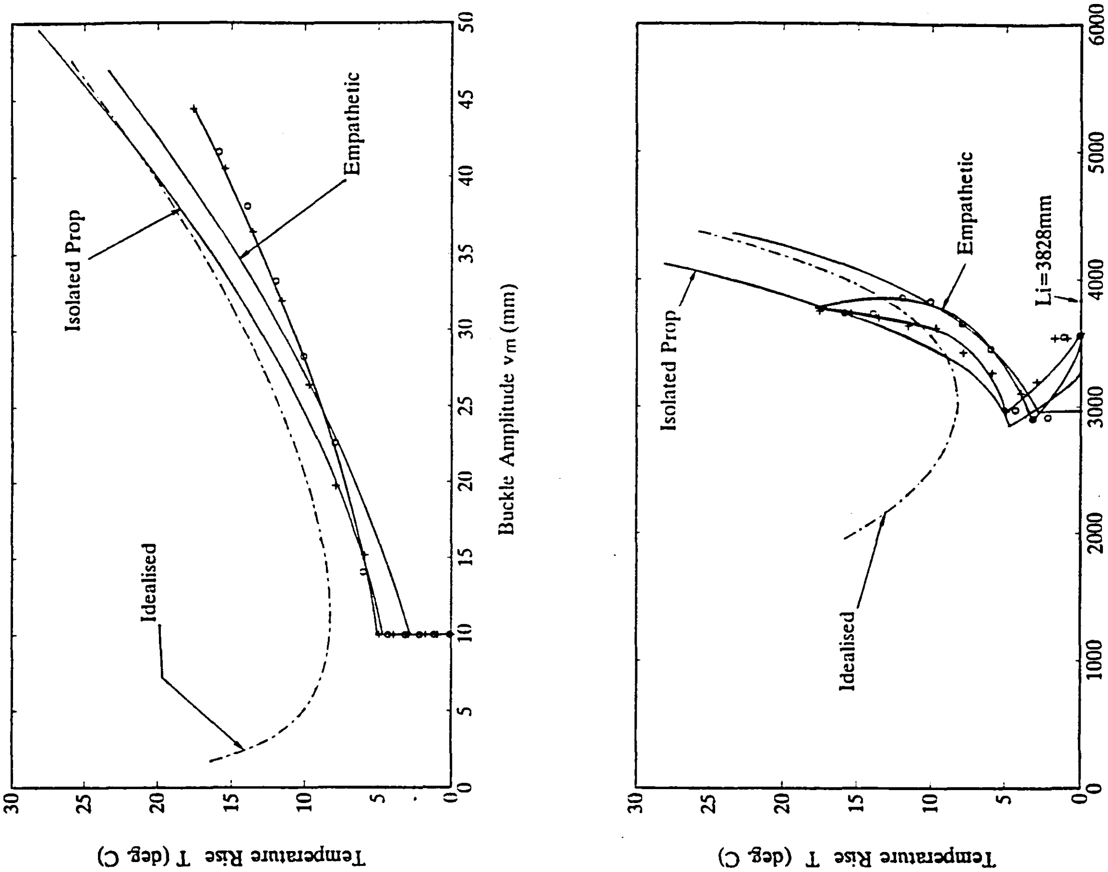

ISOLATED PROP (Snap) Heating Test No 25 v_{om} = 2 mm

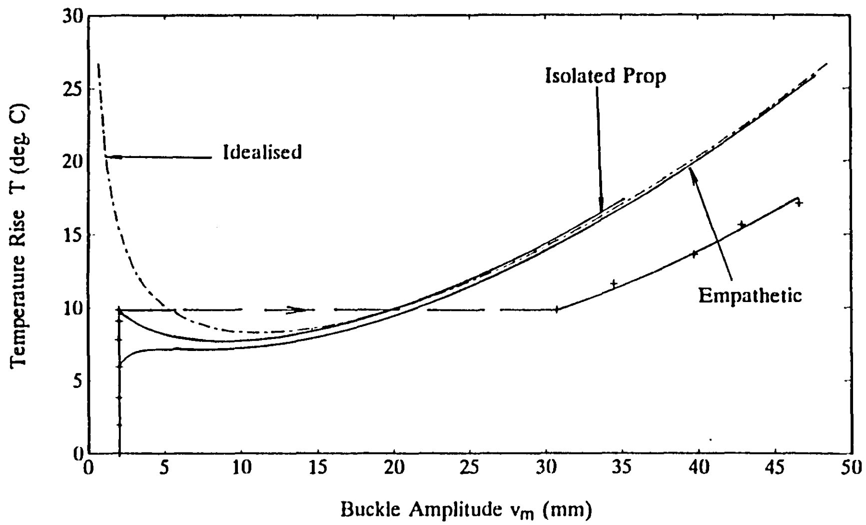

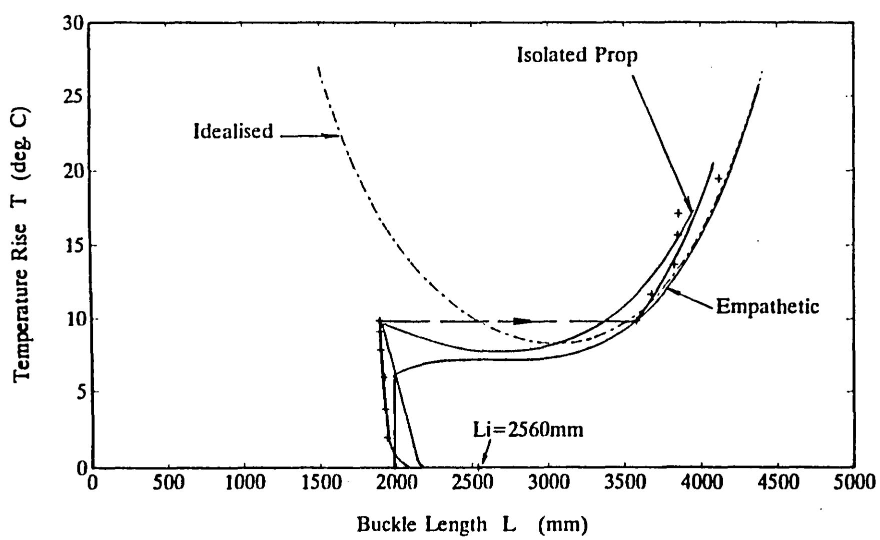

ISOLATED PROP (Snap) Heating Test No 26 v_{om} = 2 mm

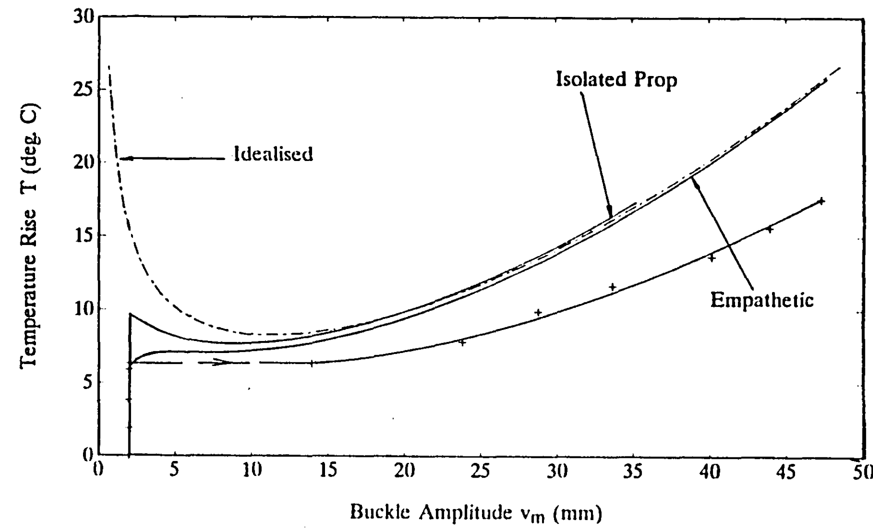

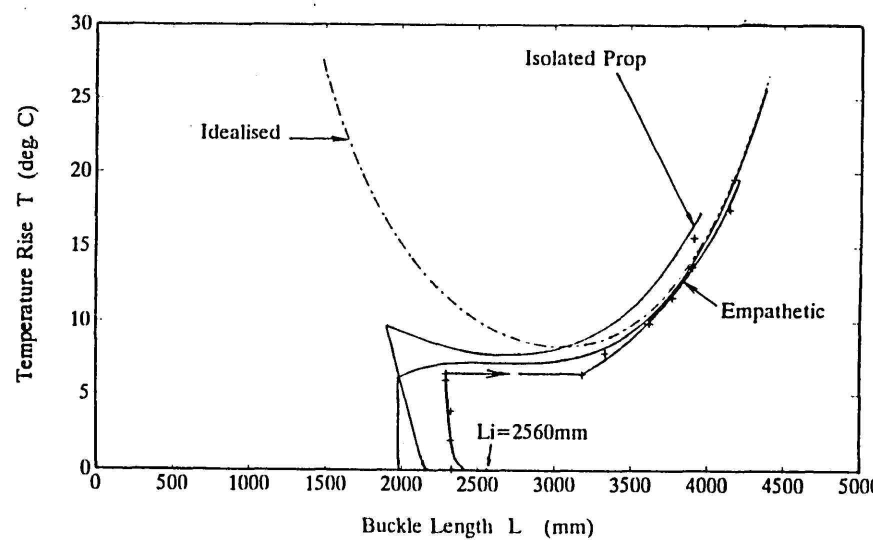

ISOLATED PROP (Snap) Heating Test No 27 v_{om} = 2 mm

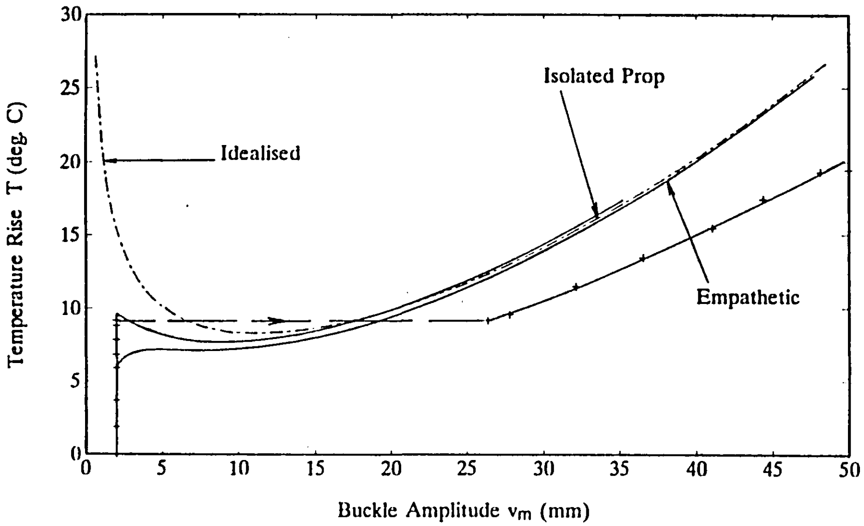

ISOLATED PROP (Snap) Heating Test No 28 v_{om} = 2 mm

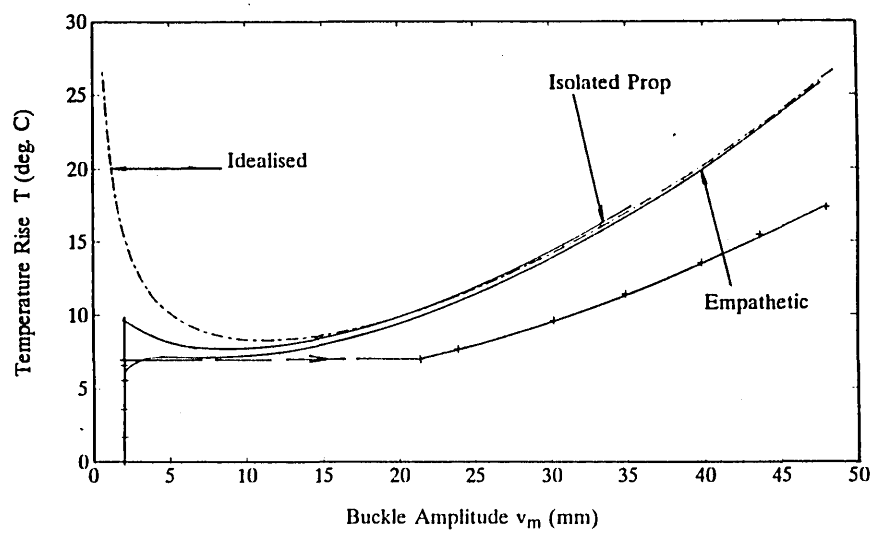

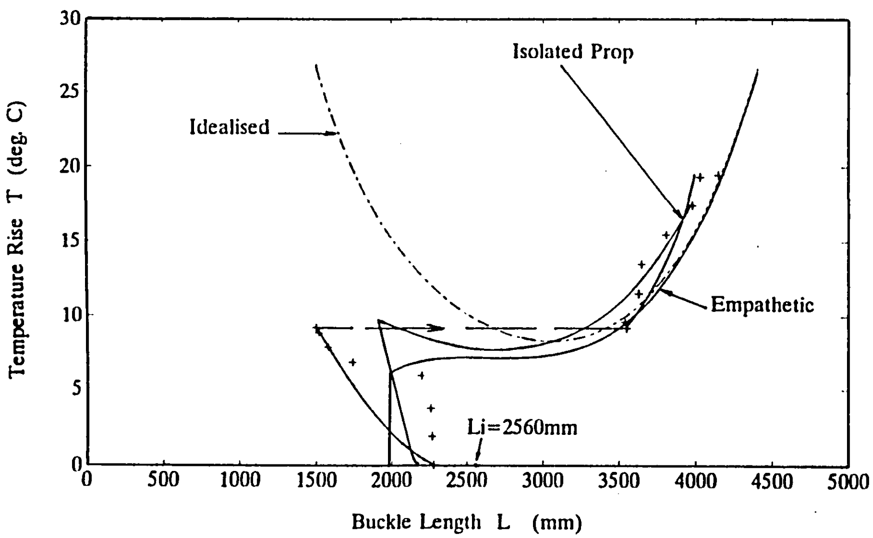

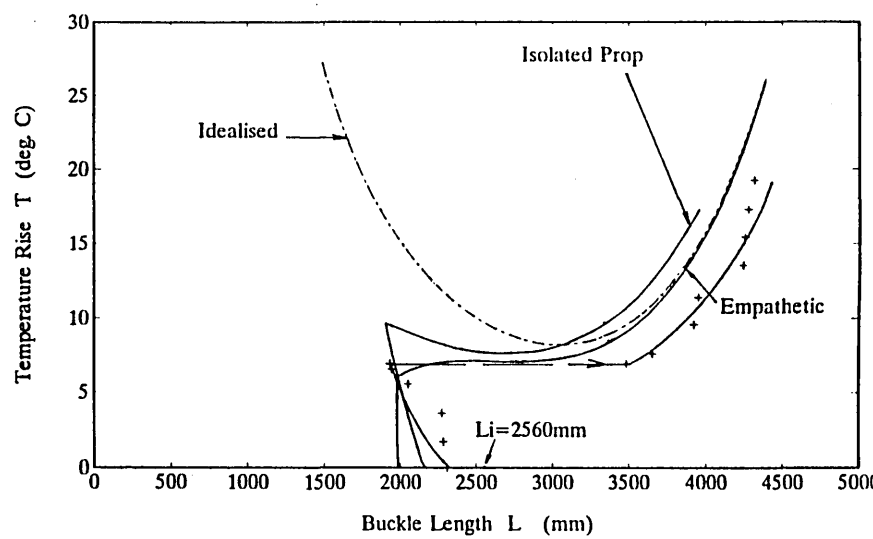

ISOLATED PROP (Snap) Heating Test No 29 v_{om} = 2 mm

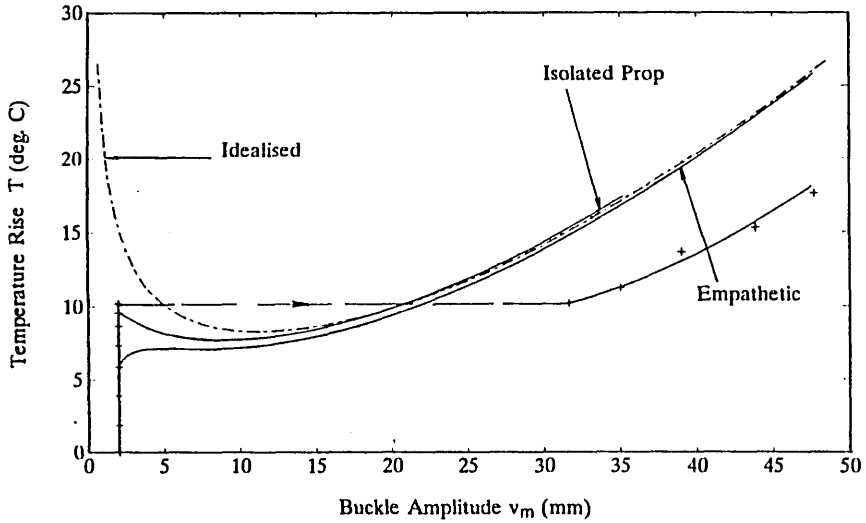

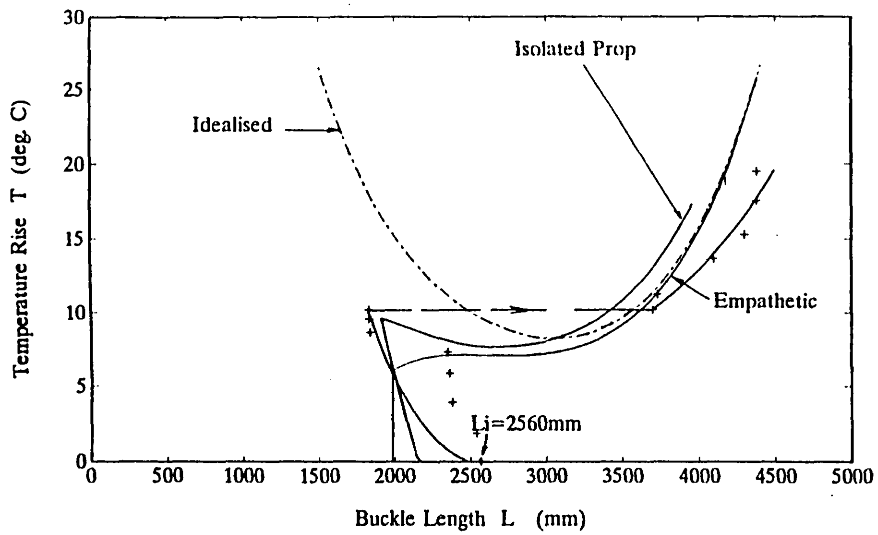

ISOLATED PROP (Snap) Heating Test No 30 v_{om} = 2 mm

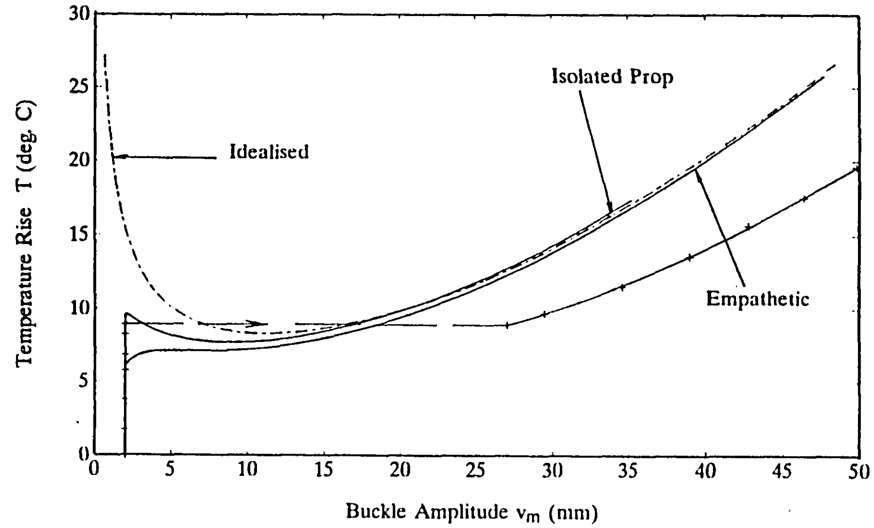

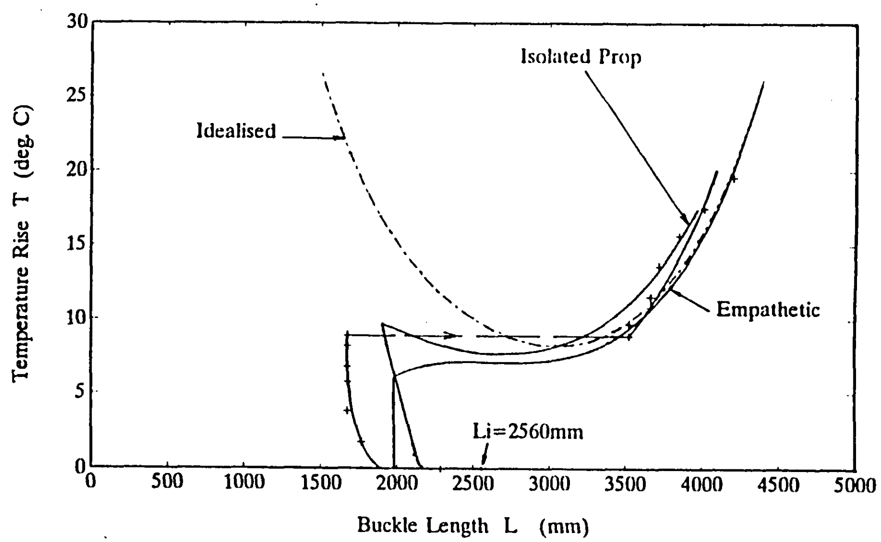

ISOLATED PROP (Snap) Heating Test No 31 v_{om} = 2 mm

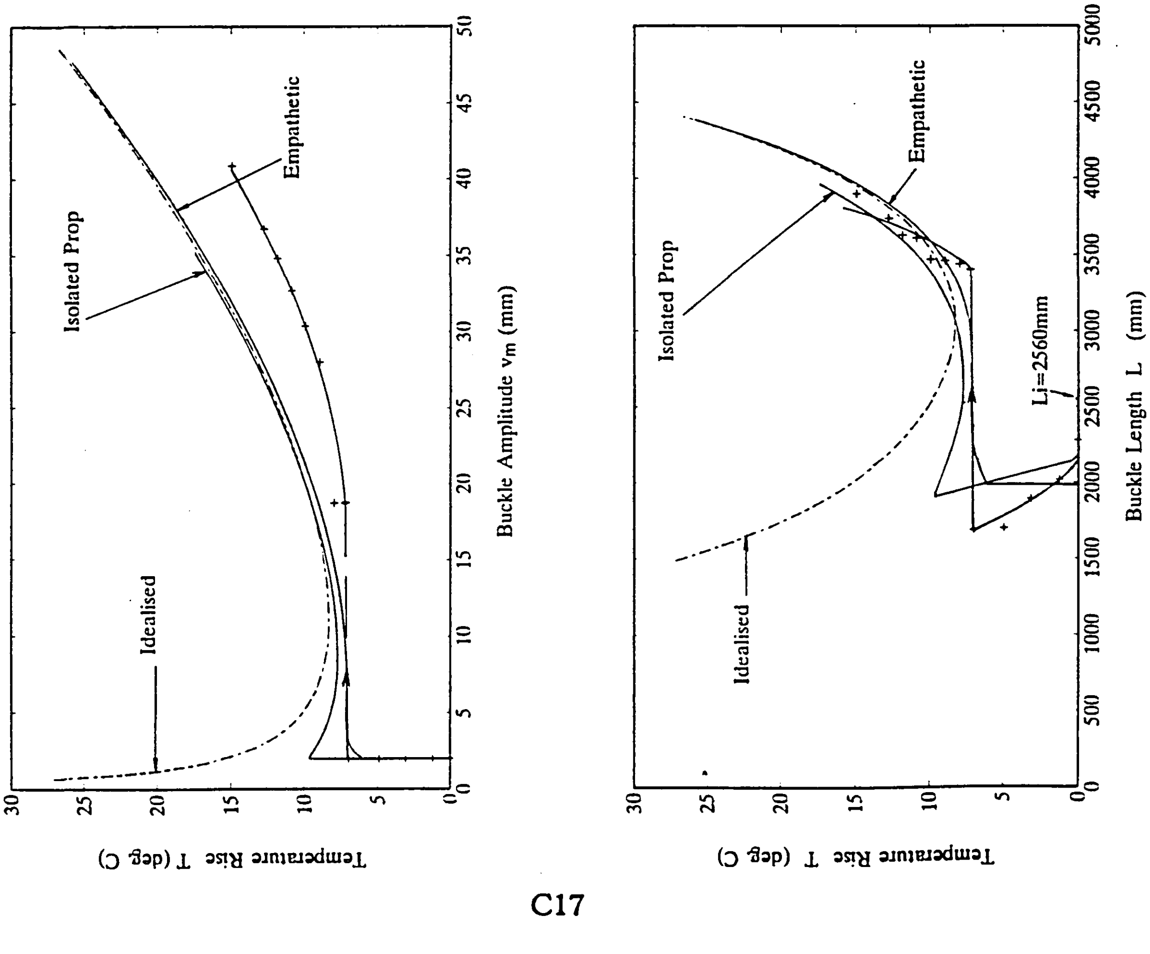

ISOLATED PROP (Snap) Heating Test No 32 v_{om} = 2 mm

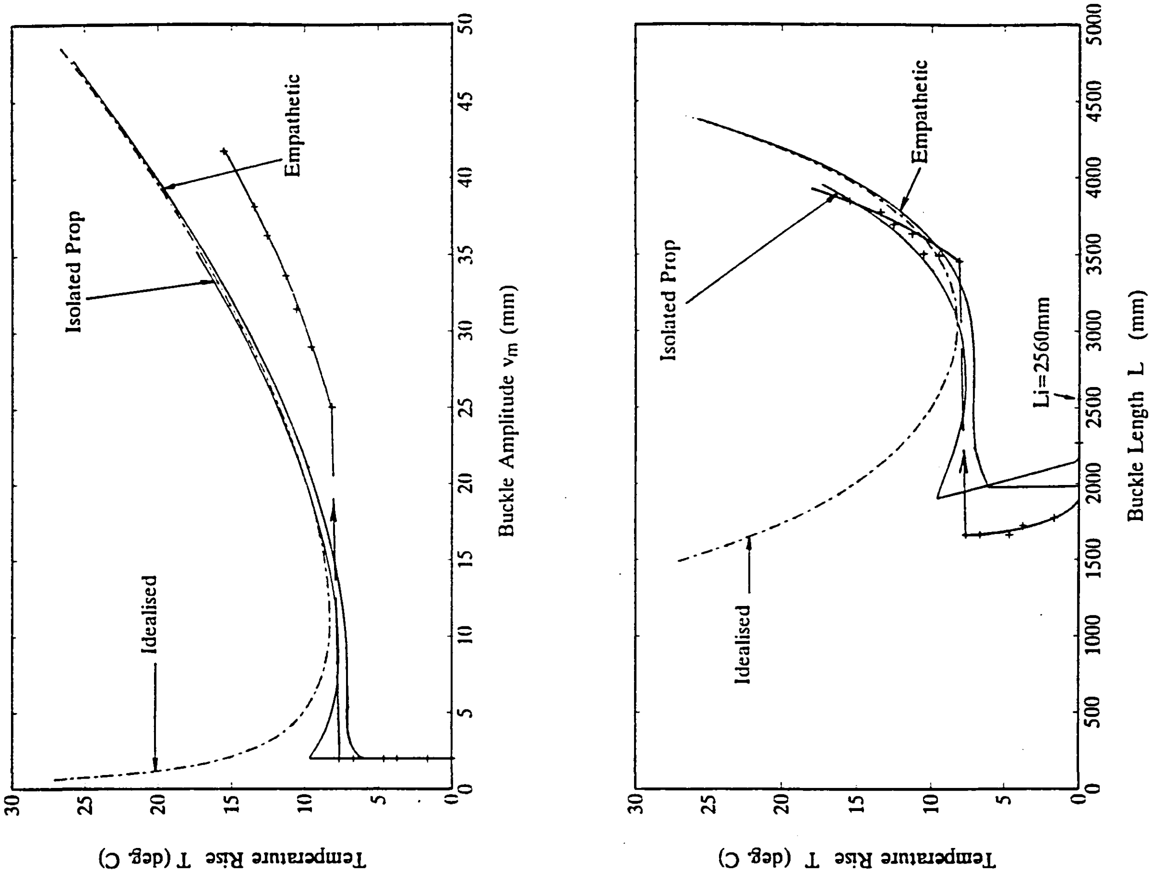

ISOLATED PROP (Snap) Heating Test No 33 v_{om} = 2 mm

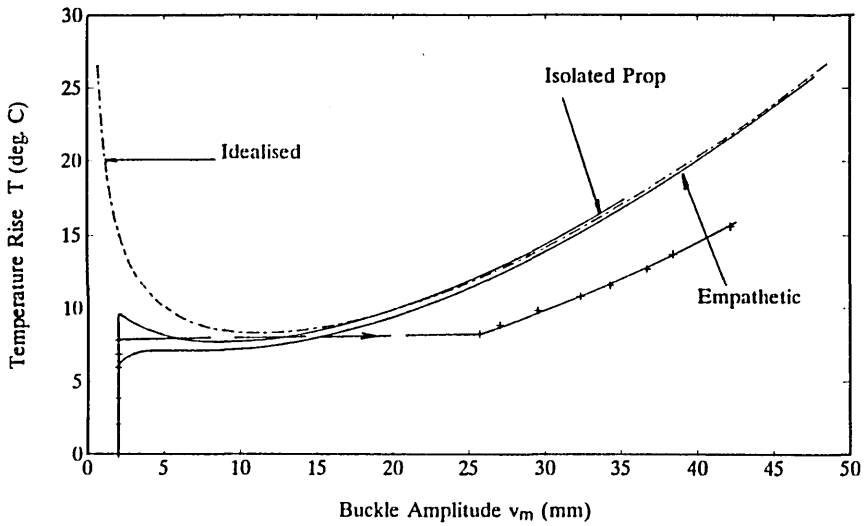

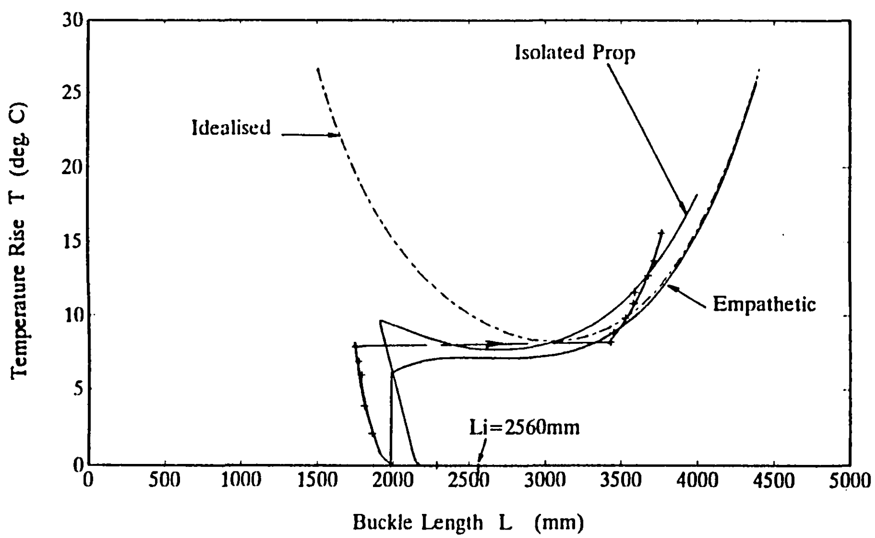

ISOLATED PROP (Snap) Cyclic Thermal Test No 34 v_{om} = 2 mm

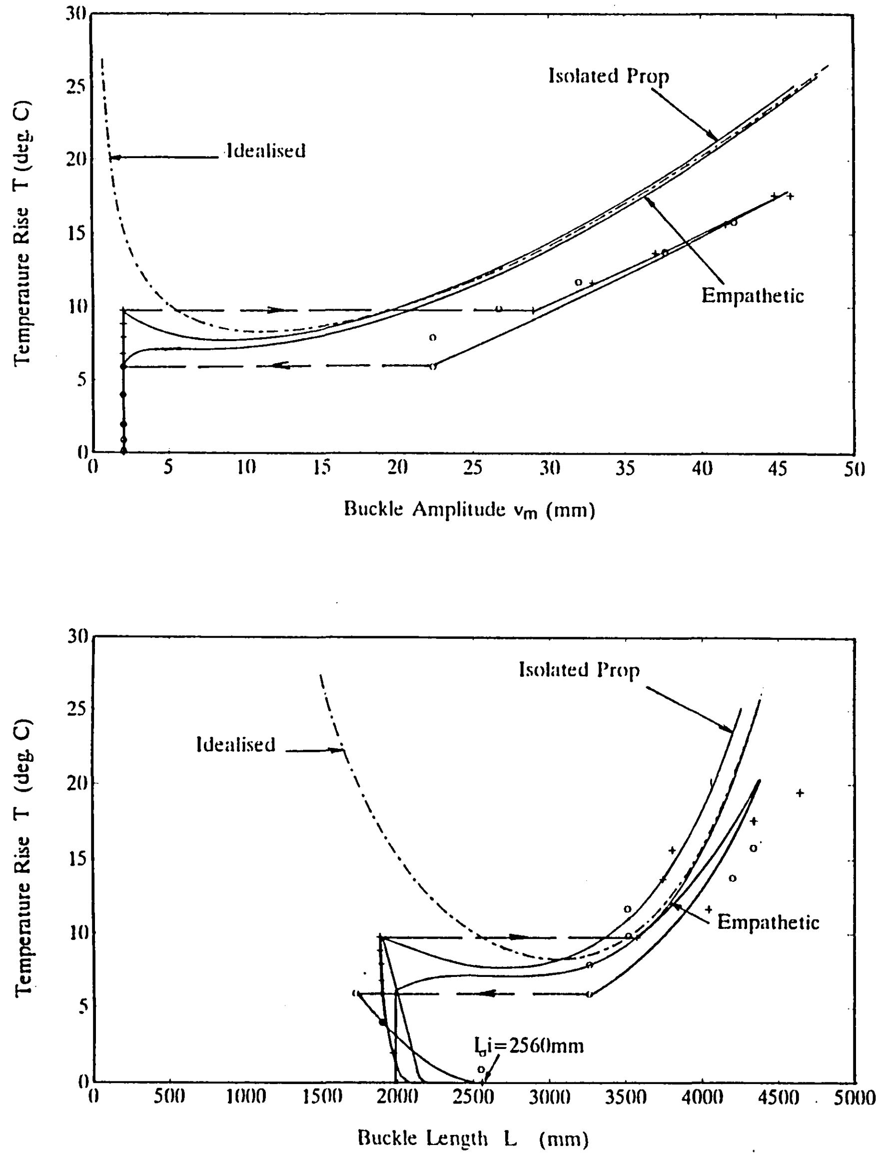

ISOLATED PROP (Snap) Cyclic Thermal Test No 35 v_{om} = 2 mm

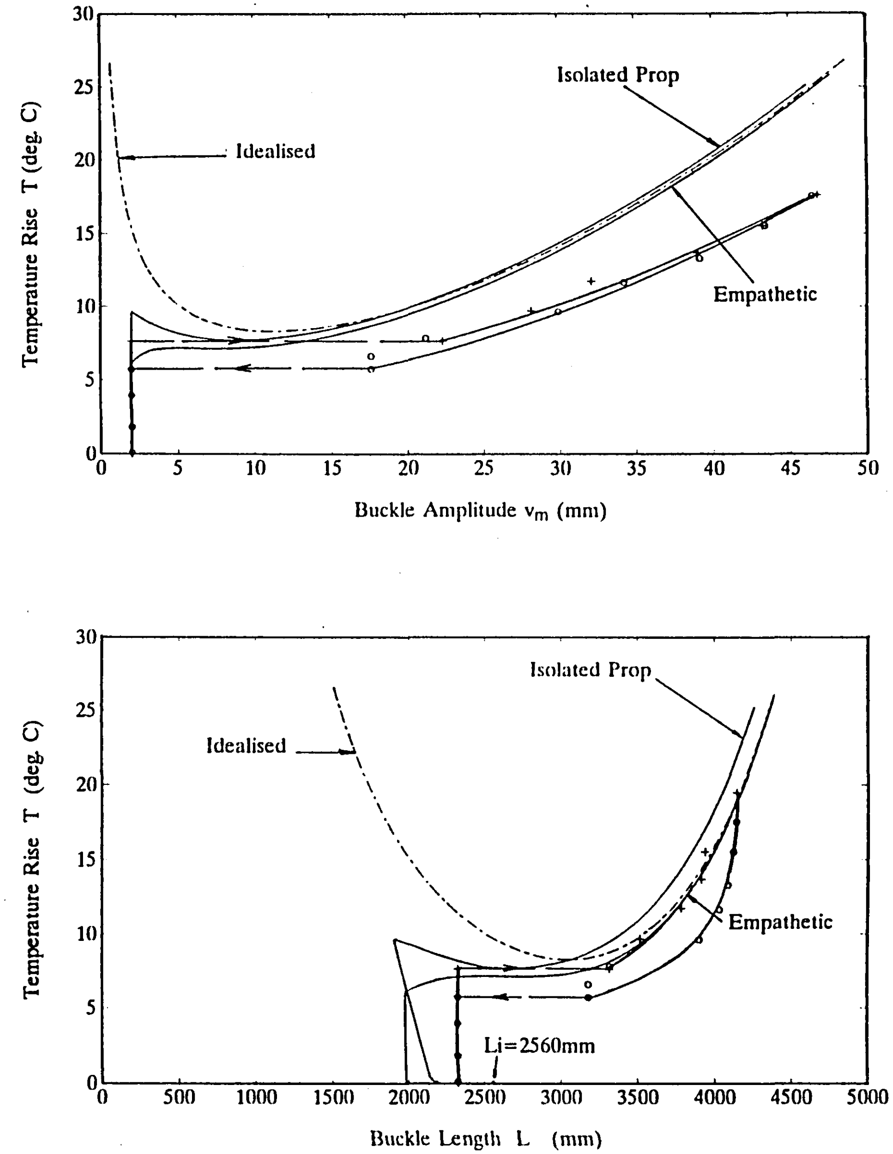

ISOLATED PROP (Snap) Cyclic Thermal Test No 36 v_{om} = 2 mm

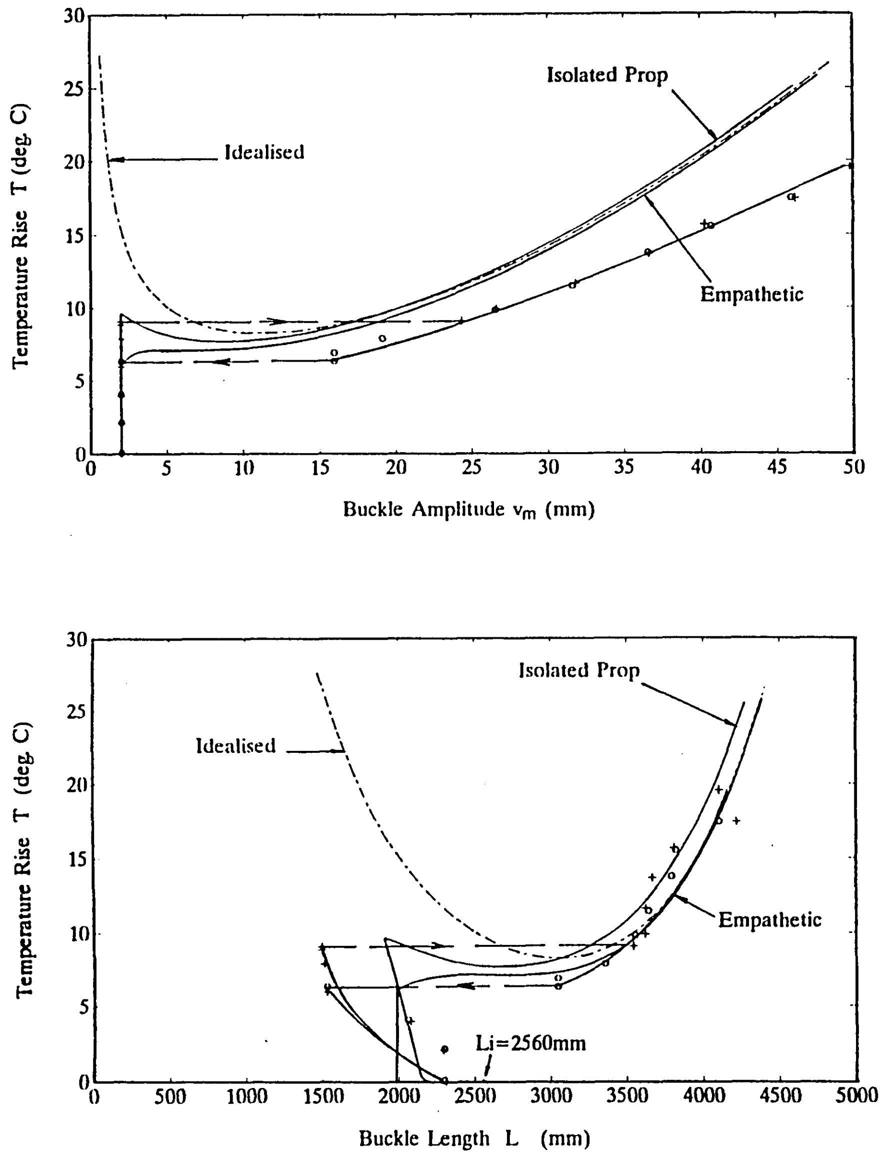

ISOLATED PROP (Snap) Cyclic Thermal Test No 37 v_{om} = 2 mm

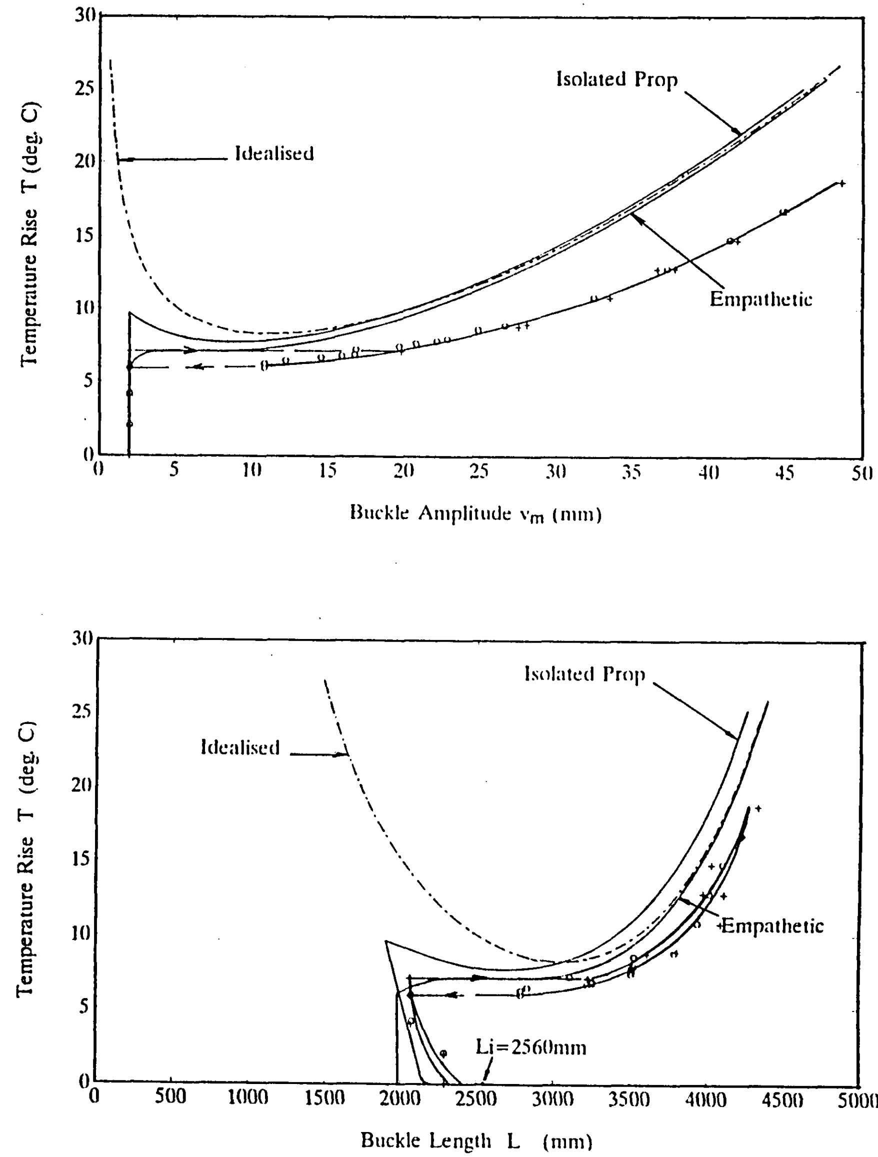

ISOLATED PROP (Snap) Cyclic Thermal Test No 38 v_{om} = 2 mm

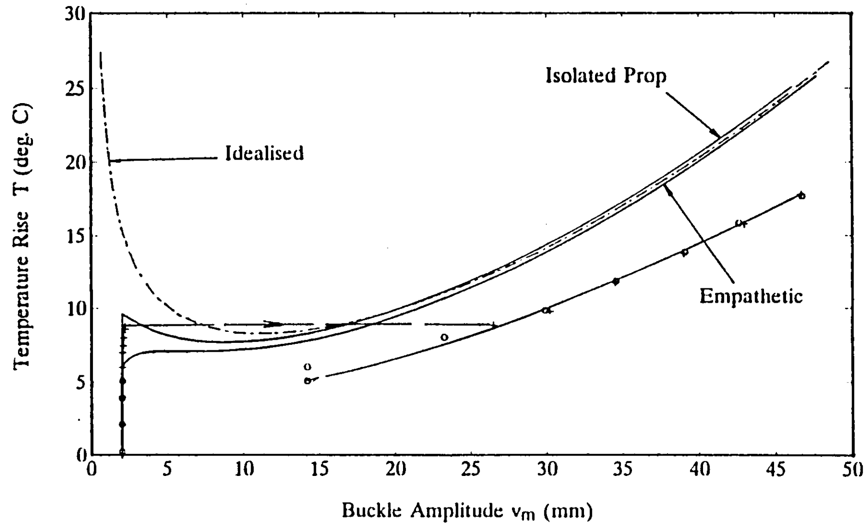

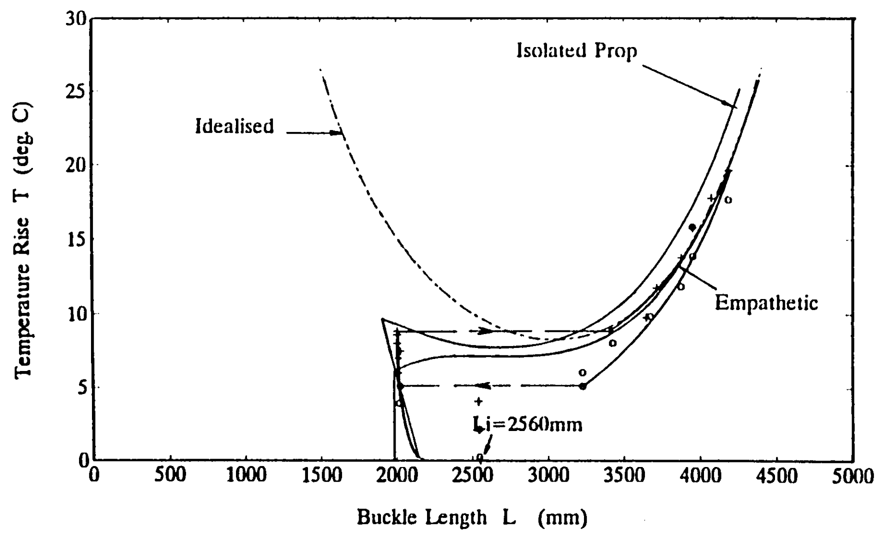

ISOLATED PROP (Snap) Cyclic Thermal Test No 39 v_{om} = 2 mm

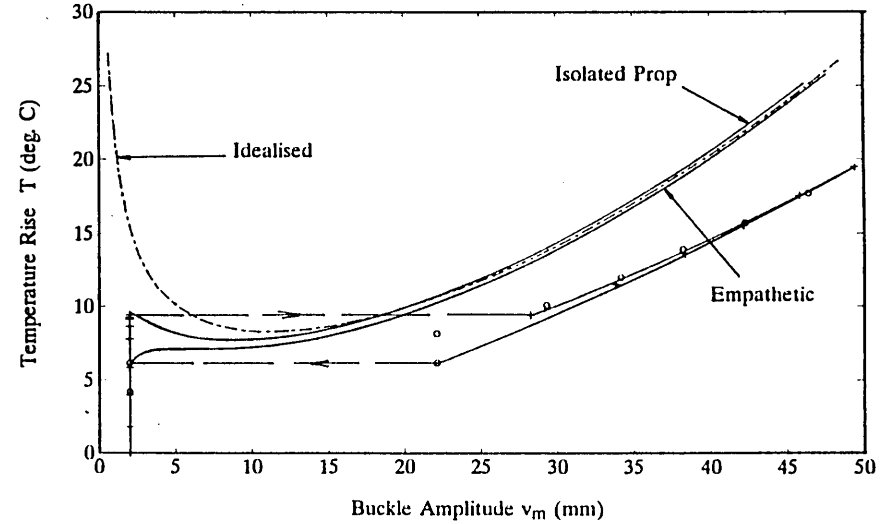

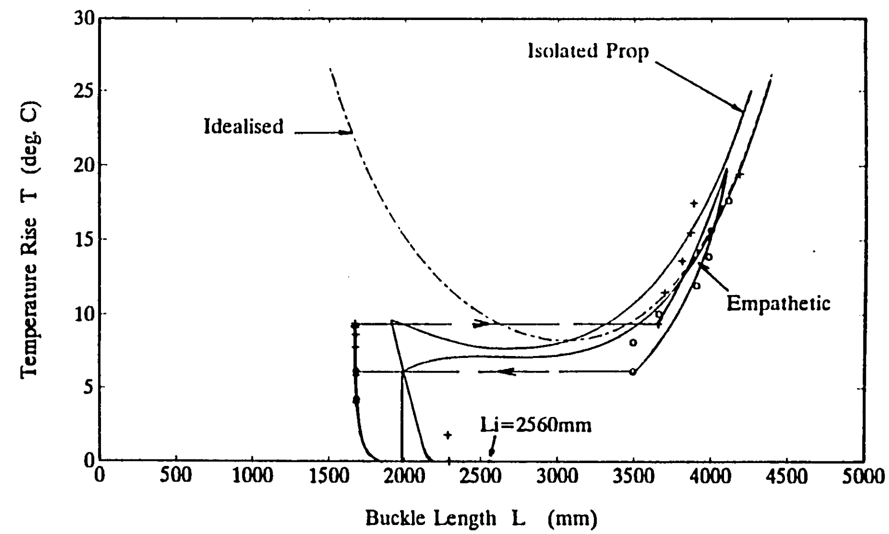

Infilled Prop (Stable) Heating Test No 40 vom = 30 mm

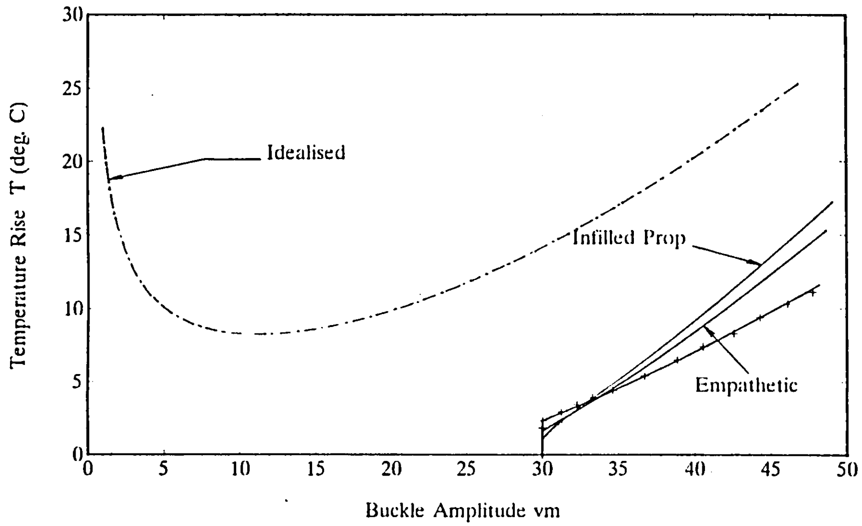

Infilled Prop (Stable) Heating Test No 41 vom = 30 mm

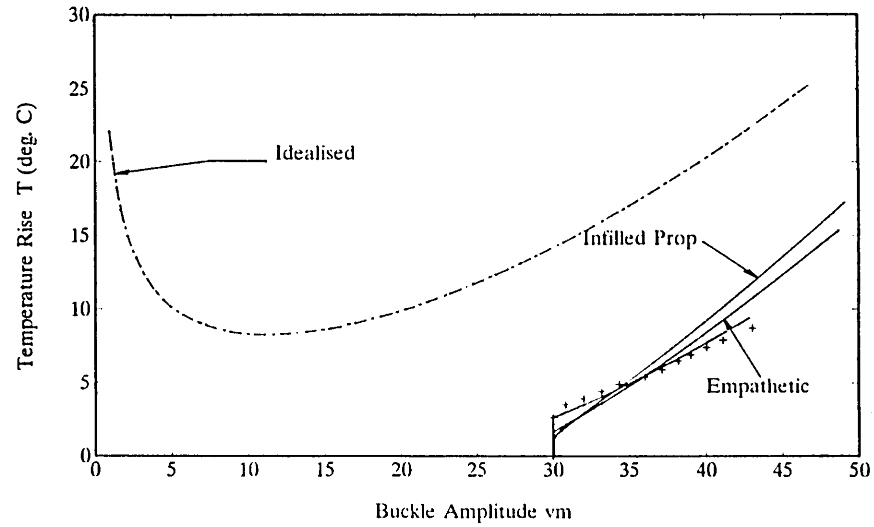

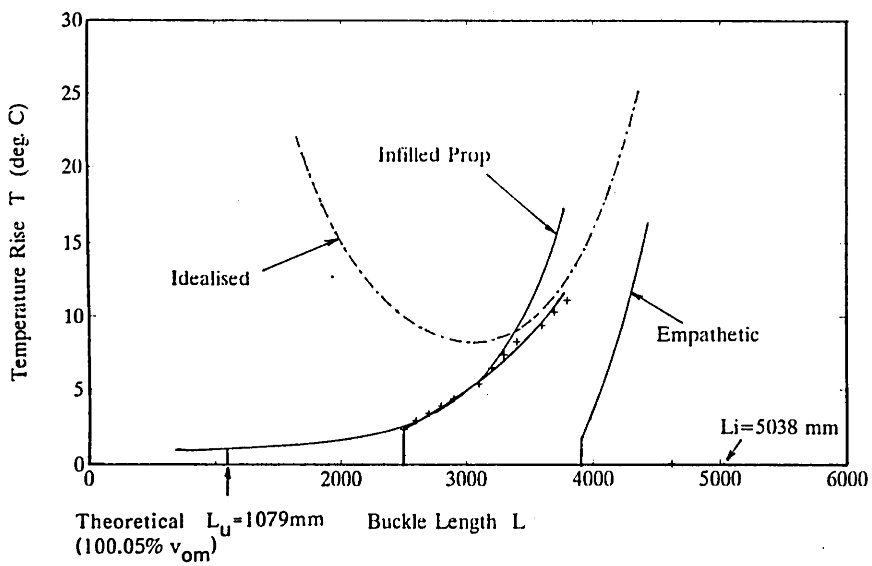

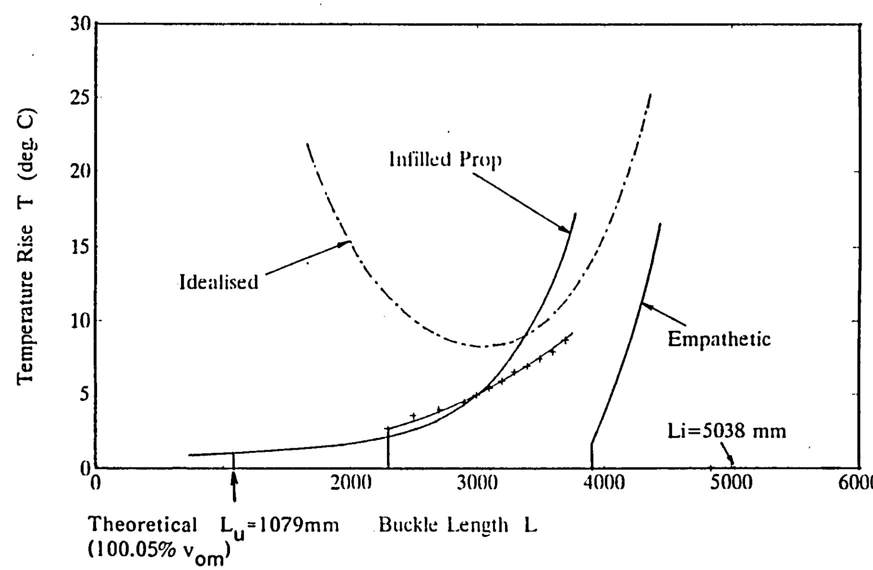

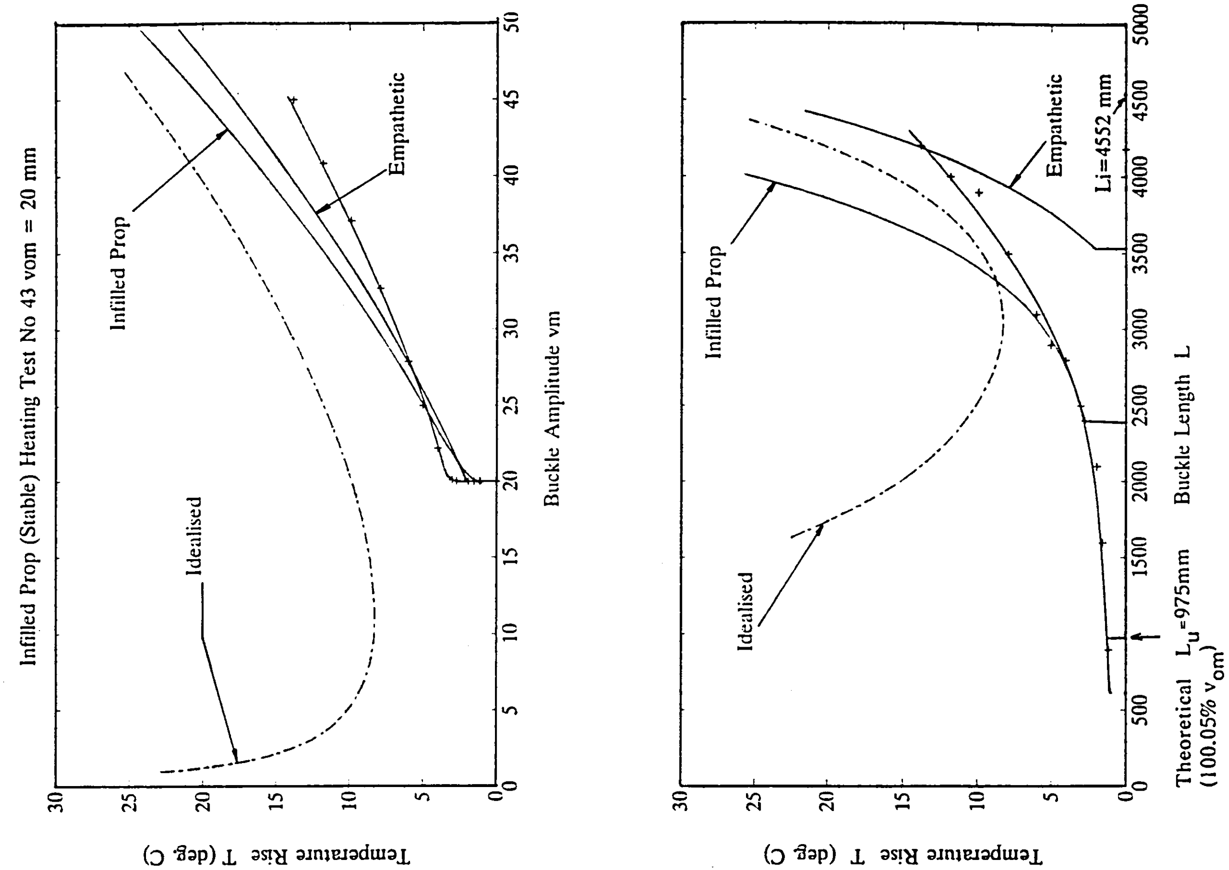

Infilled Prop (Stable) Heating Test No 43 vom = 20 mm
Temperature Rise T (deg. C)
Buckle Amplitude vm
Idealised
Infilled Prop
Empathetic
Temperature Rise T (deg. C)
Buckle Length L
Theoretical L_u=975mm
(100.05% v_{om})
Li=4552 mm

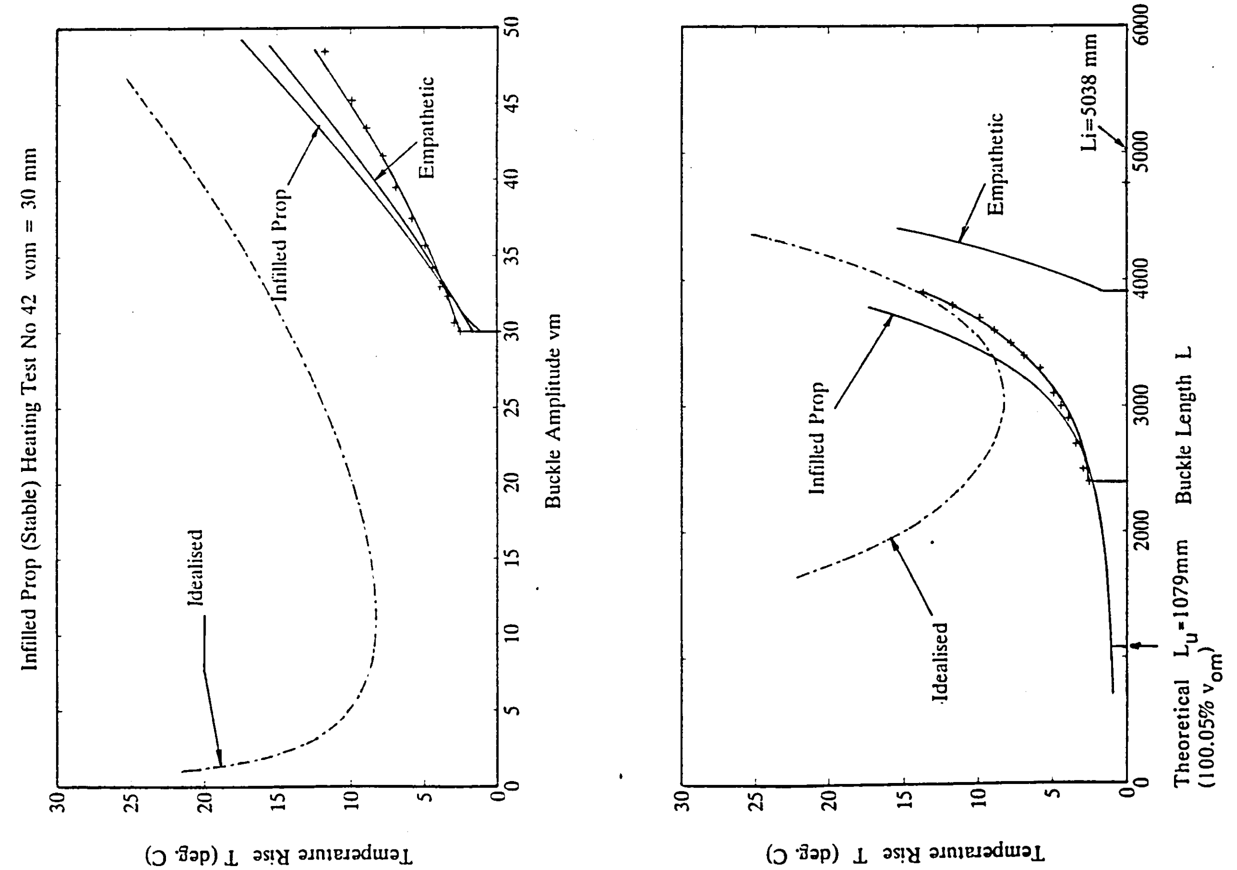

Infilled Prop (Stable) Heating Test No 42 vom = 30 mm
Temperature Rise T (deg. C)
Buckle Amplitude vm
Idealised
Infilled Prop
Empathetic
Temperature Rise T (deg. C)
Buckle Length L
Theoretical L_u=1079mm
(100.05% v_{om})
Li=5038 mm

Infilled Prop (Stable) Heating Test No 44 vom = 20 mm

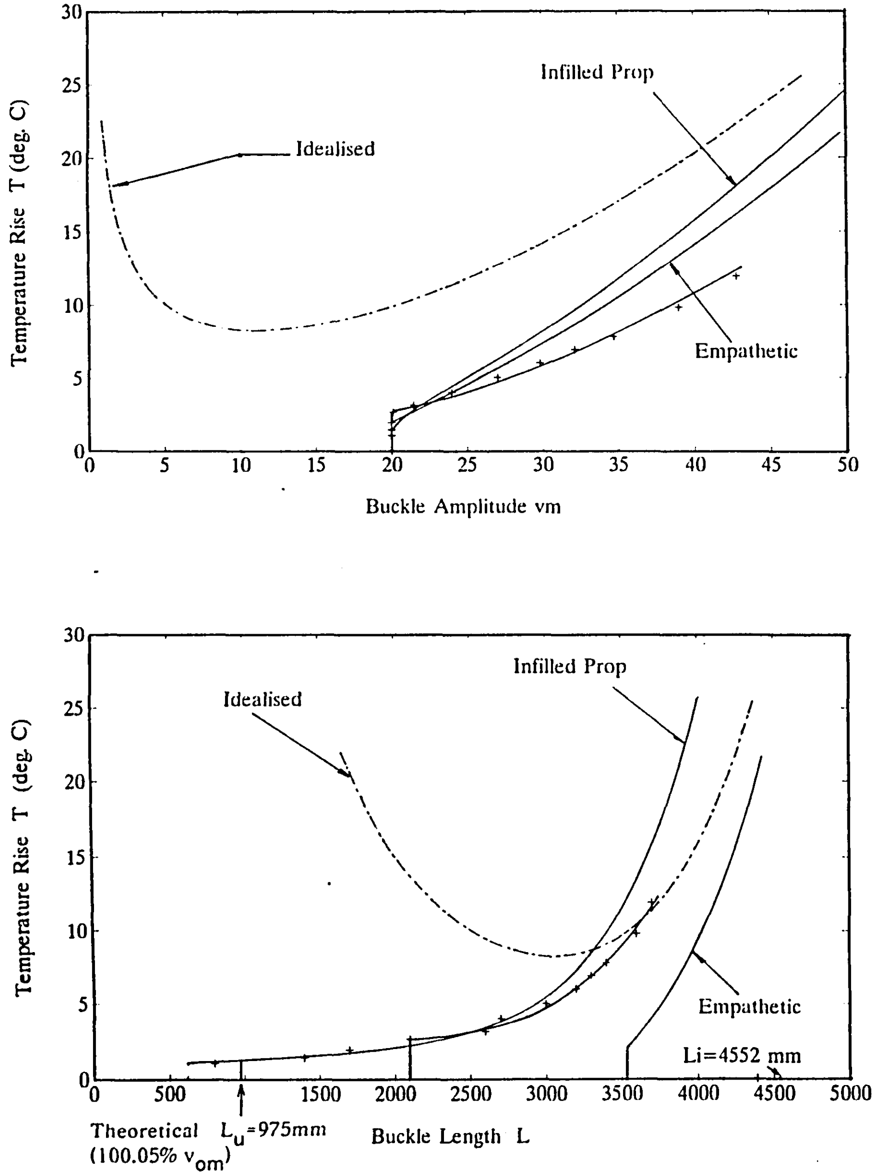

Infilled Prop (Stable) Heating Test No 45 vom = 20 mm

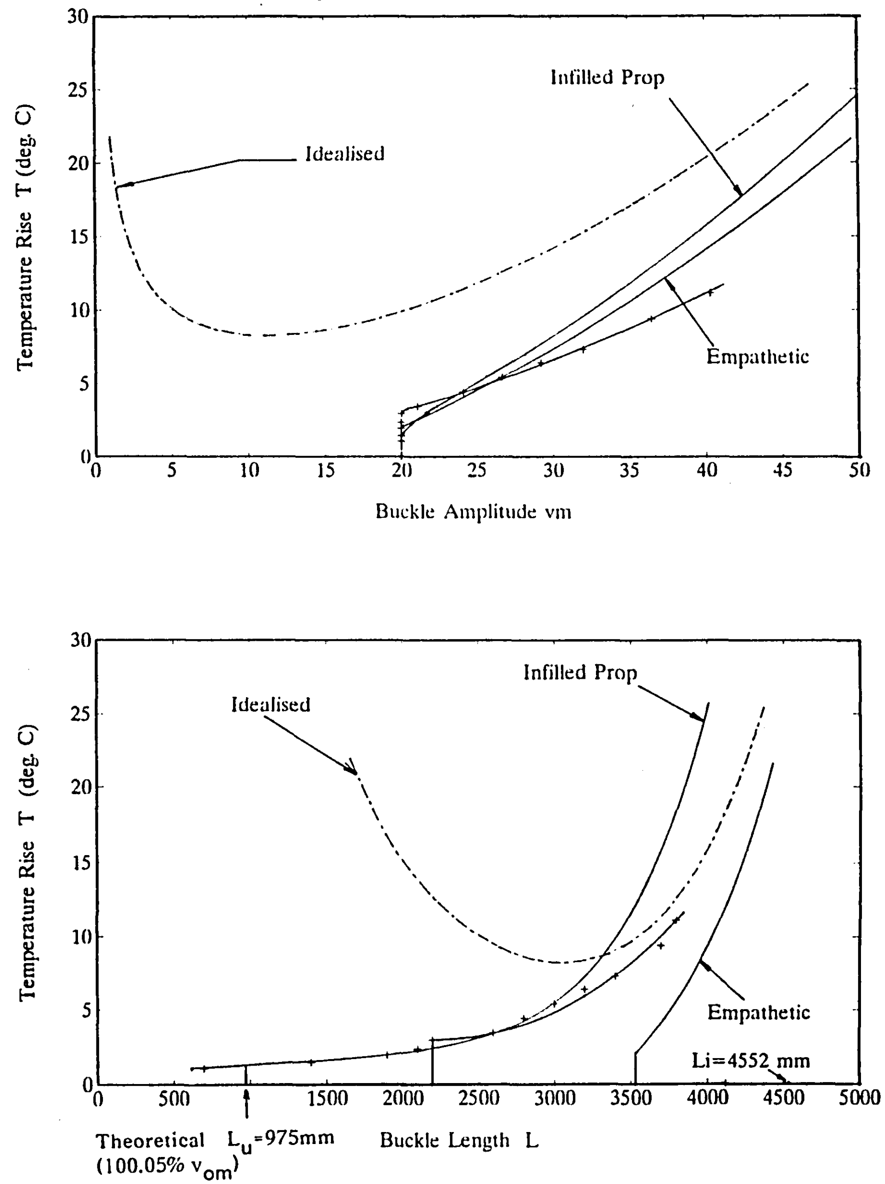

Appendix D

PUBLICATIONS

Interface Modelling for Upheaval Subsea Pipeline Buckling

Neil Taylor, Vinh Tran and Donald Richardson
School of Construction, Sheffield Polytechnic, UK

ABSTRACT

An important aspect of subsea pipeline design relates to the possible incursion of structural buckling during routine operation. Buried pipelines are susceptible to vertical mode 'upheaval' buckling and herein presented is experimental data appertaining to the resistance to movement provided by the supporting medium. Data from a set of thirty-six small scale pull-out and axial friction tests is assessed in the context of upheaval subsea pipeline buckling, comparisons being made with established seabed-mounted pipeline buckling models as appropriate.

INTRODUCTION

In-service buckling of subsea pipelines can occur due to the institution of axial compressive forces caused by the constrained thermal and pressure actions. With oil and gas temperatures up to 100°C above that of the water environment and operating pressures over $10N/mm^2$, these forces can be substantial given the ability of the pipeline/seabed interface to generate the necessary frictional resistance to axial movement. Resistance can be enhanced by burial within the seabed, and knowledge of the respective inertial - ie submerged self-weight plus cover/fill surcharge - and friction forces is crucial for design practice.

Studies into in-service subsea pipeline buckling, with particular respect to seabed-mounted topologies, have been extant since 1981 - see Hobbs[1,2], Taylor and Gan[3-7], Boer et al[8] and Friedmann[9] - and major industrially-sponsored research programmes are currently underway. Primary interest presently lies with the vertical or 'pop-up' buckling mode following the more recent exploitation of marginal fields and the concomitant employment of small-bore ($\leq$300mm OD) pipelines; offshore standards demand that these be trenched or buried within the sea-bed. These pipelines must be designed against the respective upheaval buckling and, whilst inertial and friction force data appertaining to seabed-mounted pipelines can be claimed to be reasonably well-established, that for buried pipelines is of very restricted form. Boer[8] and Traumann et al [10] consider the inertial forces in terms of geotechnical pull-out characteristics whilst Pedersen[11,12] additionally refers to the buried fully mobilised axial friction coefficient ϕ_A.

Herein presented are the findings of a recently completed experimental programme, undertaken as part of an on-going subsea pipeline stability research project, concerned with the geotechnical/structural interface aspects of upheaval subsea pipeline buckling. Pipe elements were subjected to pull-out and axial friction tests corresponding to a variety of burial topologies. Correlation of the data trends established with the restricted geotechnical data presently available is made and incorporation of this data within semi-empirical pipeline buckling design formulae discussed. Initially, a brief overview of the physical problem concerned is given.

SUBSEA PIPELINE BUCKLING

The key features of a buckled subsea pipeline are illustrated with respect to vertical mode buckling in Figure 1. Ideally, the pipeline is taken to be initially straight with vertical displacement v, possessing amplitude v_m, being null under the action of effective inertial loading q per unit length (ie submerged self-weight if seabed-mounted) and fully restrained pre-buckling axial compression force P_o.

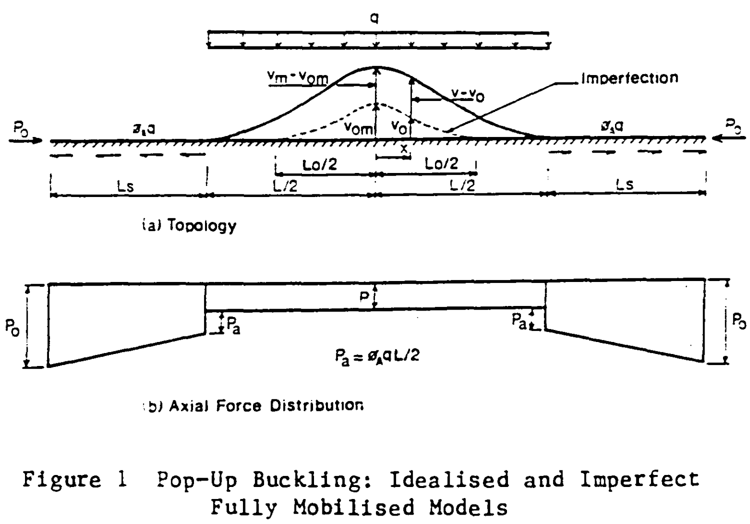

Figure 1 Pop-Up Buckling: Idealised and Imperfect Fully Mobilised Models

With the seabed taken to be rigid, deformations small and constitutive properties elastic, the force P_o is generated by the thermal and pressure actions in accordance with

$$P_o = AE\alpha T + Ap(D/2-t)(0.5-\nu)/t \tag{1}$$

where A represents the net cross-sectional area of the pipe possessing outer diameter D and wall-thickness t, E and ν are the elastic moduli, α denotes the coefficient of linear thermal expansion whilst T and p represent the thermal and pressure rises over the respective ambients.

Theoretically, buckling occurs when P_o achieves a value sufficient to provide for the necessary post-buckling force P to be established through variable buckling length L with $v_m=f(L)$; see Figure 1. The axial friction resistance $\phi_A q$ per unit length is simultaneously established through the adjacent slip lengths L_s with $P_o>P$, ϕ_A representing the fully mobilised axial friction coefficient. The key buckling regime equations take the form;

$$P_o-P-P_a = \phi_A q L_s \tag{2}$$

regarding equilibrium, where $P_a=\phi_A qL/2$ denotes the frictional component of the vertical reaction occurring at the ends of the buckle as indicated in Figure 1(b),

$$7.9883(10^{-6})(q/EI)^2L^7 - (P_o-P)L/(2AE) = \phi_A q L_s{}^2/(2AE) \tag{3}$$

regarding compatibility, where buckle length contraction is balanced by slip length extension (note pre-compression P_o) together with a buckling function, $-L/2\leq x\leq L/2$,

$$v = v_m(0.707 - 0.26176\pi^2x^2/L^2 + 0.293\pi\cos 2.86\pi x/L) \tag{4}$$

with $P=80.76EI/L^2$ and $v_m=2.407(10^{-3})qL^4/(EI)$. Solutions for P, $v_m(L)$ and L_s are determined in terms of actions T and p.

Taken together with equation (1), equations (2-4) represent the basic, idealised model for vertical mode buckling. Later imperfection studies include the presence of an imperfection-of-lie as typified in Figure 1 with initial out-of-straightness denoted by deflection v_o, of amplitude v_{om}, over length L_o. These studies result in equations (2-4) being modified in accordance with the v_{om}-L_o profile adopted; see Taylor and Gan[7], Boer[8] and Friedmann[9].

With regard to upheaval buckling, values for q which include the effective weight of cover involved are required as are buried values for axial friction force coefficient ϕ_A. It is suggested from Taylor and Gan[4] that burial cover pressure will affect the pipeline/supporting medium interface and thereby ϕ_A.

GEOTECHNICAL FACTORS

Pull-out and buried axial friction tests were undertaken to determine q and ϕ_A respectively. Small scale testing was employed to facilitate the establishment of a substantial data base for a variety of pipeline/burial topologies. Sand was chosen as the supporting medium in view of North Sea conditions, Bjerrum[13], and a sieve analysis identified the requisite medium-to-fine sand. Dry testing was employed for convenience, noting that a Coulomb medium was involved.

Figure 2 shows three typical prototype burial topologies, cover being of the order $D \lesssim h \lesssim 3D$. Testing sought to replicate type (a) given that data on type (b) already exists from Boer[8]. Throughout, tests were far longer in the preparation than the execution.

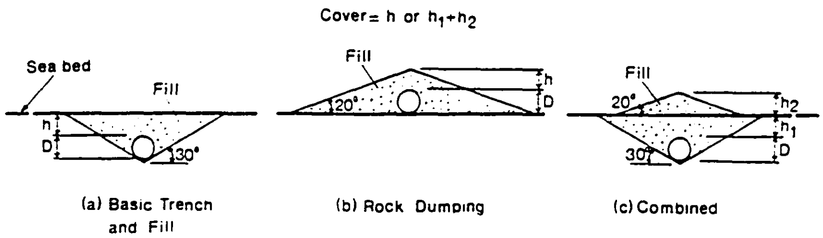

Figure 2 Typical Burial Topologies

PULL-OUT TESTS

Test Set-up The requisite experimental topology is shown in Figure 3. A discrete element of 48.3mm OD steel pipe represented the pipeline, the pipe being of 3.2mm wall-thickness and possessing a self-weight of 35.3N/m. The sand was first compacted to a typical density, ascertained later, of 1680kg/m^3. A horizontal trench was then carefully cut to the required depth and the pipe (with enclosed ends and lifting straps) emplaced, to be covered with a loose sand fill of typical density 1510kg/m^3. The lifting straps were connected to a spreader beam and transducers mounted to read directly from the buried specimen.

Clearly, as the pipe is pulled vertically, some cover will be disturbed at the ends of the pipe - so called 'end effects'. These effects must be catered for if the pipe specimen is to relate to an 'infinitely' long pipeline prototype. 'End-effects' are dealt with by ensuring the specimen is considerably shorter than the accommodating flume and by experimental identification of the ensuing effects for future deletion from the gross vertical pull values. A plane strain condition is thereby approached.

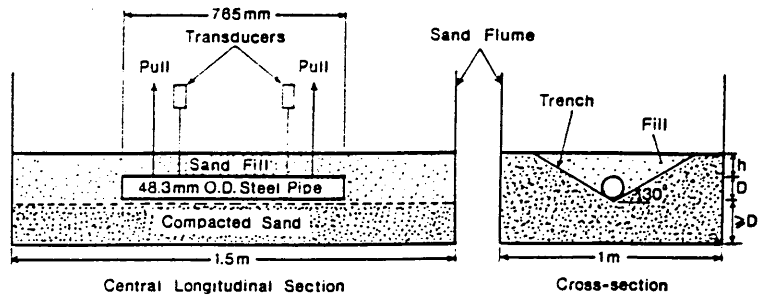

Figure 3 Pull-Out Topology

Test Procedure Stroke loading was applied to the lifting straps and the appropriate vertical pull/displacement characteristics recorded until substantial post-maximum pull-out force state deformation had been achieved. Dry testing enabled accurate assessment of the fill failure boundary on the sand surface, this boundary becoming distinct as the maximum pull-out force state was approached. Nine tests were undertaken, careful flume re-filling and sand compaction being implemented with each test.

Test Results Averaged pull-out characteristics are illustrated in normalised terms in Figure 4 for cases of h/D=1.5 and 3, strap pull being denoted by F, pipe weight by P_w. The loci show that only small deformations are onset

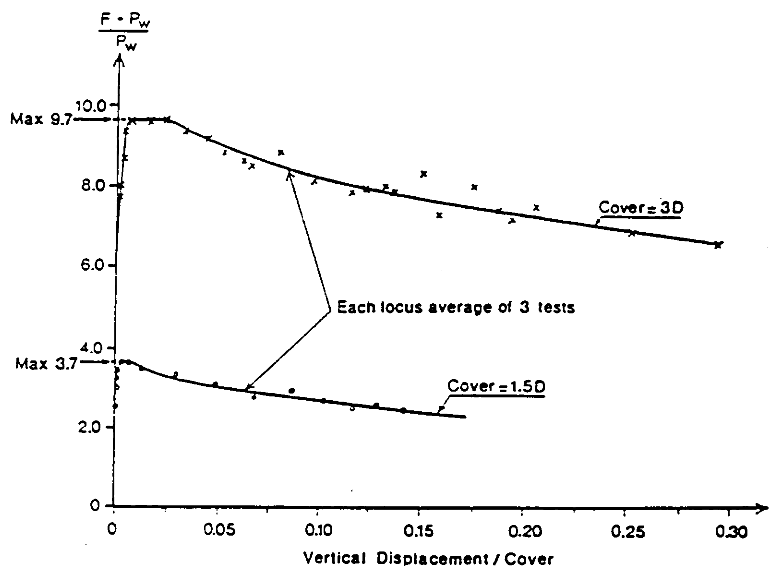

Figure 4 Pull-Out Tests Results For 48.3mm OD Pipe

up to the maximum pull-out state, deflection then increasing rapidly down the post-maximum falling branch. The loci bear comparison with that given by Boer[8]; although of generally similar form, the falling branch gradients herein are less severe, this being due to the different burial topology under investigation - recall Figures 2(a) and (b). The maximum pull-out values are indicative of the mechanical effect of pipeline burial, the submerged self-weight being effectively increased by factors of (9.7+1) and (3.7+1) for covers of 3D and 1.5D respectively; these are conservative ratios as due allowance must be made for the end-effects present in the discrete pipe test. This allowance is best undertaken when considering the maximum pull-out values in terms of cover height provided.

Figure 5 illustrates the appropriate data. The section detail shows the failure boundary rising at θ to the vertical through the sand. The net maximum pull-out force relates to the weight of cover fill, identified by shading in Figure 5, contained within the failure boundaries and above the pipe, together with the vertical component of the surface tractions active on the failure boundaries. For a discrete length L of pipe, geometry readily enables the net pull-out force to be given by

$$F-P_w-F_e = ([Dh+Dh\tan\theta+H^2\tan\theta+D^2/2+(D^2/4)\tan\theta \\ -\pi D^2/8]+[(1-k_1)\sin 2\theta(h+D/2)^2/2])L\gamma \quad (5)$$

where γ represents the specific weight of the soil, k_1 is a geotechnical constant and F_e denotes the end-effects force

$$F_e = [(Dh(\tan^2\theta+\tan\theta)+h^2\tan^2\theta+D^2(1+\tan^2\theta+2\tan\theta)/4)\pi\gamma \\ (h+D/2)/3] + [(\pi\gamma(1-k_1)\sin 2\theta\tan\theta)(h+D/2)^3/6)] \quad (6)$$

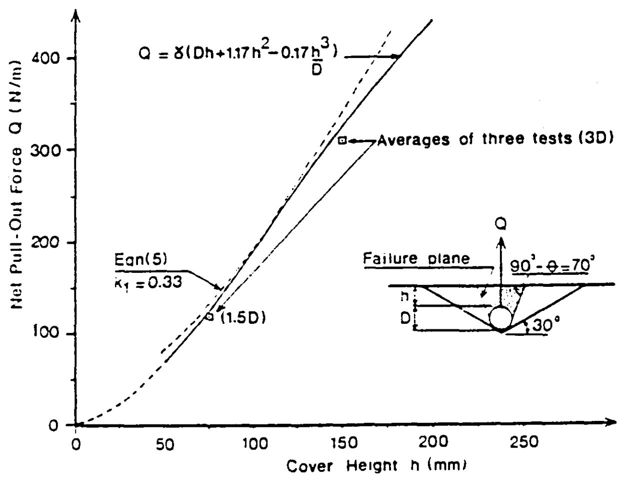

Figure 5 Pull-Out Force/Cover Height Results

F_e corresponds to sand surface semi-circular failure boundary profiles of radius $D/2+(h+D/2)\tan\theta$ being achieved at each end of the pipe. In each of equations (5) and (6), the former bracketed term refers to the fill weight component, the latter to the failure boundary tractions.

With $\theta=20°$ from observation, evaluations of equations (5) and (6) employing $k_1=0.33$ (geotechnical value for active pressure) show $100F_e/F\leq 10\%$ and a locus corresponding to equations (5) and (6) with L=1m is shown in Figure 5 together with net experimental values at h/D=1.5 and 3. These values are adjusted to take account of the end-effects term of equation (6) and to provide convenient per metre data, factoring P_w by 0.765^{-1} recalling Figure 3. That is, the graphical ordinate $Q=F-P_w-F_e$ in Figure 5 represents the net maximum pull-out resistance force per metre of pipeline and, when added to the submerged self-weight of the pipeline, represents the effective (buried) inertial loading parameter q of equations (2-4). An empirical design formula

$$Q = \gamma[Dh + 1.17h^2 - 0.17h^3/D] \qquad (7)$$

relating net pull-out force to cover depth and pipe diameter is suggested and added to the figure.

Equation (7) is similar to its equivalent in Boer[8] although the coefficient of h^2 is suitably enhanced. Further support for equation (7) comes from the general shallow anchor pull-out expression

$$Q = \gamma Dh(1 + [h/D]f) \qquad (8)$$

where f is a geotechnical variable. For the experimental values at h=1.5D and 3D, f=0.9 and 0.69 respectively, these values again being consistent with those given in Boer[8].

Finally, two wet tests were undertaken employing a water depth of D with h=D. A corresponding dry test gave a pull-out force within 10% of the average wet value.

FRICTION TESTS

Test Set-up The experimental topology is shown in Figure 6. A discrete element of pipe was again employed although in this case the pipe's length of 870mm exceeded the sand flume's corresponding dimension of 715mm providing for axial movement free from end-effects for all proposed axial movements. The sand was compacted and trenched as previously, the pipe and fill then being emplaced. The pipe was connected by wire to a weight hanger at one end, the other end's axial movement being monitored.

Test Procedure Loading was incrementally applied to the

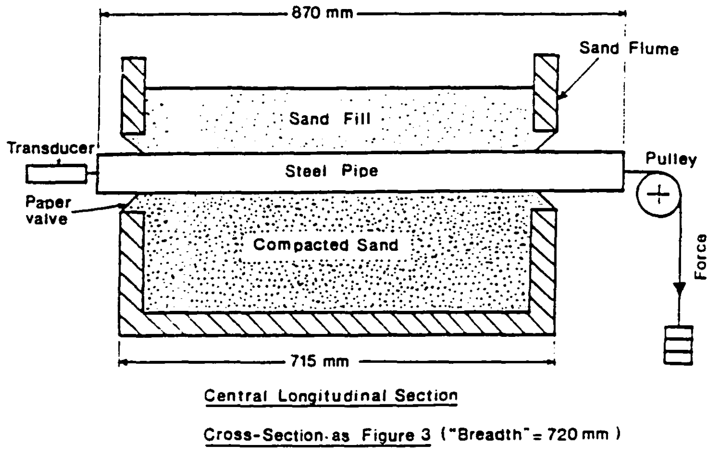

Figure 6 Axial Friction Topology

hanger and the corresponding displacement carefully monitored. This procedure was initially terminated when the frictional resistance was fully mobilised, i.e. when displacement response became dynamic. However, given that prototype pipelines experience heating/pressurising-cooling/depressurising cycles, loading was then reversed in order to detect any 'burrowing' effect whereby $\emptyset_A$ will decrease due to interface wearing, a feature perhaps particularly relevant to buried pipelines. Nine key tests were undertaken employing the same 48.3mm OD section as previously with three values of cover, h=D, 2D and 3D, each case-test being repeated three times. A significant reduction in friction resistance upon reversal of movement was observed and for h=3D, two further reversed loading half-cycles were implemented in an attempt to determine any lower limiting value for $\emptyset_A$. Eighteen additional simple load reversal tests employing D=15mm and 25mm at h=D, 2D and 3D were also undertaken.

Test Results Figure 7 displays the averaged axial friction force/displacement locus for D=48.3mm=h/3. Frictional resistance initially maximises at 191N, the corresponding displacement at which this full mobilisation of $\emptyset_A$ occurs being $u_\emptyset$=2mm. Upon reversal the maximum resistance drops by 16%. Two further reversals lead to ensuing reductions of 27% and 34% respectively; Figure 8 illustrates this effect and suggests a lower limiting value of the order of 60% original $\emptyset_A$. Reduction in friction force resistance upon reversal was obtained in all twenty-seven tests, averaged data being given in Table 1.

$\emptyset_A$ itself is obtained from

$$F_f = \emptyset_A R \tag{9}$$

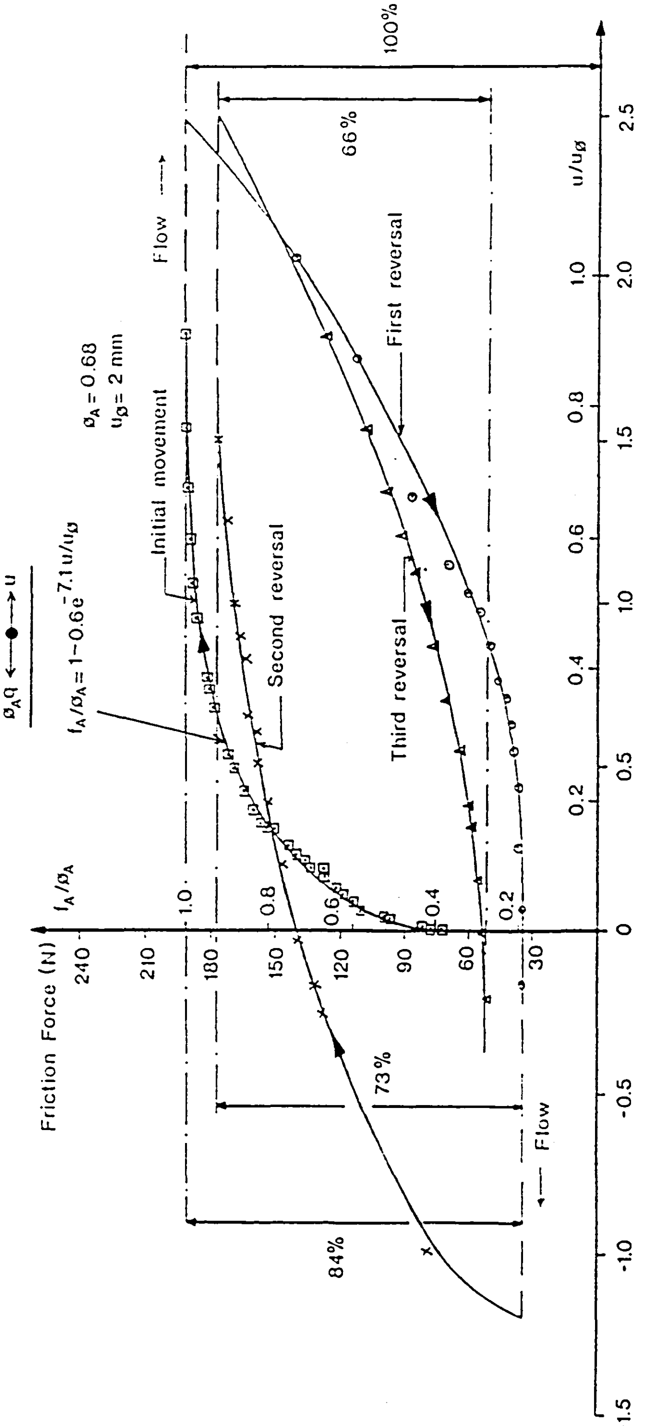

Figure 7 Axial Friction Force Characteristics under Cyclic Reversal

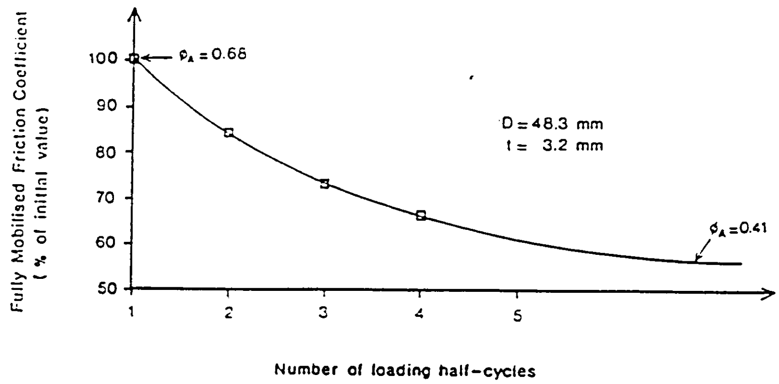

Figure 8 Cyclic Reduction in Fully-Mobilised Friction Resistance

D(mm)	h		
	D	2D	3D
15	89	87	80
25.4	86	81	75
48.3	83	85	84

Table 1; Reduced Fully Mobilised Friction Resistances upon Initial Loading Reversal (Percentages)

where F_f denotes the maximum loading or frictional resistance force and R represents the forces applied orthogonally to the pipe's surface by the surrounding medium. This is a geotechnical matter and an interpretation of piling studies, Bowles[14], suggests

$$R = (P_s)+(P_s+P_w)+2(k_2\gamma[h+D/2]\pi LD/4) \qquad (L=715mm) \quad (10)$$

where P_s represents the weight of cover lying directly above the top quarter circumference of the pipe whilst the third parenthetic term represents the lateral pressure acting on the two middle quarter circumferences lying to the sides of the pipe; k_2 is a geotechnical constant. The bottom quarter circumference carries the pipe weight P_w in addition to P_s. Vertically-oriented pipe was pulled vertically in a number of ancillary tests to evaluate k_2, general geotechnical data ranging between 0.3 and 3. With k_2=1 so determined, equations (9) and (10) afford for D=48.3mm=h/3

$$\phi_A = 191/(2[57.5] + 30.36 + 134.2) = 0.68 \qquad (11)$$

As denoted in Figure 7, an empirical curve

$$f_A = \phi_A(1-0.6e^k), \quad k = -7.1u/u_\phi \qquad (12)$$

where f_A is a friction force parameter, is employed to fit the initial loading locus data. This is suitably asymptotic to $f_A = \phi_A$ and provides in a useful design tool, as later discussed, with $f_A q$ replacing $\phi_A q$ in buckling studies to give a consistent deformation-dependent friction model. For D=48.3mm, h=D and 2D, then ϕ_A=0.55 and 0.6 respectively.

Equivalent seabed-mounted tests give values in the range 0.5-0.59 for ϕ_A; see Anand and Agarwal[15] for example. The rise in ϕ_A for buried pipes is attributed to burial pressure affecting the pipe surface/sand medium interface. This argument is supported by the observation that for surface-mounted pipes, Taylor and Gan[4] give ϕ_A=0.53 for 48.3mm OD pipe simply resting on sand against ϕ_A=0.59 for the case of the pipe having been pressed into the sand.

DESIGN CONSIDERATIONS

Two new sets of data have been set out and their potential employment in subsea upheaval pipeline buckling analysis is now illustrated. An effective inertial loading q-modelling employing equation (7) and an enhanced friction force f_A-modelling typified by equation (12) are incorporated within the otherwise established subsea seabed-mounted pipeline buckling model of Taylor and Gan[7].

It is taken that equations (7), (11) and (12) do not suffer significant scaling factors when applied to relatively small-bore prototypes. Scaling is an important matter previously discussed by Anand and Agarwal[15] and Taylor and Gan[4] with respect to seabed-mounted pipelines which can, however, typically posess upto 1m OD. The similarity of Boer's[8] equivalent expression to equation (7) is also

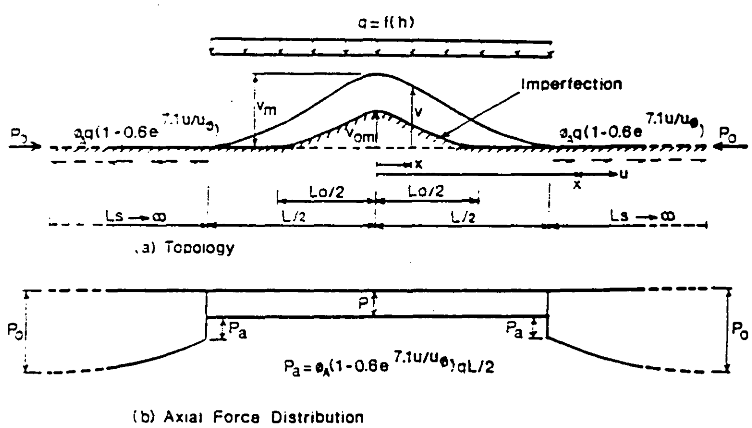

Figure 9 Upheaval Buckling Model

reassuring given the equivalent expression is based on D=442mm experimentation. Regarding friction modelling, Pedersen and Michelsen[13] quote ϕ_A=0.5 and u_ϕ=3mm for D=220mm (h/D=6), adding elsewhere[12] that alternative values for ϕ_A have also been employed. Accordingly, equations (7), (11) and (12) are employed per se, with ϕ_A=(0.55+0.6)/2=0.58 at h=1.5D.

The respective modelling topology is shown in Figure 9 and the key action/response loci are shown in Figure 10 together with the respective prototype parametric values. The effect of burial upon behaviour in terms of effective inertial loading q is clearly depicted, design being factored on snap temperature T_m. Employment of deformation-dependent friction parameter f_A as per equation (12) as opposed to the employment of fully mobilised friction parameter ϕ_A as per equation (11) shows little effect. However, a consistent deformation-dependent friction force modelling which <u>also</u> includes an integral finite slip length L_s is yet to be formulated and indications to-date are that L_s is significantly underestimated employing a fully mobilised friction model - see Taylor and Gan[4]. This is important for, if the length of slip required in practice (ie deformation-dependent) is physically unavailable, the buckling model becomes invalid. Analytical developments are thereby proceeding.

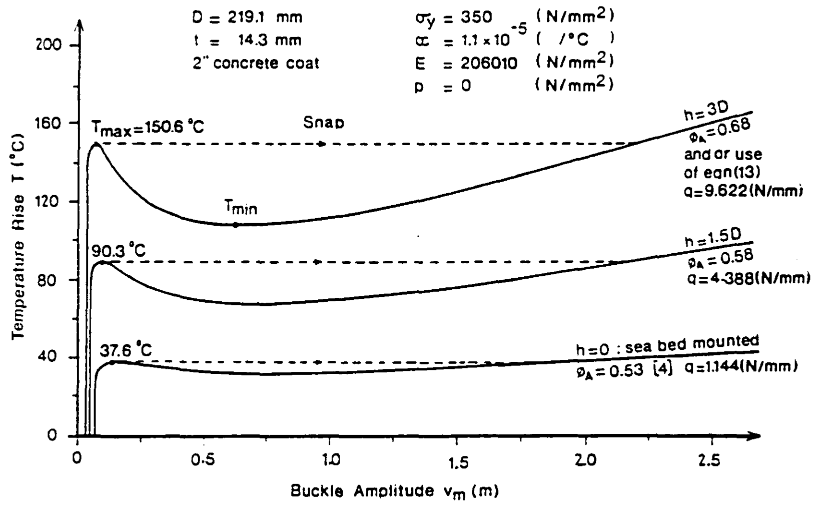

Figure 10 Thermal Action Characteristics - Upheaval Buckling

CONCLUSIONS

Pull-out and axial friction force characteristics for buried subsea pipelines have been studied and design parameters suggested. Further work is required to set up the necessary data base applicable to the various pipe sizes and burial topologies extant and proposed. The incorporation of buckling recovery characteristics, typified by Figure 7 and Table 1, together with the employment of deformation-dependent axial friction and pull-out force characteristics, form part of a forward path in subsea pipeline buckling studies.

ACKNOWLEDGEMENT

The authors wish to thank Professor A C Walker and Dr C Ellinas of AME Ltd, Guildford, UK, for advice afforded regarding subsea pipeline burial experimentation. However, the conclusions drawn are the authors' alone.

NOMENCLATURE

A; I	cross-sectional area; second moment of area
D; t	outer diameter (OD); wall thickness
E; ν	elastic constants
F	gross pull-out force
F_e	end-effects force
F_f	friction resistance
f	geotechnical variable
f_A	axial friction parameter
h	cover
k, k_1, k_2	constants
L; L_s	buckle length; slip length
L_o	initial peel length
P_a	buckle length shear reaction
P_o; P	pre-compression; buckling force
P_s; P_w	soil column weight; pipe element weight
p	pressure rise
Q	net pull-out force
q	effective inertial loading
R	orthogonal pipe loading
T	temperature rise
u	axial displacement
u_ϕ	axial displacement for fully mobilised friction
v, v_o	vertical displacements
v_m, v_{om}	amplitudes
x	spatial coordinate
α	coefficient of linear thermal expansion
γ	specific weight of sand
θ	failure plane angle
ϕ_A	axial friction coefficient, fully mobilised

REFERENCES

1. Hobbs R E, Pipeline Buckling Caused by Axial Loads, J Construct Steel Res, 1, 2, 2-10, 1981.
2. Taylor N and Gan A B, Regarding the Buckling of Pipelines Subject to Axial Loading, J Construct Steel Res, 4, 1, 45-50, 1984.
3. Hobbs R E, In-Service Buckling of Heated Pipelines, J of Transportation Engineering, Vol 110, No 2, 175-189, 1984.
4. Taylor N, Gan A B and Richardson D A R, On Submarine Pipeline Frictional Characteristics in the Presence of Buckling, 4th OMAE International Symposium, Dallas, 508-515, 1985.
5. Taylor N and Gan A B, Refined Modelling for the Lateral Buckling of Submarine Pipelines, J Construct Steel Res, 6, 2, 143-162, 1986.
6. Taylor N and Gan A B, Refined Modelling for the Vertical Buckling of Submarine Pipelines, J Construct Steel Res, 7, 1, 55-74, 1987.
7. Taylor N and Gan A B, Submarine Pipeline Buckling - Imperfection Studies, Thin-Walled Structures, 4, 4, 295-324, 1986.
8. Boer S et al, Buckling Conditions in the Design of the Gravel Cover for a High-Temperature Oil Line, Offshore Technology Conference, paper no. OTC 5294, 1986.
9. Friedmann Y, Some Aspects of the Design of Buried Hot Pipelines, 1986 European Seminar, Offshore Oil and Gas Pipeline Technology, 28-29, Jan 1986.
10. Traumann C H et al, Uplift Force - Displacement Response of Buried Pipe, ASCE Journal of Geotechnical Engineering, Vol III, No 9, Sept 1985.
11. Pedersen P and Juncher J, Upheaval Creep of Buried Heated Pipelines with Initial Imperfections, Marine Structures, Design, Construction and Safety, 1, 1, 1988.
12. Pedersen P and Michelsen J, Large Deflection Upheaval Buckling of Marine Pipelines, To be published 1988.
13. Bjerrum L, Geotechnical Problems Involved in Foundations of Structures in the North Sea, Geotechnique 23, No 3, 319-358, 1973.
14. Bowles J E, Foundation Analysis and design, 3rd Ed, McGraw-Hill, 1982.
15. Anand S and Agarwal S L, Field and Laboratory Studies for Evaluating Submarine Pipeline Frictional Resistance, Transaction of the American Society of Civil Engineers, Journal of Energy Resources Technology, Vol 103, 250-254, Sept 1981.

Marine Structures 6 (1993) 325–358

Prop-Imperfection Subsea Pipeline Buckling

Neil Taylor & Vinh Tran

School of Construction, Sheffield City Polytechnic, Pond Street, Sheffield, UK S1 1WB

(Received 16 October 1991; revised version received 1 July 1992; accepted 14 July 1992)

ABSTRACT

In-service buckling of subsea pipelines can occur due to the introduction of axial compressive forces caused by the constrained expansions set up by thermal and internal pressure actions. Proposed herein is a mathematical model relating to a pipeline, the otherwise horizontal and straight idealised lie of which is interrupted by an encounter with an isolated prop or point irregularity. The overbend produced can serve, in the presence of enhanced topologies involving trenching, burial, discrete or continuous, and fixed anchor points, to trigger vertical or upheaval buckling of the pipeline under in-service conditions. The results of a series of case studies are contrasted with data appertaining to alternative models available in the literature: experimental support is additionally noted. By questioning the implicit stress-free-when-straight assumption present in these alternative models, it is considered that a consistent, imperfection-prone isolated prop formulation is hereby provided, suitable for design application.

Key words: in-service buckling, subsea pipelines, isolated prop, trenching, burial, fixed anchor points.

NOTATION

A	Cross-sectional area
D	Pipe diameter
E	Elastic modulus
F, F_i	Shear force at prop

Marine Structures 0951-8339/93/$06.00

F_{ap}	Anchor shear capacity
h, h_1, h_2	Cover depths
I	Second moment of area of cross-section
$k_i (i = 1\text{–}6)$	Constants
L	Buckle length
L_{fap}	Anchorage spacing
L_i	Buckle length of the isolated prop imperfection topology
L_o	Buckle length of the contact undulation imperfection topology
L_s, L_{s1}, L_{s2}	Slip lengths
L_u	Buckle length at upheaval state
L^*	Lower limit on buckle length re axial friction force response through slip length
$M_x, M_i\|_x$	Bending moments
n	$\sqrt{P/EI}$
N, N_i	Maximum bending moments
p	Internal pressure rise
P	Buckle force
P_o	Pre-buckling force
P_{qi}	Buckle force at quasi-idealised state
P_u	Buckle force at upheaval
q	Submerged self-weight of pipeline per unit length
q'	Submerged self-weight of pipeline cover per unit length
t	Wall thickness of pipe
T	Temperature rise
T'	Pressure-equivalent temperature rise
u_s	Resultant longitudinal movement at buckle/slip length interface
U	Resultant flexurally induced end-shortening
v	Vertical displacement of the pipe
v_i	Vertical displacement of the imperfection topology
v_m	Maximum vertical amplitude of the buckled pipe
v_{om}	Maximum vertical amplitude of the imperfection topology
v'_x	dv/dx etc.
x	Spatial coordinate
α	Coefficient of linear thermal expansion
θ	Trench angle
ν	Poisson's ratio
σ_y	Yield stress
ϕ_A	Axial friction coefficient
ϕ'_A	Axial friction coefficient of overburden
ϕ_L	Lateral friction coefficient

INTRODUCTION

The increase in demand for hydrocarbon deposits has led, during the past two decades, to the development of substantial offshore infrastructure in the North Sea. More recently, marginal offshore fields have been exploited employing unmanned satellite facilities. Hydrocarbon export frequently employs subsea pipelines which can either simply rest on the seabed or lie in excavated trenches, with or without burial. A subsea pipeline laid at ambient temperature and subsequently employed to transport high-temperature hydrocarbons under pressure is thereby subject to the introduction of axial compressive forces caused by the constrained thermal and pressure actions and buckling can ensue.[1-3] With hydrocarbon transportation temperatures up to 100°C above that of the water environment and operating pressures over 10 N/mm^2, these forces can be substantial given the ability of the pipeline/seabed interface to generate the necessary frictional resistance to axial movement.

Pipeline installation is both sophisticated and expensive and investment is substantial. Failure of a pipeline is costly both in terms of lost production and repair, and actual in-service buckling failures have recently been recorded in the literature.[4-6]

With the later employment of smaller bore pipes for in-field hydrocarbon transportation from marginal fields employing satellite technology, the vertical or upheaval buckling mode has become of paramount importance as such pipes must be trenched and/or buried to protect them, for example, from damage by anchors and/or trawling gear — the latter can weigh up to 100 tonnes. Trenching/burial largely obviates alternative lateral mode buckling failure.[4,7,8]

Three basic types of initial imperfection can be identified as illustrated in Fig. 1. In the first case, the pipeline remains in continuous contact with some vertical undulation in an otherwise idealised horizontal and straight lie. The isolated prop alternatively features a sharp and distinct vertical irregularity such that voids (sea-filled) exist to either side. The third case occurs where the above voids become infilled with leaching sand and represents a special sub-case of the first. The initial imperfection is denoted by amplitude v_{om} and wavelength L_o or L_i as shown. Whilst L_i is determined from simple statics, L_o is subject to individual engineering judgement.[3]

Present interest is centred on the isolated prop case of Fig. 1(b). The prop represents the undercrossing of a non-parallel pipe or the presence of an intervening rock: stop–start trenching procedures can also be responsible. The overbend of the pipe serves to trigger upheaval buckling wherein the pipe lifts off the prop, resisted in these attempts by the

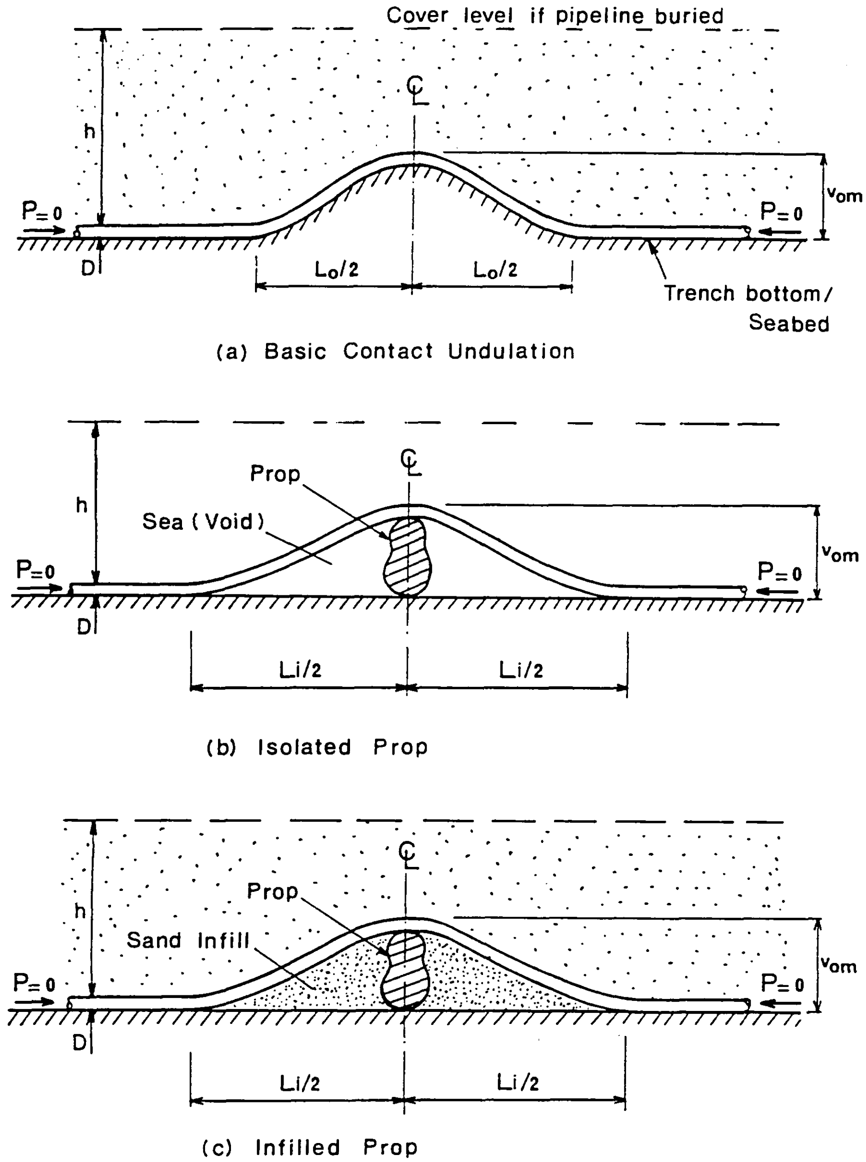

Fig. 1. Typical imperfection configurations.

effective download (i.e. self-weight, burial overburden) on the pipe and the pipe's stiffness. The following study presumes system symmetry and seabed or trench-bottom rigidity, together with indefinitely small deformations and linearly elastic constitutive properties. Essentially, four sets of equations are generated appertaining to:

(a) the interpretation of temperature and pressure rises over ambient in terms of axial compression so generated within the pipe.
(b) longitudinal equilibrium.
(c) longitudinal compatibility, and
(d) buckling relationships.

With alternative isolated prop models available in the literature,[8-10] it is worth noting that most subsea pipeline buckling models largely agree regarding the composition of factors (a)–(c); it is within (d) that most models' idiosyncracies lie. Indeed, regarding (a), the so-called pre-buckling pipe force P_0 generated by a temperature rise T and a pressure rise p can be readily represented by[1]

$$P_0 = AE\alpha T + \frac{ApD}{2t}(0{\cdot}5 - \nu) \qquad (1)$$

where A denotes the net cross-sectional area of the pipe of outer diameter D and wall thickness t, whilst E and ν are the appropriate elastic modulus and Poisson's ratio respectively. Merging the known action parameters T and p leads to computational convenience such that eqn (1) can be written

$$P_0 = AE\alpha(T + T') \qquad (2)$$

where $T' = pD(0{\cdot}5 - \nu)/(2E\alpha t)$ with $T' \approx pD/(24t)$ for typical material values (N, mm units). Here, action T alone is considered, with pressure-equivalent T' applied as a back-end reduction as necessary.

The basic isolated prop subsea pipeline buckling model is now considered with emphasis being placed upon the respective buckling relationships; trenching and/or burial details together with the employment of fixed anchor points are treated later.

ISOLATED PROP TOPOLOGIES

The proposed five key stages in buckling development are illustrated in Fig. 2. The datum state refers to the initial lie adopted by the pipeline following laying operations whereby a vertical out-of-straightness is caused by the presence of a prop. Subsea conditions are assumed to preclude effective infilling of the adjacent voids with solid matter at any stage of the pre- or post-buckling process.

As the temperature of the pipeline rises due to routine operation, the initial span or imperfection wavelength L_i suffers a reduction as the pipeline tightens up under compressive action P ($P < P_0$, see later). The

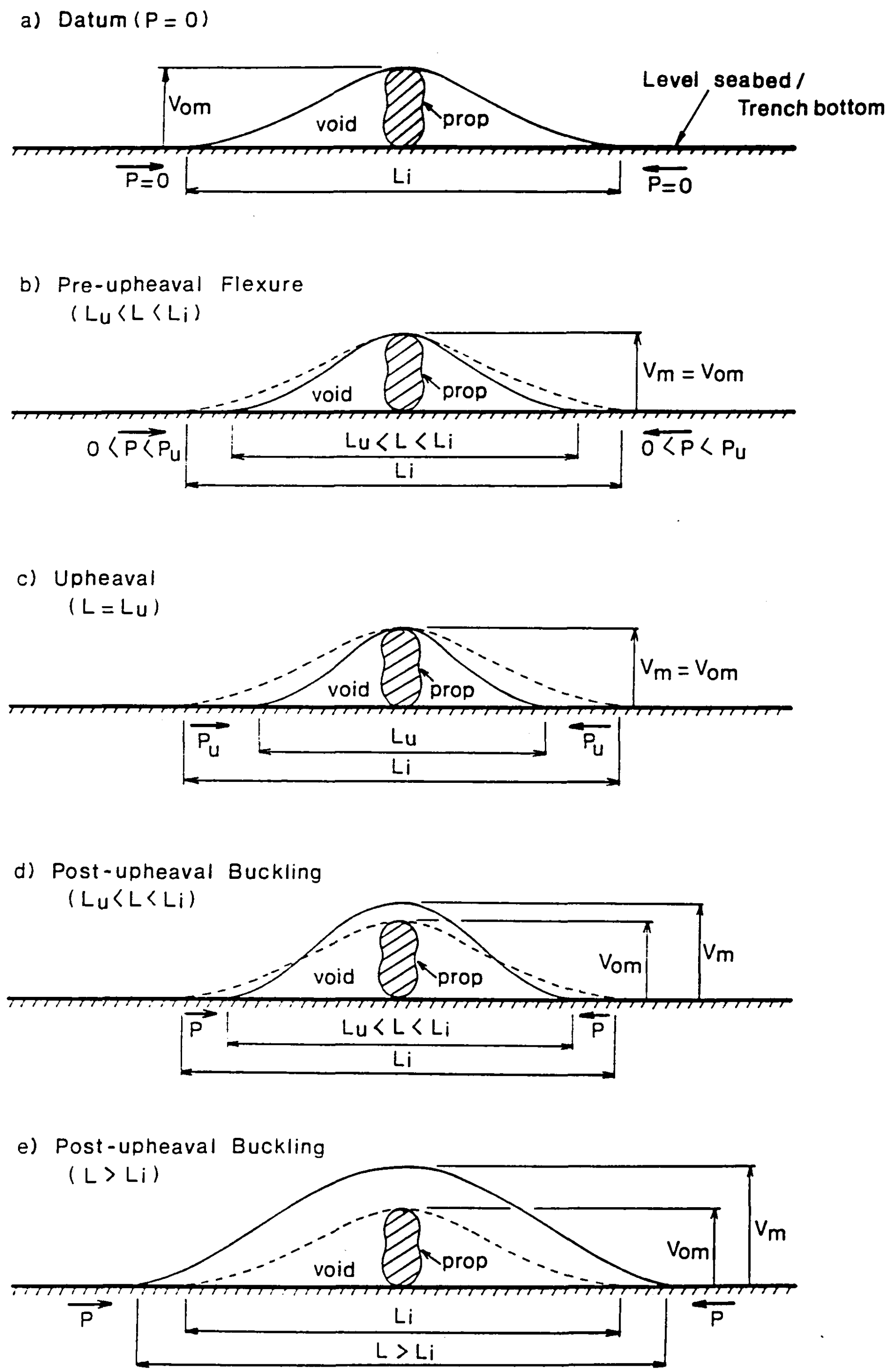

Fig. 2. Isolated prop topologies.

wavelength L reduces to some specific value L_u ($P = P_u$) whereupon the pipeline lifts off the prop. Post-upheaval buckling initially involves wavelength $L_u < L < L_i$, with $L > L_i$ ensuing if circumstances so dictate.

DATUM ESTABLISHMENT

The appropriate topology is shown in Fig. 3 with the pipeline effectively being under the contrasting actions of a prop imperfection of amplitude v_{om} and a submerged self-weight loading intensity of q (to which can be added any overburden effect in the case of buried pipes — see later). Reactions include a shear force F_i, equal to half the prop force, and a bending moment N_i acting at the crown together with a transverse reaction at the peel point. With boundary conditions

$$v_i|_{L_i/2} = v'_{i\,x}|_{L_i/2} = v'_{i\,xx}|_{L_i/2} = v'_{i\,x}|_0 = 0 \tag{3}$$

where v_i denotes initial vertical deflection and $v'_{i\,x} = \mathrm{d}v_i/\mathrm{d}x$ etc., then equilibrium affords for general bending moment $M_i|_x$, $0 \leqslant x \leqslant L_i/2$,

$$M_i|_x = EIv'_{i\,xx} = -\frac{F_iL_i}{2} + \frac{qL_i^2}{8} + F_ix - \frac{qx^2}{2} \tag{4}$$

Noting $v_i|_0 = v_{om}$, computational manipulation gives

$$v_i = \frac{q}{72EI}\left(2L_i\left[\frac{L_i}{2} - x\right]^3 - 3\left[\frac{L_i}{2} - x\right]^4\right) \tag{5}$$

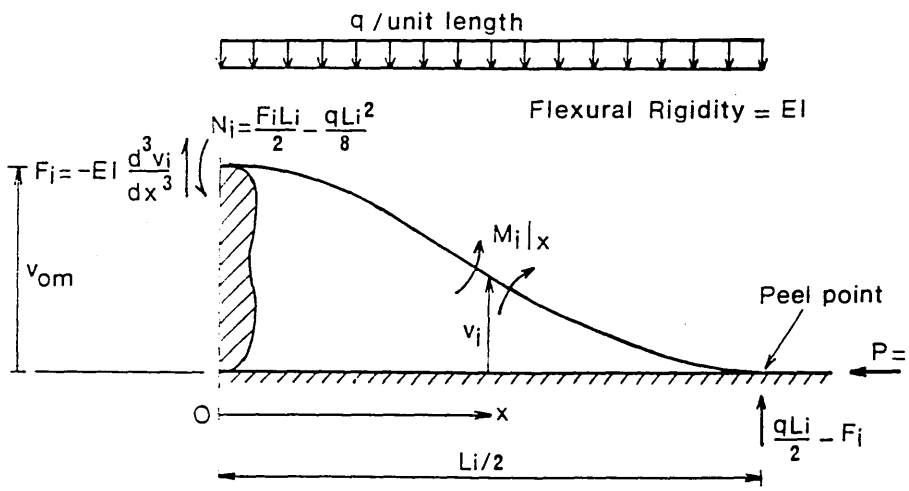

Fig. 3. Initial imperfection topology.

$$L_{\mathrm{i}} = 5{\cdot}8259\left(\frac{v_{\mathrm{om}}EI}{q}\right)^{1/4} \tag{6}$$

$$\frac{F_{\mathrm{i}}}{EI} = -v_{\mathrm{i}\,,xxx}'\big|_0 = \frac{qL_{\mathrm{i}}}{3EI} \tag{7}$$

together with

$$v_{\mathrm{i}\,,xx}'\big|_0 = v_{\mathrm{i}\,,xx}'\big|_{\max} = -\frac{qL_{\mathrm{i}}^2}{24EI} \tag{8}$$

and

$$M_{\mathrm{i}}\big|_x = \frac{q}{12}\left(\frac{L_{\mathrm{i}}}{2} - x\right)(6x - L_{\mathrm{i}}), \quad M_{\mathrm{i}}\big|_x \leqslant N_{\mathrm{i}} \tag{9}$$

The foregoing equilibrium study, whilst providing an initially curved datum $v_{\mathrm{i}}(x)$ for ensuing stability studies, actually demands a supposedly previous hypothetical stress-free-when-straight datum with q initially relating to an empty pipe. Accordingly, any prop buckling study which employs eqn (5) in conjunction with eqn (9) is effectively condemned to replicate established idealised studies.[8, 10] Here, however, whilst eqn (5) is taken to be usefully true following field observations in the North Sea,[6] eqn (9) is taken to relate to only a component of residual stress in the as-laid pipe, other components following from fabrication and laying operations.[11, 12] Given that any residual stresses are likely to be subject to in-service thermal stress relieving[6, 7, 12] and that the 'isolated' inclusion of the stress data corresponding to eqn (9) provides an effectively imperfection-free formulation which would then be non-conservative — these features are discussed further below — then the familiar engineering worst case scenario philosophy is invoked whereby the imperfection-nullifying idealised stress component given by eqn (9) is suppressed and a Perry-like datum assumption of stress-free-when-initially-deformed is employed.[13] Hereafter, in the absence of comprehensive and definitive as-laid residual stress data[11, 12], eqn (5) is employed as a kinematic imperfection of form.

PRE-UPHEAVAL FLEXURE

Figure 4 illustrates the topology adopted upon the onset of in-service axial compression P which is constant through the wavelength $L_{\mathrm{u}} \leqslant L \leqslant L_{\mathrm{i}}$; q now allows for the pipeline containing hydrocarbons. The foregoing argument leads to employment of the familiar, imperfect moment–curvature relationship

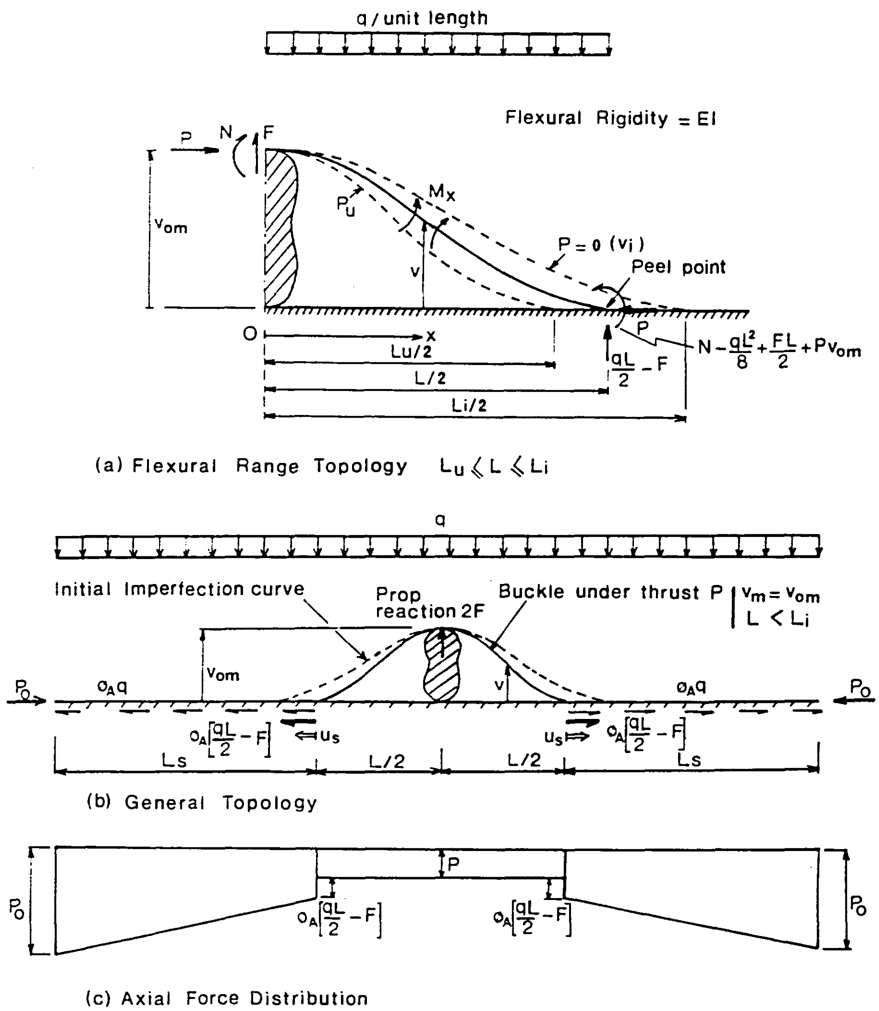

Fig. 4. Isolated prop — pre-upheaval: details of imperfect fully mobilised model.

$$\frac{M_x}{EI} = v'_{xx} - v'_{i\,xx} \tag{10}$$

where M_x represents the bending moment at x, $0 \leqslant x \leqslant L/2$, and v denotes the vertical pipe displacement at the deformed state ($P \neq 0$). The respective boundary conditions take the form

$$v|_{L/2} = v'_x|_{L/2} = v'_{xx}|_{L/2} = v'_x|_0 = 0 \tag{11}$$

together with $v|_0 = v_{om}$. The presence of the bending moment at the peel point despite the zero curvature transversality requirement is to be noted, however, with

$$M_x|_{L/2} = EIv'_{xx}|_{L/2} - EIv_{i\,xx}'|_{L/2} = -EIv_{i\,xx}'|_{L/2} \tag{12}$$

in accordance with eqn (10). Also in conjunction with eqn (10), bending moment M_x is given by

$$M_x = P(v_{om} - v) + N + Fx - \frac{qx^2}{2} \tag{13}$$

from equilibrium, N and F denoting the crown moment and shear force respectively, with F representing half the prop force.

Manipulation of eqns (5), (10), (11) and (13) affords the characteristic equation

$$\frac{L_i}{L} = \frac{5\cdot 8259}{nL}\left[\frac{4 - \frac{(nL)^2}{4}\cos(nL/2) + 2nL\sin(nL/2) - 4 - \frac{(nL)^2}{4}}{\cos(nL/2) - 1}\right]^{1/4} \tag{14}$$

where $n^2 = P/EI$. Evaluating for nL in terms of L_i/L (see Table 1) then vertical deflection v is given by

TABLE 1
Typical Buckling Force Solution for Isolated Prop Model

	L_i/L	nL	*Remarks*
Pre-upheaval	1·194 847	1·5	$P \to 0$
	1·199 31	2·0	
	1·205 182	2·5	
	1·212 541	3·0	
	1·221 515	3·5	
	1·232 263	4·0	
	1·259 967	5·0	
	1·298 091	6·0	
	1·342 1	6·857 667	Upheaval $F = 0$
Post-upheaval $L < L_i$	1·342 1	6·857 667	Upheaval $V_m = V_{om}$
	1·30	6·986 727	
	1·20	7·262 40	
	1·10	7·502 238	
	1·0	7·713 4	$L = L_i$
Post-upheaval $L > L_i$	1·0	7·713 4	$L = L_i$
	0·90	8·039 016	
	0·80	8·327 418	
	0·70	8·659 057	
	0·60	8·754 047	
	·	·	
	·	·	$P \to 80{\cdot}76EI/L^2$
	0·01	8·986 8	$(L > L_u)$

$$v = \frac{q}{n^4 EI}(-2\cos n(L/2 - x) + k_1 \sin n(L/2 - x) - n^2x^2 + k_2 nx + k_3) \tag{15}$$

where

$$\begin{aligned} k_1 &= \frac{nL}{3}\left(\frac{L_i}{L} - 3\right) + \frac{nF}{q} \\ k_2 &= k_1 + nL \\ k_3 &= \frac{(nL_i)^4}{1152} + 2\cos(nL/2) - k_1 \sin(nL/2) \end{aligned} \tag{16}$$

with the crown shear force F being expressed as

$$\begin{aligned} \frac{F}{EI} &= (-v'_{,xxx}|_0) - (-v'_{i\,,xxx}|_0) \\ &= \frac{q}{EIn(1 - \cos(nL/2))}\left[2\sin(nL/2) + \left(\frac{nL_i}{3} - nL\right)\cos(nL/2) - \frac{nL_i}{3}\right] \end{aligned} \tag{17}$$

and general bending moment being given by

$$M_x = P(v_{om} - v) + \frac{q}{n^2}\left(k_3 + \frac{L_i^2}{24} - \frac{(nL_i)^4}{1152} - 2\right) + Fx - \frac{qx^2}{2}, \quad M_x \leqslant N \tag{18}$$

noting F is available from eqn (17).

Having established the buckling force P in terms of wavelength L and amplitude $v_m = v|_0$, it is now necessary to employ longitudinal equilibrium and compatibility to relate P to the previously discussed temperature rise $T = P_0/AE\alpha$; note the system topology and axial force distribution given in Fig. 4(b) and (c). Changes in wavelength are accompanied by frictional resistance to P_0, the driving force behind the buckling mechanism, being generated in the adjacent lengths of pipe, L_s. With the slip lengths L_s undergoing fully mobilised axial friction restraint $\phi_A q$ per unit length, where ϕ_A is the axial friction coefficient between the pipe and the seabed, then familiar manipulation affords the equilibrium expression[1-3]

$$P_0 - P = [2\phi_A qAE(-u_s)]^{1/2} + \phi_A\left(\frac{qL}{2} - F\right) \tag{19}$$

where u_s denotes the longitudinal movement of the peel point given by the equally familiar longitudinal compatibility expression

$$u_s = \frac{(P_o - P)L}{2AE} - U \tag{20}$$

in which U denotes the flexural end-shortening through the wavelength such that

$$U = \frac{1}{2}\int_0^{L/2} (v'_x)^2 \mathrm{d}x - \frac{1}{2}\int_0^{L_i/2} (v'_{i\,x})^2 \mathrm{d}x \tag{21}$$

More fully, eqn (21) is

$$\begin{aligned}\int_0^{L/2} (v'_x)^2 \mathrm{d}x = \left(\frac{q}{EI}\right)^2 \frac{1}{n^7}\Big(& (4 + k_1^2)\frac{nL}{4} + \frac{nL}{2}(k_1 - nL)k_1 + \frac{(nL)^3}{6} \\ & + \frac{1}{4}(k_1^2 - 4)\sin nL - k_1(\cos nL - 1) \\ & - 4[(k_1 + nL)(1 - \cos(nL/2)) + 2\sin(nL/2) - nL] \\ & + 2k_1[2 - 2\cos(nL/2) - (k_1 + nL)\sin(nL/2)]\Big)\end{aligned} \tag{22}$$

and

$$\int_0^{L_i/2} (v'_{i\,x})^2 \mathrm{d}x = \left(\frac{q}{EI}\right)^2 \frac{L_i^7}{483\,840} \tag{23}$$

Full solution for the pre-upheaval flexure stage is now available from eqns (14)–(23) although the familiar longitudinal fully mobilised friction modelling employed above fails to allow for the early phase of this stage in which all necessary frictional resistance is (theoretically) provided for by the peel point concentrated reaction $\phi_A[qL/2 - F]$ (note Fig. 4(b) and eqn (19)). This circumstance has been accounted for elsewhere.[14, 15] Here, it is simply necessary to indicate that eqns (19) and (20) are only valid for $u_s \leqslant 0$; with $L = L^*$ denoting the wavelength at which $u_s = 0$, then L^* is found from

$$-\frac{\phi_A L^*}{2AE}\left(\frac{qL^*}{2} - F\right) + U = 0 \tag{24}$$

where U is given by eqn (21).

For $L \leqslant L^*$, $u_s = 0$ and

$$P_o = P + \phi_A\left(\frac{qL}{2} - F\right) \tag{25}$$

The above formulation is valid for $0 \leqslant P \leqslant P_u$ where P_u denotes the buckle force in the pipe at the onset of upheaval from the prop. Prior to consideration of the important upheaval state (e.g. P_u), it is pertinent to appreciate that the present analysis relates to in-service conditions. In comparison with the infilled prop case (recall Fig. 1) the pre-upheaval flexural regime represents an in-service capability for delaying the onset of upheaval: flexural and associated slip length movement can occur without upheaval being induced. In-service stress-relieving has been conceptually propounded elsewhere with respect to infilled prop studies.[6,7,12,16] Although the physical prototype presently under consideration lacks the self-weight relieving presence provided by the prop-attendent fill of the infilled case, it does share the residual stress relieving mechanism provided by the actually complex non-linear axial friction behaviour within the slip lengths,[17] ratcheting surely attending the cyclic nature of in-service activity. Given the above noted substantial degree of in-service movement herein concerned, it is contended that thermally induced residual stress-relieving is thereby similarly available. This important matter will be subject to further deliberation following presentation of the complete model. However, the above lends further support to the adoption, as herein, of a stress-free-when-initially-deformed datum.

UPHEAVAL

This state, of crucial importance to the designer, is defined as being that at which the prop reaction force ($2F$) reduces to zero. From eqn (17), therefore, with $F = 0$,

$$P_u = P|_{F=0} = 42{\cdot}027\frac{EI}{L_u^2} = 63\% P_{qi} \tag{26}$$

where $P_{qi} = 80{\cdot}76EI/L^2$ denotes the idealised buckling force value[1] ($L \equiv L_u$) and

$$L_u = L|_{F=0} = 0{\cdot}7451 L_i \tag{27}$$

Equations (26) and (27) are quite distinct from the upheaval values obtained in previous isolated prop models[8,10] and this factor requires particular consideration.

The above are explicitly based upon the familiar moment–curvature expression given by eqn (10) which incorporates initial imperfection curvature $v_i{}'_{xx}$ effects. As discussed previously, eqn (5) is taken to prescribe a stress-free-when-initially-deformed datum state, i.e. eqn (9) is suppressed. If the internal stressing of eqn (9) were to be incorporated within eqn (10) a priori with $M_i|_x = EIv_i{}'_{xx}$, the idealised[1] solutions

$$P_u^{(8,10)} = 80{\cdot}76\frac{EI}{L_u^2} = P_{qi} \quad (28)$$

where

$$L_u^{(8,10)} = 4{\cdot}5147\left(\frac{v_{om}EI}{q}\right)^{1/4} = L|_{P_{qi}} = 0{\cdot}775L_i \quad (29)$$

would ensue as eqns (5)–(9) represent the deformed state solution of a problem in which the (previous hypothetical) datum state was stress-free-when-straight. This is effectively implemented in previous isolated prop models,[8, 10] i.e. a stress-free-when-straight pipeline has been subjected to displacement v_{om} under inertial loading q and then compressed by P. These are therefore equivalent to idealised studies[1] in which the pipeline has been 'disturbed' or propelled into the idealised buckling mode at amplitude $v_m|_{P_{qi}} \equiv v_{om}|_{P_{qi}}$. (Regarding overall system modelling, thermal values may be only approximately idealised therein due to the employment of simplified compatibility assumptions.[9])

Summarising, justification for the proposed prop model's conservative philosophy which results in the 37% loss in upheaval buckling resistance identified by comparing eqns (26) and (28) is twofold. First, in the absence of comprehensive as-laid residual stress data, it is a high risk assumption to be definitive about only that component which nullifies imperfect behaviour and is based upon a historically non-existent state. Second, whilst the previous in-service considerations are not to be taken to suggest that complete relieving of all residual stress components is thereby provided,[7, 12] there is little doubt that the precise and component-only elastic interpretation given by eqn (9) fails, non-conservatively, to replicate a duly definitive in-service imperfect datum state. Should definitive residual stress data become available,[11, 12] this could be readily accommodated within the present model by suitable modification of eqn (10).

Finally, it should be noted that given the imperfect force–deformation relationship of eqn (16)

$$\frac{F}{EI} = (-v'_{xxx}|_0) - (-v'_{i\,xxx}|_0) \quad (30)$$

then for $F = 0$, there is the implicit kinematic requirement

$$v'_{xxx}|_0 = v'_{i\,xxx}|_0 \qquad (F = 0) \quad (31)$$

such that, from eqn (7),

$$v'_{xxx}|_0 = -\frac{qL_i}{3EI} \qquad (F = 0) \quad (32)$$

This is true[7] for upheaval and beyond as described in the following.

POST-UPHEAVAL BUCKLING ($L_u \leqslant L \leqslant L_i$)

Upon upheaval, the tightening-up of the wavelength is reversed with L now growing as buckling ensues with further rise in temperature. As indicated in Fig. 2, mathematical modelling of post-upheaval buckling requires a two-phase structure, first with $L < L_i$ and second with $L > L_i$ (see below).

Figure 5 illustrates the initial post-upheaval stage with Fig. 5(a) detailing the crucial flexural region, boundary conditions taking the form

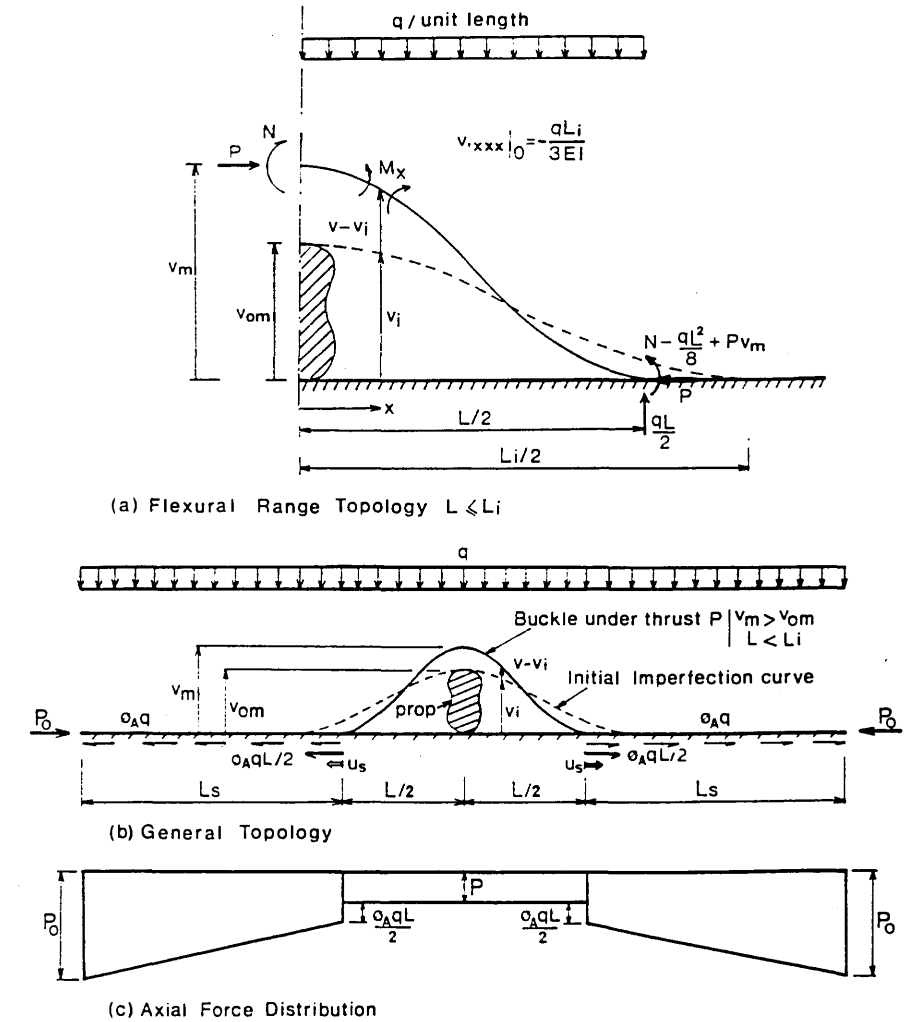

Fig. 5. Isolated prop — initial post-upheaval: details of imperfect fully mobilised model ($L < L_i$).

$$v|_{L/2} = v'_x|_{L/2} = v'_x|_0 = v'_{xx}|_{L/2} = 0 \tag{33}$$

with

$$v|_0 = v_m \tag{34}$$

Equilibrium affords for $0 \leqslant x \leqslant L/2$

$$M_x = EI(v'_{xx} - v'_{i\,xx}) = P(v_m - v) - \frac{qx^2}{2} + N \tag{35}$$

noting that eqns (12) and (32) remain valid.

Suitable manipulation of eqns (32)–(35) generates the characteristic equation

$$2\sin\frac{nL}{2} + \left(\frac{nL_i}{3} - nL\right)\cos\frac{nL}{2} - \frac{nL_i}{3} = 0 \tag{36}$$

Equation (36) is evaluated for nL for given values of L_i/L (recall the treatment of eqn (14)) and key values are given in Table 1. The deflection expression becomes

$$v = \frac{q}{EIn^4}\left(-2\cos n(L/2 - x) + \left(\frac{nL_i}{3} - nL\right)\sin n(L/2 - x)\right.$$
$$\left. + 2 - \frac{(nL)^2}{12}\left(2\frac{L_i}{L} - 3\right) + \frac{n^2L_ix}{3} - n^2x^2\right) \tag{37}$$

for $0 \leqslant x \leqslant L/2$: values for amplitude v_m are determined in turn from eqn (37), noting eqn (34).

That the present modelling smoothly interfaces, as required, with the pre-upheaval flexure modelling previously discussed at the upheaval state is available from Table 1, the respective and alternative statements for upheaval being $v_m = v_{om}$ (i.e. eqns (34) and (37)) and $F = 0$ (i.e. eqns (17) and (32)): note $0{\cdot}745 = 1/1{\cdot}3421$.

Having related buckling force P to amplitude v_m and wavelength L, it is again necessary to relate P to the temperature rise $T(P_o)$. Noting the system topology shown in Fig. 5(b) together with the axial force distribution shown in Fig. 5(c) then eqns (19), with $F = 0$, and (20) are again employed with

$$U = \frac{1}{2}\int_0^{L/2}(v'_x)^2\,dx - \frac{1}{2}\int_0^{L_i/2}(v'_{i\,x})^2\,dx$$
$$= \frac{1}{2}\left(\frac{q}{EI}\right)^2\frac{1}{n^7}\left(\frac{n^2}{36}(L_i - 3L)^2(nL + \sin nL)\sin nL - \sin nL\right.$$
$$+ \frac{nL_i}{3} - \frac{n}{3}(L_i - 3L)\cos nL + \frac{n^3L}{18}(L_i^2 - 3LL_i + 3L^2)$$

$$+ 4\left[\frac{nL_i}{3}\left(\cos\frac{nL}{2} - 1\right) - 2\sin\frac{nL}{2} + nL\right]$$

$$+ \frac{2n}{3}(L_i - 3L)\left[-\frac{nL_i}{3}\sin\frac{nL}{2} - 2\cos\frac{nL}{2} + 2\right]\Bigg)$$

$$- \left(\frac{q}{EI}\right)^2 \frac{L_i^7}{967\,680} \tag{38}$$

Figure 5 indicates that fully activated slip lengths are tacitly assumed although should the pre-upheaval flexure stage have resulted in this not being the case. eqns (24) and (25) are employed subject to $F = 0$ in place of eqns (19) and (20).

POST-UPHEAVAL BUCKLING ($L_i \leqslant L$)

The key features of this stage of buckling are illustrated in Fig. 6; proceeding as previously but noting that the transverse deflection $v = f(x, L)$ is not everywhere attended by the continuous imperfection $v_i = g(x, L_i)$, then for $0 \leqslant x \leqslant L_i/2$, equilibrium affords

$$M_x = EI(v'_{xx} - v'_{i\,xx}) = P(v_m - v) - \frac{qx^2}{2} + N \tag{39}$$

subject to boundary conditions

$$v|_0 = v_m, \quad v'_x|_0 = 0 \tag{40}$$

whilst for $L_i/2 \leqslant x \leqslant L/2$, equilibrium affords

$$M = EIv'_{xx} = P(v_m - v) - \frac{qx^2}{2} + N \tag{41}$$

subject to boundary conditions

$$v|_{L/2} = v'_x|_{L/2} = v'_{xx}|_{L/2} = 0 \tag{42}$$

together with matching conditions at $x = L_i/2$

$$v'_x = \frac{q}{EIn^3}\left(\frac{nL}{2}\cos\frac{n}{2}(L - L_i) - \sin\frac{n}{2}(L - L_i) - \frac{nL_i}{2}\right)$$

$$v'_{xx} = \frac{q}{EIn^2}\left(\frac{nL}{2}\sin\frac{n}{2}(L - L_i) + \cos\frac{n}{2}(L - L_i) - 1\right) \tag{43}$$

Manipulation of eqns (39)-(43) affords the characteristic equation

$$\sin\frac{nL}{2} - \frac{nL}{2}\cos\frac{nL}{2} + \sin\frac{nL_i}{2} - \frac{nL_i}{6}\cos\frac{nL_i}{2} - \frac{nL_i}{3} = 0 \tag{44}$$

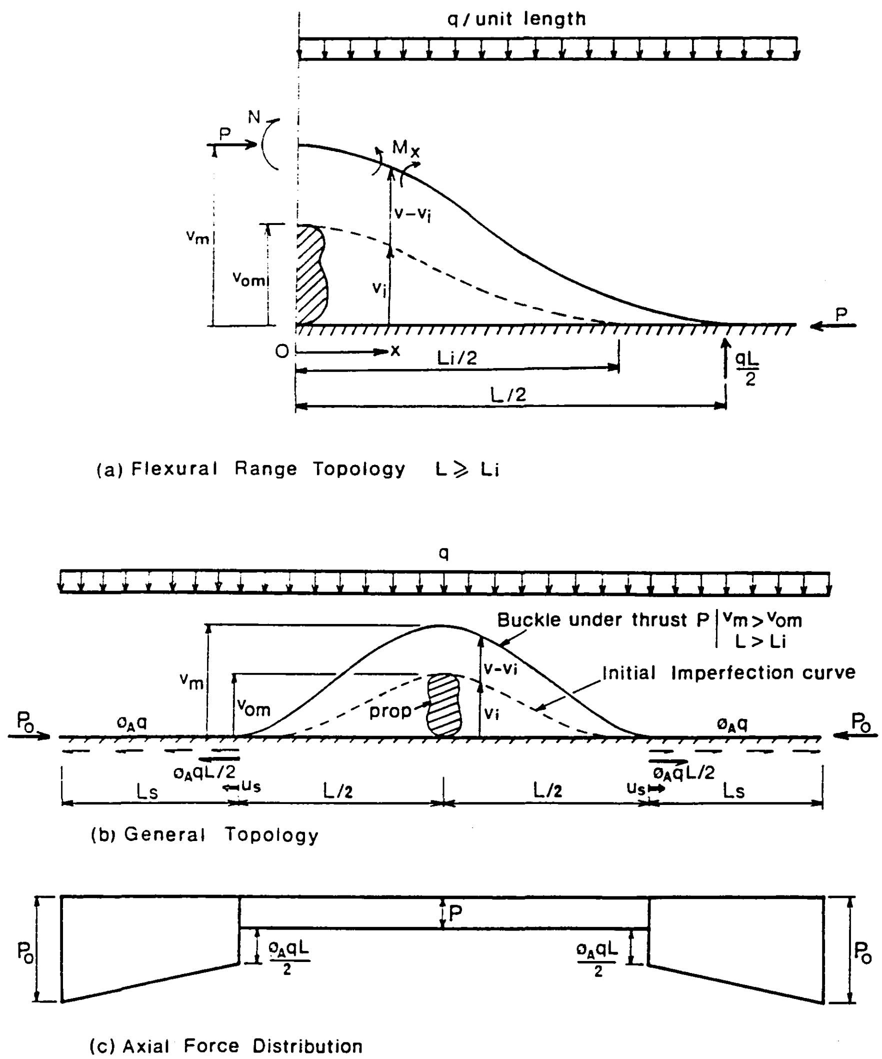

Fig. 6. Isolated prop — post-upheaval: details of imperfect fully mobilised model ($L > L_i$).

Values for nL are obtained in terms of L_i/L as previously and key values are given in Table 1. As can be seen therefrom, not only does the solution for $L > L_i$ interface smoothly with that for $L_u < L < L_i$, but also as L_i/L decreases, the imperfect (elastic) solution converges towards its idealised (elastic) envelope as anticipated.

The equations of the deflected curve take the following form: for $0 \leqslant x \leqslant L_i/2$

$$v = \frac{q}{EIn^4}\left(\left[-\frac{nL}{2}\sin\frac{nL}{2} - \cos\frac{nL}{2} - \frac{nL_i}{6}\cos\frac{nL_i}{2} - \cos\frac{nL_i}{2}\right]\cos nx\right.$$
$$\left. - \frac{nL_i}{3}\sin nx + 2 + \frac{(nL)^2}{8} - \frac{(nL_i)^2}{24} + \frac{n^2L_i}{3}x - n^2x^2\right) \quad (45)$$

and for $L_i/2 \leqslant x \leqslant L/2$

$$v = \frac{q}{EIn^4}\left(\left[-\frac{nL}{2}\sin\frac{nL}{2} - \cos\frac{nL}{2}\right]\cos nx\right.$$
$$\left. + \left[\frac{nL}{2}\cos\frac{nL}{2} - \sin\frac{nL}{2}\right]\sin nx + 1 + \frac{(nL)^2}{8} - \frac{n^2x^2}{2}\right) \quad (46)$$

The basic isolated prop modelling is concluded by the incorporation of eqns (19) ($F = 0$) and (20) — or eqns (24) and (25) if required. though by this stage it is unlikely that the slip length modelling would not have become fully established — with flexural end-shortening now of the form

$$U = \frac{1}{2}\int_0^{L/2}(v'_x)^2\mathrm{d}x + \frac{1}{2}\int_{L_i/2}^{L/2}(v'_x)^2\mathrm{d}x - \frac{1}{2}\int_0^{L_i/2}(v_i{}'_x)^2\mathrm{d}x \quad (47)$$

for $L > L_i$

where

$$\int_0^{L_i/2}(v'_x)^2\mathrm{d}x = \left(\frac{q}{EI}\right)^2\frac{1}{n^7}\left(\frac{k_4^2}{4}[nL_i - \sin nL_i] + \frac{(nL_i)^3}{18}\right.$$
$$+ \frac{(nL_i)^2}{4}[nL_i + \sin nL_i] - \frac{nL_ik_4}{6}[\cos nL_i - 1]$$
$$+ 2k_4\left[-\frac{2nL_i}{3}\cos\frac{nL_i}{2} + 2\sin\frac{nL_i}{2} - \frac{nL_i}{3}\right]$$
$$\left. + \frac{2nL_i}{3}\left[\frac{2nL_i}{3}\sin\frac{nL_i}{2} + 2\cos\frac{nL_i}{2} - 2\right]\right) \quad (48)$$

and

$$\int_{L_i/2}^{L/2}(v'_x)^2\mathrm{d}x = \left(\frac{q}{EI}\right)^2\frac{1}{n^7}\left(\frac{k_5^2}{4}[nL - \sin nL - nL_i + \sin nL_i]\right.$$
$$+ \frac{n^3}{24}[L^3 - L_i^3] + \frac{k_6^2}{4}[nL + \sin nL - nL_i - \sin nL_i]$$
$$+ \frac{k_5k_6}{2}[\cos nL - \cos nL_i]$$

$$+ 2k_5\left[-\frac{nL}{2}\cos\frac{nL}{2}+\sin\frac{nL}{2}+\frac{nL_i}{2}\cos\frac{nL_i}{2}-\sin\frac{nL_i}{2}\right]$$

$$- 2k_6\left[\frac{nL}{2}\sin\frac{nL}{2}+\cos\frac{nL}{2}-\frac{nL_i}{2}\sin\frac{nL_i}{2}-\cos\frac{nL_i}{2}\right]\Bigg) \tag{49}$$

and

$$\int_0^{L_i/2}(v_{i,x}')^2\mathrm{d}x = \left(\frac{q}{EI}\right)^2\frac{L_i^7}{483\,840} \tag{50}$$

in which constants k_4, k_5 and k_6 are determined as follows

$$k_4 = -\frac{nL}{2}\sin\frac{nL}{2}-\cos\frac{nL}{2}-\frac{nL_i}{6}\sin\frac{nL_i}{2}-\cos\frac{nL_i}{2}$$

$$k_5 = -\frac{nL}{2}\sin\frac{nL}{2}-\cos\frac{nL}{2}$$

$$k_6 = \frac{nL}{2}\cos\frac{nL}{2}-\sin\frac{nL}{2} \tag{51}$$

BASIC MODEL CASE STUDIES

The parametric data given in Table 2 have been incorporated within the foregoing formulations and Fig. 7(a) and (b) illustrate key characteristics. Two magnitudes of imperfection v_{om} have been employed to distinguish between stable and unstable responses. Note that from eqn (6)

$$L_i|_{v_{om}=100\,\mathrm{mm}} = 31{\cdot}7\ \mathrm{m} \quad \text{and} \quad L_i|_{v_{om}=250\,\mathrm{mm}} = 39{\cdot}8\ \mathrm{m} \tag{52}$$

TABLE 2
Pipeline Parameters (seabed-mounted h = 0)

Parameter	*Symbol*	*Value*	*Unit*
External diameter	D	219	mm
Wall thickness	t	14·3	mm
Elastic modulus	E	206 000	N/mm^2
Effective submerged self-weight	q	1·144	N/mm
Yield stress	σ_y	350	N/mm^2
Thermal coefficient	α	11×10^{-6}	/°C
Axial friction coefficient	ϕ_A	0·53	
Poisson's ratio[a]	ν	0·3	

[a] ν employed for evaluation of pressure component as required.

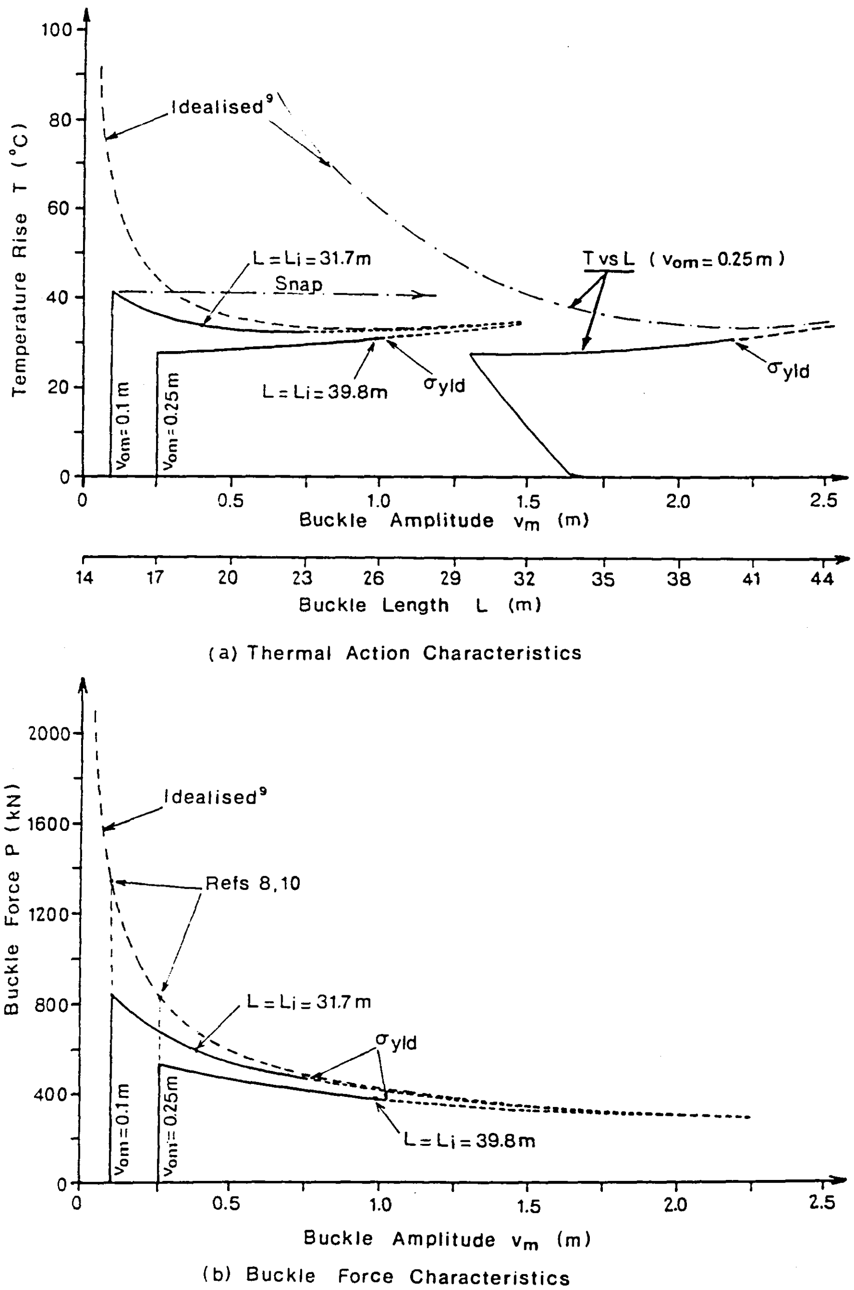

Fig. 7. Fully mobilised isolated prop models: basic model (h = 0).

The overall impression is considered to be consistent with system responses obeying the idealised envelope, being downgraded from the idealised case due to the presence of the prop imperfections, unlike elsewhere[8,10]. The smaller the imperfection (v_{om}), the more likely the occurrence of (undesirable) snap buckling with designers maintaining operating temperatures/pressures below the upheaval values for the snap cases at least. The onset of yield stress or finite rotations provides for an alternative, less demanding limitation in the case of stable post-buckling configurations: the cases illustrated in Fig. 7 involve yield stress occurring before finite rotations, the imperfect loci thereafter being shown in broken/dashed form. Further case studies follow.

ENHANCED CONSIDERATIONS

The foregoing model is applicable to a basic seabed lie topology subject to the obviation of lateral mode buckling. Indeed, advances in offshore practice include, in particular, the use of trenching and burial, continuous or discrete, together with the employment of fixed anchorages.[4] Idealised burial and fixed anchorage scenarios have been published previously.[15] The following considerations serve to expand the applicability of the present isolated prop imperfection model accordingly.

Trenching

Trenching serves to protect the pipeline, and de-trenching due to in-service buckling is to be avoided. Recalling Fig. 1(b) and Figs 4–6, then Fig. 8 illustrates an appropriate trenched section. Within the flexural or buckling wavelength L, the only effect should the pipe seek to follow the trench incline is to substitute effective inertial force m, where m is given by

$$m = q(\sin\theta + \phi_L \cos\theta) \tag{53}$$

with θ denoting the trench angle and ϕ_L representing the fully mobilised lateral friction coefficient, in place of q, the submerged self-weight of the pipe, due allowance being made for prop 'height' v_{om} as transverse deflections v and v_{om} are now inclined as suggested in Fig. 8. The effect of trenching upon buckling resistance can be gauged by the fact that with $\theta \leqslant 30°$ from a geotechnical standpoint,[18]

$$(m/q)|_{\theta=20°} = 1{\cdot}05 \quad \text{and} \quad (m/q)|_{\theta=30°} = 1{\cdot}15 \tag{54}$$

for $\phi_L = 0{\cdot}75$. Whilst upheaval temperatures are theoretically enhanced, purely vertical upheaval would actually dominate as per the basic model,

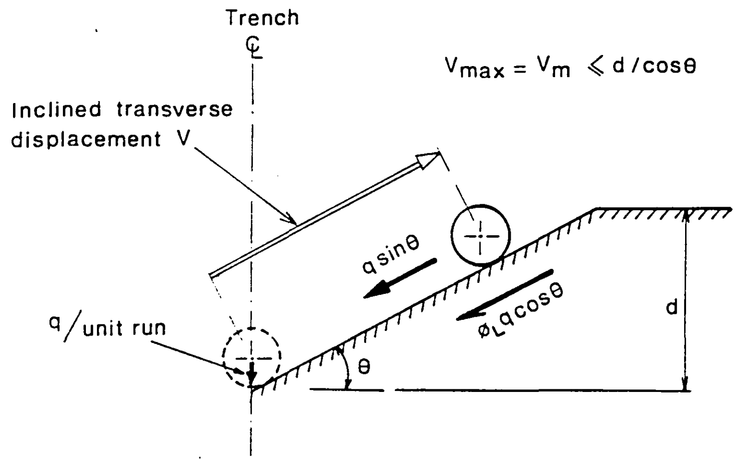

Fig. 8. Trench section.

i.e. the basic model analysis actually corresponds to a suitably trenched lie.

Burial (continuous)

Burial provides damage protection, additional insulation and enhancement of buckling resistance. Three typical burial topologies are illustrated in section in Fig. 9; two of these involve trenching as shown and, generally, cover h (or $h_1 + h_2$) $> D$. The submerged self-weight of the pipeline q is now artificially enhanced by an amount q' due to overburden pressure throughout the modelling and empirical formulae for q'/q in terms of cover (h) are available in literature regarding cases (a) and (b).[8,17] Accordingly, the effect of continuous burial upon imperfect pipeline behaviour is exhibited in Fig. 10 with regard to burial type (a). The isolated prop modelling is as given previously with the simple provision that q is replaced by $q + q'$ throughout with the axial friction coefficient numerically modified as required[17] ($\phi_A = \phi'_A$, say). Herein, for simplicity, the data of Table 2 again apply together with $q'/q = 7{\cdot}41$ for $h = 3D = 650$ mm. Clearly, extended post-upheaval buckling vertical displacement v will require $q' = f(v)$ through the buckle wavelength L as opposed to the constant value given above;[8,19] however, this constant value should suffice in the early and critical, not least to the designer, stages of upheaval itself.

It is to be recognised that continuous burial could result in the voids being in-filled to an extent that prevents pre-upheaval flexure (recall Fig. 1(c)). For this circumstance, alternative contact undulation modelling is required.[7,12]

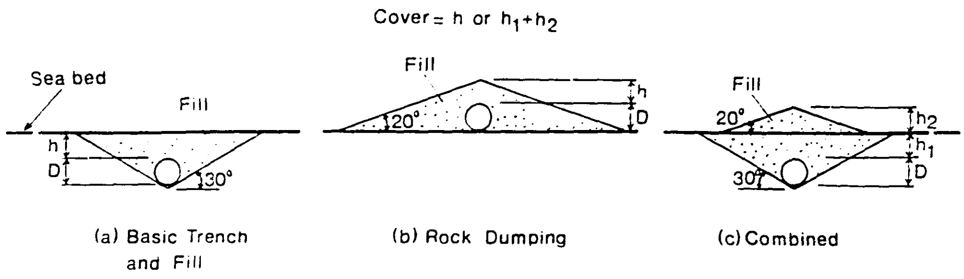

Fig. 9. Typical burial topologies.

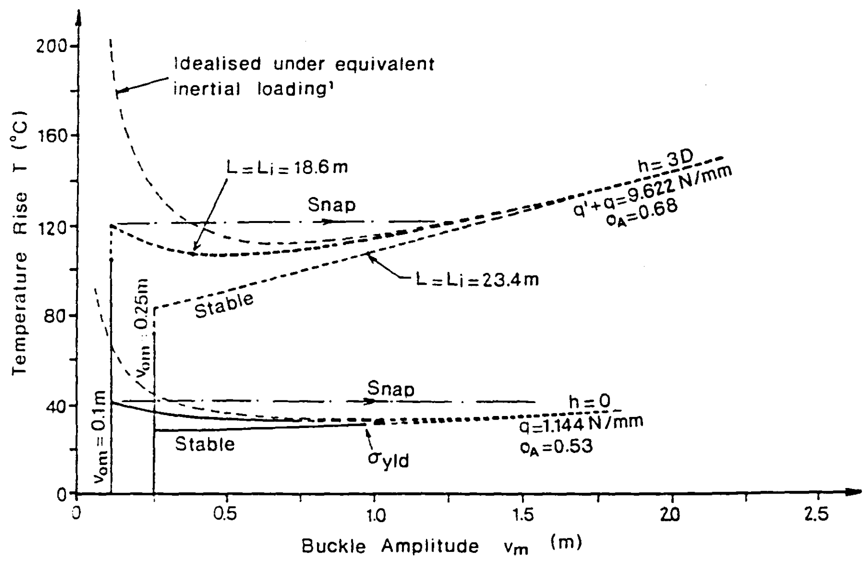

Fig. 10. Thermal action characteristics — buried pipe ($h = 3D$).

Discrete rock dumping (intermittent burial)

Continuous burial is very expensive. Costs can be reduced by the employment of intermittent burial whereby rock dumping is undertaken at judicious locations along the pipeline.[15] Cost-effectiveness is served by additional friction force generation within the slip length, i.e. $\phi'_A(q + q')$. The topology is illustrated in Fig. 11(a) whilst Fig. 11(b) shows the axial force distribution applicable upon full activation of the peel point friction reaction $\phi_A qL/2$ and of the slip length L_{s1} distributed friction force. (Prior to this stage, analysis proceeds as previously discussed for the basic topology unless the overburden slip length L_{s2} is activated for $L < L_i$ whilst checks must also be made upon the pre-upheaval flexure analysis to ascertain whether the overburden is also therein involved.)

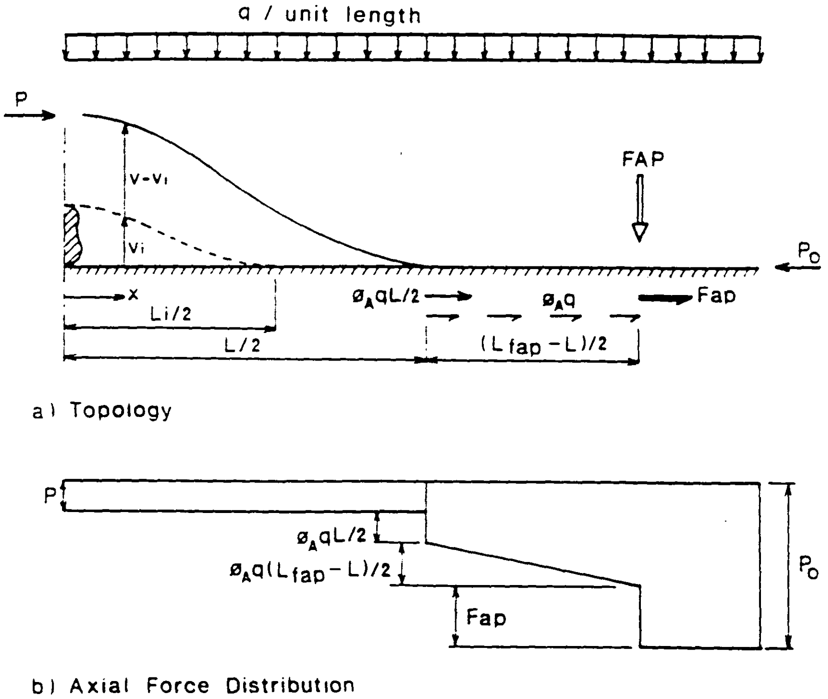

Fig. 11. Isolated prop with discrete dumping ($L > L_i$ shown).

The mechanics of the system are only modified with respect to the longitudinal equilibrium and compatibility expressions. Here, equilibrium affords

$$P_o - P = \phi_A \frac{qL}{2} + \phi_A q L_{s1} + \phi'_A q \left(1 + \frac{q'}{q}\right) L_{s2} \tag{55}$$

and longitudinal compatibility becomes

$$\frac{(P_o - P)L}{2AE} - U = -\phi_A q \left[L_{s1}^2 + (L_{s2}^2 + 2L_{s1}L_{s2})\left(1 + \frac{q'}{q}\right)\frac{\phi'_A}{\phi_A}\right] \tag{56}$$

where U can be evaluated, for $L > L_i$, from eqns (47)–(50), with

$$L_{s1} = \frac{L_D - L}{2} \tag{57}$$

and

$$L_{s2} = \frac{1}{2}\left(-L_D + \left[L_D^2 - \frac{4}{\left(1 + \frac{q'}{q}\right)}\frac{\phi_A}{\phi'_A}\left(\frac{L^2}{2} + LL_{s1} + L_{s1}^2 - \frac{2UAE}{\phi_A q}\right)\right]^{1/2}\right) \tag{58}$$

where L_D is the intermittency distance. Both L_D and q' can be varied with length of dump ($\geqslant 2L_{s2}$) then determined. The effect of intermittent burial is typified by Fig. 12 which relates to the parametric data of Table 2 together with $q'/q = 7{\cdot}41$ as previously, $\phi_A = \phi'_A$ for simplicity and $L_D = 500$ m. Note that for $L < L_i$, U can be evaluated from eqn (38) whilst for pre-upheaval studies U is determined from eqns (21)–(23); eqns (57) and (58) remain valid for both stages. It is assumed, given the purpose of intermittent burial, that $L < L_D$ and $L_i < L_D$.

There are a variety of particular slip length configurations to consider when analysing these systems, depending upon when the overburden slip length is activated: a program suite is strictly required for this purpose.

Fixed anchor points

Fixed anchor points enhance buckling resistance by simply absorbing some proportion of the pre-buckling force $P_o = AE\alpha T$. The respective topology is shown in Fig. 13 together with the appropriate axial force distribution: the figure relates to the case of the peel point friction force $\phi_A qL/2$ being fully activated, the fully mobilised axial friction force $\phi_A q$ being generated throughout the slip length $(L_{fap} - L)/2$, where L_{fap} denotes the spacing of the fixed anchors, and $L_{fap} > L > L_i$.

Longitudinal equilibrium affords

$$P_o - P = \phi_A \frac{qL}{2} + \phi_A \frac{q(L_{fap} - L)}{2} + F_{ap} \qquad (59)$$

where F_{ap} denotes anchorage capacity, whilst longitudinal compatibility becomes

$$-\left(F_{ap} + \phi_A \frac{q(L_{fap} - L)}{4}\right)\left(\frac{L_{fap} - L}{2AE}\right) = \frac{(P_o - P)L}{2AE} - U \qquad (60)$$

where evaluations for U are determined in similar manner to those relating to eqn (56).

Both the spacing L_{fap} and the capacity F_{ap} of the anchors can be varied, the latter capacities being in excess of 250 kN. The effect of employing fixed anchor points is exemplified in Fig. 14 which relates to the data given in Table 2 together with $L_{fap} = 500$ m. Comments regarding the need for a program suite as mentioned above to cater for the variety of possible slip length configurations involved again apply here.

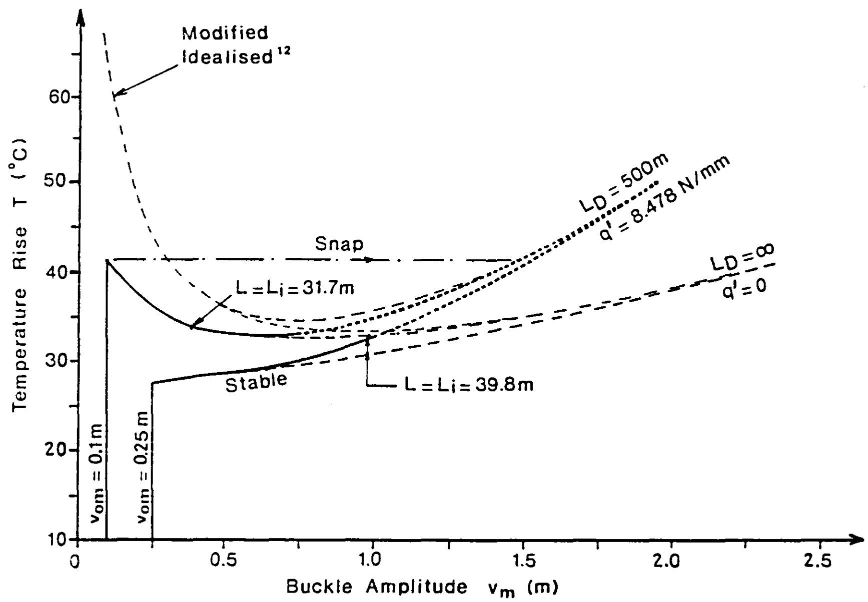

(a) Effect of varying overburden q'

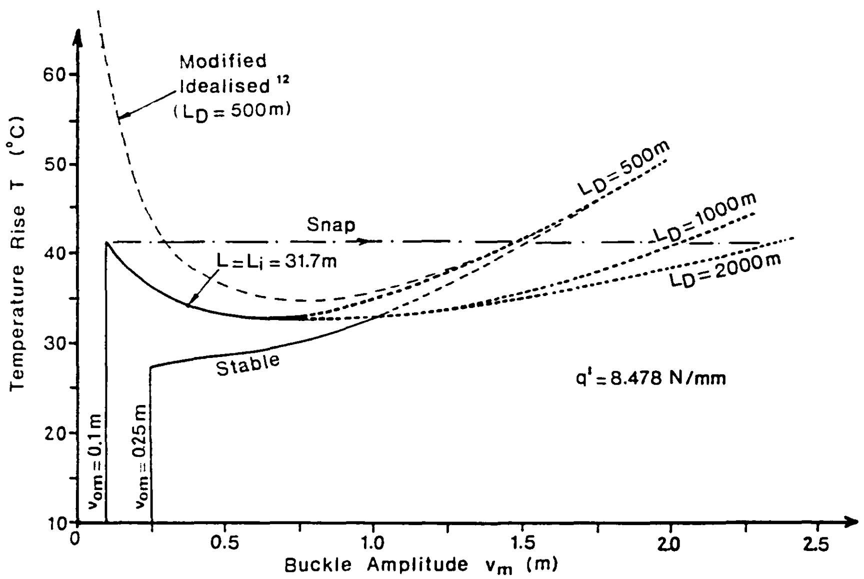

(b) Effect of varying intermittency distances L_D

Fig. 12. Thermal action characteristics — intermittent burial.

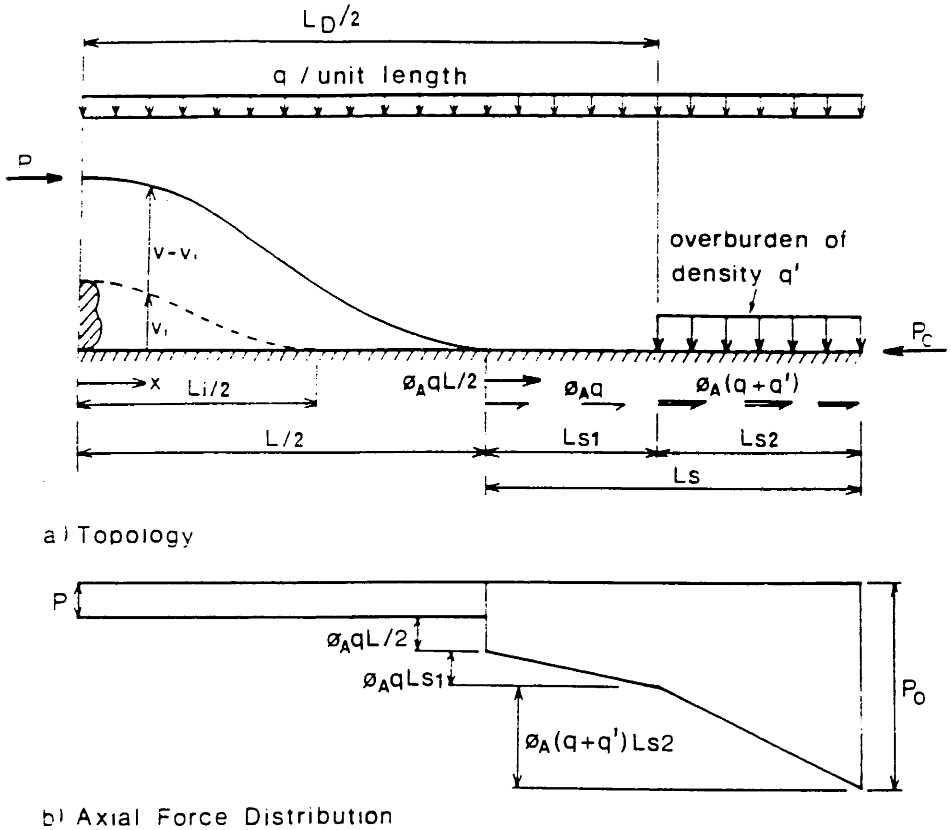

Fig. 13. Isolated prop with fixed anchor points ($L > L_i$ shown).

DISCUSSION

The basic isolated prop model proposed here is quite distinct from previously recorded formulations.[8,10] unlike these alternative models, the present proposal affords elastically imperfect behaviour, typified by Figs 7, 10, 12 and 14, consistent with the concept that conservative parametric convergence towards the corresponding idealised solutions should result as the relative effect of any initial imperfection decays with increasing system deformation. Alternative modelling[8,10] actually suggests that for any prop (imperfection) amplitude v_{om}, the lift-off buckling force corresponds identically to that afforded by idealised (i.e. non-imperfect) studies for $v_m = v_{om}$ as identified by eqns (28) and (29).[1,2] Here, the lift-off or upheaval state, so important to offshore designers, is shown to suffer a potential 37% degradation in this resistance if the existence of a supposedly previous yet totally hypothetical stress-free-when-straight

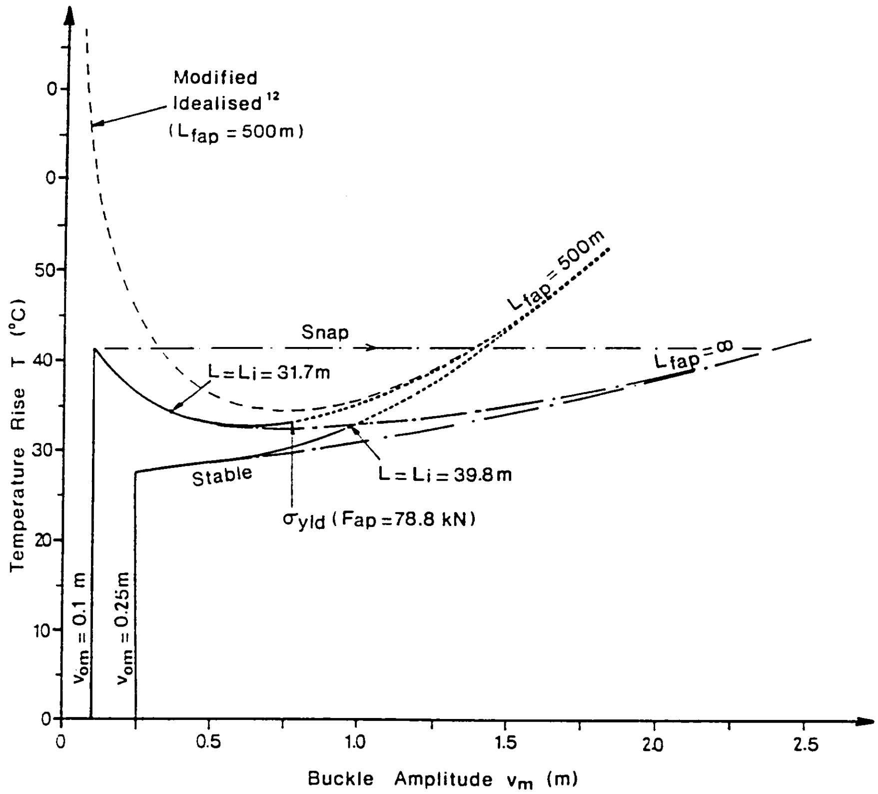

Fig. 14. Thermal action characteristics — fixed anchor points seabed-mounted/trenched lie ($h = 0$).

state is questioned. Further, the similarity in the respective upheaval lengths L_u as suggested by eqns (27) and (29) belies more substantial differences in the appropriate action/response characteristics as typified by Fig. 7.

The deformation characteristics given by eqn (5) are accepted for the present model on the basis of the support provided for eqn (6) by field observations.[6] However, the precise stressing formulation given by eqn (9) is not considered to reflect an accurate assessment of the state of residual stress in the pipe in the as-laid state. Not only does the acceptance of eqn (9) in conjunction with eqn (5) require the existence of an historically fictitious idealised lie, it also requires that residual stress due to fabrication and laying operations[11, 12] can, by comparison, be safely ignored. Given the complexities attending the hostile environment involved,[12] it is considered inappropriate and high risk to construct the analysis other than in accord with that well-established principle of elastic stability whereby the datum is prescribed as being stress-free-when-initially-deformed.[13] As noted above, the effect is duly conservative. The model could accommodate definitive and comprehensive residual stress data, should they become available.

Further support for this approach is available from infilled prop studies which similarly suppress any supposed as-laid residual stressing.[6, 7, 12, 16] Therein, such stressing is considered to be relieved under in-service conditions due to the interaction of non-linear fill accretion and slip length axial friction behaviour with thermal cyclic loading.[7, 17] The prototypes corresponding to the isolated and infilled prop topologies share the common features of actually complex non-linear axial friction behaviour and the initial bending moments supposedly suggested by eqn (9). Therein, idealised theory indicates that 50% N_i, the crown and maximum moment, is due to self-weight considerations, the remainder being due to the prop imperfection *per se* in the form $6EIv_{om}/L_i^2$. Although lacking fill support to assist in cyclic thermal stress relieving, it is surely inconceivable to suggest these components will accurately reflect in-service residual stress levels following numerous cycles of in-service non-linear axial friction response.[7, 17] Indeed, in-service pre-upheaval flexural and axial movement occurs by design with this prototype — the buckle length/temperature rise locus of Fig. 7 is particularly relevant here — and consequent as-laid stress relief due to the onset of localised plasticity under thermal loading must be considered highly probable in a manner similar to that discussed elsewhere.[12] Such 'conversion' into an imperfection of form would clearly be influenced by the out-of-straightness ratio v_{om}/L_i. Noting eqn (6), then the ratios corresponding to the case studies involving eqn (52) are 1/317 and 1/160 respectively and are considered typical of offshore practice.

Whilst the basic seabed-mounted model essentially relates to a purely trenched lie, the effects of employing enhanced burial and anchorage techniques are clearly shown in Figs 10, 12 and 14 with all-round improvements in buckling resistance being provided as anticipated.[15, 17] Imperfection-based data are thereby made available for design purposes; maximum operating temperature/pressure rises — recall the arguments concerning pressure-equivalent parameter T' in eqn (2) — clearly cannot exceed the temperature rise at upheaval, $T \equiv T_u$ say, for unstable/snap cases, whilst the onset of yield stress or finite rotations ($v'_{x\,\max} \leqslant 0{\cdot}1^r$) delimits the stable post-buckling cases studies as shown in Figs 7, 10, 12 and 14. Whilst a closed-form solution is available for the crucial upheaval buckling force P_u as given by eqn (26), a closed-form evaluation of T_u is not computationally amenable assuming the development of slip length friction forces during pre-upheaval flexure. Maximum curvature, important to the buckling mechanism, occurs at the crown throughout. It increases from the imperfection value given by eqn (8) to $-0{\cdot}106qL^2/EI(L \equiv L_u) = -0{\cdot}0588qL_i^2/EI$ at upheaval; these latter values are available from eqn (15) with $P = P_u$.

Qualitatively, the isolated prop model action/response characteristics differ from those associated with contact undulation models (recall Fig. 1) by virtue of the cusp upheaval (recall Figs 7, 10, 12 and 14). Whilst the interesting asymmetric implications (note below) have been discussed elsewhere,[9] the cusp is associated with the fact that the pre-buckling flexure phase, unavailable to contact undulation models, results in a singular change in direction of wavelength propagation (L) as amplitude commences its monotonic path. Intriguingly, solution data for the post-buckling $L > L_i$ phase correspond with those produced by an equivalent model (for common prop height v_{om}) designed to deal with the infilled prop imperfection case in which buckling initiates with a blister developing upon the overbend crown[7] (recall Fig. 1(c)). The implication is that whilst infilling of the voids reduces resistance to upheaval by preventing pre-upheaval flexural energy release, by the post-buckling state $L = L_i$, behaviour is effectively common for the two cases.

Spurred by the admission of pipeline buckling failures in the North Sea,[4–6] full thermo-mechanical system testing is presently being undertaken by several authorities. Testing upon 6-m lengths of 3/8-in o.d. pipe suffering as-delivered imperfections is presently being conducted in-house. To-date, with respect to isolated prop studies involving fixed anchor points and employing imperfection amplitudes of 20 mm and 30 mm, the theory presented here provides upheaval temperatures within 4% of the observed experimental cases (average of six tests). Theoretical buckle lengths at upheaval are within 2% of the corresponding experimental values. Qualitative observations include occurrences of asymmetry[9] and minor buckling of the supposed slip length in the proximity of the peel points. The latter questions the transversality condition, zero peel point curvature, widely adopted in contact surface modelling. Figure 15 illustrates the central region of the pipe during post-upheaval buckling with an amplitude of approximately twice the prop height; the prop takes the form of a PTFE-coated steel blade of 30 mm height visible below the pipe. Accurate upheaval specification is provided by a simple make-or-break electrical contact. Whilst it is not claimed as comprehensive proof, the above noted experimental/theoretical correlation does serve to encourage confidence in the prop model's capabilities.

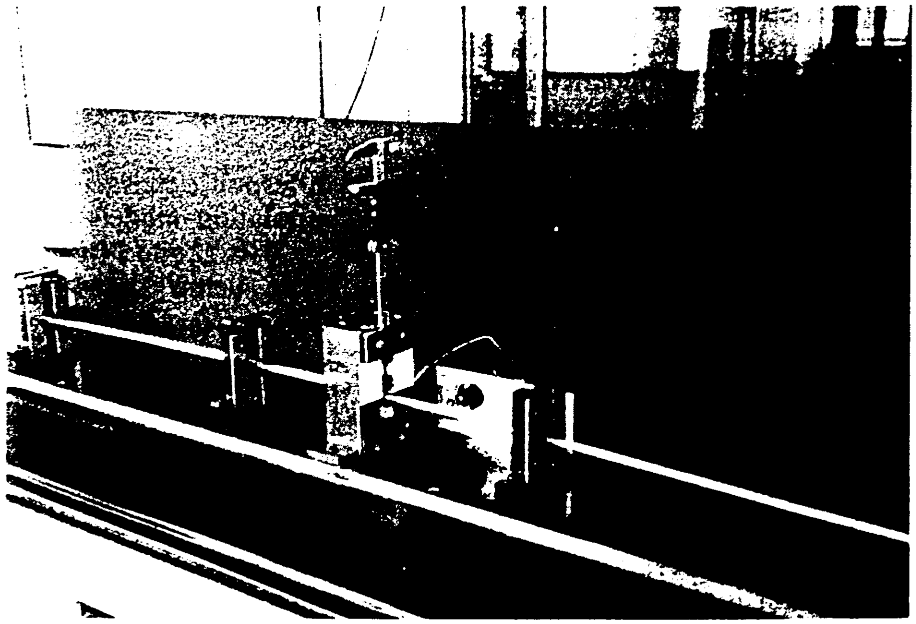

Fig. 15. Isolated prop experimentation.

CONCLUSIONS

By not requiring reference to a fictitious stress-free-when-straight datum, the isolated prop model described here is considered to present a consistent elastic interpretation of the corresponding prototype behaviour subject only to the provision of accurate residual, as-laid stressing data: this is a common feature of all elastic subsea pipeline buckling models available in the literature. However, this is a complex matter: for example, whilst residual laying tension should improve buckling resistance perhaps beyond idealised values, field observations have shown buckling failures. The proposed model thereby suggests interpreting the prop as generating an imperfection of form on the basis of a worst case scenario: whilst it is not suggested that the stress-relieving mechanism discussed would remove all as-laid, residual stressing, the fact that some degree of relief is highly probable under in-service, pre-upheaval, cyclic operation demands this stress-free-when-initially-deformed scenario must be considered given its relatively conservative implications. The proposed model is capable of dealing with the various enhanced configurations presently being employed in the North Sea and, computer mounted, is readily suitable for design application.

REFERENCES

1. Hobbs. R. E.. Pipeline buckling caused by axial loads. *Journal of Constructional Steel Research.* **1**(2) (January 1981) 2–10.
2. Taylor. N. & Gan. A. B.. Regarding the buckling of pipelines subject to axial loading. *Journal of Constructional Steel Research.* **4**(1) (January 1984) 45–50.
3. Taylor. N. & Gan. A. B.. Submarine pipeline buckling-imperfection studies. *Thin-Walled Structures.* **4**(4) (1986) 295–323.
4. Guijt. J.. Upheaval buckling of offshore pipelines: overview and introduction. In *Proceedings of the 22nd Annual OTC.* Houston. Texas. Vol. 4. May 1990. pp. 573–8.
5. Palmer. A. C.. Ellinas. C. P.. Richards. D. M. & Guijt. J.. Design of submarine pipelines against upheaval buckling. In *Proceedings of the 22nd Annual OTC.* Houston. Texas. May 1990. pp. 540–50.
6. Nielsen. N. J. R.. Lyngberg. B. & Pedersen. P. T.. Upheaval buckling failures of insulated buried pipelines — a case story. In *Proceedings of the 22nd Annual OTC.* Houston. Texas. Vol. 4. May 1990. pp. 581–600.
7. Pedersen. P. T. & Jensen. J. J.. Upheaval creep of buried heated pipeline with initial imperfections. *Journal of Marine Structures.* **1** (1988) 11–22.
8. Boer. S. *et al.*. Buckling considerations in the design of the gravel cover for a high temperature oil line. In *Proceedings of the 18th Annual OTC.* Houston. Texas. May 1986.
9. Ballet. J. P. & Hobbs. R. E.. Asymmetric effects of prop imperfections on the upheaval buckling of pipelines. *Thin-Walled Structures* (in press).
10. Ju. G. T. & Kyriakides. S.. Thermal buckling of offshore pipelines. *Journal of OMAE.* **110** (November 1988) 355–64.
11. Palmer. A. C.. Hutchinson. G. & Ellis. J. W.. Configuration of submarine pipelines during laying operations. Transaction of the American Society of Mechanical Engineers. *Journal of Engineering for Industry.* **96** (1974) 1112–18.
12. Nielsen. N. J. R. *et al.*. New design criteria for upheaval creep of buried subsea pipelines. In *Proceedings of the 22nd Annual OTC.* Houston. Texas. May 1990. 243–9.
13. Timoshenko. S. P. & Gere. J. M.. *Theory of Elastic Stability* (2nd edn). McGraw-Hill. New York. 1961. pp. 76–81.
14. Taylor. N. & Gan. A. B.. Refined modelling for the vertical buckling of submarine pipelines. *Journal of Constructional Steel Research.* **7** (1987) 55–74.
15. Hobbs. R. E. & Liang. F.. Thermal buckling of pipelines close to restraints. In *Proceedings of the Offshore Mech. Arctic Engineering Conference.* The Hague. ASME. paper OMAE-89-812. 1989.
16. Klever. F. J.. Van Helvoirt. L. C. & Sluyterman. A. C.. A dedicated finite-element model for analyzing upheaval buckling response of submarine pipelines. In *Proceedings of the 22nd Annual OTC.* Houston. Texas. Vol. 2. May 1990. 529–38.
17. Taylor. N.. Tran. V. C. & Richardson. D.. Interface modelling for upheaval subsea pipeline buckling. In *Proceedings of 4th International Conference on Computational Methods and Experimental Measurements.* Capri. Italy. Springer-Verlag. May 1989. pp. 269–82.

18. Bowles, J. E., *Foundation Analysis and Design* (3rd edn). McGraw-Hill, New York, 1982, pp. 59–60.
19. Schaminee, P. E. L., Zrn, N. F. & Schotman, G. J. M., Soil response for pipeline upheaval buckling analyses: Full-scale laboratory tests and modelling. In *Proceedings of the 22nd Annual OTC*, Houston, Texas, Vol. 4, May 1990, pp. 563–72.